# Síntesi i estudi magnètic de compostos polinuclears de Ni(II) amb lligands piridiloxima

Jordi Esteban Jarne

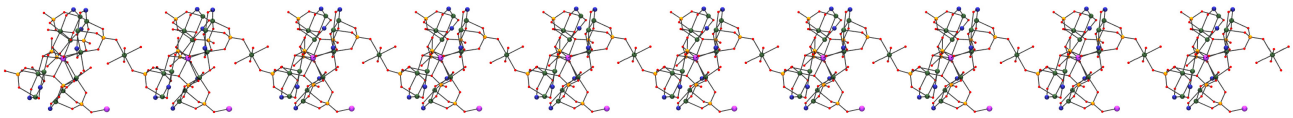

# Síntesi i estudi magnètic de compostos polinuclears de Ni(II) amb lligands piridiloxima

Jordi Esteban Jarne

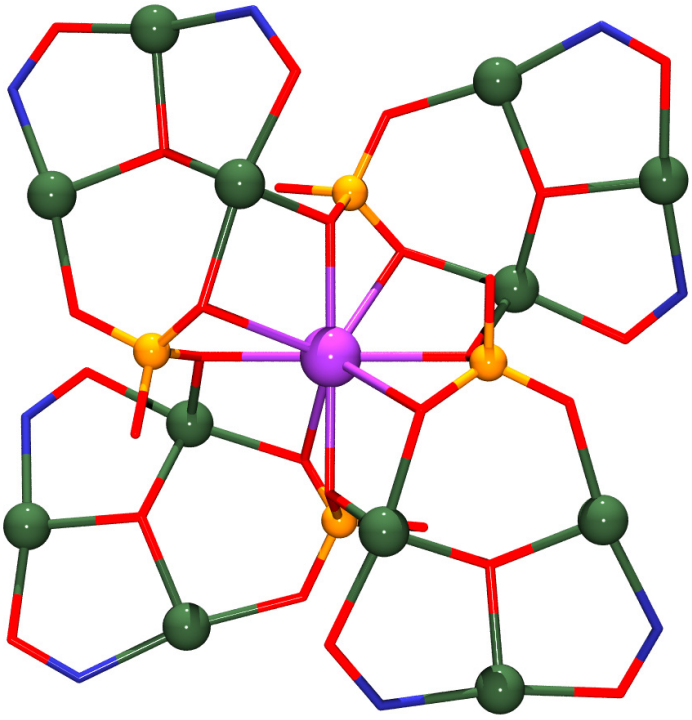

Universitat de Barcelona

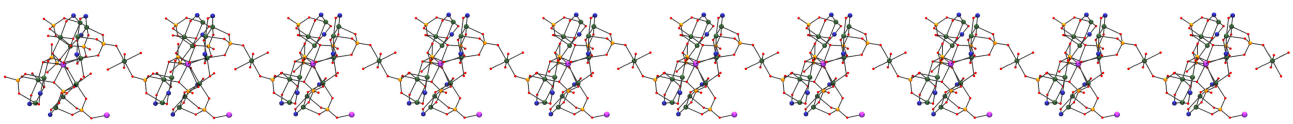

Universitat de Barcelona

Facultat de Química

Departament de Química Inorgànica

Programa de Doctorat: Química Inorgànica Molecular

# SÍNTESI I ESTUDI MAGNÈTIC DE COMPOSTOS POLINUCLEARS DE Ni(II) AMB LLIGANDS PIRIDILOXIMA

**Jordi Esteban Jarne**

Director: Dr. Albert Escuer Fité, Departament de Química Inorgànica

Albert Escuer i Fité, Catedràtic del Departament de Química Inorgànica de la Facultat de Química de la Universitat de Barcelona,

CERTIFICA: que el treball titulat *Síntesi i estudi magnètic de compostos polinuclears de Ni(II) amb lligands piridiloxima* que presenta el Sr. Jordi Esteban Jarne per optar al grau de Doctor per la Universitat de Barcelona, ha estat realitzat sota la seva direcció al departament de Química Inorgànica d'aquesta Facultat.

Barcelona, juny de 2014

Dr. Albert Escuer i Fité

*Love hides in molecular structures*

*Love hides*, The Doors

# 1

# Introducció

## 1.1. Magnetisme Molecular[1,2]

### 1.1.1. Aspectes generals

El magnetisme és un fenomen físic que descriu la resposta d'un material, a escala microscòpica, en presència de camps magnètics. Aquesta resposta pot ser, bàsicament, de dos tipus: el material pot ser atret o repel·lit pel camp magnètic. L'atracció d'un material per un camp magnètic s'anomena paramagnetisme i es produeix quan un sistema té electrons desaparellats; mentre que la repulsió del material en presència del camp s'anomena diamagnetisme i es dóna en sistemes que tenen tots els electrons aparellats.

El magnetisme molecular estudia la resposta d'un material, a escala molecular, a un camp magnètic aplicat, i en certs casos, permet observar fenòmens quàntics que no s'observen a escala macroscòpica però que són necessaris per entendre el seu funcionament.

En introduir una mostra en un camp magnètic *H* s'observa que el camp a l'interior de la mostra, anomenat inducció magnètica (*B*), és diferent del camp aplicat. Aquesta variació en el camp s'anomena magnetització, *M*.

$$B = H + 4\pi M$$

Formalment, la magnetització es defineix com la variació de l'energia interna de la mostra en ser pertorbada per un camp magnètic extern:

$$M = -\frac{\delta E}{\delta H}$$

La magnetització molar es descriu, per tant, com:

$$M_M = N\langle\mu\rangle \qquad \mu_n = -\frac{\delta E_n}{\delta H}$$

on *N* és el número d'Avogadro i $<\mu>$ la magnetització mitjana de totes les molècules (sent $\mu_n$ la magnetització de cadascuna d'elles).

Aplicant el factor de probabilitat de Boltzman ($P_n$), que indica la probabilitat de població d'un estat energètic en funció de la temperatura, obtenim l'equació:

$$M = N\underbrace{\sum_n \mu_n P_n}_{<\mu>} = N\frac{\sum_n(-\delta E_n/\delta H)\exp(-E_n/kT)}{\sum_n \exp(-E_n/kT)}$$

Per altra banda, es defineix la susceptibilitat magnètica, $\chi$, com la variació de la magnetització en funció del camp magnètic aplicat:

$$\chi = \frac{\partial M}{\partial H}$$

que és una magnitud adimensional.

Com generalment es treballa a camps en què la magnetització presenta una resposta lineal respecte d'aquest, es pot expressar $\chi$ com la relació entre la magnetització i el camp magnètic aplicat (sempre que es treballi dins el règim lineal $M/H$):

$$\chi = \frac{M}{H}$$

La susceptibilitat es pot expressar de moltes formes, però la més habitual i la que s'utilitza en aquesta memòria és la susceptibilitat magnètica molar, $\chi_M$:

$$\chi_M = \chi\frac{M_W}{\rho}$$

on $M_W$ és el pes molecular i $\rho$ és la densitat de la mostra en g/cm$^3$. D'aquesta fórmula s'extreu que les unitats de la susceptibilitat magnètica molar són cm$^3$/mol (cm$^3$·mol$^{-1}$).

La mesura de susceptibilitat magnètica ($\chi_{mes}$) és la suma de dues contribucions: la susceptibilitat diamagnètica ($\chi_{dia}$) que és independent de la temperatura, depèn dels electrons de les capes plenes del metall i dels lligands i té un valor negatiu; i la susceptibilitat paramagnètica ($\chi_{para}$), que depèn de la temperatura, prové del trencament de la simetria esfèrica dels àtoms amb electrons desaparellats en aplicar un camp magnètic extern i té un valor positiu.

La contribució paramagnètica de la susceptibilitat es calcula de la següent forma:

$$\chi_{para} = \chi_{mes} - \chi_{dia}$$

on el valor de $\chi_{dia}$ d'una mostra es calcula teòricament com la suma de les contribucions diamagnètiques dels àtoms i enllaços que la formen, que per compostos de coordinació són de l'ordre de $10^{-4}$ $cm^3 \cdot mol^{-1}$ (dos ordres de magnitud menys que $\chi_{para}$). El valor d'aquesta contribució està tabulat i es coneix com les constants de Pascal:[3]

$$\chi_{dia} = \sum \chi_{atoms}^{dia} + \sum \chi_{enllaços}^{dia}$$

A partir d'aquest moment, quan es tracti de susceptibilitat magnètica en aquesta memòria, es farà referència a la contribució paramagnètica de la susceptibilitat. El càlcul de la contribució diamagnètica i la seva resta de la susceptibilitat mesurada queda implícit.

**Equació de Van Vleck**

Tot i que la fórmula de la magnetització presentada anteriorment

$$M = \frac{\sum_n (-\delta E_n / \delta H) \exp(-E_n / kT)}{\sum_n \exp(-E_n / kT)}$$

és una fórmula general i es pot aplicar en tots els casos, la seva aplicació és difícil perquè requereix el coneixement de la variació dels diversos estats energètics $E_n$ (que depèn del camp aplicat $H$) per tots els nivells ocupats i per cada temperatura per poder calcular el conjunt de derivades $\delta E_n / \delta H$.

L'any 1932, el físic nord-americà John Hasbrouck Van Vleck va simplificar l'expressió de la susceptibilitat magnètica basant-se en el mètode de pertorbacions, suposant l'existència d'una zona en què la magnetització presentava un comportament lineal respecte al camp magnètic.[4]

Per realitzar aquesta simplificació, primer va descompondre l'energia del sistema en funció de les pertorbacions d'acord amb la següent fórmula:

$$E_n = E_n^{(0)} + E_n^{(1)} H + E_n^{(2)} H^2 + \ldots$$

on $E_n^{(0)}$ és l'energia del nivell n en absència de camp (o camp zero) i $E_n^{(1)}$ i $E_n^{(2)}$ són els coeficients Zeeman de primer i segon ordre.

En segon lloc, Van Vleck va suposar que $H/kT<<1$ per valors de camp ($H$) no molt elevats i valors de temperatura ($T$) no molt baixos, de forma que la nova fórmula de magnetització es pot expressar com:

$$M = \frac{NH\sum_n (E_n^{(1)2}/kT - 2E_n^{(2)})\exp(-E_n^{(0)}/kT)}{\sum_n \exp(-E_n^{(0)}/kT)}$$

Si se substitueix aquesta equació a la fórmula general de la magnetització s'obté l'equació de Van Vleck:

$$\chi_M = \frac{M_M}{H} = \frac{N\sum_n (E_n^{(1)2}/kT - 2E_n^{(2)})\exp(-E_n^{(0)}/kT)}{\sum_n \exp(-E_n^{(0)}/kT)}$$

que ja no conté les derivades $\delta E_n/\delta H$ i permet el càlcul de $\chi$ coneixent només $E_n^{(0)}$, $E_n^{(1)}$ i $E_n^{(2)}$. Aquesta equació se simplifica per compostos mononuclears o polinuclears formats per ions sense contribució orbital (termes energètics A i E, en què $E_n^{(2)}=0$) i s'obté l'expressió :

$$\chi_M = \frac{N\sum_n E_n^{(1)2}\exp(-E_n^{(0)}/kT)}{kT\sum_n \exp(-E_n^{(0)}/kT)}$$

Per últim, tenint en compte que

$$\sum (E_{|S,m_s>})^2 = g^2\beta^2[S^2 + (S-1)^2 + ... + (-S)^2] = g^2\beta^2[S(S+1)(2S+1)/3]$$

i substituint aquesta equació a cadascun dels nivells energètics $E_n$ s'obté la fórmula general:

$$\chi_M = \frac{Ng^2\beta^2}{3kT}\frac{\sum_n S(S+1)(2S+1)\exp(-E_S^{(0)}/kT)}{\sum_n (2S+1)\exp(-E_S^{(0)}/kT)}$$

on *N* és el número d'Avogadro, *g* és la constant giromagnètica (2,00232 per a l'electró lliure), β és el magnetó de Bohr ($4{,}668 \cdot 10^{-5}$ $cm^{-1} \cdot G^{-1}$), *k* és la constant de Boltzmann (0,695 $cm^{-1} \cdot K^{-1}$) i *S* és l'spin total de cada nivell energètic $E_S$.

**Lleis de Curie i Curie-Weiss**

Per un sistema amb un únic centre paramagnètic que presenta un únic estat d'spin, la susceptibilitat molar donada per l'equació de Van Vleck es redueix a:

$$\chi_M = \frac{Ng^2\beta^2}{3kT} S(S+1)$$

Aquesta expressió es coneix com la llei de Curie i estableix que $\chi_M$ = ct/*T* (on $N\beta^2/k$ = 0,375 $cm^3 \cdot mol^{-1}$), i per tant, $\chi_M T$ és constant per tot el rang de temperatures. Aquesta llei, però, només és aplicable a aquells compostos que no presenten acoblament spin-òrbita de primer ordre. Per tal de poder ajustar compostos amb acoblament spin-òrbita poc marcat, es va modificar la llei de Curie i es va obtenir la llei de Curie-Weiss, que s'exposa a continuació:

$$\chi_M = \frac{Ng^2\beta^2}{3k(T-\theta)} S(S+1)$$

i determina que, per un determinat rang de temperatures, $\chi_M = ct/(T-\theta)$.

**Hamiltonià de Heisenberg-Dirac-Van Vleck**

La llei de Curie permet ajustar el comportament d'un únic centre paramagnètic, però no és aplicable a compostos polinuclears. Per a tal efecte, es necessita un tractament més complex de l'equació de Van Vleck, com és el Hamiltonià de Heisenberg-Dirac-Van Vleck (HDVV).El Hamiltonià HDVV descriu la interacció entre els spins de diferents centres paramagnètics i permet calcular el valor de les interaccions que s'estableixen entre aquests, anomenades constants d'acoblament o *J* i mesurades en $cm^{-1}$.

L'exemple més senzill és per un compost dinuclear amb dos centres paramagnètics A i B, en què s'obté el Hamiltonià d'intercanvi magnètic:

$$H = -JS_A S_B$$

sent $S_A$ i $S_B$ els operadors d'spin de cadascun dels ions i $J$ la interacció entre ells. Per conveni, si els moments magnètics s'alineen en el mateix sentit, el valor de la constant d'acoblament serà positiu i es parlarà d'un acoblament ferromagnètic, mentre que si els moments magnètics es disposen en sentits contraris s'anomenarà acoblament antiferromagnètic i el valor de $J$ serà negatiu.

Matemàticament s'obté que $S = S_A + S_B$, $S^2 = S_A{}^2 + S_B{}^2 + 2S_A \cdot S_B$ i $S_A \cdot S_B = (S^2 - S_A{}^2 - S_B{}^2)/2$, de forma que es pot substituir el Hamiltonià anterior per

$$H = \frac{-J(S^2 - S_A^2 - S_B^2)}{2}$$

que té solució quàntica exacta, els valors propis de la qual són:

$$E_{(S,S_A,S_B)} = \frac{-J[S(S+1) - S_A(S_A+1) - S_B(S_B+1)]}{2}$$

Com $S_A$ i $S_B$ són valors constants es poden eliminar de l'equació d'energia modificant l'origen d'energia potencial, de forma que el valor d'energia per a cada valor de $S$ es calcula com:

$$E_{(S)} = \frac{-J[S(S+1)]}{2}$$

Els valors d'energia $E_S$ calculats a partir d'aquesta fórmula per a cadascun dels estats magnètics del sistema ($S$, $S-1$, ..., $-S$) s'introdueixen a l'equació de Van Vleck per tal de poder descriure la mesura de susceptibilitat i obtenir el valor de la constant d'acoblament $J$, que es defineix com la diferència energètica entre l'estat $E_S^{(0)}$ i l'estat excitat energèticament més proper $E_S^{(1)}$.

El límit d'aplicació del Hamiltonià HDVV i de les equacions derivades d'aquest venen donades per la nuclearitat i el número d'acoblaments magnètics presents en un compost, que poden donar equacions massa extenses com per operar amb elles. És per aquest motiu que es necessiten certes eines o programes per poder calcular aquests Hamiltonians i ajustar les mesures de susceptibilitat, com són els programes CLUMAG,[5] MAGPACK-fit[6] o PHI.[7]

Per acabar, val la pena destacar que dins la comunitat científica hi ha una certa disparitat referent al Hamiltonià HDVV i s'utilitzen indistintament els Hamiltonians $H = -J \cdot S_A \cdot S_B$ i $H = -2J \cdot S_A \cdot S_B$ (l'única diferència entre Hamiltonians és el valor de $J$, que en el primer cas serà el doble que en el segon). En aquesta memòria es tractarà sempre amb el Hamiltonià $H = -J \cdot S_A \cdot S_B$.

**Frustració d'spin i interaccions competitives**[8]

La situació en què un o més spins d'un sistema no troben una orientació que s'adigui a totes les interaccions amb spins veïns rep el nom de sistema amb interaccions competitives. Aquest fet genera diferents estats propers en energia i amb valors de $S$ diferents. El cas concret en què els estats d'spin són degenerats (d'igual energia) s'anomena frustració magnètica o d'spin.

L'exemple clàssic d'aquest fenomen és un triangle format per tres centres paramagnètics (tres cations metàl·lics) amb el mateix moment magnètic ($S_A$) acoblats antiferromagnèticament, que pot presentar dues interaccions diferents ($J_1$, $J_2$) si es tracta d'un triangle isòsceles, figura 1, o una única constant d'acoblament ($J_1 = J_2 = J$) si es tracta d'un triangle equilàter. La relació entre els dos acoblaments determinarà el sentit del moment magnètic del tercer catió metàl·lic.

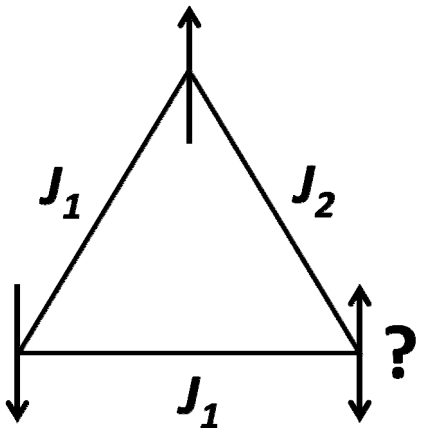


**Figura 1.** Esquema general de la frustració d'spin en triangles acoblats antiferromagnèticament.

A continuació es descriurà el cas d'un triangle format per tres àtoms amb $S_i = 1$ (com és el cas del $Ni^{II}$) acoblats antiferromagnèticament.

La figura 2, esquerra, mostra l'energia per als diferents estats energètics $E_S$ en funció de la relació entre la intensitat de les interaccions ($p = J_2/J_1$):

- en presència d'una interacció predominant, és a dir, per $J_1 >> J_2$ ($p < ½$) o $J_2 >> J_1$ ($p > 2$), el triangle presenta un estat fonamental d'spin $S = 1$. Aquest comportament es pot explicar per la cancel·lació dels dos moments acoblats per la interacció dominant, de forma que el tercer moment magnètic determina l'estat del sistema.

- per contra, quan $J_2$ i $J_1$ presenten el mateix ordre de magnitud ($J_2 \approx J_1 = J$, $½ < p < 2$), no hi ha cap interacció predominant i el sistema presenta un estat fonamental d'spin $S = 0$. La representació d'aquest estat $S = 0$ no és trivial, i només es pot entendre si els moments magnètics se situen sobre el pla del triangle i formant un angle de 120° entre ells, figura 2, dreta.

- finalment, pels valors de $p = ½$ i $p = 2$ s'observa la coexistència de dos estats degenerats amb diferent valor de $S$ ($S = 0$ i $S = 1$). Aquests dos punts són, precisament, els punts de frustració d'spin per aquest sistema. La degeneració d'estats fonamentals no es pot explicar amb la representació clàssica dels moments magnètics.

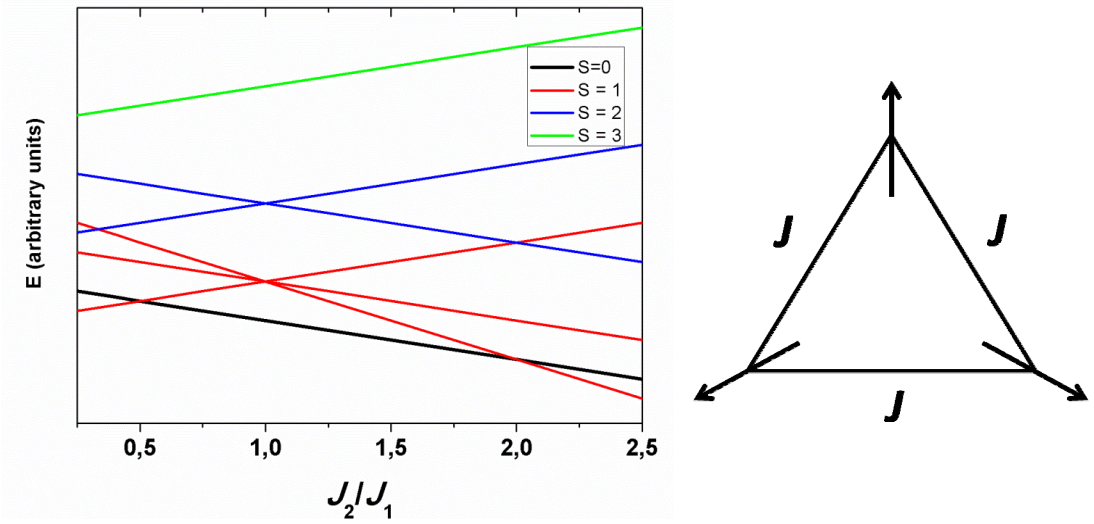


**Figura 2.** Esquerra, representació de l'energia dels diferents estats $S$ en funció de la relació $J_2/J_1$ per a un triangle amb $S_i = 1$. Dreta, disposició dels moments magnètics per tal de generar un estat fonamental $S = 0$.

Així, s'observa com un sistema format per tres centres paramagnètics amb $S_i = 1$ acoblats antiferromagnèticament entre ells pot generar un estat fonamental d'spin $S = 1$, $S = 0$ o tots dos alhora.

### 1.1.2. Mesures de magnetisme

En aquesta memòria es presentaran, principalment, dos tipus de mesures magnètiques, representades de tres formes diferents i realitzades en un SQUID (*Superconducting Quantum Interference Device*).[9] Aquestes mesures són:

Magnetització molar (*M*): També anomenada, simplement, magnetització. Aquesta mesura es realitza a temperatura baixa i fixa (2 K) variant el camp. Per tal d'expressar *M* d'una forma més senzilla i informativa, aquesta mesura es representa com $M/N\beta$ (o $M/N\mu_B$) respecte del camp (*H*), sent $N\mu_B$ el moment magnètic d'un mol d'electrons (5585 $G \cdot cm^3 \cdot mol^{-1}$) i *H* en Gauss o Tesla, indistintament.

Quan la corba de la magnetització tendeix a un valor constant de $M/N\mu_B$, anomenat magnetització a saturació, *M* es pot expressar com:

$$M = Ng\mu_B S$$

i per tant:

$$M / N\mu_B = gS$$

Si es considera que el paràmetre *g* normalment presenta un valor proper al de l'electró lliure ($g_{e^-} \approx 2{,}00$), $g \cdot S \approx 2S$ i la mesura de magnetització ($M/N\mu_B$) dóna de forma ràpida i aproximada el número d'electrons desaparellats (*n*) que determinen l'estat fonamental del sistema, es pot calcular fàcilment un valor aproximat de *S*.

A mode d'exemple, la figura 3 mostra la mesura de magnetització per a un compost amb $S = 1$, que tendeix a un valor de $M/N\mu_B \approx 2$ ($M/N\mu_B$ és adimensional).

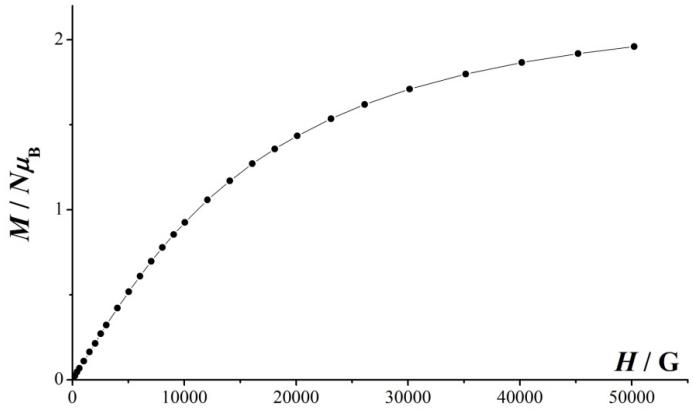


**Figura 3.** Mesura de magnetització molar d'un compost amb estat fonamental *S* = 1.

En representar diverses mesures de magnetització a diferents temperatures respecte el quocient *M*/*T* s'obté la mesura de la magnetització reduïda. Aquesta mesura permet el càlcul de l'anisotropia magnètica (paràmetre *D*), que com es veurà en breu, té una elevada rellevància en la caracterització de compostos anisotròpics.

Susceptibilitat magnètica molar ($\chi_M$): Aquesta mesura, a diferència de l'anterior, es realitza a camp constant variant la temperatura. En la caracterització dels compostos presentats en aquesta memòria, s'ha realitzat la mesura a dos camps diferents: 5000 i 400 G en els intervals 2–300 i 2–30 K, respectivament. La primera mesura dóna una resposta més intensa i amb menys soroll de fons però en ocasions pot caure fora de la zona lineal de la magnetització (la desviació respecte la linealitat augmenta a camps alts), mentre que la segona mesura té menys intensitat i més soroll de fons però generalment cau dins la zona lineal de *M*/*H*. La diferència entre mesures és més notòria quan es tracta amb compostos ferromagnètics (no presenten un màxim de $\chi_M$) o compostos amb efectes a baixa temperatura (*Zero Field Splitting* o *ZFS*, *spin canting*, interaccions intermoleculars, etc.).

Els resultats obtinguts amb aquesta mesura es poden representar de dues formes diferents: la primera és la representació de la pròpia susceptibilitat respecte de la temperatura, figura 4. Aquesta representació tendeix a 0 a temperatures elevades (per la població de tots els estats $m_S$ que fan que la magnetització mitjana sigui 0) i augmenta en disminuir la temperatura fins arribar al valor de $\chi_M$ corresponent a l'estat fonamental *S* del sistema (en cas que *S* = 0 la corba presenta un

màxim de susceptibilitat i tendeix a un valor de 0 $cm^3 \cdot mol^{-1}$ a 0 K) . La segona, i més utilitzada, és la representació de $\chi_M T$ respecte $T$, figura 4, que dóna informació a primer cop d'ull sobre la naturalesa del compost: si el compost és ferromagnètic la corba de $\chi_M T$ augmenta en disminuir la temperatura; si és antiferromagnètic $\chi_M T$ disminueix en baixar la temperatura; i si per contra es tracta d'un compost ferrimagnètic, a mesura que disminueix la temperatura el valor de $\chi_M T$ primer disminueix fins a un mínim i posteriorment augmenta. En tots tres casos, els efectes a baixa temperatura modifiquen els últims punts de la corba, provocant una desviació de $\chi_M T$ respecte del comportament esperat.

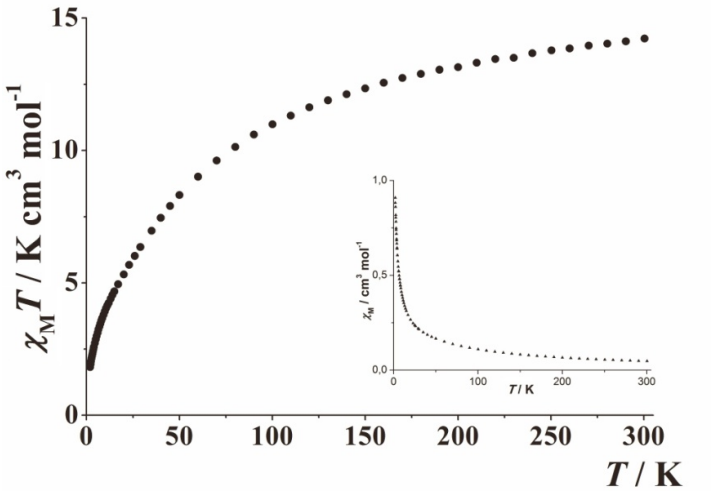


**Figura 4.** Representació de $\chi_M T$ i $\chi_M$ respecte la temperatura d'un compost antiferromagnètic amb un estat fonamental d'spin $S$ = 1.

Si es considera el cas d'un compost que presenta un estat fonamental ben separat dels seus estats excitats, s'obté que la susceptibilitat molar i la susceptibilitat molar per la temperatura, a temperatura baixa, es poden calcular com:

$$\chi_M = \frac{Ng^2\beta^2}{3kT} S(S+1) = \frac{0{,}125 g^2}{T} S(S+1) \text{ i } \chi_M T = 0{,}125 g^2 S(S+1)$$

i si, com en el cas anterior, se suposa una $g$ propera a la de l'electró lliure, s'obtenen les expressions:

$$\chi_M = \frac{S(S+1)}{2T} \text{ i } \chi_M T = \frac{S(S+1)}{2}$$

a partir de les quals es pot calcular el valor aproximat de $\chi_M$ i $\chi_M T$.

Per a l'exemple mostrat a la figura 4 (compost amb estat fonamental $S$ = 1), els valors aproximats de $\chi_M$ i $\chi_M T$ a 2 K serien $\chi_M$ = 0,5 i $\chi_M T$ = 1,0. Aquests valors són més baixos que els valors experimentals perquè s'ha suposat un valor de $g$ = 2,00, inferior al seu valor real.

Com s'ha comentat anteriorment, la mesura de $\chi_M T$ respecte $T$ és la més utilitzada. Aquest fet és degut a dos motius: la seva representació dóna una informació més intuïtiva sobre els tipus d'acoblament i la presència d'efectes a temperatura baixa i el seu ajust es pot realitzar per qualsevol mostra (a diferència de la mesura de $\chi_M$, que dóna ajustos pocs sensibles per compostos que no presenten un màxim de susceptibilitat).

### 1.1.3. Aplicacions

**Imants uni-moleculars**

S'anomena imant uni-molecular o *Single Molecule Magnet* (SMM) aquella molècula que, per sota d'una determinada temperatura, anomenada temperatura de bloqueig o *blocking temperature* ($T_B$), es comporta com un imant, és a dir, presenta una magnetització permanent. Per tal de ser considerat imant uni-molecular, cal que aquesta magnetització sigui intrínseca de la molècula i no es degui a un ordenament magnètic tridimensional.

Els requisits perquè una molècula es comporti com un SMM són:
- un estat fonamental d'spin, $S$, elevat.
- una anisotropia magnètica, $D$, elevada i negativa.

Aquests paràmetres determinen la barrera de potencial ($U$) que ha de superar l'spin de la molècula per tal d'invertir el seu moment magnètic, i que es calcula amb la fórmula $U = S^2|D|$ per spins enters o $U = S^2\,(1/4 - |D|)$ per spins fraccionaris. Tot i que el signe de $D$ no afecta la barrera de potencial (apareix en valor absolut a la fórmula), aquest paràmetre ha ser negatiu per tal d'estabilitzar l'estat fonamental de major $S$, tal com mostra la figura 5. Un valor positiu de $D$ estabilitzaria un estat fonamental $S$ = 0 que, per definició, té associada una barrera de potencial nul·la.

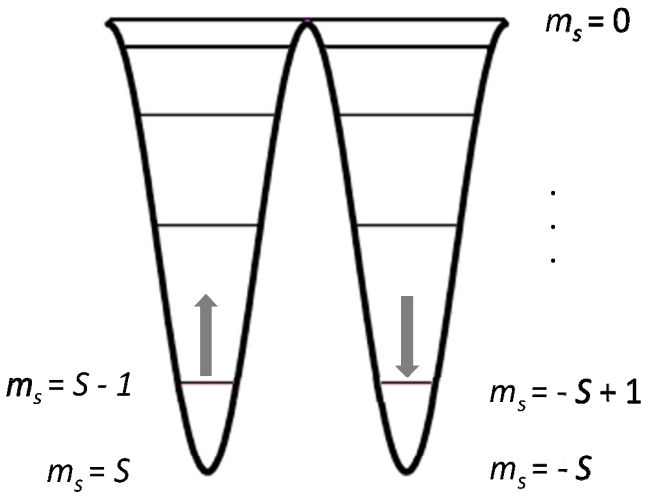


**Figura 5.** Barrera de potencial per un SMM amb estat fonamental *S*.

La determinació física d'un SMM es realitza a partir de les mesures de:

- susceptibilitat magnètica fora de fase a camp altern ($\chi''_{AC}$): en disminuir *T* s'ha d'observar un canvi en la posició i intensitat dels pics.
- magnetització respecte del camp (*M vs. H*): el compost ha de presentar magnetització en absència de camp magnètic (romanent) per sota de $T_B$ i, per tant, ha de generar un cicle d'histèresi. A causa de l'efecte túnel i de diversos processos tèrmics, la magnetització romanent d'un imant uni-molecular es va perdent amb el temps. És per aquest motiu que, quan un compost es comporta com un SMM també es diu que presenta una relaxació lenta de la magnetització.

El primer imant uni-molecular que es va descobrir, i el més estudiat a dia d'avui, és el compost $[Mn_{12}O_{12}(CH_3COO)_{16}(H_2O)_4]$ (anomenat $Mn_{12}AcO$), un compost de valència mixta format per un nucli o *core* $Mn^{IV}_4Mn^{III}_8$. Tot i que aquest compost va ser sintetitzat el 1980,[10] no va ser fins al cap de 10 anys que se'n va estudiar el comportament magnètic[11] i es va trobar que presenta un estat fonamental d'spin *S* = 10 i una barrera energètica *U* de 66 K (uns 45 $cm^{-1}$) que li confereixen una relaxació lenta de la magnetització per sota de 10 K.[12]

Des del descobriment del primer imant uni-molecular, el camp del magnetisme molecular ha viscut un important auge ja que aquestes molècules van ser considerades excel·lents candidats per substituir els materials usats en l'emmagatzematge d'informació (usant el sistema spin *up* i spin *down* de forma anàloga al sistema binari 1, 0).

Així, en els últims anys s'han sintetitzat un elevat nombre de *Single Molecule Magnets* amb nuclearitats tan variades com:[13] $\{V_4\}$,[14] $\{Mn^{III}_2\}$,[15] $\{Mn^{III}_3\}$,[16] $\{Mn^{III}_6\}$,[17] $\{Mn_{10}\}$,[18] $\{Mn_{15}\}$,[19] $\{Mn_{25}\}$,[20] $\{Mn_{84}\}$,[21] $\{Fe_4\}$,[22] $\{Fe_8\}$,[23] $\{Fe_{10}\}$,[24] $\{Fe_{19}\}$,[25] $\{Co_4\}$,[26] $\{Co_6\}$,[27] $\{Ni_4\}$,[28] $\{Ni_8\}$,[29] $\{Ni_9\}$,[30] $\{Ni_{12}\}$[31] o $\{Ni_{21}\}$,[32] entre molts d'altres, encara que pocs d'aquests milloren el comportament d'imant uni-molecular del $Mn_{12}AcO$. Més recentment, s'han caracteritzat diversos compostos derivats de lantànids, ja siguin heterometàl·lics 3d-4f[13b] o homometàl·lics 4f mono- o polinuclears,[13c,d] que es comporten com *SMM*.

Els imants uni-moleculars, gràcies a la seva exclusiva combinació de propietats quàntiques i clàssiques, han permès l'estudi de fenòmens quàntics com ara l'estudi de l'efecte túnel en la mesura de la magnetització (*quantum tunneling of the magnetization*)[33] i la supressió de l'efecte túnel a camp nul per spins fraccionaris (*spin parity effect*)[34] o per interferències (febles) entre molècules (*quantum phase interference*),[34a,35] la deflagració magnètica o inversió abrupta de la magnetització d'una mostra en aplicar un camp magnètic oposat al moment magnètic,[36] etc.

Tot i que l'ús de SMM en l'emmagatzematge d'informació no ha estat possible encara a causa de les reduïdes barreres de potencial que presenten (aquestes molècules es comporten com imants a temperatures molt baixes) i de la presència de relaxació magnètica a camp nul per efecte túnel (que comportaria una pèrdua de la informació progressiva i irreversible), se segueix treballant en la seva implementació en aquest camp, així com en spintrònica i en computació quàntica.[37]

**Refrigerants magnètics**

Aquesta aplicació es basa en l'efecte magnetocalòric, descobert el 1881[38] i descrit als voltants de 1920,[39] que es pot explicar com la disminució de l'entropia que pateix un material en ser magnetitzat (ordenació d'spins) i l'augment de l'entropia del mateix material en retirar el camp magnètic aplicat (desordenació d'spins).[40]

Per descriure el funcionament d'un refrigerador magnètic es considerarà un sistema amb un estat fonamental d'spin $S$, $2S+1$ nivells magnètics degenerats en absència de camp magnètic i una entropia magnètica ($S_m$) que es pot descriure com:

$$S_m = R\ln(2S+1)$$

En primer lloc s'aïlla el material (refrigerant magnètic) **(i)**, se li aplica un camp magnètic *H* que provoca la població de l'estat fonamental $M_S$ = - *S*, fet que comporta una disminució de l'entropia magnètica i un augment de la temperatura (ΔT) per mantenir l'entropia global del sistema; etapa anomenada *magnetització adiabàtica* **(ii)**. A continuació, mantenint el camp magnètic aplicat, es retira la calor (ΔT) del sistema (per mitjà d'un gas o líquid) i es restaura la temperatura inicial **(iii)**. Posteriorment, es torna a aïllar el material i es retira el camp magnètic, que provoca la població dels 2*S* + 1 estats, l'augment d'entropia magnètica i una disminució de *T* per tal que l'entropia global es mantingui constant; etapa anomenada *desmagnetització adiabàtica* **(iv)**. Finalment, mantenint *H* = 0, es posa en contacte la mostra que es vol refredar amb el refrigerant, de forma que aquest rep la calor de la mostra i en provoca la disminució de la temperatura **(v)**. Quan s'assoleix l'equilibri tèrmic es pot tornar a iniciar el cicle,[40d,e,f] figura 6.

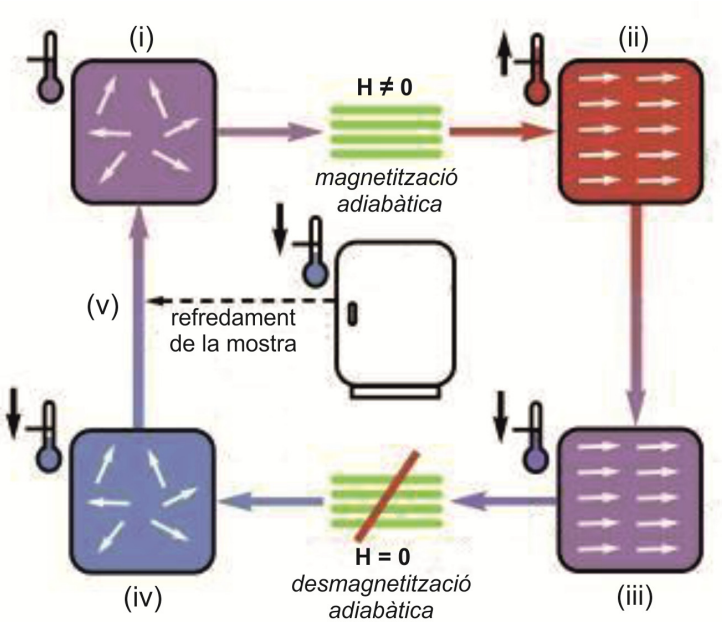


**Figura 6.** Esquema del funcionament d'un refrigerador magnètic.

Així, un refrigerant magnètic eficient ha de presentar una elevada variació de l'entropia magnètica ($\Delta S_m$) en absència i presència de camp magnètic o, el que és el mateix, en el procés d'ordenació i desordenació d'spins. Per tal que aquest $\Delta S_m$ sigui el més elevat possible, el material en qüestió ha de presentar les característiques següents:

- Un estat fonamental d'spin (*S*) elevat: l'entropia magnètica depèn directament d'aquest valor, com s'ha vist a l'equació de $S_m$ anterior.

- Una anisotropia magnètica (*D*) reduïda o nul·la: l'anisotropia magnètica trenca la degeneració d'estats d'spin a camp nul, generant diversos $m_S$ ordenats i disminuint el nombre d'estats poblats a temperatura elevada.
- Acoblaments febles entre els centres metàl·lics: la constant d'acoblament (*J*) es defineix com la diferència energètica entre un estat $E_S^{(n)}$ i l'estat excitat energèticament més proper $E_S^{(n+1)}$, de forma que la feblesa d'aquestes interaccions afavorirà la presència d'estats excitats propers que poden ser poblats, augmentant així la variació entròpica.

Tot i això, els primers estudis sobre refrigerants magnètics es van realitzar partir de tres SMMs amb un estat fonamental $S = 10$, com són el $Mn_{12}AcO$, $Mn_{12}BzO$ i el $\{Fe_8\}$,[41] i es va observar que es necessitaven camps magnètics molt elevats per poblar únicament l'estat fonamental.

Posteriorment, es van estudiar una sèrie de compostos polinuclears de metalls de transició amb baixa anisotropia magnètica ($D \approx 0$), com els compostos de nuclearitat $\{Fe_{14}\}$ i $\{Fe_{17}\}$,[42] $\{Mn_{10}\}$, $\{Mn_{17}\}$, $\{Mn_{19}\}$[43] i $\{Mn_{32}\}$.[44] L'únic exemple de clúster homometàl·lic de níquel és un compost amb nuclearitat $\{Ni_7\}$,[45] que tot i presentar estat fonamental d'spin reduït ($S = 1$), presenta una elevada frustració magnètica que provoca la degeneració de l'estat fonamental i una elevada variació de l'entropia ($\Delta S_m$).

Finalment, es va introduir la química dels lantànids en la recerca de nous refrigerants moleculars ja que aquests poden presentar estats fonamentals d'spin elevats i una anisotropia magnètica reduïda (sobretot el $Gd^{III}$, que presenta l'estat fonamental isotròpic més elevat entre els metalls: $S = 7/2$). Es va procedir a l'estudi de compostos heterometàl·lics 3d-4f, com per exemple els compostos amb nuclearitat $\{Mn_4Gd_3\}$, $\{Mn_4Gd_4\}$, $\{Mn_4Gd_6\}$ i $\{Mn_9Gd_9\}$;[46] $\{Co_4Gd_6\}$, $\{Co_6Gd_6\}$, $\{Co_8Gd_4\}$, $\{Co_8Gd_8\}$ i $\{Co_{10}Gd_{42}\}$;[47] $\{Ni_6Ln_6\}$ (Ln = Gd, Dy), $\{Ni_8Gd_4\}$, $\{Ni_{10}Gd_{42}\}$ i $\{Ni_{12}Gd_{36}\}$;[47c,48] $\{Cu_5Gd_4\}$, $\{Cu_6Gd_6\}$ i $\{Cu_{36}Gd_{24}\}$;[49] així com un elevat nombre de compostos formats per lantànids, que van des de compostos de baixa nuclearitat ($\{Gd_2\}$),[50] nuclearitat mitja ($\{Gd_5\}$ o $\{Gd_7\}$)[51] i d'elevada nuclearitat ($\{Gd_{24}\}$),[52] fins arribar a una sèrie de polioxometal·lats units a aquests metalls, com són els $\{Gd_3Ga_5O_{12}\}$, $\{GdW_{10}O_{36}\}$ o $\{GdP_5W_{30}O_{110}\}$.[53]

La incorporació dels lantànids (especialment del gadolini) ha donat un impuls important a la recerca de nous refrigerants magnètics, ja que ha permès arribar a temperatures similars a les assolides amb $^4He$ líquid. És destacable, però, que tot i que els compostos obtinguts presenten una baixa densitat que impedeix la seva aplicació en aparells quotidians, la deposició d'aquestes molècules

sobre certes superfícies (de forma que no variïn les seves propietats magnètiques) hauria de permetre la seva implementació en instruments que requereixin refredar localment a temperatures molt baixes.

## 1.2. Metodologia experimental

### 1.2.1. Aproximacions descendent i ascendent

L'augment de la demanda de dispositius electrònics cada cop més petits ha provocat, indirectament, un estudi intensiu sobre la miniaturització dels seus components, sent els imants, que actuen en l'emmagatzemament d'informació (discs durs, bandes magnètiques de targetes de crèdit, etc.), un dels seus components més importants.

La principal dificultat que presenta la miniaturització dels imants és la d'obtenir partícules de grandària reduïda i amb poca dispersió a partir de la fragmentació d'imants de majors dimensions. Aquest procés de reducció de la grandària de partícula s'anomena aproximació descendent o *top-down approach*, figura 7, i és un procés costós, laboriós i presenta límits físics en la mida de partícula.

El procés contrari, anomenat aproximació ascendent o *bottom-up approach*, consisteix en la síntesi d'un material a partir dels seus components,[54] figura 7, i ha demostrat ser un procés senzill, econòmic, altament reproduïble i capaç de generar espècies nanomètriques d'elevada uniformitat.

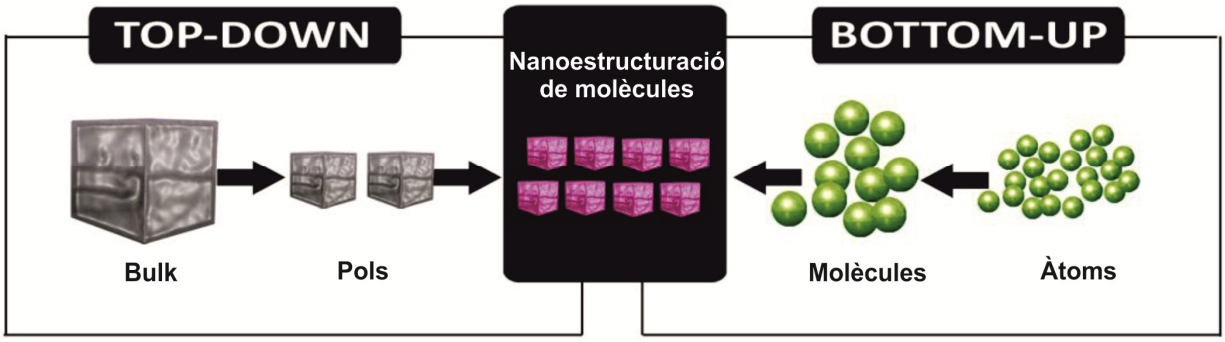


**Figura 7.** Processos descendent i ascendent per arribar a grandària de partícula desitjada.

Donat que cada cop es busquen materials magnètics de dimensions més reduïdes i menys disperses per a aplicacions més especialitzades, sembla una bona idea optar per a la síntesi d'aquests materials seguint l'aproximació *bottom-up*.

A part de l'elevada reproductibilitat i monodispersió dels productes sintetitzats seguint aquest mètode, aquests tipus de síntesi presenta altres avantatges com ara la possibilitat de funcionalitzar les molècules en qüestió i canviar-ne les propietats[54c] o dissoldre-les en solvents orgànics per tal de poder-les dipositar sobre diversos substrats adoptant les formes desitjades.[55]

### 1.2.2. Serendipitat

En química de la coordinació, s'acostuma a afrontar l'aproximació ascendent de dues formes diferents:

- la síntesi dirigida o *designed assembly*, en què s'utilitza lligands rígids per a la síntesi de polígons o poliedres moleculars, utilitzada per Lehn,[56] Fujita[57] i Raymond.[58]
- la serendipitat (síntesi fortuïta) o *serendipitous assembly*, que consisteix en usar lligands capaços de coordinar diversos cations metàl·lics en varis modes de coordinació, fet que fa pràcticament impossible predir l'estructura del compost final.[59]

La segona aproximació és, clarament, la més usada en els camps de la química de la coordinació i el magnetisme molecular. La principal limitació que presenta la síntesi dirigida és controlar l'elevat número de variables que intervenen en la formació d'un compost (modes de coordinació dels lligands i/o anions, condicions de reacció, forces d'empaquetament a l'hora de formar sòlids més o menys cristal·lins, etc.), que només es pot dur a terme treballant amb lligands de topologies fixes i predeterminades i metalls que presentin geometries de coordinació concretes. Aquests factors limiten enormement les opcions sintètiques i haguessin impossibilitat la síntesi de compostos com, per exemple, el $\{Mn_{84}\}$.[21] En paraules de Winpenny sobre la química de coordinació i la síntesi de clústers, "és només una petita exageració dir que, actualment, la síntesi dirigida té el seu punt fort en el disseny i el seu punt feble en la síntesi de molècules que tinguin algun interès més enllà del fet que la seva síntesi fos predita" i "el resultat inevitable de sintetitzar únicament molècules previsibles és que la feina sintètica serà, primer, previsible i, finalment, avorrida".[59]

### 1.2.3. Química supramolecular[60]

S'anomena química supramolecular la química basada en les interaccions no covalents i la organització de molècules en sistemes polimoleculars o supermolècules per mitjà d'aquestes forces intermoleculars febles. Es tracta d'una branca molt àmplia de la química, ja que inclou el procés sintètic dels lligands, la coordinació d'aquests lligands amb el cations metàl·lics corresponents (química de la coordinació), l'estudi experimental i teòric de les interaccions no-covalents i de l'estabilitat de la supermolècula, l'estudi de la selectivitat i energia involucrades en el reconeixement molecular entre el substrat (*guest*) i el receptor (*host*), etc.

Per tal que el reconeixement molecular *host-guest* sigui efectiu, cal que es compleixin diversos condicionants:

- complementarietat estèrica: *host* i *guest* han de presentar una forma i grandària adequades.
- interaccions complementàries: els punts d'unió han d'estar situats de forma adequada per a establir interaccions efectives: positiu/negatiu, càrrega/dipol o dipol/dipol en interaccions electrostàtiques, donador/acceptor en ponts d'hidrogen, sistemes deslocalitzats propers per apilament π-π, etc.
- multiplicitat d'interaccions: la feblesa dels enllaços no-covalents requereix un elevat nombre d'interaccions.
- estabilitat global: cal que la suma dels diferents efectes sigui capaç de generar i estabilitzar la supermolècula.

També cal tenir en compte la interacció que puguin establir receptor i substrat amb el solvent així com l'aparellament de dominis hidrofòbics i hidrofílics, que tot i no ser propietats intrínseques dels components poden afavorir o perjudicar la formació de supermolècules en determinats medis.

Com s'ha vist, els diversos receptors i substrats contenen una certa *informació* que determina l'efectivitat del reconeixement. Així, la química supramolecular ha estat anomenada *informàtica molecular*, ja que hi ha un procés de *lectura* i *processat* de la *informació* que conté cada molècula,[61] o química *LEGO*, en què cada molècula equival a un bloc de *LEGO* i l'acoblament entre molècules/blocs és feble i reversible.

L'elevada selectivitat que presenten aquests sistemes, així com les seves propietats (coordinació, transport i intercanvi d'ions o reconeixement i control molecular), han fet que la química supramolecular hagi pres una major importància en els últims anys en els camps de la biomedicina, el control mediambiental, la síntesi dirigida de compostos i l'*enginyeria cristal·logràfica*.[62]

Es poden diferenciar dues grans branques en la química supramolecular: reconeixement molecular (o interacció receptor-substrat) i auto-encaix (*self-assembly*). El primer consisteix en l'assemblatge de supermolècules a partir de l'encapsulament i coordinació per mitjà d'enllaços no-covalents de molècules petites (*substrat*) a l'interior de molècules més grans (receptors), mentre que el segon consisteix en la formació de la supermolècula a partir dels seus components per associació espontània i reversible mitjançant enllaços no-covalents.[63]

Un concepte clau en la síntesi per *self-assembly* és l'efecte plantilla o *template synthesis*,[64] que consisteix en la ordenació selectiva dels diferents components al voltant d'una espècie central, generalment un ió, que dirigeix la síntesi cap a un producte amb la geometria adequada. L'efecte plantilla dels cations metàl·lics és conegut i ha estat intensament estudiat des del descobriment dels primers èters corona l'any 1967,[65] la posterior aparició de criptands i calixarens,[61b,66] i finalment de metal·locorones;[67] mentre que la química coordinativa d'anions, tot i ser descoberta per les mateixes dates,[68] ha tingut un desenvolupament molt més lent i, tot i els treballs de Lehn i col·laboradors,[56a,69] no ha estat fins fa 15-20 anys que aquest tema ha estat estudiat més intensament.[62b,70]

Cal comentar, però, que no hi ha una frontera clara entre les dues principals branques de la química supramolecular que s'han comentat en aquest apartat. Així, en aquest treball es presenten una família de receptors aniònics que es troben en aquesta frontera: són compostos sintetitzats al voltant d'un anió central per associació espontània dels seus components (*self-assembly*), però hi ha un cert reconeixement molecular entre l'ió central (*guest*) i la molècula que l'envolta (*host*) que promou la generació del compost final per mitjà d'enllaços no-covalents (ponts d'hidrogen).

## 1.2.4. Treball al laboratori

**Mètode sintètic**

En aquesta memòria es presenten els resultats obtinguts en la síntesi de compostos polinuclears seguint l'aproximació ascendent (*bottom-up*), com sol ser habitual en el camp de la química de la coordinació. Per a formar aquests compostos s'han utilitzat diversos lligands 2-piridiloxima i el catió metàl·lic $Ni^{II}$, en absència i presència d'anions coordinants i d'altres co-lligands i en diferents condicions de reacció (solvent, pH, etc.).

La obtenció de nous compostos per totes les rutes sintètiques proposades demostra que les propietats dels lligands emprats eren les adequades per als objectius marcats inicialment, i si bé les síntesis no eren dirigides i han generat aquests compostos per serendipitat, s'ha estudiat la relació entre l'estructura dels compostos obtinguts i els reactius i el medi de reacció per a cadascun d'aquests productes.

Durant aquesta tesi, el treball de laboratori s'ha dut a terme seguint la reacció general:

lligand piridiloxima+ sal metàl·lica + base + solvent → cristal·lització → productes

En ocasions, s'ha realitzat aquesta reacció en presència de co-lligands o d'altres espècies.

S'ha estudiat l'efecte de cadascun d'aquests factors, que s'introdueixen a continuació:

- Lligands: s'han emprat diferents lligands derivats de la 2-piridiloxima, principalment la dioxima dapdo$H_2$ i el lligand pyC{CN}NOH. L'estudi d'aquests dos lligands ha estat l'eix experimental del treball i la utilització d'altres oximes, principalment la pyC{ph}NOH, s'ha limitat a una de les sèries de reaccions involucrant co-lligands aminats.
- Sals metàl·liques: s'ha estudiat la reacció de diverses sals de $Ni^{II}$ de naturalesa i propietats diferents derivades de les característiques dels seus anions. Per una banda s'han assajat les reaccions a partir de carboxilats i β-dicetonats de níquel(II) ($AcO^-$, R-$BzO^-$, $acac^-$, $tfacac^-$, $hfacac^-$), en les que s'espera la coordinació de l'anió en el producte final. Les sals inorgàniques emprades s'han escollit en funció de la capacitat coordinativa de l'anió. Així, s'ha provat la reacció amb sals d'anions potencialment coordinants (halurs, nitrat, sulfat) i amb sals d'anions poc o gens coordinants (perclorat, tetrafluoroborat).

- Base: s'han provat reaccions amb diverses bases ($NEt_3$, NaOMe, NaOH, $NMe_4(OH)$, etc.) i variant la concentració d'aquestes, i per tant, el pH de la dissolució. Si bé totes elles han estat emprades per aportar el medi bàsic necessari per desprotonar la corresponent oxima, cal tenir present que poden influir en el producte resultant ja que aporten cations ($NEt_3H^+$, $Na^+$, $NMe_4^+$) i fins i tot co-lligands addicionals (com és el cas del metòxid) a la mescla de reacció.
- Co-lligands: s'han afegit certs co-lligands per tal de combinar les propietats d'aquests amb les dels lligands 2-piridiloxima. Els co-lligands utilitzats han estat l'anió azidur ($N_3^-$), que tendeix a generar acoblaments ferromagnètics quan actua en mode $\mu_{1,1}$- (o *end-on*), l'anió dicianamida ($N\{CN\}_2^-$), que permet connectar clústers i, per últim, una sèrie d'amines bi- i tri-dentades en combinació amb $N_3^-$ per tal de bloquejar diverses posicions de coordinació.
- Solvent: s'ha treballat, bàsicament, amb 3 solvents ben diferenciats: metanol (MeOH), que presenta una elevada polaritat i capacitat coordinativa, acetonitril (MeCN), d'una polaritat intermèdia i poca capacitat donadora, i finalment diclorometà ($CH_2Cl_2$), apolar i que no té tendència a coordinar-se. El paper del solvent no és innocent, ja que pot induir a la formació de compostos determinats a causa de les seves propietats.

**Mètodes de cristal·lització**

La caracterització estructural resulta imprescindible en aquest tipus de recerca i, per tant, un dels punts clau d'aquest treball ha estat l'obtenció de monocristalls per a la seva resolució per difracció de raigs-X de monocristall. És important remarcar que el procés de cristal·lització ha de ser el més lent possible per tal d'afavorir la formació de monocristalls de forma i grandària adequada per a la seva resolució.

Amb aquest objectiu, s'han utilitzat les tècniques de cristal·lització següents:
- Cristal·lització per capes: els fonaments d'aquest mètode són la insolubilitat del compost en l'agent precipitant i la difusió lenta entre aquest i el solvent. Així, se situarà a la part inferior del tub la dissolució més densa de forma que la mescla entre dissolució i agent precipitant sigui el més lenta possible, és a dir, per difusió. En aquest treball, s'ha utilitzat dietilèter com agent precipitant quan el solvent és MeOH i MeCN, i hexà quan el solvent és $CH_2Cl_2$.

- Cristal·lització per evaporació lenta del solvent: aquest mètode consisteix, com el seu nom indica, en l'evaporació del solvent de forma lenta i controlada, de forma que la concentració dels soluts augmenti fins a propiciar la cristal·lització d'aquests.
- Cristal·lització en vial tancat: Aquest mètode es basa en el desplaçament dels equilibris termodinàmics existents a la dissolució, mantenint la concentració constant durant períodes de temps normalment llargs (setmanes) i la cristal·lització del compost més insoluble.

Com aquestes tècniques es fonamenten en conceptes diferents, el producte obtingut a partir de cadascuna d'elles pot no ser el mateix; i per tant, s'ha provat la cristal·lització utilitzant els tres mètodes per a cadascuna de les reaccions realitzades. Així, en el decurs d'aquesta tesi s'han provat prop de 500 reaccions, més d'un miler de cristal·litzacions i s'han caracteritzat adequadament prop de 50 compostos. També s'han sintetitzat cinc compostos que han resultat ser no reproduïbles.

Finalment, val la pena comentar que en aquest treball només s'han considerat productes cristal·lins, tant per a la mesura de difracció de raigs X de monocristall com per a les mesures magnètiques i l'anàlisi elemental. Per tant, és molt raonable pensar que durant aquesta tesi s'hauran obtingut diversos compostos en forma de pols que han estat descartats. Inicialment, es van recristal·litzar diversos precipitats en nous solvents per tal de millorar la cristal·linitat dels productes, però de manera general no es va apreciar una millora en la seva cristal·linitat.

## 1.3. Níquel i níquel(II): característiques principals

El níquel és un element químic de nombre atòmic 28, pes atòmic 58.70 g/mol i símbol Ni situat en el grup 10 i període 4 de la taula periòdica dels elements. És un metall de transició de color blanc platejat, conductor de l'electricitat i de la calor, dúctil, mal·leable, resistent a la corrosió i presenta ferromagnetisme a temperatura ambient.

El seu ús es remunta fins al 3500 a.C. en forma de bronzes i aliatges naturals amb Fe i Cu,[71] va ser descrit per primera vegada (com *coure blanc*) en diversos manuscrits xinesos al 1700 a.C., però no va ser fins el 1751 que va ser aïllat pel químic i mineralogista suec Axel Fredrik Cronstedt.

El nom de níquel prové dels miners alemanys de l'edat mitjana, que anomenaven *kupfernickel* un mineral vermell similar al coure (*kupfer*) però que no era coure per acció d'un follet endimoniat

(*nickel*, a l'antiga mitologia alemanya). Quan el 1751 va ser aïllat pel Baró Axel Fredrik Cronstedt, aquest li va mantenir el nom.[72]

La producció mundial (extracció i refinament) d'aquest metall va ser superior als 2 milions de tones mètriques l'any 2012,[73] i les seves principals aplicacions són en la fabricació d'acers inoxidables, imants *alnico* (que contenen Al, Ni i Co), monedes, bateries recarregables, en diversos aliatges, com a tint per vidres verds i, en menor mesura, per fer cordes per guitarres elèctriques i càpsules per micròfons.[74]

Tot i el seu abundant ús, el níquel presenta una moderada toxicitat, ja sigui per contacte, que pot provocar dermatitis o èczemes (fet que li va comportar la menció d'al·lergogen de l'any 2008 per part de l'*American Contact Dermatitis Society*), com per ingestió o inhalació, ja que és considerat un agent cancerigen.

El níquel pot presentar diferents estats d'oxidació (0, I, II, III, IV), però els més estables són $Ni^0$ ([Ar] $3d^8$ $4s^2$ o [Ar] $3d^9$ $4s^1$) i $Ni^{II}$ ([Ar] $3d^8$). L'estat d'oxidació $Ni^{II}$ és el més habitual en química de la coordinació i va ser l'escollit en aquesta tesi per tal de sintetitzar els diversos compostos polinuclears.

El catió $Ni^{II}$, que presenta una configuració $d^8$, acostuma a generar dos tipus d'entorns (o geometries) ben diferenciats: octaèdric, en què els electrons es distribueixen en els orbitals de forma $t_{2g}^6$ $e_g^2$ i es comporta com un ió paramagnètic (amb un spin local $S = 1$) o plano-quadrat, que es comporta com una espècie diamagnètica a causa de l'estabilització i aparellament dels $e^-$ de l'orbital $d_z^2$ ($a_{1g}$) i la desocupació de l'orbital $d_{x^2-y^2}$ ($b_{1g}$), esquema 1.

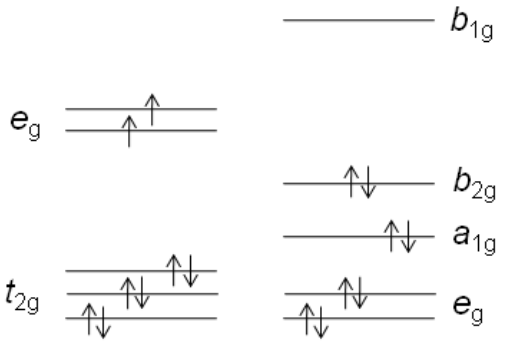


**Esquema 1.** Distribució electrònica d'un catió $d^8$ per a un entorn octaèdric (esquerra) i plano-quadrat (dreta).

A continuació es tractarà sobre el catió $Ni^{II}$ en un entorn octaèdric ($O_h$). Aquest ió té un estat fonamental de spin $S = 1$ i un terme fonamental $^3A_{2g}$ que, tot i que presenta interacció amb l'estat excitat $^3T_2$, i per tant, acoblament spin-òrbita, no mostra desdoblament a camp nul (*Zero Field Splitting, ZFS*) ni anisotropia magnètica (*D*). Aquest supòsit és considerant un entorn octaèdric "ideal". Per contra, si es considera un entorn octaèdric "no ideal", és a dir, lleugera o notòriament distorsionat per efecte dels lligands, s'observa un trencament de la degeneració orbital de l'estat fonamental (efecte Jahn-Teller de segon ordre)[2] i l'aparició del desdoblament a camp nul o *ZFS*, que juntament amb l'efecte de l'acoblament spin-òrbita creen una certa anisotropia magnètica, *D*, en el catió,[1] esquema 2.

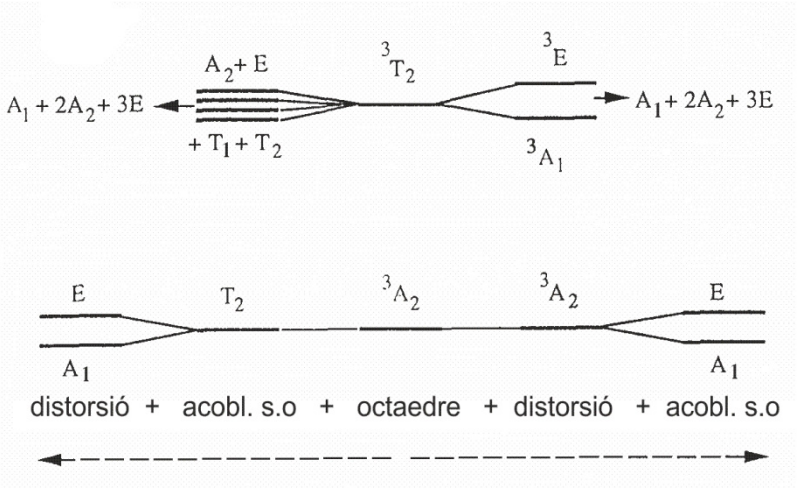


**Esquema 2.** Desdoblament a camp nul de l'estat fonamental i del primer estat excitat per un ió $Ni^{II}$ en un entorn octaèdric distorsionat.

S'ha comprovat com, per efecte dels lligands, s'ha generat una certa anisotropia magnètica (*D*) en un catió metàl·lic formalment isotròpic, de forma que queda demostrat que el catió $Ni^{II}$ és un bon candidat per a la síntesi de compostos polinuclears paramagnètics i amb anisotropia magnètica.

## 1.4. Lligands 2-piridiloxima

El grup oxima es troba present en un gran nombre de lligands àmpliament utilitzats en la química de la coordinació per la seva versatilitat i capacitat coordinativa, sobretot per metalls de la primera sèrie de transició, així com per la seva capacitat d'estabilitzar metalls en estats d'oxidació elevats.[75] Les propietats d'aquest grup són conegudes des de fa temps, com demostra el fet que el lligand dimetilglioxima va ser utilitzat el 1890 per Tschugaeff com agent per la determinació gravimètrica de Ni(II);[76] però l'interès en compostos sintetitzats a partir d'oximes ha augmentat dràsticament en els últims 15 anys a causa de la seva aplicació en models bioinorgànics,[77] en el disseny de receptors selectius de $Ca^{2+}$ i $Ba^{2+}$,[78] en el desenvolupament de nous catalitzadors,[79] del seu ús com inhibidor de la corrosió en superfícies de ferro[80] i, sobretot, en la síntesi de compostos polinuclears homometàl·lics i heterometàl·lics i el seu estudi magnètic,[75,81] entre els quals es troba algun compost amb propietats de SMM (Single Molecule Magnet)[82] i SCM (Single Chain Magnet).[83]

Els mètodes usats en la síntesi de lligands oxima en aquest treball han estat l'addició d'hidroxilamina a aldehids o cetones i la nitrosilació de carbonis units a un grup electroatraient, esquema 3.

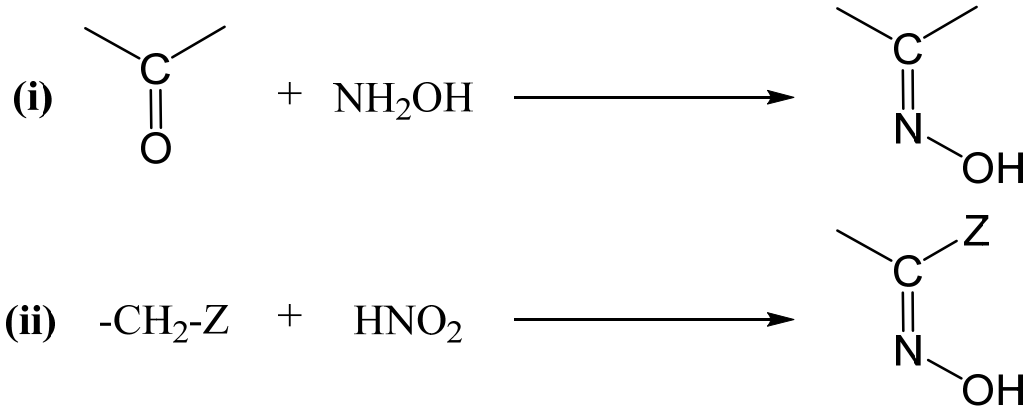


**Esquema 3.** Reacció d'addició d'hidroxilamines a aldehids o cetones **(i)** i de nitrosilació **(ii)**, on *Z* representa un grup electroatraient.

Altres mètodes coneguts per a la síntesi d'aquests lligands són l'addició de clorur de nitrosil (NOCl) a olefines i la reacció de Grignard entre un bromomagnesià (R-Mg-X) i la base conjugada d'un nitrocompost, previ tractament amb BuLi.

En els últims 15 anys s'han utilitzat dos grans conjunts de lligands que contenen grups oxima en la química de la coordinació: els lligands saliciloxima i els lligands piridiloxima. Dels últims, els més utilitzats són els de la família de lligands 2-piridiloxima, que presenten la fórmula general que es mostra a l'esquema 4, en què els substituents R i R' poden ser grups coordinants, donadors o acceptors d'electrons o hidrogen.

Els lligands 2-piridiloxima, en la seva forma desprotonada, presenten diversos modes de coordinació possibles (esquema 4) i permeten generar sistemes polinuclears amb un gran ventall de nuclearitats i topologies. Per representar els diferents modes de coordinació dels lligands 2-piridiloxima (i d'altres lligands), en aquest treball s'ha utilitzat la notació de Harris,[84] que s'expressa com $X.Y_1Y_2Y_3\cdots Y_n$, on X és el nombre total d'ions metàl·lics coordinats al lligand i cada lletra Y representa el nombre d'ions metàl·lics units a cadascun dels àtoms donadors del lligand, seguint l'ordre de prioritat establert en la llista Cahn-Ingold-Prelog (a efectes pràctics, O abans que N).

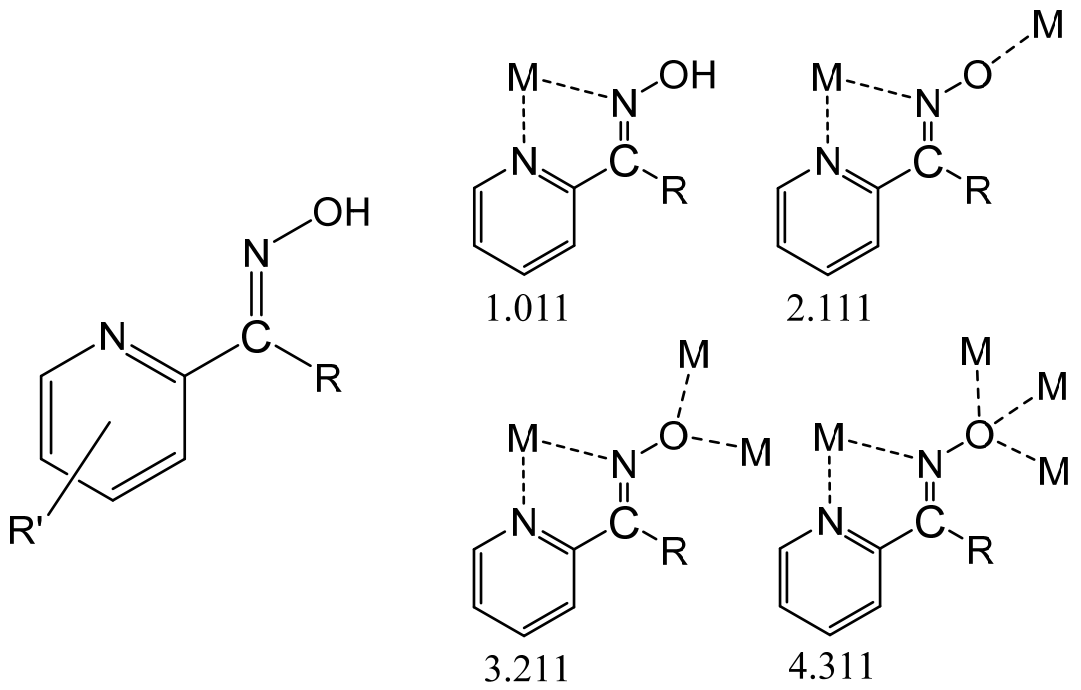


**Esquema 4.** Esquerra, estructura general pels lligands 2-piridiloxima. Dreta, modes de coordinació per un lligand 2-piridiloxima protonat i desprotonat. Els modes de coordinació s'expressen d'acord amb la notació de Harris.[84]

Com es veu a l'esquema 4, els lligands 2-piridiloxima contenen, bàsicament, dues posicions funcionalitzables, que donen a aquesta família una gran diversitat: R, coordinat al carboni unit al grup oxima, i R', sobre l'anell piridínic.

En el decurs d'aquesta tesi s'han utilitzat diversos lligands, que es descriuen breument en les següents seccions.

### 1.4.1. 2,6-diacetilpiridildioxima

El lligand 2,6-diacetilpiridildioxima, dapdo$H_2$, conté dos grups oxima situats en posició *orto* respecte l'àtom de nitrogen de l'anell piridínic, esquema 5, i és un excel·lent candidat per obtenir nous clústers, ja que els tres àtoms de N es troben situats de forma que poden unir un àtom metàl·lic per efecte quelat deixant lliure els dos àtoms d'O dels grups oxima per coordinar nous cations.

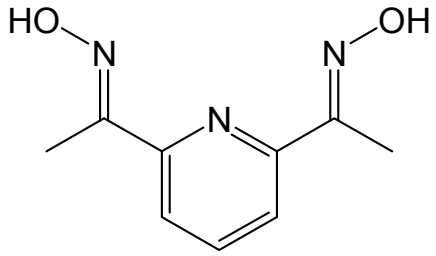


**Esquema 5.** Representació del lligand 2,6-diacetilpiridildioxima.

Aquest lligand es sintetitza fàcilment a partir de 2,6-diacetilpiridina i 2 equivalents de $NH_2OH{\cdot}HCl$ i NaOH en MeOH/$H_2O$, portant la mescla a reflux durant dues hores.[85] Els dos grups oxima presenten valors de $pK_a$ bàsics i propers ($pK_{a1}$ ~ 10.1, $pK_{a2}$ ~ 10.8) que disminueixen dràsticament en coordinar un centre metàl·lic.[86]

Tot i la gran capacitat coordinativa del lligand dapdo$H_2$ (esquema 6) i d'altres lligands piridildioxima, la major part de compostos sintetitzats a partir d'aquests lligands abans de l'inici d'aquesta tesi eren compostos mononuclears. Els compostos $[M^{II}(LH_2)]X_2$ (M = Mn,[85] Fe,[86] Ni,[87] Cu,[85,88] Zn[88b]), [MCl(dapdoH)] (M = $Pd^{II}$, $Pt^{II}$)[77c] i $[M^{IV}(dapdo)_2]$ (M = Ni,[89] Co[90]) presenten, tots ells, el mode de coordinació 1.00111, és a dir, els tres àtoms de N es troben coordinats a un àtom metàl·lic però els

àtoms d'O dels grups oxima no ho estan. L'estabilització de metalls en estats d'oxidació elevats que s'ha comentat anteriorment queda palesa en els compostos $[M^{IV}(dapdo)_2]$ (M = Ni,[89] Co[90]), en què el lligand $dapdoH_2$, en la seva forma desprotonada $dapdo^{2-}$ és capaç d'estabilitzar aquests estats d'oxidació poc habituals en níquel i cobalt. També es va trobar el compost polimèric $[Mn(dapdoH_2)Cl_2]_n$[91] i dos compostos trinuclears de $Mn^{II}$ i $Cu^{II}$ amb fórmula $[Mn_3(dapdoH_2)_2(R\text{-}COO)_6]$[92] i $[Cu_3(dapdoH_2)_2Cl_6]$[93] en què el lligand $dapdoH_2$ exhibeix el mateix mode de coordinació 1.00111 i no actua de lligand pont.

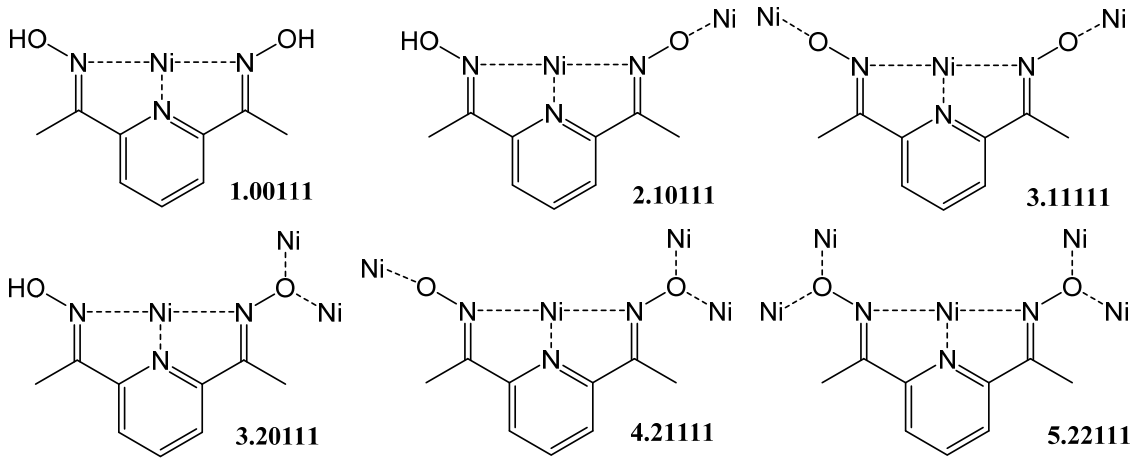


**Esquema 6.** Modes de coordinació caracteritzats per al lligand $dapdoH_2$ en la seva forma protonada, monodesprotonada ($dapdoH^-$) i totalment desprotonada ($dapdo^{2-}$).

No obstant, a la bibliografia també hi ha exemples de compostos polinuclears en què el lligand $dapdoH_2$ (en les seves formes desprotonades $dapdoH^-$ o $dapdo^{2-}$) actua de lligand pont; com per exemple dos compostos dinuclears de $Cu^{II}$ amb fórmula $[Cu(dapdoH)]_2X_2$ ($X = Cl^-, BF_4^-$)[94] en què el lligand $dapdoH^-$ es troba en el mode de coordinació 2.10111, un complex de valència mixta de Fe en què una subunitat $\{Fe^{II}(dapdoH)_2\}$ s'uneix a dos cations $Fe^{3+}$ en el mateix mode 2.10111 donant un compost de fórmula $[Fe^{II}(dapdoH)_2Fe^{III}Cl_4(O)]$,[86] el complex pentanuclear $[Mn_5O_2(N_3)_4(AcO)(dapdo)_3(py)_2]$[95] en què cada lligand coordina tres àtoms metàl·lics en el mode 3.11111, dues famílies de complexos hexanuclears de valència mixta de manganès reportades per Christou *et al.* amb fórmula general $[Mn^{II}_2Mn^{III}_4O_2(MeO)_2(dapdo)_2(dapdoH)_4]^{2+}$,[96,97] que presenten els modes de coordinació 3.11111 i 2.10111 i, finalment, dos complexos octanuclears de valència mixta de manganès que tenen per fórmula $[Mn^{II}_2Mn^{III}_6O_4(OH)_4(MeO)_2(N_3)_2(dapdo)_2(dapdoH)_2(H_2O)]$,[96] en què els lligands actuen en mateixos

modes que en el cas anterior, i $[Mn^{II}_6Mn^{III}_2O_2(dapdo)_6(NO_3)_2]$, que presenta el mode de coordinació 4.21111, el més elevat en el moment de la seva publicació.[97] El lligand $dapdoH_2$ també ha estat utilitzat en la síntesi d'un parell de compostos polinuclears heterometàl·lics: un complex $Cr^{III}_2Cu^{II}_2$ en què dues subunitats {Cu(dapdo)} uneixen dos grups crom-triazaciclononà en un mode de coordinació 3.11111[98] i un sistema trinuclear $Mn^{IV}Gd^{III}_2$ en què l'àtom de manganès uneix un lligand $dapdo^{2-}$ en mode de coordinació 3.11111 i els àtoms de gadolini es troben units a dos lligands $dapdoH^-$ en mode 2.10111.[99]

Com es pot observar, la química del lligand $dapdoH_2$ amb níquel és molt reduïda: a l'inici d'aquesta tesi únicament s'havien caracteritzat tres compostos mononuclears, un d'ells de $Ni^{IV}$, i cap compost polinuclear de $Ni^{II}$ amb aquest lligand.

En aquesta tesi es presenten els primers i únics compostos polinuclears de $Ni^{II}$ amb el lligand $dapdoH_2$ publicats a dia d'avui. S'han obtingut 14 nous compostos a partir d'anions carboxilats i no-carboxilats, amb un interval de nuclearitats que va de $Ni_2$ a $Ni_{10}$, i s'ha demostrat la gran capacitat coordinativa d'aquest lligand, ja que s'han observat fins a sis modes de coordinació diferents, esquema 6, entre els que es troben els modes 3.20111 i 5.22111, observats per primera vegada en el decurs d'aquesta tesi.

És destacable el fet que el lligand $dapdo^{2-}$ en els modes de coordinació 2.10111 i 3.11111 té tendència a generar entorns plano-quadrats en cations $Ni^{II}$ ($d^8$). Aquest fet es deu al fort camp cristal·lí que creen els grups oxima del lligand (semblant al generat per grups ciano),[100] que provoca la disminució del potencial d'oxidació de $Ni^{II}$ i en facilita l'oxidació a $Ni^{IV}$ ($d^6$) en ser coordinat per un segon lligand $dapdo^{2-}$.[89]

### 1.4.2. 2-acetonitrilpiridiloxima

En veure l'elevada tendència que presentava el lligand $dapdoH_2$ a generar entorns plano-quadrats en el catió $Ni^{II}$, que provoca que aquest es comporti com una espècie diamagnètica, es va decidir substituir-lo per un nou lligand de la familia de les 2-piridiloximes. El nou lligand havia de ser capaç d'estabilitzar un entorn octaèdric sobre aquest catió metàl·lic, de forma que tots els cations $Ni^{II}$ que formessin part dels nous compostos polinuclears fossin paramagnètics.

Per tal d'introduir una nova variable en el disseny del lligand es va decidir afegir un grup donador amb un parell d'electrons disponible en el mateix substituent en què es troba el grup oxima. Aquest parell d'electrons, en el millor dels casos, podria coordinar nous centres metàl·lics, afavorint la formació de clústers polinuclears; i en cas contrari, podria afavorir l'estabilització dels complexos formats en establir ponts d'hidrogen intramoleculars o intermoleculars.

La família de lligands ciano-oxima (RC{CN}NOH) conté un grup –CN unit a l'àtom de carboni enllaçat al grup oxima que provoca un augment de la seva acidesa entre $10^3$ i $10^5$ vegades respecte d'altres oximes amb substituents alifàtics o aromàtics.[75] Aquesta família de lligands va ser caracteritzada per primera vegada fa uns 30 anys,[101] però el seu ús ja era conegut amb anterioritat en el control del creixement de plantes,[102] com antídot contra intoxicacions per certs pesticides[103] i per la seva activitat antimicrobial i fungicida.[104] Més tard, es van obtenir els primers complexos metàl·lics derivats d'aquests lligands amb diferents cations, com ara $Na^+$,[105a] $Co^{II}$ i $Ni^{II}$,[105b] $Ag^+$,[105,106] $Cs^+$,[105b] $Tl^+$,[106] i $Pb^{II}$,[107] entre els que destaca un complex de $Ag^+$ que actua com a sensor de gasos.[105a] En els últims anys, s'han utilitzat certs lligands ciano-oxima en la teràpia contra el càncer a causa de la seva activitat antitumoral i reduïda toxicitat.[108]

El lligand 2-acetonitrilpiridiloxima o pyC{CN}NOH, esquema 7, es va sintetitzar realitzant una modificació de la síntesi trobada a la bibliografia,[109] que consisteix en fer reaccionar quantitats equimolars de $pyCH_2CN$, àcid acètic i $KNO_2$, deixar la solució en agitació durant dues hores en un bany de gel, filtrar el sòlid obtingut i rentar-lo amb aigua. Aquest lligand presenta una elevada insolubilitat en solvents polars que disminueix dràsticament en presència de cations metàl·lics.

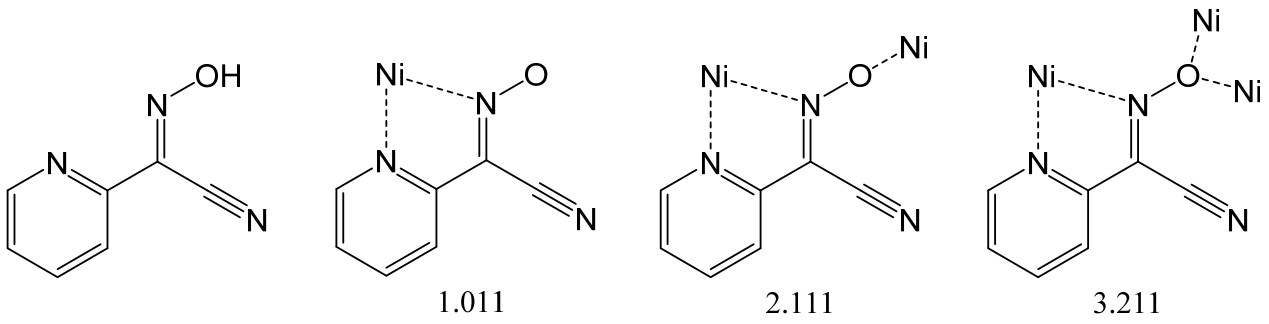


**Esquema 7.** Estructura del lligand pyC{CN}NOH i modes de coordinació caracteritzats per aquest lligand en el seu estat desprotonat.

La química de coordinació d'aquest lligand era pràcticament desconeguda a l'inici d'aquesta tesi. A part del seu ús en la determinació fotomètrica de $Fe^{2+}$ en solució,[109b,110] únicament s'havien trobat dos sistemes polimèrics de $Cs^+$ i $Tl^+$ amb fórmula $[M(pyC\{CN\}NO)]_n$[111] i una sèrie de compostos mononuclears de $Fe^{II}$, $Ni^{II}$ i $Cu^{II}$, $[M(pyC\{CN\}NO)_2L_2]$ (L = piridina o 3-picolina).[112] Paral·lelament, en el decurs de la tesi, es va estudiar al grup el seu comportament amb $Cu^{II}$,[113] i $Mn^{II,III,IV}$,[114] i es va trobar, pel què fa als compostos de coure, una sèrie de compostos amb grups $\mu_3$-O i $\mu_4$-O no observats en compostos $Cu^{II}$/oxima anteriorment,[113] mentre que per als sistemes $Mn^{n+}$/oxima es van observar noves topologies i un compost amb nuclearitat $Mn_{10}$ i el major estat fonamental de spin trobat en compostos derivats de piridiloximes, $S = 14$.[114]

En aquesta tesi s'han caracteritzat, per primera vegada, compostos derivats del lligand pyC{CN}NOH amb sals de $Ni^{II}$. S'han sintetitzat i caracteritzat un elevat nombre de compostos (21), entre els que destaquen una família de clústers formats per triangles $Ni_3/\mu_3$-OR/oxima, aïllats o units entre ells, obtinguts tots ells a partir de diverses sals carboxíliques i un compost monodimensional en què un fragment de nuclearitat $\{Ni_{12}Na_2\}$ format per efecte plantilla al voltant d'un catió $Na^+$ es propaga en l'espai en coordinar un nou catió $Ni^{II}$ i crear el compost cadena $\{Ni_{12}Na_2\text{-}Ni\text{-}\}_n$.

Els sistemes triangulars són fragments habituals en sistemes derivats d'oximes i metalls de transició d'alta nuclearitat, però a diferència del $Cu^{II}$,[113,115] $Mn^{III}$,[16,116] $Fe^{III}$,[117] i $Co^{III}$,[118] no s'havia pogut sintetitzar cap triangle $Ni_3/\mu_3$-OR/oxima aïllat. Aquests resultats suggereixen que l'augment de l'acidesa del grup oxima del lligand provoca que els cations divalents presentin comportaments més típics de cations trivalents, permeten l'ajust inequívoc d'aquests fragments i, indirectament, una millor comprensió del comportament de sistemes de major nuclearitat formats per fragments $Ni_3/\mu_3$-OR/oxima.

### 1.4.3. Sistema 2-piridiloxima / azida / amina

Posteriorment, es va decidir iniciar una nova estratègia sintètica basada en l'ús de clústers dinuclears neutres de níquel(II) amb lligands azidur i amines polidentades alifàtiques. Aquesta decisió es va prendre amb l'objectiu d'afavorir la coordinació de l'anió azidur (únic anió present en el medi de reacció) per tal d'obtenir acoblaments ferromagnètics promoguts per ponts azida o oxima/azida.[59a,119] En observar la coordinació de l'anió azidur en presència d'altres anions es va

procedir a la síntesi directa de nous compostos polinuclears amb ponts azida a partir de diverses sals de níquel(II), azidur i d'amines bi- i tridentades. Es van mantenir les amines per tal que actuessin com topalls o *stoppers* i ocupessin diverses posicions de l'esfera de coordinació.

En aquest marc, es van utilitzar diferents lligands 2-piridiloxima i amines polidentades per tal de poder analitzar la seva influència. Es van utilitzar els lligands i les amines mostrats a l'esquema 8. D'aquests, es van obtenir nous compostos per tots els lligands excepte per pyC{Me}NOH, 3-MepyC{H}NOH i pyC{$NH_2$}NOH.

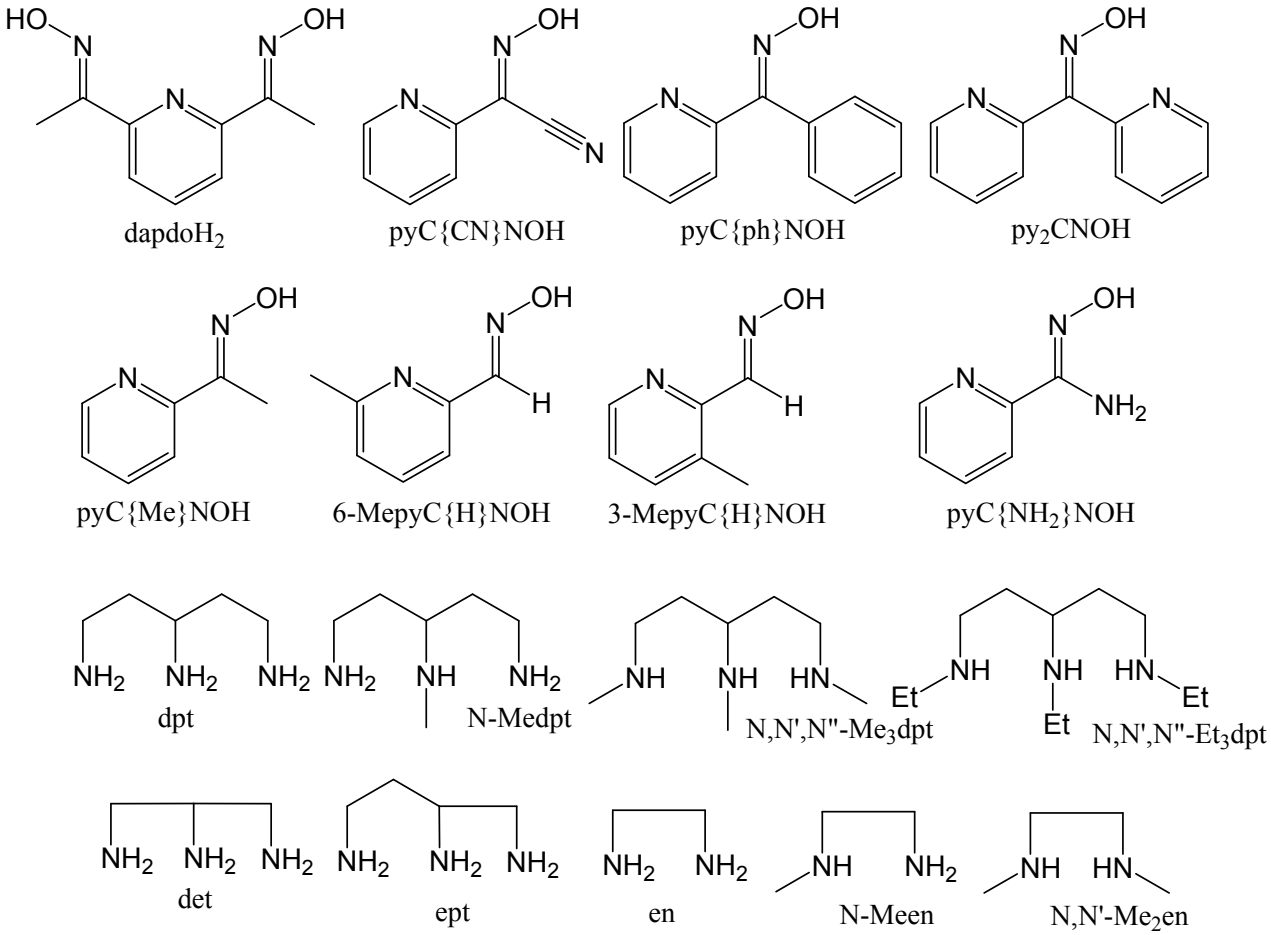


**Esquema 8.** Conjunt de lligands 2-piridiloxima i amines usades.

**pyC{ph}NOH**

Els primers compostos polinuclears sintetitzats amb el lligand fenil-2-piridilcetoxima, pyC{ph}NOH, esquema 8, van ser una família de compostos trinuclears d'osmi amb topologia triangular, obtinguda el 2002.[120] Posteriorment, s'han caracteritzat prop de 50 compostos (CCDC), entre els que destaquen un compost triangular de $Fe^{III}_3$,[121] una papallona de $Zn_4$,[122] diversos triangles de $Cu_3$[115c,123] i $Co_3$[124] i, finalment, una sèrie de compostos de manganès de nuclearitat $Mn^{III}_3$,[16,116] $Mn^{II}_4$,[125a] $Mn^{II}_3Mn^{IV}$,[125b,c] $Mn^{II}Mn^{III}_5$,[126] $Mn^{II}_4Mn^{III}_4$[127] i $Mn^{II}_4Mn^{III}_6Mn^{IV}_2$.[128]

Pel què fa a la química d'aquest lligand amb $Ni^{II}$, a la bibliografia s'han trobat 10 precedents, que consisteixen en dos compostos dinuclears units per ponts oxima[128] i sulfat,[129] respectivament, un compost trinuclear que únicament conté lligands pyC{ph}NOH i presenta la fórmula $[Ni_3(pyC\{ph\}NO)_6]$,[130] un compost tetranuclear en què els cations $Ni^{II}$ formen un tetraedre,[124b] dos compostos pentanuclears amb topologia de *bowtie*,[131] i finalment tres complexos de nuclearitat $Ni_6$,[132] dos dels quals estan formats per dos triangles paral·lels i units entre si per ponts sulfat[132a] mentre que el tercer presenta una geometria de cadira.[132b] També cal destacar un compost heterometàl·lic $Mn^{III}_4Ni^{II}_4$ que forma un quadrat en què els ions $Ni^{II}$ se situen a les cantonades mentre que els de $Mn^{III}$ es troben al centre dels costats.[127c]

**$py_2$CNOH**

Els primers compostos polinuclears sintetitzats amb el lligand di-2-piridilcetoxima, $py_2$CNOH, esquema 8, van ser tres compostos dinuclears de $Cu^{II}$ i $Ag^+$ i un complex hexanuclear de $Zn^{II}$ sintetitzats a principis dels anys 1990.[133] Posteriorment, sobretot a partir de l'any 2000, aquest lligand va ser emprat en la síntesi d'un elevat nombre de compostos polinuclears, fins a arribar als 80 compostos de coordinació caracteritzats actualment (CCDC), fent de la di-2-piridilcetoxima un dels lligands més emprats dins la família de les piridiloximes.

Un gran nombre de compostos obtinguts a partir del lligand $py_2$CNOH presenten estructura de metal·lomacrocicle, com per exemple un complex dodecanuclear de $Mn^{II}_4Mn^{III}_6Mn^{IV}_2$,[134] un complex tetranuclear de $Co^{II}_2Co^{III}_2$,[124b,135] diversos compostos di-, tri-, penta- i hexanuclears de $Cu^{II}$,[136] i dos compostos de nuclearitat $Zn_4$ i $Zn_8$.[137] Una altra característica d'aquest lligand és que ha

permès la síntesi una família de compostos trinuclears heterometàl·lics 3d – 4f,[138] la major part dels quals presenten comportament de SMM.

La química d'aquest lligand amb $Ni^{II}$ ha generat compostos de diverses nuclearitats i topologies, com són un compost trinuclear en què els àtoms de $Ni^{II}$ es troben en una disposició angular,[139] una sèrie de compostos de nuclearitat $Ni_4$ amb forma de metal·locorona[140] o cub distorsionat,[141] tres compostos pentanuclears amb topologia de metal·locorona[141] o metal·locorona coordinada a un metall central,[140a,142] un compost heptanuclear format per dos triangles units per un àtom de Ni addicional[141] i finalment un compost de nuclearitat $Ni_{10}$ format per dos metal·lomacrocicles quasi-paral·lels coordinats entre si.[143] També s'han caracteritzat un metal·lomacrocicle heterometàl·lic $Ni^{II}_2Mn^{III}_2$[140a] i una família de compostos trinuclears heterometàl·lic 3d – 4f amb *core* $Ln^{III}_2Ni^{II}$, entre els que es troba un compost de $Dy_2Ni$ que es comporta com un SMM.[144]

**pyC{Me}NOH**

El lligand metil-2-piridilcetoxima, pyC{Me}NOH, esquema 8, va ser usat per primera vegada el 1975 per Hodgson *et al.* en la síntesi d'un compost mononuclear de $Pt^{II}$ que es disposava formant cadenes.[145] Durant els anys posteriors, es va sintetitzar diversos compostos mononuclears de Rh(III),[146] Ni(II)[147] i Co(II)[148] o dinuclears de Co(II) i Ni(II)[149] o Cu(II),[150] però no va ser fins l'any 2000 que el seu ús va viure un important auge en la síntesi de compostos polinuclears de metalls de transició i el seu estudi magnètic. Des d'aquest any, s'han caracteritzat més de 60 compostos que contenen aquest lligand, 31 dels quals polinuclears, entre els quals destaquen una sèrie de compostos de $Mn^{III}_3$,[16,116] diversos compostos de valència mixta de manganès de nuclearitats $Mn_6$ i $Mn_8$[96,151] i $Mn_{13}$ i $Mn_{16}$,[152] així com un compost tetranuclear de $Fe^{III}$,[153] i un compost de valència mixta de cobalt i nuclearitat $Co^{II}Co^{III}_2$;[154] alguns dels quals presenten comportament d'imant unimolecular.[16,96,116,152]

La química del lligand pyC{Me}NOH amb $Ni^{II}$ no ha estat molt explorada i es coneixen pocs compostos polinuclears amb $Ni^{II}$, la major part dels quals són heterometàl·lics. S'ha caracteritzat una família de compostos dinuclears i trinuclears homo- i heterometàl·lics en què s'ha unit el fragment $\{Ni(pyC\{Me\}NO)_3\}^-$ a diversos cations metàl·lics 3d com $Ni^{II}$, $Ni^{III}$, $Fe^{III}$, $Mn^{II}$, $Mn^{III}$, etc.,[128] un compost trinuclear amb forma triangular en què l'àtom d'oxigen d'un grup oxima actua de lligand

central $\mu_3$-O,[130] un compost tetranuclear que forma una metal·locorona capaç d'encapsular anions[140c] i un compost hexanuclear que conté un lligand sulfat central al voltant del qual se situen els diferents àtoms de $Ni^{II}$.[132] També s'han sintetitzat diversos compostos heterometàl·lics 3d/4f amb nuclearitats $Ni^{II}Ln^{III}$, $Ni^{II}_2Ln^{III}$ i $Ni^{II}_2Ln^{III}_2$ per tal d'obtenir SMMs a partir de metalls de transició i lantànids, en què el fragment $\{Ni(pyC\{Me\}NOH)_3\}^{2+}$ (protonat, parcial o totalment desprotonat) actua de lligand i coordina els lantànids.[155]

**pyC{$NH_2$}NOH**

El lligand amino-2-piridilcetoxima és un cas molt particular entre els diversos lligands 2-piridiloxima, ja que la gran majoria de compostos polinuclears caracteritzats per aquest lligand contenen $Ni^{II}$.

El primer compost sintetitzat amb pyC{$NH_2$}NOH va ser obtingut l'any 2008 per Brechin, Perlepes *et al.* i consisteix en un compost dodecanuclear de níquel acoblat ferromagnèticament a través de ponts oxima.[156] En vista del ferromagnetisme promogut per aquest lligand, es van sintetitzar nous compostos de nuclearitat $Ni_4$, $Ni_8$ i $Ni_{12}$,[157] que presenten el mateix tipus d'acoblament. També es van sintetitzar una sèrie de compostos heterometàl·lics $Ni^{II}_2M^{III}$ (M= Fe, Cr) i $Ni^{II}_2Mn^{IV}$ en què dos fragments $\{Ni(pyC\{NH_2\}NO)_3\}$ coordinen un metall central,[158] però es va trobar que aquests compostos havien perdut les propietats ferromagnètiques trobades per sistemes de $Ni^{II}$, probablement a causa de la distorsionada coordinació dels lligands al catió $Ni^{II}$.

Els dos casos que no contenen Ni són un complex dinuclear de $Zn^{II}$ de fórmula $[Zn_2(pyC\{NH_2\}NO)_4]$[159] i una família de compostos de $Zn^{II}_2$ sintetitzats a partir de diferents anions amb interessants propietats fotoluminiscents.[160]

**3-MepyC{H}NOH i 6-MepyC{H}NOH**

Els lligands 2-(3-metil)- i 2-(6-metil)piridilaldoxima presenten una important variació respecte els altres lligands utilitzats en aquest capítol: presenten modificacions en l'anell piridínic, posicions R' a l'esquema 8. Amb aquestes modificacions, es pretén estudiar els efectes electrònics i d'impediment estèric que pot provocar la presència d'un grup metil en diverses posicions.

Aquest tipus de lligands ha estat molt poc estudiat, com demostra el fet que a l'inici d'aquesta tesi només s'hagués caracteritzat un compost pel lligand 6-MepyC{H}NOH, i que, en acabar aquesta tesi, encara no se n'ha caracteritzat cap per al lligand 3-MepyC{H}NOH.

El 1999 es va caracteritzar el primer compost sintetitzat per al lligand 6-MepyC{H}NOH, que consistia en un sistema de nuclearitat $Ni_9$ que forma un metal·lomacrocicle amb 8 cations $Ni^{II}$ i 10 lligands 6-MepyC{H}$NO^-$ i encapsula l'ió $Ni^{II}$ addicional.[161] Posteriorment, durant la realització d'aquesta tesi van aparèixer nous compostos sintetitzats a partir d'aquest lligand, com són una família de compostos penta- i hexanuclears de $Ni^{II}$,[162] una cadena de $\{Mn^{II}_2Mn^{III}_2\}_n$ que es comporta com SCM,[83b] dos compostos tetranuclears de $Co^{II}Co^{III}_3$ en què els àtoms de $Co^{III}$ formen un triangle[163] i finalment un compost trinuclear i dos compostos hexanuclears formats a partir de triangles de $Cu^{II}_3$ què presenten frustració de spin;[164] tots ells sintetitzats al grup.

# 2

# Objectius

# 2. Objectius

Els principals objectius en els camps de la química de la coordinació i el magnetisme molecular són la síntesi de nous compostos de coordinació, l'estudi de les seves propietats magnètiques i la racionalització i comprensió de la relació entre l'estructura d'aquests i seves les propietats. L'anàlisi i comparació de compostos similars afavoreix una millor comprensió d'aquests, fet que permet la síntesi dirigida de nous compostos per tal que presentin les propietats desitjades i que permetin la seva aplicació com imants unimoleculars (SMM, SCM), refrigerants magnètics, etc.

Així, els objectius marcats a l'inici d'aquest treball van ser:

- La síntesi, caracterització i estudi magnètic de compostos polinuclears de $Ni^{II}$ amb el lligand 2,6-diacetilpiridildioxima (dapdo$H_2$).

- La síntesi, caracterització i estudi magnètic de compostos polinuclears de $Ni^{II}$ amb el lligand 2-acetonitrilpiridiloxima (pyC{CN}NOH).

- La síntesi, caracterització i estudi magnètic de compostos polinuclears de $Ni^{II}$ obtinguts a partir del sistema 2-piridiloxima/azida/amina.

# 3

# Resultats

## 3.1. Article 1.

## First Structural and Magnetic Studies of Ni Clusters Containing 2,6-Diacetylpyridine-dioxime as a Ligand.

Albert Escuer, **Jordi Esteban**, Núria Aliaga-Alcaide, Mercè Font-Bardia, Teresa Calvet, Olivier Roubeau, Simon J. Teat.

*Inorganic Chemistry* **2010**, *49*, 2259-2266.

Inorganic Chemistry
Article

*Inorg. Chem.* **2010**, *49*, 2259–2266 **2259**
DOI: 10.1021/ic9020965

# First Structural and Magnetic Studies of Ni Clusters Containing 2,6-Diacetylpyridine-dioxime as a Ligand

**Albert Escuer,*,† Jordi Esteban,† Núria Aliaga-Alcalde,‡ Mercé Font-Bardia,§ Teresa Calvet,§ Olivier Roubeau,⊥ and Simon J. Teat#**

†*Departament de Química Inorgànica and Institut de Nanociència i Nanotecnologia de la Universitat de Barcelona (IN2UB), Martí I Franqués 1-11, 08028 Barcelona, Spain,* ‡*ICREA (Institut Català de Recerca i Estudis Avançants) & Departament de Química Inorgànica de la Universitat de Barcelona, Martí I Franqués 1-11, 08028 Barcelona, Spain,* §*Departament de Mineralogia I Crystalografia, Universitat de Barcelona, Martí Franqués s/n, 08028 Barcelona, Spain,* ⊥*Instituto de Ciencia de Materiales de Aragón, CSIC-Universidad de Zaragoza, Pl. San Francisco s/n, 50009 Zaragoza, Spain, and* #*Advanced Light Source, Lawrence Berkeley National Laboratory, 1 Cyclotron road, Berkeley, California 94720*

Received October 23, 2009

In the present work, coordination possibilities of the system dapdo$H_2$/$Ni^{2+}$, being dapdo$H_2$ = 2,6-diacetylpyridine dioxime, have been explored, offering as a result a number of unprecedented clusters with a variety of topologies and magnetic behaviors. Depending on the precursors and reaction conditions, several compounds named [$Ni_2$(dapdo)$_2$] (**1**), [$Ni_3$(OH)(BzO)$_3$(dapdo)(dapdoH$_2$)($H_2O$)]·1.25$H_2O$ (**2**), [$Ni_3$(AcO)$_4$(dapdoH)$_2$($H_2O$)$_2$]·$H_2O$ (**3**), and [$Ni_4$-(AcO)$_3$(dapdo)(dapdoH)$_2$($H_2O$)$_3$]·(AcO)·3$H_2O$ (**4**) were achieved and structurally well-characterized. Dc magnetic measurements were carried out in the 2−300 K range revealing antiferromagnetic interactions for (**2**−**4**) compounds and diamagnetic response for the square planar coordinated complex (**1**).

## Introduction

At present, research of oximes in coordination chemistry is a growing field. 2-pyridyl oximes are well-known ligands in this area because of their ability to generate stable first-row transition coordination compounds with a large range of nuclearities.[1] These molecules are very versatile, able to act as bidentate ligands in their neutral state or to link up to three metallic centers in their deprotonated anionic form. Self-assembly of metal-oximato fragments have yielded a large amount of high nuclearity clusters, as for example: $Ni_7$,[2] $Ni_9$,[3] $Ni_{10}$,[4] $Ni_{12}$ or $Ni_{14}$,[5] $Fe_{12}$,[6] and $Mn_8$,[7] $Mn_9$,[8] $Mn_{10}$,[9] and $Mn_{12}$,[10] exhibiting in some cases SMM response.[7,10]

One of the crucial synthetic points in the search of high nuclearity systems is the design of ligands to increase such nuclearity and/or generate new topologies. Regarding this matter, pyridyl dioximato ligands ($LH_2$, with R = various), Scheme 1, appear as excellent candidates for the achievement of polynuclear clusters in the bottom-up approach: they contain a good N-donor unit (pyridinic ring) and two meta-oximato groups capable of binding four metal centers, M in Scheme 2.

*To whom correspondence should be addressed. E-mail: albert.escuer@ub.edu.

(1) Milios, C. J.; Stamatatos, T. C.; Perlepes, S. P. *Polyhedron* **2006**, *25*, 134.
(2) Stamatatos, T. C.; Diamantopoulou, E.; Raptopoulou, C. P.; Psycharis, V.; Escuer, A.; Perlepes, S. P. *Inorg. Chem.* **2007**, *46*, 2350.
(3) (a) Khanra, S.; Weyhermuller, T.; Rentschler, E.; Chaudhuri, P. *Inorg. Chem.* **2005**, *44*, 8176. (b) Stamatatos, T. C.; Diamantopoulou, E.; Tasiopoulos, A.; Psycharis, V.; Vicente, R.; Raptopoulou, C. P.; Nastopoulos, V.; Escuer, A.; Perlepes, S. P. *Inorg. Chim. Acta* **2006**, *359*, 4149. (c) Stamatatos, T. C.; Papatriantafyllopoulou, C.; Katsoulakou, E.; Raptopoulou, C. P.; Perlepes, S. P. *Polyhedron* **2007**, *26*, 1830.
(4) Psomas, G.; Dendrinou-Samara, C.; Alexiou, M.; Tsohos, A.; Raptopoulou, C. P.; Terzis, A.; Kessissoglou, D. P. *Inorg. Chem.* **1998**, *37*, 6556.
(5) (a) Stamatatos, T. C.; Abboud, K. A.; Perlepes, S. P.; Christou, G. *Dalton Trans.* **2007**, 3861. (b) Papatriantafyllopoulou, C.; Jones, L. F.; Nguyen, T. D.; Matamoros-Salvador, N.; Cunha-Silva, L.; Paz, F. A. A.; Rocha, J.; Evangelisti, M.; Brechin, E. K.; Perlepes, S. P. *Dalton Trans.* **2008**, 3153. (c) Stamatatos, T. C.; Escuer, A.; Abboud, K. A.; Raptopoulou, C. P.; Perlepes, S. P.; Christou, G. *Inorg. Chem.* **2008**, *47*, 11825.
(6) Murugesu, M.; Abbout, K. A.; Christou, G. *Polyhedron* **2004**, *23*, 2779.
(7) (a) Milios, C. J.; Kefalloniti, E.; Raptopoulou, C. P.; Terzis, A.; Vicente, R.; Lalioti, N.; Escuer, A.; Perlepes, S. P. *Chem.Commun.* **2003**, 819. (b) Milios, C. J.; Stamatatos, T. C.; Kyritsis, P.; Terzis, A.; Raptopoulou, C. P.; Vicente, R.; Escuer, A.; Perlepes, S. P. *Eur. J. Inorg. Chem.* **2004**, 2885. (c) Stoumpos, C. C.; Stamatatos, T. C.; Psycharis, V.; Raptopoulou, C. P.; Christou, G.; Perlepes, S. P. *Polyhedron* **2008**, *27*, 3703. (d) Stoumpos, C. C.; Stamatatos, T. C.; Sartzi, H.; Roubeau, O.; Tasiopoulos, A. J.; Nastopoulos, V.; Teat, S. J.; Christou, G.; Perlepes, S. P. *Dalton Trans.* **2009**, 1004.
(8) Roubeau, O.; Lecren, L.; Li, Y. G.; Le Goff, X. F.; Clerac, R. *Inorg. Chem. Commun.* **2005**, *8*, 314.
(9) Papatriantafyllopoulou, C.; Raptopoulou, C. P.; Escuer, A.; MIlios, C. J. *Inorg. Chim. Acta* **2007**, *360*, 61.
(10) Dendrinou-Samara, C.; Zaleski, C. M.; Evagorou, A.; Kampf, J. W.; Pecoraro, V. L.; Kessissoglou, D. P. *Chem.Commun.* **2003**, 2668.


Published on Web 01/26/2010

**Scheme 1.** $LH_2$ Dioxime Ligands (R = H, Me, $NH_2$); $dapdoH_2$ Refers to the Ligand in Which R = Me

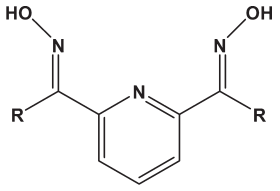

**Scheme 2.** Coordination Modes for $dapdoH_2$, $dapdoH^-$, or $dapdo^{2-}$ Ligands[a]

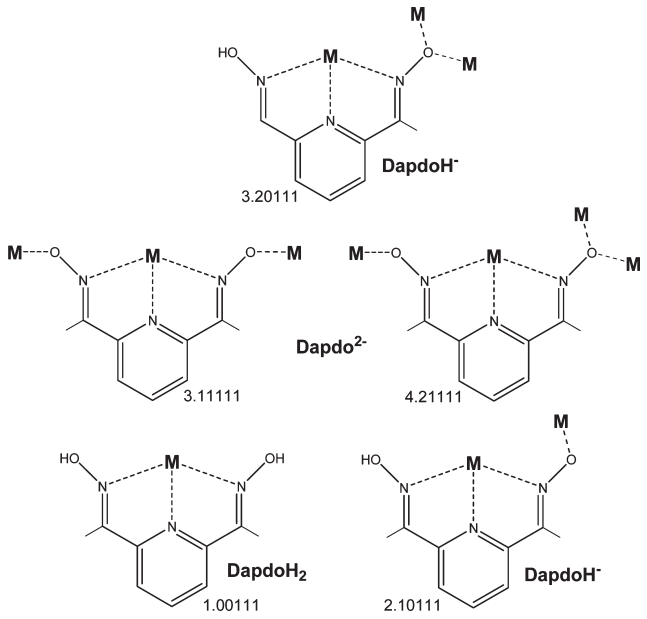


[a] A large number of unprecedented possibilities as the novel coordination mode 3.20111 reported in this work for $dapdoH^-$ are still possible.

Within this family of linkers, 2,6-diacetylpyridine dioxime ($dapdoH_2$) is the most well-studied and only a few examples using related ligands like 2,6-pyridine dioxime ($pdoH_2$) or pyridine-2,6-diamidoxime ($pdamoH_2$) have been reported to date.[1]

On the other hand, the putative capacity of $dapdoH_2$ for the development of high nuclearity systems differs from current results in the literature, where the majority of compounds happen to be mononuclear. Thus, a number of systems with general formula $[M^{II}(LH_2)_2]X_2$ (M = Cu,[11] Ni,[12] Fe,[13] Mn[11a]), including one $[Ni^{II}(pdamoH)_2]$[14] and two $[M^{IV}(dapdo)_2]$ ($M^{IV}$ = Ni,[15] Co[16]) have been described. In all of them, the six coordination sites of the metallic centers are shielded by two $LH_2$, $LH^-$, or $L^{2-}$ ligands in 1.00111 coordination modes (Harris notation),[17] respectively. In addition, several mononuclear complexes containing one $dapdoH_2$ ligand in the 1.00111 coordination mode along with anions or solvent molecules linked in the remainder positions of the coordination sphere of metal have been found with $Cu^{2+}$,[18] $Zn^{2+}$,[18a] $In^{3+}$,[19] and $Ru^{2+}$.[20] Besides, some of these coordinated anions may also bind neighboring centers giving as a result 1D systems in which $dapdoH_2$ acts exclusively as a tridentate ligand (e.g., $[Cu(pdamoH_2)(\mu\text{-}SO_4)]_n$[12] and $[Mn(dapdoH_2)(\mu\text{-}Cl)_2]_n$).[21] Recent reports show similar coordination properties for certain trinuclear systems, $[Mn_3(dapdoH_2)_2(R\text{-}COO)_6]$ (R = H, Me, Ph).[22]

Nevertheless, it should be emphasized the existence of some polynuclear clusters generated after deprotonation of $dapdoH_2$; where now, the resulting anionic species ($dapdoH^-$ and/or $dapdo^{2-}$) play a primary role. This group of compounds comprises a dinuclear copper system that contains a double oximato bridge and two $dapdoH^-$ ligands in 2.10111 coordination modes, which general formula is $[Cu_2(dapdoH)_2](BF_4)_2$;[23] a mixed valence trinuclear Fe system in which one $\{Fe^{II}(dapdoH)_2\}$ subunit is linked to two $Fe^{3+}$ cations, described as $[Fe^{II}(dapdoH)_2Fe^{III}Cl_4(O)]$;[13] an heterometallic copper−chromium compound in which {Cu(dapdo)} subunits bind chromium triazacyclononane groups in a 3.11111 coordination mode;[24] a family of $Mn^{II}_2Mn^{III}_4$ hexanuclear anionic species expressed as $[Mn_6O_2(MeO)_2(dapdo)_2(dapdoH)_4]^{2+}$;[25] a mixed valence $[Mn^{II}_2Mn^{III}_6O_4(OH)_4(MeO)_2(N_3)_2(dapdo)_2(dapdoH)_2(H_2O)]$[25a] complex and finally an heterometallic Mn/Gd trinuclear system.[26]

Here, we introduce the first polynuclear clusters achieved by reacting $dapdoH_2$ with different nickel salts in basic conditions. This approach has led to the formation of unique structures, $Ni_2$ (**1**), $Ni_3$ (**2**, **3**), and $Ni_4$ (**4**), that include the organic unit or its deprotonated forms exhibiting a variety of coordination modes. Syntheses, structures, and magnetic behaviors of these compounds are described in the following sections.

## Experimental Section

**Syntheses.** 2,6-Diacetylpyridine, $Ni(AcO)_2\cdot 4H_2O$ and Ni(acac)$_2$ (acac = acetylacetonate) were purchased from Sigma-Aldrich Inc. and Flucka AG and used without further purification. $Ni(BzO)_2\cdot 3H_2O$ was synthesized dissolving equimolar quantities (40 mmol) of benzoic acid and NaOH in 40 mL of

(11) (a) Glynn, C. W.; Turnbull, M. M. *Transition Met. Chem.* **2002**, *27*, 822. (b) Halcrow, M. A.; Kilner, C. A.; Wolowska, J.; McInnes, E. J. L.; Bridgeman, A. J. *New J. Chem.* **2004**, *28*, 228.
(12) Bovenzi, B. A.; Pearse, G. A., Jr. *J. Chem. Soc., Dalton Trans.* **1997**, 2793.
(13) Vasilevsky, I. V.; Stenkamp, R. E.; Lingafelter, E. C.; Rose, N. J. *J. Coord. Chem.* **1988**, *19*, 171.
(14) Salonen, M.; Saarinen, H.; Mutikainen, I. *J. Coord. Chem.* **2008**, *61*, 1462.
(15) Sproul, G.; Stucky, G. D. *Inorg. Chem.* **1973**, *12*, 2898.
(16) Namli, H.; Azaz, A. D.; Karabulut, S.; Çelen, S.; Kurtaran, R.; Kazak, C. *Transition Met. Chem.* **2007**, *32*, 266.
(17) Coxall, R. A.; Harris, S. G.; Henderson, D. K.; Parsons, S.; Tasker, P. A.; Winpenny, R. E. P. *J. Chem. Soc., Dalton Trans.* **2000**, 2349.
(18) (a) Nicholson, G. A.; Petersen, J. L.; McCormick, B. J. *Inorg. Chem.* **1982**, *21*, 3274. (b) Vasilevsky, I. V.; Stenkamp, R. E.; Lingafelter, E. C.; Schomaker, V.; Willett, R. D.; Rose, N. J. *Inorg. Chem.* **1989**, *28*, 2619. (c) Abboud, K. A.; Palenik, R. C.; Palenik, G. J. *Acta Crystallogr., Sect. C* **1994**, *C50*, 525.
(19) (a) Abram, S.; Maichle-Mössmer, C.; Abram, U. *Polyhedron* **1997**, *16*, 2183. (b) Abram, S.; Maichle-Mössmer, C.; Abram, U. *Polyhedron* **1997**, *16*, 2291.
(20) Singh, S. K.; Sharma, S.; Dwivedi, S. D.; Zou, R.-Q.; Xu, Q.; Pandey, D. S. *Inorg. Chem.* **2008**, *47*, 11942.
(21) (a) Unni Nair, B. C.; Sheats, J. E.; Ponteciello, R.; Van Engen, D.; Petrouleas, V.; Dismukes, G. C. *Inorg. Chem.* **1989**, *28*, 1582. (b) Marsh, R. E. *Inorg. Chem.* **1990**, *29*, 572.
(22) Escuer, A.; Cordero, B.; Solans, X.; Font-Bardia, M.; Calvet, T. *Eur. J. Inorg. Chem.* **2008**, 5082.
(23) Nicholson, G. A.; Petersen, J. L.; McCormick, B. J. *Inorg. Chem.* **1980**, *19*, 195.
(24) Khanra, S.; Weyhermüller, T.; Chaudhuri, P. *Dalton Trans.* **2007**, 4675.
(25) (a) Stamatatos, T. C.; Luisi, B. S.; Moulton, B.; Christou, G. *Inorg. Chem.* **2008**, *47*, 1134. (b) Khanra, S.; Weyhermüller, T.; Chaudhuri, P. *Dalton Trans.* **2008**, 4885.
(26) Lampropoulos, C.; Stamatatos, T. C.; Abboud, K. A.; Christou, G. *Inorg. Chem.* **2009**, *48*, 429.

$H_2O$, filtering and mixing the final solution with a commercial source of $Ni(NO_3)_2 \cdot 6H_2O$ (20 mmol) in 20 mL of water. The resulting nickel salt was obtained in good yield (>80%). $DapdoH_2$ was prepared following C.W. Glynn and M.M. Turnbull method.[11a]

**$[Ni_2(dapdo)_2]$ (1).** $DapdoH_2$ (0.193 g, 1 mmol) and $Ni(acac)_2$ (0.514 g, 2 mmol) were dissolved in 20 mL of MeOH together with $NEt_3$ (0.202 g, 2 mmol). The mixture was stirred for 2 h and then filtered. Crystals were obtained by layering the final solution with 10 mL of diethyl ether. Anal. Calcd for $C_{18}H_{18}N_6Ni_2O_4$ (**1**): C, 43.26; H, 3.63, N, 16.82%. Found: C, 43.1; H, 3.7, N, 16.6%. Relevant IR bands ($cm^{-1}$): 3421(b), 1559(w), 1512 (w), 1399(s), 1299(m), 1273(m), 1196(s), 1151(m), 1118(m), 1087(s), 788(m), 559(m).

**$[Ni_3(OH)(BzO)_3(dapdo)(dapdoH_2)(H_2O)] \cdot 1.25H_2O$ (2).** $DapdoH_2$ (0.194 g, 1.0 mmol) and $Ni(BzO)_2 \cdot 3H_2O$ (0.602 g, 2 mmol) were dissolved in 40 mL of distilled MeOH and then $NEt_3$ (0.202 g, 2 mmol) was added. The solution was stirred for 2 h, filtered and crystallized layering with diethyl ether. Anal. Calcd for $C_{39}H_{38}N_6Ni_3O_{12} \cdot 1.25\ H_2O$ (**2**): C, 47.73; H, 4.16, N, 8.56%. Found: C, 47.8; H, 4.0, N, 8.8%. Relevant IR bands ($cm^{-1}$): 3436(b), 1599(s), 1340(s), 1214(w), 1121(w), 1087(w), 1044(w), 802(w), 721(m).

**$[Ni_3(AcO)_4(dapdoH)_2(H_2O)_2] \cdot H_2O$ (3).** A slurry of $dapdoH_2$ (0.193 g, 1 mmol) was dissolved in 20 mL of distilled MeOH and $NEt_3$ (0.202 g, 2 mmol) together with $Ni(AcO)_2 \cdot 4H_2O$ (0.494 g, 2 mmol). The solution was stirred for a couple of hours, filtered and crystallized layering with diethyl ether. Anal. Calcd for $C_{26}H_{36}N_6Ni_3O_{14} \cdot H_2O$ (**3**): C, 36.70; H, 4.50, N, 9.88%. Found: C, 35.3; H, 4.6, N, 9.5%. Relevant IR bands ($cm^{-1}$): 3400(b), 1577(s), 1410(s), 1213(m), 1167(m), 1058(m), 809 (m), 661(m).

**$[Ni_4(AcO)_3(dapdo)(dapdoH)_2(H_2O)_3](AcO) \cdot 3H_2O$ (4).** $DapdoH_2$ (0.193 g, 1 mmol) and $Ni(AcO)_2 \cdot 4H_2O$ (0.494 g, 2 mmol) were added to 20 mL of $CH_2Cl_2$ together with $NEt_3$ (0.202 g, 2 mmol). The solution was stirred and after a couple of hours, filtered and layered using hexane. Anal. Calcd for $C_{35}H_{47}N_9Ni_4O_{17} \cdot 3H_2O$ (**4**); C, 36.41; H, 4.63, N, 10.92%. Found: C, 35.2; H, 4.8, N, 10.5%. Relevant IR bands ($cm^{-1}$): 3396(b), 1572(s), 1517 (m), 1489(m), 1193 (m), 1167 (m), 1085 (m), 1060 (m), 811 (w), 715 (w), 669 (w).

**Physical Measurements.** Magnetic susceptibility measurements were carried out on polycrystalline samples with a DSM5 Quantum Design susceptometer working in the range 30−300 K under magnetic fields of 0.3 T and under a field of 0.03T in the 30−2 K range to avoid saturation effects. Diamagnetic corrections were estimated from Pascal Tables. Infrared spectra (4000−400 $cm^{-1}$) were recorded from KBr pellets on a Bruker IFS-125 FT-IR spectrophotometer.

**X-ray Crystallography.** Data for compound **1** were collected on a red block using a single-axis HUBER diffractometer on station BM16 of the European Synchrotron Radiation Facility, Grenoble, France. Cell refinement, data reduction and absorption corrections were done with HKL-2000 suite.[27] The structure was solved by direct methods and the refinement and all further calculations were carried out using SHELX-TL suite.[28] All non-hydrogens were refined anisotropically. Hydrogens were found in difference Fourier maps, placed geometrically on their riding atom and refined with a riding model.

Data for compound **2** were collected on an orange plate on a Bruker APEX II CCD diffractometer on Advanced Light Source beamline 11.3.1 at Lawrence Berkeley National Laboratory, from a silicon 111 monochromator . The structure was solved by direct methods and refined on $F^2$.[28] The crystal was found to be twinned, although attempts at finding a twinning matrix were unsuccessful. Twinning was thus taken into account with TWIN/BASF instructions in shelxl. All non-hydrogens were refined anisotropically, although displacement parameters restrains were used for a number of carbon atoms and the lattice water oxygens. Hydroxyl hydrogens were found in difference Fourier maps and refined with distance restrains. The rest of hydrogens were placed geometrically on their riding atom. At the end of the refinement, large voids remained in the structure containing only diffuse electron density that could not be modeled satisfactorily. These voids were thus analyzed and taken into account by PLATON/SQUEEZE,[29] that recovered a total of 276 electrons per cell in voids occupying a total of 1476 cubic angstroms (main voids volumes are 200 and 125 $Å^3$), resulting in a significant improvement both in $R_1$ and w$R_2$ factors. The derived figures (electrons/volume) would reasonably account for a number of diffuse small solvent molecules, e.g. water or methanol.

A red prismatic crystal of (**3**) was selected and mounted on a MAR345 diffractometer with an image plate detector. Unit-cell parameters were determined from 6640 reflections ($3 < \theta < 31°$) and refined by least-squares method. Lorentz-polarization and absorption corrections were made.

The structure was solved by direct methods, using SHELXS computer program[30] and refined by full-matrix least-squares method with SHELX97 computer program.[31] All H atoms were computed and refined, using a riding model, with an isotropic temperature factor equal to 1.2 time the equivalent temperature factor of the atom which are linked.

(**4**) Data collection of the data was made on a APEX2 (BRUKER AXS, 2005) diffractometer. Unit-cell parameters were determined from 1896 reflections ($2.3 < \theta < 23.4°$) and refined by least-squares method. The structure was solved using SIR97[32] and refined with SHELX97.[31]

Unit-cell parameters, structure, and refinement data are listed in Table 1.

Plots for publication were generated with ORTEP3 for Windows and plotted with Pov-Ray programs.[33]

## Results and Discussion

**Syntheses.** There are several resemblances in the synthetic preparation of compounds **1**−**4**; however, the chemistry behind suggests a more complex picture than one may anticipate. This way, it was found that reactions using $Ni(acac)_2$ or $Ni(tfacac)_2$ (tfacac = trifluoroacetylacetonato) together with $dapdoH_2$ always yielded compound **1**, even if different reagent ratios, pH, or solvents were used. Basically, no examples of octahedral Ni compounds were achieved using acac or derivative ligands as starting materials. In contrast, compounds **2**−**4** could be easily obtained with $Ni(BzO)_2$ or $Ni(AcO)_2$ salts, correspondingly. Nevertheless, we may stress that all three complexes exhibit great dependency on other reactiońs variables. Hence, compound **2** was obtained using MeOH or 96% EtOH as solvents, and a small amount of $H_2O$ in solution was mandatory. No compounds were isolated using dry solvents. Also, of particular interest it is the necessity of $H_2O$ molecules that do not react or

(27) Otwinowski, Z.; Minor, W. *Methods in Enzymology: Macromolecular Crystallography, Part A*; Carter, C.W., Jr., Sweet, R. M., Eds.; Academic press: New York, 1997; Vol. *276*, pp 307−326.

(28) Sheldrick, G. M. *Acta Crystallogr., Sect. A* **2008**, *64*, 112.

(29) Spek, A. L. *J. Appl. Crystallogr.* **2003**, *36*, 7.

(30) Sheldrick, G. M., *SHELXS−A Computer Program for Determination of Crystal Structures*; University of Göttingen: Göttingen, Germany, 1997.

(31) Sheldrick, G. M., *SHELX97−A Computer Program for Determination of Crystal Structures*; University of Göttingen: Germany, 1997.

(32) Altomare, A.; Burla, M. C.; Camalli, M.; Cascarano, G. L.; Giacovazzo, C.; Guagliardi, A.; Moliterni, A. G. G.; Polidori, G.; Spagna, R. *J. Appl. Crystallogr.* **1999**, *32*, 115.

(33) Ortep-3 for Windows: Farrugia, L. J. *J. Appl. Crystallogr.* **1997**, *30*, 565.

**Table 1.** Crystal Data and Structure Refinement for Compounds **1**−**4**

| | (1) | (2) | (3) | (4) |
|---|---|---|---|---|
| formula | $C_{18}H_{18}N_6Ni_2O_4$ | $C_{156}H_{154}N_{24}Ni_{12}O_{53}$ | $C_{26}H_{38}N_6Ni_3O_{16}$ | $C_{35}H_{53}N_9Ni_4O_{20}$ |
| FW | 499.76 | 3917.55 | 846.72 | 1154.63 |
| space group | P21/c | P212121 | Pca21 | *C*2/*c* |
| *a* (Å) | 8.319(2) | 13.1697(9) | 13.663(6) | 17.9677(6) |
| *b* (Å) | 14.755(3) | 29.501(2) | 14.994(4) | 17.4069(7) |
| *c* (Å) | 7.123(2) | 44.867(3) | 18.343(6) | 35.032(1) |
| α (deg) | 90 | 90 | 90 | 90 |
| *ss* (deg) | 92.28(3) | 90 | 90 | 95.115(2) |
| γ (deg) | 90 | 90 | 90 | 90 |
| *V* (Å$^3$) | 873.6(4) | 17432(2) | 3758(2) | 10912.9(7) |
| *Z* | 2 | 4 | 4 | 8 |
| *T* (K) | 150 | 150 | 293(2) | 100 |
| λ(MoK$_\alpha$) (Å) | 0.75150 | 0.77490 | 0.71073 | 0.71070 |
| $\rho_{calcd}$ (g cm$^{-3}$) | 1.900 | 1.489 | | 1.407 |
| μ(MoK$_\alpha$), mm$^{-1}$ | 2.780 | 1.355 | 1.558 | 1.433 |
| *R* | 0.0344 | 0.0661 | 0.0746 | 0.0496 |
| ωR$^2$ | 0.0958 | 0.1537 | 0.2076 | 0.1299 |

deprotonated, but complete the octahedral coordination of some of the metal ions of the clusters (**2**−**4**). Even more, intramolecular hydrogen bonds between water molecules among each other or with the rest of ligands in the structure are responsible for the closure and stability of the final compounds (see structural section). The nature of the solvent is critical too, becoming evident if one compares compounds **3** and **4**. These two complexes were obtained using identical reagents and ratios. However, compound **3** was accomplished using a polar solvent, MeOH, with some drops of $H_2O$, whereas reactions in $CH_2Cl_2$ led always to big crystals of compound **4**.

Finally, experiments using sodium azide together with $H_2$dapdo were carried out in a further attempt to achieve advance architectures. In contrast, the presence of azido anions in solution under aerobic conditions gave systematically dark crystals of the already reported mononuclear Ni(IV) complex containing two deprotonated dapdo$^{2-}$ ligands, [Ni(dapdo)$_2$].[15]

In this sense, it is remarkable the coordination behavior of the deprotonated form dapdo$^{2-}$ bonded to Ni$^{2+}$ atoms. Ni$^{IV}$ complexes derived from oximato anions are well-known (e.g., [Ni(dapdo)$_2$] and [Ni(dmg)$_3$]$^{2-}$, where dmg$^{2-}$ stands for dimetylglioximato) and the stabilization of their high oxidation state has been related to strong spherical crystal fields, provided by the oximato groups themselves.[34] However, complexes **2**−**4** indicate that coordination of only one dapdo$^{2-}$ ligand is not enough to favor the oxidation of Ni$^{2+}$ to Ni$^{4+}$ while always stabilizing the square planar environment around the metallic centers.

**Description of the Structures. [Ni$_2$(dapdo)$_2$] (1).** A labeled plot of the neutral centrosymmetric dinuclear units present in compound **1** is shown in Figure 1. Selected bond parameters are listed in Table 2. The dinuclear units consist of two nickel atoms linked by two oximato bridges from two 2.10111 dapdo$^{2-}$ ligands. Each nickel atom (Ni$^{2+}$, d$^8$), is coordinated by three N atoms from one of the dapdo$^{2-}$ ligands and one O-oximato atom from the second dapdo$^{2-}$ ligand, providing a distorted square planar environment. Bond distances lies in the 1.972(2)−1.817(2) Å range and the bond angles around the nickel atoms deviates from 90° due to the low bit angle of the

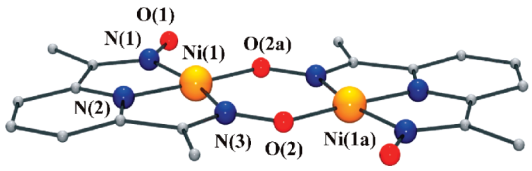


**Figure 1.** Labeled Pov-Ray plot of complex **1**. H atoms omitted for clarity.

**Table 2.** Selected Interatomic Distances (Å) and Angles (deg) for Vompound **1**

| | | | |
|---|---|---|---|
| Ni(1)−N(1) | 1.912(2) | Ni(1)−N(3) | 1.927(2) |
| Ni(1)−N(2) | 1.817(2) | Ni(1)−O(2a) | 1.832(1) |
| N(1)−O(1) | 1.282(2) | N(3)−O(2) | 1.339(2) |
| N(1)−Ni(1)−N(2) | 82.47(7) | N(3)−Ni(1)−O(2a) | 104.84(7) |
| N(1)−Ni(1)−N(3) | 164.58(7) | Ni(1)−N(1)−O(1) | 124.4(1) |
| N(1)−Ni(1)−O(2a) | 90.58(7) | Ni(1)−N(3)−O(2) | 129.6(1) |
| N(2)−Ni(1)−N(3) | 82.12(7) | Ni(1a)−O(2)−N(3) | 125.5(1) |
| N(2)−Ni(1)−O(2a) | 173.02(7) | | |

dapdo$^{2-}$ ligand, being N(1)−Ni(1)−N(2) and N(2)−Ni(1)−N(3) (82.47(7)° and 82.12(7)°, respectively), lower than the bond angles involving the oxygen atom O(2a)−Ni1−N(1) and O(2a)−Ni1−N(3) (90.58(7) and 104.84(7)°, respectively).

Both dapdo$^{2-}$ ligands are totally deprotonated and surprisingly, the noncoordinated oximato groups are neither involved in coordination nor hydrogen bonding. The molecule is practically planar with a slight distortion in the Ni(1)−N(3)−O(2)−Ni(1a) torsion angle of 1.9(2)°. A single weak intermolecular interaction is observed corresponding to a $\pi-\pi$ stacking of the pyridinic rings of neighboring molecules, with a distance between centroids of 3.721 Å.

**[Ni$_3$(OH)(BzO)$_3$(dapdo)(dapdoH$_2$)(H$_2$O)]·1.25H$_2$O (2).** The asymmetric unit of compound **2** contains four nonequivalent trinuclear units with similar core and bond parameters. A labeled plot of one of these neutral trinuclear units is shown in Figure 2. Selected bond parameters for this unit are also listed in Table 3. This trinuclear compound combines one tetracoordinated nickel atom Ni(2), in a distorted square-planar geometry, with two hexacoordinated nickel atoms, Ni(1) and Ni(3), connected together by a central $\mu_3$−OH group. Coordination sphere of Ni(2) is formed by the three N-atoms from a 3.11111 dapdo$^{2-}$ ligand and the central hydroxo ligand. Each oximato group of this deprotonated dapdo$^{2-}$ links a second Ni$^{2+}$ ion giving Ni(2)−N(5)−(O4)−Ni(1)

(34) Baucom, E. I.; Drago, R. S. *J. Am. Chem. Soc.* **1971**, *93*, 6469.

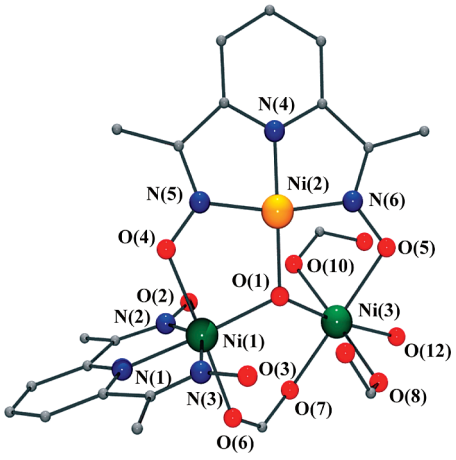


**Figure 2.** Labeled Pov-Ray plot of complex **2**. Ni atoms in octahedral or square planar environment are plotted in green and orange color in that order. Aromatic rings of the benzoate ligands and protons other than the NOH groups are omitted for clarity.

**Table 3.** Selected Interatomic Distances (Å) and Angles (deg) for Compound **2**

| | | | |
|---|---|---|---|
| Ni(1)−N(1) | 1.993(6) | Ni(1)−O(1) | 2.001(5) |
| Ni(1)−N(2) | 2.141(6) | Ni(1)−O(4) | 2.091(5) |
| Ni(1)−N(3) | 2.184(5) | Ni(1)−O(6) | 2.042(5) |
| Ni(2)−N(4) | 1.779(6) | Ni(2)−N(6) | 1.862(6) |
| Ni(2)−N(5) | 1.868(6) | Ni(2)−O(1) | 1.859(5) |
| Ni(3)−O(1) | 2.064(5) | Ni(3)−O(8) | 2.043(4) |
| Ni(3)−O(5) | 2.111(5) | Ni(3)−O(10) | 2.108(4) |
| Ni(3)−O(7) | 2.037(5) | Ni(3)−O(12) | 2.099(5) |
| N(2)−O(2) | 1.391(7) | N(3)−O(3) | 1.394(8) |
| N(5)−O(4) | 1.320(7) | N(6)−O(5) | 1.319(8) |
| Ni(1)−O(4)−N(5) | 114.0(4) | Ni(2)−N(5)−O(4) | 122.7(4) |
| Ni(3)−O(5)−N(6) | 108.7(4) | Ni(2)−N(6)−O(5) | 122.0(4) |
| Ni(1)−O(1)−Ni(2) | 113.7(2) | | |
| Ni(1)−O(1)−Ni(3) | 123.6(2) | | |
| Ni(2)−O(1)−Ni(3) | 105.4(2) | | |

and Ni(2)−N(6)−(O5)−Ni(3) bridges with torsion angles of 15.5 and 27.1°, respectively.

The core of **2** is highly asymmetrical, because of the two hexacoordinated $Ni^{2+}$ atoms organize differently: coordination sphere of Ni(1) is completed with three N-atoms from one 1.00111 dapdo$H_2$ and one O-atom from one syn−syn benzoate ligand (with a Ni(1)−O(6)···O(7)−Ni(3) torsion angle of 46.8°); meanwhile, Ni(3) coordinates two additional monocoordinated benzoate groups and completes the octahedral environment with a molecule of water. N−M−N bond angles for $dapdo^{2-}$ and dapdo$H_2$ ligands are strongly modified by deprotonation and O-coordination: N(4)−Ni(2)−N(5) and N(4)−Ni-(2)−N(6) (83.4(3) and 83.4(3)°, respectively) are considerably higher than N(1)−Ni(1)−N(2) and N(1)−Ni-(1)−N(3) (76.1(2) and 76.3(2)°, in that order). Bond angles involving the hydroxo ligand are also highly asymmetric: (Ni(1)−O(1)−Ni(2), Ni(2)−O(1)−Ni(3) Ni-(1)−O(1)−Ni(3) bond angles are 113.7(2), 105.4(2), and 123.6(2)°) giving an irregular triangle which distances: Ni(1)···Ni(2), Ni(2)···Ni(3), and Ni(1)···Ni(3) are 3.232, 3.124, and 3.583, respectively. Overall, Ni−N distances lie in a 1.779(6)−1.868(6) Å range for $dapdo^{2-}$, whereas they remain between 1.993(5) and 2.184(5) Å in the case of dapdo$H_2$. Ni−O distances lies in a shorter range comprised between 2.001 and 2.111 Å.

The orientation and distance between the centroids of the pyridinic ring of $dapdo^{2-}$ and the benzylic ring of one

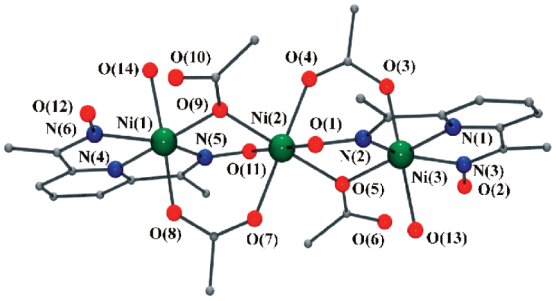


**Figure 3.** Labeled Pov-Ray plot of complex **3**.

**Table 4.** Selected Interatomic Distances (Å) and Angles (deg) for Compound **3**

| | | | |
|---|---|---|---|
| Ni(1)−N(4) | 1.996(8) | Ni(1)−O(8) | 2.053(6) |
| Ni(1)−N(5) | 2.056(8) | Ni(1)−O(9) | 2.058(6) |
| Ni(1)−N(6) | 2.201(8) | Ni(1)−O(14) | 2.127(6) |
| Ni(2)−O(1) | 2.075(6) | Ni(2)−O(7) | 2.087(6) |
| Ni(2)−O(4) | 2.084(6) | Ni(2)−O(9) | 2.182(6) |
| Ni(2)−O(5) | 2.159(6) | Ni(2)−O(11) | 2.075(6) |
| Ni(3)−N(1) | 1.998(8) | Ni(3)−O(3) | 2.017(6) |
| Ni(3)−N(2) | 2.004(8) | Ni(3)−O(5) | 2.061(6) |
| Ni(3)−N(3) | 2.197(9) | Ni(3)−O(13) | 2.152(6) |
| N(2)−O(1) | 1.335(10) | N(3)−O(2) | 1.362(13) |
| N(5)−O(11) | 1.295(11) | N(6)−O(12) | 1.316(11) |
| Ni(1)−N(5)−O(11) | 124.8(5) | Ni(2)−O(11)−N(5) | 112.3(4) |
| Ni(3)−N(2)−O(1) | 126.1(5) | Ni(2)−O(1)−N(2) | 111.5(4) |
| Ni(1)−O(9)−Ni(2) | 103.5(3) | Ni(2)−O(5)−Ni(3) | 105.1(3) |

of the terminal benzoates, >3.90 Å, may be pointed as weak $\pi-\pi$ stacking.

**$Ni_3(AcO)_4(dapdoH)_2(H_2O)_2]\cdot H_2O$ (3).** A labeled plot of the neutral trinuclear unit of **3** is depicted in Figure 3 and selected bond parameters are listed in Table 4. This linear compound contains three hexacoordinated nickel atoms, bounded to a total of two 2.10111 $dapdoH^-$ molecules, four bridging acetate anions, and two water molecules.

$DapdoH^-$ molecules act as terminal ligands, capping terminal Ni(1) and Ni(3) centers by binding them through their three nitrogen atoms, respectively. The central nickel atom is coordinated to one deprotonated O-oximato of each $dapdoH^-$. At the same time, two bridging acetate anions, in $\eta^1,\mu$-AcO and $\eta^2,\mu$-AcO modes, connect Ni(2) with each Ni(1) and Ni(3) metallic centers. Finally, there are two water molecules that complete the coordination sphere of Ni(1) and Ni(3), respectively. Four Ni−N distances close to 2 Å corresponds to the bonds with the pyridinic rings (N(4)−Ni(1) and N(1)−Ni(3)) and the deprotonated oximato group (N(5)−Ni(1) and N(2)−Ni(3)) whereas two larger bond distances close to 2.2 Å involve the links with the protonated oxime groups (N(6)−Ni(1) and N(3)−Ni(3)). Ni−O distances range between 2.017 and 2.182 Å. N−Ni−N bond angles ranged between 74.7 and 80.8° because of the low bite of the $dapdoH^-$ ligands. At last, N−O−Ni angles are 112.1(4)° for N(5)−O(11)−Ni(2) and 111.77(4)° for N(2)−O(1)−Ni(2). The molecule deviates from planarity, with the Ni(1)−N(5)−O(11)−Ni(2) and Ni(3)−N(2)−O(1)-Ni(2) torsion angles being slightly greater than 20°.

**$[Ni_4(AcO)_3(dapdo)(dapdoH)_2(H_2O)_3](AcO)\cdot 3H_2O$ (4).** Figure 4 shows the labeled plot of the cationic tetranuclear structure of this compound. Selected bond parameters are listed in Table 5. The core of **4** consists of one

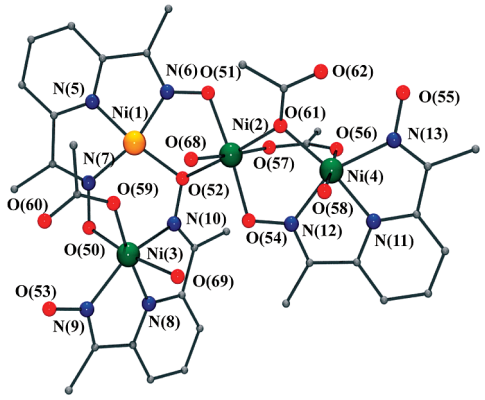


**Figure 4.** Labeled Pov-Ray plot of complex **4**. Ni atoms in octahedral and square planar environments are plotted in green and orange colors, respectively.

**Table 5.** Selected Interatomic Distances (Å) and Angles (deg) for Compound **4**

| | | | |
|---|---|---|---|
| Ni(1)−N(5) | 1.819(3) | Ni(1)−N(7) | 1.931(3) |
| Ni(1)−N(6) | 1.885(3) | Ni(1)−O(52) | 1.869(3) |
| Ni(2)−O(51) | 2.023(3) | Ni(2)−O(57) | 2.052(3) |
| Ni(2)−O(52) | 2.115(3) | Ni(2)−O(61) | 2.088(3) |
| Ni(2)−O(54) | 2.012(3) | Ni(2)−O(68) | 2.052(3) |
| Ni(3)−N(8) | 1.984(3) | Ni(3)−O(50) | 2.069(3) |
| Ni(3)−N(9) | 2.085(3) | Ni(3)−O(59) | 2.018(3) |
| Ni(3)−N(10) | 2.048(3) | Ni(3)−O(69) | 2.144(3) |
| Ni(4)−N(11) | 1.985(4) | Ni(4)−O(56) | 2.044(3) |
| Ni(4)−N(12) | 2.038(3) | Ni(4)−O(58) | 2.110(3) |
| Ni(4)−N(13) | 2.117(4) | Ni(4)−O(61) | 2.045(3) |
| N(6)−O(51) | 1.314(4) | N(7)−O(50) | 1.348(4) |
| N(9)−O(53) | 1.367(4) | N(10)−O(52) | 1.387(4) |
| N(12)−O(54) | 1.333(4) | N(13)−O(55) | 1.394(6) |
| Ni(1)−N(6)−O(51) | 124.3(2) | Ni(2)−O(51)−N(6) | 114.2(2) |
| Ni(1)−N(7)−O(50) | 127.9(2) | Ni(3)−O(50)−N(7) | 110.2(2) |
| Ni(3)−N(10)−O(52) | 124.9(2) | Ni(1)−O(52)−N(10) | 113.2(2) |
| | | Ni(2)−O(52)−N(10) | 115.9(2) |
| Ni(2)−O(54)−N(12) | 110.6(2) | Ni(4)−N(12)−O(54) | 124.3(2) |
| Ni(1)−O(52)−Ni(2) | 110.3(1) | Ni(2)−O(61)−Ni(4) | 104.2(1) |

tetracoordinated nickel atom, Ni(1), and three hexacoordinated nickel centers, Ni(2)−Ni(4). Ni(1) environment consist of three N-atoms from one 3.11111 dapdo$^{2-}$ ligand and one O-oximate bridging atom from one exhibiting a distorted square-planar geometry. The deprotonated oximato groups connect Ni(1) with Ni(2) and Ni(3) in a similar fashion of Ni(2) in complex **3**. Ni(3) is bounded to the three N-atoms of one dapdoH$^-$ ligand that displays the novel 3.20111 coordination mode (unprecedented until now), one bridging O-oximato atom, one monocoordinated acetate group, and one water molecule, giving octahedral environment. This dapdoH$^-$ ligand assist as a link among Ni(1), Ni(2) and Ni(3). A second dapdoH$^-$ ligand exhibiting a 2.10111 coordination mode, is found to be coordinated to Ni(4) by their three N-atoms. Again, the deprotonated O-oximato attaches Ni(2) and Ni(4) and the octahedral environment of both metals is completed by the coordination of two AcO$^-$ ligands in a $\eta^1$,$\mu$-AcO and $\eta^2$,$\mu$-AcO way and two molecules of water, correspondingly.

Ni−N and Ni−O distances lie in the 1.819−2.144 Å range, where the shortest correspond to the square planar Ni(1). As it was found in previous compounds, N−Ni−N angles are clearly lower than 90° lying between 75.3−82.4°, corresponding to the largest observed with deprotonated dapdo$^{2-}$ ligand.

It is remarkable that the fragment Ni(2)/Ni(4) in which the two metallic ions are linked by one syn−syn and one monocoordinated carboxylates (together with one oximato bridge from the dapdoH$^-$ ligand coordinated to Ni(4)) is identical to the Ni(2)/Ni(1) or Ni(2)/Ni(3) fragments in compound **3**, with bonds parameters very similar too, more details in Tables 4 and 5.

**H-Bond Role.** Structurally, two aspects make complexes **2** − **4** unanticipated: locally, the variety of ligands attached to each octahedral Ni$^{2+}$ ion and, in a more global sense, the noteworthy, high asymmetry of the final structures. All three compounds present as common traits protonated oxime groups from dapdoH$_2$ and/or dapdoH$^-$ ligands, coordinated H$_2$O molecules and noncoordinated O-atoms from monodentate carboxylato groups. Detailed analysis of these fragments reveals their noninnocent role, where the arrangement of such units is led by sets of strong, intramolecular H-bonds that contribute to stabilize the structures. Thus, the necessity of water in the reaction media to obtain the reported complexes can be now understood. Besides, additional crystallization water molecules provide a number of intermolecular H-bonds among the clusters generating extended networks in the crystals. Intramolecular H-bonds for compounds **2**−**4** are summarized in Table S1 in the Supporting Information (including one relevant crystallization water molecule for **3** and the carboxylate anion in **4**). A view of these H bonds within the core of these compounds is shown in Figure 5.

In compound **2** (Figure 5, top), H atoms from the protonated dapdoH$_2$ ligand, the central OH$^-$ group and the coordinated molecule of water form a set of H-bonds with O-atoms from the monocoordinated benzoate ligands. This way, benzoate O(9) atom interacts with protonated O(1)-hydroxo and O(3)-oxime atoms, O(10)-benzoate interacts with O(2)-oxime atom, and finally O(12) from the coordinated water molecule interact with O(11)-benzoate atom.

Similarly, in compound **3** (Figure 5, middle), H-atoms from the protonated oximato groups form strong intramolecular H-bonds with the noncoordinated O-atoms of the $\eta^1$,$\mu$-AcO ligands (O(2)···O(6) and O(10)···O(12) interactions). In addition, crystallization water molecules are placed between the O-carboxylato atoms coordinated to Ni(2) and coordinated water molecules providing further H-bonds, O(13)···O1w···O(7) and O(14)···O2w···O(4).

In the case of compound **4**, H-atoms from the protonated oximato groups and coordinated water molecules form a set of intramolecular H-bonds that involve the O-atoms from coordinated and anionic carboxylates. Here, the protonated oximato groups form H-bonds with the noncoordinated O-atoms of the $\eta^1$,$\mu$-AcO ligands (O(55)···O(62) and O(53)···O(60), respectively). Also, one of the coordinated water molecules interacts in a similar way with the O-atom from the carboxylato coordinated to Ni(3), O(59)···O(68). The three coordinated water molecules form strong H-bonds with the anionic acetate molecule, O(63)···O(58), O(63)···O(68), and O(64)···O(69), folding the molecule. One of the crystallization water molecules joins one deprotonated oximato groups and one monodentate carboxylato

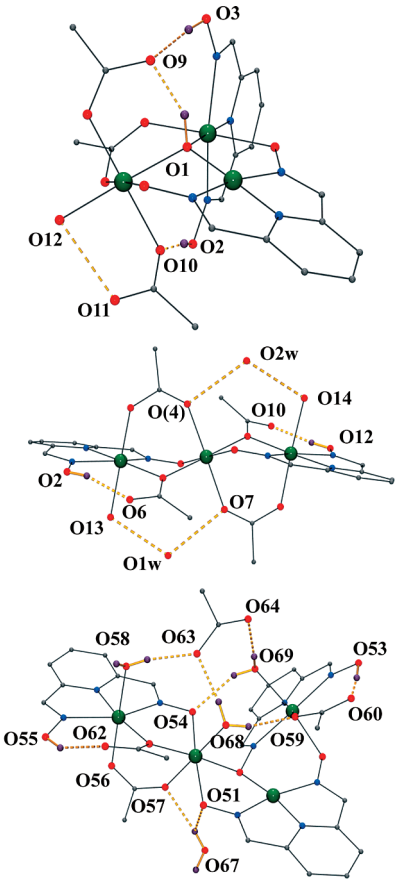


**Figure 5.** From top to bottom, partially labeled plots of the intramolecular H-bonds for compounds **2**−**4**, in that order. H-atoms not involved in H-bonds, Me groups, aromatic benzoate rings, and parentheses of the labels has been omitted for clarity.

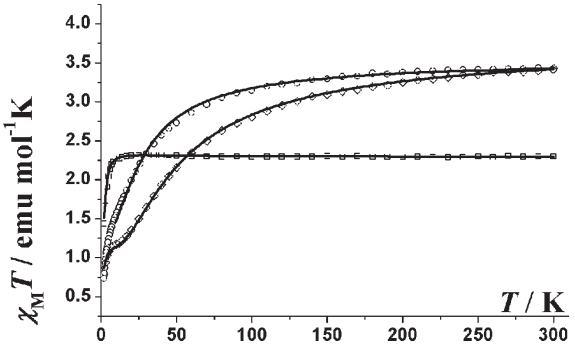


**Figure 6.** Plot of the $\chi_M T$ product vs $T$ for compounds **2** (squares), **3** (diamonds), and **4** (dot centered circles).

ligand as well, giving as a result weaker interactions, O(67)···O(51) and O(67)···O(57).

**Magnetic Measurements and Fit Procedure.** Diamagnetic response at room temperature was found for compound **1**, in agreement with the expected results for a cluster containing $Ni^{2+}$ centers with square planar environments. $\chi_M T$ product vs $T$ for compounds **2**−**4** are plotted in Figure 6. Compound **2** shows a $\chi_M T$ value nearly constant between 300 and 14 K with a maximum value of 2.32 $cm^3$ K $mol^{-1}$ at 30 K. At low temperature, $\chi_M T$ value decreases down to 1.43 $cm^3$ K $mol^{-1}$. These room-temperature values are also consistent with the structural data that indicate that one of the nickel atoms, in square planar environment, is diamagnetic. Compound **2** behaves magnetically as a dinuclear system and therefore the fitting of the experimental data was performed by means of the conventional equation derived from the Hamiltonian

$$H = -J(S_1S_3)$$

for two local $S = 1$ spin centers including an intermolecular interaction parameter $zJ'$. The subindexes of the local $S_n$ spins along this section refer to the numbers of the corresponding structures. Best fit parameters were $J = +2.16(7)$ $cm^{-1}$, $zJ' = -0.87(1)$ K, and $g = 2.141(2)$. In good agreement with the above results, magnetization experiments show a magnetization plot that reaches a nonsaturated value 3.3 electrons under an external field of 5 T with an increase versus field lower than the expected for the Brillouin plot for two isolated $S = 1$ centers.

Compound **3** exhibits a room temperature value of 3.43 $cm^3$ K $mol^{-1}$ which decreases down to 0.82 at 2 K. The $\chi_M T$ plot shows a plateau around 1.15 $cm^3$ K $mol^{-1}$ and between 5 and 13 K. Analysis of the magnetic data of compound **3** was performed by means of analytical expression derived from the Hamiltonian

$$H = -J(S_1S_2 + S_2S_3)$$

which corresponds to a symmetric linear arrangement of three paramagnetic centers where the interaction between the terminal spin carriers have been neglected. Best fit parameters were $J = -18.8(2)$ $cm^{-1}$, $zJ' = -0.90(3)$ $cm^{-1}$, and $g = 2.233(3)$. Magnetization plot shows a Brillouin shape behavior supporting the idea of having two electrons as can be expected for a well isolated $S = 1$ ground state.

Tetranuclear compound **4** contains one square planar nickel atom and therefore can be analyzed as a trinuclear system. Room temperature $\chi_M T$ value is 3.41 $cm^3$ K $mol^{-1}$, which decreases gradually upon cooling, reaching 0.73 $cm^3$ K $mol^{-1}$ at 2 K. As it occurred in the previous compound, a change in the slope of $\chi_M T$ plot at values slightly greater than the expected for an $S = 1$ ground state was observed.

In this case, structural data reveals different kind of bridges between the paramagnetic centers of compound **4** and then the experimental $\chi_M T$ plot was analyzed by means CLUMAG program[35] on the two-$J$ Hamiltonian

$$H = -J_1(S_2S_4) - J_2(S_2S_3)$$

Best-fit parameters were $J_1 = -16.7$ $cm^{-1}$, $J_2 = 1.16$ $cm^{-1}$, and $g = 2.17$. As described above, the Ni(2)/Ni(4) fragment of compound **4** is structurally similar to the one found in **3.** Therefore, $J_1$ could be related to the exchange parameter of 18.8 $cm^{-1}$ found for **3** and be assigned to the Ni(2)−Ni(4) interaction, whereas the weak interaction $J_2$ could be related to the single, high torsioned, oximato bridge between Ni(2) and Ni(3). Likewise for compound **3**, here magnetization at 5 T tends to a nonsaturated value associated to two electrons.

(35) Gatteschi, D.; Pardi, L. *Gazz. Chim. Ital.* **1993**, *123*, 231.

## Conclusions

In the present work, we have reported the results obtained using ligand dapdo$H_2$ together with different nickel salts as precursors. Earlier work with pyridyl monooximato ligands, suggested the possibility of having the neutral ligand, dapdo$H_2$, or its deprotonated anionic forms, dapdo$H^-$ and dapdo$^{2-}$, coordinated to Ni centers. The latest, dapdo$^{2-}$, contains two deprotonated oximato groups conferring the ligand with the capability of increasing the nuclearity and therefore complexity of the final compounds (fact previously observed with manganese). Compounds **1**−**4** are the first examples that corroborate that this is also possible with Ni. From all the above, one of the most relevant results in this preliminary work is the finding of a novel coordination mode for dapdo$H^-$, 3.20111, which coordinates three $Ni^{2+}$ units, arrangement that was unknown in the chemistry of this dioxime ligand. In addition, another important aspect is the tendency of dapdo$^{2-}$ to force square planar coordination around $Ni^{2+}$ ions, a trait that appears in three of the four compounds described in this paper: **1**, **2**, and **4**. We would also like to stress the capacity of dapdo$H_2$/dapdo$H^-$/dapdo$^{2-}$ to coordinate with Ni, providing high nuclearity clusters and new topologies as well as the possibility of achieving octahedral and square planar coordinations around the metallic ions with the use of this ligand. This concept directly affects the magnetic results because square planar coordination around the Ni decreases the total magnetic spin diminishing the superexchange pathways inside the clusters. From a magnetic point of view, this is indeed a limitation in the search of Ni clusters with high spin numbers. Therefore, synthetic strategies should avoid fully deprotonation of the ligand to prevent under aerobic conditions, easy oxidation to $Ni^{IV}$ or square planar coordination.

**Acknowledgment.** This work was supported by the CICYT Projects CTQ2009-07264. We acknowledge provision of time at the Advanced Light Source, which is supported by the Director, Office of Science, Office of Basic Energy Sciences of the U.S. Department of Energy under Contract DE-AC02-05CH11231.

**Supporting Information Available:** H-bond parameters (PDF); crystallographic data files for complexes **1**−**4** (CIF). This material is available free of charge via the Internet at http://pubs.acs.org.

### 3.1.1. Resum: First Structural and Magnetic Studies of Ni Clusters Containing 2,6-Diacetylpyridine-dioxime as a Ligand.

Albert Escuer, Jordi Esteban, Núria Aliaga-Alcaide, Mercè Font-Bardia, Teresa Calvet, Olivier Roubeau, Simon J. Teat.

*Inorganic Chemistry* **2010**, *49*, 2259-2266.

En aquest article es presenten el primers compostos polinuclears reportats a la bibliografia amb el lligand dapdo$H_2$ i el catió $Ni^{II}$, sintetitzats a partir de carboxilats i β-dicetonats de níquel(II).

Els compostos obtinguts van ser: $[Ni_2(dapdo)_2]$ (**1_1**), $[Ni_3(dapdoH_2)(H_2O)(OH)(BzO)_3(dapdo)]$ (**1_2**), $[Ni_3(H_2O)_2(AcO)_4(dapdoH)_2]$ (**1_3**) i $[Ni_4(H_2O)_3(AcO)_3(dapdo)(dapdoH)_2](AcO)$ (**1_4**), figura 8. El compost **1_1** presenta tots dos ions $Ni^{II}$ amb una geometria plano-quadrada lleugerament distorsionada, els compostos **1_2** i **1_4** contenen un únic catió $Ni^{II}$ amb aquesta geometria mentre que el compost **1_3** està format exclusivament per cations amb entorns octaèdrics.

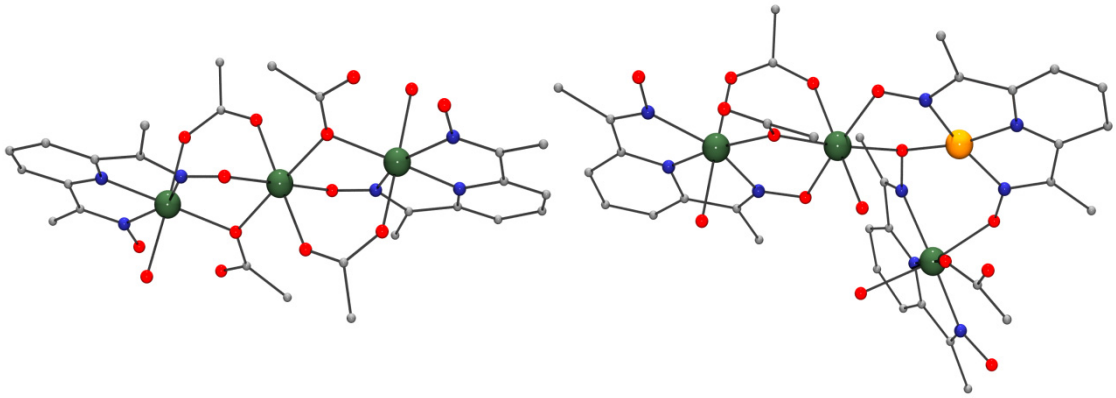

**Figura 8.** Estructura dels compostos **1_3** i **1_4**. Els cations $Ni^{II}$ amb entorn octaèdric es representen en verd, mentre que els cations amb geometria plano-quadrada es mostren en taronja.

Els resultats de les mesures magnètiques realitzades venen determinats per la presència de cations amb entorns plano-quadrats: s'ha trobat un comportament diamagnètic a temperatura ambient per **1_1**, fet que confirma el que es podia esperar per un compost format per dos cations $Ni^{II}$ ($d^8$) amb geometria plano-quadrada, **1_2** es comporta magnèticament com un compost dinuclear i, per

últim, **1_3** i **1_4** es poden descriure com compostos trinuclears. Les mesures de susceptibilitat magnètica han estat ajustades donant unes constants d'acoblament (*J*) amb valors de -18,8 i -16,7 $cm^{-1}$ pels ponts oxima/acetat amb angles i torsions semblants.

Finalment, cal remarcar que en aquest article no només es van obtenir els primers compostos polinuclears de $Ni^{II}$ amb el lligand dapdo$H_2$, sinó que també es va caracteritzar per primera vegada el mode de coordinació 3.20111 (d'acord amb la notació de Harris) per aquest lligand i es va observar la tendència del lligand dapdo$H_2$ a generar entorns plano-quadrats en cations $Ni^{II}$ quan es coordina en el mode de coordinació 3.11111, tal i com mostren els compostos **1_2** i **1_4**.

## 3.2. Article 2.

## $Ni_5$, $Ni_8$, and $Ni_{10}$ clusters with 2,6-diacetylpyridine-dioxime as a ligand.

Albert Escuer, **Jordi Esteban**, Olivier Roubeau.

*Inorganic Chemistry **2011**, 50, 8893-8901*

Inorganic Chemistry

ARTICLE

pubs.acs.org/IC

# $Ni_5$, $Ni_8$, and $Ni_{10}$ Clusters with 2,6-Diacetylpyridine-dioxime as a Ligand

Albert Escuer,*[,†] Jordi Esteban,[†] and Olivier Roubeau[‡]

[†]Departament de Química Inorgànica and Institut de Nanociència i Nanotecnologia de la Universitat de Barcelona (IN2UB), Martí i Franqués 1-11, 08028 Barcelona, Spain

[‡]Instituto de Ciencia de Materiales de Aragón (ICMA), CSIC and Universidad de Zaragoza, Departamento de Física de la Materia Condensada, Pedro Cerbuna 12, 50009 Zaragoza, Spain

Supporting Information

**ABSTRACT:** In the present work, novel coordination possibilities for the system $dapdoH_2/Ni^{II}$ ($dapdoH_2$ = 2,6-diacetylpyridine-dioxime) have been explored. Depending on the starting reagents and solution conditions, several clusters with nuclearities ranging from $Ni_5$ to $Ni_{10}$ were achieved and structurally characterized, namely, $[Ni_5(R\text{-}COO)_2(dapdo)_2(dapdoH)_2(N(CN)_2)_2(MeOH)_2]$ in which $R\text{-}COO^-$ = benzoate (**1**) or 3-chlorobenzoate (**2**), $[Ni_8(dapdo)_4(NO_3)_4(OH)_4(MeOH)_4]$ (**3**), and $[Ni_{10}(dapdo)_8(N(CN)_2)_2(MeO)(MeOH)](NO_3)$ (**4**). For the first time, pentadentate coordination for the $dapdo^{2-}$ ligand has been established. All compounds show a combination of square-planar and octahedrally coordinated nickel atoms. According to the $Ni_2(sp)Ni_3(Oh)$ (**1** and **2**), $Ni_4(sp)Ni_4(Oh)$ (**3**), and $Ni_4(sp)Ni_6(Oh)$ (**4**) environments, these systems magnetically behave as trimer, tetramer, and hexanuclear clusters, respectively. dc magnetic measurements in the 2−300 K range of temperature reveal antiferromagnetic coupling for all compounds, and the correlation of the superexchange interaction with the torsion angles involving the oximato bridges is experimentally confirmed.

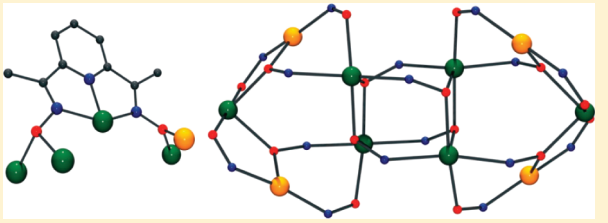

## INTRODUCTION

At present, research based on the use of oximes in coordination chemistry is a growing field. 2-Pyridyl oximes, {py}C(R)-NOH, are well-known ligands in this area due to their ability to generate stable first-row transition coordination compounds with a large range of nuclearities.[1] These molecules are very versatile and able to act as bidentate ligands in their protonated state or to link up to three metallic centers in their deprotonated anionic form. In addition, the donor properties of the {py}C-(R)NOH ligands can be tuned according to the nature of the R group (H, Me, Ph, py, $-NH_2$, etc.). Self-assembly of nickel-{py}C(R)$NO^-$ fragments have yielded a large number of medium-high nuclearity clusters, as for example, $Ni_7$,[2] $Ni_8$,[3] $Ni_9$,[4] $Ni_{10}$,[5] $Ni_{12}$, or $Ni_{14}$,[3,6] exhibiting, in some cases, slow relaxation of magnetization.[7]

One of the synthetic challenges in the search of high nuclearity systems is the design of ligands able to stabilize large nuclearities and/or generate new topologies in order to improve the desired properties. Regarding this matter, pyridyldioximato ligands ($LH_2$, with R = various) (Scheme 1) are attractive ligands for the achievement of polynuclear clusters because the three nitrogen atoms give an excellent chelate that easily coordinates one metallic center, whereas the two *ortho*-oximato groups are able to coordinate at both sides of the central cation up to four additional cations as a function of the degree of deprotonation of the ligand.

Within this family of linkers, 2,6-diacetylpyridine-dioxime ($dapdoH_2$) is the most studied among the few related ligands that have been reported to date,[1] such as 2,6-pyridinedioxime ($pdoH_2$) or pyridine-2,6-diamidoxime ($pdamoH_2$) (Scheme 1).

The most common coordination mode of these $LH_2$, $LH^-$, or $L^{2-}$ ligands is the 1.00111 mode (Harris notation, referred to as $X.Y_1Y_2Y_3...Y_n$, where $X$ is the overall number of metals bound by the whole ligand and each value of $Y$ refers to the number of metal ions attached to the different donor atoms. The ordering of $Y$ is listed by the Cahn−Ingold−Prelog priority rules, hence here O before N),[8] in which the tridentate coordination of the three nitrogen atoms yields octahedral mononuclear $[M^{II}(LH_2)_2]^{2-}$,[9] $[M^{II}(LH)_2]$,[10] or $[M^{IV}(L)_2]$[11] complexes or plays the role of terminal ligand in a number of mononuclear[12] or polynuclear[9c,13] derivatives bridged by other ligands, such as halides, pseudohalides, or carboxylates.

Larger nuclearities have been characterized, mainly in the very recent years, allowing the characterization of an increasing number of coordination modes. After the early characterization of the $LH^-$ 2.10111 mode in the double oximato bridged $Cu^{II}$ complex[14] with the formula $[Cu_2(dapdoH)_2](BF_4)_2$, several coordination modes have been reported for the deprotonated $dapdo^{2-}$ ligand ($L^{2-}$ 3.11111/4.21111) or 3.20111 for $LH^-$ in

**Received:** April 28, 2011
**Published:** August 19, 2011

**Scheme 1. Reported $LH_2$ Pyridyldioxime Ligands**

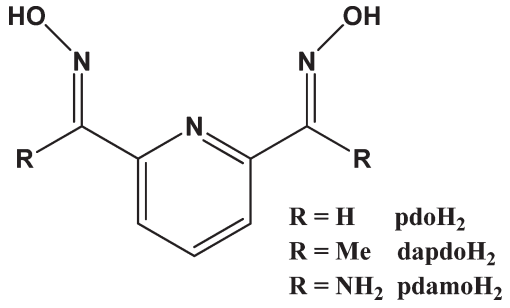


**Scheme 2. Coordination Modes for $dapdoH^-$ or $dapdo^{2-}$ Ligands Found in Compounds 1−4[a]**

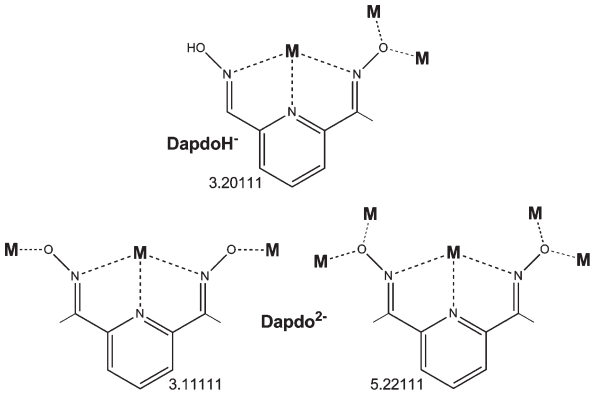


[a] The novel coordination mode 5.22111 has been observed for the first time in this work.

one mixed valence $Fe_3$ complex,[9d] several $Mn^{II}_2Mn^{III}_4$ and one $Mn^{II}_2Mn^{III}_6$ cluster,[15] or two heterometallic $Cu^{II}/Cr^{III}$ and $Mn^{IV}/Gd^{III}$ systems.[16] Our recent contribution to the knowledge of the properties of this kind of ligands comprised $Cu^{II}$−pdamoH$_2$ derivatives,[17] the first $Ni^{II}$−dapdoH$_2$ derivatives,[18] and one novel $Mn^{II}_6Mn^{III}_2$ dapdoH$_2$ complex[15c] in which the modes 2.10111/3.11111/3.20111 and 2.10111/3.11111/3.20111/4.21111 were found for $LH^-$ and $L^{2-}$, respectively.

These previously reported complexes show how the increase of nuclearity is closely related to the deprotonation of both oximato arms, reaching the larger nuclearity reported until now ($Mn_8$) for the $L^{2-}$ 4.21111 coordination mode.[15]

Following our work on pyridyldioximate ligands, we now report a series of $Ni_5$ (**1** and **2**), $Ni_8$ (**3**), and $Ni_{10}$ (**4**) new clusters containing $dapdoH^-$ and $dapdo^{2-}$ ligands. All of them exhibit nickel centers in both octahedral or square-planar coordination environments in the same compound. For the first time, the coordination mode 5.22111 has been characterized for this kind of ligand, and larger nuclearity ($M_{10}$) is achieved (Scheme 2). Syntheses, structures, and magnetic behavior of **1**−**4** are described in the following sections.

## EXPERIMENTAL SECTION

**Syntheses.** 2,6-Diacetylpyridine, $NaN(CN)_2$, and $Ni(NO_3)_2\cdot 6H_2O$ were purchased from Sigma-Aldrich Inc. and used without further purification. $Ni(BzO)_2\cdot 3H_2O$ and $Ni(3\text{-Cl-BzO})_2\cdot 3H_2O$ were synthesized by dissolving equimolar quantities (40 mmol) of benzoic acid (or 3-Cl-benzoic acid) and NaOH in 40 mL of $H_2O$, filtering, and mixing the final solution with a commercial source of $Ni(NO_3)_2\cdot 6H_2O$ (20 mmol) in 20 mL of water. The resulting nickel salt was obtained in good yield (>80%). DapdoH$_2$ was prepared following the C. W. Glynn and M. M. Turnbull method.[9a]

*$[Ni_5(RCOO)_2(dapdo)_2(dapdoH)_2(N(CN)_2)_2(MeOH)_2]$ $RCOO^-$ = benzoate (**1**) or 3-Cl-benzoate (**2**).* dapdoH$_2$ (0.193 g, 1 mmol), $Ni(BzO)_2\cdot 3H_2O$ (0.709 g, 2 mmol) or $Ni(3\text{-Cl-BzO})_2\cdot 3H_2O$ (0.847 g, 2 mmol), and $Na(N(CN)_2)_2$ (0.178 g, 2 mmol) were dissolved in 20 mL of MeOH, and $NEt_3$ (0.202 g, 2 mmol) was added. The mixture was stirred for 2 h and then filtered. Crystals were obtained by layering the final solution with 10 mL of diethylether. Anal. Calcd for $C_{56}H_{54}N_{18}Ni_5O_{14}$ (**1**): C, 44.88; H, 3.77; N, 16.82%. Found: C, 44.10; H, 3.67; N, 16.65%. Anal. Calcd for $C_{56}Cl_2H_{52}N_{18}Ni_5O_{14}$ (**2**): C, 42.91; H, 3.47; N, 16.09%. Found: C, 42.31; H, 3.39; N, 15.85%. Relevant IR bands ($cm^{-1}$): 3432 (b), 2257 (s), 2216 (m), 2156 (s), 1594 (m), 1534 (m), 1512 (m), 1490 (m), 1377 (m), 1203 (s), 1153 (m), 1122 (m), 1087 (m), 1065 (m), 807 (w), 724 (w) for **1** and 3413 (b), 2258 (s), 2215 (m), 2156 (s), 1592 (m), 1558 (m), 1484 (m), 1407 (m), 1372 (s), 1263 (m), 1154 (m), 1086 (m), 1060 (m), 813 (w), 765 (w) for **2**.

*$[Ni_8(dapdo)_4(NO_3)_4(OH)_4(MeOH)_4]\cdot 7MeOH$ (**3**$\cdot 7MeOH$).* Solid dapdoH$_2$ (0.193 g, 1 mmol) was dissolved in 20 mL of MeOH together with $Ni(NO_3)_2\cdot 6H_2O$ (0.581 g, 2 mmol) and $NEt_3$ (0.202 g, 2 mmol). The solution was stirred at room temperature for a couple of hours, filtered, and crystallized by layering with 10 mL of diethylether. Anal. Calcd for $C_{40}H_{56}N_{16}Ni_8O_{28}$ (**3**): C, 28.62; H, 3.36; N, 13.35%. Found: C, 27.89; H, 3.55; N, 13.00%. Relevant IR bands ($cm^{-1}$): 3346 (b), 1630 (w), 1591 (m), 1519 (m), 1493 (m), 1407 (s), 1384 (s), 1220 (s), 1192 (m), 1167 (w), 1131 (w), 1089 (w), 809 (m), 701 (w).

*$[Ni_{10}(dapdo)_8(N(CN)_2)_2(MeO)(MeOH)](NO_3)\cdot 3MeOH$ (**4**$\cdot 3MeOH$).* dapdoH$_2$ (0.193 g, 1 mmol), $Ni(NO_3)_2\cdot 6H_2O$ (0.581 g, 2 mmol), and $NaN(CN)_2$ (0.178 g, 2 mmol) were dissolved in 20 mL of MeOH together with $NEt_3$ (0.202 g, 2 mmol). The solution was stirred for 2 h and then filtered. Crystals were obtained by layering the final solution with 10 mL of diethylether. Anal. Calcd for $C_{81}H_{91}N_{31}Ni_{10}O_{24}$ (**4**$\cdot$3MeOH): C, 39.39; H, 3.71; N, 17.58%. Found: C, 38.58; H, 3.52; N, 17.94%. Relevant IR bands ($cm^{-1}$): 3442 (b), 2267 (w), 2227 (w), 2159 (m), 1637 (m), 1592 (m), 1534 (w), 1384 (s), 1231 (w), 1205 (m), 1155 (m), 1125 (m), 1087 (m), 1086 (m), 1046 (m), 790 (w).

**Physical Measurements.** Magnetic susceptibility measurements were carried out on polycrystalline samples with a DSM5 Quantum Design susceptometer working in the range of 30−300 K under magnetic fields of 0.3 T and under a field of 0.03 T in the 30−2 K range to avoid saturation effects. Diamagnetic corrections were estimated from Pascal tables. Infrared spectra (4000−400 $cm^{-1}$) were recorded from KBr pellets on a Bruker IFS-125 FT-IR spectrophotometer.

**X-ray Crystallography.** Data for compounds **1** and **2** were collected on red blocks at 150 K and $\lambda$ = 0.7383 Å both using a single-axis HUBER diffractometer on station BM16 of the European Synchrotron Radiation Facility, Grenoble, France. Cell refinement, data reduction, and absorption corrections were done with the HKL-2000 suite.[19] The structures were solved with SIR92,[20] and the refinement and all further calculations were carried out using SHELXL-97.[21] Data for compounds **3** and **4** were collected at 100 K on, respectively, a red plate and an orange plate both on a Bruker X8 Kappa APEX II diffractometer at the Unidade de Raios X, RIAIDT, University of Santiago de Compostela, Spain. The structures were solved by direct methods and refined on $F^2$ using the SHELX-TL suite.[21]

All non-hydrogens were refined anisotropically, whereas hydrogens were placed geometrically on their carrier atom and refined with a riding model where possible.

In the case of **1**, one strong electron density peak remained close to one phenyl ring and could not be included in the structural model and

**Table 1. Crystal Data and Structure Refinement for Compounds 2−4**

| | (2) | (3) | (4) |
|---|---|---|---|
| formula | $C_{56}Cl_2H_{54}N_{18}Ni_5O_{14}$ | $C_{40}H_{48}N_{16}Ni_8O_{28}\cdot 7MeOH$ | $C_{78}H_{79}N_{31}Ni_{10}O_{21}\cdot 3MeOH$ |
| fw | 1567.62 | 1902.95 | 2469.95 |
| space group | $P21/n$ | $P\bar{1}$ | $C2/c$ |
| $a$/Å | 16.980(4) | 11.261(2) | 15.335(3) |
| $b$/Å | 11.613(3) | 12.292(3) | 33.125(7) |
| $c$/Å | 17.846(4) | 13.577(3) | 21.821(4) |
| α/deg | 90 | 86.48(1) | 90 |
| $\beta$/deg | 118.23(3) | 67.61(1) | 108.18(3) |
| $\gamma$/deg | 90 | 84.67(1) | 90 |
| $V$/Å$^3$ | 3101(2) | 1729.4(6) | 10531(4) |
| $Z$ | 2 | 1 | 4 |
| $T$, K | 150(2) | 100(2) | 100(2) |
| $\lambda$ (Mo Kα), Å | 0.73830 | 0.71073 | 0.71073 |
| $\rho_{calc}$, g·cm$^{-3}$ | 1.679 | 1.666 | 1.558 |
| $\mu$ (Mo Kα), mm$^{-1}$ | 1.832 | 2.433 | 1.826 |
| $R$ [$I > 2s(I)$] | 0.0389 | 0.0584 | 0.0562 |
| w$R$ [all data] | 0.1113 | 0.1600 | 0.1576 |
| $S$ [all data] | 1.091 | 1.050 | 1.054 |

both $R_1$ and w$R^2$ factors remained very high at the end of the refinement, while unreasonably high EXTI and WEIGHT parameters were necessary to reach convergence. We believe the problem lies in either or both of the following: (i) strong reflections were not well treated and (ii) absorption corrections were inadequate, possibly also due to problems with strong reflections. Because compound **1** is isosutructural with compound **2**, only the structure of the latter is reported here in detail.

For compound **2**, the terminal N(6) nitrogen atom of the dicyanamide ion was highly disordered. Splitting of the atom over two positions was considered, but it did not improve the model, both half N atoms remaining highly disordered. N6 was thus refined with one sole site and displacement parameter restraints. All hydrogens were found in difference Fourier maps, and those on the oxime oxygen O(2) and methanol oxygen O(7) were refined freely with their thermal parameters 1.5 times that of their carrier O.

For compound **3**, hydrogens on the hydroxide oxygens O(3) and O(4) and on the coordinated methanol oxygens O(5) and O(8) were found in successive difference Fourier maps and refined with their thermal parameters 1.2 times that of their carrier oxygen and a soft distance restraint. Together with the four dapdo$^{2-}$ and four-coordinated nitrate, this clearly points at a neutral main complex. The solvent area was particularly disordered. After locating one methanol molecule (O1S), the remaining electron density peaks (max. ca. five electrons) occupying a rather small void of ca. 300 Å$^3$ could not be modeled satisfactorily (see CIF for details). The disordered area was thus analyzed and taken into account with PLATON/SQUEEZE that recovered a total of ca. 99 electrons per cell all in one void of ca. 275 Å$^3$. The combination of occupied volume and electrons would account reasonably with five additional lattice methanol molecules per cell, which have been included in the formula and related structural parameters.

In the case of **4**, the terminal CN group of the dicyanamide ion was highly disordered. It was considered splitting the two atoms, but the partial atoms were still highly disordered. Therefore, C(20) and N(9) were refined with displacement parameter restraints, and their remaining high max/min ratios likely correspond to their real disorder. One of the lattice methanol molecules was only half-occupied. The coordinated methanol molecule is, in fact, half methanol and half methanoate for charge compensation. The corresponding half-occupied hydroxyl hydrogen H(9) forming a hydrogen bond with the nitrate ion was found in a difference Fourier map and refined with its thermal parameter 1.5 times that of O(9) and a distance restraint. Hydrogens on the lattice methanol molecules were omitted. At the end of the refinement, there remained areas in the structure with only weak electron density peaks that could not be modeled satisfactorily as solvent molecules. This was, therefore, analyzed and taken into account by PLATON/SQUEEZE[22] that recovered, per cell, four groups of ca. 20/70 electrons in voids of 103/267 Å$^3$, respectively. These figures altogether would agree with the presence of 4 methanol and 4 diethylether diffuse molecules in addition to the 12 MeOH per cell already in the structural model.

Crystallographic and experimental details for **2**−**4** are summarized in Table 1, whereas experimental details of **1** are provided in Table S1 and Figure S1 (Supporting Information). All data can be found in the supplementary crystallographic data for this paper in CIF format with CCDC numbers 817654-817657. These data can be obtained free of charge from The Cambridge Crystallographic Data Centre via www.ccdc.cam.ac.uk/data_request/cif.

Plots for publication were generated with ORTEP3 for Windows and plotted with POV-ray programs.[23]

## RESULTS AND DISCUSSION

**Syntheses.** In our previous work,[18] we studied the reactivity of the Ni$^{2+}$/dapdoH$_2$/R-COO$^-$ system in a basic medium and several tri- and tetranuclear systems containing oximato and carboxylato bridges where reported, and different coordination modes for dapdoH$_2$, dapdoH$^-$, or dapdo$^{2-}$ were characterized. The presence of labile solvent molecules in these compounds suggested the possibility to grow their nuclearity or dimensionality by means of the adequate bridging ligands. On the other hand, it was also envisaged the possibility to generate novel "empty" coordination sites by substitution of the carboxylate ligands by less coordinating anions. With this aim, we have explored the systematic reaction of nickel carboxylates with dapdoH$_2$ and additional bridging ligands, such as azide, dicyanamide, or thiocyanate. When sodium dicyanamide was present in the reaction medium, crystalline pentanuclear compounds **1** and **2** and decanuclear **4** were obtained in good yield. However,

in these compounds, the dicyanamide ligand acts as a terminal ligand and does not provide the expected linkage between polynuclear units. In contrast, reaction in the same synthetic conditions starting from nickel benzoates and sodium azide yields a mixture of dark crystals of the already reported[11] mononuclear $Ni^{IV}$ complex $[Ni(dapdo)_2]$ containing two deprotonated $dapdo^{2-}$ ligands and red needles for which structural characterization has been unsuccessful until now. The presence of coordinated azide in its end-on coordination mode (checked by IR spectroscopy) and the ferromagnetic response of these systems suggest the probable formation of azido-containing clusters, and efforts to reach their full structural characterization are in progress.

On the other hand, the change from carboxylato anions to nitrate ones yielded the crystalline compounds **3** and **4**, which show larger nuclearity and new topologies clearly different than the carboxylato-containing complexes, suggesting a rich noncarboxylato chemistry for this ligand.

The coordination behavior of the deprotonated form $dapdo^{2-}$ bonded to $Ni^{2+}$ atoms is remarkable. Strong spherical crystal fields, provided by the oximato groups,[24] favor the easy oxidation of the $Ni^{II}$ cation to the $d^6$ low-spin $Ni^{IV}$ oxidation state (e.g., $[Ni(dapdo)_2]$ and $[Ni(dmg)_3]^{2-}$, where $dmg^{2-}$ stands for dimetylglioximato).[24] The square-planar environment is common for $Ni^{II}$ atoms linked to several deprotonated oximato groups as in glioximato derivatives. However, pyridyloximato ligands give hexacoordination systematically with the only exception of the amidoxime function attached to pyridyl, pyrazyl, or pyimidinic rings, which, as in our case, give complexes in which tetra- and hexacoordination have been characterized simultaneously in the same compound.[3,6b,25] In our previous paper, we have reported how coordination of only one 3.11111 $dapdo^{2-}$ ligand it is not enough to favor the oxidation of $Ni^{II}$ to $Ni^{IV}$ but stabilizes the square-planar environment around the nickel centers.

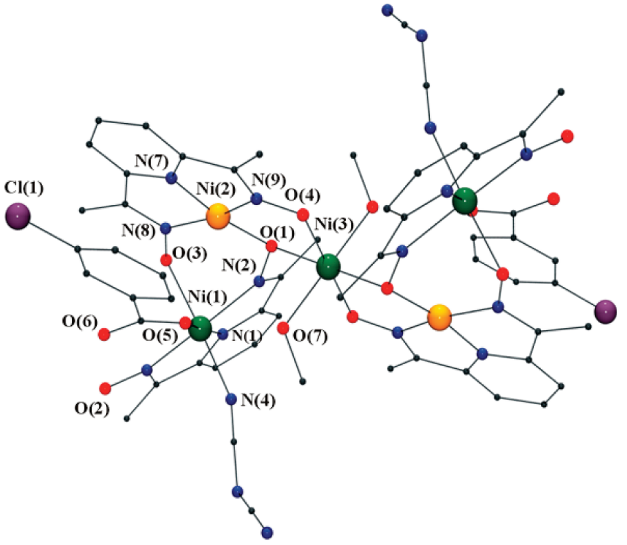


**Figure 1.** Labeled POV-ray plot of complex **2**. Ni atoms in an octahedral or square-planar environment are plotted in green and orange color, respectively. H atoms are omitted for clarity.

In agreement with these previous data, compounds **1**−**4** exhibit square-planar coordination for those nickel atoms linked to the three N atoms of one 3.11111 $dapdo^{2-}$ ligand. In contrast, characterization of the novel 5.22111 coordination mode shows an octahedral environment for the nickel atom coordinating the three N atoms of $dapdo^{2-}$. This feature suggests an important change in the electronic density and the reduction of the crystal field of the ligand due to the coordination of a second metallic atom to the oximato group at the limit between square-planar and octahedral environments.

**Description of the Structures.** *$[Ni_5(3\text{-}ClBzO)_2(dapdo)_2(dapdoH)_2(N(CN)_2)_2(MeOH)_2]$* (***2***). A labeled plot of the neutral centrosymmetric pentanuclear unit present in compound **2** is shown in Figure 1. Selected bond parameters are listed in Table 2. The pentanuclear units consist of two tetracoordinated nickel atoms Ni(2) and symmetry related Ni(2′) and three hexacoordinated nickel atoms, Ni(1), Ni(1′), and Ni(3), which are linked by the oximato groups of four ligand molecules. Each tetracoordinated cation Ni(2) is bonded to one 3.11111 $dapdo^{2-}$ molecule by its three N atoms and linked to one O-oximato atom from one neighbor $dapdoH^-$ ligand, resulting in a distorted square-planar environment. The coordination sphere of the Ni(1) cation is formed by the three N atoms of one 3.20111 $dapdoH^-$ ligand, one O-oximato atom from one neighbor $dapdo^{2-}$ ligand, one O atom from one monocoordinated benzoate group, and one N atom from one dicyanamide anion. Finally, the central Ni(3) atom is linked by four O-oximato groups (from two $dapdo^{2-}$ and two $dapdoH^-$ ligands) and by two *trans*-methanol molecules.

Ni−N bond distances are in the 1.813(2)−2.104(3) Å range, corresponding the shorter distances to the square-planar cations

**Table 2. Selected Interatomic Distances (Å) and Angles (deg) for Compound 2**

| | | | |
|---|---|---|---|
| Ni(1)−N(1) | 1.983(2) | Ni(1)−N(2) | 2.070(2) |
| Ni(1)−N(3) | 2.104(3) | Ni(1)−N(4) | 2.074(2) |
| Ni(1)−O(3) | 2.075(2) | Ni(1)−O(5) | 2.035(2) |
| Ni(2)−N(7) | 1.813(2) | Ni(2)−N(8) | 1.921(2) |
| Ni(2)−N(9) | 1.891(2) | Ni(2)−O(1) | 1.881(2) |
| Ni(3)−O(1) | 2.070 (2) | Ni(3)−O(4) | 1.991(2) |
| Ni(3)−O(7) | 2.114(2) | | |
| Ni(1)−N(2)−O(1) | 124.8(1) | Ni(1)−O(3)−N(8) | 111.4(1) |
| Ni(2)−N(8)−O(3) | 126.4(2) | Ni(1)−N(3)−O(2) | 126.9(2) |
| Ni(2)−O(1)−N(2) | 114.1(1) | Ni(2)−N(9)−O(4) | 125.1(1) |
| Ni(3)−O(4)−N(9) | 116.6(1) | Ni(3)−O(1)−N(2) | 116.9(1) |
| Ni(2)−O(1)−Ni(3) | 112.83(8) | | |
| Ni(1)−N(2)−O(1)−Ni(2) | 31.4(2) | Ni(1)−N(2)−O(1)−Ni(3) | 103.3(2) |
| Ni(2)−N(8)−O(3)−Ni(1) | 40.7(2) | Ni(2)−N(9)−O(4)−Ni(3) | 6.4(2) |



dx.doi.org/10.1021/ic200895q |*Inorg. Chem.* 2011, 50, 8893–8901

and being larger those provided by dapdoH$^-$ than dapdo$^{2-}$ ligands. $N_{oxime}-Ni-N_{pyridyl}$ angles deviate from 90° due to the low bite angle of the ligand, being larger the angles generated by the dapdo$^{2-}$ ligand (around 82°) than the angles that involve monodeprotonated dapdoH$^-$ ligands (around 77°). The torsion angle corresponding to the Ni(1)−N(1)−O(2)−Ni(3) bridge is surprisingly high, deviating only 13.3(2)° from orthogonality.

The two O atoms of the carboxylato anion participate in strong intramolecular H bonds: the coordinated O(5) atom interacts with the methanol molecule with a O(7)···O(5) distance of 2.835(3) Å, and the noncoordinated O(6) atom interacts with the protonated oximate group with a O(6)···O(2) distance of 2.635(3) Å. Aromatic rings of the dapdo$^{2-}$ and the chlorobenzoate ligands give intercluster $\pi-\pi$ interactions with a distance between centroids of 3.495(4) Å.

*[$Ni_8(dapdo)_4(NO_3)_4(OH)_4(MeOH)_4$]·3MeOH,NEt3* (***3***). Figure 2 shows a labeled plot of the neutral centrosymmetric compound **3**, while Table 3 lists the selected bond parameters. This octanuclear compound has four tetracoordinated and four hexacoordinated nickel atoms. All four tetracoordinated Ni$^{II}$ atoms (Ni(1), Ni(3), and symmetry related) are bonded to one 3.11111 dapdo$^{2-}$ ligand by its three N atoms and to one $\mu_3$-OH bridging group, exhibiting a distorted square-planar geometry. Hexacoordinated Ni$^{II}$ atoms show a $NiO_6$ environment and can be described as central Ni(2) and Ni(2a) and the peripheral Ni(4) and Ni(4a) groups. The central nickel atoms Ni(2) are linked by double oximato/hydroxo bridges to Ni(1a) and Ni(3) and by means of $\mu_3$-OH groups to Ni(1), Ni(2a), and Ni(4). The coordination sphere of Ni(2) is completed with one methanol molecule. The external Ni(4) atoms are linked by double oximato/hydroxo bridges to Ni(3) and through a single oximato bridge to Ni(1). Coordination sites around Ni(4) are completed with two monodentate nitrato ligands and one methanol solvent molecule.

A set of intramolecular H bonds contribute to stabilize the molecule: O(8) from one coordinated methanol molecule interacts with O(1a) from one of the oximato groups with an (O(8)···O(1a) distance of 2.589(7) Å) and with O(3) from one of the hydroxo ligands with an (O(8)···O(3) distance of 2.941(6) Å).

One of the O atoms from one coordinated nitrato ligand interacts with the other hydroxo ligand with an O(11)···O(4) distance of 2.704(6) Å.

*[$Ni_{10}(dapdo)_8(N(CN)_2)_2(MeO)(MeOH)](NO_3)$·3MeOH* (***4***). A plot of the decanuclear compound **4** is shown in Figure 3. These

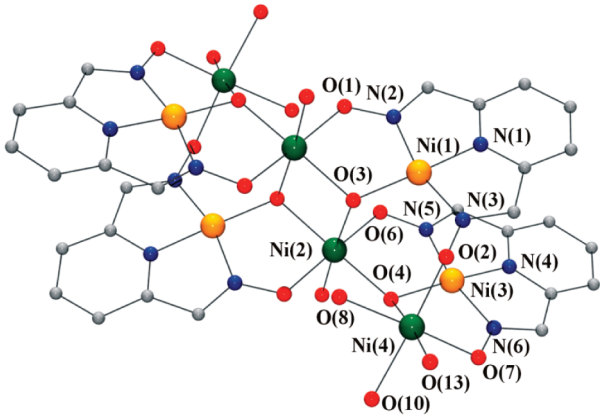


**Figure 2.** Labeled POV-ray plot of complex **3**. Ni atoms in an octahedral or square-planar environment are plotted in green and orange color, respectively. O(10) and O(13) correspond to oxygen atoms from coordinated nitrato ligands. H atoms are omitted for clarity.

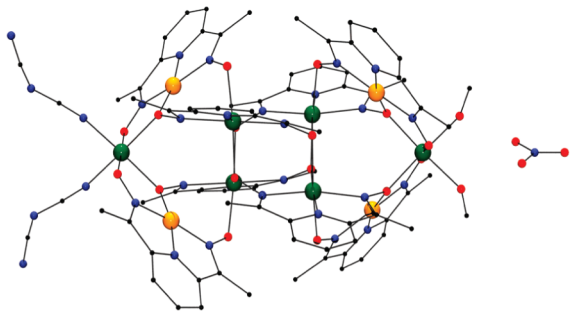

**Figure 3.** Plot of complex **4**. Ni atoms in an octahedral or square-planar environment are plotted in green and orange color, respectively. H atoms are omitted for clarity.

**Table 3. Selected Interatomic Distances (Å) and Angles (deg) for Compound 3**

| | | | |
|---|---|---|---|
| Ni(1)−N(1) | 1.812(5) | Ni(1)−N(2) | 1.885(5) |
| Ni(1)−N(3) | 1.902(6) | Ni(1)−O(3a) | 1.853(4) |
| Ni(2)−O(1) | 2.043(4) | Ni(2)−O(3) | 2.121(4) |
| Ni(2)−O(3a) | 2.060(4) | Ni(2)−O(4) | 2.067(4) |
| Ni(2)−O(5) | 2.076(4) | Ni(2)−O(6) | 2.031(4) |
| Ni(3)−N(4) | 1.790(5) | Ni(3)−N(5) | 1.880(5) |
| Ni(3)−N(6) | 1.874(6) | Ni(3)−O(4) | 1.868(4) |
| Ni(4)−O(2a) | 2.027(4) | Ni(4)−O(4) | 2.100(4) |
| Ni(4)−O(7) | 2.034(4) | Ni(4)−O(8) | 2.075(4) |
| Ni(4)−O(10) | 2.088(4) | Ni(4)−O(13) | 2.086(5) |
| Ni(1a)−O(3)−Ni(2) | 110.3(2) | Ni(1a)−O(3)−Ni(2a) | 114.0(2) |
| Ni(2)−O(1)−N(2) | 114.0(3) | Ni(2)−O(6)−N(5) | 113.0(3) |
| Ni(2)−O(3)−Ni(2a) | 95.5(2) | Ni(2)−O(4)−Ni(3) | 109.1(2) |
| Ni(2)−O(4)−Ni(4) | 131.3(2) | Ni(3)−O(4)−Ni(4) | 105.9(2) |
| Ni(4a)−O(2)−N(3) | 124.5(4) | Ni(4)−O(7)−N(6) | 111.1(3) |
| Ni(4)−O(10)−N(7) | 127.7(4) | Ni(4)−O(13)−N(8) | 127.9(5) |
| Ni(1)−N(2)−O(1)−Ni(2) | 10.0(6) | Ni(1)−N(3)−O(2)−Ni(4a) | 76.9(5) |
| Ni(3)−N(5)−O(6)−Ni(2) | 5.5(6) | Ni(3)−N(6)−O(7)−Ni(4) | 18.9(6) |



dx.doi.org/10.1021/ic200895q |*Inorg. Chem.* 2011, 50, 8893–8901

units possess a $C_2$ rotation axis that includes one N−O nitrato bond and the two peripheral nickel atoms. Each cluster contains six nonequivalent nickel atoms, organized as one inner $\{Ni_4(dapdo^{2-})_4\}$ pseudocubane surrounded by four nickel atoms distributed near each corner of the cube, and finally is capped by two additional peripheral nickel atoms. Six of the nickel atoms are hexacoordinated (inner cubane and peripheral ones), whereas the remainder tetracoordinated nickel ions exhibit a square-planar environment. The eight $dapdo^{2-}$ ligands are distributed in two groups: four of them link the nickel atoms of the inner cubane and adopt the unprecedented 5.22111 coordination mode, in contrast with the four $dapdo^{2-}$ ligands linked to the square-planar nickel atoms, which adopt the 3.11111 coordination mode. The two peripheral nickel atoms placed on the $C_2$ axis do not coordinate additional pyridyldioximato ligands.

A labeled plot of the core of the cationic decanuclear unit of **4** is depicted in Figure 4, and selected bond parameters are listed in Table 4. The octahedral coordination environment for the terminal Ni(1) atom consists of four O-oximato atoms (from two 5.22111 and two 3.11111 $dapdo^{2-}$ ligands) and two dicyanamides, giving a $NiN_2O_4$ environment, in contrast with Ni(6), which exhibits a $NiO_6$ environment from four oximato bridges (two 5.22111 and two 3.11111 $dapdo^{2-}$ ligands) and one metoxo and one methanol molecule.

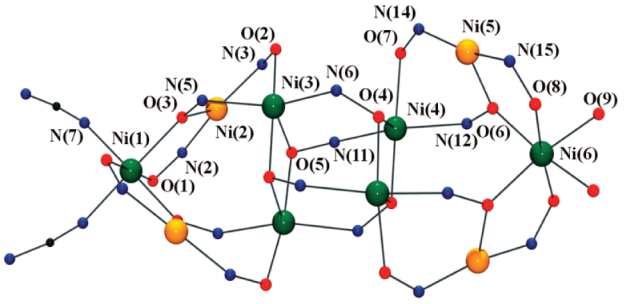


**Figure 4.** Labeled POV-ray plot of the core of complex **4**.

Tetracoordinated Ni(2), Ni(5), and symmetry related atoms show a square-planar environment. Each $Ni^{II}$ atom is bonded to one 3.1111 $dapdo^{2-}$ molecule by the three N atoms and to one O-oximato group from another $dapdo^{2-}$ molecule ($NiN_3O$ environment). Bond distances are between 1.79(1) and 1.935(7) Å, corresponding the shorter ones to the Ni−N(ring) bond. Bond angles deviate from the ideal 90° value due to the small bite of the $dapdo^{2-}$ ligand.

The hexacoordinated Ni(3), Ni(4), and symmetry related atoms form the inner $[Ni_4(NO)_4]$ pseudocubane in which each nonmetallic vertex has been substituted by one oximate bridge (Figure 5). Each oximato group provides three edges and one vertex of the pseudocube, resulting in four similar hexagonal $Ni_2(NO)_2$ faces and two conventional $Ni_2O_2$ square faces, with bond angles Ni(3)−O(5)−Ni(3a) and Ni(4)−O(4)−Ni(4a) of 101.0(3)° and 101.5(3)°, respectively. Ni−O−N−Ni torsion angles in the pseudocube are close to 70° in all cases. Ni(3) and Ni(4) are bridged by one single oximato bridge to Ni(1) and Ni(6), respectively, with a similar torsion angle close to 120°.

The anionic nitrate molecule interacts with the methanol/methanoate ligands coordinated to Ni(6) via a multicentric H bond in which the minimum distances of 2.65(1) and 2.814(9) Å correspond to O(9)···O(10) and O(9)···O(9a), respectively.

**Magnetic Measurements and Modelization.** Room-temperature $\chi_M T$ values are 3.93 and 3.95 $cm^3\,K\,mol^{-1}$, respectively,

**Table 4. Selected Interatomic Distances (Å) and Angles (deg) for Compound 4**

| | | | |
|---|---|---|---|
| Ni(1)−O(1) | 2.025(6) | Ni(1)−N(7) | 2.043(9) |
| Ni(1)−O(3) | 2.106(6) | | |
| Ni(2)−N(1) | 1.824(8) | Ni(2)−N(2) | 1.893(8) |
| Ni(2)−N(3) | 1.924(7) | Ni(2)−O(3) | 1.847(6) |
| Ni(3)−N(4) | 1.995(8) | Ni(3)−N(5) | 2.107(7) |
| Ni(3)−N(6) | 2.187(7) | Ni(3)−O(2) | 2.077(6) |
| Ni(3)−O(5) | 2.043(7) | Ni(3)−O(5a) | 2.108(6) |
| Ni(4)−N(10) | 2.005(8) | Ni(4)−N(11) | 2.175(7) |
| Ni(4)−N(12) | 2.092(7) | Ni(4)−O(4) | 2.026(7) |
| Ni(4)−O(7) | 2.064(6) | Ni(4)−O(4a) | 2.125(6) |
| Ni(5)−N(13) | 1.79(1) | Ni(5)−N(14) | 1.935(7) |
| Ni(5)−N(15) | 1.875(8) | Ni(5)−O(6) | 1.843(7) |
| Ni(6)−O(6) | 2.067(6) | Ni(6)−O(8) | 1.998(8) |
| Ni(6)−O(9) | 2.073(7) | | |
| Ni(3)−O(5)−Ni(3a) | 101.0(3) | Ni(4)−O(4)−Ni(4a) | 101.5(3) |
| Ni(1)−O(1)−N(2) | 118.9(5) | Ni(1)−O(3)−N(5) | 123.7(5) |
| Ni(2)−O(3)−N(5) | 114.2(5) | Ni(3)−O(2)−N(3) | 111.7(5) |
| Ni(3)−O(5)−N(11) | 112.0(5) | Ni(4)−O(4)−N(6) | 111.5(5) |
| Ni(4)−O(7)−N(14) | 113.9(5) | Ni(5)−O(6)−N(12) | 113.1(5) |
| Ni(6)−O(6)−N(12) | 124.3(5) | Ni(6)−O(8)−N(15) | 117.9(6) |
| Ni(1)−O(1)−N(2)−Ni(2) | 12.8(9) | Ni(1)−O(3)−N(5)−Ni(3) | 119.7(5) |
| Ni(2)−O(3)−N(5)−Ni(3) | 37.4(7) | Ni(3)−N(6)−O(4)−Ni(4) | 45.0(6) |
| Ni(2)−N(3)−O(2)−Ni(3) | 36.0(8) | Ni(4)−N(11)−O(5)−Ni(3) | 45.6(7) |
| Ni(3)−N(6)−O(4)−Ni(4a) | 69.6(6) | Ni(4)−N(11)−O(5)−Ni(3a) | 69.7(7) |
| Ni(4)−N(12)−O(6)−Ni(5) | 43.1(8) | Ni(4)−N(12)−O(6)−Ni(6) | 117.0(6) |
| Ni(5)−N(14)−O(7)−Ni(4) | 33.4(9) | Ni(5)−N(15)−O(8)−Ni(6) | 16.7(9) |



dx.doi.org/10.1021/ic200895q |*Inorg. Chem.* 2011, 50, 8893–8901

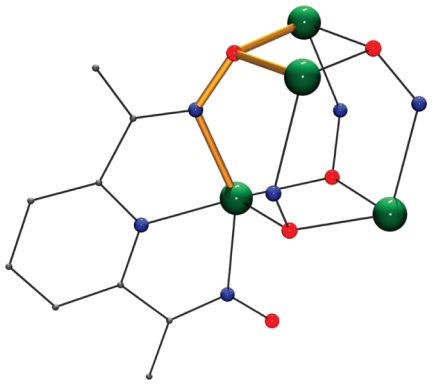

**Figure 5.** Pseudocube subunit of complex **4** generated by four dapdo$^{2-}$ ligands. Each ligand provides three edges and one vertex of the pseudocube.

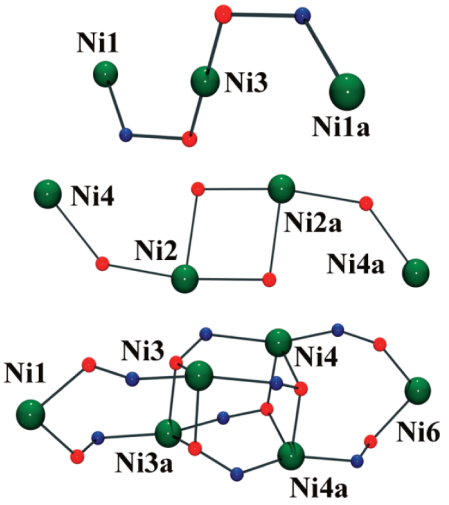


**Figure 6.** Core of the bridges between paramagnetic centers of compounds **1** and **2** (top), **3** (middle), and **4** (bottom). Nickel atom numbering corresponds to the subindexes of the local spin carriers $S_n$ employed in the corresponding Hamiltonians.

for compounds **1** and **2**, 4.82 cm$^3$ K mol$^{-1}$ for compound **3**, and 7.39 cm$^3$ K mol$^{-1}$ for **4**, in good agreement with structural data, which reveals three, four, and six octahedral paramagnetic Ni$^{II}$ centers, respectively. Numbering of the paramagnetic centers employed in the Hamiltonian expressions and the bridges between these atoms are plotted in Figure 6.

Compounds **1** and **2** show a $\chi_M T$ value nearly constant between 300 and 10 K, decreasing slightly at low temperature down to a minimum value of 1.98 cm$^3$ K mol$^{-1}$ for **1** and 1.71 cm$^3$ K mol$^{-1}$ at 1.8 K (Figure 7). The fit of the experimental data as a linear trinuclear system was calculated by means of the MAGPACK program,[26] for three local $S = 1$ spins derived from the Hamiltonian

$$H = -J(S_1 \cdot S_3 + S_3 \cdot S_{1a}) + DS_z^2$$

Best fit parameters were $J = -0.4(1)$ cm$^{-1}$, $g = 2.279(2)$, and $D = -3.7(2)$ for compound **1** and $J = -0.5(1)$ cm$^{-1}$, $g = 2.285(2)$, and $D = -3.2(2)$ for complex **2**.

The $\chi_M T$ plot for compound **3** decreases continuously on cooling and tends to zero at low temperature. $\chi_M$ increases from room temperature up to a well-defined maximum of

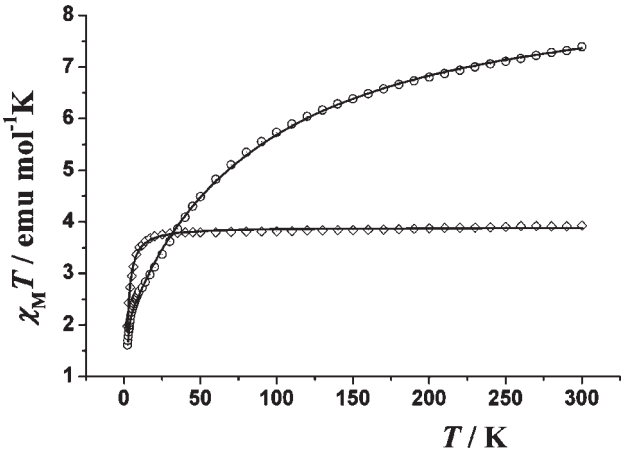


**Figure 7.** Plot of the $\chi_M T$ product vs $T$ for compounds **2** (diamonds) and **4** (dot centered circles). The solid lines show the best fit of the experimental data. Compounds **1** and **2** give practically equal magnetic responses, and only the plot of **2** is shown for clarity.

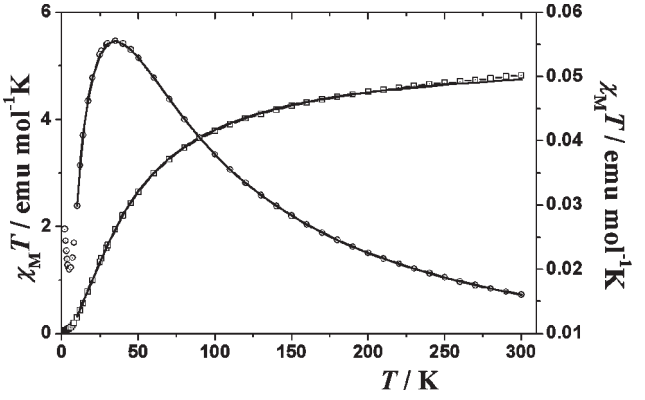


**Figure 8.** Plot of the $\chi_M T$ product vs $T$ for compound **3** (squares, left axis) and $\chi_M$ vs $T$ (dot centered circles, right axis). The solid lines show the best fit of the experimental data in the 10−300 K range of temperature.

susceptibility centered at 35 K (Figure 8). Compound **3** behaves magnetically as a tetranuclear system with two well-differentiated superexchange pathways (single or double hydroxo bridges with different Ni−O−Ni bond angles). Simulation of the experimental data was thus performed using the CLUMAG program[27] and applying the Hamiltonian

$$H = -J_1(S_2 \cdot S_4 + S_{2a} \cdot S_{4a}) - J_2(S_2 \cdot S_{2a})$$

Best fit parameters were $J_1 = -24.6$ cm$^{-1}$, $J_2 = -13.2$ cm$^{-1}$, and $g = 2.302$, with $R = 3.6 \times 10^{-5}$ ($R = (\chi_M T_{calc} - \chi_M T_{obs})^2/(\chi_M T_{obs})^2$.

The $\chi_M T$ plot for compound **4** decreases continuously on cooling from the room temperature value of 7.39 cm$^3$ K mol$^{-1}$. The plot shows a small change of slope at 13 K, reaching a value of 1.50 cm$^3$ K mol$^{-1}$ at 2 K. The $\chi_M$ plot does not exhibit a maximum of susceptibility, and magnetization measurements show a quasi saturated value equivalent to four electrons under an external field of 5 T.

According to the coupling scheme of Figure 6, this system behaves as a two-$J$ cubane capped by two additional Ni$^{II}$ atoms linked by single oximato bridges. Bond parameters for the



dx.doi.org/10.1021/ic200895q |*Inorg. Chem.* 2011, 50, 8893–8901

oximato bridges between Ni(1) with Ni(3)/Ni(3a) and Ni(6) with Ni(4)/Ni(4a) are very similar, and thus, to minimize the number of coupling constants in the fitting process, we have assumed greater symmetry than that experimentally found in the structure. Simulation was performed by means of the CLUMAG program[27] applying the three-$J$ Hamiltonian

$$H = -J_1(S_1 \cdot S_3 + S_1 \cdot S_{3a} + S_6 \cdot S_4 + S_6 \cdot S_{4a}) - J_2(S_3 \cdot S_{3a} + S_4 \cdot S_{4a}) - J_3(S_3 \cdot S_4 + S_3 \cdot S_{4a} + S_{3a} \cdot S_4 + S_{3a} \cdot S_{4a})$$

Best fit parameters were $J_1 = -4.8$ cm$^{-1}$, $J_2 = -26.2$ cm$^{-1}$, $J_3 = -24.6$ cm$^{-1}$, and $g = 2.390$ with $R = 2.1 \times 10^{-5}$.

Correlations for the coupling in Cu$^{II}$ or Mn$^{III}$ oximato bridged systems have been well-established in the last recent years and taking into account the orbitals of the Ni$^{II}$ cation involved in the superexchange interaction has been widely assumed a response closer to Cu$^{II}$ (decrease of the antiferromagnetic interaction with the increase of the M−O−N−M torsion angle)[28] than Mn$^{III}$ (strong dependence of $J$ with the torsion with even reversal of the sign of the coupling constants for torsion angles around 30° in triangular compounds).[29] Very recently, on the basis of experimental correlations on the Ni−O−N−Ni pathway, an intermediate response between Cu$^{II}$ and Mn$^{III}$ has been proposed,[30] suggesting a decrease of the antiferromagnetic interaction for increasing torsions up to around 75−80°, at which point the switch to ferromagnetic interaction may be possible. The quasi negligible values of $J$ found for compounds **1** and **2** provide a nice example of the magnetic response of the system Ni−O−N−Ni with large torsion angles close to orthogonality. As was suggested, this superexchange pathway experimentally reveals to transmit a quasi negligible interaction in contrast with the well-established medium-strong antiferromagnetic coupling widely reported for planar or weakly distorted bridges.[1]

Compound **4** contains two kinds of oximato bridges with different torsion angles: large Ni−O−N−Ni torsions are found for the bridges between the peripheral atoms and the central cubane unit (117.0° and 119.7°) and lower torsions (around 45° and 69°) inside the cubane. In agreement with the above general trends, the found $J$ values show weak antiferromagnetic coupling for the bridges mediated by large torsion angles (−4.8 cm$^{-1}$) and medium interactions with mean $J$ values around −25 cm$^{-1}$ for the less-distorted bridges.

The remainder of interactions in compound **4** and those found in **3** follow the well-established correlations for Ni−O−Ni bond angles with increasing antiferromagnetic interaction for larger bond angles.[26]

## CONCLUSIONS

In the present work, we have reported a new series of Ni$^{II}$ clusters obtained using the dioximato ligand dapdoH$_2$ in carboxylato and noncarboxylato chemistry. The most relevant features have been the characterization of the larger cluster reported until now containing pyridyldioximato ligands and the new 5.22111 coordination mode characterized for the deprotonated form dapdo$^{2-}$, which spreads the picture of the coordination possibilities of this kind of ligand. It becomes also relevant that, in contrast with the well-known 3.11111 coordination mode that systematically generates a square-planar coordination around the Ni$^{II}$ cations or even favors the easy oxidation to Ni$^{IV}$, the new 5.22111 mode stabilizes octahedral environments. Analysis of the calculated coupling constants provides experimental examples of the predicted response of the Ni−O−N−Ni pathway with large torsion angles.

## ASSOCIATED CONTENT

**Supporting Information.** Crystallographic data files (CIF format) for complexes **2**−**4**, crystal data (Table S1), and plot of compound **1** (Figure S1). This material is available free of charge via the Internet at http://pubs.acs.org.

## AUTHOR INFORMATION

**Corresponding Author**
*E-mail: albert.escuer@ub.edu.

## ACKNOWLEDGMENT

This work was supported by the CICYT projects CTQ2009-07264. A.E. acknowledges the support of the ICREA-Academia Research Award. The authors are grateful to Dr. G. Aromí, Universitat de Barcelona, and to the Spanish MCI for facilitating access to BM16 at ESRF (EXP16-01-739).

## REFERENCES

(1) Milios, C. J.; Stamatatos, T. C.; Perlepes, S. P. *Polyhedron* **2006**, *25*, 134.

(2) Stamatatos, T. C.; Diamantopoulou, E.; Raptopoulou, C. P.; Psycharis, V.; Escuer, A.; Perlepes, S. P. *Inorg. Chem.* **2007**, *46*, 2350.

(3) Ji, C.-M.; Yang, H.-J.; Zhao, C.-C.; Tangoulis, V.; Cui, A.-L.; Kou, H.-Z. *Cryst. Growth Des.* **2009**, *9*, 4607.

(4) (a) Pajunen, A.; Mutikainen, I.; Saarinen, H.; Orama, M. *Z. Kristallogr. - New Cryst. Struct.* **1999**, *214*, 217. (b) Khanra, S.; Weyhermuller, T.; Rentschler, E.; Chaudhuri, P. *Inorg. Chem.* **2005**, *44*, 8176. (c) Stamatatos, T. C.; Diamantopoulou, E.; Tasiopoulos, A.; Psycharis, V.; Vicente, R.; Raptopoulou, C. P.; Nastopoulos, V.; Escuer, A.; Perlepes, S. P. *Inorg. Chim. Acta* **2006**, *359*, 4149. (d) Stamatatos, T. C.; Papatriantafyllopoulou, C.; Katsoulakou, E.; Raptopoulou, C. P.; Perlepes, S. P. *Polyhedron* **2007**, *26*, 1830.

(5) Psomas, G.; Dendrinou-Samara, C.; Alexiou, M.; Tsohos, A.; Raptopoulou, C. P.; Terzis, A.; Kessissoglou, D. P. *Inorg. Chem.* **1998**, *37*, 6556.

(6) (a) Stamatatos, T. C.; Abboud, K. A.; Perlepes, S. P.; Christou, G. *Dalton Trans.* **2007**, 3861. (b) Papatriantafyllopoulou, C.; Jones, L. F.; Nguyen, T. D.; Matamoros-Salvador, N.; Cunha-Silva, L.; Paz, F. A. A.; Rocha, J.; Evangelisti, M.; Brechin, E. K.; Perlepes, S. P. *Dalton Trans.* **2008**, 3153. (c) Stamatatos, T. C.; Escuer, A.; Abboud, K. A.; Raptopoulou, C. P.; Perlepes, S. P.; Christou, G. *Inorg. Chem.* **2008**, *47*, 11825.

(7) Papatriantafyllopoulou, C.; Stamatatos, T. C.; Wernsdorfer, W.; Teat, S. J.; Tasiopoulos, A.; Escuer, A.; Perlepes, S. P. *Inorg. Chem.* **2010**, *49*, 10486.

(8) Coxall, R. A.; Harris, S. G.; Henderson, D. K.; Parsons, S.; Tasker, P. A.; Winpenny, R. E. P. *J. Chem. Soc., Dalton Trans.* **2000**, 2349.

(9) (a) Glynn, C. W.; Turnbull, M. M. *Transition Met. Chem.* **2002**, *27*, 822. (b) Halcrow, M. A.; Kilner, C. A.; Wolowska, J.; McInnes, E. J. L.; Bridgeman, A. J. *New J. Chem.* **2004**, *28*, 228. (c) Bovenzi, B. A.; Pearse, G. A., Jr. *J. Chem. Soc., Dalton Trans.* **1997**, 2793. (d) Vasilevsky, I. V.; Stenkamp, R. E.; Lingafelter, E. C.; Rose, N. J. *J. Coord. Chem.* **1988**, *19*, 171.

(10) Salonen, M.; Saarinen, H.; Mutikainen, I. *J. Coord. Chem.* **2008**, *61*, 1462.

(11) (a) Sproul, G.; Stucky, G. D. *Inorg. Chem.* **1973**, *12*, 2898. (b) Namli, H.; Azaz, A. D.; Karabulut, S.; ÇElen, S.; Kurtaran, R.; Kazak, C. *Transition Met. Chem.* **2007**, *32*, 266.

(12) (a) Nicholson, G. A.; Petersen, J. L.; McCormick, B. J. *Inorg. Chem.* **1982**, *21*, 3274. (b) Vasilevsky, I. V.; Stenkamp, R. E.; Lingafelter, E. C.; Schomaker, V.; Willett, R. D.; Rose, N. J. *Inorg. Chem.* **1989**, *28*, 2619. (c) Abboud, K. A.; Palenik, R. C.; Palenik, G. J. *Acta Crystallogr., Sect. C* **1994**, *C50*, 525. (d) Abram, S.; Maichle-Mössmer, C.; Abram, U. *Polyhedron* **1997**, *16*, 2183. (f) Abram, S.; Maichle-Mössmer, C.; Abram, U. *Polyhedron* **1997**, *16*, 2291. (g) Singh, S. K.; Sharma, S.; Dwivedi, S. D.; Zou, R.-Q.; Xu, Q.; Pandey, D. S. *Inorg. Chem.* **2008**, *47*, 11942.

(13) (a) Unni Nair, B. C.; Sheats, J. E.; Ponteciello, R.; Van Engen, D.; Petrouleas, V.; Dismukes, G. C. *Inorg. Chem.* **1989**, *28*, 1582. (b) Marsh, R. E. *Inorg. Chem.* **1990**, *29*, 572. (c) Escuer, A.; Cordero, B.; Solans, X.; Font-Bardia, M.; Calvet, T. *Eur. J. Inorg. Chem.* **2008**, 5082.

(14) Nicholson, G. A.; Petersen, J. L.; McCormick, B. J. *Inorg. Chem.* **1980**, *19*, 195.

(15) (a) Stamatatos, T. C.; Luisi, B. S.; Moulton, B.; Christou, G. *Inorg. Chem.* **2008**, *47*, 1134. (b) Khanra, S.; Weyhermüller, T.; Chaudhuri, P. *Dalton Trans.* **2008**, 4885. (c) Escuer, A.; Cordero, B.; Font-Bardia, M.; Calvet, T.; Roubeau, O.; Teat, S. J.; Fedi, S.; Fabrizi di Biani, F. *Dalton Trans.* **2010**, *39*, 4817.

(16) (a) Khanra, S.; Weyhermüller, T.; Chaudhuri, P. *Dalton Trans.* **2007**, 4675. (b) Lampropoulos, C.; Stamatatos, T. C.; Abboud, K. A.; Christou, G. *Inorg. Chem.* **2009**, *48*, 429.

(17) Escuer, A.; Vlahopoulou, G.; Perlepes, S. P.; Font-Bardia, M.; Calvet, T. *Dalton Trans.* **2011**, *40*, 225.

(18) Escuer, A.; Esteban, J.; Aliaga-Alcalde, N.; Font-Bardia, M.; Calvet, T.; Roubeau, O.; Teat, S. J. *Inorg. Chem.* **2010**, *39*, 2259.

(19) Otwinowski, Z.; Minor, W. *Methods in Enzymology*; Carter, C. W., Jr., Sweet, R. M., Eds.; Academic Press: New York, 1997; Vol. 276: Macromolecular Crystallography, part A, pp 307−326.

(20) Altomare, A.; Burla, M. C.; Camalli, M.; Cascarano, G. L.; Giacovazzo, C.; Guagliardi, A.; Polidori, G. *J. Appl. Crystallogr.* **1994**, *27*, 475.

(21) Sheldrick, G. M. *Acta Crystallogr.* **2008**, *A64*, 112.

(22) Spek, A. L. *J. Appl. Crystallogr.* **2003**, *36*, 7.

(23) Ortep-3 for Windows: Farrugia, L. J. *J. Appl. Crystallogr.* **1997**, *30*, 565.

(24) Baucom, E. I.; Drago, R. S. *J. Am. Chem. Soc.* **1971**, *93*, 6469.

(25) (a) Kou, H.-Z.; An, G.-Y.; Ji, C.-M.; Wang, B.-W.; Cui, A.-L. *Dalton Trans.* **2010**, *39*, 9604. (b) Gole, B.; Chakrabarty, R.; Mukherjee, S.; Song, Y.; Mukherjee, P. S. *Dalton Trans.* **2010**, *39*, 9766. (c) An, G.-Y.; Ji, C.-M.; Cui, A.-L.; Kou, H.-Z. *Inorg. Chem.* **2011**, *50*, 1079.

(26) Borras-Almenar, J. J.; Clemente-Juan, J. M.; Coronado, E.; Tsukerblat, B. S. *J. Comput. Chem.* **2001**, *22*, 985.

(27) Gatteschi, D.; Pardi, L. *Gazz. Chim. Ital.* **1993**, *123*, 231.

(28) (a) Escuer, A.; Vlahopoulou, G.; Perlepes, S. P.; Font-Bardia, M.; Calvet, T. *Dalton Trans.* **2011**, *40*, 225. (b) Ruiz, R.; Lloret, F.; Julve, M.; Munoz, M. C.; Bois, C. *Inorg. Chim. Acta* **1994**, *219*, 179. (c) Colacio, E.; Dominguez-Vera, J. M.; Escuer, A.; Klinga, M.; Kivekas, R.; Romerosa, A. *J. Chem. Soc., Dalton Trans.* **1995**, 343. (d) Dominguez-Vera, J. M.; Colacio, E.; Escuer, A.; Klinga, M.; Kivekäs, R.; Romerosa, A. *Polyhedron* **1997**, *16*, 281.

(29) (a) Milios, C. J.; Inglis, R.; Vinslava, A.; Bagai, R.; Wernsdorfer, W.; Parsons, S.; Perlepes, S. P.; Christou, G.; Brechin, E. K. *J. Am. Chem. Soc.* **2007**, *129*, 12505. (b) Inglis, R.; Jones, L. F.; Milios, C. J.; Datta, S.; Collins, A.; Parsons, S.; Wernsdorfer, W.; Hill, S.; Perlepes, S. P.; Piligkos, S.; Brechin, E. K. *Dalton Trans.* **2009**, 3403.

(30) Palacios, M. A.; Mota, A. J.; Perea-Buceta, J. E.; White, F. J.; Brechin, E. K.; Colacio, E. *Inorg. Chem.* **2010**, *49*, 10156.

### 3.2.1. Resum: $Ni_5$, $Ni_8$, and $Ni_{10}$ clusters with 2,6-diacetylpyridine-dioxime as a ligand.

Albert Escuer, Jordi Esteban, Olivier Roubeau.

*Inorganic Chemistry* **2011**, *50*, 8893-8901.

Aquest article descriu una nova sèrie de clústers de $Ni^{II}$ obtinguts amb el lligand $dapdoH_2$. A diferència del treball anterior, es van utilitzar carboxilats de níquel(II) en presència d'un co-lligand (dicianamida, $N(CN)_2^-$) com a reactius i es van presentar els primers intents amb sals que contenen anions no carboxilats, com és el nitrat (en absència i presència del mateix co-lligand).

Així, es van caracteritzar els complexos $[Ni_5(MeOH)_2(R\text{-}COO)_2(dapdo)_2(dapdoH)_2(N(CN)_2)_2]$ ($R\text{-}COO^-$ = benzoat (**2_1**) o 3-clorobenzoat (**2_2**)), $[Ni_8(MeOH)_4(dapdo)_4(NO_3)_4(OH)_4]$ (**2_3**) i $[Ni_{10}(MeOH)(dapdo)_8(N(CN)_2)_2(MeO)](NO_3)$ (**2_4**). Aquests productes presenten una major nuclearitat que els obtinguts en l'article anterior i en tots ells hi ha presència d'ions $Ni^{II}$ en geometria octaèdrica i plano-quadrada, figura 9.

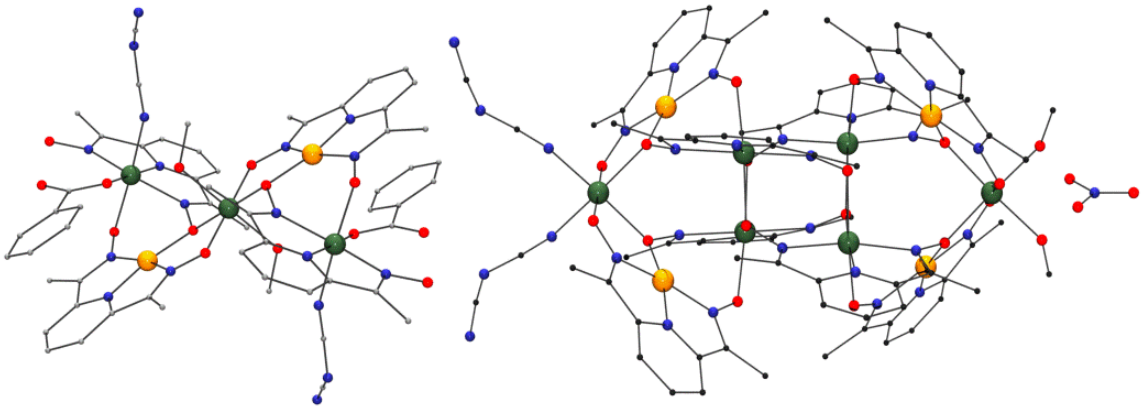

**Figura 9.** Estructura dels compostos **2_1** i **2_4**.

Es va realitzar l'estudi magnètic per tots ells i es va trobar que tots quatre compostos presenten un comportament antiferromagnètic: disminueix el valor de $\chi_M T$ en baixar la temperatura. També és destacable el fet que es va observar una forta dependència entre la intensitat de l'acoblament i els paràmetres d'enllaç dels ponts oxima: els ponts amb torsió Ni-N-O-Ni entre 45° i 69° generen una

constant d'acoblament moderada (al voltant de -25 $cm^{-1}$), els ponts amb una torsió lleugerament superior a la ortogonalitat (al voltant de 100°) tenen associada una *J* pràcticament negligible (-0,4 i -0,5 $cm^{-1}$) i finalment els ponts amb una torsió més elevada (propera a 120°) donen una interacció feble (d'uns -5 $cm^{-1}$).

La relació entre l'angle de torsió M-N-O-M i la intensitat de l'acoblament en interaccions mitjançant ponts oxima era coneguda per sistemes de $Cu^{II}$ (disminució de *J* en augmentar la torsió)[165] i $Mn^{III}$ (forta dependència de *J* amb la torsió, que pot arribar a canviar de signe per determinats angles)[166] però no per $Ni^{II}$, pel qual només s'havia realitzat una correlació basada en fets experimentals que proposava un comportament semblant a $Cu^{II}$.[167]

En conclusió, en aquest article es van presentar quatre nous productes obtinguts a partir del lligand dapdo$H_2$, que confirmen alguns trets observats anteriorment, com ara la generació d'entorns plano-quadrats en coordinar-se en el mode 3.1111 o l'acoblament antiferromagnètic per interaccions basades en ponts oxima. Es va observar per primera vegada el mode de coordinació 5.22111 en el lligand $dapdo^{2-}$ que, a diferència del mode 3.1111, estabilitza un entorn octaèdric, i es va realitzar l'estudi magnètic dels diferents compostos, que va proporcionar nous exemples experimentals que confirmen la relació entre el valor de la constant d'acoblament i l'angle de torsió Ni-N-O-Ni.

## 3.3. Article 3.

## Polynuclear pyridyldioximato-nickel(II) clusters: Synthesis, structure and magnetic study.

**Jordi Esteban**, Albert Escuer, Mercè Font-Bardia, Olivier Roubeau, Simon J. Teat.

*Polyhedron* **2013***, 52,* 339-345.

Polyhedron 52 (2013) 339–345

Contents lists available at SciVerse ScienceDirect

Polyhedron

journal homepage: www.elsevier.com/locate/poly

# Polynuclear pyridyldioximato-nickel(II) clusters: Synthesis, structure and magnetic study

Jordi Esteban [a,*], Albert Escuer [a,*], Mercé Font-Bardia [b], Olivier Roubeau [c], Simon J. Teat [d]

[a] Departament de Química Inorgànica, Institut de Nanociència i Nanotecnologia de la Universitat de Barcelona (IN2UB), Av. Diagonal 645, 08028 Barcelona, Spain
[b] Departament de Mineralogia I Cristal·lografia, Universitat de Barcelona, Martí Franqués s/n, 08028 Barcelona, Spain
[c] Instituto de Ciencia de Materiales de Aragón (ICMA), CSIC-Universidad de Zaragoza, Pl. San Francisco s/n, 50009 Zaragoza, Spain
[d] Advanced Light Source, Berkeley Laboratory, 1 Cyclotron road, Berkeley, CA 94720, USA

ARTICLE INFO

*Article history:*
Available online 13 September 2012

Dedicated to Professor Alfred Werner on the occasion of the 100th anniversary of his Nobel Prize Award in Chemistry in 1913.

*Keywords:*
Crystal structures
Pyridyl dioximato ligands
Magnetic properties
Nickel(II)
Sulfato ligand

ABSTRACT

In the present work, new polynuclear complexes with nuclearities ranging from $Ni_3$ to $Ni_{10}$, have been obtained by reaction of a variety of nickel salts and dapdo$H_2$ ligand, (dapdo$H_2$ = 2,6-diacetylpyridine dioxime). Depending on the precursors and reaction conditions the compounds with formula $[Ni_3(3\text{-Cl-BzO})(dapdo)(dapdoH)OH(dapdoH_2)](3\text{-Cl-BzO})$ (**1**), $(Et_2NH_2)_6[Ni_8(dapdoH)_4(SO_4)_9(H_2O)_2]$ (**2**) and $(Et_3NH)_2[Ni_{10}(dapdo)_8(MeOH)_4](BF_4)_6$ (**3**) were achieved and structurally characterized. The octanuclear compound **2** provides an unprecedented sulfato cluster with a new topology and connectivity. Dc magnetic measurements were carried out in the 2–300 K range revealing antiferromagnetic interactions for all compounds.



## 1. Introduction

Currently, use of oxime ligands in coordination chemistry is a growing research field and specifically, 2-pyridyl oximes, {py}C(R)-NOH, have proven to be adequate to generate stable first-row transition coordination compounds with different nuclearities [1]. These ligands are very versatile, able to act as bidentate ligand in the protonated form or to link up to three metallic centers in the deprotonated form. Self-assembly of metal-oximato fragments resulted in several high nuclearity $Ni^{II}$ clusters, as for example, $Ni_7$ [2], $Ni_8$ [3], $Ni_9$ [4], $Ni_{10}$ [5], $Ni_{12}$, $Ni_{13}$ or $Ni_{14}$ [3,6] exhibiting, in some cases, slow relaxation of magnetization [7]. In order to increase the nuclearity and to generate and stabilize new topologies, pyridyl dioximato ligands ($LH_2$, with R = various), Scheme 1, appear as excellent candidates for the achievement of polynuclear clusters through the bottom-up approach: their three N atoms close to each other give an excellent chelate that easily coordinates one metallic center, while the two *ortho*-oximato groups are capable of coordinating up to four additional cations at both sides of the central chelating group, Scheme 2. Among these ligands, 2,6-diacetylpyridine-dioxime (dapdo$H_2$) has been the most studied over the years. Despite being studied in Mn [8], Cu [9], Fe [10] and heterometallic [11] chemistry, Ni-dapdo$H_2$ chemistry has not been a hot topic and only few polynuclear compounds have been reported until now, all of them synthesized in our group [12].

Continuing our work on Ni-dapdo$H_2$ chemistry, we present a series of trinuclear $[Ni_3(3\text{-Cl-BzO})(dapdo)(dapdoH)OH(dapdoH_2)](3\text{-Cl-BzO})$ (**1**), octanuclear $(Et_2NH_2)_6[Ni_8(dapdoH)_4(SO_4)_9(H_2O)_2]$ (**2**) and decanuclear $(Et_3NH)_2[Ni_{10}(dapdo)_8(MeOH)_4](BF_4)_6$ (**3**) new clusters. Compounds **1** and **3** exhibit nickel centers in both octahedral and square-planar coordination environments in the same compound. We also have been able to reproduce the 5.22111 coordination mode (Harris notation) [13], firstly observed in our last work, and also the larger nuclearity for this ligand ($M_{10}$), having **3** the same motif than the previously $Ni_{10}$ reported compound [12b]. It should be emphasized that compound **2** gives a nuclearity and topology unprecedented in sulfato chemistry [14]. Syntheses, structures and magnetic behavior of these compounds are described in the following sections.

## 2. Experimental

### 2.1. Materials and methods

2,6-Diacetylpyridine, $NiSO_4{\cdot}7H_2O$ and $Ni(BF_4)_2{\cdot}6H_2O$ were purchased from Sigma–Aldrich Inc., Probus and Strem Chemicals Inc., respectively, and used without further purification. $Ni(3\text{-Cl-BzO})_2{\cdot}3H_2O$ was synthesized by dissolving equimolar quantities (40 mmol) of 3-Cl-benzoic acid and NaOH in 40 mL of $H_2O$,

* Corresponding authors. Tel.: +34 93 4039138.
*E-mail address:* albert.escuer@qi.ub.es (A. Escuer).

0277-5387/$ - see front matter © 2012 Elsevier Ltd. All rights reserved.
http://dx.doi.org/10.1016/j.poly.2012.09.008

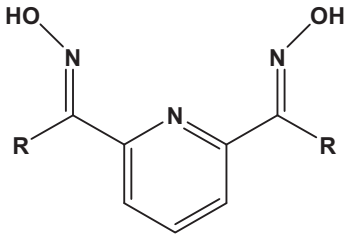


**Scheme 1.** $LH_2$ dioxime ligands (R = H, Me, $NH_2$). $DapdoH_2$ refers to the ligand in which R = Me.

filtering, and mixing the final solution with a commercial source of $Ni(NO_3)_2{\cdot}6H_2O$ (20 mmol) in 20 mL of water. The resulting nickel salt was obtained in good yield (>80%). $DapdoH_2$ was prepared following the Glynn and Turnbull method [9a].

### 2.2. Syntheses

#### 2.2.1. $[Ni_3(3\text{-}Cl\text{-}BzO)(dapdo)(dapdoH)OH(dapdoH_2)](3\text{-}Cl\text{-}BzO){\cdot}2.5CH_2Cl_2$ (**1**$\cdot 2.5CH_2Cl_2$)

20 mL of dichloromethane are poured over $DapdoH_2$ (1 mmol, 0.193 g) and $Ni(3\text{-}Cl\text{-}BzO)_2{\cdot}3H_2O$ (2 mmol, 0.847 g) and then $NEt_3$ was added (2 mmol, 0.202 g). The solution was stirred for 2 h, filtered, and layered with 10 mL of hexane for slow crystallization that provided red crystals. *Anal.* Calc. for $C_{41}Cl_2H_{39}N_9Ni_3O_{11}$ (1): C, 45.5; H, 3.7; N, 11.7. Found: C, 43.6; H, 3.8; N, 12.5%. Relevant IR bands ($cm^{-1}$): 3417(br), 3071(m), 2845(m), 1592(s), 1560(s), 1515(m), 1478(m), 1389(s), 1327(m), 1257(w), 1216(m), 1127(w), 1151(m), 1089(w), 1047(s), 806(w), 764(m), 734(m), 700(m).

#### 2.2.2. $(Et_2NH_2)_6[Ni_8(dapdoH)_4(SO_4)_9(H_2O)_2]$ (**2**)

$DapdoH_2$ (1 mmol, 0.193 g) and $NiSO_4{\cdot}7H_2O$ (2 mmol, 0.560 g) were dissolved in 20 mL of MeCN, and then $NEt_3$ was added (2 mmol, 0.202 g). The solution was stirred for 2 h and then filtered. Prismatic yellow crystals were obtained layering the final solution with 10 mL of diethylether. *Anal.* Calc. for $C_{60}H_{120}N_{18}Ni_8S_9O_{48}$ (**2**): C, 27.5; H, 4.61; N, 9.62; S, 11.02. Found: C, 26.5; H, 4.5; N, 8.5; S, 11.0%. Relevant IR bands ($cm^{-1}$): 3293(br), 2678(m), 2491(w), 1590(m), 1520(m), 1457(m), 1398(m), 1325(w), 1272(w), 1144(s), 1104(s), 984(m), 813(m), 653(w).

#### 2.2.3. $(Et_3NH)_2[Ni_{10}(dapdo)_8(MeOH)_4](BF_4)_6$ (**3**)

$DapdoH_2$ (1 mmol, 0.193 g) was dissolved in 20 mL of MeOH together with $Ni(BF_4)_2{\cdot}6H_2O$ (2 mmol, 0.680 g) and $NEt_3$ (2 mmol, 0.202 g). The solution was stirred at room temperature for a couple of hours and filtered. Red crystals were obtained by layering the filtrate with 10 mL of diethylether. *Anal.* Calc. for $B_6C_{88}F_{24}H_{120}N_{26}Ni_{10}O_{20}$ (3): C, 35.58; H, 4.07; N, 12.26. Found: C, 32.2; H, 3.6; N, 12.3%. Relevant IR bands ($cm^{-1}$): 3420(br), 1635(m), 1594(m), 1533(m), 1456(m), 1405(m), 1231(w), 1197(m), 1124(s), 1084(s), 1049(s), 722(w), 670(w).

### 2.3. Physical measurements

Magnetic susceptibility measurements were carried out on polycrystalline samples with a DSM5 Quantum Design susceptometer working in the range 30–300 K under magnetic fields of 0.3 T and under a field of 0.03 T in the 30–2 K range to avoid saturation effects. Diamagnetic corrections were estimated from Pascal Tables. Infrared spectra (4000–400 $cm^{-1}$) were recorded from KBr pellets on a Bruker IFS-125 FT-IR spectrophotometer.

### 2.4. X-ray crystallography

Data for compound **1** were collected on a red prismatic crystal on a Bruker APEX II CCD diffractometer with graphite monochromatized Mo Kα radiation. The structure was solved by Direct methods, using SHELXS computer program and refined by full-matrix least-squares method with SHELX97 computer program [15]. 2 H atoms were located from a difference map and refined with an overall isotropic thermal factor and 76 H atoms were placed at calculated positions on their carrier atom and refined using a riding model with an isotropic thermal factor 1.2 times that of their carrier atom.

Data for compounds **2** and **3** were collected on respectively yellow and red block on a Bruker APEX II CCD diffractometer on Advanced Light Source beamline 11.3.1 at Lawrence Berkeley National Laboratory, from a silicon 111 monochromator ($T$ = 100 K, $\lambda$ = 0.7749 Å). The structures were solved by direct methods and the refinement on $F^2$ and all further calculations were carried out using SHELX-TL suite [15]. In both cases, a huge portion of the cell has only very diffuse and disordered content, that could not be modeled. The contribution to the structure factors of the corresponding contents was taken into account with the SQUEEZE routine as implemented in PLATON program [16]. In both cases, the (relatively) small number of electrons found in one huge void confirms the very diffuse nature of the content, that could be reasonably ascribed to, respectively diethtlyammonium and triethylammonium cations, on basis of charge considerations and elemental analysis. While improving the quality of the structural parameters of the $[Ni_8]$ and $[Ni_{10}]$ complexes, this treatment impedes any discussion of packing and intermolecular interactions aspects. Crystallographic and experimental details of **1**–**3** are provided in Table 1.

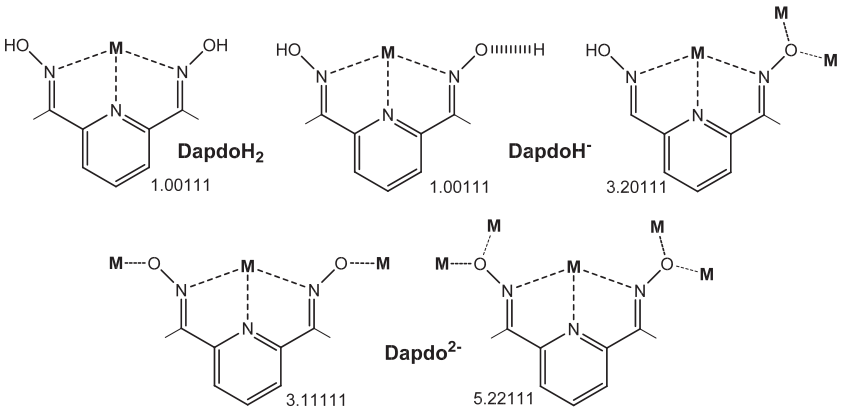


**Scheme 2.** Coordination modes for $dapdoH_2$, $dapdoH^-$ or $dapdo^{2-}$ ligands present in this work.

## 3. Results and discussion

### 3.1. Description of structures

#### 3.1.1. $[Ni_3(3\text{-Cl-BzO})(dapdo)(dapdoH)OH(dapdoH_2)](3\text{-Cl-BzO})\cdot 2.5CH_2Cl_2$ (**1**)

A labeled plot of the cationic trinuclear unit of **1** is shown in Fig. 1, and selected bond parameters are list in Table 2. This compound contains two similar but crystallographically non-equivalent molecules, **1a** and **1b**, and for clarity only **1a** will be described. The trinuclear unit consists of one tetracoordinated nickel atom, Ni(3), connected to two hexacoordinated Ni atoms, Ni(1,2), through a central $\mu_3$-OH group and one oximato group each. The tetracoordinated Ni atom, Ni(3), exhibits a distorted square-planar environment generated by the three N atoms of one 3.11111 $dapdo^{2-}$ ligand and by the central $\mu_3$-OH group. The hexacoordinated Ni atoms, Ni(1,2), are coordinated by the three N atoms of one 1.00111 $dapdoH_2$ and 1.00111 $dapdoH^-$ ligands, respectively, the central $\mu_3$-OH group and one oxime group from the first 3.11111 $dapdo^{2-}$ ligand. Finally, they complete their coordination sphere with one *syn–syn* 3-Cl-benzoate group that connects both hexacoordinated atoms, generating a slightly distorted octahedral environment. The two $dapdoH^-$ and $dapdoH_2$ ligands can also be seen as two $dapdoH^-$ ligands sharing the third hydrogen atom by means of one strong hydrogen bond (distance between O(12) and O(14) of 2.442(4) Å) as often is found in oxime chemistry [1].

Ni–N bond distances are in the 1.795(3)–2.237(3) Å range, corresponding the shorter ones to the square-planar Ni atom (bounded to the $dapdo^{2-}$ ligand) and the larger ones to the hexacoordinated Ni atoms, which are connected to the *pseudo-equivalent* $dapdoH^-dapdoH_2$. $N_{oxime}$–Ni–$N_{pyridyl}$ angles deviate from 90° due to the low bite angle of the ligand, being larger the angles generated by the $dapdo^{2-}$ ligand (around 83°) than the ones generated by the *pseudo-equivalent* $dapdoH^-dapdoH_2$ ligands (around 76°). Ni3–N–O–Ni1 and Ni3–N–O–Ni2 torsion angles deviate 27.6(3)° and 20.7(3)° from the planarity, respectively.

There is one 3-Cl-benzoate anion located over the Ni atoms plane (deviating 16.3° from that plane), which establishes, through only one oxygen atom (O(1 1 0)), strong hydrogen-bonds with the central $\mu_3$-OH group and both $dapdoH^-$ and $dapdoH_2$, O–H···O distances of 2.672(4), 2.617(4) and 2.623(4) Å, respectively. Packing of compound **1** reveals well isolated molecules which interacts by means of weak H-bonds with dichloromethane solvent molecules.

#### 3.1.2. $(NEt_2H_2)_6[Ni_8(dapdoH)_4(SO_4)_9(H_2O)_2]$ (**2**)

Fig. 2 shows a labeled plot of the anionic unit of **2**, while Table 3 lists selected bond parameters. This octanuclear compound can be described as two tetranuclear equivalent subunits linked through one $\mu_4$:$\eta^1$,$\eta^1$,$\eta^1$,$\eta^1$ (or 4.1111) sulfate group that binds two Ni atoms of each subunit.

Both tetranuclear subunits contain four hexacoordinated Ni atoms, two 3.20111 $dapdoH^-$ ligands, two $\mu_3$:$\eta^2$,$\eta^1$ (3.2100) and two $\mu_2$:$\eta^1$,$\eta^1$ (2.1100) sulfate groups and finally two water molecules. There are two kinds of metallic atoms: four central atoms (two in each subunit), linked to the 4.1111 $SO_4^{2-}$ group, and four peripheral ones. External atoms bind one $dapdoH^-$ ligand by its three N atoms, and three O atoms from two 3.2100 and one 2.1100 sulfate bridging ligands; giving a $NiN_3O_3$ coordination sphere. In contrast, each central Ni atom exhibits a $NiO_6$ environment, arising from two oxime bridging groups (that link both central Ni atoms), three different sulfate groups: the central 4.111, one 3.2100 and one 2.1100; and finally one water molecule.

Ni–N distances and N–Ni–N angles are between 1.972(6)–2.149(7) Å and 74.8(3) and 78.4(2)°, respectively (very similar to $dapdoH^-$ related in compound **1**), but Ni–N–O–Ni torsion angles are higher: Ni(3)–N–O–Ni(4), Ni(2)–N–O–Ni(1), Ni(1)–N–O–Ni(3) and Ni(4)–N–O–Ni(2) are 24.1(5), 30.3(5)°, 83.8(5)° and 85.4(5)°, respectively.

3.2100 and 2.1100 sulfate groups establish several intramolecular H bonds, with both protonated oxime groups and coordinated water molecules, with O–H···O distances around 2.586(7) Å for the first contacts and between 2.653(7) and 2.787(7) Å for $H_2O$–$SO_4^{2-}$ ones.

Finally, several intermolecular bonds are set between the $NEt_2H_2^+$, likely generated *in situ* by a $Ni^{2+}$ catalyzed reaction [17], and different sulfates groups, with N–H···O distances compressed in the 2.62(1)–2.955(9) Å range.

#### 3.1.3. $(Et_3NH)_2[Ni_{10}(dapdo)_8(MeOH)_4](BF_4)_6$ (**3**)

A plot of the cationic decanuclear compound **3** is shown in Fig. 3 and selected bond parameters are listed in Table 4. This compound can be described as an inner $\{Ni_4(dapdo^{2-})_4\}$ cubane surrounded by two trinuclear angular units. All inner nickel atoms altogether with two peripheral ones present hexacoordinated environment, while the remainder nickel atoms assemble a tetracoordinated environment. Each inner Ni atom is coordinated by one 5.22111 $dapdo^{2-}$ ligand through its three N atoms and three O atoms of three different oxime bridging groups (that come from two

**Table 1**
Crystal data and structure refinement for compounds **1**–**3**.

| | (**1**) | (**2**) | (**3**) |
|---|---|---|---|
| Formula | $C_{41}Cl_2H_{39}N_9Ni_3O_{11}\cdot 2.5CH_2Cl_2$ | $C_{60}H_{120}N_{18}Ni_8S_9O_{48}$ | $B_6C_{88}F_{24}H_{120}N_{26}Ni_{10}O_{20}$ |
| FW | 1293.118 | 2619.83 | 2969.82 |
| Space group | $P2_1/c$ | $P2_1/n$ | $F222$ |
| $a$ (Å) | 23.0119(9) | 14.6113(9) | 13.712(3) |
| $b$ (Å) | 21.8059(8) | 59.7516(4) | 28.474(5) |
| $c$ (Å) | 21.2374(9) | 32.9343(2) | 54.233(10) |
| $\alpha$ (°) | 90 | 90 | 90 |
| $\beta$ (°) | 100.180(3) | 92.908(10) | 90 |
| $\gamma$ (°) | 90 | 90 | 90 |
| $V$ (Å$^3$) | 10489.1(9) | 28716(3) | 21174(7) |
| $Z$ | 2 | 8 | 4 |
| $T$ (K) | 100(2) | 100(2) | 100(2) |
| $\lambda$ (Mo K$\alpha$) (Å) | 0.71073 | 0.7749 | 0.7749 |
| $d_{calc}$ (g cm$^{-3}$) | 1.665 | 1.212 | 0.932 |
| $\mu$ (Mo K$\alpha$) (mm$^{-1}$) | 1.515 | 1.548 | 1.173 |
| $R$ [$I > 2s(I)$] | 0.0442 | 0.0901 | 0.0908 |
| $wR$ [all data] | 0.1393 | 0.2383 | 0.2475 |
| $S$ [all data] | 1.065 | 1.049 | 1.022 |

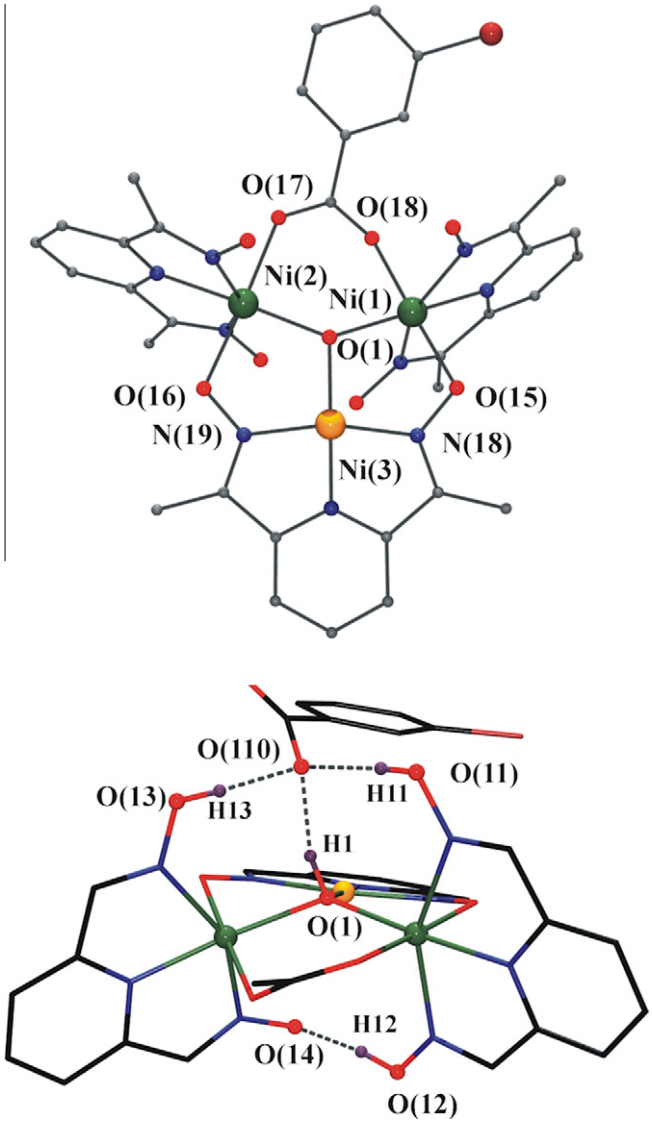


**Fig. 1.** Labeled plot of complex **1** (Top). Set of intra- and intermolecular H bonds (Bottom). Ni atoms in an octahedral or square-planar environment are plotted in green and orange color, respectively. H-atoms not involved in H-bonds, Me groups and coordinated benzoate ring have been omitted for clarity. (Color online.)

5.22111 and one 3.11111 dapdo$^{2-}$ ligands), resulting in a distorted octahedral $NiN_3O_3$ coordination sphere. The tetracoordinated Ni atoms adopt a square-planar $NiN_3O$ geometry given by the three N atoms of one 3.11111 dapdo$^{2-}$ ligand and one O-oximato atom from the 5.22111 dapdo$^{2-}$.

Finally, the hexacoordinated peripheral Ni atoms present a $NiO_6$ distorted octahedral environment arising from 4 oxime bridges of two 5.22111 and two 3.11111 dapdo$^{2-}$ ligands and two coordinated methanol molecules.

Ni–N distances are between 1.80(1) and 1.94(1) Å for 3.11111 dapdo$^{2-}$ ligands, and slightly higher for the ligand with 5.22111 coordinative mode (between 2.003(9) and 2.162(9) Å); while N–Ni–N angles are higher for 3.1111 ligand (around 82°) than for 5.22111 dapdo$^{2-}$ (around 76°).

### 3.2. Magnetic measurements and modelization

The temperature dependance of the $\chi_M T$ product for compound **1** is plotted in Fig. 4. The room-temperature $\chi_M T$ value is 2.24 cm$^3$ K cm$^{-1}$, slightly higher than the expected value of 2.00 cm$^3$ K cm$^{-1}$ for two Ni$^{II}$ atoms and $g = 2.00$, bearing in mind that one of the nickel atoms, in square-planar environment, is diamagnetic.

**Table 2**
Selected interatomic distances (Å) and angles (°) for compound **1**.

| | | | |
|---|---|---|---|
| Ni(1)–N(14) | 1.990(3) | Ni(1)–N(15) | 2.204(3) |
| Ni(1)–N(16) | 2.034(3) | Ni(1)–O(1) | 2.065(2) |
| Ni(1)–O(15) | 2.065(2) | Ni(1)–O(18) | 2.059(2) |
| Ni(2)–N(11) | 1.998(3) | Ni(2)–N(12) | 2.146(3) |
| Ni(2)–N(13) | 2.237(3) | Ni(2)–O(1) | 2.043(2) |
| Ni(2)–O(16) | 2.063(2) | Ni(2)–O(17) | 2.054(2) |
| Ni(3)–N(17) | 1.795(3) | Ni(3)–N(18) | 1.870(3) |
| Ni(3)–N(19) | 1.872(3) | Ni(3)–O(1) | 1.873(3) |
| Ni(4)–N(24) | 2.008(3) | Ni(4)–N(25) | 2.233(4) |
| Ni(4)–N(26) | 2.175(4) | Ni(4)–O(2) | 2.054(3) |
| Ni(4)–O(25) | 2.073(2) | Ni(4)–O(28) | 2.043(2) |
| Ni(5)–N(27) | 1.803(3) | Ni(5)–N(28) | 1.870(3) |
| Ni(5)–N(29) | 1.877(3) | Ni(5)–O(2) | 1.878(3) |
| Ni(6)–N(21) | 1.986(3) | Ni(6)–N(22) | 2.199(4) |
| Ni(6)–N(23) | 2.019(4) | Ni(6)–O(2) | 2.046(3) |
| Ni(6)–O(26) | 2.089(3) | Ni(6)–O(27) | 2.054(3) |
| N(14)–Ni(1)–N(15) | 75.1(1) | N(14)–Ni(1)–N(16) | 78.8(1) |
| N(11)–Ni(2)–N(12) | 76.7(1) | N(11)–Ni(2)–N(13) | 74.9(1) |
| N(17)–Ni(3)–N(18) | 82.8(1) | N(17)–Ni(3)–N(19) | 83.5(1) |
| Ni(1)–O(1)–Ni(2) | 127.6(1) | Ni(1)–O(1)–Ni(3) | 103.9(1) |
| Ni(2)–O(1)–Ni(3) | 110.4(1) | | |
| N(24)–Ni(4)–N(25) | 74.9(1) | N(24)–Ni(4)–N(26) | 76.1(1) |
| N(27)–Ni(5)–N(28) | 83.6(1) | N(27)–Ni(5)–N(29) | 82.4(1) |
| N(21)–Ni(6)–N(22) | 75.5(1) | N(21)–Ni(6)–N(23) | 79.4(1) |
| Ni(4)–O(2)–Ni(5) | 110.5(1) | Ni(4)–O(2)–Ni(6) | 126.6(1) |
| Ni(5)–O(2)–Ni(6) | 103.3(1) | | |
| Ni(1)–O(15)–N(18)–Ni(3) | 27.6(3) | Ni(2)–O(16)–N(17)–Ni(3) | 20.7(3) |
| Ni(4)–O(25)–N(28)–Ni(5) | 19.5(3) | Ni(6)–O(26)–N(29)–Ni(5) | 26.2(3) |

$\chi_M T$ decreases on cooling, first slowly ($\chi_M T$ value of 1.93 cm$^3$ K cm$^{-1}$ at 50 K) and then more sharply, until it reaches a value of 0.5 cm$^3$ K cm$^{-1}$ at 2 K. This decay indicates weak antiferromagnetic interaction, probably mixed with ZFS effects. The fit of the experimental data was made assuming isotropic interaction, using CLUMAG [18] program and applying the Hamiltonian:

$$H = -J(S_1 \cdot S_2)$$

where $S_1$ and $S_2$ are the spins carried by the hexacoordinated Ni(II) ions. The best fit parameters were $J = -5.75$ cm$^{-1}$ and $g = 2.11$, with $R = 4.40 \times 10^{-4}$ ($R = (\chi_M T_{calc} - \chi_M T_{obs})^2/(\chi_M T_{obs})^2$)). In good agreement with this antiferromagnetic interaction, magnetization versus field plot reaches a non-saturated value equivalent to 1.5 electrons under an external field of 5 T, slightly lower than expected for the Brillouin function of two uncoupled $S = 1$ centers.

Compound **2** was described before as two tetranuclear subunits linked by one 4.1111 sulfate group implying 16 interactions and five different coupling constants which means a clear overparametrization. Being known that the superexchange Ni–O–X–O–Ni interactions mediated by tetrahedral anions with electronegative central atoms (e.g. sulfate, perchlorate, phosphate, etc.) are weak or even negligible [14,19], to simplify the fit, this compound was treated as two separated tetramers.

The room temperature $\chi_M T$ value is 4.64 cm$^3$ K cm$^{-1}$, very close to the expected value of 4 cm$^3$ K cm$^{-1}$ for four Ni$^{2+}$ atoms, Fig. 4. Upon cooling, $\chi_M T$ gradually decreases down to a value of 0.74 cm$^3$ K cm$^{-1}$ at 2 K. Experimental data were fitted with CLUMAG program and the Hamiltonian built on Scheme 3:

$$H = -J_1(S_2 \cdot S_3) - J_2(S_2 \cdot S_1 + S_3 \cdot S_4) - J_3(S_2 \cdot S_4 + S_3 \cdot S_1) - J_4(S_1 \cdot S_4)$$

The best fit parameters obtained were $J_1 = -11.12$ cm$^{-1}$, $J_2 = -6.34$ cm$^{-1}$, $J_3 = -6.59$ cm$^{-1}$, $J_4 = -3.31$ cm$^{-1}$ and $g = 2.19$. Taking into account that $J_2$ and $J_3$ have similar values, a new fit was performed to adjust the plot with the three-J Hamiltonian:

$$H = -J_1(S_2 \cdot S_3) - J_2(S_2 \cdot S_1 + S_2 \cdot S_4 + S_3 \cdot S_1 + S_3 \cdot S_4) - J_3(S_1 \cdot S_4)$$

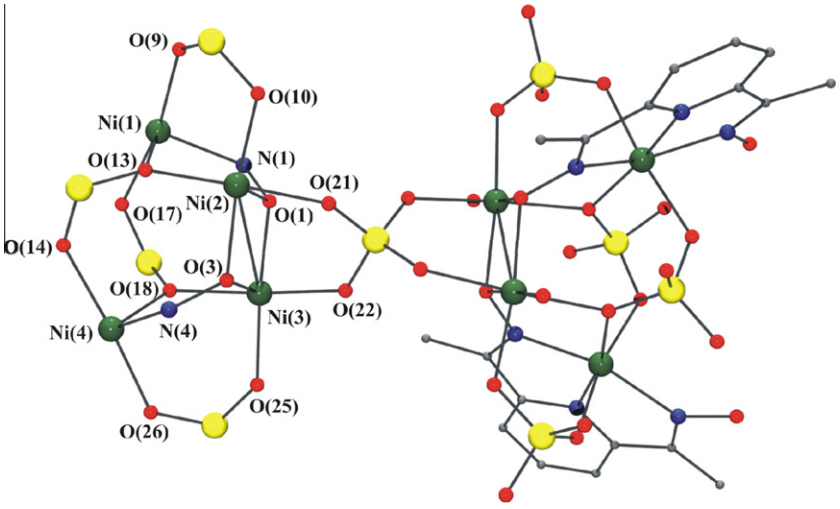


**Fig. 2.** Partially labeled plot of complex **2**. Ni atoms in octahedral environment are plotted in green and sulfur atoms in orange color. Complete oximato ligands have been plotted only in the right side of the complex whereas left side shows only the core. (Color online.)

**Table 3**
Selected interatomic distances (Å) and angles (deg) for one tetrameric subunit of compound **2**.

| | | | |
|---|---|---|---|
| Ni(1)–N(1) | 2.039(5) | Ni(1)–N(2) | 2.149(6) |
| Ni(1)–N(3) | 1.973(6) | Ni(1)–O(9) | 2.120(5) |
| Ni(1)–O(13) | 2.058(5) | Ni(1)–O(17) | 2.089(5) |
| Ni(2)–O(1) | 2.025(5) | Ni(2)–O(3) | 2.045(5) |
| Ni(2)–O(10) | 2.044(4) | Ni(2)–O(13) | 2.134(5) |
| Ni(2)–O(21) | 2.066(4) | Ni(3)–O(1) | 2.042(4) |
| Ni(3)–O(3) | 2.047(5) | Ni(3)–O(18) | 2.151(4) |
| Ni(3)–O(22) | 2.046(4) | Ni(3)–O(25) | 2.050(4) |
| Ni(4)–N(4) | 2.033(5) | Ni(4)–N(5) | 2.136(5) |
| Ni(4)–N(6) | 1.975(6) | Ni(4)–O(14) | 2.088(5) |
| Ni(4)–O(18) | 2.032(5) | Ni(4)–O(26) | 2.088(5) |
| N(1)–Ni(1)–N(3) | 78.4(2) | N(2)–Ni(1)–N(3) | 75.3(3) |
| N(4)–Ni(4)–N(6) | 78.3(2) | N(4)–Ni(4)–N(6) | 75.6(2) |
| Ni(1)–O(13)–Ni(2) | 107.9(2) | Ni(2)–O(1)–Ni(3) | 94.7(2) |
| Ni(2)–O(3)–Ni(3) | 93.9(2) | | |
| Ni(1)–N(1)–O(1)–Ni(2) | 30.3(5) | Ni(1)–N(1)–O(1)–Ni(3) | 83.8(5) |
| Ni(1)–O(17) ···O(18)–Ni(3) | 29.4(3) | Ni(1)–O(14) ···O(13)–Ni(4) | 99.8(2) |
| Ni(1)–O(17) ···O(18)–Ni(4) | 98.6(2) | Ni(2)–O(13) ···O(14)–Ni(4) | 29.2(4) |
| Ni(3)–O(25) ···O(26)–Ni(4) | 27.3(3) | Ni(4)–N(4)–O(3)–Ni(2) | 85.4(5) |
| Ni(4)–N(4)–O(3)–Ni(3) | 24.1(5) | | |

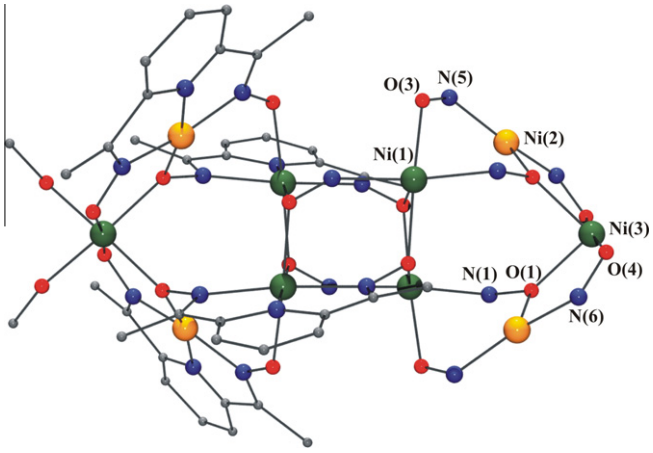


**Fig. 3.** Partially labeled plot of complex **3**. Ni atoms in octahedral or square planar environment are plotted in green and orange color in that order. Complete oximato ligands have been plotted only in the left side of the complex whereas right side shows only the core. (Color online.)

**Table 4**
Selected interatomic distances (Å) and angles (°) for compound **3**.

| | | | |
|---|---|---|---|
| Ni(1)–N(1) | 2.070(9) | Ni(1)–N(2) | 2.162(9) |
| Ni(1)–N(3) | 2.003(9) | Ni(1)–O(2) | 2.079(9) |
| Ni(1)–O(2′) | 2.099(7) | Ni(1)–O(3) | 2.103(7) |
| Ni(2)–N(5) | 1.94(1) | Ni(2)–N(6) | 1.91(1) |
| Ni(2)–N(7) | 1.80(1) | Ni(2)–O(1) | 1.830(9) |
| Ni(3)–O(1) | 2.081(9) | Ni(3)–O(4) | 1.984(8) |
| Ni(3)–O(5) | 2.04(1) | | |
| N(1)–Ni(1)–N(3) | 75.4(4) | N(2)–Ni(1)–N(3) | 76.0(4) |
| N(5)–Ni(2)–N(7) | 81.2(5) | N(6)–Ni(2)–N(7) | 82.2(5) |
| Ni(1)–O(2)–Ni(1′) | 100.3(3) | Ni(2)–O(1)–Ni(3) | 117.9(4) |
| Ni(1)–N(1)–O(1)–Ni(2) | 42(1) | Ni(1)–N(1)–O(1)–Ni(3) | 117.8(7) |
| Ni(1)–N(2)–O(2)–Ni(1′) | 66(1) | Ni(1)–N(2)–O(2)–Ni(1″) | 50.0(9) |
| Ni(2)–N(5)–O(3)–Ni(1) | 33(1) | Ni(2)–N(6)–O(4)–Ni(3) | 16(1) |

Best fit parameters with this second Hamiltonian were: $J_1 = -10.84\ cm^{-1}$, $J_2 = -6.52\ cm^{-1}$, $J_3 = -3.17\ cm^{-1}$, $g = 2.19$ and $R = 4.17 \times 10^{-4}$, consistent with the ones obtained before.

Magnetization plot shows a non-saturated value equivalent to of 1.4 electrons at 5 T, due to the existence of several low-energy excited states. The moderately weak antiferromagnetic interactions found for **2** are in good agreement with the poorly efficient

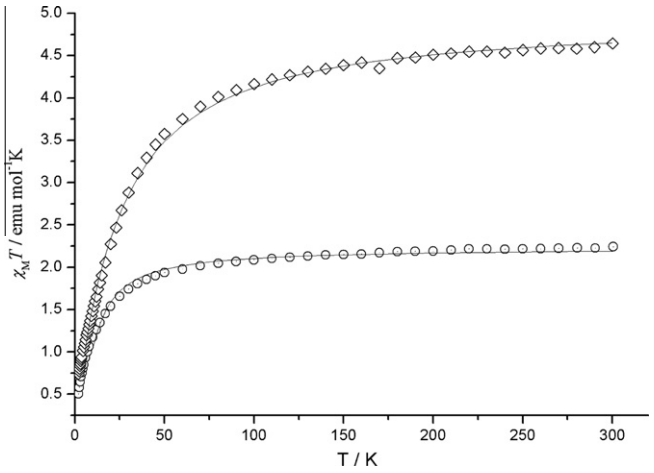


**Fig. 4.** Plot of the $\chi_M T$ product vs. $T$ for compounds **1** (dot centered circles) and **2** (diamonds). Data plotted for **2** corresponds to one tetrameric subunit. The solid lines show the best fit of the experimental data.

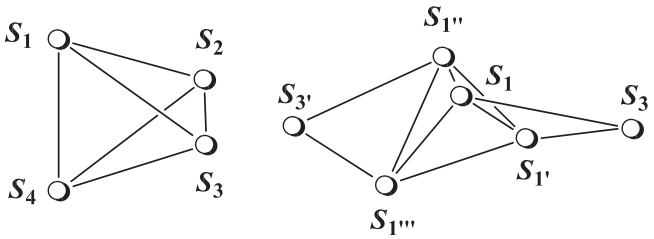


**Scheme 3.** Coupling scheme for compounds **2** (left) and **3** (right).

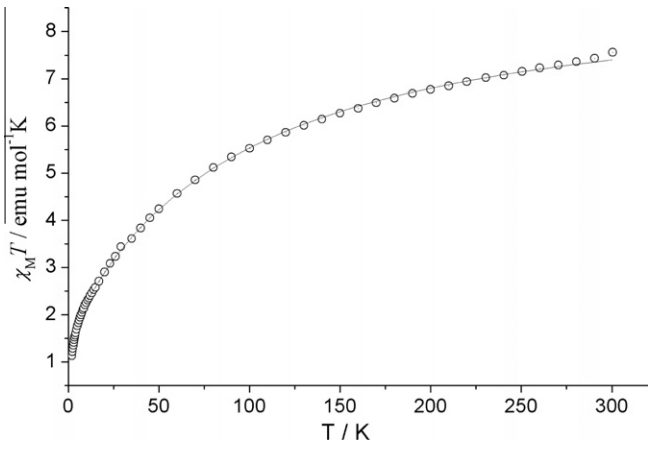


**Fig. 5.** Plot of the $\chi_M T$ product vs. T for compound **3**.

coupling mediators present in the molecule (sulfates and oximate bridges with large torsion angles close to 90°).

The $\chi_M T$ versus $T$ plot for compound **3**, Fig. 5, decreases continuously on cooling, from 7.55 $cm^3\,K\,cm^{-1}$ at 300 K to 1.10 $cm^3\,K\,cm^{-1}$ at 2 K.

Experimental data was fitted with CLUMAG [18] program and the Hamiltonian

$$H = -J_1(S_1\cdot S_3 + S_{1'}\cdot S_3 + S_{1''}\cdot S_{3'} + S_{1'''}\cdot S_{3'}) - J_2(S_1\cdot S_{1''} + S_{1'}\cdot S_{1'''}) - J_3(S_1\cdot S_{1'''} + S_{1'}\cdot S_{1''}) - J_4(S_1\cdot S_{1'} + S_{1''}\cdot S_{1'''})$$

which considers four different coupling constants, Scheme 3, and takes into account that the four square-planar Ni atoms are diamagnetic. Best fit parameters obtained were $J_1 = -7.79\ cm^{-1}$, $J_2 = -27.16\ cm^{-1}$, $J_3 = -28.61\ cm^{-1}$, $J_4 = -21.69\ cm^{-1}$ and $g = 2.43$. Considering the similar value of $J_2$ and $J_3$, and the comparable torsion angles (51.85° and 62.76°, respectively), we assumed that $J_2 = J_3$ in order to minimize the number of coupling constants in the fitting process, so a new adjustment was made with CLUMAG program and the three-$J$ Hamiltonian:

$$H = -J_1(S_1\cdot S_3 + S_{1'}\cdot S_3 + S_{1''}\cdot S_{3'} + S_{1'''}\cdot S_{3'}) - J_2(S_1\cdot S_{1''} + S_{1'}\cdot S_{1'''} + S_1\cdot S_{1'''} + S_{1'}\cdot S_{1''}) - J_3(S_1\cdot S_{1'} + S_{1''}\cdot S_{1'''})$$

New best fit parameters were: $J_1 = -8.37\ cm^{-1}$, $J_2 = -29.61\ cm^{-1}$, $J_3 = -25.49\ cm^{-1}$, $g = 2.44$ and $R = 4.75 \times 10^{-5}$; consistent with the calculated previously. Due to the energetic proximity of excited states, the magnetization plot of **3** shows a non-saturated value of 3 electrons at 5 T, much higher than the expected for an $S = 0$ system.

## 4. Conclusions

The reported compounds provided a new example of the ability of pyridyldioximato ligands to promote interesting molecular architectures. Comparison of the new structures with the previously reported nickel compounds confirms that this ligand tends to low nuclearity clusters with triangular motifs when carboxylates act as additional bridges whereas is prone to large nuclearities with unusual topology in non-carboxylato chemistry.

## Acknowledgements

This work was supported by the CICYT Project CTQ2009-07264. A.E. thanks financial support from excellence in research ICREA-Academia award. The Advanced Light Source is supported by the Director, Office of Science, Office of Basic Energy Sciences of the US Department of Energy under Contract No. DE-AC02-05CH11231.

## Appendix A. Supplementary material

CCDC 882559, 882560 and 882561 contain the supplementary crystallographic data for compounds **1**–**3**. These data can be obtained free of charge via http://www.ccdc.cam.ac.uk/conts/retrieving.html, or from the Cambridge Crystallographic Data Centre, 12 Union Road, Cambridge CB2 1EZ, UK; fax: (+44) 1223-336-033; or e-mail: deposit@ccdc.cam.ac.uk.

## References

[1] C.J. Milios, T.C. Stamatatos, S.P. Perlepes, Polyhedron 25 (2006) 134.
[2] T.C. Stamatatos, E. Diamantopoulou, C.P. Raptopoulou, V. Psycharis, A. Escuer, S.P. Perlepes, Inorg. Chem. 46 (2007) 2350.
[3] C.-M. Ji, H.-J. Yang, C.-C. Zhao, V. Tangoulis, A.-L. Cui, H.-Z. Kou, Cryst. Growth Des. 9 (2009) 4607.
[4] (a) A. Pajunen, I. Mutikainen, H. Saarinen, M.Z. Orama, Kristallogr. New Cryst. Struct. 214 (1999) 217;
(b) S. Khanra, T. Weyhermuller, E. Rentschler, P. Chaudhuri, Inorg. Chem. 44 (2005) 8176;
(c) T.C. Stamatatos, E. Diamantopoulou, A. Tasiopoulos, V. Psycharis, R. Vicente, C.P. Raptopoulou, V. Nastopoulos, A. Escuer, S.P. Perlepes, Inorg. Chim. Acta 359 (2006) 4149;
(d) T.C. Stamatatos, C. Papatriantafyllopoulou, E. Katsoulakou, C.P. Raptopoulou, S.P. Perlepes, Polyhedron 26 (2007) 1830.
[5] G. Psomas, C. Dendrinou-Samara, M. Alexiou, A. Tsohos, C.P. Raptopoulou, A. Terzis, D.P. Kessissoglou, Inorg. Chem. 37 (1998) 6556.
[6] (a) T.C. Stamatatos, K.A. Abboud, S.P. Perlepes, G. Christou, Dalton Trans. (2007) 3861;
(b) C. Papatriantafyllopoulou, L.F. Jones, T.D. Nguyen, N. Matamoros-Salvador, L. Cunha-Silva, F.A.A. Paz, J. Rocha, M. Evangelisti, E.K. Brechin, S.P. Perlepes, Dalton Trans. (2008) 3153;
(c) T.C. Stamatatos, A. Escuer, K.A. Abboud, C.P. Raptopoulou, S.P. Perlepes, G. Christou, Inorg. Chem. 47 (2008) 11825;

(d) J. Esteban, L. Alcázar, M. Torres-Molina, M. Monfort, M. Font-Bardia, A. Escuer, Inorg. Chem. 51 (2012) 5503.
[7] C. Papatriantafyllopoulou, T.C. Stamatatos, W. Wernsdorfer, S.J. Teat, A. Tasiopoulos, A. Escuer, S.P. Perlepes, Inorg. Chem. 49 (2010) 10486.
[8] (a) C.J. Milios, E. Kefalloniti, C.P. Raptopoulou, A. Terzis, R. Vicente, N. Lalioti, A. Escuer, S.P. Perlepes, Chem. Commun. (2003) 819;
(b) C.J. Milios, T.C. Stamatatos, P. Kyritsis, A. Terzis, C.P. Raptopoulou, R. Vicente, A. Escuer, S.P. Perlepes, Eur. J. Inorg. Chem. (2004) 2885;
(c) C.C. Stoumpos, T.C. Stamatatos, V. Psycharis, C.P. Raptopoulou, G. Christou, S.P. Perlepes, Polyhedron 27 (2008) 3703;
(d) C.C. Stoumpos, T.C. Stamatatos, H. Sartzi, O. Roubeau, A.J. Tasiopoulos, V. Nastopoulos, S.J. Teat, G. Christou, S.P. Perlepes, Dalton Trans. (2009) 1004;
(e) O. Roubeau, L. Lecren, Y.G. Li, X.F. Le Goff, R. Clerac, Inorg. Chem. Commun. 8 (2005) 314;
(f) C. Papatriantafyllopoulou, C.P. Raptopoulou, A. Escuer, C.J. Milios, Inorg. Chim. Acta 360 (2007) 61;
(g) C. Dendrinou-Samara, C.M. Zaleski, A. Evagorou, J.W. Kampf, V.L. Pecoraro, D.P. Kessissoglou, Chem. Commun. (2003) 2668;
(h) B.C. Unni Nair, J.E. Sheats, R. Ponteciello, D. Van Engen, V. Petrouleas, G.C. Dismukes, Inorg. Chem. 28 (1989) 1582;
(i) R.E. Marsh, Inorg. Chem. 29 (1990) 572;
(j) A. Escuer, B. Cordero, X. Solans, M. Font-Bardia, T. Calvet, Eur. J. Inorg. Chem. (2008) 5082;
(k) T.C. Stamatatos, B.S. Luisi, B. Moulton, G. Christou, Inorg. Chem. 47 (2008) 1134;
(l) S. Khanra, T. Weyhermüller, P. Chaudhuri, Dalton Trans. (2008) 4885.
[9] (a) C.W. Glynn, M.M. Turnbull, Transition Met. Chem. 27 (2002) 822;
(b) M.A. Halcrow, C.A. Kilner, J. Wolowska, E.J.L. McInnes, A.J. Bridgeman, New J. Chem. 28 (2004) 228;
(c) B.A. Bovenzi, G.A. Pearse Jr., J. Chem. Soc., Dalton Trans. (1997) 2793;
(d) G.A. Nicholson, J.L. Petersen, B.J. McCormick, Inorg. Chem. 21 (1982) 3274;
(e) I.V. Vasilevsky, R.E. Stenkamp, E.C. Lingafelter, V. Schomaker, R.D. Willett, N.J. Rose, Inorg. Chem. 28 (1989) 2619;
(f) K.A. Abboud, R.C. Palenik, G.J. Palenik, Acta Crystallogr., Sect. C C50 (1994) 525;
(g) G.A. Nicholson, J.L. Petersen, B.J. McCormick, Inorg. Chem. 19 (1980) 195.
[10] (a) M. Murugesu, K.A. Abboud, G. Christou, Polyhedron 23 (2004) 2779;
(b) I.V. Vasilevsky, R.E. Stenkamp, E.C. Lingafelter, N.J. Rose, J. Coord. Chem. 19 (1988) 171.
[11] (a) S. Khanra, T. Weyhermüller, P. Chaudhuri, Dalton Trans. (2007) 4675;
(b) C. Lampropoulos, T.C. Stamatatos, K.A. Abboud, G. Christou, Inorg. Chem. 48 (2009) 429.
[12] (a) A. Escuer, J. Esteban, N. Aliaga-Alcalde, M. Font-Bardia, T. Calvet, O. Roubeau, S.J. Teat, Inorg. Chem. 39 (2010) 2259;
(b) A. Escuer, J. Esteban, O. Roubeau, Inorg. Chem. 50 (2011) 8893.
[13] R.A. Coxall, S.G. Harris, D.K. Henderson, S. Parsons, P.A. Tasker, R.E.P. Winpenny, J. Chem. Soc., Dalton Trans. (2000) 2349.
[14] C. Papatriantafyllopoulou, E. Manessi-Zoupa, A. Escuer, S.P. Perlepes, Inorg. Chim. Acta 362 (2009) 634.
[15] (a) G.M. Sheldrick, SHELXTL, Bruker AXS Inc., Madison, Wisconsin, USA.;
(b) G.M. Sheldrick, Acta Crystallogr., Sect. A 64 (2008) 112.
[16] (a) A.L. Spek, PLATON, A Multipurpose Crystallographic Tool, Utrecht University, Utrecht, The Netherlands, 2008;
(b) A.L. Spek, J. Appl. Crystallogr. 36 (2003) 7.
[17] B.-Q. Xu, T. Yamaguchi, K. Tanabe, Chem. Lett. (1988) 281.
[18] D. Gatteschi, L. Pardi, Gazz. Chim. Ital. 123 (1993) 231.
[19] (a) C. Papatriantafyllopoulou, G. Aromi, A.J. Tasiopoulos, V. Nastopoulos, V.C. Raptopoulou, S.J. Teat, A. Escuer, S.P. Perlepes, Eur. J. Inorg. Chem. (2007) 2761;
(b) C. Papatriantafyllopoulou, C.G. Efthymiou, C.P. Raptopoulou, R. Vicente, E. Manessi-Zoupa, V. Psycharis, A. Escuer, S.P. Perlepes, J. Mol. Struct. 829 (2007) 176.

### 3.3.1. Resum: Polynuclear pyridyldioximato-nickel(II) clusters: Synthesis, structure and magnetic study.

Jordi Esteban, Albert Escuer, Mercè Font-Bardia, Olivier Roubeau, Simon J. Teat.

*Polyhedron* **2013**, *52*, 339-345.

En aquest treball es presenten els últims resultats obtinguts pel lligand dapdo$H_2$ emprant tres sals de níquel(II) amb anions de característiques molt diferents: un carboxilat, un anió no carboxilat coordinant i un anió no carboxilat no coordinant. Com a resultat es va obtenir el complex catiònic $[Ni_3(dapdoH_2)(3\text{-}ClBzO)(dapdo)(dapdoH)OH](3\text{-}ClBzO)$ amb l'anió 3-clorobenzoat (**3_1**), el complex aniònic $(Et_2NH_2)_6[Ni_8(H_2O)_2(dapdoH)_4(SO_4)_9]$ a partir de $NiSO_4$ (**3_2**) i per últim el compost $(Et_3NH)_2[Ni_{10}(MeOH)_4(dapdo)_8](BF_4)_6$ (**3_3**) a partir de l'anió tetrafluoroborat.

Els aspectes més destacables d'aquests clústers són la topologia que presenta el compost **3_2** (dos subunitats tetranuclears equivalents unides entre elles per un anió sulfat central, unit a dos cations $Ni^{II}$ de cada fragment, figura 10) i la connectivitat de l'anió sulfat: $\mu_4{:}\eta_1,\eta_1,\eta_1,\eta_1$ o 4.1111. El compost **3_1** presenta una estructura molt similar a **1_2**, mentre que **3_3** genera un *core* semblant a **2_4**, en què els dos co-lligands dicianamida són substituïts per metanol i el canvi de càrrega es compensa amb anions tetrafluoroborat (el compost cristal·litza amb dos cations $NEt_3H^+$ i dos anions $BF_4^-$ addicionals).

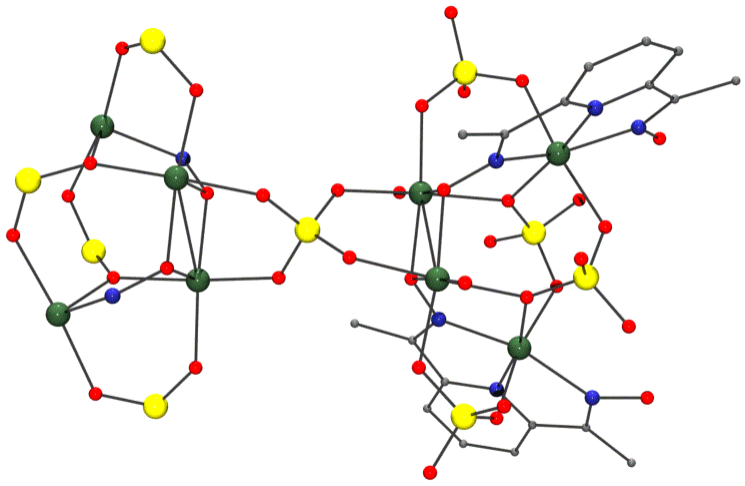

**Figura 10.** Estructura del compost **3_2**. S'han eliminat els lligands $dapdoH^-$ al fragment de l'esquerra per a una millor visió dels ponts sulfat i oxima.

Pel què fa a l'estudi magnètic d'aquests compostos, tots presenten un comportament antiferromagnètic que provoca la disminució de $\chi_M T$ en baixar la temperatura. L'acoblament per mitjà de ponts sulfat no es va contemplar ja que el superintercanvi magnètic per mitjà d'anions tetraèdrics (fosfats, perclorats, sulfats, etc.) es pot estimar negligible.[132,168]

Cal remarcar que en aquest article es va provar novament la capacitat coordinativa d'aquest lligand i la forta dependència entre les característiques de la sal de partida (lligands carboxilat o no carboxilat, ja siguin coordinants o no coordinants) i la topologia del clúster resultant.

## 3.4. Article 4.

## Triangular nickel complexes derived from 2-pyridylcyanoxime: An approach to the magnetic properties of the $[Ni_3(\mu_3\text{-}OH)\{pyC(R)NO\}_3]^{2+}$ core.

**Jordi Esteban**, Eliseo Ruiz, Mercè Font-Bardia, Teresa Calvet, Albert Escuer.

*Chemistry, A European Journal* **2012**, *18*, 3637-3648.

FULL PAPER

DOI: 10.1002/chem.201102987

# Triangular Nickel Complexes Derived from 2-Pyridylcyanoxime: An Approach to the Magnetic Properties of the $[Ni_3(\mu_3\text{-}OH)\{pyC(R)NO\}_3]^{2+}$ Core

**Jordi Esteban,[a] Eliseo Ruiz,[b] Mercé Font-Bardia,[c] Teresa Calvet,[c] and Albert Escuer*[a]**

**Abstract:** A series of nickel complexes with nuclearity ranging from $Ni_3$ to $Ni_6$ have been obtained by treatment of a variety of nickel salts with the 2-pyridylcyanoxime ligand. The reported compounds have as a common structural feature the triangular arrangement of nickel cations bridged by a central $\mu_3$-oxo/alkoxo ligand. These compounds are simultaneously the first nickel derivatives of the 2-pyridylcyanoxime ligand and the first examples of isolated, $\mu_3$-O triangular pyridyloximate nickel complexes. Magnetic measurements reveal antiferromagnetic interactions promoted by the $\mu_3$-O and oximato superexchange pathways and comparison of the experimental structural and magnetic data with DFT calculations give an in-depth explanation of the factors that determine the magnetic interaction in this kind of system.

**Keywords:** cluster compounds · coordination chemistry · density functional calculations · magnetic properties · nickel

## Introduction

Triangular arrangement of paramagnetic cations is a significant topology in cluster chemistry either on account of their intrinsic properties or as common fragments in larger cages or extended structures such as Kagome networks. Equilateral triangular systems exhibit spin frustration[1] and become adequate systems for the study of subtle phenomena such as the antisymmetric exchange interaction.[1] A particular class of triangles are those that contain a central $\mu_3$-O donor (oxo, hydroxo or alkoxo groups) and bridging oximato ligands that define the sides of the triangle (Scheme 1). Most of the reported complexes with the $[M_3(\mu_3\text{-}O)\{pyC(R)NO\}_3]^{n+}$ core (in which $pyC(R)NO^- = $ pyridyloximate ligands) are $Cu^{II}$ derivatives[2] in contrast with the very rare examples of isolated triangular clusters reported with manganese,[3] iron[4] or cobalt.[5] It is surprising that similar triangular units can only be found as a recognisable fragment in a few larger-nuclearity nickel clusters.[6] Related $[Mn_3(\mu_3\text{-}O)(R\text{-salox})]^{n+}$ (salox = salicyloxime) complexes derived from salicyloximate ligands and that include trivalent manganese cations have been widely studied in the search for single-molecule magnets (SMMs) in recent years.[7]

In recent years, nickel–oximato clusters derived from 2-pyridyloximes, (py)C(R)NOH,[8] have yielded a surprisingly rich chemistry: clusters with a large variety of nuclearities and topologies have been reported for R = H,[9] Me,[6a,9d,10] Ph[6a,9d,e,10,11] or py;[9h,12] nuclearities of up to $Ni_{14}$[9g,h] have been reached by employing the ligands summarised in Scheme 1.

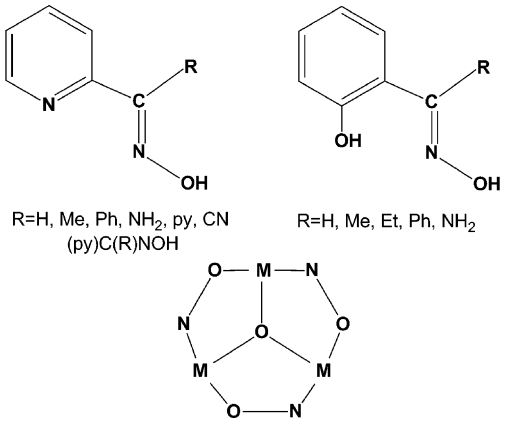


Scheme 1. Top: 2-Pyridyloxime ((py)C(*R*)NOH) and salicyloxime (R-salox) ligands referenced in the text. Bottom: Equilateral arrangement of an $\{M_3(\mu_3\text{-}O)(\mathbf{L}\text{-}NO)_3\}$ fragment.

[a] J. Esteban, Prof. A. Escuer
Departament de Química Inorgànica
Universitat de Barcelona, Av. Diagonal 645
08028 Barcelona (Spain)
Fax: (+34) 934907725
E-mail: albert.escuer@qi.ub.es

[b] Prof. E. Ruiz
Departament de Química Inorgànica and
Institut de Química Teòrica i Computacional
Universitat de Barcelona, Av. Diagonal 645
08028 Barcelona (Spain)

[c] Dr. M. Font-Bardia, Dr. T. Calvet
Departament de Cristallografia
Mineralogia i Diposits
Universitat de Barcelona, Martí I Franqués s/n
08028 Barcelona (Spain)

  

CHEMISTRY
A EUROPEAN JOURNAL

In the search for new properties in pyridyloxime chemistry, the choice of the ligand plays a fundamental role, and the properties induced by the R group of (py)C(R)NOH-type ligands is far from negligible. Coordination chemistry of 2-pyridylcyanoxime remains unexplored and only some copper derivatives with unusual $\mu_3$-O and $\mu_4$-O bridges have been recently reported by the authors.[2g] Following our work with the 2-pyridylcyanoxime ligand, we report the syntheses and structural characterisation of the first series of nickel complexes derived from 2-pyridylcyanoxime with the formulas $[Ni_3(MeOH)_2(BzO)(OH)\{pyC(CN)NO\}_4]$ (**1**), $(NEt_3H)\{\mu_{1,5}\text{-}N(CN)_2\}[Ni_6(H_2O)(MeOH)(3\text{-}ClBzO)_2(OH)_2\{pyC(CN)NO\}_8]$ (**2**), $[Ni_4(MeOH)_2(tfacac)_2(MeO)_2\{pyC(CN)NO\}_4]$ (**3**), $[Ni_5(MeOH)_4(3\text{-}ClBzO)_4(OH)_2\{pyC(CN)NO\}_4]$ (**4**) and $[Ni_5(H_2O)_4(N_3)_2(BzO)_2(OH)_2\{pyC(CN)NO\}_4]$ (**5**) in which $pyC(CN)NO^-$ is the deprotonated form of 2-pyridylcyanoxime, $BzO^-$ is benzoate and tfacac is trifluoroacetylacetonate. Complexes **1**–**5** exhibit a variety of topologies that are composed of different combinations of $\mu_3$-O triangular subunits (Scheme 2).

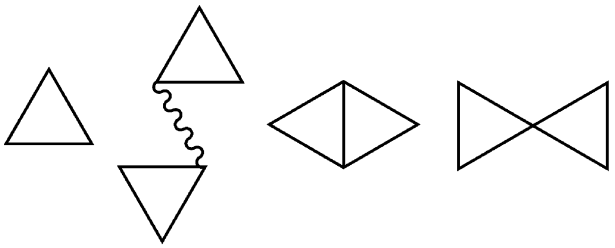

Scheme 2. Triangular-based core for the $Ni_3$ (**1**), $(Ni_3)_2$ (**2**), $Ni_4$ (**3**) and $Ni_5$ (**4**, **5**) compounds reported in this work.

Bearing in mind that the magnetic properties for this kind of nickel triangular topology system have not been established, we have devoted our attention to elucidating their magnetic response by combining experimental magnetic susceptibility measurements and DFT calculations, from which a complete description of the magnetic response of the $\mu_3$-O nickel–oximate system is proposed.

## Results and Discussion

**Synthetic comments**: In the search for ligands that can induce new structural features, the adequate addition of one R function to ligands that have previously proved to be adequate for the syntheses of cluster compounds becomes a rational way to design new ligands. The influence of the added R function can be effective in several aspects, the steric hindrance or the electronic effects being among the most relevant. We have taken 2-pyridylaldoximate (paoH) as a reference ligand; an adequate position to place additional R groups is on the carbon atom in the vicinity of the oximato function. With this idea in mind, we started a systematic exploration of the 2-pyridylcyanoxime ligand. When R = −CN, the acidity of the cyanoxime function becomes $10^3$–$10^5$ times greater than that of common oximes in which R is an aliphatic or aromatic group[8b] and thus it can induce strong electronic effects. Very recently, we reported the first derivatives of the 2-pyridylcyanoxime ligand in copper chemistry and the rare coordination of deprotonated $\mu_3$-O and $\mu_4$-O oxo donors was characterised,[2g] thereby suggesting that the strong increase in acidity of the donors enhances the properties of clusters with divalent cations to those typical of the trivalent ones. For $Ni^{II}$, this ligand easily promotes $\mu_3$-OH coordination into triangular units, which is extremely rare when employing other pyridyloximato ligands.

### Structural descriptions

*$[Ni_3(MeOH)_2(BzO)(OH)\{pyC(CN)NO\}_4]\cdot 3MeOH$ (**1**·3MeOH)*: A view of the core of complex **1** is illustrated in Figure 1. Selected interatomic distances and angles for **1** are listed in Table 1. The core of this neutral compound can be described as a distorted trinuclear isosceles arrangement of octahedrally coordinated $Ni^{II}$ atoms linked by one $\mu_3$-OH ligand with its oxygen atom placed 0.621(2) Å out of the plane defined by the three nickel atoms. Two sides of the triangle are defined by single oximato bridges, which link Ni(2) with Ni(1) and Ni(3), and the third side is defined by one oximato and one *syn–syn* carboxylato bridge between Ni(1) and Ni(3). Coordination spheres for Ni(1) and Ni(3) contain the $\mu_3$-OH ligand, one O atom from the *syn--syn*

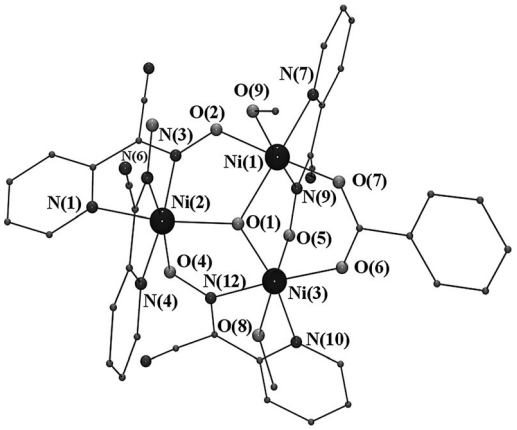


Figure 1. Partially labelled molecular structure of the triangular compound **1**. Hydrogen atoms of the organic ligands and the central OH group and solvent molecules have been suppressed for clarity.

Table 1. Selected distances [Å] and angles [°] of the core of compound **1**.

| | | | |
|---|---|---|---|
| Ni(1)−O(1) | 2.060(2) | Ni(1)-O(1)-Ni(2) | 116.28(8) |
| Ni(2)−O(1) | 2.053(2) | Ni(2)-O(1)-Ni(3) | 115.11(7) |
| Ni(3)−O(1) | 2.052(2) | Ni(1)-O(1)-Ni(3) | 102.16(7) |
| Ni(1)-O(2)-N(3) | 117.5(1) | Ni(1)-N(9)-O(5) | 123.7(1) |
| Ni(2)-O(4)-N(12) | 116.2(1) | Ni(2)-N(3)-O(2) | 126.9(1) |
| Ni(3)-O(5)-N(9) | 110.5(1) | Ni(3)-N(12)-O(4) | 125.3(1) |
| Ni(1)···Ni(2) | 3.465(2) | Ni(1)-O(2)-N(3)-Ni(2) | 3.3(2) |
| Ni(2)···Ni(3) | 3.494(2) | Ni(2)-O(4)-N(12)-Ni(3) | 17.0(2) |
| Ni(1)···Ni(3) | 3.199(2) | Ni(3)-O(5)-N(9)-Ni(1) | 16.7(2) |

  

benzoato ligand, one oximato bridge with Ni(2), one pyC(CN)NO$^-$ ligand and one methanol solvent molecule, whereas Ni(2) links two pyC(CN)NO$^-$ ligands, the central OH$^-$ group and one O-oximato atom, thereby resulting in an $N_2O_4$ environment for Ni(1) and Ni(3) and an $N_4O_2$ environment for Ni(2). Bond angles that involve the central $\mu_3$-OH group are 116.28(8)° for Ni(1)-O(1)-Ni(2), 115.11(7)° for Ni(3)-O(1)-Ni(2) and 102.16(7)° for Ni(1)-O(1)-Ni(3); the corresponding Ni···Ni distances are 3.465(2), 3.494(2) and 3.199(2) Å, respectively.

The four oximato ligands are deprotonated, but one of them, which is coordinated to Ni(2), acts as a terminal ligand and interacts by means of one strong hydrogen bond with one of the coordinated solvent molecules; there is an O(3)···O(9) distance of 2.682(3) Å. Ni-O-N-Ni torsion angles are moderate (close to 17°) for two of them and close to planar for Ni(1)-O(2)-N(3)-Ni(2) (Table 1). One of the crystallisation solvent molecules is involved in a set of hydrogen bonds and interacts with one of the coordinated methanol molecules to Ni(3) (O(11)···O(8) 2.797(3) Å) and with the OH$^-$ ligand (O(11)···O(1) 3.190(3) Å). An additional intermolecular hydrogen bond links the nitrile groups of one neighbouring trinuclear molecule (O(11)···N(2) 2.925(4) Å).

*$(NEt_3H)\{\mu_{1,5}$-$N(CN)_2\}[Ni_6(H_2O)(MeOH)(3$-$ClBzO)_2(OH)_2$-$\{pyC(CN)NO\}_8]\cdot 3.5\,MeOH\cdot 0.5\,H_2O$*

*(**2**$\cdot NEt_3H\cdot 3.5\,MeOH\cdot 0.5\,H_2O$)*: The structure of **2** consists of two triangles, closely related to complex **1**, in which two labile methanol donors have been substituted by one dicyanamide bridging ligand. The extra negative charge is compensated by one triethylammonium countercation. A view of the core of both triangles of complex **2** is shown in Figure 2. Selected interatomic distances and angles for **2** are listed in Table 2. Bond parameters inside each triangular unit are very similar to those found in **1** without significant differences in the parameters related to the central OH$^-$ groups, which are placed 0.612(3) and 0.644(3) Å out of the plane defined by Ni(1,2,3) and Ni(4,5,6), respectively. The main nickel planes are quasi-parallel, with an angle between the planes of 1.47(2)°. The only differences as a result of the coordination of the dicyanamide ligand are related to the Ni-N-O-Ni torsion angles, which take values around 9, 11 and 25° (Table 2). The dicyanamide ligand is coordinated in the $\mu_{1,5}$ mode with an Ni(1)···Ni(5) distance of 8.552(3) Å. In a similar manner to **1**, solvent molecules are involved in hydrogen bonds with the uncoordinated O-oximato and hydroxo groups. Intercluster hydrogen bonds are provided through one of the solvent molecules that links the triethylammonium cation and two cyano groups of neighbouring molecules.

*$[Ni_4(MeOH)_2(tfacac)_2(MeO)_2\{pyC(CN)NO\}_4]\cdot 2\,MeOH$*

*(**3**$\cdot 2\,MeOH$)*: The neutral core of the tetranuclear compound **3** can be described as a butterfly arrangement of four Ni$^{II}$ atoms, or alternatively, as two $\mu_3$-methoxo-centred triangles that share one side. A labelled plot and selected interatomic distances and angles for **3** are reported in Figure 3 and

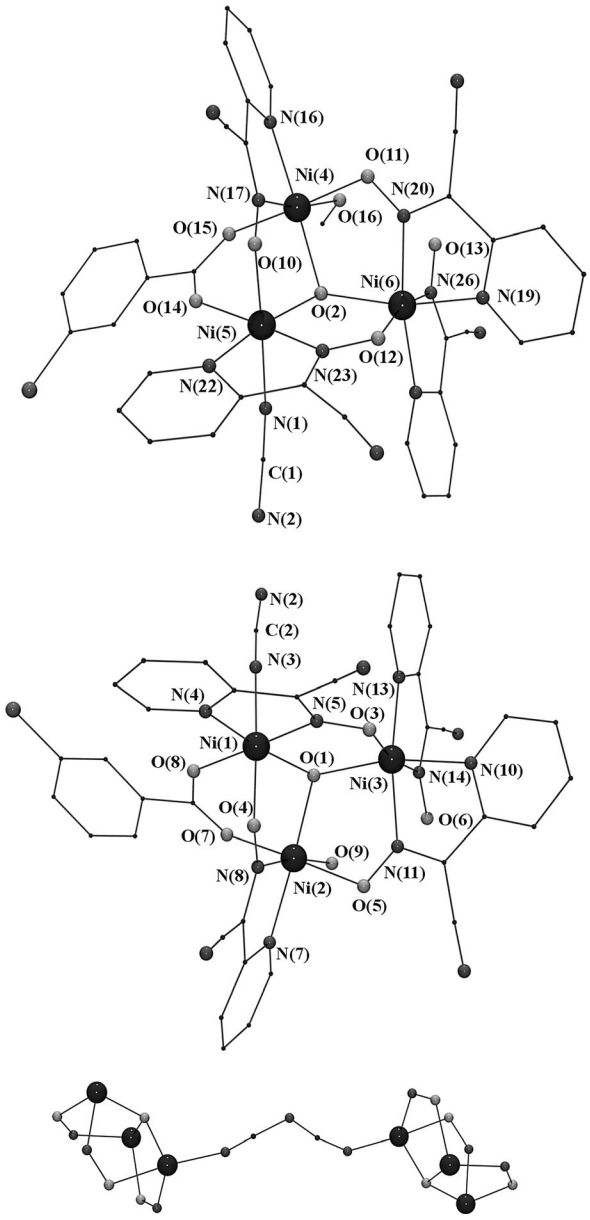


Figure 2. Top: Partially labelled molecular structure of the triangular units of compound **2**. Bottom: Plot of the linkage of the two triangles by means of the dicyanamido bridging ligand. The hydrogen atoms of the organic ligands and the central OH group, solvent molecules and $NEt_3H^+$ countercation have been suppressed for clarity.

Table 3, respectively. Ni(1) and its equivalent Ni(1′) atoms are placed in the wing sites of the butterfly and their $N_2O_4$ coordination sphere is defined by one pyC(CN)NO$^-$ ligand coordinated by its two N atoms, two O atoms from one bidentate tfacac ligand, one O atom from one oximato bridge and the central methoxo group. The $N_4O_2$ environment of Ni(2) is defined by two pyC(CN)NO$^-$ ligands coordinated by its N atoms and the two methoxo groups, whereas Ni(3) coordinates six O atoms from two oximato bridges, the two methoxo groups and two methanol molecules. The four pyC(CN)NO ligands are deprotonated. Bond angles that involve the central $\mu_3$-OMe donor group are 115.0(2)° for

  

CHEMISTRY
A EUROPEAN JOURNAL



Table 2. Selected distances [Å] and bond and torsion angles [°] of the core of compound **2**.

| | | | |
|---|---|---|---|
| Ni(1)−O(1) | 2.043(3) | Ni(1)-O(1)-Ni(2) | 103.3(1) |
| Ni(2)−O(1) | 2.052(3) | Ni(2)-O(1)-Ni(3) | 116.3(2) |
| Ni(3)−O(1) | 2.052(3) | Ni(1)-O(1)-Ni(3) | 114.6(2) |
| Ni(4)−O(2) | 2.071(3) | Ni(4)-O(2)-Ni(5) | 102.7(1) |
| Ni(5)−O(2) | 2.051(3) | Ni(4)-O(2)-Ni(6) | 115.6(2) |
| Ni(6)−O(2) | 2.066(3) | Ni(5)-O(2)-Ni(6) | 113.7(2) |
| Ni(1)-O(4)-N(8) | 108.2(2) | Ni(1)-N(5)-O(3) | 124.9(3) |
| Ni(2)-O(5)-N(11) | 116.3(3) | Ni(2)-N(8)-O(4) | 124.4(3) |
| Ni(3)-O(3)-N(5) | 117.3(3) | Ni(3)-N(11)-O(5) | 127.2(3) |
| Ni(4)-O(11)-N(20) | 117.2(3) | Ni(4)-N(17)-O(10) | 124.1(2) |
| Ni(5)-O(10)-N(17) | 108.9(2) | Ni(5)-N(23)-O(12) | 125.5(3) |
| Ni(6)-O(12)-N(23) | 116.1(3) | Ni(6)-N(20)-O(11) | 127.3(3) |
| Ni(1)···Ni(2) | 3.212(1) | Ni(1)-O(4)-N(8)-Ni(2) | 26.5(4) |
| Ni(2)···Ni(3) | 3.487(1) | Ni(2)-O(5)-N(11)-Ni(3) | 8.4(5) |
| Ni(1)···Ni(3) | 3.445(1) | Ni(3)-O(3)-N(5)-Ni(1) | 9.5(5) |
| Ni(4)···Ni(5) | 3.200(1) | Ni(4)-O(11)-N(20)-Ni(6) | 10.7(5) |
| Ni(4)···Ni(6) | 3.500(1) | Ni(5)-O(10)-N(17)-Ni(4) | 24.9(4) |
| Ni(5)···Ni(6) | 3.446(1) | Ni(6)-O(12)-N(23)-Ni(5) | 12.8(4) |

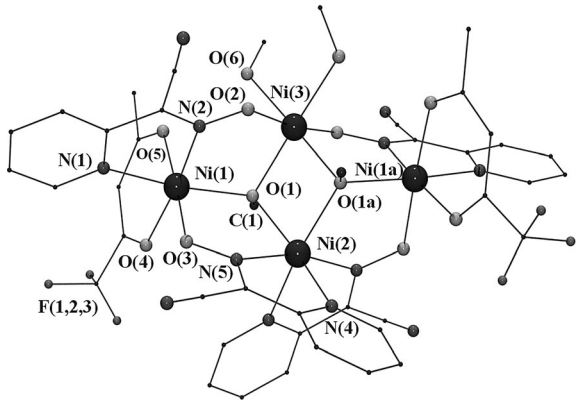


Figure 3. Partially labelled molecular structure of the tetranuclear structure of compound **3**. Hydrogen atoms of the organic ligands and solvent molecules have been suppressed for clarity.

Table 3. Selected distances [Å] and bond and torsion angles [°] of the core of compound **3**.

| | | | |
|---|---|---|---|
| Ni(1)−O(1) | 2.082(4) | Ni(1)-O(1)-Ni(2) | 115.0(2) |
| Ni(2)−O(1) | 2.095(4) | Ni(2)-O(1)-Ni(3) | 96.2(2) |
| Ni(3)−O(1) | 2.064(4) | Ni(1)-O(1)-Ni(3) | 108.1(2) |
| Ni(1)-O(3)-N(5) | 117.2(4) | Ni(1)-N(2)-O(2) | 125.1(4) |
| Ni(3)-O(2)-N(2) | 113.8(4) | Ni(2)-N(5)-O(3) | 126.0(4) |
| Ni(1)···Ni(2) | 3.523(1) | Ni(1)-O(3)-N(5)-Ni(2) | 19.2(6) |
| Ni(2)···Ni(3) | 3.097(2) | Ni(3)-O(2)-N(2)-Ni(1) | 20.8(6) |
| Ni(1)···Ni(3) | 3.3554(9) | | |

Ni(1)-O(1)-Ni(2), 108.1(2)° for Ni(1)-O(1)-Ni(3) and 96.2(2)° for Ni(2)-O(1)-Ni(3), the corresponding Ni···Ni distances being 3.523(1), 3.3554(9) and 3.097(2) Å, respectively. Ni-O-N-Ni torsion angles show moderate values around 20°. Oxygen atoms of the $\mu_3$-OH groups are placed 0.785(4) Å out of the planes defined by Ni(1,2,3). No significant hydrogen bonds or intercluster interactions could be found.

*$[Ni_5(MeOH)_4(3\text{-}ClBzO)_4(OH)_2[pyC(CN)NO]_4]\cdot 7MeOH$ (**4**·7MeOH)*: The centrosymmetric molecule of **4** consists of two vertex-sharing $\mu_3$-OH-centred triangles (bowtie topology). The oxygen atom of the $\mu_3$-OH ligand is placed 0.707(2) Å out of the plane defined by the three nickel atoms. A labelled plot and selected interatomic distances and angles for **4** are reported in Figure 4 and Table 4, respectively. In a similar manner to **1** and **2**, the sides of the triangles are defined by single oximato bridges between the central Ni(1) atom and the peripheral Ni(2) and Ni(3). These latter nickel atoms are bridged by one oximato, one O-carboxylato and one *syn–syn* carboxylato bridge. The $NiO_6$ environment of the central Ni(1) atom is formed by four O-oximato atoms and the two hydroxo groups, whereas the $NiN_2O_4$ environment of the remaining nickel atoms include the two N atoms of one $pyC(CN)NO^-$ ligand, the hydroxo ligand, two O atoms from the carboxylato ligands and one methanol molecule. Each diatomic oximate group links the central $Ni^{II}$ atom and one peripheral metallic ion with Ni-N-O-Ni torsion angles close to zero. The base of the triangles is bridged by one $\mu_3$-OH group, one O-carboxylato atom with an Ni(2)-O(6)-Ni(3) bond angle of 89.61(7)° and one *syn–syn* carboxylato. Each triangle is nearly isosceles, with the Ni(1)···Ni(2), Ni(1)···Ni(3) and Ni(2)···Ni(3) distances being 3.3894(8), 3.3906(8) and 2.9609(7) Å, respectively. These intermetallic distances reflect the different Ni-O-Ni bond angles with the central $\mu_3$-OH ligand: Ni(1)-O(1)-Ni(2) and Ni(1)-O(1)-Ni(3) are similar (114.43(8) and

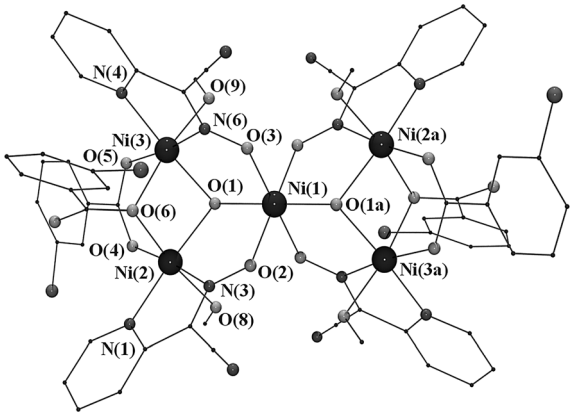


Figure 4. Partially labelled molecular structure of the pentanuclear structure of compound **4**. Hydrogen atoms of the organic ligands and the central OH groups and solvent molecules have been suppressed for clarity.

Table 4. Selected distances [Å] and bond and torsion angles [°] of the core of compound **4**.

| | | | |
|---|---|---|---|
| Ni(1)−O(1) | 2.023(2) | Ni(1)-O(1)-Ni(2) | 114.43(8) |
| Ni(2)−O(1) | 2.008(2) | Ni(2)-O(1)-Ni(3) | 95.13(7) |
| Ni(3)−O(1) | 2.003(2) | Ni(1)-O(1)-Ni(3) | 114.71(7) |
| Ni(1)-O(2)-N(3) | 114.7(1) | Ni(2)-N(3)-O(2) | 125.9(1) |
| Ni(1)-O(3)-N(6) | 114.6(1) | Ni(3)-N(6)-O(3) | 126.0(1) |
| Ni(1)···Ni(2) | 3.3894(8) | Ni(2)-O(6)-Ni(3) | 89.61(7) |
| Ni(2)···Ni(3) | 2.9609(7) | Ni(1)-O(3)-N(6)-Ni(3) | 1.0(2) |
| Ni(1)···Ni(3) | 3.3906(8) | Ni(1)-O(2)-N(3)-Ni(2) | 0.5(2) |

  

114.71(7)°) and much larger than Ni(2)-O(1)-Ni(3) (95.13(7)°).

The O(1) atom from the $\mu_3$-OH groups and the uncoordinated O(7) atom of the carboxylato ligands are connected by means of hydrogen bonds to ten crystallisation methanol molecules, which define an $(MeOH)_8$ ring. This "drop" of methanol connects four $Ni_5$ molecules (Figure 5).

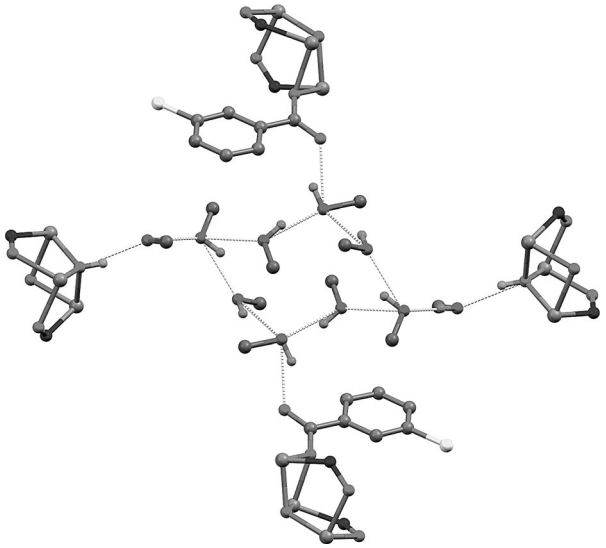

Figure 5. Plot of the hydrogen bonds promoted by the ten methanol molecules found between four pentanuclear units of **4**. Only three nickel atoms of each molecule and the OH or 3-Cl-benzoate ligands directly involved in the hydrogen-bonding network have been plotted.

*$[Ni_5(H_2O)_4(N_3)_2(BzO)_2(OH)_2\{pyC(CN)NO\}_4]\cdot 2MeCN\cdot 10H_2O$* (***5***·*$2MeCN\cdot 10H_2O$*): A labelled plot and selected interatomic distances and angles for compound **5** are reported in Figure 6 and Table 5, respectively. The neutral core of this centrosymmetric pentanuclear compound can be described as a bowtie arrangement of five $Ni^{II}$ ions. The structure of **5** is very similar to that reported for compound

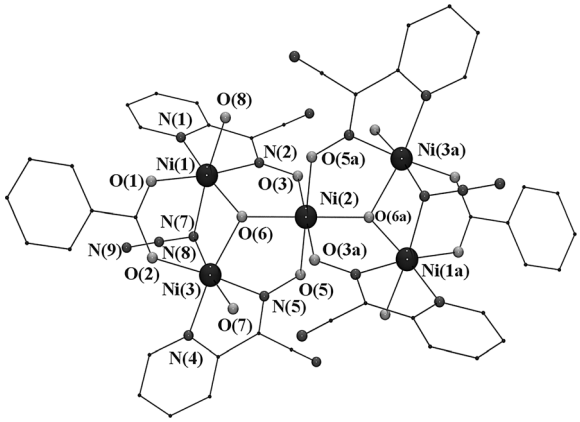


Figure 6. Partially labelled molecular structure of the pentanuclear structure of compound **5**. Hydrogen atoms of the organic ligands and the central OH groups and solvent molecules have been suppressed by clarity.

Table 5. Selected distances [Å] and bond and torsion angles [°] of the core of compound **5**.

| | | | |
|---|---|---|---|
| Ni(1)−O(6) | 2.017(1) | Ni(1)-O(6)-Ni(2) | 113.71(6) |
| Ni(2)−O(6) | 2.023(1) | Ni(2)-O(6)-Ni(3) | 114.41(6) |
| Ni(3)−O(6) | 2.022(1) | Ni(1)-O(6)-Ni(3) | 95.23(6) |
| Ni(2)-O(3)-N(2) | 114.9(1) | Ni(1)-N(2)-O(3) | 125.8(1) |
| Ni(2)-O(5)-N(5) | 114.7(1) | Ni(3)-N(5)-O(5) | 126.4(1) |
| Ni(1)···Ni(2) | 3.3825(3) | Ni(1)-N(7)-Ni(3) | 89.20(6) |
| Ni(2)···Ni(3) | 3.3999(2) | Ni(2)-O(3)-N(2)-Ni(1) | 2.6(2) |
| Ni(1)···Ni(3) | 2.9835(3) | Ni(2)-O(5)-N(5)-Ni(3) | 7.3(2) |

**4**, but the O-carboxylato bridge is changed for one $\mu_{1,1}$-$N_3^-$ ligand with a similar Ni(1)-N(7)-Ni(3) bond angle of 89.20(6)°. The complete description and bond parameters are very similar to **4** with minor changes in the out-of-plane Ni(1,2,3) deviation of the O atom of the hydroxo group (0.720(1) Å) and slightly larger Ni-N-O-Ni torsion angles.

**Magnetic measurements and fit procedure**: Oxo-, hydroxo- or methoxo-centred triangles of $Cu^{II}$ or $Mn^{III}$ with oximato bridges have been previously studied and it has been stated from the experimental work and DFT calculations that their magnetic properties exhibit a strong dependence upon the bond parameters inside the triangular core. Oxo or methoxo $Cu_3$-centred triangles are always strongly antiferromagnetically coupled with $-J$ coupling constants typically greater than 500 $cm^{-1}$.[2] For these systems, it has been demonstrated that the main contribution to the antiferromagnetic coupling is correlated with the out-of-plane displacement of the central $\mu_3$-O atom (or alternatively to the related Cu-O-Cu bond angles) with a minor contribution of the torsion of the oximato bridges.[2g] In contrast, for R-salox$^-$/$Mn^{III}$ triangles, ferro- or antiferromagnetic coupling has been reported as a function of the Mn-N-O-Mn torsion angles, with the ferro-/antiferromagnetic boundary around torsion angles of 30°.[3,7] Studies of triangular nickel systems have not been reported up to now and compounds **1**–**5** provide enough experimental data to propose their magneto-structural trends on the basis of their different kinds of magnetic responses as a function of their topologies and nuclearity.

As has been described above, complexes **1** to **5** have key structural common features that provide us with the possibility to establish a detailed study of the superexchange pathways. The five complexes consist of isolated or linked isosceles or quasi-isosceles $\mu_3$-O-centred triangles in which the equivalent sides are defined by one diatomic oximato bridge and the base of the triangle is formed by a variety of bridging ligands (Scheme 3).

As can be observed in Table 6, the described complexes cover all combinations of Ni-O-Ni bond and Ni-N-O-Ni torsion angles including a third oximato bridge in the base of the triangle for **1** and **2**. In addition, complexes **4** and **5** provide a nice comparison of the influence on the superexchange interaction of one O-carboxylato or one end-on azido bridge with the same Ni-X-Ni bond angle of 89°.

The numbering of all the spin carriers in the Hamiltonians applied to **1**–**5** and in the subsequent discussion is provided

  

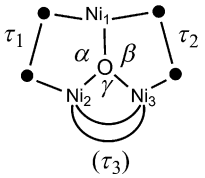


Scheme 3. Common triangular-based core for compounds **1**–**5**. Symbols $\alpha$, $\beta$ and $\gamma$ represent the Ni-O-Ni bond angles and $\tau_1$ and $\tau_2$ the corresponding Ni-N-O-Ni torsion angles. For **1** and **2**, a third oximato bridge is present in the base of the triangle and in this case the torsion is labelled as $\tau_3$.

in Scheme 4. Compounds **1** and **2** show a very similar magnetic response that agrees with antiferromagnetic interactions inside one triangular arrangement of three $S=1$ local spins (Figure 7). Room-temperature $\chi_M T$ values (by the $Ni_3$ unit) are 3.05 and 2.92 $cm^3K^{-1}mol^{-1}$ for **1** and **2**, respectively. Upon cooling, $\chi_M T$ plots gradually decrease down to a plateau below 50 K and after a final decrease at low temperature (greater for compound **2**) reach values of 1.05 and 0.51 $cm^3K^{-1}mol^{-1}$. On the basis of the data summarised in Table 7, which shows different bond parameters for the three interactions inside the triangle, the fit of the experimental data for compound **1** was initially performed on the basis of the superexchange pathways indicated in Scheme 4 using the CLUMAG program[13] and by applying the Hamiltonian [Eq. (1)]:

Table 6. Core parameters for compounds **1** to **5**. Data for **2** corresponds to the triangle defined by Ni(1,2,3).

| | 1 | 2 | 3 | 4 | 5 |
|---|---|---|---|---|---|
| $\alpha$ | 116.28(8) | 116.3(2) | 115.0(2) | 114.71(7) | 113.71(6) |
| $\beta$ | 115.11(8) | 114.6(2) | 108.1(2) | 114.43(8) | 114.41(6) |
| $\gamma$ | 102.16(7) | 103.3(1) | 96.2(2) | 95.13(7) | 95.23(6) |
| $\tau_1$ | 3.3(2) | 8.4(5) | 19.2(6) | 1.0(2) | 7.3(2) |
| $\tau_2$ | 17.0(2) | 9.5(5) | 20.8(6) | 0.5(2) | 2.6(2) |
| $\tau_3$ | 16.7(2) | 26.5(4) | – | – | – |

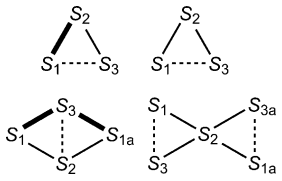


Scheme 4. Coupling schemes applied in the fit procedure of compounds **1**–**5**. Different coupling constants in the corresponding Hamiltonians are indicated as dotted lines, bold lines and solid lines, corresponding in all cases $J_1$ to the base of the triangles.

$$H = -J_1(S_1 \cdot S_3) - J_2(S_1 \cdot S_2) - J_3(S_2 \cdot S_3) \quad (1)$$

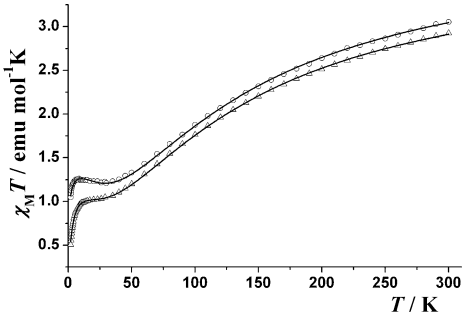


Figure 7. Product of $\chi_M T$ versus $T$ for compounds **1** (dot-centred circles) and **2** (triangles). Solid lines show the best obtained fit.

The fit was performed by discarding the low $T$ values (<8 K) to avoid intercluster or zero-field splitting (ZFS) deviations. Best-fit parameters indicate a quasi-isosceles response with values of −14.5, −52.9 and −49.7 $cm^{-1}$, which indicate a similar value for $J_2$ and $J_3$ and clearly a lower value for the $J_1$ coupling constant.

Assuming that the two greater coupling constants are practically undistinguishable ($J_2=J_3$), a new fit was performed by including all data in the 2–300 K range with the conventional analytical equations, including a $\theta$ parameter to correct the low $T$ decay, derived from the Hamiltonian [Eq. (2)]:

$$H = -J_1(S_1 \cdot S_3) - J_2(S_1 \cdot S_2 + S_2 \cdot S_3) \quad (2)$$

Best-fit parameters were $J_1=-16.8(8)$ $cm^{-1}$, $J_2=-55.2(5)$ $cm^{-1}$, $g=2.322(5)$ and $\theta=-0.53(2)$ K.

In light of the results obtained for **1**, the fit for compound **2** was performed by applying the Hamiltonian in Equation (2). Best-fit parameters were $J_1=-19.8(4)$ $cm^{-1}$, $J_2=-53.9(4)$ $cm^{-1}$, $g=2.280(5)$ and $\theta=-2.80(3)$ K, which are fully consistent with compound **1**. The greater $\theta$ value and the more pronounced low-temperature decay should be attributed to the typically very weak interaction mediated between both triangular units by the dicyanamide bridge[14] (Figure 7).

Compound **3** shows an $\chi_M T$ value of 4.27 $cm^3K^{-1}mol^{-1}$ at room temperature, which decreases upon cooling and tends toward zero at low temperature. The $\chi_M$ plot exhibits a broad maximum at 80 K, which is in good agreement with an even number of local $S=1$ spins antiferromagnetically coupled (Figure 8). Structural data show two sets of Ni-O-Ni bond angles for the wing–body interactions. The fit of the experimental data was then performed on the basis of Scheme 4 and by applying the Hamiltonian [Eq. (3)]:

$$H = -J_1(S_2 \cdot S_3) - J_2(S_2 \cdot S_1 + S_2 \cdot S_{1a}) - J_3(S_3 \cdot S_1 + S_3 \cdot S_{1a}) \quad (3)$$

Best-fit parameters obtained with the CLUMAG program[13] were $J_1=+1.6$ $cm^{-1}$, $J_2=-63.1$ $cm^{-1}$, $J_3=-26.9$ $cm^{-1}$ and $g=2.352$ with paramagnetic impurities of 1%.

As is explained below, the DFT-calculated values differ strongly from the above fit. To have a complete overview of the response of the fit procedure, we performed an additional fit and assumed that $J_2=J_3$. Under these conditions, a new excellent fit was obtained for $J_1=+0.3$ $cm^{-1}$, $J_2=J_3=-37.1$ $cm^{-1}$, and $g=2.00$. The $g$ value seems too low but $J_2$ and $J_3$ agree very well with the DFT-calculated values. These fits indicate that the system has multiple analytical solutions and that the most reliable values should be assumed to be the calculated ones.

The calculated value for $J_1$ has a high degree of uncertainty because of the dominant strong antiferromagnetic coupling promoted by $J_2$ and $J_3$ that leads to the $S=0$ ground state independently of $J_1$ when $J_2$, $J_3 \gg J_1$. This feature was

  

Table 7. Structural parameters [Å and °] and calculated exchange coupling constants [$cm^{-1}$] corresponding to the $Ni_3$ (**1**; see Figure 1), $Ni_4$ (**3**; see Figure 3) and $Ni_5$ (**5**; see Figure 6) complexes. The subscript numbers for the calculated coupling constants corresponds to the numbering employed in Scheme 4 and structural data. Two sets of values are indicated for complex **3** (see fit procedure).

| | Bridges | $d$(Ni···Ni) | Ni-O-Ni | Ni-O-N | Ni-N-O-Ni | $J_{exptl}$ | $J_{calcd}$ |
|---|---|---|---|---|---|---|---|
| $Ni_3$ complex **1** | | | | | | | |
| $J_{1,2}$ | NO, OH | 3.465 | 116.3 | 117.5 | 3.3 | −52.9 | −40.4 |
| $J_{2,3}$ | NO, OH | 3.494 | 115.1 | 116.2 | 17.0 | −49.7 | −34.4 |
| $J_{1,3}$ | NO, RCOO, OH | 3.199 | 102.2 | 110.5 | 16.7 | −14.5 | −13.3 |
| $Ni_4$ complex **3** | | | | | | | |
| $J_{1,2}$ | NO, $OCH_3$ | 3.523 | 115.0 | 117.2 | 19.2 | −63.1 (−37.1) | −38.5 |
| $J_{1,3}$ | NO, $OCH_3$ | 3.355 | 108.1 | 113.8 | 20.8 | −26.9 (−37.1) | −32.7 |
| $J_{2,3}$ | 2 $OCH_3$ | 3.097 | 96.2 | – | – | +1.6 (+0.3) | +18.1 |
| $Ni_5$ complex **5** | | | | | | | |
| $J_{1,2}$ | NO, OH | 3.382 | 113.7 | 114.9 | 2.7 | −24.5 | −28.2 |
| $J_{2,3}$ | NO, OH | 3.400 | 114.4 | 114.7 | 7.3 | −24.5 | −32.1 |
| $J_{1,3}$ | RCOO, $N_3$, OH | 2.984 | 95.2 | – | – | +10.1 | +34.3 |

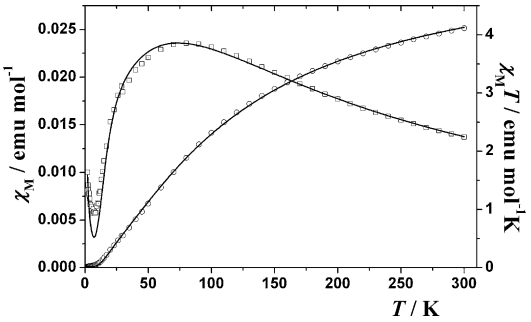


Figure 8. Product of $\chi_M$ (squares) and $\chi_M T$ (dot-centred circles) versus $T$ for compound **3**. Solid lines show the best fit.

checked by performing a set of simulations, which have shown that the quality of the fit is practically constant, even when changing the fixed $J_1$ value by one order of magnitude. Therefore we can only conclude that $J_2$ and $J_3$ indicate moderately strong antiferromagnetic coupling; for the body interaction $J_1$ we can only propose a weak coupling, probably ferromagnetic.

Complexes **4** and **5** exhibit a similar shape with an $\chi_M T$ decrease from the room-temperature values of 4.74 and 5.28 $cm^3 K^{-1} mol^{-1}$ down to minimum values of 3.00 and 4.33 $cm^3 K^{-1} mol^{-1}$ at 44 K for **4** and 80 K for **5**, respectively (Figure 9). Below the minimum, the two plots increase up to

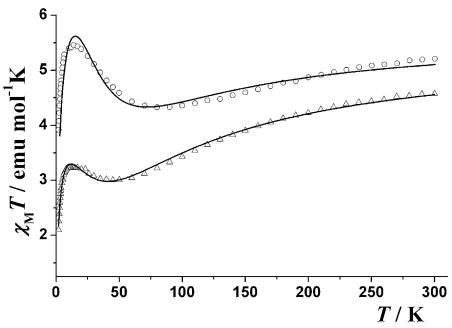


Figure 9. Product of $\chi_M T$ versus $T$ for compounds **4** (triangles) and **5** (dot-centred circles). Solid lines show the best obtained fit.

maximum $\chi_M T$ values of 3.20 and 5.46 $cm^3 K^{-1} mol^{-1}$ placed at 13 K (for **4**) and 14 K (for **5**), thereby suggesting a ferrimagnetic response with greater antiferromagnetic components for **4**. At low temperature, the $\chi_M T$ value decreases and reaches 2.07 and 3.90 $cm^3 K^{-1} mol^{-1}$ for **4** and **5**, respectively, due to intercluster interactions or ZFS effects. These compounds exhibit the quasi-isosceles core; a fit of the experimental data was performed by applying the interaction (Scheme 4) and by assuming only two coupling constants with the conventional analytical equation derived from the Hamiltonian [Eq. (4)]:

$$H = -J_1(S_1 \cdot S_3 + S_{1a} \cdot S_{3a}) - J_2(S_2 \cdot S_1 + S_2 \cdot S_3 + S_2 \cdot S_{1a} + S_2 \cdot S_{3a}) \quad (4)$$

Best-fit parameters were $J_1 = -13.4(2)$ $cm^{-1}$, $J_2 = -27.2(4)$ $cm^{-1}$, $g = 2.084(3)$ for **4** and $J_1 = +10(2)$ $cm^{-1}$, $J_2 = -24.5(8)$ $cm^{-1}$, $g = 2.13(1)$ for **5**. Dominant antiferromagnetic interactions between the central and peripheral $S = 1$ spins in a bowtie topology led to an $S = 3$ ground state for both compounds. As expected from the structural data, $J_2$ values are similar, whereas the replacement of an oxo bridging ligand by one end-on azido bridge switches the sign of $J_1$ and introduces ferromagnetic components into the core of this pentanuclear system.

Some of the coupling constants obtained in the above fits are unreliable (as $J_1$ in compound **3**), are indistinguishable by symmetry ($J_2$ and $J_3$ also in compound **3**) or have been assumed to be equivalent to minimise the number of variables in the fit process. To have a more precise picture of the coupling constant values and to rationalise the effect of the main structural parameters, DFT calculations were performed.

The calculated $J$ values by using DFT methods for complexes **1**, **3** and **5** (see the computational details in the Experimental Section) show a good agreement with the experimentally fitted $J$ values (Table 7). In Figure 10, the comparison between the experimental susceptibility curves and those obtained directly using the calculated $J$ values also confirms the accuracy of the employed methodology to reproduce the magnetic properties of such complexes. The analysis of the $J$ values indicates that cases with one oximato bridging ligand combined with one hydroxo or alkoxo bridging ligand result in a moderate antiferromagnetic coupling. To analyse the effect of the presence of alkoxo or hydroxo bridging ligand, the $Ni_4$ complex (**3**) was calculated again by replacing the methoxo group with a hydroxo ligand. The three calculated $J_1$–$J_3$ values are −31.7, −27.6 and

  

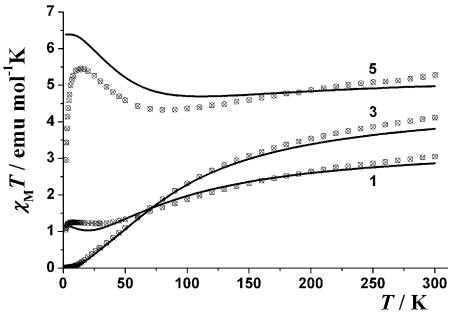


Figure 10. Magnetic-susceptibility curves for the $Ni_3$ (**1**), $Ni_4$ (**3**), $Ni_5$ (**5**) complexes. Squares represent the experimental data, whereas the solid line was calculated with DFT *J* values.

+17.2 $cm^{-1}$. The inverse procedure was followed for the $Ni_5$ complex (**5**) by replacing the original hydroxo group with a methoxo ligand to give the following $J_1$–$J_3$ values: −32.7, −39.0 and +38.7 $cm^{-1}$. The results for both systems confirm that the presence of the methoxo group slightly enhances the strength of the exchange interactions relative to the hydroxo ligand.

Traditionally, for the oximato transition-metal complexes, the M-O-N-M torsion angle was proposed to be the key structural parameter that primarily controls the magnetic properties.[15] To analyse the effect of such a geometrical parameter in our family of complexes, the $Ni_3$ complex (**1**) was selected and we focused in the $J_{2,3}$ interaction (Scheme 4). We prepared some model complexes by changing the Ni(2)-O-N-Ni(3) torsion angle but keeping all the remaining bond parameters of the triangular complex. The dependence of $J_{2,3}$ on such a torsion angle is shown in Figure 11. The obtained results indicate that the increase of the Ni-O-N-Ni torsion angle induces a slightly larger antiferromagnetic coupling. At first glance, this result seems surprising, because for single oximato bridges between two nickel centres a decrease in the antiferromagnetic interaction has recently been proposed[16] for large torsion angles. For the well-studied equivalent $Mn^{III}$ triangles, the opposite behaviour was found. In the case of the $Mn_3$ complexes, there is a "magic" Mn-N-O-Mn torsion angle. Thus if the value is larger than 31°, the coupling is ferromagnetic, whereas smaller values lead to antiferromagnetic couplings.[7,15] To explain the difference between the $Mn^{III}$ and $Ni^{II}$ complexes, we have to keep in mind the different nature of the orbitals that bear the unpaired electrons. Thus, for the $Ni^{II}$ complexes, those orbitals are $d_{z^2}$ and $d_{x^2-y^2}$, whereas for $d^4$ $Mn^{III}$ there is one unpaired electron on each d orbital with the exception of the $d_{x^2-y^2}$ that remains empty. Assuming the validity of the Kahn–Briatt model, we can expect that for $Ni^{II}$ complexes the maximum coupling should be reached for a perfect octahedral coordination sphere of the two involved $Ni^{II}$ cations. This fact can be easily understood because for a perfect octahedral coordination, the lobes of $d_{z^2}$ and $d_{x^2-y^2}$ orbitals will have the maximum overlap with those of the bridging ligand that favours the interaction between the two paramagnetic centres. To measure the degree of distortion of the coordination sphere of the $Ni^{II}$ cations from a perfect octahedron, we have employed the continuous shape measures (*S*(Q); see the computational details in the Experimental Section).

This approach allows us to quantify the distortion. Thus a *S*(OC6) value equal to zero indicates a perfect octahedral coordination. The smaller the *S*(OC6) value is, the smaller the structural distortion from the perfect octahedron. In Figure 12, there is the dependence of the calculated $J_{2,3}$ value upon changing the Ni(2)-O-N-Ni(3) torsion angle (the same as those represented in Figure 11) with the sum of the S(OC6) values for the two $Ni^{II}$ cations involved in the $J_{2,3}$ exchange interaction. The curve nicely corroborates the fact that the larger Ni-O-N-Ni torsion angle values lead to coordination spheres closer to the perfect octahedron (smaller S(OC6) values) and consequently larger antiferromagnetic couplings for a better overlap with the bridging ligands that facilitate the interaction between the paramagnetic centres.

The complete analysis of the magnetic response of this kind of triangular system allows us to propose a behaviour closer to the copper triangles than to the manganese ones and to confirm the Ni-O-Ni bond angle that involves the

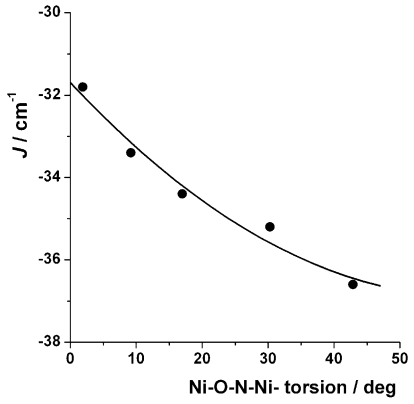


Figure 11. Dependence of the $J_{2,3}$ value for some model systems on the $Ni_3$ complex (**1**) changing the Ni(2)-O-N-Ni(3) torsion angle.

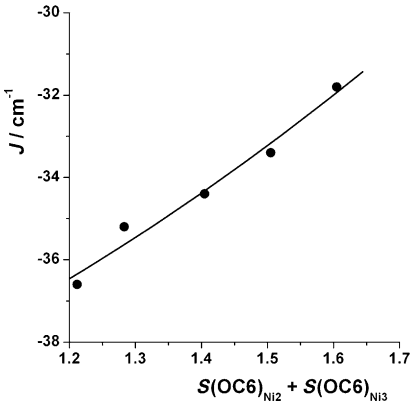


Figure 12. Dependence of the $J_{2,3}$ value for some model systems on the $Ni_3$ complex (**1**) changing the Ni(2)-O-N-Ni(3) torsion angle with the sum of the continuous shape measurement parameter S(OC6) corresponding to the two $Ni^{II}$ cations involved in the $J_{2,3}$ interaction.

  

central hydroxo or alkoxo ligand as a major factor. The amount of experimental data is still limited, but to check the validity of the above conclusions and to compare the coupling constants in larger clusters, we have selected the previously reported hexanuclear systems $[Ni_6(SO_4)_4(OH)\{pyC(R)NO\}_3\{pyC(R)NOH\}_3(MeOH)_2(H_2O)]$ (R = Me, Ph),[6a] which are the only ones with available magnetic data that contain the fragment $[Ni_3(\mu_3\text{-}OH)\{pyC(R)NO\}_3]^{3+}$ in a quasi-equilateral arrangement. These complexes exhibit Ni-O-Ni bond angles around 110° (lower than those found in **1**–**5**) and medium Ni-O-N-Ni torsion angles around 25°. From the above calculations we would expect moderately weak antiferromagnetic coupling and in excellent agreement, the reported $J$ values were $-20.5$ and $-17.0\,cm^{-1}$, which are lower than those found in **1**–**5** for similar torsions and larger Ni-O-Ni bond angles.

## Conclusion

The employment of the relatively acidic 2-pyridylcyanoxime ligand in nickel chemistry has allowed us to synthesise a series of $Ni_3$, $Ni_4$ and $Ni_5$ complexes that can be described as topologically derived from isolated, side- or vertex-sharing $\mu_3$-OR isosceles triangles. Analysis of the experimental and DFT-calculated sign and magnitude of the coupling constants gives a complete description of the magnetic properties of this kind of system, which can be summarised as follows. 1) Moderate antiferromagnetic interactions should be expected in all cases for the $[Ni_3(\mu_3\text{-}O)\{pyC(R)NO\}_3]^{n+}$ core. 2) Antiferromagnetic interactions are enhanced for −OR = alkoxo relative to hydroxo bridges. 3) In contrast to isolated single oximato bridges, the effect of the torsion angle in the case of μ-OR-centred triangles is a minor effect and the magnitude of the antiferromagnetic interaction should be attributed to the Ni-O-Ni bond angles. d) The structural dependence of the $J$ value for the double oximato and hydroxo exchange pathway on the torsion Ni-N-O-Ni angle is rather small and an opposite trend is found to that of the equivalent $Mn^{III}$ systems. For the $Ni^{II}$ systems, the increase of the Ni-N-O-Ni angle enhances the antiferromagnetic coupling. Such a difference can be explained by the different magnetic orbitals of the $Ni^{II}$ and $Mn^{III}$ cations involved in the exchange interactions.

## Experimental Section

**General**: Magnetic susceptibility measurements were carried out on polycrystalline samples using a Quantum Design DSM5 susceptometer working in the range 2–300 K under magnetic fields of 0.3 T. Diamagnetic corrections were estimated from Pascal tables. Infrared spectra (4000–400 $cm^{-1}$) were recorded from KBr pellets. 2-Pyridylacetonitrile, sodium azide and sodium dicyanamide were purchased from Sigma–Aldrich and used without further purification. $Ni(BzO)_2{\cdot}3H_2O$ and $Ni(3\text{-}Cl\text{–}BzO)_2{\cdot}xH_2O$ were synthesised by dissolving equimolar quantities (40 mmol) of NaOH and benzoic acid or 3-chlorobenzoic acid, respectively, in water (40 mL). The final solution was filtered and mixed with a commercial source of $Ni(NO_3)_2{\cdot}6H_2O$ (20 mmol) in water (20 mL). The resulting salts were obtained in good yields (>80%). $Ni(tfacac)_2{\cdot}xH_2O$ was synthesised by mixing trifluoroacetylacetonate (40 mmol), $Ni(NO_3)_2{\cdot}6H_2O$ (20 mmol) and $NaAcO{\cdot}3H_2O$ (40 mmol) in water (100 mL). The precipitate was filtered, dissolved in ethanol (40 mL) and recrystallized by the addition of water (100 mL). The resulting salt was obtained in low yield (≈30%). The py-(CN)NOH ligand was prepared according to the literature.[17]

**Single-crystal X-ray structure analyses**: Details of crystal data, data collection and refinement are given in Table 8. X-ray data were collected using a MAR345 diffractometer with an image-plate detector for **1**, **2** and

Table 8. Crystal data, data collection and structure refinement details for the X-ray structure determination of compounds **1**–**5**.

| | **1** | **2** | **3** | **4** | **5** |
|---|---|---|---|---|---|
| formula | $C_{40}H_{42}N_{12}Ni_3O_{12}$ | $C_{83}H_{70}Cl_2N_{28}Ni_6O_{20}$ | $C_{44}H_{48}F_6N_{12}Ni_4O_{14}$ | $C_{67}H_{78}Cl_4N_{12}Ni_5O_{25}$ | $C_{46}H_{52}N_{20}Ni_5O_{24}$ |
| $M_r$ [g mol$^{-1}$] | 1058.99 | 2202.83 | 1317.78 | 1889.76 | 1562.63 |
| space group | triclinic | triclinic | monoclinic | monoclinic | monoclinic |
| crystal system | $P\bar{1}$ | $P\bar{1}$ | $C2/c$ | $P21/n$ | $P21/n$ |
| $a$ [Å] | 11.093(6) | 13.718(4) | 22.622(1) | 14.369(3) | 13.8290(3) |
| $b$ [Å] | 14.064(5) | 13.886(2) | 15.945(1) | 15.814(2) | 13.8139(3) |
| $c$ [Å] | 15.945(6) | 14.229(4) | 16.0496(8) | 19.039(3) | 19.3703(4) |
| $\alpha$ [°] | 90.07(3) | 75.67(2) | 90 | 90 | 90 |
| $\beta$ [°] | 72.72(2) | 85.08(2) | 90.944(2) | 92.68(2) | 101.534(1) |
| $\gamma$ [°] | 89.20(3) | 79.20(2) | 90 | 90 | 90 |
| $V$ [Å$^3$] | 2375(2) | 2577(1) | 5788.6(8) | 4321(1) | 3625.6(1) |
| $Z$ | 2 | 1 | 4 | 2 | 2 |
| $T$ [K] | 293(2) | 293(2) | 100(2) | 293(2) | 100(2) |
| $D_{calcd}$ [g cm$^{-3}$] | 1.481 | 1.419 | 1.512 | 1.450 | 1.416 |
| $F(000)$ | 1092 | 1126 | 2696 | 1944 | 1568 |
| $\mu(Mo_{K\alpha})$ [mm$^{-1}$] | 1.248 | 1.202 | 1.369 | 1.269 | 1.356 |
| measured reflns | 24989 | 18625 | 5670 | 35134 | 11132 |
| unique reflns | 12836 | 16224 | 5670 | 10978 | 11132 |
| $R_{int}$ | 0.0344 | 0.0364 | 0.0000 | 0.0641 | 0.0324 |
| $\theta_{min}/\theta_{max}$ [°] | 2.65/32.33 | 1.48/28.93 | 1.56/26.02 | 1.67/29.93 | 1.66/30.61 |
| $R(F^2)$ | 0.0424 | 0.0397 | 0.0609 | 0.0535 | 0.0356 |
| w$R(F^2)$ | 0.1198 | 0.1260 | 0.1797 | 0.1507 | 0.1038 |
| variables | 622 | 1323 | 372 | 563 | 460 |
| $\Delta\rho_{max}/\Delta\rho_{min}$ [e Å$^{-3}$] | 0.577/−0.525 | 0.666/−0.723 | 1.596/−1.091 | 1.570/−0.573 | 1.200/−0.722 |

  

**4** and using a Bruker Kappa ApexII CCD diffractometer for **3** and **5** with $Mo_{K\alpha}$ radiation ($\lambda = 0.71073$ Å). The structures were solved by direct methods using the SHELXS computer program[18] and refined by full-matrix least-squares methods with the SHELXS97 computer program.[19] Three hydrogen atoms for **1** and one for **3**, respectively, were located from difference synthesis, whereas all the remaining hydrogen atoms were computed and refined by using a riding model, using in all cases a temperature factor equal to 1.2 times the equivalent temperature factor of the atom which was linked. Lorentz polarisation and absorption corrections were applied.

CCDC-844624 (**1**), 844625 (**2**), 844626 (**3**), 844627 (**4**) and 844628 (**5**) contain the supplementary crystallographic data for this paper. These data can be obtained free of charge from The Cambridge Crystallographic Data Centre via www.ccdc.cam.ac.uk/data_request/cif.

**$[Ni_3(MeOH)_2(BzO)(OH)\{py\text{-}(CN)NO\}_4]\cdot 3MeOH$ (1)**: py-(CN)NOH (0.073 g, 0.5 mmol), $Ni(BzO)_2\cdot 3H_2O$ (0.301 g, 1 mmol) and $NaN(CN)_2$ (0.089 g, 1 mmol) were dissolved in MeOH (20 mL) and then $NEt_3$ (0.101 g, 1 mmol) was added. The solution was stirred for 2 h, filtered and crystallised by layering with diethyl ether (10 mL). Relevant IR bands: $\tilde{\nu} = 3446$ (br), 2210 (w), 1601 (s), 1558 (m), 1460 (s), 1416 (m), 1399 (m), 1296 (w), 1266 (w), 1225 (m), 1154 (w), 1102 (w), 1057 (w), 1037 (m), 780 (w), 712 $cm^{-1}$ (m); elemental analysis calcd (%) for **1** ($C_{37}H_{30}N_{12}Ni_3O_9$): C 46.16, H 3.14, N 17.46; found: C 46.87, H 3.04, N 17.11.

**$(NEt_3H)[Ni_6(H_2O)(MeOH)(3\text{-}ClBzO)_2\{N(CN)_2\}(OH)_2\{py\text{-}(CN)NO\}_8]\cdot 0.5H_2O\cdot 3.5MeOH$ (2)**: py-(CN)NOH (0.073 g, 0.5 mmol), $Ni(3\text{-}ClBzO)_2\cdot xH_2O$ (0.369 g, 1 mmol) and $NaN(CN)_2$ (0.089 g, 1 mmol) were added to MeOH (20 mL) together with $NEt_3$ (0.101 g, 1 mmol). The solution was stirred for 2 h, filtered and crystallised by layering with diethyl ether. Relevant IR bands: $\tilde{\nu} = 3412$ (br), 2294 (w), 2217 (m), 2187 (s), 1601 (s), 1558 (s), 1460 (s), 1422 (s), 1390 (s), 1302 (m), 1264 (m), 1227 (s), 1155 (m), 1107 (m), 1062 (w), 1036 (s), 1005 (w), 777 (m), 741 (w), 712 $cm^{-1}$ (m); elemental analysis calcd (%) for **2**·($NEt_3H$) ($C_{79}Cl_2N_{28}Ni_6O_{16}H_{64}$): C 45.62, H 3.08, N 18.86; found: C 45.94, H 2.98, N 18.38.

**$[Ni_4(MeOH)_2(MeO)_2\{py\text{-}(CN)NO\}_4(tfacac)_2]\cdot 2MeOH$ (3)**: py-(CN)NOH (0.073 g, 0.5 mmol), $Ni(tfacac)_2\cdot xH_2O$ (0.362 g, 1 mmol) and $NaN(CN)_2$ (0.089 g, 1 mmol) were added to MeOH (20 mL) together with $NEt_3$ (0.101 g, 1 mmol). The solution was stirred and after a couple of hours filtered and layered by using diethyl ether (10 mL). Relevant IR bands: $\tilde{\nu} =$ 3411 (b), 2220 (w), 1626 (s), 1602 (m), 1521 (w), 1464 (s), 1428 (m), 1299 (s), 1266 (w), 1223 (s), 1190 (m), 1141 (m), 1108 (w), 1038 (m), 777 (m), 713 $cm^{-1}$ (m); elemental analysis calcd (%) for **3** ($C_{42}H_{40}F_6N_{12}Ni_4O_{12}$): C 40.24, H 3.22, N 13.41; found: C 40.61, H 3.09, N 13.56.

**$[Ni_5(MeOH)_4(3\text{-}ClBzO)_4(OH)_2\{py\text{-}(CN)NO\}_4]\cdot 7MeOH$ (4)**: py-(CN)NOH (0.073 g, 0.5 mmol) and $Ni(3\text{-}ClBzO)_2\cdot xH_2O$ (0.369 g, 1 mmol) were dissolved in commercial MeOH (20 mL) and $NEt_3$ (0.101 g, 1 mmol). The solution was stirred for 2 h, filtered and crystallised by layering with diethyl ether. Relevant IR bands: $\tilde{\nu} = 3417$ (br), 2219 (w), 1602 (s), 1559 (s), 1456 (s), 1428 (m), 1392 (s), 1341 (m), 1217 (m), 1036 (m), 766 (m), 739 (m), 711 $cm^{-1}$ (m); elemental analysis calcd (%) for **4** ($C_{60}Cl_4N_{12}Ni_5O_{18}H_{50}$): C 43.35, H 3.03, N 10.11; found: C 42.98, H 2.94, N 10.12.

**$[Ni_5(MeOH)_4(BzO)_2(N_3)_2(OH)_2\{py\text{-}(CN)NO\}_4]\cdot 2CH_3CN\cdot 10H_2O$ (5)**: py-(CN)NOH (0.073 g, 0.5 mmol), $Ni(BzO)_2\cdot 3H_2O$ (0.301 g, 1 mmol) and $NaN_3$ (0.065 g, 1 mmol) were dissolved in MeOH (20 mL) together with $NEt_3$ (0.101 g, 1 mmol). The solution was stirred for a couple of hours and filtered. Crystals were obtained by layering the final solution with diethyl ether (10 mL). Relevant IR bands: $\tilde{\nu} = 3400$ (br), 2221 (w), 2063 (s), 1601 (s), 1553 (s), 1463 (s), 1400 (s), 1299 (w), 1214 (m), 1104 (w), 1035 (m), 778 (w), 711 $cm^{-1}$ (m); elemental analysis calcd (%) for **5**·$6H_2O$ ($C_{42}N_{18}Ni_5O_{20}H_{48}$): C 35.56, H 3.41, N 17.78; found: C 35.74, H 3.35, N 17.46.

**Computational details**: Electronic structure calculations based on density functional theory provide an excellent estimation of the exchange coupling constants in polynuclear transition-metal complexes when taking into account the tiny involved energy differences.[20] Since a detailed description of the computational strategy used to calculate the exchange coupling constants in polynuclear complexes is outside the scope of this paper, we will focus our discussion here to its most relevant aspects. Previously, we published a series of papers devoted to such a purpose and in which more details can be found.[21–23] For the studied $Ni_3$ complex **1**, there are three exchange interactions, and we employed four spin configurations to estimate these three $J$ values: the high spin solution ($S = 3$) and three $S = 1$ wave functions obtained with the spin inversion of each nickel centre. In the case of the $Ni_4$ complex **3**, with three $J$ values, they were obtained by fitting the equations that involved the following spin configurations: the high-spin $S = 4$, two $S = 1$ spin configurations for the inversion of Ni(1) and Ni(3) and three $S = 0$ for the inversion of the following pairs: {Ni(1), Ni(2)}, {Ni(1), Ni(3)} and {Ni(2), Ni(3)}. Finally, the $Ni_5$ complex **5**, with three different $J$ values, the high-spin $S = 5$, one $S = 3$ spin configuration for the inversion of Ni(1) and three $S = 1$ for the inversion of the following pairs {Ni(1), Ni(2)}, {Ni(2), Ni(2a)} and {Ni(3), Ni(3a)} were employed.

In previous papers, we have analysed the effect of the basis set and the choice of the functional on the accuracy of the determination of the exchange coupling constants.[22–24] Thus, we found that the hybrid B3LYP functional,[25] together with the all electron basis set proposed by Schaefer et al., provide $J$ values in excellent agreement with the experimental ones. The hybrid character of the B3LYP, which is due to the inclusion of some contribution of exact exchange, reduces the self-interaction error and improves the calculated $J$ values relative to non-hybrid functionals. We have employed a basis set of triple-$\zeta$ quality as proposed by Schaefer et al.[26] The calculations were performed with the Gaussian 09 code[27] by using guess functions generated with the Jaguar 7.0 code[28] and introducing the ligand-field effects[29] to control the local charge and multiplicity of each atom.

A brief description of continuous shape measures is presented in this section. More detailed information on this stereochemical tool and its applications to transition-metal compounds can be found in previous publications.[30] Continuous shape measures were proposed by Avnir and coworkers to provide a quantitative evaluation of the degree of distortion of a set of atoms (e.g., the coordination sphere of a transition metal) from a given ideal polyhedral shape.[31] In short, the proposed method consists of finding the ideal structure that has the desired shape that is closest to the observed structure. The ideal and real polyhedra are superimposed in such a way as to minimise the expression in Equation (5),[20] the value of which is the shape measure of the investigated structure Q relative to the ideal shape P, in which $\vec{q}_i$ are $N$ vectors that contain the $3N$ Cartesian coordinates of the problem structure Q, $\vec{p}_i$ contain the coordinates of the ideal polyhedron P, and $\vec{q}_0$ is the position vector of the geometric centre that is chosen to be the same for the two polyhedra:

$$S(\mathrm{P}) = \min\left[\frac{\sum_{i=1}^{N}|\vec{q}_i - \vec{p}_i|^2}{\sum_{i=1}^{N}|\vec{q}_i - \vec{q}_0|^2}\right] \times 100 \qquad (5)$$

$S(\mathrm{P}) = 0$ corresponds to a structure Q fully coincident in shape with the reference polyhedron P, regardless of size and orientation. Thus, in this case this approach was employed to estimate the distortion of the quasi-octahedral coordination of the $Ni^{II}$ cations with respect to a perfect octahedron by using the $S$(OC6) value. Shape measures were calculated with version 2.0 of the SHAPE program.[32]

## Acknowledgements

A.E. thanks the Ministerio de Ciencia e Innovación (Spain), project CTQ2009-07264 and an Excellence in Research ICREA-Academia Award for financial support. E.R. offers thanks for the grants CTQ2008-06670-C02-01 and 2009SGR-1459 from the Ministerio de Ciencia e Innovación and the Generalitat de Catalunya, respectively, and thankfully acknowledges the computer resources, technical expertise and assistance provided by the Centre de Supercomputació de Catalunya.

  

[1] a) J. Yoon, E. I. Solomon, *Coord. Chem. Rev.* **2007**, *251*, 379–400.
[2] a) R. Beckett, B. F. J. Hoskins, *Chem. Soc. Dalton Trans.* **1972**, 291–295; b) T. C. Stamatatos, J. C. Vlahopoulou, Y. Sanakis, C. Raptopoulou, V. Psycharis, A. K. Boudalis, S. P. Perlepes, *Inorg. Chem. Commun.* **2006**, *9*, 814–818; c) T. Afrati, C. M. Zaleski, C. Dendrinou-Samara, G. Mezei, J. W. Kampf, V. L. Pecoraro, D. P. Kessissoglou, *Dalton Trans.* **2007**, 2658–2668; d) T. Afrati, C. Dendrinou-Samara, C. Raptopoulou, A. Terzis, V. Tangoulis, D. P. Kessissoglou, *Dalton Trans.* **2007**, 5156–5164; e) T. Afrati, C. Dendrinou-Samara, C. Raptopoulou, A. Terzis, V. Tangoulis, A. Tsipis, D. P. Kessissoglou, *Inorg. Chem.* **2008**, *47*, 7545–7555; f) A. Escuer, B. Cordero, M. Font-Bardia, T. Calvet, *Inorg. Chem.* **2010**, *49*, 9752–9754; g) A. Escuer, G. Vlahopoulou, S. P. Perlepes, F. A. Mautner, *Inorg. Chem.* **2011**, *50*, 2468–2478.
[3] a) T. C. Stamatatos, D. Foguet-Albiol, C. C. Stoumpos, C. P. Raptopoulou, A. Terzis, W. Wernsdorfer, S. P. Perlepes, G. Christou, *J. Am. Chem. Soc.* **2005**, *127*, 15380–15381; b) T. C. Stamatatos, D. Foguet-Albiol, C. C. Stoumpos, C. P. Raptopoulou, A. Terzis, W. Wernsdorfer, S. P. Perlepes, G. Christou, *Polyhedron* **2007**, *26*, 2165–2168; c) T. C. Stamatatos, D. Foguet-Albiol, S.-C. Lee, C. C. Stoumpos, C. P. Raptopoulou, A. Terzis, W. Wernsdorfer, S. O. Hill, S. P. Perlepes, G. Christou, *J. Am. Chem. Soc.* **2007**, *129*, 9484–9499.
[4] Y.-L. Miao, J.-L. Liu, Z.-J. Lin, Y.-C. Ou, J.-D. Leng, M.-L. Tong, *Dalton Trans.* **2010**, *39*, 4893–4902.
[5] C. P. Raptopoulou, V. Psycharis, *Inorg. Chem. Commun.* **2008**, *11*, 1194–1197.
[6] a) C. Papatriantafyllopoulou, G. Aromi, A. Tasiopoulos, V. Nastopoulos, C. P. Raptopoulou, S. J. Teat, A. Escuer, S. P. Perlepes, *Eur. J. Inorg. Chem.* **2007**, 2761–2774; b) B. Biswas, U. Pieper, T. Weyhermuller, P. Chaudhuri, *Inorg. Chem.* **2009**, *48*, 6781–6793.
[7] a) C. J. Milios, C. P. Raptopoulou, A. Terzis, F. Lloret, R. Vicente, S. P. Perlepes, A. Escuer, *Angew. Chem.* **2004**, *116*, 212–214; *Angew. Chem. Int. Ed.* **2004**, *43*, 210–212; b) C. J. Milios, R. Inglis, A. Vinslava, R. Bagai, W. Wernsdorfer, S. Parsons, S. P. Perlepes, G. Christou, E. K. Brechin, *J. Am. Chem. Soc.* **2007**, *129*, 12505–12511; c) R. Inglis, L. F. Jones, C. J. Milios, S. Datta, A. Collins, S. Parsons, W. Wernsdorfer, S. Hill, S. P. Perlepes, S. Piligkos, E. K. Brechin, *Dalton Trans.* **2009**, 3403–3412; d) B. Cordero, A. Escuer, S. J. teat, O. Roubeau, *Dalton Trans.* **2011**, *40*, 7127–7129; e) E. Cremades, J. Cano, E. Ruiz, G. Rajaraman, C. J. Milios, E. K. Brechin, *Inorg. Chem.* **2009**, *48*, 8012–8019; f) A.-R. Tomsa, J. Martinez-Lillo, Y. Li, L.-M. Chamoreau, K. Boubekeur, F. Farias, M. Novak, E. Cremades, E. Ruiz, A. Proust, M. Verdaguer, P. Gouzerh, *Chem. Commun.* **2010**, *46*, 5106–5108.
[8] a) P. Chaudhuri, *Coord. Chem. Rev.* **2003**, *243*, 143–190; b) C. J. Milios, T. C. Stamatatos, S. P. Perlepes, *Polyhedron* **2006**, *25*, 134–194.
[9] a) T. Weyhermüller, R. Wagner, S. Khanra, P. Chaudhuri, *Dalton Trans.* **2005**, 2539–2546; b) S. Khanra, T. Weyhermuller, E. Rentschler, P. Chaudhuri, *Inorg. Chem.* **2005**, *44*, 8176–8178; c) T. C. Stamatatos, E. Diamantopoulou, A. Tasiopoulos, V. Psycharis, R. Vicente, C. P. Raptopoulou, V. Nastopoulos, A. Escuer, S. P. Perlepes, *Inorg. Chim. Acta* **2006**, *359*, 4149–4157; d) P. Chaudhuri, T. Weyhermuller, R. Wagner, S. Khanra, B. Biswas, E. Bothe, E. Bill, *Inorg. Chem.* **2007**, *46*, 9003–9016; e) T. C. Stamatatos, C. Papatriantafyllopoulou, E. Katsoulakou, C. P. Raptopoulou, S. P. Perlepes, *Polyhedron* **2007**, *26*, 1830–1834; f) S. Zhang, L. Zhen, B. Xu, R. Inglis, K. Li, W. Chen, Y. Zhang, K. F. Konidaris, S. P. Perlepes, E. K. Brechin, Y. Li, *Dalton Trans.* **2010**, *39*, 3563–3571; g) T. C. Stamatatos, K. A. Abboud, S. P. Perlepes, G. Christou, *Dalton Trans.* **2007**, 3861–3863; h) T. C. Stamatatos, A. Escuer, K. A. Abboud, C. P. Raptopoulou, S. P. Perlepes, G. Christou, *Inorg. Chem.* **2008**, *47*, 11825–11838.
[10] C. G. Efthymiou, C. P. Raptopoulou, A. Terzis, S. P. Perlepes, A. Escuer, C. Papatriantafyllopoulou, *Polyhedron* **2010**, *29*, 627–633.
[11] a) C. Papatriantafyllopoulou, C. G. Efthymiou, C. P. Raptopoulou, A. Terzis, E. Manessi-Zoupa, S. P. Perlepes, *Spectrochim. Acta Part A* **2008**, *70*, 718–728; b) C. G. Efthymiou, A. A. Kitos, C. P. Raptopoulou, S. P. Perlepes, A. Escuer, C. Papatriantafyllopoulou, *Polyhedron* **2009**, *28*, 3177–3184; c) C. Papatriantafyllopoulou, T. C. Stamatatos, W. Wernsdorfer, S. J. Teat, A. Tasiopoulos, A. Escuer, S. P. Perlepes, *Inorg. Chem.* **2010**, *49*, 10486–10496.
[12] a) G. Psomas, C. Dendrinou-Samara, M. Alexiou, A. Tsohos, C. P. Raptopoulou, A. Terzis, D. P. Kessissoglou, *Inorg. Chem.* **1998**, *37*, 6556–6557; b) G. Psomas, A. J. Stemmler, C. Dendrinou-Samara, J. J. Bodwin, M. Schneider, M. Alexiou, J. W. Kampf, D .P. Kessissoglou, V. L. Pecoraro, *Inorg. Chem.* **2001**, *40*, 1562–1570; c) M. Alexiou, I. Tsivikas, C. Dendrinou-Samara, A. A. Pantazaki, P. Trikalitis, N. Lalioti, D. A. Kyriakidis, D. P. Kessissoglou, *J. Inorg. Biochem.* **2003**, *93*, 256–264; d) M. Alexiou, C. Dendrinou-Samara, C. P. Raptopoulou, A. Terzis, V. Tangoulis, D. P. Kessissoglou, *Eur. J. Inorg. Chem.* **2004**, 3822–3827; e) T. C. Stamatatos, E. Diamantopoulou, C. P. Raptopoulou, V. Psycharis, A. Escuer, S. P. Perlepes, *Inorg. Chem.* **2007**, *46*, 2350–2352.
[13] D. Gatteschi, L. Pardi, *Gazz. Chim. Ital.* **1993**, *123*, 231–240.
[14] A. Escuer, F. A. Mautner, N. Sanz, R. Vicente, *Inorg. Chem.* **2000**, *39*, 1668–1673.
[15] J. Cano, T. Cauchy, E. Ruiz, C. J. Milios, C. C. Stoumpos, T. C. Stamatos, S. P. Perlepes, G. Christou, E. K. Brechin, *Dalton Trans.* **2008**, 234–240.
[16] a) M. A. Palacios, A. J. Mota, J. E. Perea-Buceta, F. J. White, E. K. Brechin, E. Colacio, *Inorg. Chem.* **2010**, *49*, 10156–10165; b) A. Escuer, J. Esteban, O. Roubeau, *Inorg. Chem.* **2011**, *50*, 8893–8901; c) A. Escuer, G. Vlahopouluo, F. A. Mautner, *Dalton Trans.* **2011**, *40*, 10109–10116.
[17] A. A. Mokhir, K. V. Domasevich, N. K. Dalley, X. Kou, N. N. Gerasimchuk, O. A. Gerasimchuk, *Inorg. Chim. Acta* **1999**, *284*, 85–98.
[18] G. M. Sheldrick, SHELXS - *A computer program for determination of crystal structures*, University of Göttingen, Germany, **1997**.
[19] G. M. Sheldrick, SHELX97 - *A computer program for determination of crystal structures*, University of Göttingen, Germany, **1997**.
[20] a) E. Ruiz, P. Alemany, S. Alvarez, J. Cano, *J. Am. Chem. Soc.* **1997**, *119*, 1297–1303; b) E. Ruiz, J. Cano, S. Alvarez, *Chem. Eur. J.* **2005**, *11*, 4767–4771; c) E. Ruiz, T. Cauchy, J. Cano, R. Costa, J. Tercero, S. Alvarez, *J. Am. Chem. Soc.* **2008**, *130*, 7420–7426.
[21] a) E. Ruiz, *Struct. Bonding (Berlin)* **2004**, *113*, 71–102; b) E. Ruiz, S. Alvarez, J. Cano, V. Polo, *J. Chem. Phys.* **2005**, *123*, 164110.
[22] E. Ruiz, J. Cano, S. Alvarez, P. Alemany, *J. Comp. Chem.* **1999**, *20*, 1391- 1400.
[23] E. Ruiz, A. Rodríguez-Fortea, J. Cano, S. Alvarez, P. Alemany, *J. Comp. Chem.* **2003**, *24*, 982–989.
[24] E. Ruiz, A. Rodríguez-Fortea, J. Tercero, T. Cauchy, C. Massobrio, *J. Chem. Phys.* **2005**, *123*, 074102.
[25] A. D. Becke, *J. Chem. Phys.* **1993**, *98*, 5648–5652.
[26] A. Schäfer, C. Huber, R. Ahlrichs, *J. Chem. Phys.* **1994**, *100*, 5829–5835.
[27] *Gaussian 09 (Revision A.1)*: M. J. Frisch, G. W. Trucks, H. B. Schlegel, G. E. Scuseria, M. A. Robb, J. R. Cheeseman, G. Scalmani, V. Barone, B. Mennucci, G. A. Petersson, H. Nakatsuji, M. Caricato, X. Li, H. P. Hratchian, A. F. Izmaylov, J. Bloino, G. Zheng, J. L. Sonnenberg, M. Hada, M. Ehara, K. Toyota, R. Fukuda, J. Hasegawa, M. Ishida, T. Nakajima, Y. Honda, O. Kitao, H. Nakai, T. Vreven, J. A. Montgomery, Jr., J. E. Peralta, F. Ogliaro, M. Bearpark, J. J. Heyd, E. Brothers, K. N. Kudin, V. N. Staroverov, R. Kobayashi, J. Normand, K. Raghavachari, A. Rendell, J. C. Burant, S. S. Iyengar, J. Tomasi, M. Cossi, N. Rega, J. M. Millam, M. Klene, J. E. Knox, J. B. Cross, V. Bakken, C. Adamo, J. Jaramillo, R. Gomperts, R. E. Stratmann, O. Yazyev, A. J. Austin, R. Cammi, C. Pomelli, J. W. Ochterski, R. L. Martin, K. Morokuma, V. G. Zakrzewski, G. A. Voth, P. Salvador, J. J. Dannenberg, S. Dapprich, A. D. Daniels, Ö. Farkas, J. B. Foresman, J. V. Ortiz, J. Cioslowski, D. J. Fox Wallingford, CT, **2009**.
[28] *Jaguar 7.0*: Schrödinger, LLC, New York, **2007**.
[29] G. Vacek, J. K. Perry, J.-M. Langlois, *Chem. Phys. Lett.* **1999**, *310*, 189–194.
[30] a) D. J. Avnir, O. Katzenelson, S. Keinan, M. Pinsky, Y. Pinto, Y. Salomon, H. Zabrodsky, in *Hel-Or Concepts in Chemistry: A Contemporary Challenge. Research Studies*, Press Ltd.: Tauton, England,

  

**1997**; b) S. Alvarez, P. Alemany, D. Casanova, J. Cirera, M. Llunell, D. J. Avnir, *Coord. Chem. Rev.* **2005**, *249*, 1693–1708.
[31] a) S. Zabrodsky, D. J. Peleg, D. J. Avnir, *J. Am. Chem. Soc.* **1992**, *114*, 7843–7851; b) J. Cirera, P. Alemany, S. Alvarez, *Chem. Eur. J.* **2004**, *10*, 190–207.
[32] SHAPE version 2.0: M. Llunell, D. Casanova, J. Cirera, P. Alemany, S. Alvarez, Barcelona, **2010**.

Received: September 22, 2011
Published online: February 15, 2012

  

### 3.4.1. Resum: Triangular nickel complexes derived from 2-pyridylcyanoxime: An approach to the magnetic properties of the $[Ni_3(\mu_3\text{-}OH)\{pyC(R)NO\}_3]^{2+}$ core.

Jordi Esteban, Eliseo Ruiz, Mercè Font-Bardia, Teresa Calvet, Albert Escuer.

*Chemistry, A European Journal* **2012**, *18*, 3637-3648.

En aquest article es va introduir el lligand 2-acetonitrilpiridiloxima (pyC{CN}NOH) en la química del $Ni^{II}$ i es va estudiar la seva reactivitat amb sals d'anions carboxilat i β-dicetonat.

Es van caracteritzar els compostos $[Ni_3(MeOH)_2(BzO)(OH)(pyC\{CN\}NO)_4]$ (**4_1**), $(NEt_3H)[Ni_6(H_2O)(MeOH)(3\text{-}ClBzO)_2(OH)_2(\mu_{1,5}\text{-}N(CN)_2)(pyC\{CN\}NO)_8]$ (**4_2**), $[Ni_4(MeOH)_2(tfacac)_2(MeO)_2(pyC\{CN\}NO)_4]$ (**4_3**), $[Ni_5(MeOH)_4(3\text{-}ClBzO)_4(OH)_2(pyC\{CN\}NO)_4]$ (**4_4**) i $[Ni_5(H_2O)_4(N_3)_2(BzO)_2(OH)_2(pyC\{CN\}NO)_4]$ (**4_5**), que presenten com a fragment estructural comú una disposició triangular de tres cations $Ni^{II}$ units per un lligand central $\mu_3$-OR (R= H, Me) i, com a mínim, dos ponts oxima. Aquests compostos es poden classificar en triangles aïllats (**4_1**); triangles units per un co-lligand (dicianamida, **4_2**); triangles que comparteixen un costat o aresta, topologia coneguda com papallona o *butterfly* (**4_3**); i finalment en triangles que comparteixen un vèrtex, disposició anomenada llacet o *bowtie* (**4_4** i **4_5**), esquema 9.

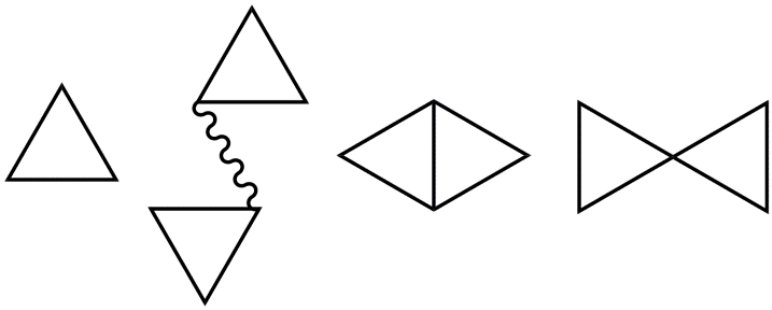

**Esquema 9.** Topologies dels compostos **4_1** – **4_5**.

Els fragments triangulars $Ni_3/\mu_3$-OR/oxima formen part d'un gran nombre de compostos, però no s'havia pogut determinar el seu comportament magnètic ni els factors que hi influeixen perquè no s'havia caracteritzat cap d'aquests sistemes aïllats. Els productes **4_1** i **4_2** són els primers exemples de sistemes $Ni_3/\mu_3$-OR/oxima i permeten identificar de forma inequívoca els factors que

determinen les constants d'acoblament per aquest sistema. Tot i que el compost **4_2** conté dos triangles units per un co-lligand, el superintercanvi magnètic promogut per aquest és negligible i, per tant, els dos triangles es poden considerar magnèticament quasi independents. Els compostos **4_3 – 4_5** són exemples senzills de topologies basades en triangles i compleixen les directrius trobades per **4_1** i **4_2**.

Així, es va realitzar l'estudi magnètic dels diferents compostos i, juntament amb un estudi per DFT, es va poder determinar que:

- els acoblaments mitjançant un grup $\mu_3$-OR i un lligand oxima promouen un acoblament moderadament antiferromagnètic. Aquest acoblament és més antiferromagnètic quan el lligand central és un grup alcoxo ($\mu_3$-OR) que no pas quan es tracta d'un grup hidroxo ($\mu_3$-OH).
- el paràmetre estructural clau per entendre el comportament d'aquestes interaccions és l'angle Ni-O-Ni. L'angle de torsió Ni-N-O-Ni té una incidència molt menor en el valor de *J*.

En comparar el comportament dels sistemes $Ni_3/\mu_3$-OR/oxima amb d'altres semblants com ara $Cu^{II}$ i $Mn^{III}$, s'observa que el valor de la constant d'acoblament en els sistemes de $Ni^{II}$ depèn de l'angle M-O-M com en els sistemes de $Cu^{II}$,[113] mentre que pel cas del $Mn^{III}$ el factor determinant és la torsió M-N-O-M.[169]

## 3.5. Article 5.

## $Ni^{II}$-pyridyloximato triangles with a central $\mu_3$-OH ligand: Magnetostructural correlations

**Jordi Esteban**, Mercè Font-Bardia, Albert Escuer.

*European Journal of Inorganic Chemistry* **2013**, 5274-5280.

EurJIC European Journal of Inorganic Chemistry
ChemPubSoc Europe
FULL PAPER

DOI:10.1002/ejic.201300814

# $Ni^{II}$-Pyridyloximato Triangles with a Central $\mu_3$-OH Ligand: Magnetostructural Correlations

**Jordi Esteban,*[a] Mercè Font-Bardia,[b] and Albert Escuer[a]**

**Keywords:** Cluster compounds / Coordination modes / Magnetic properties / Nickel

New examples of unusual $\mu_3$-OR/oximato-$Ni_3$ isolated triangles have been obtained by treatment of different nickel carboxylato salts with 2-pyridylcyanoxime, pyC{CN}NOH. Depending on the precursor and reaction conditions, compounds $[Ni_3(MeOH)_2(AcO)(OH)(pyC\{CN\}NO)_4]$ (**1**), $(NEt_4)$-$[Ni_3(H_2O)(3\text{-}ClBzO)_2(OH)(pyC\{CN\}NO)_4]$ (**2**) and $(NEt_3H)$-$[Ni_3(H_2O)_3(OH)(Ph_2CHCOO)_3(pyC\{CN\}NO)_3]$ (**3**) were characterized. Direct current magnetic measurements performed in the 2–300 K temperature range revealed antiferromagnetic interactions induced by the $\mu_3$-OR/oximato superexchange pathway, quasi-frustration for **1** and **2**, and an $S = 0$ ground state for **3**. Magnetostuctural correlations derived from the experimental data confirmed the previous DFT predictions relating the magnitude of the superexchange interaction with the Ni–O–Ni bond angle.

## Introduction

The use of pyridyloximate ligands and paramagnetic 3d metal ions in coordination chemistry has been a hot topic in the last decade due to their ability to generate a large number of clusters (254 entries in the CCDC database) with a wide range of properties and interest in a variety of research fields such as in bioinorganic modelling[1] and the design of selective receptors[2] or catalysts,[3] with the magnetic response being the most studied, often in the search for single-molecule magnets (SMMs).[4]

Among the pyridyloximate ligands, the 2-pyridyloximate ligands with general formula pyC{R}NOH are modulable, very versatile, can be easily functionalized and have proven to be suitable for generating stable first-row transition coordination compounds with a wide range of nuclearities and topologies.[5] Focusing our attention on nickel chemistry, all nuclearities from $Ni_3$ to $Ni_{14}$ (except for $Ni_{11}$) have been generated,[6] presenting in some cases out-of-phase signals.[7]

A common trend in medium-to-high nuclearity oximato clusters is the presence of $\mu_3$-OR (R = H, Me)-centred triangular fragments or isolated triangular compounds with the generic $\{M_3(\mu_3\text{-}OR)(R'\text{-}NO)_3\}^{n+}$ core. The study of the magnetostructural correlations of these molecules is important for understanding the magnetic response of larger clusters and, as an example, the dependence of the coupling with the oximato torsion angles in the case of $\{Mn_3(\mu_3\text{-}OR)(R'\text{-salox})\}^{n+}$ (R′-salox = substituted salicyloximato) has been crucial in the search for SMMs in recent years.[4a,8]

Isolated triangles derived from pyridyloximates with the $\{M_3(\mu_3\text{-}OR)(pyC\{R'\}NO)_3\}^{n+}$ core have been well characterized in $Cu^{II}$ chemistry[9] and, despite being less common, for manganese,[10] iron[11] and cobalt.[12] The magnetic response of these small molecules is useful for determining univocally the factors that influence the magnetic coupling and, in some cases, for studying phenomenon such as spin frustration. Note, isolated triangles with the $\{Ni_3(\mu_3\text{-}OR)(pyC\{R'\}NO)_3\}^{n+}$ core were unprecedented and only very recently have two examples been reported by our group together with DFT calculations to determine the factors that influence the superexchange pathway in the nickel case.[6b]

The first isolated $Ni_3$ $\mu_3$-OR/oximato triangles were synthesized with 2-pyridylcyanoxime, pyC{CN}NOH, depicted in Scheme 1, which possesses unique properties in comparison with related ligands due to the presence of the cyano substituent on the C atom vicinal to the oximate function. This cyano group induces an increased acidity in the oxime (3–5 units of $pK_a$ with respect to ligands with

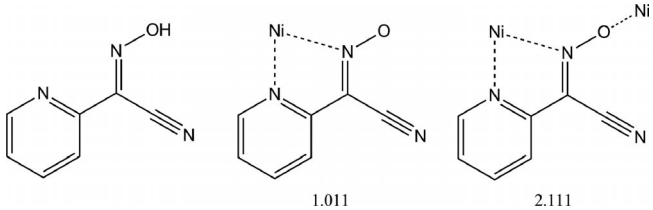


1.011 2.111

Scheme 1. Left: 2-pyridylcyanoxime ligand. Right: coordination modes, in Harris notation,[14] of the deprotonated pyC{CN}NO⁻ ligand found in compounds **1**–**3**.

[a] Departament de Química Inorgànica, Universitat de Barcelona, Av. Diagonal 645, 08028 Barcelona, Spain
E-mail: jordi.esteban@qi.ub.edu
http://www.ub.edu/inorgani/recerca/MagMol/magmol.htm
[b] Department de Cristallografia, Mineralogia i Dipòsits, Universitat de Barcelona, Martí Franquès s/n, 08028 Barcelona, Spain

Supporting information for this article is available on the WWW under http://dx.doi.org/10.1002/ejic.201300814.

EurJIC European Journal of Inorganic Chemistry



other substituents) and significant changes in electronic effects that have led to rare and unprecedented topologies in Cu[9g] and Mn[13] chemistry.

In the search for new examples of isolated $\{Ni_3(\mu_3\text{-}OR)(pyC\{R'\}NO)_3\}^{n+}$ triangles that allow us to validate experimentally the previous DFT predictions, a set of reactions with the pyC{CN}NOH ligand under different conditions have been performed and in this work we report the synthesis, structural characterization and magnetic study of $[Ni_3(MeOH)_2(AcO)(OH)(pyC\{CN\}NO)_4]$ (**1**), $(NEt_4)[Ni_3(H_2O)(3\text{-}ClBzO)_2(OH)(pyC\{CN\}NO)_4]$ (**2**) and $(NEt_3H)[Ni_3(H_2O)_3(OH)(Ph_2CHCOO)_3(pyC\{CN\}NO)_3]$ (**3**). Susceptibility measurements showed moderately strong antiferromagnetic coupling for **1**–**3**. Complexes **1** and **2** are close to magnetically frustrated triangles, whereas complex **3** is an unusual example of an equilateral axial triangle with three-fold symmetry and the $S = 0$ ground state. Correlation of the magnetostructural parameters of these three new examples of $\mu_3$-OR/oximato-$Ni_3$ isolated triangles and the previously reported[6b] $[Ni_3(MeOH)_2(BzO)(OH)(py\{CN\}NO)_4]$ (**4**) and the linked triangles $(NEt_3H)\{\mu_{1,5}\text{-}N(CN)_2\}[Ni_6(H_2O)(MeOH)(3\text{-}ClBzO)_2(OH)_2(py\{CN\}NO)_8]$ (**5**) has confirmed that the Ni–O–Ni bond angles involving the central $RO^-$ bridge are the main factors influencing the magnitude of the superexchange interaction, as was predicted by DFT calculations.

## Results and Discussion

### Structural Description

#### *$[Ni_3(MeOH)_2(AcO)(OH)(pyC\{CN\}NO)_4]\cdot 2.5MeOH$ ($1\cdot 2.5MeOH$)*

A view of the core of complex **1** is illustrated in Figure 1 and selected interatomic distances and angles are listed in Table 1. The core of this compound consists of a nearly isosceles arrangement of three $Ni^{II}$ cations linked by one central $\mu_3$-OH ligand with the O atom placed 0.600(2) Å out of the $Ni_3$ plane.

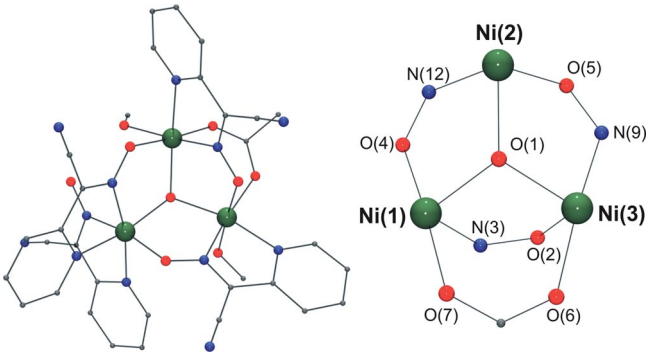


Figure 1. Left: molecular structure of compound **1**. Right: labelled core of **1**. All hydrogen atoms have been omitted for clarity.

Two sides of the triangle are defined by single oximato bridges that link Ni(2) with Ni(1) and Ni(3), and the third side, between Ni(1) and Ni(3), is defined by one oximato and one *syn-syn* carboxylato bridge. This third side, involving the carboxylato bridge, has the smallest Ni···Ni distance and Ni–O–Ni bond angle (Table 1).

Table 1. Selected distances [Å] and angles [°] for the core of compound **1**.

| | | | |
|---|---|---|---|
| Ni(1)–N(1) | 2.080(3) | Ni(1)–N(3) | 2.040(3) |
| Ni(1)–O(1) | 2.041(3) | Ni(1)–O(4) | 2.036(2) |
| Ni(1)–O(7) | 2.048(2) | Ni(1)–O(9) | 2.073(2) |
| Ni(2)–N(4) | 2.100(4) | Ni(2)–N(6) | 2.066(3) |
| Ni(2)–N(10) | 2.119(3) | Ni(2)–N(12) | 2.051(3) |
| Ni(2)–O(1) | 2.057(2) | Ni(2)–O(5) | 2.075(2) |
| Ni(3)–N(7) | 2.064(3) | Ni(3)–N(9) | 2.041(3) |
| Ni(3)–O(1) | 2.026(2) | Ni(3)–O(2) | 2.062(2) |
| Ni(3)–O(6) | 2.034(2) | Ni(3)–O(8) | 2.128(3) |
| Ni(1)–O(1)–Ni(2) | 116.1(1) | Ni(1)–N(3)–O(2)–Ni(3) | 15.0(3) |
| Ni(2)–O(1)–Ni(3) | 114.9(1) | Ni(3)–N(9)–O(5)–Ni(1) | 26.6(3) |
| Ni(1)–O(1)–Ni(3) | 104.0(1) | Ni(2)–N(12)–O(4)–Ni(1) | 3.2(3) |
| Ni(1)···Ni(2) | 3.4769(7) | Ni(1)···Ni(3) | 3.4427(6) |
| Ni(1)···Ni(3) | 3.2056(6) | | |

Ni(1) and Ni(3) exhibit a $NiN_2O_4$ environment generated by one pyC{CN}$NO^-$ ligand (bonded through its two N atoms), the central $\mu_3$-OH group, one O atom from an oximato bridge, one monodentate acetato ligand and one coordinated MeOH, whereas Ni(2) exhibits a $NiN_4O_2$ environment formed from two pyC{CN}$NO^-$ ligands (both bonded by their two N atoms), one *O*-oximato bridge and the central $\mu_3$-OH group. The three bridging oximato ligands are coordinated in the 2.111 coordination mode (see Scheme 1), and the fourth deprotonated 2-pyridylcyanoximato ligand, coordinated to Ni(2), is coordinated in the 1.011 coordination mode and forms a strong hydrogen bond with the MeOH molecule linked to Ni(1). One of the lattice methanol molecules also generates strong hydrogen bonds with the $\mu_3$-OH group and the methanol molecule coordinated to Ni(3) (see Figure S1 and Table S1 in the Supporting Information). Molecules of **1** are linked by means of intermolecular hydrogen bonds mediated by one of the lattice methanol molecules, resulting in a 1D arrangement of trimers along the *a* direction of the cell (see Figure S1).

#### *$(NEt_4)[Ni_3(H_2O)(3\text{-}ClBzO)_2(OH)(pyC\{CN\}NO)_4]\cdot H_2O\cdot 2CH_2Cl_2$ ($2\cdot H_2O\cdot 2CH_2Cl_2$)*

A labelled structure and selected interatomic distances and angles for **2** are presented in Figure 2 and Table 2, respectively. The structure of the core of **2** is similar to that of complex **1** with a central $\mu_3$-OH group located 0.556(2) Å out of the $Ni_3$ plane, with three 2.111- and one 1.011-coordinated 2-pyridylcyanoximato ligands and one *syn-syn* carboxylate bridge. The main difference lies in the fact that one of the coordinated solvent molecules has been substituted by one monodentate carboxylate ligand, resulting in an anionic triangle with extra negative charge that is compensated by one tetraethylammonium counter cation. The coordination environments, similar to compound **1**, are $NiN_2O_4$ for Ni(1) and Ni(2) and $NiN_4O_2$ for Ni(3) with the only difference being the coordination of one water molecule and one monodentate carboxylato ligand on Ni(3) and Ni(2), respectively. Intramolecular hydrogen bonds are



 

EurJIC European Journal of Inorganic Chemistry



formed between the monodentate 3-ClBzO$^-$ and central hydroxo group and the non-coordinated oximate ligand and the coordinated water molecule. One lattice water molecule forms a number of intramolecular hydrogen bonds with the water molecule on Ni(1) and the non-coordinated O atom of the carboxylato ligand (see Figure S2 and Table S1 in the Supporting Information). Intermolecular interactions are negligible, the trimers being well isolated by the dichloromethane and tetraethylammonium molecules.

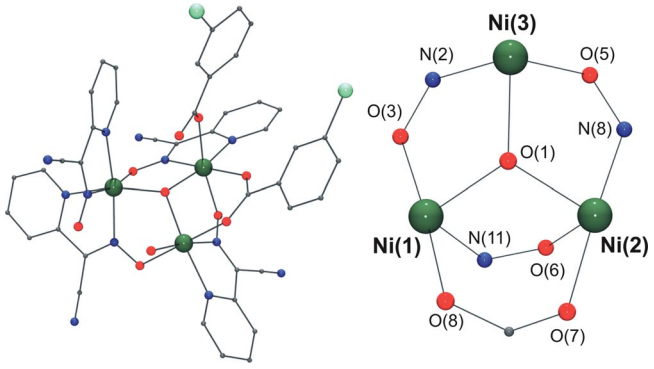


Figure 2. Left: molecular structure of compound **2**. Right: labelled core of **2**. All hydrogen atoms have been omitted for clarity.

Table 2. Selected distances [Å] and angles [°] for the core of compound **2**.

| | | | |
|---|---|---|---|
| Ni(1)–N(10) | 2.086(2) | Ni(1)–N(11) | 2.057(2) |
| Ni(1)–O(1) | 2.010(2) | Ni(1)–O(2) | 2.110(2) |
| Ni(1)–O(3) | 2.091(2) | Ni(1)–O(8) | 2.086(2) |
| Ni(2)–N(7) | 2.088(2) | Ni(2)–N(8) | 2.085(2) |
| Ni(2)–O(1) | 2.041(2) | Ni(2)–O(6) | 2.099(2) |
| Ni(2)–O(7) | 2.069(2) | Ni(2)–O(9) | 2.080(2) |
| Ni(3)–N(1) | 2.080(2) | Ni(3)–N(2) | 2.052(2) |
| Ni(3)–N(4) | 2.131(3) | Ni(3)–N(5) | 2.109(2) |
| Ni(3)–O(1) | 2.030(2) | Ni(3)–O(5) | 2.086(2) |
| Ni(1)–O(1)–Ni(2) | 106.35(8) | Ni(1)–N(11)–O(6)–Ni(2) | 25.2(2) |
| Ni(2)–O(1)–Ni(3) | 114.52(9) | Ni(2)–N(8)–O(5)–Ni(3) | 16.6(2) |
| Ni(1)–O(1)–Ni(3) | 117.34(9) | Ni(3)–N(2)–O(3)–Ni(1) | 2.1(2) |
| Ni(1)···Ni(2) | 3.2426(9) | Ni(1)···Ni(3) | 3.451(1) |
| Ni(2)···Ni(3) | 3.4248(8) | | |

### *(NEt$_3$H)[Ni$_3$(H$_2$O)$_3$(OH)(Ph$_2$CHCOO)$_3$(pyC{CN}NO)$_3$]·3.5H$_2$O (3·3.5H$_2$O)*

The labelled structure of **3** is depicted in Figure 3 and selected interatomic distances and angles are listed in Table 3. The anionic equilateral triangular unit of **3** is formed by one central $\mu_3$-OH group located 0.585(3) Å out of the Ni$_3$ plane, three 2.111-coordinated pyC{CN}NO$^-$ ligands, three monodentate carboxylates and three coordinated water molecules. All three Ni centres, related by the $C_3$ axis, possess a NiN$_2$O$_4$ environment generated by the two N atoms of a pyC{CN}NO$^-$ ligand, one *O*-oximato bridge, the central $\mu_3$-OH group, the monodentate Ph$_2$CHCOO$^-$ and one water molecule. Charge balance is achieved by one trimethylammonium cation. Each coordinated water molecule forms an intramolecular hydrogen bond with the uncoordinated arm of the neighbouring carboxylate, and one water molecule is trapped in the cavity generated by the aromatic rings of the Ph$_2$CHCOO$^-$ ligands, establishing a strong hydrogen bond with the central $\mu_3$-OH group. One of the lattice water molecules forms a hydrogen bond with the –NH donor group of the triethylammonium cation, and the remaining ones are interlinked by very strong hydrogen bonds forming an unusual hexagonal "drop" of water with a boat configuration (see Figure S3 and Table S1 in the Supporting Information).

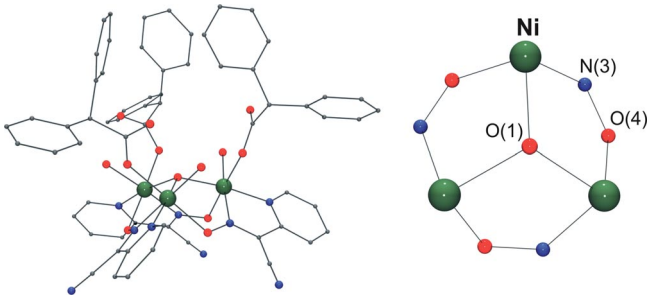


Figure 3. Left: molecular structure of compound **3**. Right: labelled core of **3**. All hydrogen atoms have been omitted for clarity.

Table 3. Selected distances [Å] and angles [°] for the core of compound **3**.

| | | | |
|---|---|---|---|
| Ni–N(1) | 2.054(3) | Ni–N(3) | 2.055(3) |
| Ni–O(1) | 2.033(1) | Ni–O(2) | 2.085(2) |
| Ni–O(4) | 2.082(2) | Ni–O(5) | 2.071(3) |
| Ni–O(1)–Ni′ | 112.1(1) | N(1)–Ni–N(3) | 79.75(9) |
| Ni–N(3)–O(4)–Ni′ | 13.9(3) | | |

### Magnetic Measurements and Modeling

The temperature dependence of the $\chi_M T$ product for trinuclear compounds **1** and **2** are plotted in Figure 4. For compounds **1** and **2**, the $\chi_M T$ product behaves very similarly, as can be expected from their similar structures and bond parameters. The room temperature $\chi_M T$ value is 2.87 and 2.77 cm$^3$ K mol$^{-1}$ for **1** and **2**, respectively. These values decrease continuously on cooling to 0.48 and 0.51 cm$^3$ K mol$^{-1}$ at 2 K, exhibiting a plateau at around 30 K with similar values of 0.95 and 1.05 cm$^3$ K mol$^{-1}$. The experimental data was fitted by using the PHY program.[15]

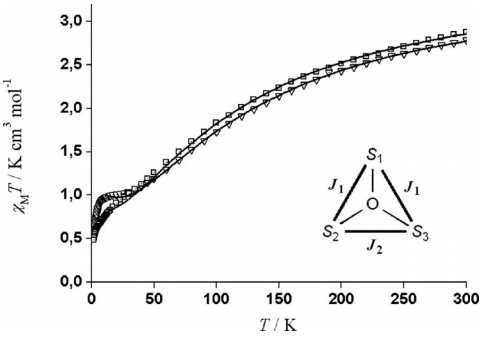


Figure 4. $\chi_M T$ product vs. $T$ for compounds **1** (dot-centred squares) and **2** (dot-centred triangles). Solid lines show the best obtained fit. Inset: two-$J$ interaction scheme (see text).



 

On the basis of the quasi-isosceles core of these compounds, the two-*J* model schematized in Figure 4 (inset) was assumed applying the derived Hamiltonian in Equation (1).

$$H = -J_1(S_1S_2 + S_1S_3) - J_2(S_2S_3) \quad (1)$$

The best-fit parameters are $J_1$ = –44.6 cm$^{-1}$, $J_2$ = –24.4 cm$^{-1}$, $g$ = 2.21 and $R = 2.57 \times 10^{-4}$ [$R = (\chi_M T_{exp} - \chi_M T_{calcd.})^2/(\chi_M T_{exp})^2$] for **1** and $J_1$ = –49.5 cm$^{-1}$, $J_2$ = –22.9 cm$^{-1}$, $g$ = 2.20 and $R = 1.02 \times 10^{-4}$ for **2**. Trials to differentiate the three coupling constants by means of a 3-*J* Hamiltonian gave an isosceles response with practically identical values and thus the two-*J* calculation was assumed to be reliable.

Compound **3** shows a $\chi_M T$ value of 2.91 cm$^3$ K mol$^{-1}$ at room temperature, which diminishes constantly upon cooling and, in contrast to **1** and **2**, tends to zero at low temperatures ($\chi_M T$ value of 0.05 cm$^3$ K mol$^{-1}$ at 2 K; Figure 5). The experimental data was fitted by using the PHY program[15] and, due to the $C_3$ symmetry of the cluster, a Hamiltonian was applied with only one exchange coupling constant [Equation (2)]. The best-fit parameters are $J$ = –26.16 cm$^{-1}$, $g$ = 2.15 and $R = 2.46 \times 10^{-4}$.

$$H = -J(S_1S_2 + S_1S_3 + S_2S_3) \quad (2)$$

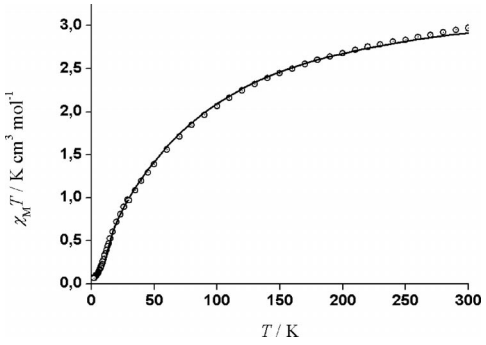


Figure 5. $\chi_M T$ product vs. $T$ for compound **3**. Solid line shows the best obtained fit.

Note that three $S$ = 1 paramagnetic metal centres, each coupled antiferromagnetically, exhibit a $\chi_M T$ value at 2 K of around 0.5 cm$^3$ K mol$^{-1}$ for **1** and **2** and nearly 0 for **3**, when classical magnetic spin vectors would predict the lowest possible ground state of $S$ = 1 (with its $\chi_M T$ product of 0.99 cm$^3$ K mol$^{-1}$ at 2 K for $g$ = 2.00). However, the results are not surprising on the basis of the dependence of the spin energy levels of isosceles and equilateral triangles on the magnitude of the coupling constants[16] (Figure 6). The $J_1$ and $J_2$ notation is illustrated in Figure 4, and in the case of equilateral triangles, $J_1$ and $J_2$ are the same and thus the $J_2/J_1$ ratio is equal to 1.

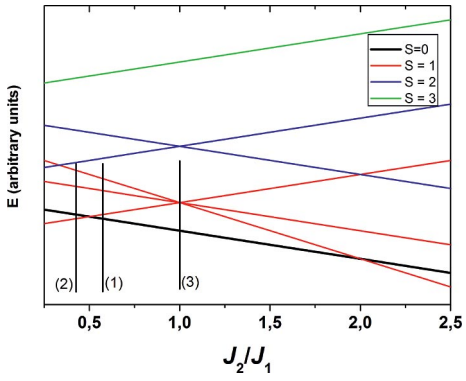


Figure 6. Variation of the spin-state energies for an antiferromagnetic triangle vs. the $J_2/J_1$ ratio for local spins $S_1 = S_2 = S_3 = 1$. Vertical lines show the $J_2/J_1$ ratios for compounds **1**–**3**.

The calculated coupling constants for compounds **1** and **2** give $J_2/J_1$ values close to 0.5 (0.55 and 0.46, respectively) and, according to the energy diagram, they have almost degenerate $S$ = 1 and $S$ = 0 ground spin states (calculated gaps are 4.2 and 3.7 cm$^{-1}$ for **1** and **2**), and thus both spin states are populated even at low temperature, resulting in the $\chi_M T$ intermediate value of around 0.5 cm$^3$ K mol$^{-1}$ at 2 K (between the $\chi_M T$ values of 0 and 0.99 cm$^3$ K mol$^{-1}$ expected for $S$ = 0 and $S$ = 1, respectively, and $g$ = 2.00). Furthermore, for the equilateral system **3**, all the coupling constants have the same value and the $J_2/J_1$ ratio is equal to 1. The gap between $S$ = 0 and the degenerate set of $S$ = 1 spin states is equal to $|J|$, and in this case is 26.2 cm$^{-1}$. This gap is large enough that only the $S$ = 0 ground state is populated at low temperatures, leading to this unusual ground state and its associated diamagnetic response at low temperature.

## Magnetostructural Correlations

The key structural parameters and calculated exchange coupling constants for **1**–**3** and the previously reported systems[6b] $[Ni_3(MeOH)_2(BzO)(OH)(pyC\{CN\}NO)_4]$ (**4**) and $(NEt_3H)\{\mu_{1,5}\text{-}N(CN)_2\}[Ni_6(H_2O)(MeOH)(3\text{-}ClBzO)_2(OH)_2(pyC\{CN\}NO)_8]$ (**5**) are listed in Table 4. Complexes **1**, **2**, **4** and **5** have a common isosceles core with one additional *syn-syn* carboxylato bridge on one side, whereas the sides of **3** are defined exclusively by oximato bridges in an equilateral arrangement. From the analysis of these data we realize that the magnitude of the antiferromagnetic interaction has a wide range of values (–55.2 to –16.8 cm$^{-1}$). The main structural parameters involving the bridges between the nickel atoms also show a wide variation (102.2–117.3° for the Ni–O–Ni bond angle and 2.1–26.6° for the Ni–O–N–Ni torsion angle).

In good agreement with previous DFT calculations,[6b] the isosceles response of the magnetic interactions and structural data from Table 4 suggest that the Ni–O–Ni bond angles correlate with the magnitude of the coupling constants whereas there is no evident correlation with the Ni–O–N–Ni torsion angles. This becomes evident in Figure 7,

 

Table 4. Structural parameters and calculated exchange coupling constants for compounds **1**–**3** and the previously reported complexes **4** and **5**.[a]

| Bridges | ∠Ni–O–Ni [°] | ∠Ni–N–O–Ni [°] | $J_{exp}$ [cm$^{-1}$] | Ref. |
|---|---|---|---|---|
| Compound **1** | | | | |
| $J_1$ NO, OH | 116.1 | 3.2 | –44.6 | |
| $J_1$ NO, OH | 114.9 | 26.6 | –44.6 | |
| $J_2$ NO, OH, RCOO | 104.0 | 15.0 | –24.4 | |
| Compound **2** | | | | |
| $J_1$ NO, OH | 117.3 | 2.1 | –49.5 | |
| $J_1$ NO, OH | 114.5 | 16.6 | –49.5 | |
| $J_2$ NO, OH, RCOO | 106.4 | 25.2 | –22.9 | |
| Compound **3** | | | | |
| $J$ NO, OH | 112.1(1) | 13.9 | –26.2 | |
| Compound **4**[a] | | | | |
| $J_1$ NO, OH | 116.3 | 3.3 | –55.2 | [6b] |
| $J_1$ NO, OH | 115.1 | 17.0 | –55.2 | |
| $J_2$ NO, OH, RCOO | 102.2 | 16.7 | –16.8 | |
| Compound **5**[a] | | | | |
| $J_1$ NO, OH | 116.0 | 9.6 | –53.9 | [6b] |
| $J_1$ NO, OH | 114.2 | 11. 2 | –53.9 | |
| $J_2$ NO, OH, RCOO | 103.0 | 25.7 | –19.8 | |

[a] Average values.

which shows a linear dependence of $J$ with the Ni–O–Ni bond angle, whereas the plot of $J$ as a function of the Ni–O–N–Ni torsion angle shows very different values of $J$ for similar torsion angles and similar $J$ values for any torsion.

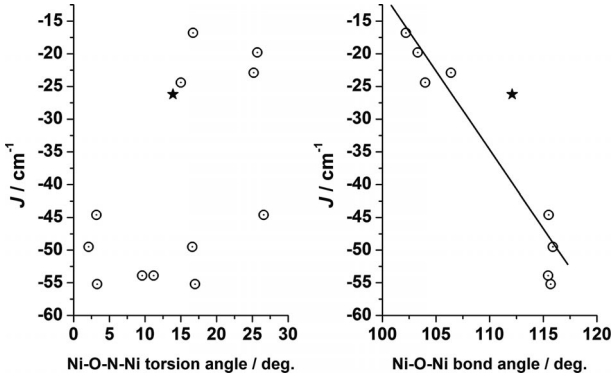


Figure 7. Plots of the experimental $J$ values for **1**–**5** as a function of the oximato torsion angle (left) or the Ni–O–Ni bond angle (average value for angles with the same $J_1$) involving the central hydroxo ligand (right). The points plotted as solid stars correspond to the equilateral triangle **3**.

For the $\{Cu_3(\mu_3\text{-OR})(R'\text{-NO})_3\}^{n+}$ triangles it has been demonstrated by DFT calculations and proven experimentally that the main contribution to the antiferromagnetic coupling is correlated with the Cu–O–Cu bond angles with a minor contribution of the torsion of the oximato bridges,[9e] whereas for R-salox$^-$/Mn$^{III}$ triangles, ferro- or antiferromagnetic coupling has been reported as a function of the Mn–N–O–Mn torsion angle, the ferro/antiferromagnetic limit lying at a torsion angle of around 30°.[8] The study of the superexchange interactions for **1**–**5** provides enough experimental data to confirm the expected magneto-structural trends, resulting in behaviour similar to Cu$^{II}$ analogous systems.

From the above data emerges an important consequence: as a function of the magnitude of the coupling constants inside the triangular fragments, their ground state will be $S = 1$, a mixture of $S = 1$ and $S = 0$, or even $S = 0$ for three-fold symmetry. Thus, the presence of $\{Ni_3(\mu_3\text{-OR})(R'\text{-NO})_3\}$ fragments in larger clusters does not contribute to an enlargement of the $S$ ground state and it can be assumed as unfavourable in the search for a SMM response.

## Conclusions

2-Pyridylcyanoxime ligand is the only pyridyloximate able to generate the highly unusual $\mu_3$-OR/oximato-Ni$_3$ isolated triangles so far. In this work, starting from the same oximate ligand, three new Ni$_3$ triangles have been characterized. Analysis of the structural and magnetic data has confirmed previous DFT predictions that indicated that the antiferromagnetic interaction depends fundamentally on the Ni–O–Ni angle, whereas the Ni–N–O–Ni torsion angle has little effect on the magnetic coupling. The presence of $\{Ni_3(\mu_3\text{-OR})(R'\text{-NO})_3\}$ fragments in larger nuclearity clusters does not contribute to an enlargement of the spin ground state in contrast to a related Mn$^{III}$ case.

## Experimental Section

**Synthesis:** 2-Pyridylacetonitrile and nickel acetate were purchased from Sigma–Aldrich and used without further purification. The pyC{CN}NOH ligand was prepared according to the procedure reported in the literature.[17] $[Ni(3\text{-Cl-BzO})_2]\cdot 2.5H_2O$ and $[Ni(Ph_2CHCOO)_2]\cdot xH_2O$ were synthesized by dissolving equimolar quantities (40 mmol) of 3-chlorobenzoic acid and diphenylbenzoic acid, respectively, and NaOH in $H_2O$ (40 mL), filtering and mixing the final solution with a commercial source of $Ni(NO_3)_2\cdot 6H_2O$ (20 mmol) in water (20 mL). The resulting nickel salts were obtained as green precipitates in good yields (>80%). Samples for analyses were gently ground and vacuum-dried to remove volatile solvents. The yields of **1**–**3** were around 40% as well-formed crystalline products, which were employed in the physical measurements. Further powder fractions were discarded.

**$[Ni_3(MeOH)_2(AcO)(OH)(pyC\{CN\}NO)_4]\cdot 2.5MeOH$ (1·2.5MeOH):** Solid 2-pyridylcyanoxime (0.074 g, 0.5 mmol) was dissolved in MeOH (20 mL) together with $Ni(AcO)_2\cdot 4H_2O$ (0.246 g, 1 mmol) and $NEt_3$ (0.051 g, 0.5 mmol). The solution was stirred for 2 h, then filtered and crystallized by layering with diethyl ether (10 mL). Relevant IR bands: $\tilde{\nu}$ = 3419 (br), 2219 (w), 1602 (s), 1571 (m), 1462 (s), 1421 (m), 1301 (w), 1266 (w), 1225 (s), 1157 (w), 1108 (w), 1060 (w), 1037 (m), 779 (m), 711 (m) cm$^{-1}$. Elemental analysis for dried **1**: $C_{32}H_{28}N_{12}Ni_3O_9$ (**1**: 900.78): calcd. C 42.67, H 3.13, N 18.66; found C 41.9, H 3.3, N 19.0.

**$(NEt_4)[Ni_3(H_2O)(3\text{-ClBzO})_2(OH)(pyC\{CN\}NO)_4]\cdot H_2O\cdot 2CH_2Cl_2$ ($2\cdot H_2O\cdot 2CH_2Cl_2$):** pyC{CN}NOH (0.074 g, 0.5 mmol), $Ni(3\text{-ClBzO})_2\cdot xH_2O$ (0.369 g, 1 mmol) and $NEt_3$ (0.051 g, 0.5 mmol)



 

were dissolved in dichloromethane (20 mL). The solution was stirred for 2 h and then filtered. Crystals were obtained by layering this final solution with hexane (10 mL). Relevant IR bands: $\tilde{\nu}$ = 3392 (br), 2216 (w), 1601 (s), 1561 (m), 1458 (s), 1419 (m), 1390 (m), 1302 (w), 1266 (w), 1228 (s), 1155 (w), 1106 (w), 1037 (m), 1006 (w), 777 (w), 737 (w), 711 (m) $cm^{-1}$. Elemental analysis for dried **2**: $C_{50}Cl_2H_{47}N_{13}Ni_3O_{10}$ (**2**·$H_2O$: 1237.04 + 18.0): calcd. C 47.85, H 3.93, N 14.51; found C 46.8, H 3.7, N 14.9.

$Et_4N^+$ is the counter cation of complex **2** and $Et_3N$ was employed as the base in its synthesis. The reactivity of di- or trialkylamines with dichloromethane under mild conditions was established early[17a] and the use of triethylamine as base and $CH_2Cl_2$ as solvent in nickel or manganese chemistry can lead, probably catalysed by the cation, to a wide variety of products such as $Et_4N^+$, $Et_2NH_2^+$ or chloroalkyl derivatives.[13,18b]

**$(NEt_3H)[Ni_3(H_2O)_3(OH)(Ph_2CHCOO)_3(pyC\{CN\}NO)_3]\cdot 3.5H_2O$ (3·3.5$H_2O$):** pyC{CN}NOH (0.074 g, 0.5 mmol) and $[Ni(Ph_2CHCOO)_2]\cdot xH_2O$ (0.369 g, 1 mmol) were added to dichloromethane (10 mL) together with $NEt_3$ (0.051 g, 0.5 mmol). The solution was stirred for 2 h, then filtered and finally layered with hexane (10 mL). Relevant IR bands: $\tilde{\nu}$ = 3427 (br), 2920 (w), 2216 (w), 1603 (s), 1457 (s), 1424 (m), 1378 (m), 1302 (w), 1229 (m), 1154 (w), 1058 (w), 1036 (m), 779 (w), 747 (m), 711 (m) $cm^{-1}$. Elemental analysis for dried **3**·3.5$H_2O$: $C_{69}H_{68}N_{10}Ni_3O_{13}$ (**3**·3.5$H_2O$: 1421.49 + 63.1): calcd. C 55.82, H 5.09, N 9.44; found C 54.2, H 5.3, N 9.7.

**Physical Measurements:** Magnetic susceptibility measurements were carried out on polycrystalline samples using a Quantum Design MPMS-5 SQUID susceptometer working in the range 2–300 K under magnetic fields of 0.3 (300–30 K) and 0.03 T (30–2 K) to avoid saturation effects. Diamagnetic corrections were estimated from Pascal's tables. IR spectra (4000–400 $cm^{-1}$) were recorded as KBr pellets with a Bruker IFS-125 FT-IR spectrometer.

### Single-Crystal X-ray Structure Analyses

Details of crystal data, data collection and refinement are given in Table 5. X-ray data were collected with a Bruker CCD SMART1000 diffractometer for **1** and a MAR345 diffractometer with an image plate detector for **2** and **3**, all three with graphite-monochromated Mo-$K_\alpha$ radiation ($\lambda$ = 0.71073 Å). All structures were solved by direct methods by using the SHELXS computer program[19] and refined by the full-matrix least-squares method by using the SHELX97 computer program.[20] Five hydrogen atoms for **1** and three for **2** were located from a difference synthesis, whereas all the remaining hydrogen atoms were computed and refined by using a riding model with an overall isotropic temperature factor equal to 1.2 times the equivalent temperature factor of the atom to which it is linked. Lorentzian, polarization and absorption corrections were applied.

Table 5. Crystal data, data collection and structure refinement details for the X-ray structure determination of compounds **1**–**3**.

| | **1**·2.5MeOH | **2**·$H_2O$·2$CH_2Cl_2$ | **3**·3.5$H_2O$ |
|---|---|---|---|
| Formula | $C_{69}H_{76}N_{24}Ni_6O_{23}$ | $C_{52}Cl_6H_{53}N_{13}Ni_3O_{13}$ | $C_{138}H_{150}N_{20}Ni_6O_{33}$ |
| $M_r$ | 1961.80 | 1424.90 | 2968.99 |
| System | Triclinic | Triclinic | Trigonal |
| Space group | $P\bar{1}$ | $P\bar{1}$ | $P\bar{3}$ |
| $a$ [Å] | 9.7760(12) | 14.339(5) | 14.404(3) |
| $b$ [Å] | 12.4096(16) | 14.681(4) | 14.404(3) |
| $c$ [Å] | 17.711(2) | 14.800(3) | 20.6310(10) |
| $\alpha$ [°] | 78.084(2) | 81.64(2) | 90 |
| $\beta$ [°] | 89.742(2) | 80.71(2) | 90 |
| $\gamma$ [°] | 86.745(2) | 87.84(2) | 120 |
| $V$ [Å$^3$] | 2098.9(5) | 3041.7(15) | 3707.0(11) |
| $Z$ | 1 | 2 | 1 |
| $T$ [K] | 100(1) | 293(2) | 203(2) |
| $\lambda$(Mo-$K_\alpha$) [Å] | 0.71073 | 0.71073 | 0.71073 |
| $\rho_{calcd.}$ [g cm$^{-3}$] | 1.552 | 1.556 | 1.327 |
| $\mu$ [mm$^{-1}$] | 1.405 | 1.251 | 0.824 |
| $R$[a] | 0.0390 | 0.0469 | 0.0733 |
| $wR^2$[b] | 0.1151 | 0.1402 | 0.2438 |

[a] Author, please give footnote. [b] Author, please give footnote.

**Supporting Information** (see footnote on the first page of this article): Plots and bond parameters for the main hydrogen-bonding interactions for **1**–**3**.

## Acknowledgments

Funds from the Ministerio de Economia y Competitividad Project (CTQ2012-30662) are acknowledged. A. E. is thankful for financial support from the Institució Catalana de Recerca i Estudis Avançats through an ICREA Academia Award for excellence in research.

[1] D. T. Rosa, J. A. Krause Bauer, M. J. Baldwin, *Inorg. Chem.* **2001**, *40*, 1606–1613.
[2] S. Akine, T. Taniguchi, T. Saiki, T. Nabeshima, *J. Am. Chem. Soc.* **2005**, *127*, 540–541.
[3] M. J. Goldcamp, S. E. Robison, J. A. Krause Bauer, M. J. Baldwin, *Inorg. Chem.* **2002**, *41*, 2307–2309.
[4] a) P. Chaudhuri, *Coord. Chem. Rev.* **2003**, *243*, 143–190; b) C. J. Milios, C. P. Raptopoulou, A. Terzis, F. Lloret, R. Vicente, S. P. Perlepes, A. Escuer, *Angew. Chem.* **2004**, *116*, 212; *Angew. Chem. Int. Ed.* **2004**, *43*, 210–212; c) C. J. Milios, E. Kefalloniti, C. P. Raptopoulou, A. Terzis, R. Vicente, N. Lalioti, A. Escuer, S. P. Perlepes, *Chem. Commun.* **2003**, 819–821; d) C. J. Milios, T. C. Stamatatos, P. Kyritsis, A. Terzis, C. P. Raptopoulou, R. Vicente, A. Escuer, S. P. Perlepes, *Eur. J. Inorg. Chem.* **2004**, 2885–2901; e) R. Clérac, H. Miyasaka, M. Yamashita, C. Coulon, *J. Am. Chem. Soc.* **2002**, *124*, 12837–12844.
[5] C. J. Milios, T. C. Stamatatos, S. P. Perlepes, *Polyhedron* **2006**, *25*, 134–194.
[6] a) A. Escuer, J. Esteban, N. Aliaga-Alcalde, M. Font-Bardia, T. Calvet, O. Roubeau, S. J. Teat, *Inorg. Chem.* **2010**, *49*, 2259–2266; b) J. Esteban, E. Ruiz, M. Font-Bardia, T. Calvet, A. Escuer, *Chem. Eur. J.* **2012**, *18*, 3637–3648; c) T. C. Stamatatos, E. Diamantopoulou, C. P. Raptopoulou, V. Psycharis, A. Escuer, S. P. Perlepes, *Inorg. Chem.* **2007**, *46*, 2350–2352; d) A. Escuer, J. Esteban, O. Roubeau, *Inorg. Chem.* **2011**, *50*, 8893–8901; e) A. Escuer, J. Esteban, M. Font-Bardia, *Chem. Commun.* **2012**, *48*, 9777–9779; f) T. C. Stamatatos, K. A. Abboud, S. P. Perlepes, G. Christou, *Dalton Trans.* **2007**, 3861–3863; g) T. C. Stamatatos, A. Escuer, K. A. Abboud, C. P. Raptopoulou, S. P. Perlepes, G. Christou, *Inorg. Chem.* **2008**, *47*, 11825–11838; h) J. Esteban, L. Alcázar, M. Torres-Molina, M. Monfort, M. Font-Bardia, A. Escuer, *Inorg. Chem.* **2012**, *51*, 5503–5505.
[7] C. Papatriantafyllopoulou, T. C. Stamatatos, W. Wernsdorfer, S. J. Teat, A. J. Tasiopoulos, A. Escuer, S. P. Perlepes, *Inorg. Chem.* **2010**, *49*, 10486–10496.
[8] a) C. J. Milios, C. P. Raptopoulou, A. Terzis, F. Lloret, R. Vicente, S. P. Perlepes, A. Escuer, *Angew. Chem.* **2004**, *116*, 212–214; b) C. J. Milios, R. Inglis, A. Vinslava, R. Bagai, W. Wernsdorfer, S. Parsons, S. P. Perlepes, G. Christou, E. K. Bre-

 

chin, *J. Am. Chem. Soc.* **2007**, *129*, 12505–12511; c) R. Inglis, L. F. Jones, C. J. Milios, S. Datta, A. Collins, S. Parsons, W. Wernsdorfer, S. Hill, S. P. Perlepes, S. Piligkos, E. K. Brechin, *Dalton Trans.* **2009**, 3403–3412; d) B. Cordero, A. Escuer, S. J. Teat, O. Roubeau, *Dalton Trans.* **2011**, *40*, 7127–7129; e) E. Cremades, J. Cano, E. Ruiz, G. Rajaraman, C. J. Milios, E. K. Brechin, *Inorg. Chem.* **2009**, *48*, 8012–8019; f) A.-R. Tomsa, J. Martinez-Lillo, Y. Li, L.-M. Chamoreau, K. Boubekeur, F. Farias, M. Novak, E. Cremades, E. Ruiz, A. Proust, M. Verdaguer, P. Gouzerh, *Chem. Commun.* **2010**, *46*, 5106–5108.

[9] a) R. Beckett, B. F. J. Hoskins, *J. Chem. Soc., Dalton Trans.* **1972**, 291–295; b) T. C. Stamatatos, J. C. Vlahopoulou, Y. Sanakis, C. Raptopoulou, V. Psycharis, A. K. Boudalis, S. P. Perlepes, *Inorg. Chem. Commun.* **2006**, *9*, 814–818; c) T. Afrati, C. M. Zaleski, C. Dendrinou-Samara, G. Mezei, J. W. Kampf, V. L. Pecoraro, D. P. Kessissoglou, *Dalton Trans.* **2007**, 2658–2668; d) T. Afrati, C. Dendrinou-Samara, C. Raptopoulou, A. Terzis, V. Tangoulis, D. P. Kessissoglou, *Dalton Trans.* **2007**, 5156–5164; e) T. Afrati, C. Dendrinou-Samara, C. Raptopoulou, A. Terzis, V. Tangoulis, A. Tsipis, D. P. Kessissoglou, *Inorg. Chem.* **2008**, *47*, 7545–7555; f) A. Escuer, B. Cordero, M. Font-Bardia, T. Calvet, *Inorg. Chem.* **2010**, *49*, 9752–9754; g) A. Escuer, G. Vlahopoulou, S. P. Perlepes, F. A. Mautner, *Inorg. Chem.* **2011**, *50*, 2468–2478.

[10] a) T. C. Stamatatos, D. Foguet-Albiol, C. C. Stoumpos, C. P. Raptopoulou, A. Terzis, W. Wernsdorfer, S. P. Perlepes, G. Christou, *J. Am. Chem. Soc.* **2005**, *127*, 15380–15381; b) T. C. Stamatatos, D. Foguet-Albiol, C. C. Stoumpos, C. P. Raptopoulou, A. Terzis, W. Wernsdorfer, S. P. Perlepes, G. Christou, *Polyhedron* **2007**, *26*, 2165–2168; c) T. C. Stamatatos, D. Foguet-Albiol, S.-C. Lee, C. C. Stoumpos, C. P. Raptopoulou, A. Terzis, W. Wernsdorfer, S. O. Hill, S. P. Perlepes, G. Christou, *J. Am. Chem. Soc.* **2007**, *129*, 9484–9499.

[11] Y.-L. Miao, J.-L. Liu, Z.-J. Lin, Y.-C. Ou, J.-D. Leng, M.-L. Tong, *Dalton Trans.* **2010**, *39*, 4893–4902.

[12] C. P. Raptopoulou, V. Psycharis, *Inorg. Chem. Commun.* **2008**, *11*, 1194–1197.

[13] L. Alcázar, B. Cordero, J. Esteban, V. Tangoulis, M. Font-Bardia, T. Calvet, A. Escuer, *Dalton Trans.* **2013**, *42*, 12334–12345.

[14] R. A. Coxall, S. G. Harris, D. K. Henderson, S. Parsons, P. A. Tasker, R. E. P. Winpenny, *J. Chem. Soc., Dalton Trans.* **2000**, 2349–2356.

[15] N. F. Chilton, R. P. Anderson, L. D. Turner, A. Soncini, K. S. Murray, *J. Comput. Chem.* **2013**, *34*, 1164–1175.

[16] O. Kahn, *Molecular Magnetism*, VCH, New York, **1993**, ch. 10.

[17] a) N. N. Gerasimchuk, V. V. Skopenko, K. V. Domasevich, O. A. Zhmurko, *Ukrainskii Khim. Zh.* **1992**, *58*, 935–949 *(Russian Edition)*; b) A. A. Mokhir, K. V. Domasevich, N. K. Dalley, X. Kou, N. N. Gerasimchuk, O. A. Gerasimchuk, *Inorg. Chim. Acta* **1999**, *284*, 85–98.

[18] a) W. C. Davies, G. B. Evans, F. L. Hulbert, *J. Chem. Soc.* **1939**, 412–418; b) C. Lampropoulos, K. A. Abboud, T. C. Stamatatos, G. Christou, *Inorg. Chem.* **2009**, *48*, 813–815.

[19] G. M. Sheldrick, *SHELXS – A Computer Program for the Determination of Crystal Structures*, University of Göttingen, Göttingen, **1997**.

[20] G. M. Sheldrick, *SHELX97 – A Program for Crystal Structure Refinement*, University of Göttingen, Göttingen, **1997**.

Received: June 28, 2013
Published Online: August 26, 2013

 

## 3.5.1. Resum: $Ni^{II}$-pyridyloximato triangles with a central $\mu_3$-OH ligand: Magnetostructural correlations

Jordi Esteban, Mercè Font-Bardia, Albert Escuer.

*European Journal of Inorganic Chemistry* **2013**, 5274-5280.

Aquest treball es va presentar com una continuació de l'article anterior, l'objectiu del qual era la recerca de nous exemples de sistemes triangulars aïllats. Per obtenir aquests nous compostos es va partir del lligand pyC{CN}NOH i anions carboxilat per tal d'aprofitar la seva tendència a donar sistemes triangulars amb pont $\mu_3$-OH, utilitzant nous anions carboxilat en alguns casos i en d'altres modificant les condicions de síntesis anteriors.

Així, es van sintetitzar i caracteritzar tres nous sistemes triangulars $Ni_3/\mu_3$-OR/oxima amb fórmula: $[Ni_3(MeOH)_2(AcO)(OH)(pyC\{CN\}NO)_4]$ (**5_1**), $(NEt_4)[Ni_3(H_2O)(3\text{-}ClBzO)_2(OH)(pyC\{CN\}NO)_4]$ (**5_2**) i $(NEt_3H)[Ni_3(H_2O)_3(OH)(Ph_2CHCOO)_3(pyC\{CN\}NO)_3]$ (**5_3**), que es mostren a la figura 11.

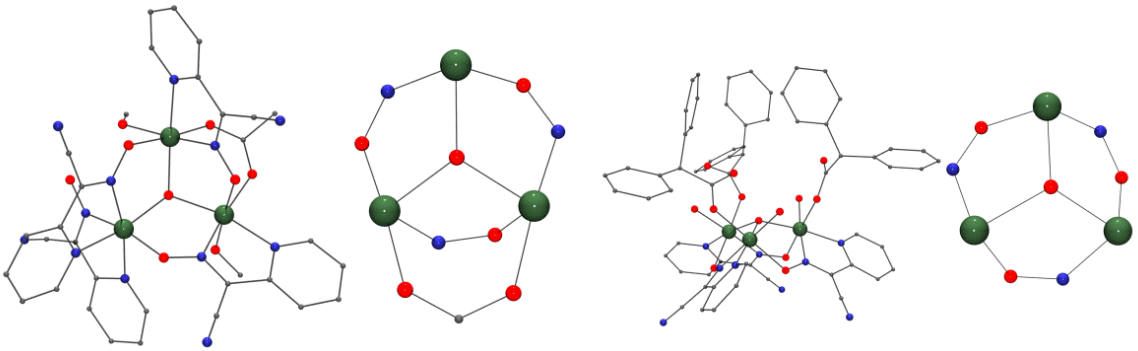

**Figura 11.** Estructura i *core* magnètic dels compostos **5_1** (esquerra) i **5_3** (dreta).

Aquests tres compostos es poden classificar en dos grups diferents: compostos que contenen dos ponts $\mu_3$-OH/oxima i un pont $\mu_3$-OH/oxima/carboxilat (**5_1** i **5_2**) i compostos que només contenen ponts $\mu_3$-OH/oxima (**5_3**). La presència d'aquest pont $\mu_3$-OH/oxima/carboxilat genera un segon camí d'intercanvi magnètic entre cations $Ni^{II}$ i provoca que els dos grups de compostos presentin un comportament magnètic molt diferenciat:

- la susceptibilitat magnètica dels compostos **5_1** i **5_2** disminueix amb la temperatura fins arribar a *ca.* 0,5 K·cm$^3$·mol$^{-1}$, valor associat a la població de l'estat fonamental $S = 1$ i d'un estat excitat $S = 0$ energèticament poc separat. Les dades experimentals van ser ajustades amb un Hamiltonià amb dues constants d'acoblament.
- la corba de $\chi_M T$ *vs.* $T$ pel compost **5_3** també decreix amb la temperatura però, en aquest cas, arriba a 0 K cm$^3$ mol$^{-1}$, que correspon a un estat fonamental $S = 0$. Les dades experimentals es van ajustar amb un Hamiltonià amb una única $J$.

L'estat fonamental d'spin ve determinat per la relació entre les constants d'acoblament que es troben al triangle ($J_2/J_1$).[1] Per un triangle de Ni$^{II}$ acoblat antiferromagnèticament, l'estat fonamental pot ser $S = 1$, $S = 0$ o tots dos alhora.

També es va confirmar amb nous exemples que el paràmetre estructural que determina la intensitat de l'acoblament magnètic en sistemes $Ni_3/\mu_3$-OR/oxima és l'angle Ni-O-Ni (com ja s'havia apuntat a l'article anterior per mitjà de càlculs DFT) realitzant una correlació magnetoestructural basada en dades experimentals.

Finalment, val la pena comentar que tots els triangles aïllats de níquel(II) basats en el sistema $\mu_3$-OR/oxima han estat obtinguts únicament amb el lligand pyC{CN}NOH, probablement a causa de les propietats úniques d'aquest lligand. També cal remarcar que, a diferència d'altres metalls com el Mn$^{III}$, els fragments triangulars $\{Ni_3(\mu_3\text{-OR})(\text{oxima})_3\}$ no són un *building block* útil en la síntesi de compostos de major nuclearitat amb propietats SMM, ja que no contribueixen a augmentar l'estat fonamental d'spin del sistema.

## 3.6. Article 6.

## New topologies in pentanuclear nickel/oximato clusters: Structural and magnetic characterization.

**Jordi Esteban**, Mercè Font-Bardia, José Sánchez Costa, Simon J. Teat, Albert Escuer.

*Inorganic Chemistry* **2014**, *53*, 3194-3203.

Inorganic Chemistry

Article

pubs.acs.org/IC

# New Topologies in Pentanuclear Nickel/Oximato Clusters: Structural and Magnetic Characterization

Jordi Esteban,*[,†] Mercè Font-Bardia,[‡,§] José Sánchez Costa,[†,⊥] Simon J. Teat,[∥] and Albert Escuer*[,†]

[†]Departament de Química Inorgànica, Universitat de Barcelona, Avinguda Diagonal 645, 08028 Barcelona, Spain

[‡]Departament de Mineralogia, Cristal·lografia i Dipòsits Minerals, Universitat de Barcelona, Martí Franqués s/n, 08028 Barcelona, Spain

[§]Unitat de Difracció de R-X. Centre Científic i Tecnològic de la Universitat de Barcelona (CCiTUB). Universitat de Barcelona, Solé i Sabarís 1−3, 08028 Barcelona, Spain

[∥]Advanced Light Source, Lawrence Berkeley National Laboratory, 1 Cyclotron Road, Berkeley, California 94720, United States

Supporting Information

**ABSTRACT:** In the present work, five new $Ni_5$ clusters employing the versatile 2-pyridylcyanoxime ligand have been synthesized and chemically, structurally, and magnetically characterized. The crystallographic examination of these $Ni_5$ clusters together with those already published in the literature, giving a total number of 14 complexes, exhibiting up to 8 different topologies for which the relationship between topology, reaction conditions and magnetic response has been analyzed. DC magnetic measurements were carried in the 300−2 K range for the new complexes and the analysis of the experimental data revealed an antiferromagnetic response for the oximato mediated interactions with a variety of ground states ($S$ = 0, 1, 3) as function of the cluster topology.

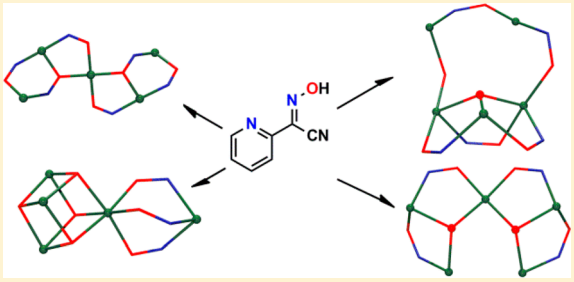


## INTRODUCTION

Chemistry of 3D metallic clusters is a continuously growing research field due its intrinsic interest in coordination chemistry and the relevance in research fields, such as bioinorganic chemistry[1] or molecular nanomagnetism.[2]

Rational design of clusters and tailoring of the derived properties has been reached in some cases employing rigid ligands and the "designed assembly" approach to obtain polygons or polyhedral compounds by Lehn,[3] Fujita,[4] and other authors.[5] However, most of the reported cluster chemistry is obtained following the named "serendipitous assembly", consisting of one-pot reactions of the adequate ligands, pH, solvents, and metallic salts. This approach has proven to be extremely successful, but fundamental aspects, such as nuclearity, topology, or the derived properties, become largely unpredictable, and only the analysis of the properties of large series of complexes can give an approach to improve future synthetic work.[6]

2-Pyridyloximes have been widely employed in cluster chemistry and molecular magnetism studies along the last years because of their ability to coordinate several metallic centers, to stabilize discrete clusters and their efficient behavior as magnetic coupler.[7] These ligands are also attractive to experimental coordination chemists by their apparently unpredictable coordinative properties, which are reflected in the large number of nuclearities and topologies characterized to date, which are often modified even as response to small changes in the reaction conditions. As example, nickel clusters of 2-pyridyloximes show practically all nuclearities between $Ni_3$ and $Ni_{14}$ (except for $Ni_{11}$)[8] and a surprising variety of topologies considering that a CCDC database search results in 78 entries, reflecting the specially "serendipitous" character of this family of ligands.

Given the fact that the chances of identifying new types of coordination clusters with improved or novel properties can be increased by the development of new reaction systems with suitable metal precursors and ligands, and following our work in this field, we have chosen the 2-pyridylcyanoxime ligand, pyC{CN}NOH, Scheme 1, to continue the exploration of the synthesis of oximate metallic clusters.

This choice has been made on the basis of the unique properties of pyC{CN}NOH ligand related to the cyano substituent on the vicinal C-atom to the oximate function, which gives a much more acidic oxime (3−5 units of $pK_a$) respect to ligands with other substituents.[7] PyC{CN}NOH ligand has proven to be a valid ligand to synthesize complexes with unusual topologies (as we have reported in previous copper,[9] nickel,[8a,10] and manganese[11] studies), and in contrast with all the other members of this family of ligands, we have observed its specific tendency to generate $\mu_3$-OR/oximato triangular-based complexes and clusters with $Ni_3$ and $Ni_5$

**Received:** January 9, 2014
**Published:** March 4, 2014

  

**Scheme 1. PyC{CN}NOH Ligand and Coordination Modes for pyC{CN}NO$^-$ Found in Compounds 1−5 (in Harris Notation[12])**

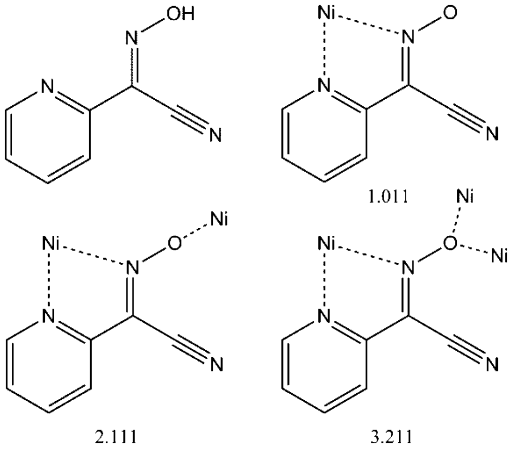


nuclearity.[8a,10] Notably, 7 of the 14 compounds obtained with this ligand in Ni$^{II}$ chemistry, including the five new clusters presented in this paper, exhibit the $Ni_5$ nuclearity.[8a,10]

In this Article, we report the characterization of series of pentanuclear nickel clusters obtained by reaction of Ni$^{II}$ salts and pyC{CN}NOH ligand with formula $(NEt_4)[Ni_5(OH)_2(Ph_2CHCOO)_5(pyC\{CN\}NO)_4(H_2O)]$ (**1**), $[Ni_5Cl_2(pyC\{CN\}NO)_8(H_2O)_2]$ (**2**), $[Ni_5Br_3(MeO)_4(pyC\{CN\}NO)_3(MeOH)_6]$ (**3**), $[Ni_5(NCS)_2(OH)_2(pyC\{CN\}NO)_6(H_2O)_3]$ (**4**), and $[Ni_5(MeO)_2(OH)_{1.5}(pyC\{CN\}NO)_6(H_2O)_{2.5}(MeOH)](NO_3)_{0.5}$ (**5**).

The reported complexes provide several new cores for the $Ni_5$/2-pyridyloximato system and, therefore, the aim of this work is not only to present the new compounds but to review the different topologies for this nuclearity in the search of some relationship between the structural data, the reaction conditions and the magnetic properties, which can be useful in order to rationalize the "serendipitous" behavior of this kind of ligands.

## EXPERIMENTAL SECTION

2-Pyridylacetonitrile and the nickel salts were purchased from Sigma-Aldrich Inc. and used without further purification. $Ni(Ph_2CHCOO)_2{\cdot}xH_2O$ was synthesized dissolving equimolar quantities (40 mmol) of diphenylbenzoic acid and NaOH in 40 mL of $H_2O$, filtering, and mixing the final solution with a commercial source of $Ni(NO_3)_2{\cdot}6H_2O$ (20 mmol) in 20 mL of water. The resulting nickel salt was obtained in good yield (>80%). Samples for analysis were dried to remove the volatile crystallization solvents.

**pyC{CN}NOH.** The ligand was prepared following a modification of the procedure[13] reported in the literature: reaction of equimolar ratio of $pyCH_2CN$, acetic acid, and $KNO_2$ was set under stirring for two hours in an ice-bath, and then the brown product was filtered and cleaned with abundant water. The ligand was collected as a brown solid in 40% yield.

**$(NEt_4)[Ni_5(OH)_2(Ph_2CHCOO)_5(pyC\{CN\}NO)_4(H_2O)]{\cdot}3CH_2Cl_2{\cdot}H_2O$ (1·3$CH_2Cl_2$·$H_2O$).** PyC{CN}NOH (0.073 g, 0.5 mmol), $Ni(Ph_2CHCOO)_2{\cdot}xH_2O$ (0.240 g, 0.5 mmol), and $NaN(CN)_2$ (0.089 g, 1 mmol) were dissolved in 20 mL of dichloromethane together with $NEt_3$ (0.101 g, 1 mmol). The mixture was stirred for 2 h and then filtered. Crystals were obtained by layering the final solution with 10 mL of hexane. Green bricks adequate for X-ray diffraction appeared a week after. Anal. Calcd for $C_{106}H_{97}N_{13}Ni_5O_{18}$ (**1**·$H_2O$): C, 59.65; H, 4.58; N, 8.53%. Found: C, 59.1; H, 4.3; N, 8.7%. Relevant IR bands ($cm^{-1}$): 3420(br), 2211(w), 1601(s), 1457(s), 1419(m), 1392(m), 1302(w), 1269(w), 1230(m), 1154(w), 1105(w), 1037(w), 781(w), 745(m), 708(m).

**$[Ni_5Cl_2(pyC\{CN\}NO)_8(H_2O)_2]{\cdot}2CH_2Cl_2{\cdot}H_2O$ (2·2$CH_2Cl_2$·$H_2O$).** Twenty mL of $CH_2Cl_2$ were poured over pyC{CN}NOH (0.073 g, 0.5 mmol), $NiCl_2{\cdot}6H_2O$ (0.238 g, 1 mmol) and $NEt_3$ (0.101 g, 1 mmol). The mixture was stirred for a couple of hours, then filtered and finally layered with 10 mL of hexane. Red prismatic crystals were collected after two weeks. Anal. Calcd for $C_{56}Cl_2H_{38}N_{24}Ni_5O_{11}$ (**2**·$H_2O$): C, 42.37; H, 2.41; N, 21.18%. Found: C, 42.4; H, 2.6; N, 20.7%. Relevant IR bands ($cm^{-1}$): 3425(br), 2217(w), 1601(s), 1460(s), 1426(m), 1399(m), 1302(m), 1266(w), 1221(s), 1155(m), 1107(m), 1061(w), 1037(s), 1007(w), 780(m), 746(w), 709(s).

**$[Ni_5Br_3(MeO)_4(pyC\{CN\}NO)_3(MeOH)_6]{\cdot}1.5MeOH{\cdot}0.5H_2O$ (3·1.5MeOH·0.5$H_2O$).** PyC{CN}NOH (0.073 g, 0.5 mmol) was dissolved in 20 mL of MeOH with $NiBr_2{\cdot}xH_2O$ (0.218 g, 1 mmol) and $NEt_3$ (0.101 g, 1 mmol). The mixture was stirred for two hours, filtered and left for slow evaporation in an open vial. Dark prismatic crystals adequate for X-ray diffraction were obtained after two weeks. Anal. Calcd for $C_{31}Br_3H_{49}N_9Ni_5O_{13.5}$ (**3**·0.5$H_2O$): C, 28.71; H, 3.81;

**Table 1. Crystal Data, Data Collection, and Structure Refinement Details for the X-ray Structure Determination of Compounds 1−5**

| | 1 | 2 | 3 | 4 | 5 |
|---|---|---|---|---|---|
| formula | $C_{109}H_{102}Cl_6N_{13}Ni_5O_{18}$ | $C_{58}Cl_6H_{42}N_{24}Ni_5O_{11}$ | $C_{65}H_{104}Br_6N_{18}Ni_{10}O_{30}$ | $C_{217}H_{208}N_{100}Ni_{20}O_{62}S_8$ | $C_{191}H_{216}N_{74}Ni_{20}O_{74}$ |
| fw | 2388.19 | 1575.41 | 2684.22 | 6639.51 | 5906.58 |
| system | monoclinic | monoclinic | trigonal | monoclinic | tetragonal |
| space group | $P2_1/c$ | $P2_1/c$ | $R\bar{3}$ | $C2/c$ | $P4_2/n$ |
| $a$ (Å) | 16.734(2) | 15.674(2) | 15.210(7) | 32.360(2) | 34.0083(4) |
| $b$ (Å) | 24.440(3) | 14.767(2) | 15.210(7) | 23.188(1) | 34.0083(4) |
| $c$ (Å) | 28.002(3) | 18.470(2) | 40.38(2) | 23.240(1) | 12.0595(2) |
| $\alpha$ (deg) | 90 | 90 | 90 | 90 | 90 |
| ß (deg) | 112.758(5) | 108.501(2) | 90 | 101.395(3) | 90 |
| $\gamma$ (deg) | 90 | 90 | 120 | 90 | 90 |
| $V$ (Å$^3$) | 10561(2) | 4054.0(8) | 8090(7) | 17095(2) | 13947.6(3) |
| $Z$ | 4 | 2 | 3 | 2 | 2 |
| $T$ (K) | 100(2) | 100(2) | 105(2) | 293(2) | 100(1) |
| $\lambda$(Mo$K_\alpha$) (Å) | 0.77490 | 0.71073 | 0.71073 | 0.71073 | 1.54178 |
| $\rho_{calcd}$ (g·cm$^{-3}$) | 1.502 | 1.440 | 1.653 | 1.290 | 1.406 |
| $\mu$(Mo$K_\alpha$), mm$^{-1}$ | 1.374 | 1.403 | 3.999 | 1.196 | 2.120 |
| $R$ | 0.0725 | 0.0335 | 0.0517 | 0.0521 | 0.0684 |
| $\omega R^2$ | 0.2217 | 0.0914 | 0.1441 | 0.2148 | 0.2190 |



dx.doi.org/10.1021/ic500057j | Inorg. Chem. 2014, 53, 3194−3203

N, 9.72%. Found: C, 28.3; H, 3.7; N, 10.0%. Relevant IR bands ($cm^{-1}$): 3427(br), 2221(w), 1602(m), 1467(s), 1427(m), 1303(w), 1263(w), 1220(m), 1157(w), 1108(m), 1032(w), 1037(m), 779(w), 711(m). Reaction starting from $NiCl_2·6H_2O$ gives a product with the same IR spectrum but crystals adequate for diffraction were not obtained and thus the sample will no further discussed.

**$[Ni_5(NCS)_2(pyC\{CN\}NO)_6(OH)_2(H_2O)_3]·5MeCN·4H_2O$ (4·5MeCN·4H$_2$O).** PyC{CN}NOH (0.073 g, 0.5 mmol) was dissolved in 20 mL of MeCN with $Ni(SCN)_2$ (0.174 g, 1 mmol), $NaN(CN)_2$ (0.089 g, 1 mmol), and $NEt_3$ (0.101 g, 1 mmol). The mixture was stirred for 2 h and then filtered. Crystals were obtained by layering the final solution with 10 mL of diethyl ether. Crystals were collected after a couple of weeks. Anal. Calcd for $C_{44}H_{40}N_{20}Ni_5O_{15}S_2$ (**4**·4H$_2$O): C, 36.53; H, 2.78; N, 19.37; S, 4.43%. Found: C, 37.3; H, 2.8; N, 18.9; S, 4.2%. Relevant IR bands ($cm^{-1}$): 3441(br), 2223(w), 2101(w), 1971(w), 1602(s), 1466(s), 1428(m), 1303(w), 1265(w), 1222(m), 1157(w), 1108(m), 1061(w), 1037(m), 778(w), 712(m).

**$[Ni_5(MeO)_2(OH)_{1.5}(pyC\{CN\}NO)_6(H_2O)_{2.5}(MeOH)](NO_3)_{0.5}$·2.75MeOH·1.25H$_2$O (5·2.75MeOH·1.25H$_2$O).** PyC{CN}NOH (0.073 g, 0.5 mmol) and $Ni(NO_3)_2·6H_2O$ (0.290 g, 1 mmol) were dissolved in 20 mL of MeOH and $NEt_3$ (0.101 g, 1 mmol). The mixture was stirred for two hours, filtered and left for slow evaporation in an open vial. Red crystals appeared after a month. Anal. Calcd for $C_{45}H_{43}N_{18.5}Ni_5O_{15.75}$ (**5**·1.25H$_2$O): C, 38.93; H, 3.12; N, 18.66%. Found: C, 38.2; H, 3.3; N, 18.1%. Relevant IR bands ($cm^{-1}$): 3397(br), 2222(w), 1602(m), 1465(s), 1427(m), 1384(s), 1302(w), 1266(w), 1226(m), 1157(w), 1109(w), 1062(w), 1036(m), 779(w), 711(m).

**Physical Measurements.** Magnetic susceptibility measurements were carried out on polycrystalline samples with a MPMS5 Quantum Design susceptometer working in the range 30−300 K under external magnetic field of 0.3 T and under a field of 0.03 T in the 30−2 K range to avoid saturation effects. Diamagnetic corrections were estimated from Pascal Tables. Infrared spectra (4000−400 $cm^{-1}$) were recorded from KBr pellets on a Bruker IFS-125 FT-IR spectrophotometer.

**X-ray Crystallography.** Details of crystal data, data collection, and refinement for **1**−**5** are given in Table 1. Data for compound **1** was measured from dark green crystals at 100 K and $\lambda$ = 0.7749 Å using a Bruker APEX II CCD diffractometer on Advanced Light Source beamline 11.3.1 at Lawrence Berkeley National Laboratory.

Collection of data for compound **2**, **3**, **4**, and **5** was made on a Bruker CCD SMART1000, a MAR345 diffractometer with an image plate detector, a Bruker X8 KappaAPEXII diffractometer with a CCD detector and a Bruker-Nonius FR591 Kappa CCD 2000, respectively. All structures were solved by direct methods, using SHELXS computer program[14] and refined by full-matrix least-squares method with SHELX97 computer program,.[15] International Tables of X-ray Crystallography[16] were used to minimize the $\Sigma w||F_o|^2 - |F_c|^2|^2$ function. Lorentz-polarization, and absorption corrections were made.

For compound **1**, $\sin(\theta_{max}/\lambda)$ is lower than 0.5 (0.4587) because of the relatively low scattering and the small size of the crystals which limited the observed reflections. For complex **2**, 2H atoms were located from a difference synthesis and refined with an isotropic temperature factor equal to 1.2 times the equivalent temperature factor of the atoms which are linked and 18H atoms were computed and refined, using a riding model, with an isotropic temperature factor equal to 1.2 times the equivalent temperature factor of the atoms which are linked. **3**, **4**, **5**: all H atoms were computed and refined, using a riding model, with an isotropic temperature factor equal to 1.2 times the equivalent temperature factor of the atom which are linked.

All data can be found in the Supporting Information for this paper in cif format with CCDC numbers 970384−970388. These data can also be obtained free of charge from The Cambridge Crystallographic Data Centre via www.ccdc.cam.ac.uk/data_request/cif.

Plots for publication were generated with ORTEP3 for Windows and plotted with Pov-Ray programs.[17]

## RESULTS AND DISCUSSION

**Description of the Structures.** *$(NEt_4)$-$[Ni_5(OH)_2(Ph_2CHCOO)_5(pyC\{CN\}NO)_4(H_2O)]·3CH_2Cl_2·H_2O$ (1·3CH$_2$Cl$_2$·H$_2$O).* A view of the core of complex **1** is illustrated in Figure 1. Selected interatomic distances and angles for **1** are

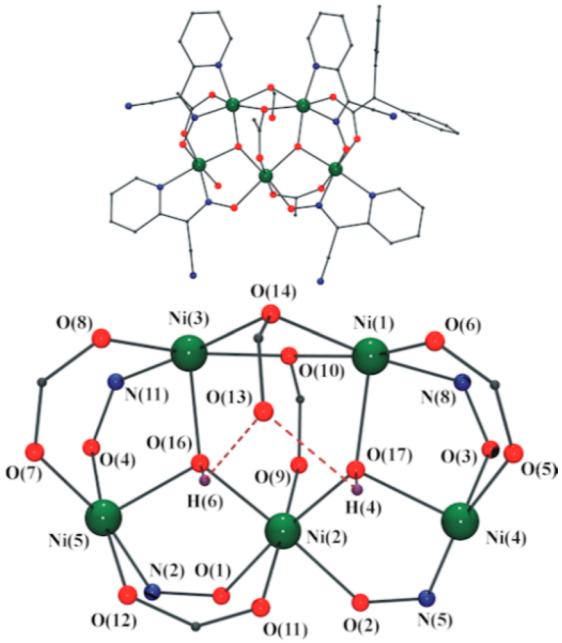


**Figure 1.** Top: View of complex **1**. Phenyl groups have been omitted for clarity except for the Ph2CCOO$^-$ ligand linked to Ni(3)/Ni(5). Bottom: Partially labeled Pov-Ray plot of complex **1**, showing the H bonds involving the $\mu_3$-OH ligands as red dashed bonds.

listed in Table 2. The core of this anionic compound can be described like two $\mu_3$-OH centered triangles formed by Ni(1,2,4) and Ni(2,3,5) cations sharing the Ni(2) vertex. Both $\mu_3$-OH groups are placed slightly out of the plane formed by the three $Ni^{II}$ atoms (0.470 and 0.502 Å, respectively). Ni(1) and Ni(3) are linked together by two $Ph_2CHCOO^-$ bridging ligands in 2.20 and 3.21 coordination mode (or $\eta^1$,$\mu$-*R*-$COO^-$ and $\eta^2$:$\eta^1$,$\mu$-*R*-$COO^-$ respectively) resulting in a three edge-sharing triangles topology.

Ni(1,2,4) triangle shows Ni(1)···Ni(2), Ni(1)···Ni(4) and Ni(2)···Ni(4) distances of 3.571(2), 3.271(3) and 3.324(2) Å, respectively. The sides of the triangles are defined by one double oximato and syn−syn carboxylato bridge between Ni(1) and Ni(4), one single oximato bridge between Ni(2) and Ni(4) and the $\eta^2$:$\eta^1$,$\mu$-carboxylato ligand between Ni(1) and Ni(2); whereas Ni(2,3,5) triangle exhibits Ni(2)···Ni(3), Ni(2)···Ni(5), and Ni(3)···Ni(5) Ni−Ni distances of 3.606(2), 3.226(2), and 3.290(3) Å, respectively, and is defined by two double oximato/syn−syn carboxylato bridges between Ni(5) and Ni(2,3) and one $\eta^2$:$\eta^1$,$\mu$-carboxylato bridge between Ni(2) and Ni(3). In the inner triangle, the Ni(1)···Ni(3) distance is 3.236(2) Å.

The coordination environment of Ni(2) (the shared vertex) is $NiO_6$, provided by the two $\mu_3$-OH groups, two O-oximato bridges, one syn−syn $Ph_2CHCOO^-$ ligand and the $\eta^2$:$\eta^1$,$\mu$-diphenylacetate bridge, whereas each remaining nickel centers is linked to one pyC{CN}NO$^-$ ligand by their two N atoms exhibiting a $NiN_2O_4$ environment. All pyC{CN}NO$^-$ ligands exhibit the same 2.111 coordination mode.



dx.doi.org/10.1021/ic500057j | Inorg. Chem. 2014, 53, 3194−3203

**Table 2. Selected Interatomic Distances (Å) and Angles (deg) for Compound 1**

| | | | |
|---|---|---|---|
| Ni(1)–N(7) | 2.07(1) | Ni(1)–N(8) | 2.037(9) |
| Ni(1)–O(6) | 2.042(7) | Ni(1)–O(10) | 2.172(7) |
| Ni(1)–O(14) | 2.114(7) | Ni(1)–O(17) | 2.012(9) |
| Ni(2)–O(1) | 2.038(9) | Ni(2)–O(2) | 2.063(9) |
| Ni(2)–O(9) | 2.075(8) | Ni(2)–O(11) | 2.10(1) |
| Ni(2)–O(16) | 2.043(7) | Ni(2)–O(17) | 2.046(7) |
| Ni(3)–N(10) | 2.10(1) | Ni(3)–N(11) | 2.05(1) |
| Ni(3)–O(8) | 2.035(7) | Ni(3)–O(10) | 2.117(7) |
| Ni(3)–O(14) | 2.170(7) | Ni(3)–O(16) | 1.983(9) |
| Ni(4)–N(4) | 2.08(1) | Ni(4)–N(5) | 2.03(1) |
| Ni(4)–O(3) | 2.056(9) | Ni(4)–O(5) | 2.028(8) |
| Ni(4)–O(15) | 2.16(1) | Ni(4)–O(17) | 2.013(8) |
| Ni(5)–N(1) | 2.06(1) | Ni(5)–N(2) | 2.04(1) |
| Ni(5)–O(4) | 2.056(9) | Ni(5)–O(7) | 2.041(8) |
| Ni(5)–O(12) | 2.069(9) | Ni(5)–O(16) | 2.010(8) |
| Ni(1)–O(17)–Ni(2) | 123.3(4) | Ni(1)–O(17)–Ni(4) | 108.7(4) |
| Ni(2)–O(17)–Ni(4) | 110.0(4) | Ni(2)–O(16)–Ni(3) | 127.2(4) |
| Ni(2)–O(16)–Ni(5) | 105.5(3) | Ni(3)–O(16)–Ni(5) | 111.0(4) |
| Ni(1)–O(10)–Ni(3) | 98.0(3) | Ni(1)–O(14)–Ni(3) | 98.1(4) |
| Ni(1)–N(8)–O(3)–Ni(4) | 20(1) | Ni(3)–N(11)–O(4)–Ni(5) | 18(1) |
| Ni(4)–N(5)–O(2)–Ni(2) | 4(1) | Ni(5)–N(2)–O(1)–Ni(2) | 8(1) |

Complex **1** contains three different $Ph_2CHCOO^-$ coordination modes: three carboxylates are coordinated in the syn–syn mode, one links three metallic centers in its tridentate 3.21 mode and the last one links two nickel ions in its 2.20 mode. The noncoordinated O(13) atom from the 2.20 $Ph_2CHCOO^-$ ligand establishes two strong intramolecular H-bonds with the hydroxo ligands with O(13)···O(16) and O(13)···O(17) distances of 3.02(1) and 2.904(9) Å, respectively).

Ni–O–Ni bond angles involving the $\mu_3$–OH group show one large and two smaller angles in each triangle (123.3(4)/110.0(4)/108.7(4)° and 127.2(4)/111.0(4)/105.5(3)°, Table 2). The crystallization water molecule forms two additional intramolecular H bonds with the water molecule bonded to Ni(4) and the O(13) atom. Relevant H-bonds or other intermolecular interactions were not found.

Charge balance is achieved by means of one tetraethylammonium cation, which was the product of the reaction of the triethylamine (employed as base in the synthesis) and the dichloromethane solvent. Reactivity of di- or trialkylamines with dichloromethane in mild conditions was early established[18a] and the use of triethylamine as base and $CH_2Cl_2$ as solvent in nickel or manganese chemistry can lead, probably catalyzed by the cation, to a wide variety of products such as $Et_4N^+$, $Et_2NH_2^+$, or chloro-alkyl derivatives.[18b,c]

*$[Ni_5Cl_2(pyC\{CN\}NO)_8(H_2O)_2]\cdot 2CH_2Cl_2\cdot H_2O$ (**2**·$2CH_2Cl_2\cdot H_2O$).* The centrosymmetric molecule of **2** consists on a central $Ni^{II}$ atom connected to the four peripheral $Ni^{II}$ centers via four oximato bridges and can be described like a distorted bowtie, Figure 2. Selected interatomic distances and angles for **2** are listed in Table 3. The $NiO_6$ environment of the central Ni(1) atom arises from four O-oximato atoms and two trans water molecules, whereas all peripheral nickel atoms exhibit $NiClN_4O$ environments formed by two $pyC\{CN\}NO^-$ ligands, one bridging chloride atom and one O-oximato donor.

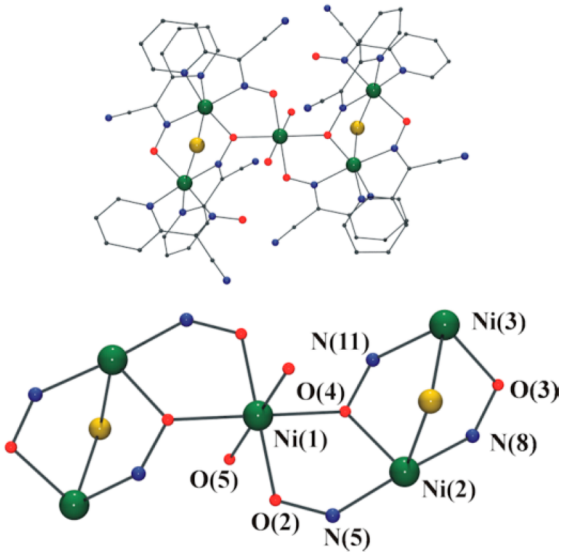


**Figure 2.** Top: View of complex **2**. Bottom: Partially labeled Pov-Ray plot of complex **2**. All hydrogen atoms have been omitted for clarity.

**Table 3. Selected Interatomic Distances (Å) and Angles (deg) for Compound 2**

| | | | |
|---|---|---|---|
| Ni(1)–O(2) | 2.033(2) | Ni(1)–O(4) | 2.108(2) |
| Ni(1)–O(5) | 2.038(2) | | |
| Ni(2)–O(4) | 2.062(2) | Ni(2)–N(7) | 2.075(2) |
| Ni(2)–N(4) | 2.058(2) | Ni(2)–N(8) | 2.053(2) |
| Ni(2)–N(5) | 2.030(3) | Ni(2)–Cl(1) | 2.413(1) |
| Ni(3)–O(3) | 2.076(2) | Ni(3)–N(10) | 2.073(2) |
| Ni(3)–N(1) | 2.049(3) | Ni(3)–N(11) | 2.070(2) |
| Ni(3)–N(2) | 2.054(2) | Ni(3)–Cl(1) | 2.404(1) |
| Ni(1)–O(4)–Ni(2) | 112.06(9) | Ni(2)–Cl(1)–Ni(3) | 87.72(3) |
| Ni(2)–N(5)–O(2)–Ni(1) | 16.2(3) | Ni(2)–N(8)–O(3)–Ni(3) | 20.9(3) |
| Ni(3)–N(11)–O(4)–Ni(1) | 104.0(2) | Ni(3)–N(11)–O(4)–Ni(2) | 27.1(2) |

Each triangular Ni(1,2,3) subunit contains four pyridyloximate ligands that show three different coordination modes: one 1.011 ligand is coordinated to Ni(3), two oximate ligands in the 2.111 coordinative mode link Ni(1)/Ni(2) and Ni(2)/Ni(3) and finally one oximate in its 3.211 coordination mode acts as tridentate bridge between the three nickel atoms. Ni–O–N–Ni torsion angles are relatively low except for Ni(1)–O(4)–N(11)-Ni(3), which takes a value of 104.0(2)°. As consequence of the different ligands that define the sides of the triangular subunits the Ni(1)···Ni(2), Ni(1)···Ni(3), and Ni(2)···Ni(3) distances are 3.4583(5), 4.5577(6), and 3.3375(5) Å, respectively

The water molecules coordinated to the central Ni(1) generate a set of intramolecular H-bonds with the 1.011 pyridyloximate ligands (distance O(5)–H(5AO)···O(1) of 2.677(3) Å) and the chloride bridging atoms (distance O(5)–H(5BO)···Cl(1) of 3.090(3) Å). The pyridyl rings belonging to the oximate ligand N(8)–O(3) establish weak intermolecular $\pi$-stacking interactions (distance between centroids is 3.727 Å) with the pyridyl rings of the N(5)–O(2) oximate ligands.

*$[Ni_5Br_3(MeO)_4(pyC\{CN\}NO)_3(MeOH)_6]\cdot 1.5MeOH\cdot 0.5H_2O$ (**3**·1.5MeOH·0.5$H_2O$).* Compound **3** can be described like a $\{Ni_4(MeO)_4\}^{4+}$ cubane with an additional $Ni^{II}$ ion linked to



dx.doi.org/10.1021/ic500057j | Inorg. Chem. 2014, 53, 3194–3203

one of its corners through three oximato bridges, as shown in Figure 3. Selected distances and angles for **3** are listed in Table

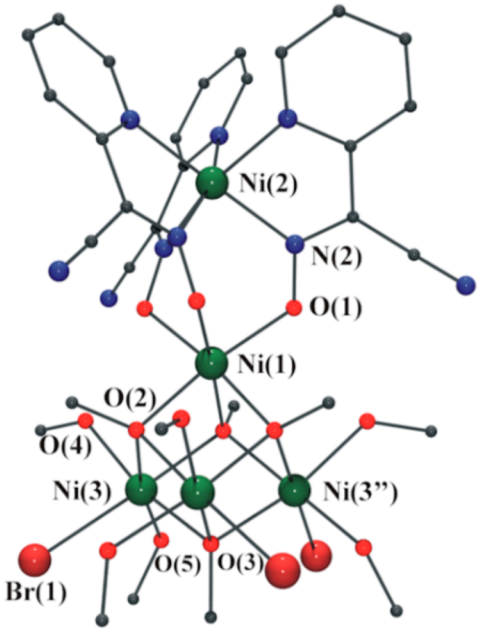


**Figure 3.** Partially labeled Pov-Ray plot of complex **3**. All hydrogen atoms have been omitted for clarity.

**Table 4. Selected Interatomic Distances (Å) and Angles (deg) for Compound 3**

| | | | |
|---|---|---|---|
| Ni(1)–O(1) | 2.087(2) | Ni(1)–O(2) | 2.050(2) |
| Ni(2)–N(1) | 2.117(3) | Ni(1)–N(2) | 2.044(4) |
| Ni(3)–Br(1) | 2.587(1) | Ni(3)–O(3) | 2.068(2) |
| Ni(3)–O(2) | 2.050(2) | Ni(3)–O(4) | 2.089(3) |
| Ni(3)-O(2′) | 2.075(2) | Ni(3)–O(5) | 2.066(3) |
| Ni(1)–O(2)–Ni(3) | 97.2(1) | Ni(3)–O(2)–Ni(3′) | 97.54(9) |
| Ni(1)–O(2)–Ni(3″) | 96.45(9) | Ni(3)–O(3)–Ni(3′) | 97.2(1) |
| Ni(2)–N(2)–O(1)–Ni(1) | 38.3(3) | | |

4. The external Ni(2) cation is coordinated to three pyridyloximate ligands by their six nitrogen atoms, exhibiting in consequence a $NiN_6$ environment. All three oximato bridges bind the same metallic center, Ni(1), that together with three $\mu_3$-$MeO^-$ groups provide a $NiO_6$ environment. Remaining nickel atoms (Ni(3) and symmetry related) have a $NiBrO_5$ environment formed by three $\mu_3$-$MeO^-$ groups, one bromide and two coordinated MeOH molecules. Bond angles in the cubane subunit show values in the short 96.5–97.5° range and Ni(1)–O(1)–N(2)–Ni(2) torsion angles are 38.3(3)°.

The methanol molecules coordinated to Ni(3) promote intramolecular H-bonds with the oximato ligands coordinated to Ni(2) with O(4)–H(4O)···O(1) distance of 2.760(4) Å and the bromine atoms with O(5)–H(5O)···Br(1) distance of 3.235(3) Å.

*$[Ni_5(OH)_2(pyC\{CN\}NO)_6(SCN)_2(H_2O)_3]\cdot 5MeCN\cdot 4H_2O$ (**4**·5MeCN·4$H_2O$).* The core of neutral complex **4** is depicted in Figure 4 and selected interatomic distances and angles are listed in Table 5. This compound can be described like a $[Ni_3(\mu_3$–OH$)(pyC\{CN\}NO)_3]^{2+}$ triangular fragment in which two $Ni^{II}$ atoms are linked to a dinuclear subunit, providing the triangle a handle. The triangle binds the dinuclear subunit through two double oximato/aquo-hydroxo bridges (two hydroxo groups sharing one additional H atom by means of a strong H-bond, O(2)–H(2OB)···O(3) distance of 2.443(5) Å) and the $Ni_2$ subunit itself is linked by an oximato/thiocyanato bridge.

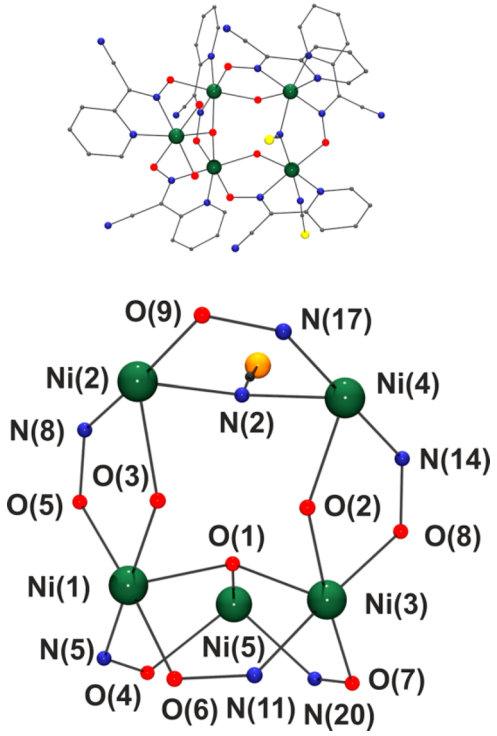


**Figure 4.** Partially labeled Pov-Ray plot of complex **4**. All hydrogen atoms have been omitted for clarity. Compound **5** exhibits a similar structure with a methoxo bridge instead the thiocyanate ligand between Ni(2) and Ni(4).

**Table 5. Selected Interatomic Distances (Å) and Angles (deg) for Compound 4**

| | | | |
|---|---|---|---|
| Ni(1)–N(3) | 2.092(4) | Ni(1)–N(5) | 2.041(4) |
| Ni(1)–O(1) | 2.036(4) | Ni(1)–O(3) | 2.075(3) |
| Ni(1)–O(5) | 2.106(4) | Ni(1)–O(6) | 2.067(4) |
| Ni(2)–N(1) | 2.018(5) | Ni(2)–N(2) | 2.121(4) |
| Ni(2)–N(6) | 2.062(5) | Ni(2)–N(8) | 2.066(4) |
| Ni(2)–O(3) | 2.096(4) | Ni(2)–O(9) | 2.047(3) |
| Ni(3)–N(9) | 2.065(5) | Ni(3)–N(11) | 2.048(5) |
| Ni(3)–O(1) | 2.052(3) | Ni(3)–O(2) | 2.055(3) |
| Ni(3)–O(7) | 2.047(3) | Ni(3)–O(8) | 2.069(4) |
| Ni(4)–N(12) | 2.105(5) | Ni(4)–N(14) | 2.053(4) |
| Ni(4)–N(15) | 2.076(4) | Ni(4)–N(17) | 2.039(4) |
| Ni(4)–N(2) | 2.107(4) | Ni(4)–O(2) | 2.027(4) |
| Ni(5)–N(18) | 2.060(5) | Ni(5)–N(20) | 2.049(5) |
| Ni(5)–O(1) | 2.032(3) | Ni(5)–O(4) | 2.050(4) |
| Ni(1)–O(3)–Ni(2) | 114.8(2) | Ni(1)–O(1)–Ni(3) | 111.9(2) |
| Ni(1)–O(1)–Ni(5) | 112.4(2) | Ni(2)–N(2)–Ni(4) | 109.7(2) |
| Ni(3)–O(2)–Ni(4) | 115.8(2) | Ni(3)–O(1)–Ni(5) | 112.7(2) |
| Ni(1)–N(5)–O(4)–Ni(5) | 14.6(5) | Ni(2)–N(8)–O(5)-Ni(1) | 0.5(5) |
| Ni(3)–N(11)–O(6)–Ni(1) | 13.8(5) | Ni(4)–N(17)–O(9)–Ni(2) | 12.1(5) |
| Ni(4)–N(14)–O(8)–Ni(3) | 4.0(5) | Ni(5)–N(20)–O(7)–Ni(3) | 2.5(5) |



dx.doi.org/10.1021/ic500057j | Inorg. Chem. 2014, 53, 3194–3203

All three metal centers from the triangle, Ni(1), Ni(3), and Ni(5), have a $NiN_2O_4$ environment, while the remaining Ni(2) and Ni(4) present a $NiN_4O_2$ and $NiN_5O$ environment, respectively. Ni(1) and Ni(3) bind one pyC{CN}NO$^-$ ligand by its two N atoms, the $\mu_3$−OH group, one aquo−hydroxo bridge and two O-oximato bridges; Ni(5) is bound to one pyridyloximato ligand also by its two N atoms, to the $\mu_3$-OH group, to one O-oximato bridge and finally to two coordinated water molecules. Ni(2) coordinates one pyC{CN}NO$^-$ ligand by the two N atoms, two thiocyanate ligands (one acting as a terminal group, the other one acting as a end-on bridging group), one aquo-hydroxo bridge, and two O-oximato bridges; and finally Ni(4) is tied to four N atoms from two different pyC{CN}NO$^-$ ligands, to the end-on bridging SCN$^-$ and to one aquo-hydroxo bridge.

The $[Ni_3(\mu_3\text{-OH})(pyC\{CN\}NO)_3]^{2+}$ triangular fragment is roughly isosceles (Ni···Ni distances and Ni−O−Ni bond angles are comprised between 3.380 and 3.401 Å and 111.9−112.7°, respectively). The O-hydroxo atom is placed 0.577(3) Å out of the plane defined by the Ni(1,3,5) cations. The hydroxo and the N(2)-atom of the thiocyanate ligand establish an H-bond with O(1)-H(1O)···N(2) distance of 2.992(6) Å.

*$[Ni_5(MeO)_2(OH)_{1.5}(pyC\{CN\}NO)_6(H_2O)_{2.5}(MeOH)](NO_3)_{0.5}\cdot 2.75MeOH\cdot 1.25H_2O$ (**5**·2.75MeOH·1.25$H_2O$).* Compound **5** presents a very similar core to **4**, Figure 4. The main differences lie in the presence of a bridging methoxo group instead of the thiocyanate bridging ligand, the substitution of the terminal thiocyanate ligand by one methanol molecule and finally the coordinative change of the N(15)/N(17) containing pyridyloximato ligand from Ni(4) to Ni(2), so the O-oximato bridge now links Ni(4) instead of Ni(2). The charge difference generated by the substitution of the anionic SCN$^-$ ligand by the neutral methanol group is compensated with an aquo/hydroxo group with a 50% occupancy and the anionic nitrate, also exhibiting a 50% occupancy.

Further structural details of **5** are not mentioned to avoid repetitive descriptions. Table 6 lists selected interatomic distances and angles for **5**.

**Comments on the $Ni_5$ Topologies.** In this work, we have presented five new complexes from the $Ni_5$/2-pyridyloxime system. Considering the complexes reported in this work and those previously reported, there are a total of 14 $Ni_5$/2-pyridyloximato complexes which surprisingly exhibit up to 8 different topologies, Scheme 2.

In the search for a relationship between reactants (mainly the 2-pyridyloxime ligand and the Ni$^{II}$ counteranions) and the resulting topologies, some trends can be drawn: (i) 4-Hydroxysalicylhydroxamate leads to stabilize 12-MC cyclic molecules in which the metallacrown is formed by four metallic centers linked through four oximato bridges that generate a $\{-M-N-O-\}_4$ ring. These rings are able to coordinate a fifth central metallic cation employing the O-oximato atoms, Scheme 2A, as has been observed in Cu,[20] Mn[21], and heterometallic chemistry.[22] Similar centered metallacrowns were obtained when using the rigid Indane-1,2,3-trione-trioxime or Indane-1,2,3-trione-dioxime ligands. The stability of these metallacrowns arises from the bridges provided by the presence of an extra O-donor atom from the hydroxo groups located near the C-oximato atom.[23]

When 4-hydroxysalicylhydroxamate was combined with di-2-pyridyloxime ($py_2CNOH$), a similar centered $Ni_4$-metallacrown,[19] Scheme 2A, was obtained. In this case, the complex contains two salicyl and two pyridyloximates and the second N-pyridyl donor of the $py_2CNO^-$ ligand plays the same role than the hydroxo group of the 4-hydroxysalicylhydroxamate, helping to stabilize the macrocyclic arrangement.

Reaction of $py_2CNOH$ ligand with nickel nitrate leads to a similar metallacrown[8h] but with an extra oximato bond between the metallacrown and the central Ni$^{II}$ cation, Scheme 2B. In this

**Table 6. Selected Interatomic Distances (Å) and Angles (deg) for Compound 5**

| | | | |
|---|---|---|---|
| Ni(1)−N(3) | 2.112(4) | Ni(1)−N(5) | 2.042(4) |
| Ni(1)−O(1) | 2.043(3) | Ni(1)−O(3) | 2.049(3) |
| Ni(1)−O(5) | 2.109(4) | Ni(1)−O(6) | 2.068(4) |
| Ni(2)−N(6) | 2.097(4) | Ni(2)−N(8) | 2.044(4) |
| Ni(2)−N(15) | 2.122(4) | Ni(2)−N(17) | 2.049(4) |
| Ni(2)−O(3) | 2.078(4) | Ni(2)−O(12) | 2.009(3) |
| Ni(3)−N(9) | 2.066(5) | Ni(3)−N(11) | 2.053(4) |
| Ni(3)−O(1) | 2.049(3) | Ni(3)−O(2) | 2.121(4) |
| Ni(3)−O(7) | 2.060(4) | Ni(3)−O(8) | 2.069(4) |
| Ni(4)−N(12) | 2.059(5) | Ni(4)−N(14) | 2.032(5) |
| Ni(4)−O(2) | 2.089(4) | Ni(4)−O(9) | 2.032(4) |
| Ni(4)−O(12) | 2.038(3) | Ni(4)−O(13) | 2.105(4) |
| Ni(5)−N(18) | 2.076(4) | Ni(5)−N(20) | 2.032(4) |
| Ni(5)−O(1) | 2.036(3) | Ni(5)−O(4) | 2.088(4) |
| Ni(1)−O(3)−Ni(2) | 113.3(2) | Ni(1)−O(1)−Ni(3) | 110.9(2) |
| Ni(1)−O(1)−Ni(5) | 112.1(2) | Ni(2)−O(12)−Ni(4) | 111.1(2) |
| Ni(3)−O(2)−Ni(4) | 111.5(2) | Ni(3)−O(1)−Ni(5) | 111.3(2) |
| Ni(1)−N(5)−O(4)−Ni(5) | 14.5(4) | Ni(2)−N(8)−O(5)−Ni(1) | 7.1(4) |
| Ni(2)−N(17)−O(9)−Ni(4) | 16.5(4) | Ni(3)−N(11)−O(6)−Ni(1) | 10.6(4) |
| Ni(4)−N(14)−O(8)−Ni(3) | 0.8(5) | Ni(5)−N(20)−O(7)−Ni(3) | 9.1(4) |

**Scheme 2. Pov-Ray Plot of the Cores of the Different Topologies for the $Ni_5$/2-Pyridyloximes System[a]**

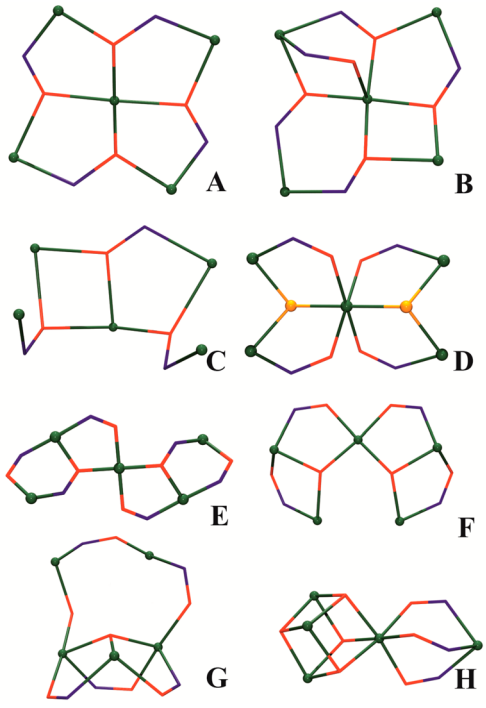


[a]Ni atoms are plotted in green, nitrogen in blue, oxygen in red, and orange atoms in topology D can be oxygen or N-azide atoms.



dx.doi.org/10.1021/ic500057j | Inorg. Chem. 2014, 53, 3194−3203

case, all the bridges were provided by the oximate groups and the additional coordination of the second N-pyridyl donor.

(ii) The reaction of $py_2CNOH$ ligand in acetone/aqueous medium with nickel acetate generates an irregular core Scheme 2C, formed by only three 3.2110 or 3.2111 oximates and six carboxylate bridges.[8c] In this case, most of the coordination sites of the $Ni^{II}$ cations are occupied by O-carboxylate bridges avoiding the coordination of the secondary N-pyridyl donor atoms and so the metallacrown is no longer formed.

(iii) The use of 2-pyridyloxime ligands in presence of carboxylic groups mainly generates bowtie cores,[8b,d,f,24] as diacetylpyridyldioxime ($dapdoH_2$), phenyl-2-pyridyloxime ({ph}{py}CNOH), 6-methyl-2-pyridyloxime (6-MepyCNOH), and 2-pyridylcyanoxime (pyC{CN}NOH) ligands have proved. All these clusters can be separated into two main groups: $\mu_3$-OR or $\mu_3$-$N_3$ centered triangles, Scheme 2D and O-oximato centered ones, in which the oximato ligand itself binds the triangles from the outside and the inside, Scheme 2E. The presence of squareplanar Ni(II) ions or the absence of available $OH^-$ and $N_3^-$ ligands cause the 2-E type of bowtie cores instead 2-D.

(iv) Finally, three new topologies have been shown in this Article: In the first place, coordination of the highly hindered $Ph_2CHCOO^-$ carboxylate ligands yields a distorted trapezium, Scheme 2F. In second place, the reaction of inorganic nickel salts (thiociante or nitrate in methanolic medium) leads to additional thiocyanate or methoxide bridges, resulting in two triangles with a $Ni_2$ grip or handle, Scheme 2G. In the last place, a new and surprising $Ni_4(MeO)_4$ cubane coordinated by three oximato bridges to an extra $Ni^{2+}$ ion has been discovered, Scheme 2H, when the reaction was set with pyC{CN}NOH and $NiBr_2$.

Despite that the relationship between the reactants and the resulting topology is highly serendipitous it could be pointed out that topologies 2-A and -B are dependent on additional O,N-donor groups attached to the vicinity of the oximate groups, which provide additional bridges in de adequate direction and that the most common structure 2-D, is related to the presence of carboxylate counteranions. The effect of the solvent is difficult to predict but in some cases the resulting product can be justified a posteriori: as example the reaction starting from nickel halides yields topology 2-E employing a coordinating solvent as methanol, whereas topology 2-H was obtained when the solvent ($CH_2Cl_2$) is unable to link the nickel cations. Oximate, carboxylate and alcoxo/hydroxo bridges induce typically antiferromagnetic interactions and low spin ground states are usually found for all the analyzed topologies, being $S = 1$ the expected ground state. Interestingly, competitive interactions can lead to diamagnetic $S = 0$ ground states despite the odd number of paramagnetic centers as will be further discussed. Larger spin states, up to the maximum $S = 5$, have been reported only for the 2-D bowtie topology when additional $\mu_3$-1,1,1 azido bridges are involved in the center of the shared triangles.

**Magnetic Measurements and Modeling.** The numbering of all the spin carriers in the Hamiltonians applied to **1**–**5** and in the subsequent discussion is provided in Scheme 3. The fit of the experimental data was made using CLUMAG program[25] for all complexes and applying the Hamiltonians derived from the corresponding interaction scheme. The number of coupling constants for each topology has been minimized as possible in basis to structural considerations to avoid overparametrization.

**Scheme 3. Schematic of the Magnetic Interactions for 1–5 (See Text for the Corresponding Hamiltonians)**

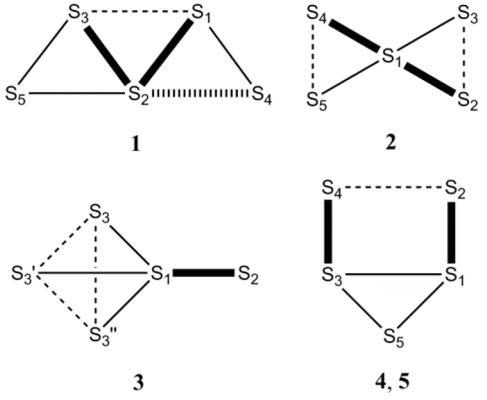


The room temperature $\chi_M T$ value for **1** is 4.96 $cm^3$ K $mol^{-1}$, which on cooling decreases continuously down to 0.75 $cm^3$ K $mol^{-1}$ at 2 K, Figure 5. The complex has seven interaction

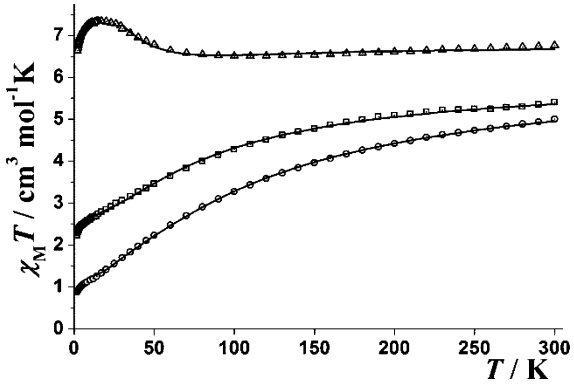


**Figure 5.** Product of $\chi_M T$ vs $T$ for compounds **1** (dot centered circles), **2** (dot centered squares), and **3** (triangles). Solid lines show best obtained fit.

pathways but the number superexchange pathways can be reduced attending to the kind of bridges: double oxo bridge ($J_1$), double hydroxo/oximato ($J_2$), triple hydroxo/oximate/carboxylate ($J_3$), and single hydroxo bridge ($J_4$). The 4-$J$ Hamiltonian was

$$H = -J_1(S_1 \cdot S_3) - J_2(S_2 \cdot S_4) - J_3(S_2 \cdot S_5 + S_1 \cdot S_4 + S_3 \cdot S_5) - J_4(S_1 \cdot S_2 + S_2 \cdot S_3)$$

The best fit parameters were $J_1 = +5.9$ $cm^{-1}$, $J_2 = -29.0$ $cm^{-1}$, $J_3 = -22.0$ $cm^{-1}$, $J_4 = -12.9$ $cm^{-1}$, and $g = 2.14$, with $R = 1.75 \times 10^{-5}$ ($R = (\chi_M T_{exp} - \chi_M T_{calcd})^2/(\chi_M T_{exp})^2$). Calculation of the energy of the lower spin states indicates an $S = 1$ ground state followed by one $S = 0$ with a gap of 10.6 $cm^{-1}$ and well isolated of larger spin states (the gap with the nearest $S = 2$ level is 26.0 $cm^{-1}$). Magnetization experiments show a nonsaturated value equivalent to 1.8 electrons, consistent with the population of the $S = 1$ ground state and a partial population of the low-lying $S = 0$ level.

Compound **2** presents a room temperature $\chi_M T$ value of 5.40 $cm^3$ K $mol^{-1}$ that drops when cooling down to 2.23 $cm^3$ K $mol^{-1}$ at 2 K, Figure 5. In this case there are three very different superexchange pathways and thus the applied Hamiltonian for the centrosymmetric compound **2** is



dx.doi.org/10.1021/ic500057j | Inorg. Chem. 2014, 53, 3194–3203

$$H = -J_1(S_1 \cdot S_2 + S_1 \cdot S_4) - J_2(S_1 \cdot S_3 + S_1 \cdot S_5) - J_3(S_2 \cdot S_3 + S_4 \cdot S_5)$$

Best fit parameters were $J_1 = -19.8$ cm$^{-1}$, $J_2 = -16.6$ cm$^{-1}$, $J_3 = -12.3$ cm$^{-1}$, and $g = 2.20$, with $R = 3.36 \times 10^{-5}$. Calculation of the energy of the lower spin states indicates an $S = 1$ ground state, but in this case, quasi degenerate with an $S = 0$ and two $S = 2$ spin levels. Effective population of the ground state only is possible below 2 K, explaining the shape and value of the lower $\chi_M T$ experimental plot and its value of 2.23 cm$^3$ K mol$^{-1}$ at 2 K. In good agreement, magnetization plot tends to the equivalent value of 3.5 electrons as result of the partial population of the low lying $S = 2$ spin levels at this temperature.

The $\chi_M T$ product at room temperature for compound **3** is 6.76 cm$^3$ K mol$^{-1}$ and then the curve diminishes to 6.52 cm$^3$ K mol$^{-1}$ at 100 K. Below this minimum the plot increases up to a maximum $\chi_M T$ value of 7.34 cm$^3$ K mol$^{-1}$ at 17 K suggesting a ferrimagnetic response with predominant ferromagnetic coupling. Finally, at lower temperatures, the $\chi_M T$ value decreases and reaches 6.64 cm$^3$ K mol$^{-1}$ at 2 K, due to ZFS or weak intercluster interactions, Figure 5.

Complex **3** clearly shows three different interaction pathways and on basis on the structural parameters the experimental data were fitted (in the 300−30 K temperature range) with the 3-$J$ Hamiltonian:

$$H = -J_1(S_1 \cdot S_2) - J_2(S_1 \cdot S_3 + S_1 \cdot S_{3'} + S_1 \cdot S_{3''}) - J_3(S_3 \cdot S_{3'} + S_3 \cdot S_{3''} + S_{3'} \cdot S_{3''})$$

Best parameters obtained were $J_1 = -51.4$ cm$^{-1}$, $J_2 = +3.9$ cm$^{-1}$, $J_3 = +11.0$ cm$^{-1}$, and $g = 2.32$, with $R = 4.10 \times 10^{-5}$. Fit values justify the ferrimagnetic response of **3**, pointed out by the minimum in the $\chi_M T$ plot: between room temperature and 100 K the dominant interaction corresponds to the strong antiferromagnetic interaction mediated by $J_1$ whereas at lower temperatures the ferromagnetic interactions inside the cubane fragment increase the $\chi_M T$ value, resulting in an $S = 3$ ground state. The magnetization plot shows a quasi saturated value of 6.5 $\mu_B$ at 5 T, that arises from the population of the well isolated $S = 3$ ground state.

$\chi_M T$ product versus $T$ for compounds **4** and **5** are depicted in Figure 6. Room temperature $\chi_M T$ value for **4** is 5.00 cm$^3$ K mol$^{-1}$ and decreases on cooling down to 0.88 cm$^3$ K mol$^{-1}$ at 2 K. Compound **5** shows a $\chi_M T$ value of 4.36 cm$^3$ K mol$^{-1}$ at 300 K and surprisingly, tends to zero at low temperature and the $\chi_M$ plot exhibit a well-defined maximum at 11 K.

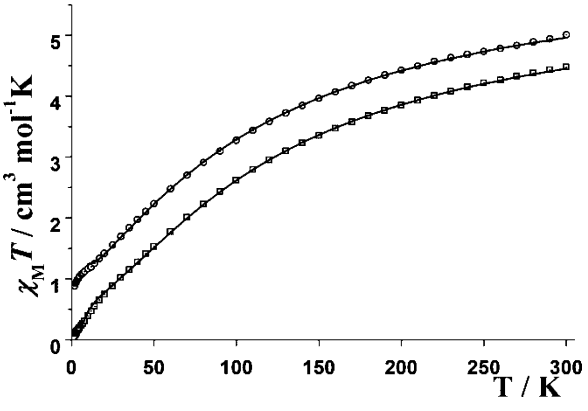


**Figure 6.** Product of $\chi_M T$ vs $T$ for compounds **4** (dot centered circles) and **5** (dot centered squares). Solid lines show best obtained fit.

As was pointed out in the structural description, Ni−O−Ni and Ni−O−N−Ni angles inside the $\mu_3$-OH centered triangle Ni(1,3,5) are practically identical and thus these three interactions were joined as $J_1$. By the same reasons the interaction between Ni(1)/Ni(2) and Ni(3)/Ni(4) were joined in a common $J_2$ coupling constant. The interaction between Ni(2) and Ni(4) corresponds to a very different pathway for each compound: in **4** is a double oximate/$\mu_{1,1}$-NCS bridge whereas for **5** is a double oximate/alkoxo bridge. The corresponding 3-$J$ Hamiltonian is

$$H = -J_1(S_1 \cdot S_5 + S_3 \cdot S_5 + S_1 \cdot S_3) - J_2(S_1 \cdot S_2 + S_3 \cdot S_4) - J_3(S_2 \cdot S_4)$$

The best obtained fit corresponds to $J_1 = -37.6$ cm$^{-1}$, $J_2 = -41.4$ cm$^{-1}$, $J_3 = -0.7$ cm$^{-1}$, and $g = 2.23$, with $R = 3.78 \times 10^{-5}$ for **4** and $J_1 = -39.6$ cm$^{-1}$, $J_2 = -40.4$ cm$^{-1}$, $J_3 = -35.9$ cm$^{-1}$ and $g = 2.19$, with $R = 2.91 \times 10^{-4}$ for **5** (in the range of 300 − 10 and 300 - 2 K, respectively). From these data, a simplified fit assuming $J_1 = J_2 \neq J_3$ for **4** and $J_1 = J_2 = J_3$ for **5** gives average values of $J_1 = J_2 = -41.4$ cm$^{-1}$, $J_3 = -1.6$ cm$^{-1}$, and $g = 2.27$ for **4** and $J_1 = J_2 = J_3 = -37.2$ cm$^{-1}$, and $g = 2.17$ for **5** with a similar quality. As could be expected from structural data, $J_1$ and $J_2$ take similar values in the two compounds. It should be pointed out that the value of $J_3$ is poorly reliable for compound **4**: its low value in comparison with the strong coupling mediated by $J_1$ and $J_2$ do not influence the shape of the plot as was checked fixing its value in the ±5 cm$^{-1}$ range. Thus, for the interaction mediated by the double oximate/thiocyanate bridges we are only able to propose a non quantified very weak magnetic interaction, probably antiferromagnetic. Magnetization plot for **4** shows a nonsaturated value equivalent to 1.8 electrons under the maximum applied field of 5 T. In contrast, no magnetization was obtained for compound **5** in agreement with the overall antiferromagnetic coupling.

Magnetic properties of complexes **4** and **5** become unusual and the different low-temperature response is not evident for this new $Ni_5$ topology. To justify the $S = 1$ (for **4**) and $S = 0$ (for **5**) ground states suggested by the susceptibility measurements we performed a more detailed analysis of the energy dependence of the low energy spin levels as function of the coupling constants.

According to the obtained fit values, the main difference among **4** and **5** lies in the very different value of $J_3$: for complex **4** $J_1$ and $J_2$ have similar values but $J_1 \approx J_2 \gg J_3$ and the ground state is apparently $S = 1$ whereas for complex **5** the three constants have similar values ($J_1 \approx J_2 \approx J_3$) and the ground state is clearly $S = 0$. Thus, it appears an evident relationship between $J_3$ and the stabilization of the diamagnetic ground state and to analyze this effect, the system was modeled as is shown in the coupling scheme plotted in Figure 7 (right), assuming $J_A = J_1 = J_2$ and $J_B = J_3$ Thus the analyzed Hamiltonian was

$$H = -J_A(S_1 \cdot S_5 + S_3 \cdot S_5 + S_1 \cdot S_3 + S_1 \cdot S_2 + S_3 \cdot S_4) - J_B(S_2 \cdot S_4)$$

The $J_A$ value was fixed to −40 cm$^{-1}$ (close to the fit value of $J_1$ and $J_2$) and $J_B$ was systematically explored between 0 and −40 cm$^{-1}$ range of values. The energy for the low lying spin levels $S = 0$, 1, and 2 are plotted in Figure 7 right, as function of the $J_B/J_A$ ratio. Analysis of this plot shows that $S = 0$ is the



dx.doi.org/10.1021/ic500057j | Inorg. Chem. 2014, 53, 3194−3203

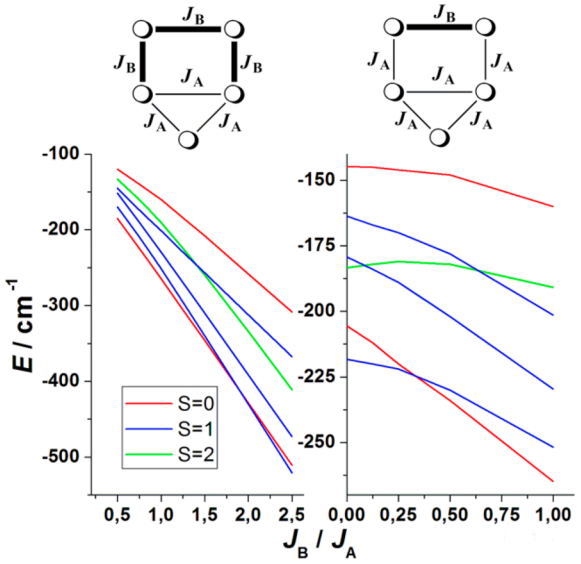


**Figure 7.** Coupling scheme and plot of energy of the low-lying spin levels for the optimized triangle-with-handle topology (left) and for complexes **4** and **5** (right). The values for $J_B/J_A$ = 1 are a common point in both plots.

ground state for larger $J_B/J_A$ ratios. In contrast, for lower $J_B/J_A$ ratios one well isolated $S$ = 1 becomes the ground state, being the frustration point at $J_B/J_A$ = 1/3.

For **4**, the calculated value of $J_3$ leads to one $J_B/J_A$ ratio on the lower limit of the plot with its associated $S$ = 1 ground state. At low temperature, both spin levels are populated explaining the intermediate value of 0.88 cm$^3$ K mol$^{-1}$ at 2 K and the low and nonsaturated value of magnetization.

For **5**, the calculated value of $J_3$ is similar to $J_1$ and $J_2$ ($J_B$ is similar to $J_A$) and the $J_B/J_A$ ratio is close to 0.9. This $J_B/J_A$ ratio leads to an $S$ = 0 ground state that confirms the quasi-diamagnetic behavior observed in the magnetization measurement at 2 K. In simple terms, complex **5** can be envisaged as an equilateral triangle antiferromagnetically coupled (local $S$ = 0) and a dimeric unit also antiferromagnetically coupled.

The topology of compounds **4** and **5** consists of a nearly equilateral triangle sharing one of its sides with a square arrangement of spin carriers (triangle-with-handle). To check if the diamagnetic ground state is inherent to this topology or if it could be dependent on the relative strength of the interactions inside each fragment, a new simulation was performed in order to give a wide characterization of this unusual $Ni_5$ arrangement.

Thus, the system was modeled according the coupling scheme plotted in Figure 7 left with the Hamiltonian:

$$H = -J_A(S_1\cdot S_5 + S_3\cdot S_5 + S_1\cdot S_3) - J_B(S_1\cdot S_2 + S_3\cdot S_4 + S_2\cdot S_4)$$

As in the above case, the $J_A$ value was fixed to −40 cm$^{-1}$ (close to the fit values of $J_1$) and $J_B$ was systematically explored between −20 and −100 cm$^{-1}$ range of values. Figure 7 left shows the energy trends for the low lying spin levels $S$ = 0, 1, and 2 as function of the $J_B/J_A$ ratio for triangle-with-handle compounds in which $J_A = J_1 \neq J_B = J_2 = J_3$.

Analysis of this plot shows how for the larger $J_B/J_A$ ratios the ground state is $S$ = 0, well isolated from the nearest $S$ = 1 spin level. In contrast, for lower $J_B/J_A$ ratios $S$ = 1 becomes the ground state but relatively close to the $S$ = 0 with the frustration point placed at $J_B/J_A$ = 2.0. In short, the ground state is function of the relative strength of the antiferromagnetic interaction inside the triangle and the handle and for similar interactions (as occurs in compound **5**, $S$ = 0 should be expected.

**Magnetic Correlations.** DFT calculations previously reported by the authors,[8b,10] have shown that the antiferromagnetic interaction inside triangular $[Ni_3(\mu_3\text{-OH})(\text{R-NO})_3]^{2+}$ fragments is strongly dependent on the Ni−O−Ni bond angle involving the central $\mu_3$-OH bridge. All the hydroxo/oximato mediated coupling constants reported in this paper present $J$ values that lie in the calculated range (between −15 and −50 cm$^{-1}$) and the values around −40 cm$^{-1}$ for the triangular subunits of **4** and **5** with Ni−O−Ni bond angles in the short 110.9−112.7 range of values are fully consistent with the correlations and the recently reported $[Ni_3(\mu_3\text{-OH})(\text{R-NO})_3]^{2+}$ triangles.[10] In the same way, the antiferromagnetic coupling associated to hydroxo/oximato bridges with lower Ni−O−Ni bond angles present in compound **1** show weaker antiferromagnetic interaction ($J_2$ = 29.0 cm$^{-1}$ and $J_3$ = 22.0 cm$^{-1}$) in good agreement with the expected values, providing additional proofs of the validity of the proposed model. Ni−O−Ni and Ni−O−O−N-Ni bond and torsion angles involved in these superexchange pathways are very similar and thus, the lower value obtained for $J_3$ should be related with the anticomplementary interaction of the syn−syn carboxylate bridge.

The oximate/pseudohalide bridges have been characterized only for the oximate/$\mu_{1,1}$-$N_3$ case for which we proved its moderate ferromagnetic response.[8e] Compound **4** gives the first example of oximate/N-thiocyanate double bridge. Magnetically, this double bridge behaves different of the azido case showing a weak and probably antiferromagnetic response.

Finally, it should be pointed out that the series of topologies reported for the $Ni_5$/oximate system tends to give low S ground states, mainly $S$ = 0 and 1, as corresponds with the oximate or oximate/hydroxo bridges that give moderate or strong antiferromagnetic interactions. The combination of oximates with $\mu_{1,1}$-$N_3$ or $\mu_{1,1,1}$-$N_3$ (bowtie topology D, Scheme 2), gives the unique examples in which the maximum $S$ = 5 ground state has been reached, arising as the best combination of ligands to obtain large spins that could lead to SMM response.

## ■ CONCLUSIONS

The employment of 2-pyridylcyanoxime ligand with different carboxylate and noncarbolxylate $Ni^{2+}$ salts has led to five new $Ni_5$/2-pyridyloxime clusters. These new complexes provided three new topologies together with the first example of the oximate/*N*-thiocyanate double bridge.

Magnetic measurements were carried in the 300 − 2 K range and revealed antiferromagnetic response for **1**, **2**, **4**, and **5** and ferrimagnetic behavior for **3**. All OH/oximato mediated magnetic interactions present coupling constant values that agree with the expected ones from previous DFT calculations. The oximate/N-thiocyanate double bridge proves to be a poorly efficient superexchange pathway in contrast with the clearly ferromagnetic character of the oximate/$\mu_{1,1}$-$N_3$ case.

Analysis of this system is an excellent example for serendipitous assembly: among the 14 $Ni_5$/2-pyridyloxime clusters that have been characterized, 8 different topologies have been observed and only for three of them an approach to rational design could be suggested. These variations come from small changes in the ligand (substitution on the vicinal C-atom to the oximate function), solvent coordination and the counteranion of the starting $Ni^{II}$ salt.



dx.doi.org/10.1021/ic500057j | Inorg. Chem. 2014, 53, 3194−3203

## ■ ASSOCIATED CONTENT

### Supporting Information

Crystallographic data in CIF format for compounds **1**−**5**. This material is available free of charge via the Internet at http://pubs.acs.org.

## ■ AUTHOR INFORMATION


### Corresponding Authors

*E-mail: jordi.esteban@qi.ub.edu.
*E-mail: albert.escuer@ub.edu.

### Present Address

⊥José Sánchez Costa: LCC, CNRS, and Université de Toulouse (UPS, INP), 205 route de Narbonne, 31077, Toulouse, France.


### Author Contributions

The manuscript was written through contributions of all authors.

### Notes

The authors declare no competing financial interest.

## ■ ACKNOWLEDGMENTS

Funds from CICYT Project CTQ2012-30662 are acknowledged. A.E. is thankful for financial support from the Excellence in Research ICREA-Academia Award. The Advanced Light Source is supported by the Director, Office of Science, Office of Basic Energy Sciences, of the U.S. Department of Energy under Contract No. DE-AC02-05CH11231.

## ■ REFERENCES


(1) (a) Rosa, D. T.; Krause Bauer, J. A.; Baldwin, M. J. *Inorg. Chem.* **2001**, *40*, 1606. (b) Akine, S.; Taniguchi, T.; Saiki, T.; Nabeshima, T. *J. Am. Chem. Soc.* **2005**, *127*, 540. (c) Goldcamp, M. J.; Robison, S. E.; Krause Bauer, J. A.; Baldwin, M. J. *Inorg. Chem.* **2002**, *41*, 2307.

(2) (a) Boyd, P. D. W.; Li, Q.; Vincent, J. B.; Folting, K.; Chang, H. R.; Streib, W. E.; Huffman, J. C.; Christou, G.; Hendrickson, D. N. *J. Am. Chem. Soc.* **1988**, *110*, 8537. (b) Milios, C. J.; Inglis, R.; Vinslava, A.; Bagai, R.; Wernsdorfer, W.; Parsons, S.; Perlepes, S. P.; Christou, G.; Brechin, E. K. *J. Am. Chem. Soc.* **2007**, *129*, 12505. (c) Choi, H. J.; Sokol, J. J.; Long, J. R. *Inorg. Chem.* **2004**, *43*, 1606. (d) Bogani, L.; Wernsdorfer, W. *Nat. Mater.* **2008**, *7*, 179. (e) Aromı, G.; Parsons, S.; Wernsdorfer, W.; Brechin, E. K.; McInnes, E. J. L. *Chem. Commun.* **2005**, 5038.

(3) (a) Dietrich, B.; Guilhem, J.; Lehn, J. M.; Pascard, C.; Sonveaux, E. *Helv. Chim. Acta* **1984**, *67*, 91. (b) Ulrich, S.; Petitjean, A.; Lehn, J. M. *Eur. J. Inorg. Chem.* **2010**, 1913.

(4) (a) Yoneya, M.; Yamaguchi, T.; Sato, S.; Fujita, M. *J. Am. Chem. Soc.* **2012**, *134*, 14401. (b) Fujita, D.; Suzuki, K.; Sato, S.; Yagi-Utsumi, M.; Yamaguchi, Y.; Mizuno, N.; Kumasaka, T.; Takata, M.; Noda, M.; Uchiyama, S.; Kato, K.; Fujita, M. *Nat. Commun.* **2012**, *3*, 1093.

(5) (a) Biros, S. M.; Yeh, R. M.; Raymond, K. N. *Angew. Chem., Int. Ed.* **2008**, *47*, 6062. (b) Brown, C. J.; Miller, G. M.; Johnson, M. W.; Bergman, R. G.; Raymond, K. N. *J. Am. Chem. Soc.* **2011**, *133*, 11964.

(6) (a) Winpenny, R. E. P. *J. Chem. Soc., Dalton Trans.* **2002**, 1. (b) Aromí, G.; Bell, A. R.; Helliwell, M.; Raftery, J.; Teat, S. J.; Timco, G. A.; Roubeau, O.; Winpenny, R. E. P. *Chem.—Eur. J.* **2003**, *9*, 3024. (c) Mukherjee, P.; Mukherjee, S. *Acc. Chem. Res.* **2013**, *46* (11), 2556 DOI: 10.1021/ar400059q.

(7) Milios, C. J.; Stamatatos, T. C.; Perlepes, S. P. *Polyhedron* **2006**, *25*, 134.

(8) (a) Escuer, A.; Esteban, J.; Aliaga-Alcalde, N.; Font-Bardia, M.; Calvet, T.; Roubeau, O.; Teat, S. J. *Inorg. Chem.* **2010**, *49*, 2259. (b) Esteban, J.; Ruiz, E.; Font-Bardia, M.; Calvet, T.; Escuer, A. *Chem.—Eur. J.* **2012**, *18*, 3637. (c) Stamatatos, T. C.; Diamantopoulou, E.; Raptopoulou, C. P.; Psycharis, V.; Escuer, A.; Perlepes, S. P. *Inorg. Chem.* **2007**, *46*, 2350. (d) Escuer, A.; Esteban, J.; Roubeau, O. *Inorg. Chem.* **2011**, *50*, 8893. (e) Escuer, A.; Esteban, J.; Font-Bardia, M. *Chem. Commun.* **2012**, *48*, 9777. (f) Esteban, J.; Font-Bardia, M.; Escuer, A. *Inorg. Chem.* **2014**, *53*, 1113. (g) Stamatatos, T. C.; Abboud, K. A.; Perlepes, S. P.; Christou, G. *Dalton Trans.* **2007**, 3861. (h) Stamatatos, T. C.; Escuer, A.; Abboud, K. A.; Raptopoulou, C. P.; Perlepes, S. P.; Christou, G. *Inorg. Chem.* **2008**, *47*, 11825. (i) Esteban, J.; Alcázar, L.; Torres-Molina, M.; Monfort, M.; Font-Bardia, M.; Escuer, A. *Inorg. Chem.* **2012**, *51*, 5503.

(9) Escuer, A.; Vlahopoulou, G.; Perlepes, S. P.; Mautner, F. A. *Inorg. Chem.* **2011**, *50*, 2468.

(10) (a) Esteban, J.; Font-Bardia, M.; Escuer, A. *Eur. J. Inorg. Chem.* **2013**, 5274. (b) Esteban, J.; Font-Bardia, M.; Escuer, A. *Inorg. Chem. Commun.* **2014**, DOI: 10.1016/j.inoche.2014.02.033.

(11) Alcazar, L.; Cordero, B.; Esteban, J.; Tangoulis, V.; Font-Bardia, M.; Calvet, T.; Escuer, A. *Dalton Trans.* **2013**, *42*, 12334.

(12) Coxall, R. A.; Harris, S. G.; Henderson, D. K.; Parsons, S.; Tasker, P. A.; Winpenny, R. E. P. *Chem. Soc., Dalton Trans.* **2000**, 2349.

(13) (a) Gerasimchuk, N. N.; Skopenko, V. V.; Domasevich, K. V.; Zhmurko, O. A. *Ukr. Khim. Zh. (Russ. Ed.)* **1992**, *58*, 935. (b) Mokhir, A. A.; Domasevich, K. V.; Dalley, N. K.; Kou, X.; Gerasimchuk, N. N.; Gerasimchuk, O. A. *Inorg. Chim. Acta* **1999**, *284*, 85.

(14) Sheldrick, G. M. *SHELXS—A Computer Program for Determination of Crystal Structures*: University of Göttingen: Göttingen, Germany, 1997.

(15) Sheldrick, G. M. *SHELX97—A Program for Crystal Structure Refinement*; University of Göttingen: Göttingen, Germany, 1997.

(16) *International Tables of X-Ray Crystallography*, Vol. *IV*; Kynoch Press: Witton, Birmingham, U.K., 1974, 99−100 and 149.

(17) Ortep-3 for Windows: Farrugia, L. J. *J. Appl. Crystallogr.* **1997**, *30*, 565.

(18) (a) Davies, W. C.; Evans, G. B.; Hulbert, F. L. *J. Chem. Soc.* **1939**, 412. (b) Alcazar, L.; Cordero, B.; Esteban, J.; Tangoulis, V.; Font-Bardia, M.; Calvet, T.; Escuer, A. *Dalton Trans.* **2013**, *42*, 12334. (c) Lampropoulos, C.; Abboud, K. A.; Stamatatos, T. C.; Christou, G. *Inorg. Chem.* **2009**, *48*, 813.

(19) Psomas, G.; Stemmler, A. J.; Dendrinou-Samara, C.; Bodwin, J. J.; Schneider, M.; Alexiou, M.; Kanpf, J. W.; Kessissoglou, D. P.; Pecoraro, V. L. *Inorg. Chem.* **2001**, *40*, 1562.

(20) Herring, J.; Zeller, M.; Zaleski, C. M. *Acta Crystallogr.* **2011**, *E67*, m41.

(21) (a) Lah, M. S.; Pecoraro, V. L. *J. Am. Chem. Soc.* **1989**, *111*, 7258. (b) Dendrinou-Samara, C.; Papadopoulos, A. N.; Malamatri, D. A.; Tarushi, A.; Raptopoulou, C. P.; Terzis, A.; Samaras, E.; Kessissoglou, D. P. *J. Inorg. Biochem.* **2005**, *99*, 864.

(22) Mezei, G.; Zaleski, C. M.; Pecoraro, V. L. *Chem. Rev.* **2007**, *107*, 4933.

(23) Che, Z.; Jia, M.; Zhang, Z.; Liang, F. *Cryst. Growth Des.* **2010**, *10*, 4807.

(24) (a) Papatriantafyllopoulou, C.; Stamatatos, T. C.; Wensdorfer, W.; Teat, S. J.; Tasiopoulos, A. J.; Escuer, A.; Perlepes, S. P. *Inorg. Chem.* **2010**, *49*, 10486. (b) Escuer, A.; Vlahopoulou, G.; Mautner, F. A. *Dalton Trans.* **2011**, *40*, 10109.

(25) Gatteschi, D.; Pardi, L. *Gazz. Chim. Ital.* **1993**, *123*, 231.

### 3.6.1. Resum: New topologies in pentanuclear nickel/oximato clusters: Structural and magnetic characterization.

Jordi Esteban, Mercè Font-Bardia, José Sánchez Costa, Simon J. Teat, Albert Escuer.

*Inorganic Chemistry* **2014**, *53*, 3194-3203.

Després d'obtenir una família de compostos de nuclearitat entre $Ni_3$ i $Ni_5$ basats en els fragments triangulars $Ni_3/\mu_3$-OR/oxima, es va provar de modificar les síntesis per tal d'obtenir nous productes a partir d'anions carboxilat així com la síntesi de nous compostos a partir de sals no carboxíliques de níquel(II), totes elles coordinants.

Es van estudiar cinc nous compostos, tots ells de nuclearitat $Ni_5$, que presenten quatre topologies diferents. Aquests són: $NEt_4[Ni_5(H_2O)(OH)_2(Ph_2CHCOO)_5(pyC\{CN\}NO)_4]$ (**6_1**), format per dos triangles que comparteixen un vèrtex i generen un trapezi (o un llacet o *bowtie* fortament distorsionat); $[Ni_5(H_2O)_2Cl_2(pyC\{CN\}NO)_8]$ (**6_2**), amb forma de *bowtie*; un cubà de $\{Ni_4(MeO)_4\}^{4+}$ unit a un cinquè catió $Ni^{II}$ mitjançant tres ponts oxima, $[Ni_5(MeOH)_6Br_3(MeO)_4(pyC\{CN\}NO)_3]$ (**6_3**) i $Ni_5(MeOH)_6Cl_3(MeO)_4(pyC\{CN\}NO)_3]$ (**6_3b**) (l'espectre d'IR d'aquest producte és totalment coincident amb l'anterior, però no s'ha pogut resoldre l'estructura d'aquest compost a causa de la seva baixa cristal·linitat); i finalment dos compostos que es poden descriure com triangles units a una subunitat dinuclear o com triangles amb *nansa*, $[Ni_5(H_2O)_3(NCS)_2(OH)_2(pyC\{CN\}NO)_6]$ (**6_4**) i $[Ni_5(H_2O)_{2,5}(MeOH)(MeO)_2(OH)_{1,5}(pyC\{CN\}NO)_6](NO_3)_{0,5}$ (**6_5**).

Aprofitant aquesta variabilitat topològica, es va dur a terme una cerca bibliogràfica i es va trobar un total de 9 compostos sintetitzats a partir de lligands 2-piridiloxima i nuclearitat $Ni_5$, que presentaven fins a 5 topologies diferents. A la vista d'aquests resultats, es va intentar racionalitzar el comportament del sistema $Ni_5$/2-piridiloxima en funció dels diferents anions emprats.

Es va estudiar el comportament magnètic dels diversos compostos i es va trobar que els compostos **6_1**, **6_2**, **6_4** i **6_5** són antiferromagnètics, mentre que el compost **6_3** presenta un comportament ferrimagnètic (conté acoblaments ferromagnètics i antiferromagnètics). És destacable el fet que els compostos **6_4** i **6_5**, tot i presentar la mateixa topologia (triangle amb *nansa*), tenen estats fonamentals d'spin diferents: $S = 1$ i $S = 0$, respectivament. Es va trobar que el valor de l'estat fonamental ve donat per la relació d'intensitats entre la constant d'acoblament de la *nansa* dinuclear i la constant d'acoblament dins del triangle.

En resum, es van obtenir cinc nous compostos de nuclearitat $Ni_5$ a partir del lligand 2-acetonitrilpiridiloxima i diferents sals carboxíliques i no carboxíliques. Aquests compostos presenten una elevada variabilitat topològica, de forma que es va estudiar la relació entre l'anió de partida i la topologia del compost i es va determinar que el factor més rellevant és la presència d'anions carboxilat, que generen estructures basades en triangles, poc o molt distorsionats, en funció del seu volum.

## 3.7. Article 7.

## Template arrangement of $\{Ni_3(\mu_3\text{-}OH)(SO_4)(R\text{-}NO)_2\}^+$ fragments around $Na^+$ cations: an unprecedented $\{Ni_{12}Na\}$ unit linked by oximate and sulfate bridges.

**Jordi Esteban**, Mercè Font-Bardia, Albert Escuer.

*Inorganic Chemistry Communications* **2014**, *43*, 169-172.

Inorganic Chemistry Communications 43 (2014) 169–172

Contents lists available at ScienceDirect

Inorganic Chemistry Communications

journal homepage: www.elsevier.com/locate/inoche

# Template arrangement of $\{Ni_3(\mu_3\text{-}OH)(SO_4)(R\text{-}NO)_2\}^+$ fragments around $Na^+$ cations: An unprecedented $\{Ni_{12}Na\}$ unit linked by oximate and sulfate bridges

Jordi Esteban [a,*], Mercè Font-Bardia [b,c], Albert Escuer [a,*]

[a] Departament de Química Inorgànica, Universitat de Barcelona, Av. Diagonal 645, Barcelona 08028, Spain
[b] Departament de Mineralogia, Cristal·lografia i Dipòsits Minerals, Universitat de Barcelona, Martí Franqués s/n, 08028 Barcelona, Spain
[c] Unitat de Difracció de R-X, Centre Científic i Tecnològic de la Universitat de Barcelona (CCiTUB), Universitat de Barcelona, Solé i Sabarís 1-3, 08028 Barcelona, Spain

ARTICLE INFO

*Article history:*
Received 25 January 2014
Accepted 22 February 2014
Available online 3 March 2014

*Keywords:*
Supramolecular
Template synthesis
Sulfato complexes
Metallamacrocycle
Magnetic measurements

ABSTRACT

A novel $\{-Ni_{12}Na_2\text{-}Ni\text{-}\}_n$ chain has been characterized from the reaction between 2-pyridylcyanoxime, (pyC{CN}NOH), and nickel(II) sulfate. The template synthesis around a $Na^+$ cation gives an unprecedented arrangement of four nickel triangles coordinated to the central sodium ion by sulfato bridges.



The use of 2-pyridyloximate ligands and paramagnetic first-row transition metal ions has been a growing field in the last years due to their ability to generate stable polynuclear compounds with a wide range of nuclearities [1]. Among them, 2-pyridylcyanoxime ligand, pyC{CN}NOH, Scheme 1, has proven to possess unique reactivity that arises from the coordination of the cyano substituent to the vicinal C-atom to the oximate function, which gives a much more acidic oxime (3–5 units of pKa with respect to ligands with other substituents) [1], and has lead to unique topologies, as we have reported in the previous copper [2], nickel [3] and manganese [4] studies. One of the specific properties of this ligand is that, as has been recently reported, it is prone to generate isolated triangular clusters with $\{Ni_3(\mu_3\text{-}OH)(R\text{-}NO)_3\}^{2+}$ core [3].

Although sulfate anions present great coordinative possibilities (they can bind up to 10 metal ions) [5], and have shown interesting properties in different fields such as catalysis, medicinal, bioinorganic and environmental chemistry [5], its use in coordination chemistry is limited and currently, only six entries were found in CCDC containing the simultaneous sulfate and oximate bridges being practically all of them are $Ni^{II}$ derivatives such as $Ni_4$ [6], two $Ni_5$ [7], a family of $Ni_6$ [8] and one $Ni_8$ [9] clusters.

In this work we have explored the combination of the pyC{CN}NOH ligand and sulfate anions with the aim of triggering the aggregation of preformed smaller species into new high-nuclearity clusters; and we report the synthesis, characterization and magnetic study of a $\{-Ni_{12}Na_2\text{-}Ni\text{-}\}_n$ chain with the formula $[Ni_{13}Na_2(H_2O)_2(MeOH)_{14}(OH)_4(pyC\{CN\}NO)_8(SO_4)_8]_n\cdot$solvent (**1**·solvent) in which four $\{Ni_3(\mu_3\text{-}OH)(SO_4)(R\text{-}NO)_2\}^+$ triangles template around a central Na(1) ion. This fragment links a peripheral Na(2) cation and the chain is the result of further linkage of the $\{Ni_{12}Na_2\}$ units by one additional bridging $Ni^{II}$ cation.

Noteworthy, the $\{Ni_{13}Na_2\}$ fragment is the largest oximate–sulfate cluster and the second highest nuclearity in Ni-oximate chemistry (only surpassed by a family of $Ni_{14}$ clusters [10]) and in Ni-sulfate chemistry (just outstripped by one $Ni_{30}$ compound [11]).

Reaction of nickel sulfate and 2-pyridyloximate (2:1 ratio) in methanolic solution and NaOH as base yields compound **1** by slow evaporation [12,13]. Compound **1** consists of one central Na(1) cation surrounded by four $[Ni_3(OH)(pyC\{CN\}NO)_2(SO_4)_2(MeOH)_2(H_2O)]^-$ triangles and a second Na(2) cation linked by a sulfato bridge. One additional nickel atom links the $\{Ni_{12}Na_2\}$ units generating a one-dimensional $\{-(Ni_{12}Na_2)\text{-}Ni\}_n$ system. The four triangular subunits are not crystallographically equivalent but their bond parameters are very similar and to simplify the discussion only one of them will be described on detail. The triangular subunit formed by Ni(1,2,3) is defined by one central $\mu_3$-OH ligand, two oximate and one sulfato bridges that determine the main plane of the triangle, Fig. 1 top. The two sides defined by the oximate bridges show close bond parameters (Ni–O(1a)–Ni bond angles are 106.8(2) and 109.5(2)° and Ni···Ni distances of 3.274(1)

* Corresponding authors. Tel.: +34 934039144; fax: +34 934907725.
*E-mail address:* jordi.esteban@qi.ub.edu (J. Esteban).

http://dx.doi.org/10.1016/j.inoche.2014.02.033
1387-7003/

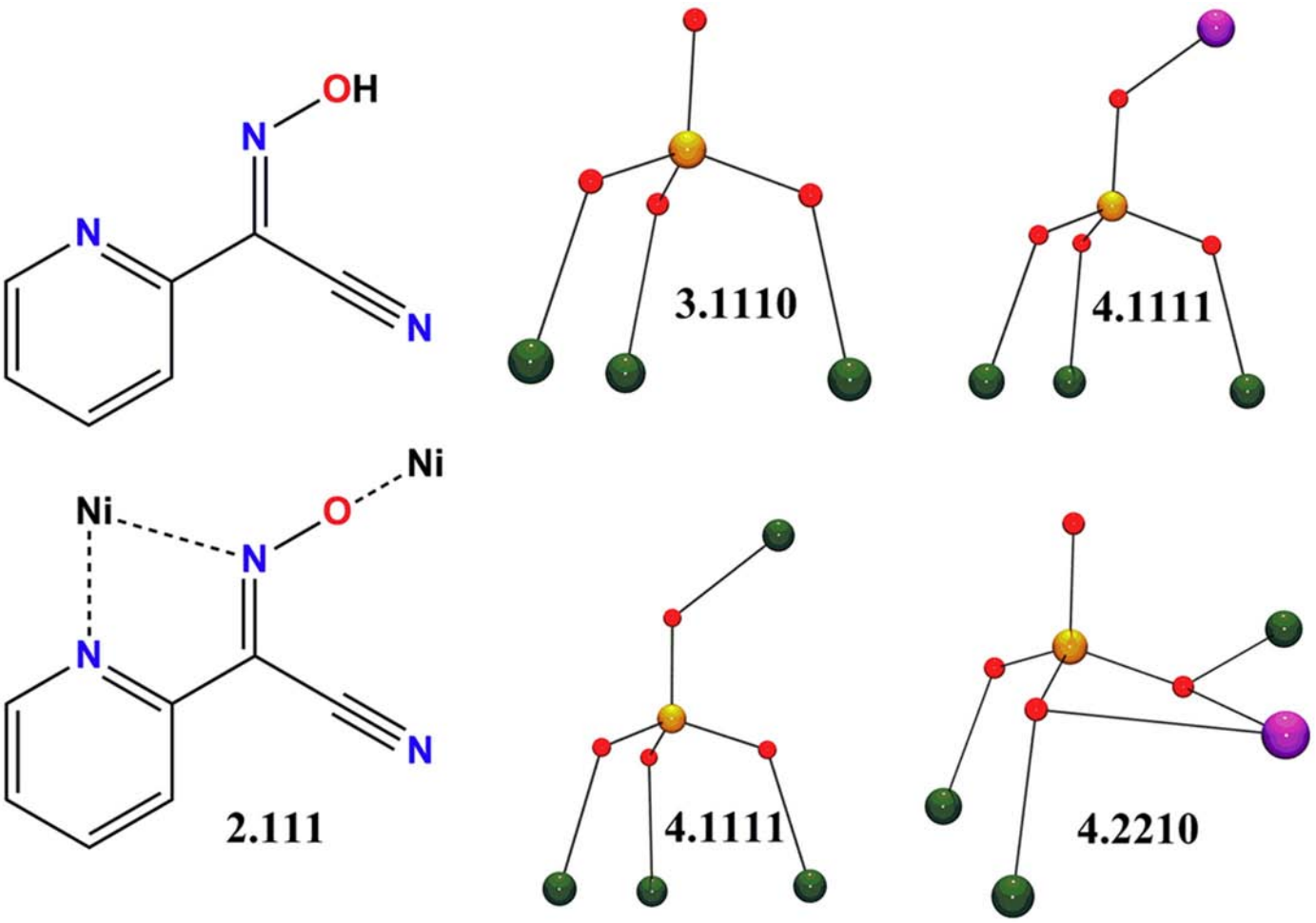


**Scheme 1.** Left, pyC{CN}NOH ligand and the coordination mode for pyC{CN}NO$^-$ present in this communication, in Harris notation [14]. Right, sulfate coordination modes presented in this work. Color code: Ni$^{II}$, green; O, red, N, blue; S, orange; Na$^+$ purple. (For interpretation of the references to color in this figure legend, the reader is referred to the web version of this article.)

and 3.325(1) Å) whereas the parameters for the side defined by the sulfato bridge are 123.3(2)° and 3.585(1) Å, respectively. Ni–N–O–Ni torsion angles are 7.8(5) and 17.9(5)°. One capping tridentate sulfate ligand links three axial coordination sites and the coordination spheres of the nickel atoms are completed by solvent molecules except for O(10) atom, which comes from one sulfate of the neighbor triangle. The O(10) atom is equivalent to O(33): they both bridge two triangles and link the central Na(1) cation.

The four linked triangles are arranged in a roughly $S_4$ symmetry around the central Na(1) cation, Fig. 1 bottom, determining the tridecanuclear {$Ni_{12}Na$} unit. The sodium cation is linked by four pentadentate 4.2210 sulfates resulting in a *girobifastigium* coordination polyhedron (Johnson 26) [15], Fig. 2. The four Na–O distances of the central square plane, O(10,12,28,33), are comprised in the 2.277–2.328 Å range whereas the other four sites O(9,15,26,34), related by an $S_4$ axis, exhibit larger bond distances in the 2.710–2.871 Å range. Focusing in the environment of the sodium atom, its coordination can alternatively be described as the center of a 16-MC8 metallacrown formed by four nickel atoms, four sulfurs and eight oxygen donors, Fig. 2.

The discrete {$Ni_{12}Na_2$} units are linked to the Ni(13) atom. This nickel atom exhibits a $NiO_6$ coordination environment that arises from four methanol molecules and two *trans* 4.1111 sulfate anions that generate the final 1D {−($Ni_{12}Na_2$)-Ni-}$_n$ system, Fig. 3.

Factors that lead to the stabilization of **1** are the combination of the properties of the chosen reagents. In fact, other 2-pyridyloximes with R = H, Me or Ph instead of the nitrile function do not tend to give triangular clusters and when combined with sulfato ligand give a variety of $Ni_6$ topologies. A second feature is related with the great coordinative flexibility of the sulfato ligand, which exhibits their 4.2110, 4.1111 and 3.1110 modes coordinating Ni$^{II}$ and Na$^+$ cations, Scheme 1. The sodium cation plays a crucial role in the syntheses of **1** as a templating agent. Noteworthy, reaction performed employing $Et_3N$ as base does not give isolable compounds whereas the same reaction with CsOH as base leads to the equivalent compound with Cs$^+$ instead of the central Na$^+$ cation.

The temperature dependence of the $\chi_M T$ product of compound **1** is plotted in Fig. 4 [16]. The room temperature $\chi_M T$ value is 14.2 K cm$^3$ mol$^{-1}$, which decreases gradually on cooling, down to 1.8 K cm$^3$ mol$^{-1}$ at 2 K.

In view of the negligible magnetic exchange promoted by sulfato anions [5] no intertriangle interactions were considered and thus the fitting of the experimental data was done using the conventional analytical equation derived from the two-*J* Hamiltonian:

$$H = -J_1(S_1 \cdot S_2 + S_2 \cdot S_3) - J_2(S_1 \cdot S_3)$$

considering four triangles plus one isolated Ni$^{II}$ for molar formula. Best fit parameters obtained were $J_1 = -22.8(4)$ cm$^{-1}$, $J_2 = -14.3(2)$ cm$^{-1}$ and $g = 2.204(5)$.

According to DFT calculated correlation for $\mu_3$-OH/NO bridges as superexchange pathway presented in a previous paper [3a], the main factor that contributes to tune the AF interaction are the Ni–O–Ni bond angles involving the central $\mu_3$-OH bridge. The estimated *J* value for an average Ni–O–Ni angle of ~108° would be around −25 cm$^{-1}$ in

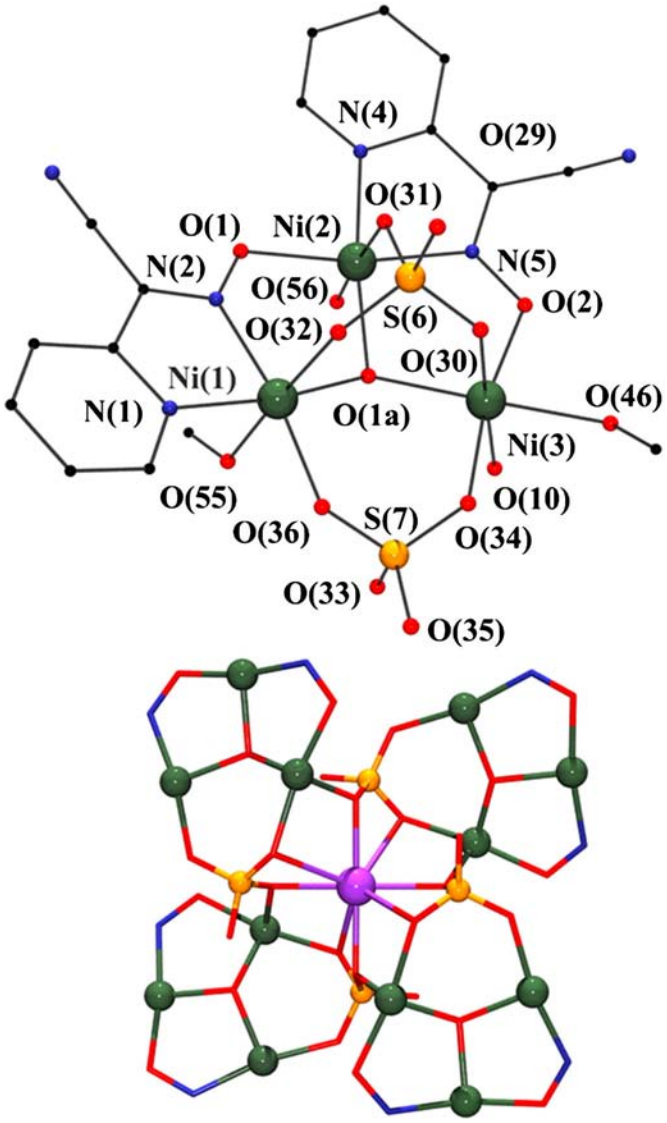


**Fig. 1.** Top, labeled plot of a $Ni_3$ triangular subunit. Bottom, view along the pseudo-$S_4$ axis of the {$Ni_{12}Na$} unit of compound **1**.

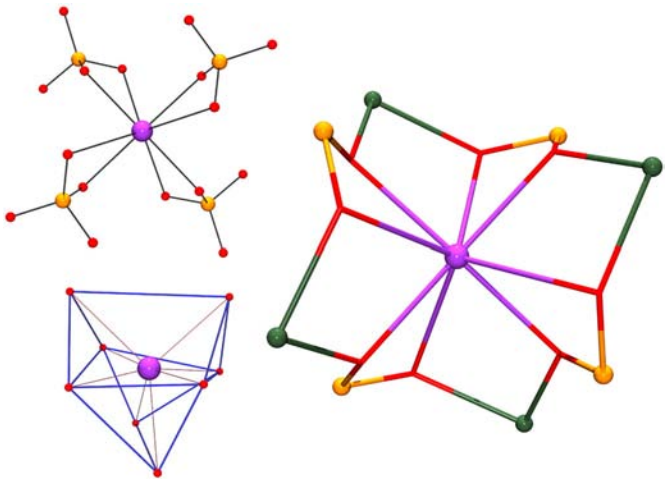

**Fig. 2.** Left, environment of the central Na(1) cation generating the *girobifastigium* coordination polyhedron. Right, View of the 16-MC8 metallacrown generated around the $Na^+$ cation.

excellent agreement with the estimated value of $J_1$. The weaker interaction, mediated by the countercomplementary $SO_4^{2-}$/OH bridges, should be mainly attributed to the interaction mediated by the Ni–O–Ni pathway with a bond angle of 123.4(2)°. Ground state for a triangular arrangement of $Ni^{II}$ cations depends on the $J_2/J_1$ ratio, being $S = 1$ for ratios comprised between 0 and 0.5 and $S = 0$ for ratios larger than 0.5 (which is a frustration point). The $J_2/J_1$ ratio for **1** is around 0.62 and the ground state of each triangle is $S = 0$. Thus, the low $\chi_M T$ value at 2 K can be rationalized like four $S = 0$ triangles plus one isolated $Ni^{2+}$ atom.

In conclusion, the employment of 2-pyridylcianoxime ligand with nickel sulfate in the presence of sodium cations has lead to one 1D system containing four triangular units template around the sodium cation resulting in {$Ni_{12}Na$} fragments. Compound **1** provides a new example of the unusual reactivity of 2-pyridylcianoxime and the relevant and poorly explored role of the sulfato ligands to generate large nuclearity clusters.

## Acknowledgments

Funds from the Ministerio de Economia y Competitividad Project CTQ2012-30662 are acknowledged. A.E. is thankful for the financial support from the Excellence in Research ICREA-Academia Award.

## Appendix A. Supplementary material

Supplementary data to this article can be found online at http://dx.doi.org/10.1016/j.inoche.2014.02.033.

## References

[1] C.J. Milios, T.C. Stamatatos, S.P. Perlepes, Polyhedron 25 (2006) 134–194.
[2] A. Escuer, G. Vlahopoulou, S.P. Perlepes, F.A. Mautner, Inorg. Chem. 50 (2011) 2468–2478.
[3] a) J. Esteban, E. Ruiz, M. Font-Bardia, T. Calvet, A. Escuer, Chem. Eur. J. 18 (2012) 3637–3648;
b) J. Esteban, M. Font-Bardia, A. Escuer, Eur. J. Inorg. Chem. (2013) 5274–5280.
[4] L. Alcazar, B. Cordero, J. Esteban, V. Tangoulis, M. Font-Bardia, T. Calvet, A. Escuer, Dalton Trans. 42 (2013) 12334–12345.
[5] C. Papatriantafyllopoulou, E. Manessi-Zoupa, A. Escuer, S.P. Perlepes, Inorg. Chim. Acta 362 (2009) 634–650.
[6] E. Moushi, C.G. Efthymiou, S.P. Perlepes, C. Papatriantafyllopoulou, Int. J. Inorg. Chem. (2011) 606271–606279.
[7] Z. Chen, M. Jia, Z. Zhang, F. Liang, Cryst. Growth Des. 10 (2010) 4806–4814.
[8] a) C. Papatriantafyllopoulou, G. Aromi, A.J. Tasiopoulos, V. Nastopoulos, C.P. Raptopoulou, S.J. Teat, A. Escuer, S.P. Perlepes, Eur. J. Inorg. Chem. (2007) 2761–2774;
b) C.G. Efthymiou, A.A. Kitos, C.P. Raptopoulou, S.P. Perlepes, A. Escuer, C. Papatriantafyllopoulou, Polyhedron 28 (2009) 3177–3184.
[9] J. Esteban, A. Escuer, M. Font-Bardia, O. Roubeau, S.J. Teat, Polyhedron 52 (2013) 339–345.
[10] a) T.C. Stamatatos, K.A. Abboud, S.P. Perlepes, G. Christou, Dalton Trans. (2007) 3861–3863;
b) T.C. Stamatatos, A. Escuer, K.A. Abboud, C.P. Raptopoulou, S.P. Perlepes, G. Christou, Inorg. Chem. 47 (2008) 11825–11838;
c) J. Esteban, L. Alcázar, M. Torres-Molina, M. Monfort, M. Font-Bardia, A. Escuer, Inorg. Chem. 51 (2012) 5503–5505.
[11] L. Dong, R. Huang, Y. Wei, W. Chu, Inorg. Chem. 48 (2009) 7528–7530.
[12] Reaction of $Ni(SO_4)\cdot 6H_2O$ (0.280 g, 1 mmol) with 2-pyridylcyanoxime (0.073 g, 0.5 mmol) an NaOH (0.040 g, 1 mmol) in 20 mL of methanol yields compound **1** by slow evaporation as orange bricks. Anal. calcd for dried $C_{70}H_{96}N_{24}Na_2Ni_{13}O_{60}S_8$ (**1**): C, 25.48; H, 2.94; N, 10.19; S, 7.77%. Found: C, 25.0; H, 3.1; N, 9.8; S, 7.6 %. Relevant IR bands ($cm^{-1}$): 3315(br), 2226(w), 1603(m), 1468(s), 1432(w), 1303(w), 1266(w), 1224(m), 1142(s), 1107(s), 1037(m), 781(w), 712(w), 632(w). Reaction performed with CsOH instead NaOH yields the equivalent compound as tin needles (not adequate for X-ray determination) with the same IR spectra. Infrared spectra (4000–400 $cm^{-1}$) were recorded from KBr pellets on a Brucker IFS-125 FT-IR spectrophotometer.
[13] Data for compound **1** was measured from orange crystals at 273 K and $\lambda = 0.71073$ Å using a Bruker APEX-II CCD diffractometer with graphite monochromator. Crystal data and structural parameters for **1**: [$C_{70}H_{96}N_{24}Na_2Ni_{13}O_{60}S_8$], MW: 3299.39, triclinic space group *P-1*, $a = 14.0686(18)$ Å, $b = 22.314(3)$ Å, $c = 29.223(4)$ Å, $\alpha = 93.991(2)°$, $\beta = 103.354(2)°$, $\gamma = 108.295(2)°$, $V = 8373.6(2.18)$ $Å^3$, $Z = 2$, $Dc = 1.306$ $g\cdot cm^{-3}$, $\mu$(Mo-K$\alpha$) = 1.605 $mm^{-1}$, $T = 273(2)$ K, 34,029 reflections measured, 17,825 independent reflections ($R_{int} = 0.0782$), final $R_1$[IN2 σ(I)] = 0.0622 and final $wR_2 = 0.1569$. Program SQUEEZE, part of the PLATON package of crystallographic software, was used to calculate the solvent disorder area and

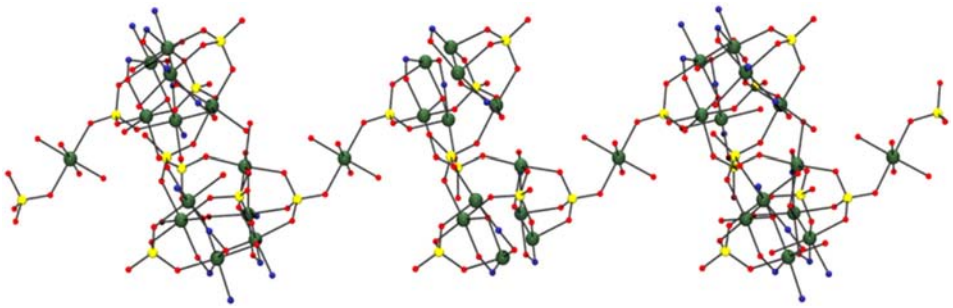

**Fig. 3.** View of the $\{-Ni_{12}Na_2\text{-}Ni\text{-}\}_n$ chain showing the bridging Ni(13) ion and the position of Na(2) linked to one of the 4.1111 sulfates.

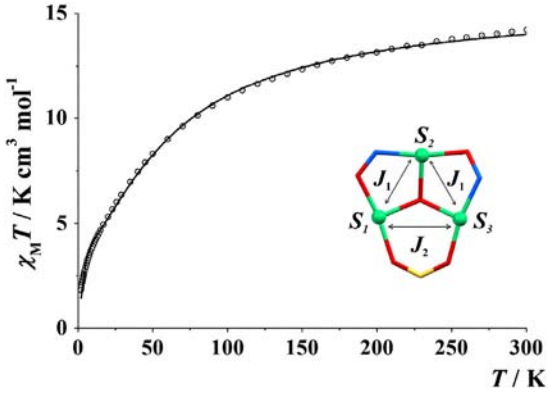


**Fig. 4.** $\chi_M T$ product vs. $T$ for compound **1**. Solid line shows the best obtained fit. Inset: coupling scheme for each of the triangles (see text).

remove its contribution to the overall intensity data; as consequence methanol and water molecules around Na(2) were not determined. CCDC 972518.

[14] Harris notation, referred as X.Y1Y2Y3…Yn, where X is the overall number of metals bound by the whole ligand and each value of Y refers to the number of metal ions attached to the different donor atoms. The ordering of Y is listed by the Cahn–Ingold–Prelog priority rules, hence here O before N. R.A. Coxall, S.G. Harris, D.K. Henderson, S. Parsons, P.A. Tasker, R.E.P. Winpenny, Chem. Soc. Dalton Trans. (2000) 2349–2356.

[15] M. Llunell, D. Casanova, J. Cirera, P. Alemany, S. Alvarez, SHAPE version 2.0, 2010. (Barcelona) The program can be obtained free of charge by request to the authors.

[16] Magnetic susceptibility measurements were carried out on polycrystalline samples using a Quantum Design MPMS-5 SQUID susceptometer working in the range 2–300 K under magnetic fields of 0.3 T (300–30 K) and 0.03 T (30–2 K) to avoid saturation effects. Diamagnetic corrections were estimated from Pascal tables.

### 3.7.1. Resum: Template arrangement of $\{Ni_3(\mu_3\text{-}OH)(SO_4)(R\text{-}NO)_2\}^+$ fragments around $Na^+$ cations: an unprecedented $\{Ni_{12}Na\}$ unit linked by oximate and sulfate bridges.

Jordi Esteban, Mercè Font-Bardia, Albert Escuer.

*Inorganic Chemistry Communications* **2014**, *43*, 169-172.

Aquesta comunicació conté el resultat obtingut en fer reaccionar el lligand pyC{CN}NOH amb $NiSO_4$, utilitzant NaOH com a base.

Es va sintetitzar un compost monodimensional amb fórmula $[Ni_{13}Na_2(H_2O)_2(MeOH)_{14}(OH)_4(pyC\{CN\}NO)_8(SO_4)_8]_n$ (**7_1**) que es pot descriure com un fragment $\{Ni_{12}Na_2\}$ format per quatre triangles $\{Ni_3(\mu_3\text{-}OH)(SO_4)(pyC\{CN\}NO)_2\}^+$ disposats al voltant d'un catió $Na^+$ central (per efecte plantilla o *template synthesis*) i units entre ells per mitjà d'anions sulfats en mode de coordinació 4.2110, figura 12. La subunitat $\{Ni_{12}Na_2\}$ s'uneix, a través d'un lligand sulfat axial, a un catió $Ni^{II}$ addicional que es troba coordinat, al seu torn, amb un nou fragment $\{Ni_{12}Na_2\}$, generant així el sistema monodimensional $\{Ni_{12}Na_2\text{-}Ni\text{-}\}_n$, figura 13.

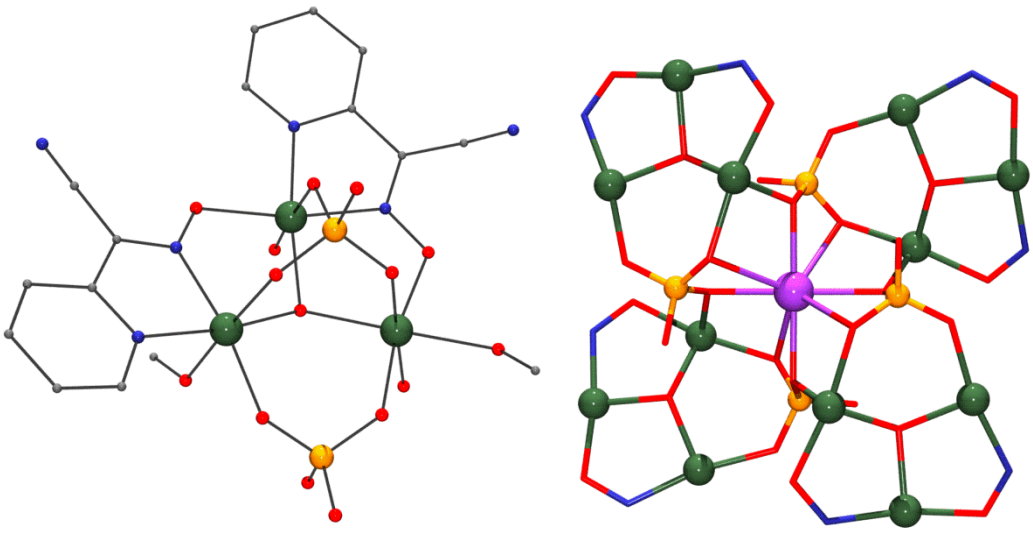

**Figura 12.** Estructura del triangle $\{Ni_3(\mu_3\text{-}OH)(SO_4)(pyC\{CN\}NO)_2\}^+$ (esquerra) i disposició dels triangles al voltant de l'ió $Na^+$ central (dreta).

Des d'un punt de vista magnètic, el sistema es va estudiar com quatre triangles aïllats (l'acoblament a través d'anions sulfat es pot considerar negligible)[132,168] i un catió $Ni^{II}$ també aïllat. L'ajust de les dades experimentals amb un Hamiltonià amb dues *J* va donar un estat fonamental d'spin per als triangles de $S = 0$, de forma que el valor de la susceptibilitat (o $\chi_M T$) a baixa temperatura es deu únicament a la presència del catió $Ni^{II}$ de la unitat monomèrica.

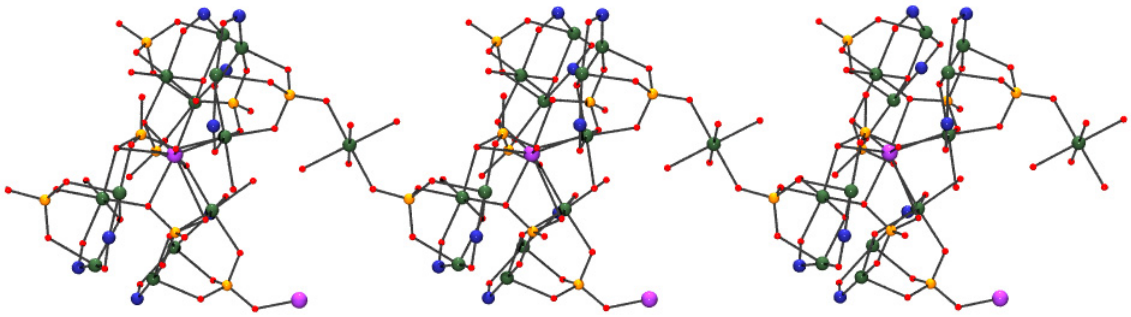

**Figura 13.** Vista de la cadena $\{\text{-}Ni_{12}Na_2\text{-}Ni\text{-}\}_n$. Els lligands piridiloxima han estat eliminats per tenir una imatge més clara del sistema.

Així, es pot dir que es va obtenir un nou compost, a partir del sistema $Ni^{II}$/oxima/$SO_4$, creat al voltant d'un catió $Na^+$ per efecte plantilla i que s'estén formant la cadena monodimensional $\{Ni_{12}Na_2\text{-}Ni\text{-}\}_n$ en coordinar-se el fragment $\{Ni_{12}Na_2\}$ a un catió $Ni^{II}$ que actua de pont. Les característiques més destacables del fragment $\{Ni_{13}Na_2\}$ són que es tracta del compost de major nuclearitat pel sistema oxima/sulfat i el segon major pels sistemes Ni/oxima i Ni/$SO_4$.

## 3.8. Article 8.

## High nuclearity in azido/oximate chemistry: $Ni_{14}$ and $Ni_{13}$ clusters with *S* = 6 and 9 ground states.

**Jordi Esteban**, Laura Alcázar, Maria Torres-Molina, Montserrat Monfort, Mercè Font-Bardia, Albert Escuer.

*Inorganic Chemistry* **2012**, *51*, 5503-5505.

Inorganic Chemistry

Communication

pubs.acs.org/IC

# High Nuclearity in Azido/Oximate Chemistry: $Ni_{14}$ and $Ni_{13}$ Clusters with $S$ = 6 and 9 Ground States

Jordi Esteban,[†] Laura Alcázar,[†] Maria Torres-Molina,[†] Montserrat Monfort,[†] Mercè Font-Bardia,[‡] and Albert Escuer*,[†]

[†]Departament de Química Inorgànica, Universitat de Barcelona, Av. Diagonal 645, 08028 Barcelona, Spain

[‡]Departament de Mineralogia i Cristal·lografia, Universitat de Barcelona, Martí Franqués s/n, 08028 Barcelona, Spain

Supporting Information

**ABSTRACT:** In the present work, we report a family of $Ni_{14}$ and unprecedented $Ni_{13}$ clusters linked by end-on azido and oximato bridges. Ferrimagnetic response gives $S$ = 6 and 9 ground states, resulting in the largest nuclearities and spins in nickel oximato chemistry.

Coordination chemistry of salicyl[1] or pyridyl[2] oximate ligands has grown in the past decade in relation to their ability to generate high-nuclearity metallic clusters with single-molecule-magnet (SMM) response. Blending of different bridging ligands (other than carboxylates) is a synthetic strategy widely employed in cluster chemistry to increase the nuclearity or to improve the magnetic properties of the resulting complexes. The azido anion (in its end-on coordination mode) has been intensely studied to obtain ferro- or ferrimagnetic high-spin systems with a large variety of coligands.[3]

Following our previous work in nickel/oximato/azide chemistry, we have centered our attention on the poorly explored ligand 6-methylpyridine-2-carbaldehydeoxime (6-MepaoH; Chart 1), for which, in addition to one early reported[4] $Ni^{II}_9$ cluster, only some $Ni_5$ and $Ni_6$ cages[5] and one $(Mn^{II}_2Mn^{III}_2)_n$ chain[6] have been recently characterized by us. The reaction of 6-MepaoH with $Ni^{II}$ salts in the presence of sodium azide yields clusters with the formulas $[Ni_{13}(6\text{-Mepao})_{12}(N_3)_8(OH)_6(N\text{-Meen})_2(MeOH)_4]$ (**1**·7MeOH·2-$H_2O$; N-Meen = *N*-methylethylenediamine), $[Ni_{13}(6\text{-Mepao})_{12}(N_3)_8(OH)_6(MeOH)_8]$ (**2**), and $[Ni_{14}(6\text{-Mepao})_{12}(N_3)_8(Cl)_2(OH)_4(MeOH)_4(H_2O)_4]Cl_2$ (**3**·7MeOH·2.5$H_2O$).

**Chart 1. 6-MepaoH Ligand and Coordination Modes Found in 1−3**

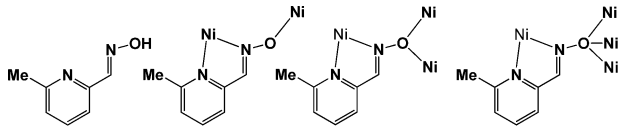


Compounds **1**−**3**, together with the previously reported complexes $[Ni_{12}Na_2(OH)_4(N_3)_8(pao)_{12}(H_2O)_{10}](OH)_2$ (**4**) and $[Ni_{14}(OH)_4(N_3)_8(pao)_{14}(paoH)_2(H_2O)_2](ClO_4)_2$ (**5**),[7] form a family of ferrimagnetic clusters with common structural features. The maximum ground state $S$ = 9 has been found for the $Ni_{13}$ compounds **1** and **2**.

The largest nuclearities reported until now in nickel oximato chemistry were $Ni_{12}$ and $Ni_{14}$, which also exhibit the previous record spin $S$ = 6.[7,8] It is worth noting that the nuclearity for $Ni_{13}$ is extremely rare, and to our knowledge, only one nickel triazole cluster exhibiting this nuclearity has been reported until now.[9]

A first approach to the family of clusters **1**−**5** can be made by attending to their common structural motifs. All of them contain two hexanuclear $Ni_6$ rings, which acting as complex as the ligand link two $Na^+$ cations ($Ni_6Na_2Ni_6$, **4**), one $Ni^{2+}$ cation ($Ni_6NiNi_6$, **1** and **2**), or two $Ni^{2+}$ cations ($Ni_6Ni_2Ni_6$, **3** and **5**); see Figure 1. In addition to **1**−**5**, one hexanuclear $[Mn^{III}Ni_5(N_3)_4(pao)_6(paoH)_2(OH)_2](ClO_4)$ system with the same local topology and $pao^-$ ligands has recently been reported.[10]

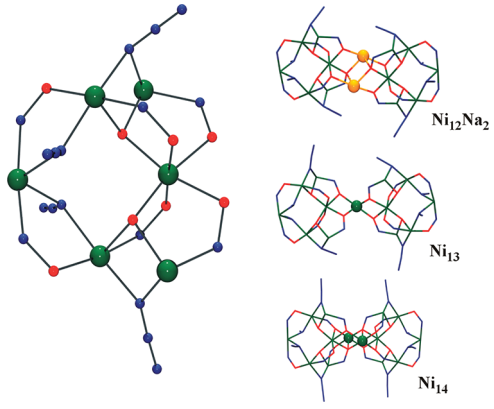


**Figure 1.** (Left) Plot of the common $Ni_6$ ring for **1**−**5**. (Right) Schematic core of $Ni_{12}Na_2$, $Ni_{13}$, and $Ni_{14}$ clusters exhibiting a very similar pattern. Color key: Ni, green; O, red; N, blue; Na, orange.

Complexes **1** and **2** are isostructural,[11] and thus only **1** will be described in detail. Complex **1** consists of two $\{Ni_5(6\text{-Mepao})_6(N_3)_4\}$ fragments connected by one nickel linear trinuclear unit (Figure 2). The nickel atoms of these $Ni_5$ fragments are linked by end-on azido/oximato bridges between

**Received:** February 22, 2012
**Published:** May 7, 2012

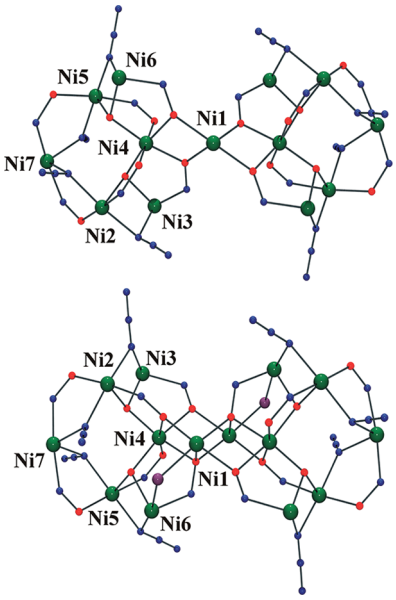


**Figure 2.** (Top) Core of clusters **1** and **2**. (Bottom) Core of cluster **3**. Color key: Ni, green; O, red; N, blue; Cl, violet.

Ni(2)/Ni(7) and Ni(5)/Ni(7) or end-on azido/hydroxo bridges between Ni(2)/Ni(3) and Ni(5)/Ni(6). Two $\eta^1{:}\eta^1{:}\eta^1{:}\mu_2$-oximates and two $\mu_3$-OH bridges link Ni(2,5) with Ni(4), and the core is completed with two $\eta^1{:}\eta^1{:}\eta^2{:}\mu_3$-oximate bridges [linking Ni(3,6) with Ni(4) and the central Ni(1) atom] and solvent molecules. The N-Meen ligand is linked to Ni(6). The Ni−N−Ni bond angles involving azido ligands show values of 94.6(3)° and 99.0(3)° for Ni(2)−N−Ni(3) and Ni(5)−N−Ni(6) and larger ones [111.0(3)° and 117.3(3)°] for Ni(7)−N−Ni(2) and Ni(7)−N−Ni(5). Ni−N−O−Ni torsion angles are lower than 7° except for Ni(3)−N−O−Ni(4), which has a value of 28.5(7)°. The only difference among **1** and **2** lies in the substitution of the bidentate amine on Ni(6) by two methanol molecules.

Tetradecacomplex[11] **3** is very similar to the previously reported **5**, and the reader can find a detailed description of its core in a corresponding publication.[7] The main differences are substitution of the neutral bidentate paoH ligands on Ni(2) and the bridging pao$^-$ bridges in **5** by two methanol molecules and two chloride bridges in **3**. The remaining bond parameters are very similar in both compounds.

The differences between the $Ni_{13}$ (**1** and **2**) and $Ni_{14}$ (**3** and **5**) cores are induced by the subtle change in the coordination mode of the 6-Mepao$^-$ ligands linked to Ni(2) and Ni(6). In the $Ni_{13}$ cluster, the oxime coordinated to Ni(2) ($\eta^1{:}\eta^1{:}\eta^1{:}\mu_2$ mode) does not interact with the central nickel atom and the oxime coordinated to Ni(6) ($\eta^1{:}\eta^1{:}\eta^2{:}\mu_3$ mode) links Ni(6) with Ni(4) and the central Ni(1) cation. In contrast, in the $Ni_{14}$ cluster, the oximes coordinated to the Ni(2) and Ni(6) clusters adopts the $\eta^1{:}\eta^1{:}\eta^2{:}\mu_3$ and $\eta^1{:}\eta^1{:}\eta^3{:}\mu_4$ modes, linking Ni(4) and two central atoms Ni(1) and Ni(1′) (Figure 3). The increase of the coordination sites in the central fragment of the cluster is fulfilled with the chloro bridges and solvent molecules.

The room temperature $\chi_M T$ value for **1** is 13.7 cm$^3$ K mol$^{-1}$, close to the expected value for 13 isolated $Ni^{2+}$ ions (13.0 cm$^3$ K mol$^{-1}$). Upon cooling, $\chi_M T$ decreases very slightly, exhibiting a broad minimum at 160 K and suggesting ferrimagnetic response. Below the minimum, the plot reaches a maximum $\chi_M T$ value of 20.1 cm$^3$ K mol$^{-1}$ at 9 K, followed by a fast decrease to 12.6 cm$^3$ K mol$^{-1}$ (Figure 4). Compound **2** shows a quasi-identical behavior (Figure S2 in the Supporting Information).

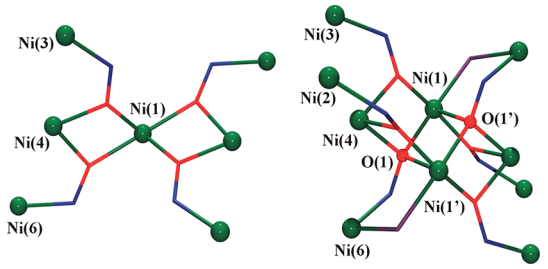


**Figure 3.** Coordination to the central nickel atoms of the oximate bridging ligands for the $Ni_{13}$ (left) and $Ni_{14}$ (right) clusters.

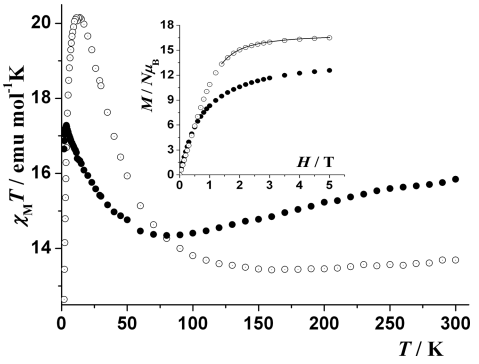


**Figure 4.** $\chi_M T$ product versus $T$ plot for compounds **1** (open circles) and **3** (solid circles). Inset: magnetization experiments at 2 K showing the high-field fit of the data (solid line).

Compound **3** shows a room temperature $\chi_M T$ value of 15.8 cm$^3$ K mol$^{-1}$ (slightly larger than that expected for 14 $Ni^{2+}$ isolated ions, 14.0 cm$^3$ K mol$^{-1}$). $\chi_M T$ decreases upon cooling, exhibiting a clear minimum of 14.3 cm$^3$ K mol$^{-1}$ at 80 K. Below the minimum, the plot increases up to a maximum $\chi_M T$ value of 17.3 cm$^3$ K mol$^{-1}$ at 3.7 K and finally slightly diminishes to 16.4 cm$^3$ K mol$^{-1}$ at 2 K. The size of **1**−**3** and the large number of superexchange pathways exclude fit of the data, but an approach to the main interactions can be made on the basis of the structural parameters.

As described, these compounds can be envisaged as two pentanuclear $Ni^{II}$ wings linked by a linear $Ni_3$ or butterfly-like $Ni_4$ subunits. Nickel atoms from both wings are connected by double oximato/end-on azido or $\mu_3$-OH/end-on azido bridges. There is experimental evidence that the double oximato/end-on azido bridges promote ferromagnetic coupling,[12] and experimental and theoretical density functional theory calculations also indicate that ferromagnetic coupling should be expected for the double $\mu_3$-OH/end-on azido bridges.[13] Thus, we have that each wing should be ferromagnetically coupled with an $S = 5$ local spin. The interaction of Ni(2,3,5,6) with Ni(4), mediated by double $\mu_{2,3}$-oximato and $\mu_3$-OH bridges (with Ni−O−Ni angles of around 111° in all cases), should provide an antiferromagnetic contact, and finally the interaction between Ni(4) and Ni(4′) with the central Ni(1) atom should be antiferromagnetic in nature according the double Ni−O−Ni linkage with bond angles of 103.2(2)° and 109.9(2)°. Given all of these coupling interactions, we assume that **1** must have a



dx.doi.org/10.1021/ic3004036 | Inorg. Chem. 2012, 51, 5503−5505

ground state of $S = 9$ according the spin alignment shown in Chart 2, left.

**Chart 2. Scheme of the Spin Alignment of 1 and 2 (Left) and 3 (Right) and the Proposed Spin Ground States**

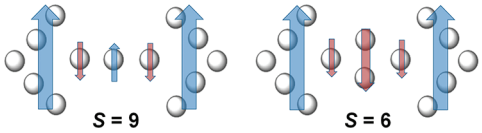


The lower $\chi_M T$ value observed for **3** is compatible with an $S = 6$ ground state arising from the antiferromagnetic coupling between the ferromagnetic $Ni_5$ wings and the ferromagnetic central $Ni_4$ butterfly. This proposal agrees with the $S = 6$ ground state proposed by Christou et al.[7] for complex **5** and the $S = 3$ ground state reported for the $\{Mn^{III}Ni_5\}$ related system.[10] From experimental evidence, substitution of the oximate bridge in **5** by one bridging chloride in **3** does not modify the magnetic response of the cluster.

This proposal was confirmed by magnetization experiments at 2 K. Magnetization of **1** and **2** shows a fast increase with quasi-saturated values equivalent to 16.5 and 17.2 electrons (Figures 4 and S2 in the Supporting Information). The low-field magnetization of **1** is slightly sigmoidal, showing a maximum at 0.3 T in its first derivative and suggesting an intercluster interaction close to $-0.3$ cm$^{-1}$. A fit of the magnetization data above 1.5 T (to discard the intercluster interaction effect) gives an excellent fit for an $S = 9$ spin with a low $D$ value of $-0.15$ cm$^{-1}$ (Figure 4, inset). Thus, the low-$T$ decay in the $\chi_M T$ plot can be attributed to intercluster interactions mainly mediated by hydrogen bonds. Magnetization for **3** tends to be equivalent to 12.6 electrons, in good agreement with the proposed $S = 6$ ground state and the reported data for **5**.

Despite the large $S = 9$ ground state, the low $D$ value, arising partially from the $C_2$ symmetry of the molecule, excludes the observation of out-of-phase signals and a SMM response of over 2 K, as was experimentally checked by alternating-current susceptibility measurements.

In conclusion, the new topology of the $\{Ni_{13}\}$ clusters completes a family of clusters exhibiting the largest nuclearity and spin ground states in nickel/oximate chemistry. These complexes provide new examples of the relevant versatility of the oxime ligands to generate high-nuclearity systems and the ability of the azido ligand to promote selective ferromagnetic interactions.

## ■ ASSOCIATED CONTENT

### Supporting Information

X-ray crystallographic data for complexes **1** and **3** in CIF format, experimental procedures, and structural and magnetic data for compound **2** (Figures S1 and S2). This material is available free of charge via the Internet at http://pubs.acs.org.

## ■ AUTHOR INFORMATION

### Corresponding Author

*E-mail: albert.escuer@ub.edu.

### Notes

The authors declare no competing financial interest.

## ■ ACKNOWLEDGMENTS

This work was supported by CICYT Project CTQ2009-07264. A.E. is thankful for financial support from the Excellence in Research ICREA-Academia Award.

## ■ REFERENCES

(1) (a) Milios, C. J.; Raptopoulou, C. P.; Terzis, A.; Lloret, F.; Vicente, R.; Perlepes, S. P.; Escuer, A. *Angew. Chem., Int. Ed.* **2004**, *43*, 210. (b) Milios, C. J.; Vinslava, A.; Wood, P. A.; Parsons, S.; Wernsdorfer, W.; Christou, G.; Perlepes, S. P.; Brechin, E. K. *J. Am. Chem. Soc.* **2007**, *129*, 8. (c) Milios, C. J.; Vinslava, A.; Wernsdorfer, W.; Prescimone, A.; Wood, P. A.; Parsons, S.; Perlepes, S. P.; Christou, G.; Brechin, E. K. *J. Am. Chem. Soc.* **2007**, *129*, 6547.

(2) (a) Milios, C. J.; Stamatatos, Th. C.; Perlepes, S. P. *Polyhedron* **2006**, *25*, 134 (Polyhedron Report). (b) Tasiopoulou, A. J.; Perlepes, S. P. *Dalton Trans.* **2008**, 5537 (Perspective).

(3) Escuer, A.; Aromi, G. *Eur. J. Inorg. Chem.* **2006**, 4721 (Microreview).

(4) Pajunen, A.; Mutikainen, I.; Saarinen, H.; Orama, M. *Z. Kristallogr.—New Cryst. Struct.* **1999**, *214*, 217.

(5) Escuer, A.; Vlahopoulou, G.; Mautner, F. A. *Dalton Trans.* **2011**, *40*, 10109.

(6) Escuer, A.; Vlahopoulou, G.; Mautner, F. A. *Inorg. Chem.* **2011**, *50*, 2717.

(7) (a) Stamatatos, T. C.; Abboud, K. A.; Perlepes, S. P.; Christou, G. *Dalton Trans.* **2007**, 3861. (b) Stamatatos, T. C.; Escuer, A.; Abboud, K. A.; Raptopoulou, C. P.; Perlepes, S. P.; Christou, G. *Inorg. Chem.* **2008**, *47*, 11825.

(8) (a) Papatriantafyllopoulou, C.; Jones, L. F.; Nguyen, T. D.; Matamoros-Salvador, N.; Cunha-Silva, L.; Almeida-Paz, F. A.; Evangelisti, M.; Brechin, E. K.; Perlepes, S. P. *Dalton Trans.* **2008**, 3153. (b) Ji, C.-M.; Yang, H.-J.; Zhao, C.-C.; Tangoulis, V.; Cui, A.-L.; Kou, H.-Z. *Cryst. Growth Des.* **2009**, *9*, 4607. (c) Kou, H.-Z.; An, G.-Y.; Ji, C.-M.; Wang, B.-W.; Cui, A.-L. *Dalton Trans.* **2010**, *39*, 3153.

(9) (a) Papatriantafyllopoulou, C.; Diamantopoulou, E.; Terzis, A.; Lalioti, N.; Tangoulis, V.; Perlepes, S. P. *Inorg. Chem. Commun.* **2008**, *11*, 454. (b) Papatriantafyllopoulou, C.; Diamantopoulou, E.; Terzis, A.; Tangoulis, V.; Lalioti, N.; Perlepes, S. P. *Polyhedron* **2009**, *28*, 1903.

(10) Chen, H.; Ma, C.-B.; Yuan, D.-Q.; Hu, M.-Q.; Wen, H.-M.; Liu, Q.-T.; Chen, C.-N. *Inorg. Chem.* **2011**, *50*, 10352.

(11) Crystal data for $1 \cdot 7MeOH \cdot 2H_2O$: $C_{94}N_{52}Ni_{13}O_{22}H_{116} \cdot (CH_4O)_7(H_2O)_2$ (3353.98), monoclinic, $C2/c$, $a = 24.582(13)$ Å, $b = 22.488(8)$ Å, $c = 27.802(10)$ Å, $\beta = 91.96(2)°$, $V = 15360(11)$ Å$^3$, $Z = 4$, $T = 100(2)$ K, $\lambda$(Mo K$\alpha$) = 0.71073 Å, 23067 reflections collected, 14280 unique ($R_{int} = 0.0446$), $R = 0.0611$, $R_w^2 = 0.1587$. Crystal data for $3 \cdot 7MeOH \cdot 2.5H_2O$: $C_{88}H_{96}Cl_4N_{48}Ni_{14}O_{24} \cdot (CH_4O)_7(H_2O)_{2.5}$ (3497.25), triclinic, $P\bar{1}$, $a = 16.227(1)$ Å, $b = 16.709(2)$ Å, $c = 19.201(2)$ Å, $\alpha = 108.409(5)°$, $\beta = 92.219(5)°$, $\gamma = 115.014(4)°$, $V = 4385.7(7)$ Å$^3$, $Z = 1$, $T = 100(2)$ K, $\lambda$(Mo K$\alpha$) = 0.71073 Å, 17249 reflections collected, 17249 unique ($R_{int} = 0.0426$), $R = 0.0424$, $R_w^2 = 0.1380$. Cell data for **2**: monoclinic, $C2/c$, $a = 24.525(5)$ Å, $b = 22.274(5)$ Å, $c = 27.632(6)$ Å, $\beta = 92.96(1)°$, $V = 15074(1)$ Å$^3$. CCDC deposition numbers for **1** and **3**: 867793 and 867794.

(12) (a) Stamatatos, T. C.; Diamantopoulou, E.; Raptopoulou, C. P.; Psycharis, V.; Escuer, A.; Perlepes, S. P. *Inorg. Chem.* **2007**, *46*, 2350. (b) Papatriantafillopoulou, C.; Stamatatos, T. C.; Wernsdorfer, W.; Teat, S. J.; Tasiopoulos, A.; Escuer, A.; Perlepes, S. P. *Inorg. Chem.* **2010**, *49*, 10486.

(13) Esteban, J.; Ruiz, E.; Font-Bardia, M.; Calvet, T.; Escuer, A. *Chem.—Eur. J.* **2012**, *18*, 3637.

### 3.8.1. Resum: High nuclearity in azido/oximate chemistry: $Ni_{14}$ and $Ni_{13}$ clusters with *S* = 6 and 9 ground states.

Jordi Esteban, Laura Alcázar, Maria Torres-Molina, Montserrat Monfort, Mercè Font-Bardia, Albert Escuer.

*Inorganic Chemistry* **2012**, *51*, 5503-5505.

En aquesta comunicació es van presentar els resultats obtinguts pel lligand 6-MepyC{H}NOH amb $Ni^{II}$, sintetitzats a partir de diferents sals metàl·liques, azidur de sodi i, en un cas, una amina bidentada.

Els compostos caracteritzats són: $[Ni_{13}(N\text{-Meen})_2(MeOH)_4(6\text{-MepyC}\{H\}NO)_{12}(N_3)_8(OH)_6]$ (**8_1**) (N-Meen: N-metiletilendiamina), $[Ni_{13}(MeOH)_8(6\text{-MepyC}\{H\}NO)_{12}(N_3)_8(OH)_6]$ (**8_2**) i $[Ni_{14}(MeOH)_4(H_2O)_4(6\text{-MepyC}\{H\}NO)_{12}(N_3)_8(Cl)_2(OH)_4]Cl_2$ (**8_3**). Tots ells, juntament amb dos compostos de nuclearitat $\{Ni_{12}Na_2\}$ (**8_4**) i $\{Ni_{14}\}$ (**8_5**) prèviament estudiats per Christou *et al.*,[142,170] presenten en comú el fragment $\{Ni_6(oxima)_6(N_3)_4(OH)_2\}$ que es pot descriure com un anell hexanuclear que conté quatre ponts amb azida i un spin local *S* = 4. Aquests fragments són capaços de coordinar diversos metalls, de forma que els compostos prèviament descrits es poden entendre com sistemes $\{Ni_6Na_2Ni_6\}$ (**8_4**), $\{Ni_6NiNi_6\}$ (**8_1** i **8_2**) i $\{Ni_6Ni_2Ni_6\}$ (**8_3** i **8_5**), figura 14.

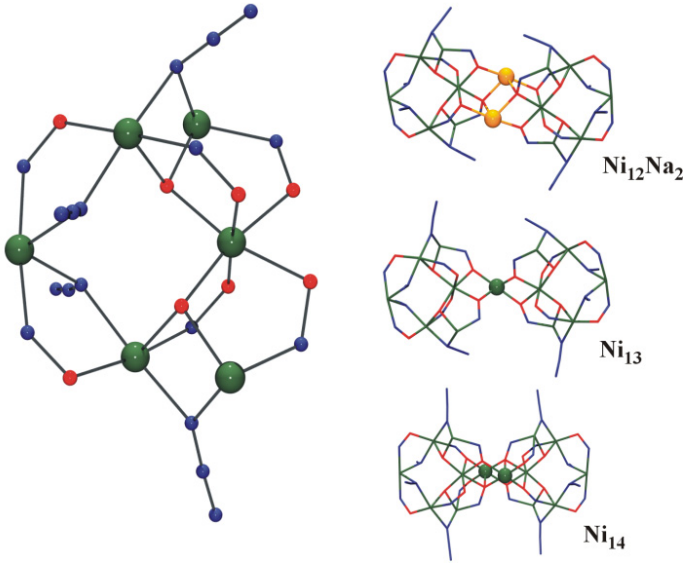


**Figura 14.** Fragment $\{Ni_6(oxima)_6(N_3)_4(OH)_2\}$ comú en tots els compostos (esquerra) i *core* esquemàtic dels compostos $\{Ni_{12}Na_2\}$, $\{Ni_{13}\}$ i $\{Ni_{14}\}$ (dreta).

No es va poder realitzar l'ajust de les dades de susceptibilitat magnètica d'aquests compostos a causa de l'elevat nombre de centres paramagnètics i de camins de superintercanvi magnètic, però en base a les dades experimentals de susceptibilitat magnètica i magnetització i per comparació amb dades bibliogràfiques es van determinar els tipus d'interacció presents: ferromagnètica per interaccions $\mu_3$-OH/$N_3$ i oxima/$N_3$ i antiferromagnètica per ponts $\mu_3$-OH/oxima. Aquesta assignació va revelar un estat fonamental $S$ = 9 per **8_1** i **8_2** i $S$ = 6 per **8_3**, d'acord amb l'esquema d'acoblament que es mostra a la figura 15.

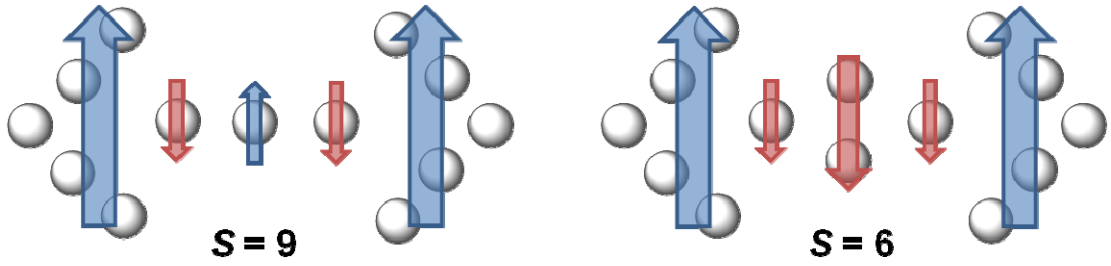


**Figura 15.** Esquema d'acoblaments per **8_1** i **8_2** (esquerra) i **8_3** i **8_5** (dreta).

L'ajust de la mesura de magnetització reduïda de **8_1** a camps superiors a 1,5 T (per eliminar les possibles interaccions intermoleculars) va confirmar l'estat fonamental $S$ = 9 i va donar un valor de $D$ = -0,15 $cm^{-1}$. Tot i l'elevat estat fonamental d'spin de **8_1**, el sistema {$Ni_{13}$} no es comporta com un imant unimolecular (SMM) a temperatures superiors a 2 K a causa del reduït valor de $D$ (que es deu a la simetria $C_2$ que presenta el compost), ja que no s'observen senyals fora de fase a la mesura de susceptibilitat magnètica amb corrent altern.

Per acabar, cal destacar que el compost **8_3**, {$Ni_{14}$}, presenta la nuclearitat més elevada trobada per al sistema Ni/oxima juntament amb **8_5**, i que els productes **8_1** i **8_2** presenten l'estat fonamental d'spin més elevat per aquest mateix sistema, $S$ = 9, però no exhibeixen un comportament de SMM a causa de la seva elevada simetria.

## 3.9. Article 9.

## Anion coordination by metallamacrocycles: A cryptand-like cavity.

**Jordi Esteban**, Mercè Font-Bardia, Albert Escuer.

*Chemical Communications* **2012**, *48*, 9777-9979.

Cite this: *Chem. Commun.*, 2012, **48**, 9777–9779

www.rsc.org/chemcomm

**COMMUNICATION**

# Anion coordination by metallamacrocycles: a cryptand-like cavity†

**Albert Escuer,*[a] Jordi Esteban[a] and Mercè Font-Bardia[b]**

***Received 6th June 2012, Accepted 1st August 2012***
**DOI: 10.1039/c2cc34061e**



**A $\{Ni_9(N_3)_9\}$ metallamacrocycle is able to coordinate azide and halide anions in trigonal prismatic cavities by means of H-bond interactions. It provides an unprecedented example of a self-assembled cryptand-like cavity.**

Supramolecular chemistry of anionic species has been a hot subject over the last few decades and its role in biology, selective anion transport, molecular recognition and sensing, crystal engineering and template self-assembly syntheses has been intensely studied.[1] Molecular recognition and selective coordination of anions have been traditionally performed on the basis of organic preformed cavities of the adequate size which, by themselves[2] or involving transition cations in cascade reactions,[3] are able to link a variety of anions. In contrast, selective inclusion of anions in discrete supramolecular metallocapsules, obtained by self-assembly of their specific components, is an emerging field and in addition to preformed organic receptors, a number of metallocages hosting polynuclear anions ($CF_3SO_3^-$, $BF_4^-$, $PF_6^-$ or $SO_4^{2-}$) have been reported.[3,4]

Despite that coordination of the azide anion was established early by Lehn *et al.* in the well known $(N_3) \subset [BT\text{-}6H^+]$ bis-trend hexaprotonated cryptand[5] the number of X-ray characterized specific receptors for this anion is surprisingly low. In addition to the cryptand in which the azido anion is linked by six H-bonds, only one planar[6] and one polycyclic[7] organic receptor (containing only four H-bonds) and one pseudospherical metallocage in which the interaction with the guest involves C–H···N bonds[8] have been recently characterized.

Pyridyloximes are versatile ligands able to bridge up to four metallic centres and have been widely employed in recent years in coordination cluster chemistry.[9] In the case of nickel, chemistry of 2-pyridyloximes, (py)C{*R*}NOH, has yielded a large variety of topologies and nuclearities up to $Ni_{14}$.[10] An interesting class of systems are those combining pyridyloximes and end-on azido bridges which are adequate to obtain high spin ground states and SMM response.[11]

In search of new synthetic routes, we have combined for the first time aliphatic polydentate amines with the nickel–oximato–azido system and we report the syntheses and characterization (ESI†) of the trinuclear complex $[Ni_3(Medpt)_2(py_2CNO)_2(N_3)_4]\cdot MeOH$ (**1·MeOH**) and the rational syntheses of the enneanuclear metallacycles $(N_3) \subset [Ni_9(dpt)_6(pyC\{ph\}NO)_6(N_3)_9](A)_2\cdot MeCN$ (A = $NO_3^-$, **2·MeCN**; $Cl^-$, **3·$H_2O$**) and $(X) \subset [Ni_9(dpt)_6(pyC\{ph\}NO)_6(N_3)_9]\ X_2\cdot H_2O$ (X = $Br^-$, **4·$H_2O$**; $I^-$, **5·2$H_2O$**) in which $py_2CNOH$ is dipyridylketoneoxime, pyC{ph}NOH is phenyl-pyridylketoneoxime and dpt is dipropyltriamine. Complexes **2–5** provide a nice example of anionic conformational control in which the $\{Ni_9\}$ oligocycle is a template around one azide or halide guest anion in a trigonal prismatic cavity whereas **1** is an isolated fragment of the metallamacrocycle. H-bond coordination of cationic $R_2NH_2^+$ guests in metallamacrocyclic wheels has been widely studied by Winpenny and colleagues[12] but the inverse situation exhibited by **2–5** (ring-NH···guest interaction) is extremely unusual.

Compound **1**, obtained from the anion free dinuclear neutral precursor $[Ni_2(N_3)_4(Medpt)_2]$ (Medpt = *N*-methyldipropylenetriamine),[13] consists of neutral angular trinuclear units linked by double oximato–end-on azide bridges. The central Ni2 atom coordinates two $py_2CNO^-$ ligands whereas the external Ni1 and Ni3 atoms coordinate one tridentate *mer*-Medpt. Coordination is completed with two terminal azido ligands (Fig. 1). Ni–N–Ni bond angles are relatively large (112.8° and 112.2°) and Ni–O–N–Ni torsion angles are 17.0(3)° and 4.3(3)°.

The terminal azides in the neutral complex **1** are potentially bridging ligands and to explore this possibility a set of reactions modifying the amine, the oxime and adding different counteranions were performed. Successfully, starting from $[Ni_2(N_3)_4(dpt)_2]$ and the analogous pyC{ph}NOH oxime, in the presence of

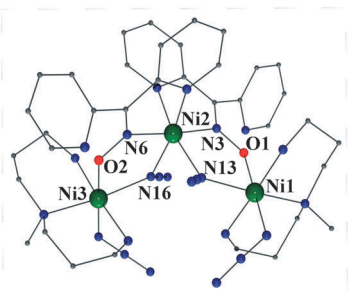


**Fig. 1** Partially labelled plot of the trinuclear compound **1**.

[a] *Departament de Química Inorgánica, Universitat de Barcelona, Av. Diagonal 645, 08028-Barcelona, Spain. E-mail: albert.escuer@qi.ub.es; Fax: +34 934907725*
[b] *Departament de Cristal lografia, Mineralogia i Diposits Minerals, Universitat de Barcelona, Martí I Franqués s/n, 08028-Barcelona, Spain*

† Electronic supplementary information (ESI) available: S1 – Details of the synthetic procedure; S2 – Additional crystallographic information; S3 – Magnetic data for **3**; S4 – Additional data about the tuning of the host cavity. CIF for the crystal structures. CCDC 859276–859278, 876039 and 876040. For ESI and crystallographic data in CIF or other electronic format see DOI: 10.1039/c2cc34061e

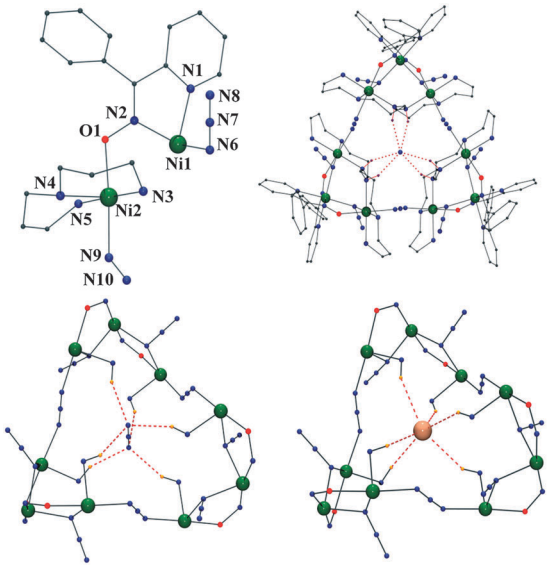


**Fig. 2** Top: partially labelled plot of the asymmetric unit and a view along the $C_3$ axis for **2–5**. Bottom: a view of the guest azido (left, **2** and **3**) and halide (right, **4** and **5**) inside the ring. Dashed lines show the H-bonds formed by the guest anions.

additional nitrate anions, the "trimer of trimers" **2** was obtained. Compound **2** can be envisaged as a $\{Ni_9\}$ ring formed by three trimeric angular units linked by end-to-end azido bridges, Fig. 2. Bond parameters of the angular subunit (Ni1–N6–Ni2′ 110.89(7)° and Ni1–N2–O1–Ni2 torsion angle 17.6(2)°) are very similar to those found in **1**.

The shorter connectivity along the ring determines a rare example of metallamacrocycle[14] in which the linkage between metallic centres is generated exclusively by azide ligands. The 24-membered ring contains six monoatomic bridges (end-on azido) and three triatomic bridges (end-to-end azido), with the repeating pattern $\{–Ni–(\mu_{1,1}N_3)–Ni–(\mu_{1,1}N_3)–Ni–(\mu_{1,3}N_3)–\}_3$.

The *zig-zag* ring conformation determines a large prismatic internal cavity. Six $–NH_2$ groups from dpt ligands functionalize this cavity establishing six H-bonds with the central azido ion which is trapped in the middle of the ring along the $C_3$ axis of the molecule. The three positive charges on the ring are thus compensated by the guest azide anion and two ionic nitrates.

The most fascinating feature of **2** is the H-bond interactions with the central azide ion. The only preformed molecule exhibiting anion recognition property towards the azido anion and involving six H-bonds is the well known $[(N_3) \subset BT\text{-}6H^+]$ bis-tren cryptate reported by Lehn and co-workers.[5] The set of six NH···$N_3$ interactions for $[(N_3) \subset BT\text{-}6H^+]$ and complex **2** are plotted in Fig. 3. In both cases, the six NH donors are arranged closely to a trigonal prism with $N_{amine}\cdots N_{azido}\cdots N_{amine}$ bond angles of around 96° and 115° respectively. The different degree of pyramidalization determines a less elongated prism for compound **2** (distance of 5.396 Å between the bases of the prisms for the cryptate and 3.933 Å for **2**) and a minor size of the base for the cryptate (mean N···N edge of 4.439 Å for the cryptate and 5.122 Å for **2**), Fig. 3.

Connectivity between the NH donors is established in both cases by five atom chains, HN–CCOCC–NH for $[(N_3) \subset BT\text{-}6H^+]$ and HN–NiNNNNi–NH for **2**. For $[(N_3) \subset BT\text{-}6H^+]$ these five-atom strings determine the three larger edges of the prism whereas for **2** they link vertices placed at 120°. Thus for **2**, the connectivity between the bases of the prism generates an H-bond quiral helicate, Fig. 3 and 4.

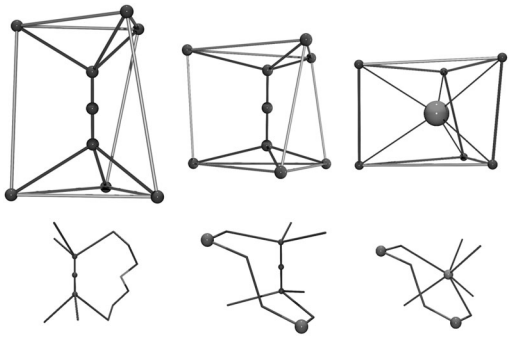

**Fig. 3** Prismatic arrangement of the N atoms around the anionic guest and one of the strings connecting the NH-donors for the cryptand $[(N_3) \subset BT\text{-}6H^+]$ (left), compounds **2** and **3** (middle) and compounds **4** and **5** (right).

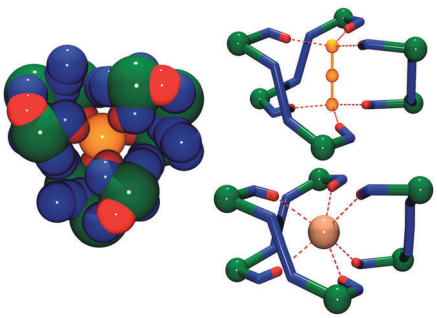

**Fig. 4** Left: details of the coordination of the guest halide atom for **4** and **5**. Right: helical arrangement around the guest anions for **2–5**.

The centroid of the aminated functions is placed in a cavity with a radius of 3.55 Å (measured as centroid···N-atoms distance), which is lower than the value of 3.70 Å found in the cryptate. The compressed prism found in compound **2**, Fig. 3, is closer to a spherical distribution and then it could be appropriate for monoanionic halides.

To check the selectivity of the system, we performed reactions starting from a variety of $NiX_2$ salts other than nitrates (X = F, Cl, Br, I, $ClO_4^-$, $BF_4^-$) and sodium azide in a ratio of 1 : 2. Complexes $N_3 \subset \{Ni_9\}X_2$ analogous to **2** (X = $Cl^-$ (**3**) for example) were formed for the smaller anions ($F^-$ or $Cl^-$) and for the larger anions ($ClO_4^-$ and $BF_4^-$) which do not fit into the cavity. In contrast, $Br \subset \{Ni_9\}Br_2$ (**4**) and $I \subset \{Ni_9\}I_2$ (**5**), including a halide atom as a guest, were obtained starting from $NiBr_2$ and $NiI_2$, Fig. 2. It is worth noting that the system exhibits selectivity for bromide and iodide in the presence of azide in the reaction medium. Bond parameters in the corners of **4–5** are very close to **1–3** (Ni1–N6–Ni2′ is 111.2(5)° and Ni1–N2–O1–Ni2 torsion angle is 16(1)° for **4** and Ni1–N6–Ni2′ is 111.3(2)° and Ni1–N2–O1–Ni2 torsion angle is 17.7(6)° for **5**).

Coordination around the halide anions in **4–5** is also prismatic, Fig. 3, and helical as in complexes **2–3**, Fig. 4. It is interesting to stress that for $[(N_3) \subset BT\text{-}6H^+]$ the highly flexible cryptand cage gives octahedral coordination around the halides and

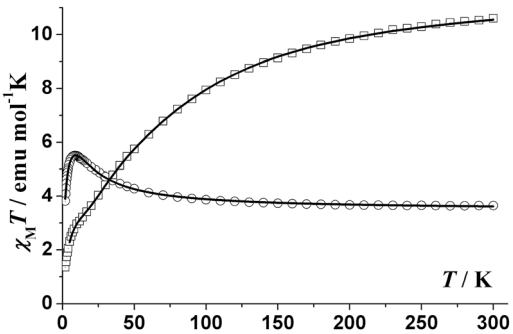


**Fig. 5** $\chi_M T$ *vs.* $T$ plot for complexes **1** (circles) and **2** (squares). Solid lines show the best fit obtained.

prismatic coordination in the elongated conformation around the azide, whereas the {$Ni_9$} metallamacrocycle exhibits always a similar trigonal prismatic cavity. The $Ni_3$ corners of the ring are rigid and then a slight tuning of the cavity size is performed by means of small changes in the Ni–N–N bond and Ni–NNN–Ni torsion angles involving the end-to-end azido ligands. As a consequence of the limited flexibility of the cavity, polyatomic $D_{3h}$ or $T_d$ anions as well as the smaller monoatomic chloride and fluoride anions are inadequate guests for this system.

As could be expected from the three labile end-to-end single bridges which link the trimeric subunits, the {$Ni_9$} rings are not stable in solution. Mass spectroscopy experiments prove a high degree of fragmentation with the predominant presence of monomeric and dimeric species.

The $\chi_M T$ plot for compound **1** shows the typical shape of ferromagnetically coupled $Ni_3$ systems and experimental data were fitted to the analytical expression derived from the conventional Hamiltonian for a linear arrangement of three $S = 1$ spins:

$$H = -J_1(S_1S_2 + S_1S_3) - J_2(S_2S_3)$$

Best fit parameters were $J_1 = +9.8$ cm$^{-1}$, $J_2 = -0.3$ cm$^{-1}$ and $g = 2.155$, Fig. 5. The interaction promoted between the $Ni^{II}$ ions by the double oximato–end-on azide bridges is ferromagnetic in agreement with previously reported results for larger nuclearity systems in which this fragment can be recognised.[10,11,15] Compound **1** gives the first example of isolated oximato–end-on azide bridges confirming unambiguously its ferromagnetic response.

Compound **2** was fitted by means of CLUMAG[16] program as one $(J_1–J_1–J_2)_3$ ring according to the two-$J$ Hamiltonian:

$$H = -J_1(S_9S_1 + S_1S_2 + S_3S_4 + S_4S_5 + S_6S_7 + S_7S_8) - J_2(S_2S_3 + S_5S_6 + S_8S_9)$$

Best fit parameters were $J_1 = +9.9$ cm$^{-1}$, $J_2 = -62.5$ cm$^{-1}$ and $g = 2.289$ for **2** and $J_1 = +8.9$ cm$^{-1}$, $J_2 = -53.5$ cm$^{-1}$ and $g = 2.211$ for **3**, Fig. 5. $J_1$ shows an excellent agreement with compound **1** and $J_2$ lies in the normal range for one $Ni^{II}$–$Ni^{II}$ interaction mediated by one end-to-end azido bridge with Ni–N–N bond angles of 128° and Ni–N–N–N–Ni torsion angles close to planarity. It should be emphasized that this magnetic ring topology (ferromagnetic corners related by antiferromagnetic interactions) is a frustrated system as is evidenced by the typical change of slope near 10 K, nicely reproduced in the fit plot. Thus, in spite of the odd number of paramagnetic centers, the ground state of the system is $S = 0$.

In conclusion, the employment of aminated ligands reveals to be a powerful tool in oximate–azido chemistry. The $–NH_2$ functions are able to establish H-bonds which can determine the nuclearity and topology of the new complexes. Azido or bromide anion inclusion provides the first coordination chemistry system with analogous cavities to the classical preformed cryptands and its quiral helical arrangement is maintained for spherical and linear anions. $NO_3^-$, $Cl^- < N_3^- < Br^-$, $I^-$ selectivity is justified by the size and flexibility of the prismatic cavity.

## Notes and references


1 (*a*) P. A. Gale and T. Gunnlaugsson, *Chem. Soc. Rev.*, 2010, **39**, 3595; (*b*) K. Bowman-James, *Acc. Chem. Res.*, 2005, **38**, 671; (*c*) S. O. Kang, R. a. Begum and K. Bowman-James, *Angew. Chem., Int. Ed.*, 2006, **45**, 7882.
2 S. O. Kang, J. M. Llinares, V. W. Day and K. Bowman-James, *Chem. Soc. Rev.*, 2010, **39**, 3980.
3 P. Ballester, *Chem. Soc. Rev.*, 2010, **39**, 3810.
4 (*a*) G. A. Lawrance, *Chem. Rev.*, 1986, **86**, 17; (*b*) R. W. Saalfrank, B. Demleitner, H. Glaser, H. Maid, D. Bathelt, F. Hampel, W. Bauer and M. Teichert, *Chem.–Eur. J.*, 2002, **8**, 2679; (*c*) M. Albrecht, I. Janser, S. Meyer, P. Weis and R. Frohlich, *Chem. Commun.*, 2003, 2854; (*d*) C. R. K. Glasson, G. V. Meehan, J. K. Clegg, L. F. Lindoy, P. Turner, M. B. Duriska and R. Willis, *Chem. Commun.*, 2008, 1190; (*e*) R. Custelcean, J. Bosano, P. V. Bonnesen, V. Kertesz and B. P. Hay, *Angew. Chem., Int. Ed.*, 2009, **48**, 4025; (*f*) V. S. Bryantsev and B. P. Hay, *J. Am. Chem. Soc.*, 2006, **128**, 2035.
5 B. Dietrich, J. Guilhem, J. M. Lehn, C. Pascard and E. Sonveaux, *Helv. Chim. Acta*, 1984, **67**, 91.
6 N.-K. Kim, K.-J. Chang, D. Moon, M. S. Lah and K.-S. Jeong, *Chem. Commun.*, 2007, 3401.
7 S. O. Kang, V. W. Day and K. Bowman-James, *Inorg. Chem.*, 2010, **49**, 8629.
8 V. Amendola, M. Boiocchi, B. Colasson, L. Fabbrizzi, M. J. Rodriguez-Douton and F. Ugozzoli, *Angew. Chem., Int. Ed.*, 2006, **45**, 6920.
9 (*a*) C. J. Milios, Th. C. Stamatatos and S. P. Perlepes, *Polyhedron*, 2006, **25**, 134 (polyhedron report); (*b*) A. J. Tasiopoulos and S. P. Perlepes, *Dalton Trans.*, 2008, 5537 (perspective).
10 (*a*) T. C. Stamatatos, K. A. Abboud, S. P. Perlepes and G. Christou, *Dalton Trans.*, 2007, 3861; (*b*) T. C. Stamatatos, A. Escuer, K. A. Abboud, C. P. Raptopoulou, S. P. Perlepes and G. Christou, *Inorg. Chem.*, 2008, **47**, 11825; (*c*) J. Esteban, L. Alcazar, M. Torres-Molina, M. Monfort, M. Font-Bardia and A. Escuer, *Inorg. Chem.*, 2012, **51**, 5503.
11 C. Papatriantafyllopoulou, T. C. Stamatatos, W. Wernsdorfer, S. J. Teat, A. Tasiopoulos, A. Escuer and S. P. Perlepes, *Inorg. Chem.*, 2010, **49**, 10486.
12 (*a*) M. Affronte, S. Carretta, G. A. Timco and R. E. P. Winpenny, *Chem. Commun.*, 2007, 1789; (*b*) C.-F. Lee, D. A. Leigh, R. G. Pritchard, D. Schultz, S. J. Teat, G. A. Timco and R. E. P. Winpenny, *Nature*, 2009, **458**, 314.
13 A. Escuer, R. Vicente, J. Ribas and X. Solans, *Inorg. Chem.*, 1995, **34**, 1793.
14 G. Mezei, C. M. Zaleski and V. L. Pecoraro, *Chem. Rev.*, 2007, **107**, 4933.
15 T. C. Stamatatos, E. Diamantopoulou, C. P. Raptopoulou, V. Psycharis, A. Escuer and S. P. Perlepes, *Inorg. Chem.*, 2007, **46**, 2350.
16 CLUMAG program: D. Gatteschi and L. Pardi, *Gazz. Chim. Ital.*, 1993, **123**, 231.

### 3.9.1. Resum: Anion coordination by metallamacrocycles: A cryptand-like cavity.

Albert Escuer, Jordi Esteban, Mercè Font-Bardia.

*Chemical Communications* **2012**, *48*, 9777-9979.

Aquesta comunicació presenta els primers resultats d'una nova estratègia sintètica, que va consistir en l'addició d'amines polidentades al sistema $Ni^{II}$/oxima/azida, sent la dipropilentriamina (dpt) i el seu derivat N-Medpt les primeres amines utilitzades.

Es va partir del compost dinuclear $[Ni_2(N\text{-}Medpt)_2(N_3)_4]$ (sintetitzat anteriorment al grup i que conté l'ió azidur com únic anió),[171] es va fer reaccionar amb el lligand $py_2CNOH$ i es va obtenir el compost trinuclear $[Ni_3(N\text{-}Medpt)_2(py_2CNO)_2(N_3)_4]$ (**9_1**), que té una topologia angular, dos ponts oxima/azida (en mode $\mu_{1,1}$, *end-on* o 2.20) i dues azides terminals aptes per coordinar nous centres metàl·lics, figura 16. La coordinació de les azides terminals (en mode $\mu_{1,3}$, *end-to-end* o 2.11) es va obtenir a partir del compost dinuclear anàleg $[Ni_2(dpt)_2(N_3)_4]$, el lligand pyC{ph}NOH en presència d'anions nitrat, donant així el compost $(N_3)\subset[Ni_9(dpt)_6(pyC\{ph\}NO)_6(N_3)_9](NO_3)_2$ (**9_2**), figura 16, que es pot descriure com tres fragments **9_1** units formant un anell de $\{Ni_9\}$ o un trímer de trímers ordenats selectivament al voltant d'un anió $N_3^-$, per auto-encaix o *self-assembly*.

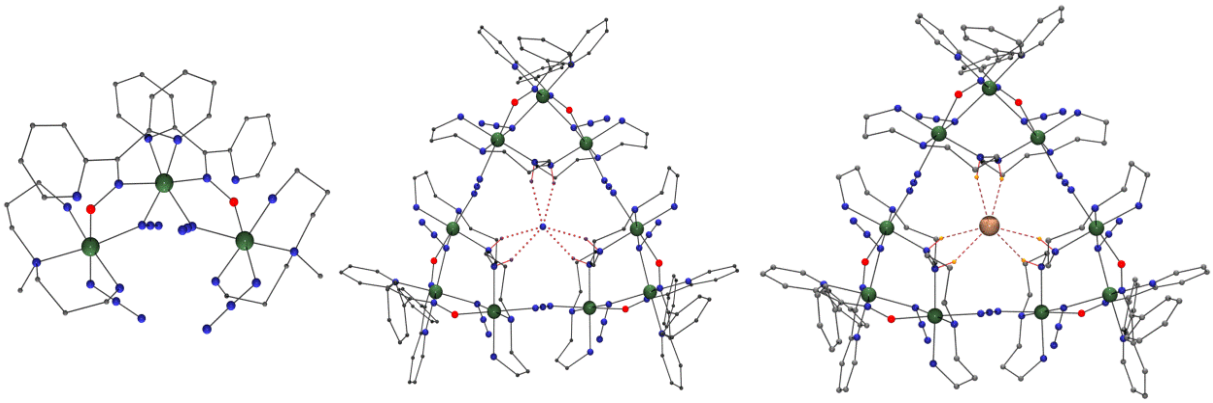

**Figura 16.** Estructura dels compostos **9_1** (esquerra), **9_2** i **9_3** (centre) i **9_4** i **9_5** (dreta).

Posteriorment, es va procedir a la síntesi del compost **9_2** directament a partir dels seus components i en comprovar l'èxit de la operació, es va repetir la síntesi amb diferents halurs de $Ni^{II}$ ($Cl^-$, $Br^-$ i $I^-$) per tal d'intentar encapsular aquests anions esfèrics. La reacció amb $NiCl_2$ va generar

l'estructura $(N_3)\subset[Ni_9(dpt)_6(pyC\{ph\}NO)_6(N_3)_9]Cl_2$ (**9_3**), però el producte obtingut a partir de $NiBr_2$ i $NiI_2$ encapsula l'halur, $X\subset[Ni_9(dpt)_6(pyC\{ph\}NO)_6(N_3)_9]X_2$ (X = $Br^-$, **9_4**; $I^-$, **9_5**), figura 16.

L'encapsulament dels anions azidur i halur es realitza a través de sis ponts d'hidrogen que provenen dels lligands aminats, disposats en forma de *zig-zag* i que generen un entorn prismàtic en tots dos anions, figura 17.

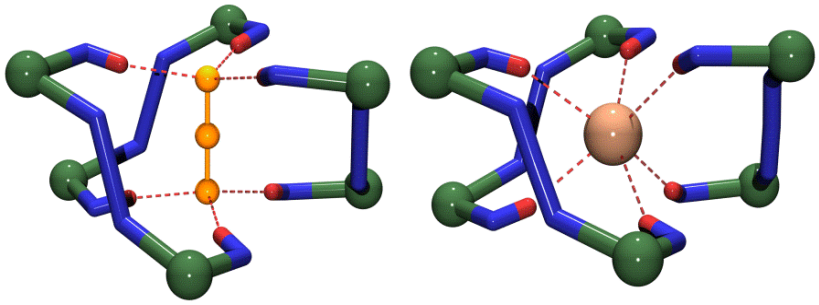

**Figura 17.** Disposició en *zig-zag* dels lligands dpt i entorn prismàtic generat pels ponts d'hidrogen.

L'estudi magnètic dels compostos **9_1**, **9_2** i **9_4** va revelar un acoblament ferromagnètic per **9_1** a través dels ponts oxima/$\mu_{1,1}$-azida, que genera un estat fonamental *S* = 3, i un comportament antiferromagnètic pels $\{Ni_9\}$ generat pels ponts $\mu_{1,3}$-$N_3$ (més intensos que les interaccions ferromagnètiques mediades pels ponts oxima/$\mu_{1,1}$-$N_3$) que dóna un spin global *S* = 0.

En conclusió, es va sintetitzar un compost de nuclearitat $Ni_3$ i una família de compostos $\{Ni_9\}$ que contenen lligands aminats polidentats. Es va trobar que els anells de $\{Ni_9\}$ estan formats per fragments trinuclears units per ponts azida i disposats selectivament al voltant de diversos anions (azidur, bromur, iodur) i que aquests anells presenten una major afinitat per anions esfèrics (de la grandària adequada), justificada per la selectivitat $Br^-$, $I^- > N_3^- > NO_3^-$, $Cl^-$.

## 3.10. Article 10.

## Anionic guests in prismatic cavities generated by enneanuclear nickel metallacycles.

**Jordi Esteban**, Mercè Font-Bardia, Albert Escuer.

*Inorganic Chemistry* **2014**, *53,* 1113-1121.

Inorganic Chemistry

Article

pubs.acs.org/IC

# Anionic Guests in Prismatic Cavities Generated by Enneanuclear Nickel Metallacycles

Jordi Esteban,*[,†] Mercè Font-Bardia,[‡,§] and Albert Escuer*[,†]

[†]Departament de Química Inorgànica, Universitat de Barcelona, Av. Diagonal 645, 08028 Barcelona, Spain

[‡]Departament de Mineralogia, Cristal·lografia i Dipòsits Minerals, Universitat de Barcelona, Martí Franqués s/n, 08028 Barcelona, Spain

[§]Unitat de Difracció de R-X, Centre Científic i Tecnològic de la Universitat de Barcelona (CCiTUB), Universitat de Barcelona, Solé i Sabarís 1-3, 08028 Barcelona, Spain

Supporting Information

**ABSTRACT:** The combination of polydentate aminated ligands with the 2-pyridyloxime-nickel-azide system leads to series of clusters with unprecedented topologies. Among them, a remarkable family of {$Ni_9$} metallacycles that are capable of selective encapsulation of azide/halide anions in a cryptand-like cavity through hydrogen-bond interactions has been characterized.

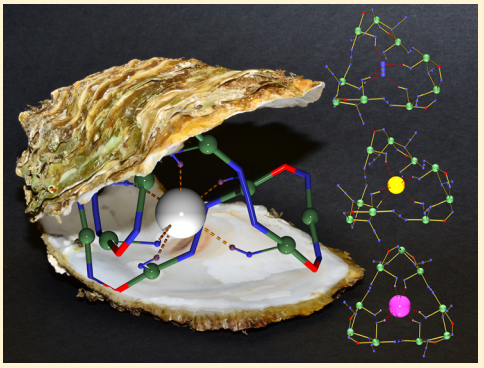

## INTRODUCTION

Anion binding and sensing is an expanding field within supramolecular chemistry, because of its applications in anion exchange and transport, biomedical and environmental monitoring, molecular recognition, and crystal engineering.[1] Among the different supramolecular strategies to synthesize this receptors, chemical (anion) template[2] offers a rational and efficient approach to molecular and supramolecular assemblies, but also allows the preparation of unusual topologies, such as rotaxanes, helicates, and catenanes.[3]

Despite the fact that most anion receptors are preformed organic molecules,[2a,4] the number of hosts that incorporate metallic centers in its structure is increasing.[5] Typical functions for metal centers in anion hosts have been structure-organizing and binding groups but, furthermore, the positive charge of the metal center contributes to a more favorable binding via columbic interaction, which is added to other host−guest interactions. One of the most useful noncovalent host−guest interactions are hydrogen bonds, because of their directionality and relative strength. In addition, the presence of nearby electron-withdrawing metal centers can boost the hydrogen-bond donor ability of the group and, consequently, enhance the host−guest interaction.

Coordination of azide anion by the well-known ($N_3$) ⊂ [BT-6H$^+$] bis-trend hexaprotonated cryptand[6] was established by the Lehn group in his seminal work in 1984. However, after this early work, the number of X-ray characterized specific receptors for this anion is surprisingly reduced in comparison with oxoanions or halides: in addition to the preformed [BT-6H$^+$] cryptand in which the azide anion is linked by six hydrogen bonds in a prismatic arrangement, only five preformed organic receptors[7] and one pseudo-spherical metallocage in which the interaction with the guest involves weak C−H···N bonds,[8] have been recently characterized.

Pyridyloximes have been extensively employed in recent years in cluster coordination chemistry,[9] because of their coordinative versatility, that allows them to bridge up to four metallic centers and their easy functionalization. Focusing on nickel derivatives, the chemistry of 2-pyridyloximes, (py)C{R}-NOH, has yielded a large variety of topologies and nuclearities up to $Ni_{14}$.[10] Combination of pyridyloximes and $\mu$-1,1-azido bridges has proven an adequate method to obtain high-spin ground states and with SMM response in some cases.[11]

In the search of new synthetic routes, we have combined aliphatic polydentate amines with the nickel−oximato−azido system (Chart 1), and we report the syntheses and characterization (see details and Scheme S1 in the Supporting Information) of the trinuclear complex $[Ni_3(Medpt)_2(py_2CNO)_2(N_3)_4]$ (**1**·MeOH); the tetranuclear compounds $[Ni_4(Medpt)_2(N_3)_4(dapdo)_2]$ (**2**·MeOH), $[Ni_4(dpt)_2(N_3)_4(py_2CNO)_4]$ (**3**·2MeCN), and $[Ni_4(Me_3dpt)_2(N_3)_4(pyC\{ph\}NO)_4]$ (**4**·4MeCN); the pentanuclear complex $[Ni_5(H_2O)_4(AcO)_2(N_3)_2(OH)_2(pyC\{ph\}-$

**Received:** October 22, 2013
**Published:** December 30, 2013

   dx.doi.org/10.1021/ic402651k | *Inorg. Chem.* 2014, 53, 1113−1121

**Chart 1. Pyridyloximate and Tridentate Aminated Ligands Discussed in the Text**

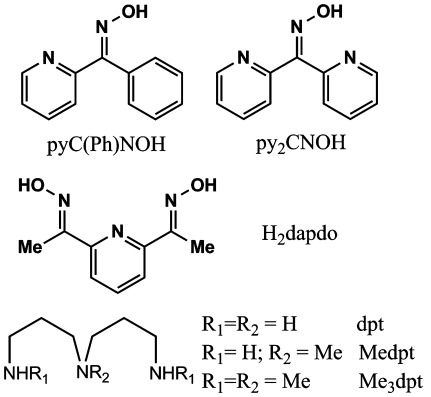


$NO)_4]$ (**5**·5MeCN,$H_2O$); and a series of enneanuclear metallacycles with formula: $(N_3) \subset [Ni_9(dpt)_6(pyC\{ph\}NO)_6(N_3)_9](A)_2$ (where A = $NO_3^-$ (**6**·MeCN), $BF_4^-$ (**7**·$2H_2O$), $F^-$ (**8**·MeOH), and $Cl^-$ (**9**·$H_2O$)), $(X) \subset [Ni_9(dpt)_6(pyC\{ph\}NO)_6(N_3)_9](X)_2$ (X = $Br^-$ (**10**·$H_2O$) and $I^-$ (**11**·$2H_2O$)), and $(N_3) \subset [Ni_9(dpt)_6(py_2CNOH)_6(N_3)_9](ClO_4)_2$ (**12**·2MeOH), in which $py_2CNO^-$, $pyC\{ph\}NO^-$, and $dapdo^{2-}$ are the deprotonated forms of dipyridylketoneoxime, phenyl-pyridyl-ketoneoxime and 2,6-diacetylpyridinedioxime, respectively, and dpt is dipropyltriamine.

This work focuses on two types of compounds derived from the new synthetic strategy of blending of 2-pyridyloximates with aliphatic amines: (i) the complete description of series of low-nuclearity complexes ($Ni_3$, $Ni_4$, and $Ni_5$); and (ii) the description of unprecedented series of nonanuclear metal-lacrowns able to coordinate a variety of anions in a similar way to classic cryptands. An exhaustive structural analysis of the $\{Ni_9\}$ family has been carried out, and some comments about the system selectivity are pointed out. Unfortunately, the labile bis-monodentate $\mu$-1,3-azido bridge is broken in solution as was proven by mass spectroscopy,[12] and then these complexes are only stable in solid state, preventing the study of association constants. Finally, DC susceptibility measurements carried in the 2−300 K temperature range have been realized for all the reported topologies. Compounds **1**, **6**, and **9**−**11** were previously described in a short communication.[12]

## EXPERIMENTAL SECTION

**Syntheses.** $py_2CNOH$ and pyC{ph}NOH ligands, as well as the aminated groups, were purchased from Sigma−Aldrich, Inc., and used without further purification. Nickel salts were purchased form Sigma−Aldrich, Inc., Fluka AG, and Strem Chemicals, Inc.

*$[Ni_3(Medpt)_2(py_2CNO)_2(N_3)_4]$·MeOH (**1**).* Compound **1**, which is defined as $[Ni_3(Medpt)_2(py_2CNO)_2(N_3)_4]$·MeOH, was obtained in good yield via reaction in methanolic medium of $py_2CNOH$ ligand (199 mg, 1 mmol), $[Ni_2(Medpt)_2(N_3)_4]$ (576 mg, 1 mmol), and triethylamine (202 mg, 2 mmol). The resulting solution was left to slow evaporation and prismatic dark crystals appeared after a week. Anal. Calcd for $C_{37}H_{58}N_{24}Ni_3O_3$ (**1·MeOH**): C, 41.8%; H, 5.5%; N, 31.6%. Found: C, 40.9%; H, 5.3%; N, 31.5%.

*$[Ni_4(Medpt)_2(N_3)_4(dapdo)_2]$·MeOH (**2**).* Compound **2**, which is defined as $[Ni_4(Medpt)_2(N_3)_4(dapdo)_2]$·MeOH, was obtained from the reaction of $[Ni_2(Medpt)_2(N_3)_4]$ (576 mg, 1 mmol), $dapdoH_2$ ligand (178 mg, 1 mmol) and $NEt_3$ (202 mg, 2 mmol) in 20 mL of MeOH. The mixture was stirred, filtered, and left for slow crystallization in a closed vial. Red prismatic crystals were collected a month later. Anal. Calcd for $C_{32}H_{56}N_{24}Ni_4O_4$ (**2**): C, 35.7%; H, 5.2%; N, 31.2%. Found: C, 35.2%; H, 5.0%; N, 31.6%.

*$[Ni_4(dpt)_2(N_3)_4(py_2CNO)_4]$·2MeCN (**3**) and $[Ni_4(Me_3dpt)_2(N_3)_4(pyC\{ph\}NO)_4]$·4MeCN (**4**).* Compounds **3** ($[Ni_4(dpt)_2(N_3)_4(py_2CNO)_4]$·2MeCN) and **4** ($[Ni_4(Me_3dpt)_2(N_3)_4(pyC\{ph\}NO)_4]$·4MeCN) were synthesized from $NiCl_2·6H_2O$ (474 mg, 2 mmol), dipropylene triamine (262 mg, 2 mmol) with $py_2CNOH$ (199 mg, 1 mmol); and $Ni(BF_4)_2·6H_2O$ (680 mg, 2 mmol), $Me_3dpt$ (346 mg, 2 mmol) with pyC{ph}NOH (198 mg, 1 mmol), respectively, together with $NaN_3$ (260 mg, 4 mmol) and $NEt_3$ (202 mg, 2 mmol) in 20 mL of MeCN. The resultant mixtures were stirred, filtered, and left for slow evaporation. Red prismatic crystals were collected after a month. Anal. Calcd for $C_{56}H_{66}N_{30}Ni_4O_4$ (**3**): C, 46.1%; H, 4.6%; N, 28.8%. Found: C, 45.5%; H, 4.8%; N, 28.3%.

*$[Ni_5(H_2O)_4(AcO)_2(N_3)_2(OH)_2(pyC\{ph\}NO)_4]$·5MeCN,$H_2O$ (**5**).* Compound **5**, which is defined as $[Ni_5(H_2O)_4(AcO)_2(N_3)_2(OH)_2(pyC\{ph\}NO)_4]$·5MeCN,$H_2O$, was obtained as red brick-shaped crystals from the slow evaporation of the resultant solution of $Ni(AcO)_2·4H_2O$ (594 mg, 2 mmol), pyC{ph}NOH (199 mg, 1 mmol), $Me_3dpt$ (346 mg, 2 mmol), $NaN_3$ (260 mg, 4 mmol), and $NEt_3$ (202 mg, 2 mmol) in 20 mL of MeCN. Anal. Calcd for $C_{52}H_{52}N_{14}Ni_5O_{14}$ (**5**): C, 46.1%; H, 4.5%; N, 28.8%. Found: C, 43.8%; H, 4.2%; N, 27.1%.

*$(N_3) \subset [Ni_9(dpt)_6(pyC\{ph\}NO)_6(N_3)_9](NO_3)_2$·MeCN (**6**).* Compound **6**, which is defined as $(N_3) \subset [Ni_9(dpt)_6(pyC\{ph\}NO)_6(N_3)_9](NO_3)_2$·MeCN, was synthesized via reaction of pyC{ph}NOH (198 mg, 1 mmol), $Ni(NO_3)_2$ (580 mg, 2 mmol), dipropylene triamine (162 mg, 2 mmol), $NaN_3$ (260 mg, 4 mmol), and $NEt_3$ (202 mg, 2 mmol) in 20 mL of acetonitrile. The solution was left to evaporate slowly and brown prisms were obtained after a week. Anal. Calcd for $C_{108}H_{156}N_{62}Ni_9O_{12}$ (**6**): C, 42.6%; H, 5.2%; N, 28.5%. Found: C, 42.4%; H, 5.2%; N, 29.0%.

*$(N_3) \subset [Ni_9(dpt)_6(pyC\{ph\}NO)_6(N_3)_9](A)_2$ (A = $BF_4$ (**7**), F (**8**), and Cl (**9**); $(X) \subset [Ni_9(dpt)_6(pyC\{ph\}NO)_6(N_3)_9](X)_2·nH_2O$ (X = Br (**10**), I (**11**); and $(N_3) \subset [Ni_9(dpt)_6(py_2CNO)_6(N_3)_9](ClO_4)_2·2MeOH$ (**12**).* Compounds **7**, **8**, and **9** (defined as $(N_3) \subset [Ni_9(dpt)_6(pyC\{ph\}NO)_6(N_3)_9](A)_2$ (where A = $BF_4$ (**7**), F (**8**), and Cl (**9**)), **10** and **11** (defined as $(X) \subset [Ni_9(dpt)_6(pyC\{ph\}NO)_6(N_3)_9](X)_2·nH_2O$ (where X = Br (**10**) and I (**11**)), and **12** (which is defined as $(N_3) \subset [Ni_9(dpt)_6(py_2CNO)_6(N_3)_9](ClO_4)_2·2MeOH$) were obtained following the same procedure as that for compound **6** in methanolic solution, starting from the corresponding nickel salt and using the $py_2CNOH$ ligand instead of pyC{ph}NOH for **12**. Dark prisms crystallized one week later. Anal. Calcd for $C_{108}H_{160}B_2F_8N_{60}Ni_9O_8$ (**7·2H$_2$O**): C, 41.5%; H, 5.1%; N, 26.8%. Found: C, 37.5%; H, 4.7%; N, 23.7%. Anal. Calcd for $C_{108}H_{158}Cl_2N_{60}Ni_9O_7$ (**9·H$_2$O**): C, 43.1%; H, 5.3%; N, 28.0%. Found: C, 42.3%; H, 5.1%; N, 28.1%. Anal. Calcd for $C_{108}H_{158}Br_3N_{57}Ni_9O_7$ (**10·H$_2$O**): C, 41.4%; H, 5.1%; N, 25.5%. Found: C, 41.5%; H, 5.2%; N, 25.7%. Anal. Calcd for $C_{108}H_{160}I_3N_{57}Ni_9O_8$ (**11·2H$_2$O**): C, 39.4%; H, 4.9%; N, 24.4%. Found: C, 39.8%; H, 5.0%; N, 24.1%. Anal. Calcd for $C_{104}Cl_2H_{154}I_3N_{66}Ni_9O_{16}$ (**12·2MeOH**): C, 38.8%; H, 4.8%; N, 29.2%. Found: C, 39.8%; H, 5.0%; N, 28.1%.

All samples were obtained in good yield (~40%) as well-formed large crystals. The yield of the reactions is greater than 40%, but it was not quantified, because the collection of the samples for instrumental measures was limited to the well-formed first crystalline fraction.

**Physical Measurements.** Magnetic susceptibility measurements were carried out on polycrystalline samples with a MPMS5 Quantum Design susceptometer working in the range of 30−300 K under an external magnetic field of 0.3 T and under a magnetic field of 0.03 T in the temperature range of 30−2 K, to avoid saturation effects. Diamagnetic corrections were estimated from the Pascal tables. Infrared spectra (4000−400 $cm^{-1}$) were recorded from KBr pellets on a Bruker IFS-125 FT-IR spectrophotometer.

**X-ray Crystallography.** Details of crystal data, data collection, and refinement are given in Tables S1, S2, and S3 in the Supporting Information, whereas experimental details for all compounds are provided in Tables S4−S8 and Figures S1−S5 in the Supporting Information. X-ray data were collected on a MAR345 diffractometer with an image plate detector for compounds **1**, **2**, **3**, and **7**, on a Bruker



dx.doi.org/10.1021/ic402651k | Inorg. Chem. 2014, 53, 1113−1121

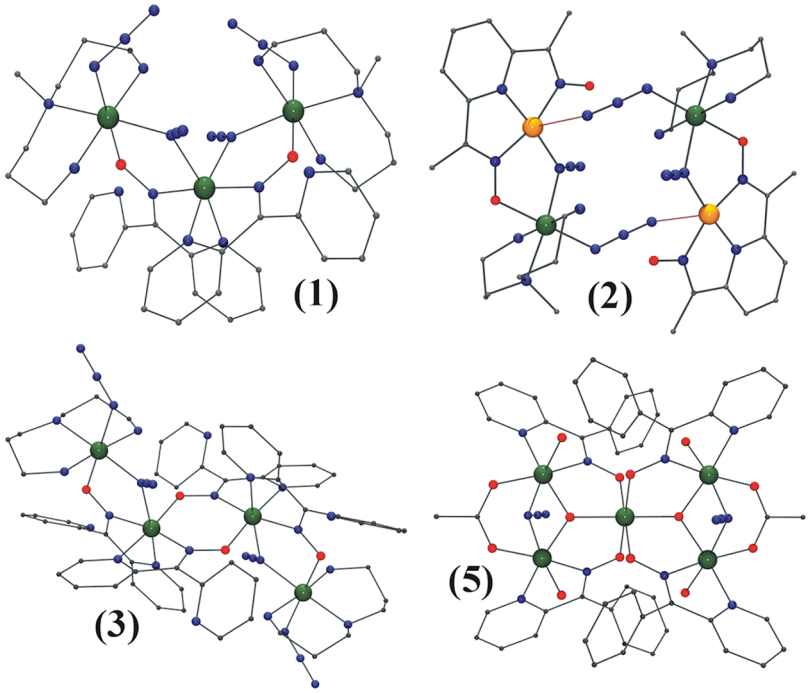


**Figure 1.** View of the molecular structure of complexes **1**, **2**, **3**, and **5**. The weak axial azido−nickel interaction in compound **2** is depicted in orange color. Color key: O, red; N, blue; C, black; octahedral $Ni^{II}$, green; and square planar $Ni^{II}$, orange.

Kappa ApexII CCD diffractometer for compounds **6** and **8**−**12**, on a Supernova ssytem for compound **4**, and on a Bruker D8 Venture system for **5**, with Mo K$\alpha$ radiation ($\lambda$ = 0.71073 nm). The structures were solved by direct methods using SHELXS computer program[13] and refined using a full-matrix least-squares method with the SHELXS97 computer program.[14]

All data can be found in the supplementary crystallographic data for this paper in CIF format with CCDC Nos. 859276−859278, 876039−876040, and 948759−948765. These data can be obtained free of charge from The Cambridge Crystallographic Data Centre via www.ccdc.cam.ac.uk/data_request/cif.

Plots for publication were generated with ORTEP3 for Windows and plotted with Pov-Ray programs.[15]

## RESULTS AND DISCUSSION

**Comments to the Syntheses.** Our initial synthetic strategy was to employ, as the nickel source, the neutral dinuclear complex $[Ni_2(Medpt)_2(N_3)_4]$ (previously reported by us[16]), which contains the aminated ligand Medpt and preformed $\mu$-1,1-azido bridges. Our objective was to avoid the presence of counteranions other than azide, in order to reach the syntheses of ferromagnetic clusters containing $\mu$-1,1-azido bridges. As result of the reaction of $[Ni_2(Medpt)_2(N_3)_4]$ with a variety of pyridyloximes (Chart 1), neutral complexes **1** and **2** were characterized.

In light of the structural data, we realized that, despite the presence of terminal azido ligands, the nuclearity of cluster **1** is limited to the low nuclearity $Ni_3$ entity. This complex is neutral and in order to bind these terminal azido ligands, additional counteranions were needed to balance the resulting positive charge. Thus, the same reaction was tried from $[Ni_2(Medpt)_2(N_3)_4]$ and $[Ni_2(dpt)_2(N_3)_4]$ adding small amounts of sodium nitrate and then, enneanuclear complex **6** was obtained. Further synthetic work revealed that the $\{Ni_9\}$ ring **6** can be obtained in high yield from the direct reaction of nickel nitrate, the aminated ligand, and sodium azide, and the direct synthesis was assumed to be preferable, as described in the Syntheses section for **6**−**12**.

From this result, similar reactions with series of different starting reagents were performed in order to elucidate three questions: (i) the effect of the anion on the final structure, (ii) the influence of the aminated ligand, and (iii) the ability of this system to encapsulate spherical anions as halides.

In addition to the medium nuclearity compounds **3**−**5**, reaction with $BF_4^-$ or $ClO_4^-$ salts gave structures similar to that of the nitrate complex **6** (complexes **7** and **12**). Reaction starting from $Ni^{II}$ halides yields the same structure for fluoride and chloride (**8** and **9**) but successful incorporation of the halide anion as a guest was achieved starting from $NiBr_2$ and $NiI_2$ salts (complexes **10** and **11**). Complex **5** is the only one that does not incorporate the tridentate amine in its structure, which gives proof of the stability of the bowtie topology[11,17] for the oximato/azide/carboxylato blend of ligands and is closely related to $[Ni_5(MeOH)_4(AcO)_2(N_3)_2(\mu_3\text{-}N_3)_2(pyC\{ph\}NO)_4]$ which contains a $\mu_3$-$N_3$ ligand instead the $\mu_3$-OH central donor.[11]

**Description and Magnetic Study.** Plots of the structure of the neutral complexes **1**−**5** are shown in Figure 1. Labeled plots and selected structural parameters are given in Figures S1−S5 and Tables S4−S8 in the Supporting Information.

Compound **1** consists of a neutral angular trinuclear unit linked by double oximato/$\mu$-1,1-azide bridges (Figure 1). The central Ni-atom exhibits a $NiN_6$ coordination sphere from two $py_2CNO^-$ ligands (each one bound by two of their N atoms) and the two $N_3^-$ binding groups whereas external Ni atoms present a $NiN_5O$ environment that comes from one Medpt ligand, which acts as tridentate ligand in *mer* coordination, one bridging and one terminal azide group and finally an O-oximato ligand. Ni−N−Ni bond angles are relatively large with values of 112.9(1)° and 112.2(1)° and the Ni−O−N-Ni torsion angles are 17.0(3)° and 4.3(3)°.



dx.doi.org/10.1021/ic402651k | *Inorg. Chem.* 2014, 53, 1113−1121

Complex **2** consists of two dinuclear subunits linked by means of $\mu$-1,3-azido bridges. Each subunit is formed by two Ni atoms (one of them linking one tridentate Medpt ligand and the other linking one dapdo$^{2-}$ dioximate), bridged as in the previous complex by a double oximato/$\mu$-1,1-$N_3^-$ bridge, which exhibits similar Ni−N−Ni and Ni−O−N-Ni angles of 112.36(9)° and 14.6(2)°, respectively. The Ni atom linked to the Medpt ligand shows an octahedral environment, whereas the Ni atom coordinated to the dapdo$^{2-}$ ligand exhibits a square planar environment in agreement the high field induced by the fully deprotonated dapdo$^{2-}$ dioximate.[18] Weak Ni−N(azide) interaction with bond distance of 2.820(3) Å (Figure 1) and a set of hydrogen bonds link the two subunits to give the tetranuclear system (see details given in Figure S2 in the Supporting Information).

A view of the core of compound **3** is illustrated in Figure 1. The centrosymmetric tetranuclear complex **3** can be described as being similar to two oximato/$\mu$-1,1-$N_3^-$ bridged dinuclear subunits (similar to compound **1**), linked together by a double oximato bridge. As in the previous case, the central Ni atoms are coordinated by the N atoms of the pyridyloximate ligands, whereas the peripheral nickels bind the aminated tridentate ligands. Ni−N−Ni bond angle is 111.4(1)° and Ni−O−N−Ni torsion angles are 20.0(2)° and 24.0(2)°. The different ligands employed in **3** (Medpt and py$_2$CNO$^-$) and **4** (Me$_3$dpt and pyC{ph}NO$^-$) are not relevant from structural point of view and the two complexes show the same topology and very close bond parameters (see Tables S6 and S7 in the Supporting Information).

The neutral core of the centrosymmetric pentanuclear compound **5** can be described as a bowtie arrangement of five Ni$^{II}$ ions, or, in other words, it is similar to two isosceles triangles sharing one vertex (Figure 1). Each triangle is $\mu_3$−OH centered with the OH bridging group being displaced 0.725(2) Å out of the plane formed by the three Ni atoms. Two sides of the triangles are defined by single oximato bridges between the central and the peripheral nickel atoms whereas the external Ni$^{II}$ atoms are bridged by one *syn*−*syn* acetate ligand and one $\mu_{1,1}$-$N_3^-$ bridging group. Ni−N−Ni bond angle is 90.51(7)° and Ni−O−N−Ni torsion angles are quasiplanar (1.2(2)° and 3.4(2)°).

Central Ni(1) atom presents a $NiO_6$ environment that proceeds from the two $\mu_3$-OH and four O-oximato ligands. Parallely, peripheral Ni(2,3) atoms exhibit a $NiN_3O_3$ environment that arises from one pyridyloxime ligand linked by its two N atoms, the $\mu$-1,1 azide, the $\mu_3$-OH central group, one *syn-syn* acetate ligand and finally one coordinated water molecule. Four intramolecular hydrogen bonds between the water molecules and the oxygen atom of the oximate groups help to stabilize the structure (Figure S5 in the Supporting Information). The crystallization water molecule establish intermolecular hydrogen bonds involving the coordinated water molecules giving a supramolecular 1D arrangement.

$\chi_M T$ vs. $T$ plot for complexes **1**, **3**, and **5** are shown in Figure 2 (**3** and **4** show quasi identical bond parameters and **2** contains diamagnetic square planar nickel atoms and then, **2** and **4** were not measured). Complex **1** is ferromagnetically coupled; **3** shows an overall antiferromagnetic response whereas **5** exhibits the typical $\chi_M T$ minimum characteristic of ferrimagnetic behavior.

The experimental data was fitted according to the interaction patterns shown in Chart 2A for **1**, Chart 2B for **3**, Chart 2C for **5**, and the derived Hamiltonians:

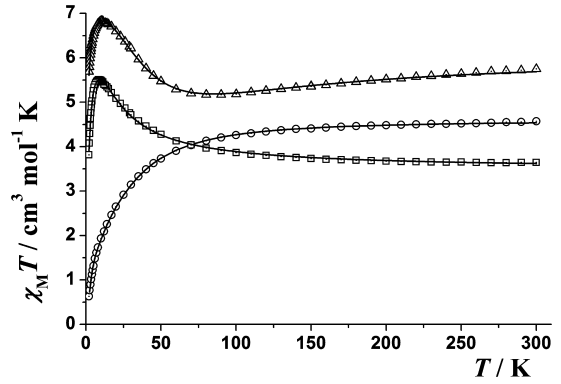


**Figure 2.** $\chi_M T$ vs $T$ plot for complexes **1** (squares, □), **3** (circles, ○) and **5** (triangles, △). Solid lines show the best fit obtained.

**Chart 2. Interaction Pattern with the Spin and Coupling Constant Labels for Topologies (A) 1, (B) 3, (C) 5, and (D) Metallacrowns 6 and 10**[a]

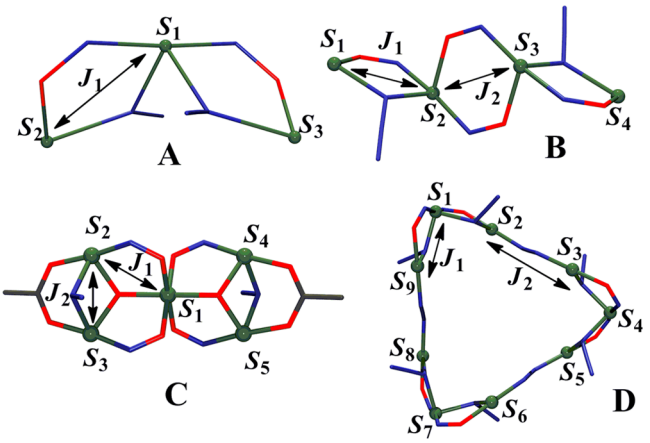


[a]See the text for the corresponding Hamiltonians.

$$H = -J_1(S_1 \cdot S_2 + S_1 \cdot S_3) \quad \text{for (1)}$$

$$H = -J_1(S_1 \cdot S_2 + S_3 \cdot S_4) - J_2(S_2 \cdot S_3) \quad \text{for (3)}$$

$$H = -J_1(S_1 \cdot S_2 + S_1 \cdot S_3 + S_1 \cdot S_4 + S_1 \cdot S_5) - J_2(S_2 \cdot S_3 + S_4 \cdot S_5) \quad \text{for (5)}$$

Compounds **1** and **5** were fitted with the derived analytical equations, whereas, for **3**, the CLUMAG program[19] was employed. Best-fit parameters were $J_1$ = +9.8(1) cm$^{-1}$ and $g$ = 2.155(3) for the trimeric complex **1**, $J_1$ = +10.2 cm$^{-1}$, $J_2$ = −28.7 cm$^{-1}$, $g$ = 2.120 and $R = 3.56 \times 10^{-5}$ ($R = (\chi_M T_{exp} - \chi_M T_{calc})^2/(\chi_M T_{exp})^2$) for the tetranuclear complex **3** and $J_1$ = −24.3(1) cm$^{-1}$, $J_2$ = +23.1(4) cm$^{-1}$ and $g$ = 2.209(1) for the pentanuclear complex **5**.

The double oximato/$\mu$-1,1-azide bridges between two Ni$^{II}$ cations have been observed as fragments of larger clusters and overall ferromagnetic interaction was proposed for these fragments. However, complex **1** provides the unambiguous assignation of ferromagnetic coupling for this combination of superexchange pathways and it is confirmed by the value of $J_1$ obtained for complex **3**, which is in full agreement with **1**. From the sign and magnitude of the calculated coupling constants, the proposed ground states are $S$ = 3 for **1**, $S$ = 0 for **3**, and $S$ = 3 for **5**.



dx.doi.org/10.1021/ic402651k | Inorg. Chem. 2014, 53, 1113−1121

Compounds **6**–**9**, and **12**, present the same structure except for the substitution pyC{ph}CNOH for $py_2CNOH$ in **12** and the variation of the corresponding anion in each case. Thus, we only describe the structural details of **6** to avoid repetitive descriptions.

This compound can be described to be similar to three trimeric angular subunits linked by $\mu$-1,3-azido bridges generating a $\{Ni_9\}$ ring, with Ni(1)–N(6)–Ni(2) bond angle of 110.89(7)° and Ni(1)–N(2)–O(1)–Ni(2) torsion angle of 17.6(2)°. Coordination of two oximate ligands to Ni(1) and the tridentate amines to Ni(2) are fully comparable with complex **1** and thus, the $\{Ni_9\}$ ring can be structurally described as a trimer of trimers (see Figure 3). The $\mu$-1,3 bridges show Ni(2)–N(9)–N(10) bond angles of 128.2(2)° and a quasi planar Ni–NNN–Ni torsion angle of 171.8(1)°.

The shorter linkage sequence $\{-Ni-(\mu_{1,1}N_3)-Ni-(\mu_{1,1}N_3)-Ni-(\mu_{1,3}N_3)-\}_3$ determines a 24-membered ring containing six monatomic bridges ($\mu$-1,1-azide) and three triatomic bridges ($\mu$-1,3-azide), which gives the larger azido metallacrown reported to date.

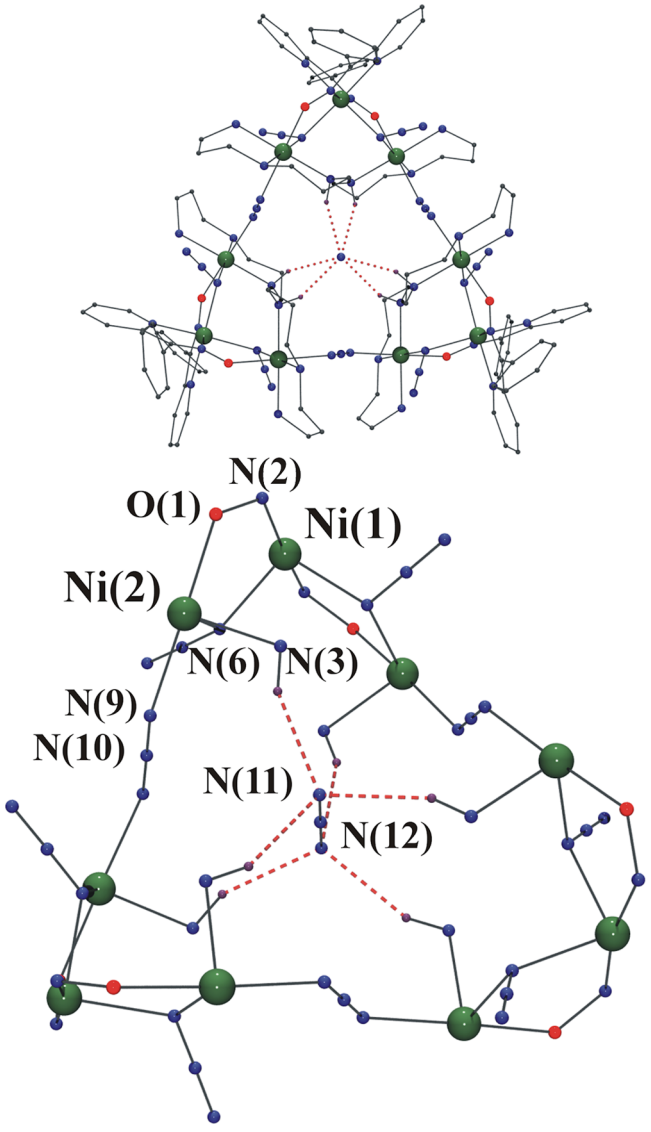


**Figure 3.** (Top) View of the molecular structure of complexes **6**–**9**, and **12**. (Bottom) Partially labeled core for all of them. Dashed bonds show the hydrogen bonds between the $-NH_2$ aminated functions and the coordinated azido guest.

The ring is not planar due to the arrangement of the $\mu$-1,3-azido bridges, exhibiting a zig-zag ring conformation that generates a large internal prismatic cavity functionalized by six $-NH_2$ groups from the six dpt ligands (see Figure 4). These-$NH_2$ functions establish six hydrogen bonds with one azide anion trapped inside the cavity along the $C_3$ axis. N(3)–H(3a)···N(11) distance is 3.037(2) Å. In addition, a set of hydrogen bonds involving the N(6) atom from the $\mu$-1,1-azide bridges and the aminated functions (N(3)–H(3b)···N(6), 3.117(2) Å and N(5)–H(5b)···N(6), 3.016(3) Å) helps to stabilize the *zig-zag* conformation of the ring. Relevant intermolecular interactions were not found.

Finally, the three positive charges on the ring are compensated by the guest azide anion and two ionic nitrates.

Compounds **10** and **11** exhibit the same metallacrown structure than the previous ones; however, in these cases, the $\{Ni_9\}$ rings encapsulate a bromide (**10**) or iodide (**11**) anion, also stabilized in this position by six hydrogen bonds. As in the above complexes **6**–**9**, and **12**, the cavity is a trigonal prism and the main bond parameters related with the bridging azide and oximato ligands are fully comparable, indicating that the conformation of the ring is poorly flexible (Figure 5). Detailed parameters for the hydrogen bonds are reported in Table S9 in the Supporting Information.

On basis of the common bond parameters in the bridging region for all the enneanuclear rings (Table 1), magnetic measurements were performed on a representative complex encapsulating one azide and one halide anion. $\chi_M T$ vs. $T$ plot for complexes **6** and **10** are shown in Figure 6. Both of them exhibit a very similar shape and values indicating that, as should be expected, the guest anion does not influence the superexchange interactions.

The experimental data was fitted with the CLUMAG program,[19] according to the interaction pattern shown in Chart 2D and the derived Hamiltonian:

$$H = -J_1(S_9 \cdot S_1 + S_1 \cdot S_2 + S_3 \cdot S_4 + S_4 \cdot S_5 + S_6 \cdot S_7 + S_7 \cdot S_8) - J_2(S_2 \cdot S_3 + S_5 \cdot S_6 + S_8 \cdot S_9)$$

Best-fit parameters were $J_1 = +9.9\ cm^{-1}$, $J_2 = -62.5\ cm^{-1}$, $g = 2.289$, and $R = 1.25 \times 10^{-5}$ for **6** and $J_1 = +8.9\ cm^{-1}$, $J_2 = -53.5\ cm^{-1}$, $g = 2.211$, and $R = 1.57 \times 10^{-5}$ for **10**.

As expected from the similar bond parameters of the double oximato/$\mu$-1,1-azide bridges, $J_1$ gives very close values to complexes **1** and **3**. The sign and magnitude of $J_2$ is indicative of strong antiferromagnetic coupling, which lies in the expected range[20] of values for a single $\mu$-1,3-azido bridge with torsion angles of ~175° and Ni–N–N bond angles close to 129°. The lower AF interaction for **10** can be attributed to the larger Ni–N bond distance.

It should be emphasized that the coupling constants $(-J_1 - J_1 - J_2)_3$ alternating with ferromagnetic $J_1$ and antiferromagnetic $J_2$ in a closed ring is unusual from a magnetic point of view. The strong AF interaction $J_2$ cancels three pairs of spins but remain three $S = 1$ corners leading to a situation similar to a $Ni^{II}$ triangle with diamagnetic $S = 0$ ground state, despite the odd number of spins (see Figure S6 in the Supporting Information).

**Host–Guest Interactions.** Synthesis by self-assembly of the metallacrowns **6**–**12** is the result of the subtle combination of several factors as charge balance, anionic effects, guest



dx.doi.org/10.1021/ic402651k | *Inorg. Chem.* 2014, 53, 1113–1121

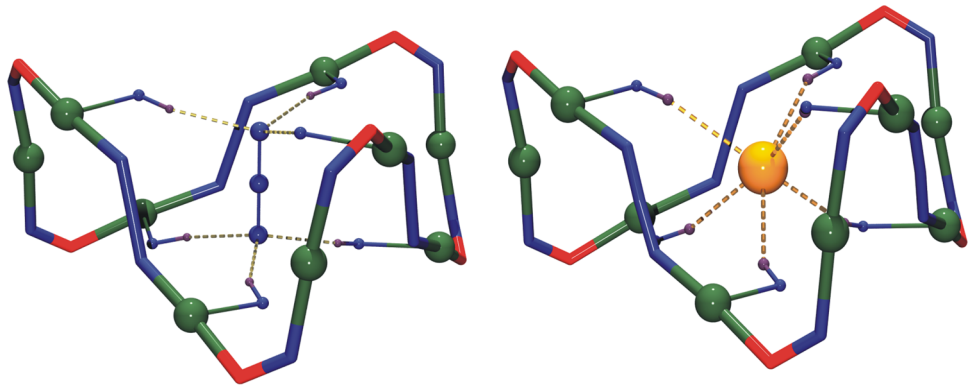

**Figure 4.** View of the *zig-zag* conformation of the ring and the prismatic cavity hosting the azide anion for compounds **6**–**9** as **12** (left), and compounds **10** and **11** (right).

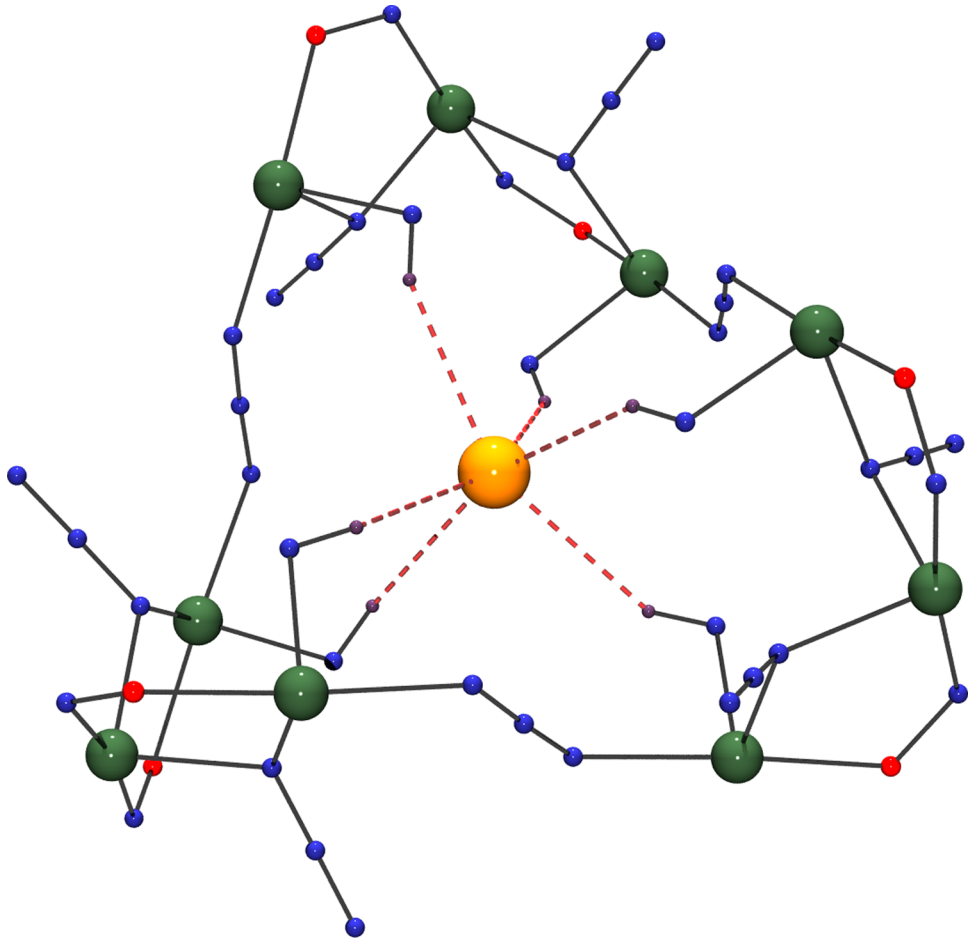

**Figure 5.** View of the metallacrown and the set of hydrogen bonds (dashed bonds) that coordinate the halide guests in compounds **10** and **11**. Atom labeling is the same as that for compounds **6**–**9**, and **12**.

coordination and hydrogen-bond interactions, which lead to the stabilization of this unusual supramolecular system. The detailed analysis of these factors will be the subject of this section.

*Anion Effect.* The reaction of $Ni^{II}$, tridentate amines, and 2-pyridyloximes without other anions in the reaction medium than azido or oximate lead to neutral low nuclearity systems ($Ni_3$, $Ni_4$), which contain the nickel centers bonded by double azido/oximato bridges. In contrast, the presence in the reaction medium of a large variety of anions stabilizes the cationic nonanuclear metallacronws **6**–**12** independently of the shape or size of the anions ($NO_3^-$, $BF_4^-$, $ClO_4^-$, $F^-$, $Cl^-$, $Br^-$, $I^-$). The structure of the metallacrowns **6**–**12** shows an evident relationship with trimeric complex **1** and they can be described as "trimers of trimers", which are linked by $\mu$-1,3-azido bridges. Two factors emerge as driving force for these reactions: on one hand, counteranions are necessary to balance the positive charge of the ring, and on the other hand, the reaction needs a small anion (azide or halide) to give a template assembly around it. The anionic guest and the counteranion become equally crucial to determine the stability and topology of the enneanuclear metallacrowns.



dx.doi.org/10.1021/ic402651k | *Inorg. Chem.* 2014, 53, 1113–1121

**Table 1. Selected Interatomic Angles Related with the Azido Bridges and Oximate Torsion for Compounds 6−12**

| | Interatomic Angles (deg) | | |
|---|---|---|---|
| compound | Ni(1)−N(6)−Ni(2) | Ni(2)−N(9)−N(10) | Ni(1)−N(2)−O(1)−Ni(2) |
| **6** | 110.89(7) | 128.2(2) | 17.6(2) |
| **7** | 110.8(1) | 127.6(2) | 17.6(3) |
| **8** | 110.9(1) | 127.9(3) | 17.3(4) |
| **9** | 111.1(1) | 130.0(2) | 14.8(4) |
| **10** | 111.0(1) | 129.2(3) | 15.2(4) |
| **11** | 111.3(2) | 129.7(4) | 17.8(5) |
| **12** | 111.1(1) | 127.0(2) | 18.6(4) |

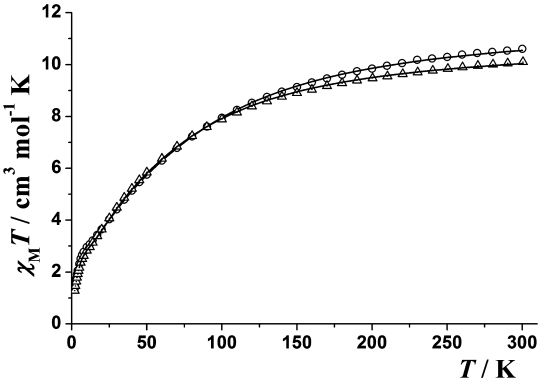


**Figure 6.** $\chi_M T$ vs $T$ plot for complexes **6** (circles) and **10** (triangles). Solid lines show the best fit obtained.

**Scheme 1. *Stoichiometric* Relationship between Complex 1 and Complexes 6−9, as Well as 12**

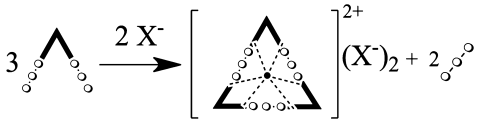


Although Scheme 1 does not correspond to one real reaction, it illustrates the "*stoichiometric*" relationship and the anion role between trinuclear complex **1** and enneanuclear complexes **6−9**, and **12**, which contain one azide as an anionic guest.

*Azide as a Guest.* Compounds **6−9**, and **12**, coordinate the guest azide in a manner similar to that of Lehn's [BT-6H$^+$] cryptand[6] (trigonal prismatic arrangement). This arrangement arises from six hydrogen bonds established between six $-NH_2$ amino functions of the dpt ligands. The trigonal prisms and even their distortions are surprisingly similar between the cryptand and the {Ni$_9$} rings, being the main difference the degree of pyramidalization of the hydrogen bonds, which determines the bases of the prisms (see Chart 3 and Table 2).

**Table 2. Comparison between [BT-6H$^+$] and {Ni$_9$} Prism Parameters**

| compound | $H^a$ | $T$ | $S$ | $D^b$ | N−N$_{az}$−N (deg) | N−H···N |
|---|---|---|---|---|---|---|
| **6** | 3.933 | 5.022 | 4.013 | 3.552 | 114.98 | 3.037 |
| **7** | 3.940 | 5.096 | 4.023 | 3.541 | 113.49 | 3.047 |
| **8** | 3.954 | 5.149 | 4.025 | 3.570 | 113.23 | 3.083 |
| **9** | 3.876 | 5.136 | 3.949 | 3.542 | 114.23 | 3.058 |
| **12** | 3.994 | 5.086 | 4.064 | 3.551 | 113.12 | 3.048 |
| **A**$^c$ | 5.396 | 4.364 | 5.528 | 3.693 | 95.03 | 2.959 |
| **10** | 3.786 | 5.176 | 3.861 | 3.538 | | |
| **11** | 3.922 | 5.207 | 4.013 | 3.590 | | |
| **B**$^{d,e}$ | 4.226 | 4.580 | 4.922 | 3.390 | | |

$^a$Polyhedron height measured as the distance between the centroids of the opposite triangular faces. $^b$Distance from the N-donor atoms to the centroid of the cavity. $^c$**A** = ($N_3$) ⊂ [BT-6H$^+$]. $^d$**B** = (Br) ⊂ [BT-6H$^+$]. $^e$Average values.

Analysis of the above data points out that the prismatic cavity is practically identical in all **6−12** cases. Comparison with compound **A** shows that, although the cavity is clearly compressed in complexes **6−9**, and **12**, the N−H···N distances serve as evidence that the hydrogen bonds are equally effective in the cryptand than in the {Ni$_9$} metallacrowns.

*Halides as Guest.* The [BT-6H$^+$] cryptand is able to coordinate azido anions but also spherical anions as halides. The highly flexible cryptand can rearrange its conformation by rotation in opposite sense of their two moieties along its main edge and then generate an octahedral environment that fits spherical guests more adequately.[6] The reported {Ni$_9$} metallacrown is much more rigid and unable to change its conformation.

**Chart 3. Prismatic Coordination of the Anionic Guests in (A) ($N_3$) ⊂ [BT-6H$^+$] Cryptand, (B) Compounds 6−9 and 12, and (C) 10 and 11 (the Image to the Far Right Describes the Structural Parameters Summarized in Table 2)$^a$**

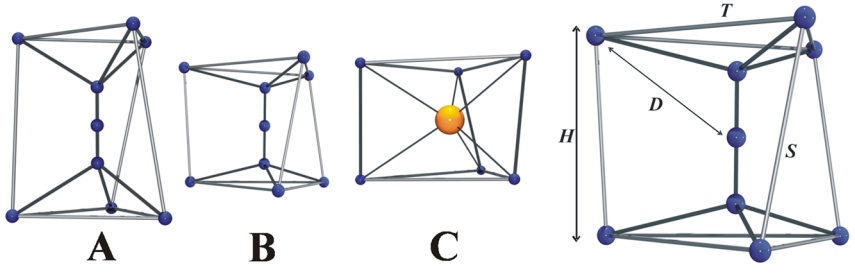


$^a$All distances refer to positions of the N atoms involved in the six hydrogen bonds.



dx.doi.org/10.1021/ic402651k | *Inorg. Chem.* 2014, 53, 1113−1121

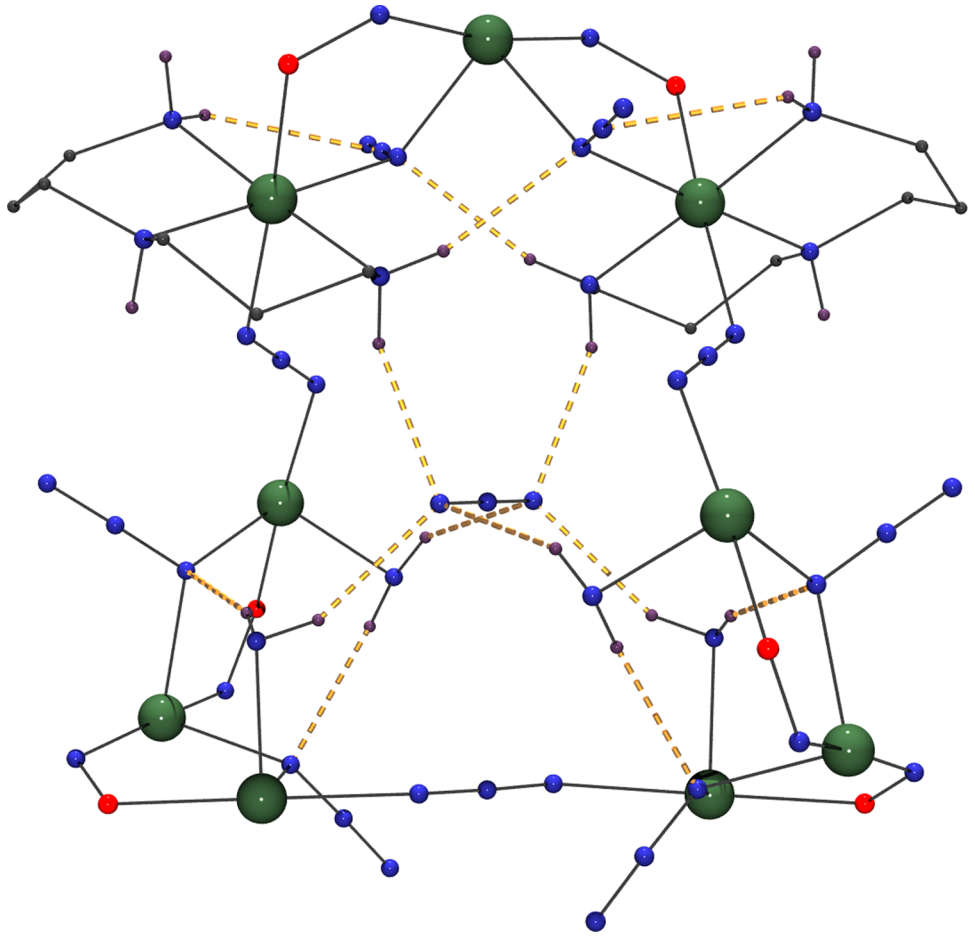

**Figure 7.** Set of hydrogen bonds promoted by the $-NH_2$ functions in **6**−**12**.

However, the compressed prisms **6**−**9**, and **12**, show distances to the centroid of the cavity that are only slightly larger than those found in (Br)[BT-6H$^+$] (see Table 2), suggesting that halides could fit into these prismatic cavities. This possibility was explored and complexes **10** and **11**, containing one bromide and one iodide guest in the unprecedented prismatic trigonal coordination (see Chart 3) were successfully characterized showing that the shape of the cavity is not a determinant factor. In contrast, reactions with nickel fluoride or chloride yielded the above-described complexes **8** and **9** in which the smaller halides act only as counteranions and the cavity is occupied by one guest azide, evidencing that the main factor involved with encapsulating the halides is their size.

*Tridentate Amines Role.* The tridentate aminated ligands establish a pack of six hydrogen bonds with both central azide and halide guest anions, but the role of these ligands can be considered not only to trap the central anion, but also to stabilize the {Ni$_9$} ring. As it can be seen in Figure 7, the $-NH_2$ functions pointing to the center of the cavity link the guest anion with one of their H atoms, whereas they establish another hydrogen bond employing their second H atom with the N(6) atom of the $\mu$-1,1-azido ligand. N(6) is also the receptor of a second hydrogen bond from the $-NH_2$ function in *trans* to the inner $-NH_2$ group. Thus, the *mer* coordination of the ligand becomes essential to stabilize the entire ring, pointing out that dpt is the optimal choice to generate these types of rings.

As experimental proof, the change of dpt ligand by *N*,*N*′,*N*″-Me$_3$dpt, which is unable to establish some of the hydrogen-bond interactions, stabilizes complex **4** instead of the {Ni$_9$} ring. Equally, experiments trying the substitution of the dpt tridentate amine by the bidentate *N*-Meen (*N*-methylethylenediamine), capable of establishing hydrogen-bond interactions with the central anion host but not with the nearby $\mu$-1,1-azide ligands leads to completely different topologies and nuclearities.[10c]

*Selectivity.* One should remember that these complexes are not stable in solution and the selectivity considerations concern the complexes in solid state exclusively. As has been proven, the {Ni$_9$} ring is able to encapsulate one azide/halide anion. However, it is noteworthy that, in all reactions involving **6**−**12**, there exists a competition between the azide, which is always present in the reaction medium, and the corresponding $Ni^{2+}$ counterion ($NO_3^-$, $BF_4^-$, $ClO_4^-$, or the halides) to fill the guest site. Tetrahedral anions as $BF_4^-$ or $ClO_4^-$ can coordinate in prismatic environments but they require larger cavities to fit adequately,[21] and their inclusion in the {Ni$_9$} cavity should be discarded as well for the smaller halides (F, $Cl^-$) for which the rigid cavity is too large to give effective hydrogen bonds. Thus, experimental results indicate that the encapsulation inside the {Ni$_9$} metallacrown is controlled by the size of the cavity and that $Br^-$ and $I^-$ ions are preferred to the $N_3^-$ species.



dx.doi.org/10.1021/ic402651k | *Inorg. Chem.* 2014, 53, 1113−1121

## CONCLUSIONS

Tridentate amines and 2-pyridyloximate blend of ligands have been demonstrated to be adequate for the syntheses of new and unprecedented topologies in oximato chemistry, such as compound **1**, which provided unambiguous experimental evidence of the ferromagnetic interaction promoted by double oximate/azide bridges. Also, a series of $Ni_3$, $Ni_4$, and $Ni_5$ complexes have been synthesized, as well as a family of self-assembled cryptand-like $\{Ni_9\}$ rings that are able to selectively encapsulate azide/halide anions, by reaction of different $Ni^{2+}$ salts, azide, and dipyridylketoneoximate or phenylpyridylketoneoximate ligands.

The azide/halide coordination takes place around six hydrogen bonds and generates a quiral helical arrangement of the cavity of the $\{Ni_9\}$ ring. $N_3^-$, $Br^-$, and $I^-$ adequately fit the cavity size, excluding other larger or smaller anions. The *mer* coordination of the aminated tridentate ligand determines the stabilization of the $\{Ni_9\}$ rings by means of a set of additional hydrogen bonds involving the two $-NH_2$ functions.

## ASSOCIATED CONTENT

### Supporting Information

Crystallographic data (CIF format), synthetic details, crystallographic information for compounds **1**−**12**, and $Ni_9$ ring spin levels energy diagram. This material is available free of charge via the Internet at http://pubs.acs.org.

## AUTHOR INFORMATION


### Corresponding Author

*E-mail: albert.escuer@qi.ub.es.


### Notes

The authors declare no competing financial interests.

## ACKNOWLEDGMENTS

Funding from the CICYT (Project No. CTQ2012-30662) are acknowledged. A.E. is thankful for financial support from the Excellence in Research ICREA-Academia Award.

## REFERENCES


(1) (a) Gale, P. A.; Gunnlaugsson, T. *Chem. Soc. Rev.* **2010**, *39*, 3595. (b) Steed, J. *Chem. Soc. Rev.* **2009**, *38*, 506. (c) Sessler, J. L.; Gale, P. A.; Cho, W.-S. *Anion Receptor Chemistry*; Royal Society of Chemistry: Cambridge, U.K., 2006. (d) Kang, S. O.; Begum, R. A.; Bowman-James, K. *Angew. Chem., Int. Ed.* **2006**, *45*, 7882. (e) Bowman-James, K. *Acc. Chem. Res.* **2005**, *38*, 671.

(2) (a) Ballester, P. *Chem. Soc. Rev.* **2010**, *39*, 3810. (b) Lawrance, G. A. *Chem. Rev.* **1986**, *86*, 17. (c) Saalfrank, R. W.; Demleitner, B.; Glaser, H.; Maid, H.; Bathelt, D.; Hampel, F.; Bauer, W.; Teichert, M. *Chem.—Eur. J.* **2002**, *8*, 2679. (d) Albrecht, M.; Janser, I.; Meyer, S.; Weis, P.; Frohlich, R. *Chem. Commun.* **2003**, 2854. (e) Glasson, C. R. K.; Meehan, G. V.; Clegg, J. K.; Lindoy, L. F.; Turner, P.; Duriska, M. B.; Willis, R. *Chem. Commun.* **2008**, 1190. (f) Custelcean, R.; Bosano, J.; Bonnesen, P. V.; Kertesz, V.; Hay, B. P. *Angew. Chem., Int. Ed.* **2009**, *48*, 4025. (g) Bryantsev, V. S.; Hay, B. P. *J. Am. Chem. Soc.* **2006**, *128*, 2035.

(3) Diederich, F., Slang, P. J., Eds. *Templated Organic Synthesis*; Wiley−VCH: Weinheim, Germany, 2000.

(4) Kang, S. O.; Llinares, J. M.; Day, V. W.; Bowman-James, K. *Chem. Soc. Rev.* **2010**, *39*, 3980.

(5) (a) Beer, P. D.; Gale, P. A. *Angew. Chem., Int. Ed.* **2001**, *40*, 486. (b) Rice, C. R. *Coord. Chem. Rev.* **2006**, *250*, 3190. (c) Pérez, J.; Riera, L. *Chem. Soc. Rev.* **2008**, *37*, 2658. (d) Fabbrizzi, L.; Poggi, A. *Chem. Soc. Rev.* **2013**, *42*, 1861.

(6) Dietrich, B.; Guilhem, J.; Lehn, J. M.; Pascard, C.; Sonveaux, E. *Helvet. Chim. Acta* **1984**, *67*, 91.

(7) (a) Kim, N.-K.; Chang, K.-J.; Moon, D.; Lah, M. S.; Jeong, K.-S. *Chem. Commun.* **2007**, 3401. (b) Kang, S. O.; Day, V. W.; Bowman-James, K. *Inorg. Chem.* **2010**, *49*, 8629. (c) Serpell, C. J.; Cookson, J.; Thompson, A. L.; Beer, P. D. *Chem. Sci.* **2011**, *2*, 494. (d) Wang, X.; Jia, C.; Huang, X.; Wu, B. *Inorg. Chem. Commun.* **2011**, *14*, 1508. (e) Bushmarinov, I. S.; Nabiev, O. G.; Kostyanovsky, R. G.; Antipina, M. Y.; Lyssenko, K. A. *Cryst. Eng. Commun.* **2011**, *13*, 2930.

(8) Amendola, V.; Boiocchi, M.; Colasson, B.; Fabbrizzi, L.; Rodriguez-Douton, M. J.; Ugozzoli, F. *Angew. Chem., Int. Ed.* **2006**, *45*, 6920.

(9) (a) Milios, C. J.; Stamatatos, T. C.; Perlepes, S. P. *Polyhedron* **2006**, *25*, 134. (b) Tasiopoulos, A. J.; Perlepes, S. P. *Dalton Trans.* **2008**, 5537.

(10) (a) Stamatatos, T. C.; Abboud, K. A.; Perlepes, S. P.; Christou, G. *Dalton Trans.* **2007**, 3861. (b) Stamatatos, T. C.; Escuer, A.; Abboud, K. A.; Raptopoulou, C. P.; Perlepes, S. P.; Christou, G. *Inorg. Chem.* **2008**, *47*, 11825. (c) Esteban, J.; Alcazar, L.; Torres-Molina, M.; Monfort, M.; Font-Bardia, M.; Escuer, A. *Inorg. Chem.* **2012**, *51*, 5503.

(11) Papatriantafyllopoulou, C.; Stamatatos, T. C.; Wernsdorfer, W.; Teat, S. J.; Tasiopoulos, A. J.; Escuer, A.; Perlepes, S. P. *Inorg. Chem.* **2010**, *49*, 10486.

(12) Escuer, A.; Esteban, J.; Font-Bardia, M. *Chem. Commun.* **2012**, *48*, 9777.

(13) Sheldrick, G. M. *SHELXS—A Computer Program for Determination of Crystal Structures*; University of Göttingen: Göttingen, Germany, 1997.

(14) Sheldrick, G. M. *SHELX97—A Computer Program for Determination of Crystal Structures*; University of Göttingen: Göttingen, Germany, 1997.

(15) Farrugia, L. J. *J. Appl. Crystallogr.* **1997**, *30*, 565 (Ortep-3 for Windows).

(16) Escuer, A.; Vicente, R.; Ribas, J.; Solans, X. *Inorg. Chem.* **1995**, *34*, 1793.

(17) Esteban, J.; Ruiz, E.; Font-Bardia, M.; Calvet, T.; Escuer, A. *Chem.—Eur. J.* **2012**, *18*, 3637.

(18) (a) Escuer, A.; Esteban, J.; Aliaga-Alcalde, N.; Font-Bardia, M.; Calvet, T.; Roubeau, O.; Teat, S. J. *Inorg. Chem.* **2010**, *39*, 2259. (b) Escuer, A.; Esteban, J.; Roubeau, O. *Inorg. Chem.* **2011**, *50*, 8893. (c) Esteban, J.; Escuer, A.; Font-Bardia, M.; Roubeau, O.; Teat, S. J. *Polyhedron* **2013**, *52*, 339.

(19) Gatteschi, D.; Pardi, L. *Gazz. Chim. Ital.* **1993**, *123*, 231 (CLUMAG program).

(20) Escuer, A.; Vicente, R.; Ribas, J.; El Fallah, M. S.; Solans, X.; Font-Bardia, M. *Inorg. Chem.* **1994**, *33*, 1842.

(21) Paul, R. L.; Bell, Z. R.; Jeffery, J. C.; McCleverty, J. A.; Ward, M. D. *Proc. Natl. Acad. Sci. U.S.A.* **2002**, *99*, 4883.

### 3.10.1. Resum: Anionic guests in prismatic cavities generated by enneanuclear nickel metallacycles.

Jordi Esteban, Mercè Font-Bardia, Albert Escuer.

*Inorganic Chemistry* **2014**, *53,* 1113-1121.

En aquest article es va presentar la síntesi, caracterització estructural i estudi magnètic de dotze complexos de $Ni^{II}$ obtinguts a partir de diversos lligands 2-piridiloxima, amines tridentades i $NaN_3$. Els compostos **9_1 – 9_5** havien estat presentats en forma de comunicació a l'article 9.

Es van obtenir una sèrie de compostos de nuclearitat $Ni_3$, $Ni_4$ i $Ni_5$ de fórmula $[Ni_3(N\text{-}Medpt)_2(py_2CNO)_2(N_3)_4]$ (**9_1**), $[Ni_4(N\text{-}Medpt)_2(N_3)_4(dapdo)_2]$ (**10_2**), $[Ni_4(dpt)_2(N_3)_4(py_2CNO)_2]$ (**10_3**), $[Ni_4(N,N',N''\text{-}Me_3dpt)_2(N_3)_4(pyC\{ph\}NO)_4]$ (**10_4**) i $[Ni_5(H_2O)_4(AcO)_2(N_3)_2(OH)_2(pyC\{ph\}NO)_4]$ (**10_5**), figura 18, així com una família d'anells $\{Ni_9\}$ generats per *self-assembly* que encapsulen un anió azidur o halur, introduïda en la comunicació anterior: $(N_3)\subset[Ni_9(dpt)_6(pyC\{ph\}NO)_6(N_3)_9]A_2$ (A = $NO_3^-$ , **9_2**; $BF_4^-$, **10_7**; $F^-$, **10_8**; $Cl^-$, **9_3**), $X\subset[Ni_9(dpt)_6(pyC\{ph\}NO)_6(N_3)_9]X_2$ (X = $Br^-$, **9_4**; $I^-$, **9_5**) i $(N_3)\subset[Ni_9(dpt)_6(py_2CNO)_6(N_3)_9](ClO_4)_2$ (**10_12**).

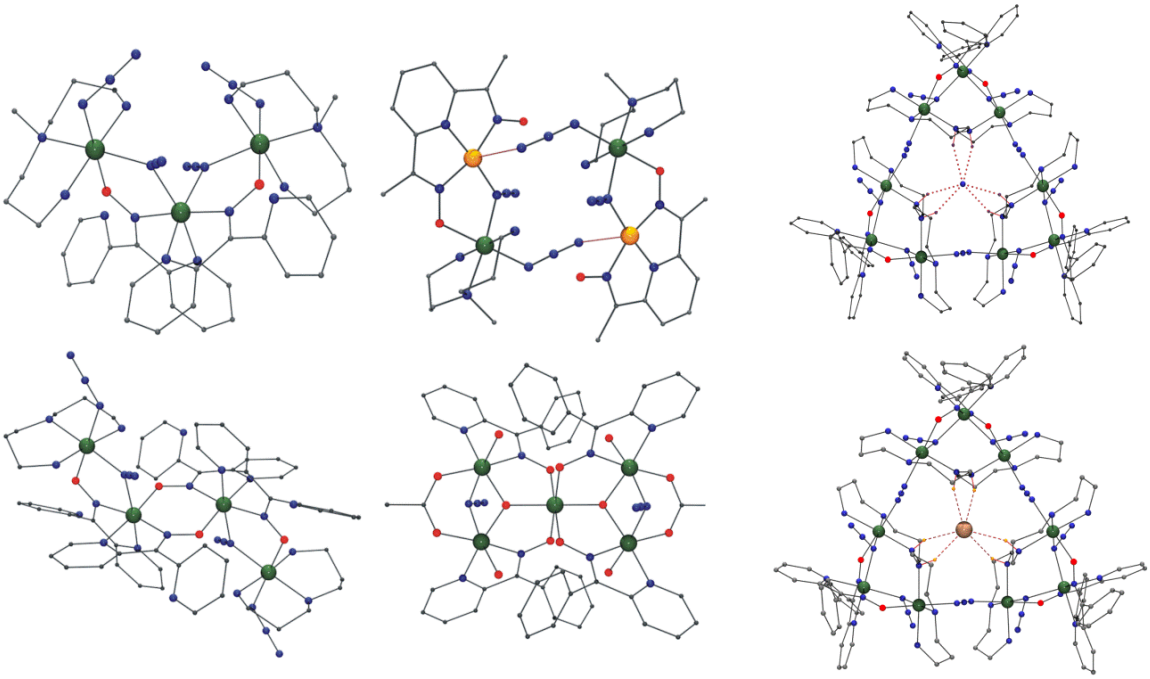

**Figura 18.** Estructura dels compostos **9_1**, **10_2**, **10_3** i **10_5** (esquerra) i **9_2** i **9_4** (dreta) presentats en aquest article.

L'estudi magnètic dels diferents compostos va mostrar que el compost trinuclear **9_1** presenta un acoblament ferromagnètic i un estat fonamental *S* = 3, mentre que el compost tetranuclear **10_3**, tot i contenir dos enllaços oxima/azida, és antiferromagnètic i té un estat fonamental *S* = 0. El compost pentanuclear **10_5** és ferrimagnètic (conté interaccions ferromagnètiques i antiferromagnètiques) i presenta un estat fonamental *S* = 3. Finalment, els compostos $(N_3)\subset\{Ni_9\}$ (**9_2**) i $(Br)\subset\{Ni_9\}$ (**9_4**) també contenen ponts azida/oxima però la interacció predominant és l'acoblament antiferromagnètic a través del pont azida *end-to-end*, de forma que el sistema es pot descriure com un triangle de $Ni^{II}$ antiferromagnèticament acoblat que deriva en un estat fonamental de spin *S* = 0 a causa de la competitivitat entre les interaccions.

També es va realitzar un estudi detallat sobre la influència dels diferents factors (anions, amines, etc.) en la obtenció dels diferents compostos.

Les principals conclusions que es poden extreure d'aquest article són que el sistema 2-piridiloxima/azida/amina tridentada demostra ser adequat per a la síntesi de nous compostos i noves topologies, entre les quals es troba una família de metal·lomacrocicles de nuclearitat $Ni_9$ capaç d'encapsular selectivament un anió azidur o halur. La coordinació d'aquests es realitza a través de sis interaccions per ponts d'hidrogen que generen les amines tridentades i que poden ajustar-se lleugerament per tal de generar un entorn més adient per a la coordinació de l'anió central. Per últim, es va trobar que el paper de les amines no és només coordinar l'anió central, sinó que també estableixen una sèrie de ponts d'H intramoleculars que estabilitzen l'anell $\{Ni_9\}$ sense els quals aquesta estructura no es manté.

## 3.11. Compostos no publicats

En aquest apartat es descriuen els compostos que no han estat publicats en el moment de redactar la memòria. Aquests compostos es poden separar en dues categories: en primer lloc, els compostos totalment caracteritzats que, per diferents motius, no han estat publicats i que per tant no es troben descrits en el compendi de publicacions i, en segon lloc, aquells compostos que han pogut ser caracteritzats estructuralment però o bé no han resultat reproduïbles en síntesis posteriors o la seva caracterització per espectroscòpia d'infraroig (IR), anàlisi elemental i per les mesures de magnetisme no ha resultat coherent.

Cal comentar que tots els compostos publicats, així com els compostos del primer bloc d'aquest apartat, són compostos totalment reproduïbles. En tots els casos s'han repetit les seves síntesi per tal de disposar de les quantitats de mostra adient per a la seva caracterització per les tècniques anomenades anteriorment.

### 3.11.1. Compostos caracteritzats

**pyC{CN}NOH**

**$[Ni(MeOH)_2(pyC\{CN\}NOH)_2]$**. Un dels primers assajos amb el lligand pyC{CN}NOH va ser la síntesi del compost $[Ni(MeOH)_2(pyC\{CN\}NOH)_2]$ (**11_1**), figura 19, a partir del lligand pyC{CN}NOH (3 mmol, 438 mg), $NiSO_4 \cdot 6H_2O$ (1 mmol, 280mg) i $NEt_3$ (3 mmols, 303 mg) en 20 mL de MeOH, deixant agitar la reacció durant unes dues hores, filtrant la mescla i deixant cristal·litzar la solució en un vial tancat. IR ($cm^{-1}$): 3452 (br), 2218 (w), 1635 (m), 1602 (m), 1457 (m), 1405 (m), 1305 (w), 1267 (w), 1231 (m), 1159 (w)m 1106 (w), 1064 (w), 1033 (m), 780 (w), 708 (w). Anàlisi elemental calculat per **11_1** ($C_{16}N_6NiO_4H_{16}$): C, 46,30; H, 3,89; N, 20,25 %; trobat: C, 47,5; H, 4,0; N, 20,8 %.

En el compost obtingut, el catió $Ni^{II}$ presenta un entorn octaèdric $NiN_4O_2$ generat pels dos lligands coordinats al pla equatorial i per dues molècules de metanol coordinades en *trans*.

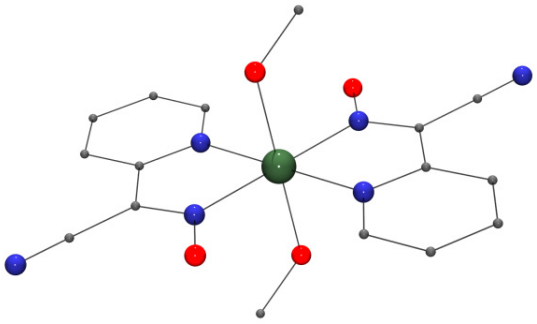

**Figura 19.** Estructura del compost mononuclear **11_1**.

La relació $Ni^{II}$/lligand/base (1:3:3) es va escollir per tal d'obtenir un compost mononuclear amb fórmula similar a $[Ni(pyC\{CN\}NO)_3]^-$, en què tres lligands coordinessin el catió $Ni^{II}$ pels seus àtoms de nitrogen, deixant disponibles els àtoms d'oxigen dels grups oxima, per tal d'utilitzar aquest compost de reactiu de partida o *starting material* en posteriors reaccions. En no obtenir el compost buscat i donat el baix rendiment del compost **11_1**, es va descartar el seu ús com a *starting material*.

És destacable el fet que, durant el transcurs de la tesi, es va observar l'aparició del fragment $[Ni(pyC\{CN\}NO)_3]^-$ en el compost **6_3**.

**$[Ni_3(MeOH)_2(CF_3COO)(OH)(pyC\{CN\}NO)_4]\cdot 2{,}5MeOH$.** Es va caracteritzar un nou compost triangular amb fórmula $[Ni_3(MeOH)_2(CF_3COO)(OH)(pyC\{CN\}NO)_4]$ (**11_2**), obtingut en fer reaccionar en 20 mL de metanol i durant dues hores, el lligand 2-acetonitrilpiridiloxima (0,5 mmols, 73 mg), $Ni(hfacac)_2\cdot H_2O$ (1 mmol, 472 mg) i trietilamina (1 mmol, 101 mg). Passat aquest temps, es va filtrar la mescla i es va deixar cristal·litzar lentament en un vial tancat. IR ($cm^{-1}$): 3456 (br), 2223 (w), 1650 (s), 1602 (m), 1464 (s), 1430 (m), 1303 (w), 1257 (s), 1201 (m), 1150 (s), 1109 (w), 1039 (w), 781 (w), 712 (w), 672 (w). Anàlisi elemental calculat per **11_2** ($C_{32}F_3N_{12}Ni_3O_9H_{25}$): C, 40,25; H, 2,64; N, 17,61 %; trobat: C, 39,2; H, 2,7; N, 17,5 %.

Aquest compost triangular és isoestructural amb el compost **5_1**. La única diferència entre els dos resideix en la substitució del lligand acetat pel trifluoroacetat ($CF_3COO^-$), figura 20. L'anió $CF_3COO^-$ prové de la descomposició del reactiu hexafluoroacetilacetonat seguint una reacció de condensació retro-Claisen,[172] possiblement catalitzada per cations metàl·lics:

$$CF_3COCHCOCF_3^- \longrightarrow CF_3COO^- + CH_3COCF_3$$

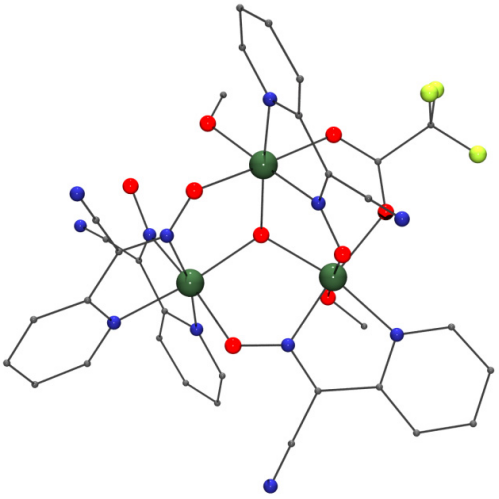

**Figura 20.** Estructura del compost **11_2**.

La mesura de susceptibilitat magnètica per al compost **11_2** presenta un valor de $\chi_M T$ a temperatura ambient proper a 3,2 $cm^3 \cdot K \cdot mol^{-1}$, que disminueix progressivament en refredar fins arribar a un valor de 0,07 $cm^3 \cdot K \cdot mol^{-1}$ a 2 K, figura 21.

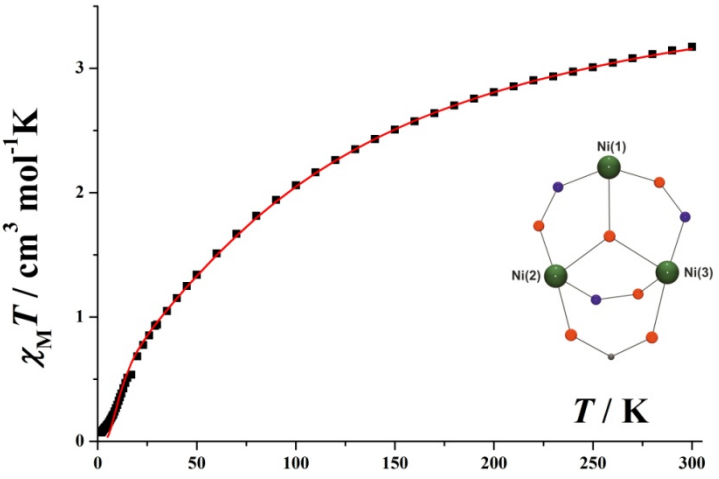


**Figura 21.** Representació de $\chi_M T$ *vs. T* i del *core* magnètic del compost **11_2**. La línia vermella representa el millor ajust obtingut.

L'ajust de les dades experimentals es va realitzar amb el programa PHI[7] aplicant el Hamiltonià amb dues constants d'acoblament:

$$H = -J_1 (S_1 S_2 + S_1 S_3) - J_2 (S_2 S_3)$$

i els valors obtinguts per al millor ajust són: $J_1$ = -40,4 $cm^{-1}$, $J_2$ = -28,4 $cm^{-1}$, $g$ = 2,31 i $R = 3{,}35 \cdot 10^{-4}$. La relació entre $J_1$ i $J_2$ ($J_2/J_1$ = 0,70) genera un estat fonamental $S$ = 0.

A la taula 1 es comparen els paràmetres estructurals més importants des del punt de vista del superintercanvi magnètic i les constants d'acoblament associades dels compostos **5_1** i **11_2**:

**Taula 1.** Angles i torsions [°] i constants d'acoblament [$cm^{-1}$] seleccionats per als compostos **5_1** i **11_2**. L'angle de torsió Ni(2)-O···O-Ni(3) fa referència al pont acetat.

| | **5_1** | **11_2** |
|---|---|---|
| Ni(1)-O-Ni(2) | 116,1(1) | 114,9(1) |
| Ni(1)-O-Ni(3) | 114,9(1) | 114,0(1) |
| Ni(2)-O-Ni(3) | 104,0(1) | 106,0(1) |
| Ni(2)-O···O-Ni(3) | 14,5(1) | 13,3(1) |
| $J_1$ | -44,6 | -40,4 |
| $J_2$ | -24,4 | -28,4 |

La variació de ± 4 $cm^{-1}$ en el valor de les constants d'acoblament es pot explicar per la variació dels angles Ni-O-Ni: la disminució dels angles dels dos costats iguals del triangle isòsceles (Ni(1)-O-Ni(2) i Ni(1)-O-Ni(3)) i l'augment del tercer angle (Ni(2)-O-Ni(3)) en passar del compost **5_1** a **11_2** provoca una disminució del valor de $J_1$ i un augment de $J_2$, de forma coherent amb la tendència observada en els articles 4 i 5.

Un altre factor que pot afectar els valors de $J_1$ i $J_2$ és la naturalesa del carboxilat coordinat: la presència del grup trifluorometil al compost **11_2** retira una certa densitat electrònica dels àtoms d'oxigen del carboxilat, de manera que aquests contribueixen en menor mesura en l'orbital molecular. Si es té en compte que les interaccions per ponts oxima i carboxilat són anticomplementàries,[162] es pot entendre que la disminució de la contribució del carboxilat a l'orbital magnètic provoca un augment de la intensitat de l'acoblament (en aquest cas, més antiferromagnètic).

**2-piridiloxima / azida / amina**

**[Ni(dpt)($N_3$)(pyC{CN}NO]**. Una de les primeres reaccions realitzades per aquest sistema va ser el compost mononuclear [Ni(dpt)($N_3$)(pyC{CN}NO] (**11_3**), sintetitzat a partir del lligand pyC{CN}NOH (1 mmol, 146 mg), el compost dinuclear [$Ni_2$(dpt)$_2$($N_3$)$_4$] (1 mmol, 576 mg) i $NEt_3$ (1 mmols, 101 mg) en 20 mL de metanol. La solució es va agitar durant un parell d'hores, es va filtrar i es va deixar evaporar lentament en un vial, apareixent uns cristalls petits i foscos al cap d'una setmana. IR ($cm^{-1}$): 3320 (s), 3294 (s), 3245 (m), 3175 (m), 2931 (m), 2857 (w), 2209 (m), 2051 (s), 1598 (s), 1481 (m), 1443 (s), 1394 (s), 1317 (m), 1298 (w), 1279 (w), 1151 (m), 1123 (w), 1104 (w), 1030 (s), 771 (m), 708 (w). Anàlisi elemental calculat per **11_3** ($C_{13}N_9NiOH_{21}$): C, 41,30; H, 5,60; N, 33,34 %; trobat: C, 40,6; H, 5,6; N, 34,2 %.

En aquest compost, el catió $Ni^{II}$ presenta un entorn $NiN_6$ generat per l'amina dpt, que es coordina en disposició *mer*, per dos nitrògens del lligand pyC{CN}$NO^-$ i finalment per l'azidur terminal, figura 22, esquerra.

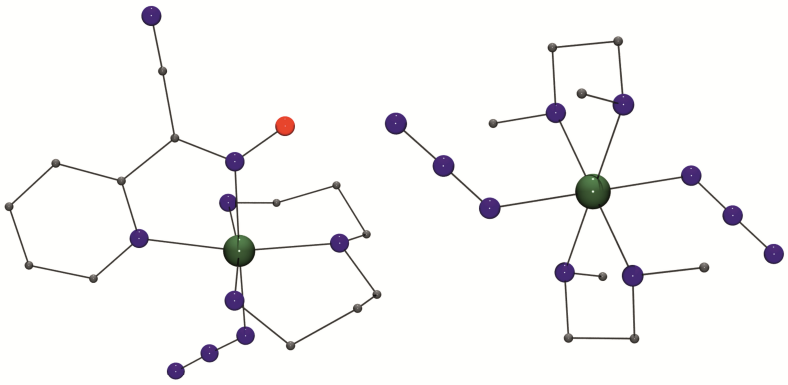

**Figura 22.** Compostos mononuclears **11_3**, esquerra, i **11_4**, dreta.

**[Ni(N,N'-$Me_2$en)$_2$($N_3$)$_2$]**. També es va obtenir un compost mononuclear amb fórmula [Ni(N,N'-$Me_2$en)$_2$($N_3$)$_2$] (**11_4**) en fer reaccionar el lligand 6-MepyC{H}NOH (1 mmol, 136 mg), $Ni(NO_3)_2{\cdot}6H_2O$ (2 mmols, 580 mg), N,N'-$Me_2$en (2 mmols, 184 mg), $NaN_3$ (4 mmols, 260 mg) i $NEt_3$ (1 mmol, 101 mg) en 20 mL de MeOH. Es va deixar reaccionar la mescla durant 2 h, es va filtrar i deixar cristal·litzar per capes amb 10 mL de dietilèter durant una setmana fins l'aparició d'uns petits prismes foscos. IR ($cm^{-1}$): 3308 (m), 3251 (m), 2920 (m), 2047 (s), 1470 (m), 1093 (w), 1071 (w),

1030 (w), 1010 (w), 944 (m), 857 (w). Anàlisi elemental calculat per **11_4** ($C_8N_{10}NiH_{24}$): C, 30,11; H, 7,58; N, 43,90 %; trobat: C, 29,0; H, 7,2; N, 42,6 %.

Com es mostra a la figura 22, dreta, l'entorn de coordinació del metall torna a ser $NiN_6$, en aquest cas generat per dues azides coordinades en *trans* i dues amines bidentades que es troben al pla equatorial.

**$[Ni_3(N,N'\text{-}Me_2en)(dapdo)_2(N_3)_2]\cdot x MeOH,H_2O$.** A partir d'una reacció molt semblant a l'anterior ($Ni(NO_3)_2$, N,N'-$Me_2$en i $NaN_3$ en les mateixes quantitats) però emprant el lligand $dapdoH_2$ (1 mmol, 198 mg), 2 equivalents de $NEt_3$ (2 mmols, 202 mg) i deixant cristal·litzar la solució en un vial tancat, es va obtenir el compost trinuclear $[Ni_3(N,N'\text{-}Me_2en)(dapdo)_2(N_3)_2]$ (**11_5**), que presenta una geometria angular. IR ($cm^{-1}$): 3405 (br), 2917 (w), 2073 (s), 1591 (m), 1503 (w), 1453 (m), 1397 (s), 1289 (m), 1252 (m), 1221 (s), 1156 (m), 1134 (m), 1088 (w), 787 (w). Anàlisi elemental calculat per **11_5** ($C_{22}N_{14}Ni_3O_4H_{28}$): C, 36,26; H, 3,87; N, 26,91 %; trobat: C, 35,9; H, 4,0; N, 26,3 %.

Els dos $Ni^{II}$ terminals es troben coordinats als lligands $dapdo^{2-}$ adoptant un entorn plano-quadrat i s'uneixen al catió central per mitjà d'un pont oxima/azida. Les dues posicions de coordinació restants del catió $Ni^{II}$ central estan ocupades per l'amina bidentada N,N'-$Me_2$en, figura 23.

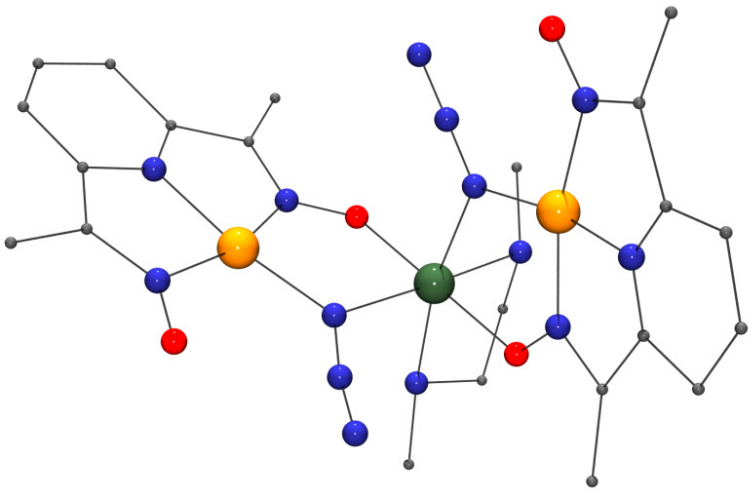

**Figura 23.** Estructura del compost **11_5**.

Aquest compost presenta dos aspectes remarcables: en primer lloc, s'ha generat un entorn plano-quadrat per coordinació amb un lligand 2.10111 dapdo$^{2-}$, de forma anàloga al compost **1_1**, i en segon lloc, aquest és el primer compost en què s'ha aconseguit la coordinació simultània del grup azidur i del lligand dapdo$H_2$ (en qualsevol dels seus estats protonat, mono- o di-desprotonat).

Des del punt de vista del magnetisme, aquest compost es comporta com un compost mononuclear, com demostra la mesura de la magnetització, que tendeix a un valor de saturació de 2 electrons ($S$ = 1).

**$[Ni_{12}Na_2(H_2O)_4(MeOH)_4(6\text{-}MepyC\{H\}NO)_{12}(N_3)_{10}(OH)_4]\cdot 4MeOH,H_2O$.** Finalment, es va obtenir un compost amb nuclearitat $\{Ni_{12}Na_2\}$ que pertany a la mateixa família de compostos $\{Ni_{12}Na_2\}$, $\{Ni_{13}\}$ i $\{Ni_{14}\}$ descrits a l'article 8 i que consisteix en dos anells de $\{Ni_6\}$ units per dos cations $Na^+$, generant un compost amb fórmula $[Ni_{12}Na_2(H_2O)_4(MeOH)_4(6\text{-}MepyC\{H\}NO)_{12}(N_3)_{10}(OH)_4]$ (**11_6**). Aquest compost va ser sintetitzat afegint a 20 mL de MeOH el lligand 6-MepyC{H}NOH (1 mmol, 136 mg), $Ni(NO_3)_2\cdot 6H_2O$ (2 mmols, 580 mg), dpt (2 mmols, 262 mg), $NaN_3$ (4 mmols, 240 mg) i $NEt_3$ (1 mmol, 101 mg), deixant agitar la mescla durant dues hores, filtrant-la i deixant cristal·litzar la solució resultant en un vial tancat durant dues setmanes fins l'aparició de cristalls adequats per a la seva resolució per difracció de raigs-X de monocristall. IR (cm$^{-1}$): 3417 (br), 2055 (s), 1604 (s), 1541 (s), 1463 (m), 1384 (m), 1350 (w), 1220 (w), 1117 (m), 1087 (s), 787 (m), 743 (w), 667 (m). Anàlisi elemental calculat per **11_6** ($C_{88}N_{54}Na_2Ni_{12}O_{24}H_{112}$): C, 34,54; H, 3,69; N, 24,71 %; trobat: C, 34,1; H, 3,8; N, 24,0 %.

Estructuralment, aquest compost és molt semblant al compost **8_4**, sent la principal diferència la presència d'un pont azida entre la subunitat $\{Ni_6\}$ i un $Na^+$ central, figura 24, de forma que els fragments externs s'uneixen als cations centrals per tres ponts oxima i un pont azida. Com es pot veure, l'amina dpt no forma part de l'estructura del compost.

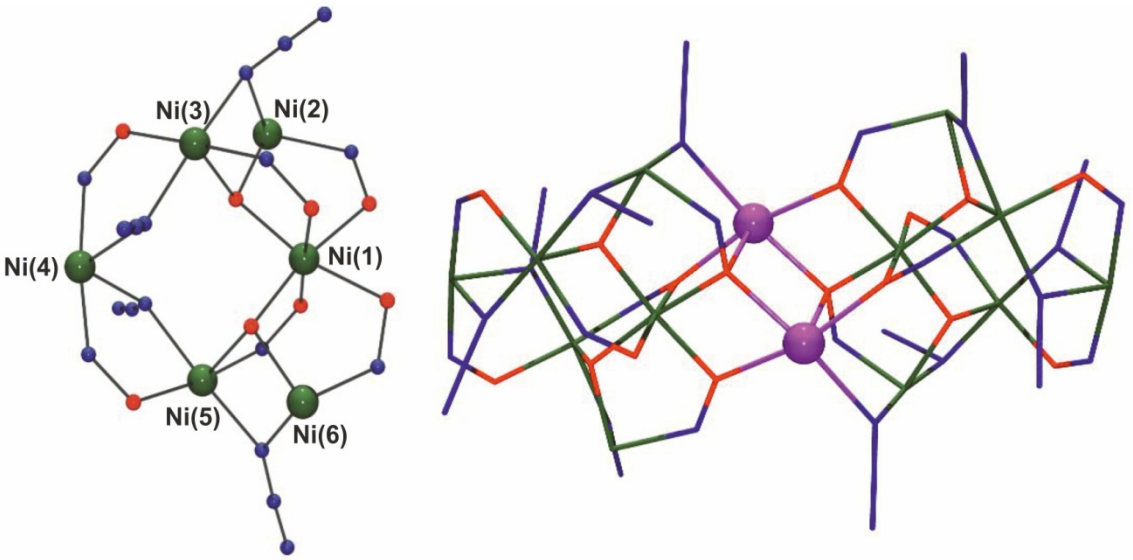


**Figura 24.** Esquerra, subunitat $\{Ni_6\}$ comú en els compostos amb nuclearitats $\{Ni_{12}Na_2\}$, $\{Ni_{13}\}$ i $\{Ni_{14}\}$. Dreta, estructura del compost **11_6**. Els cations sodi es mostren de color violeta.

El compost **11_6** presenta un valor de $\chi_M T$ a temperatura ambient de 7,32 $cm^3 \cdot K \cdot mol^{-1}$, que decreix lleugerament en disminuir la temperatura fins arribar a 7,26 $cm^3 \cdot K \cdot mol^{-1}$ al voltant de 150 K, temperatura a partir de la qual augmenta fins arribar a un màxim de 10,75 $cm^3 \cdot K \cdot mol^{-1}$ a 10 K. A partir d'aquesta temperatura, el valor de $\chi_M T$ disminueix novament amb la temperatura, fins arribar a un valor de 8,43 $cm^3 \cdot K \cdot mol^{-1}$ a 2 K, figura 25.

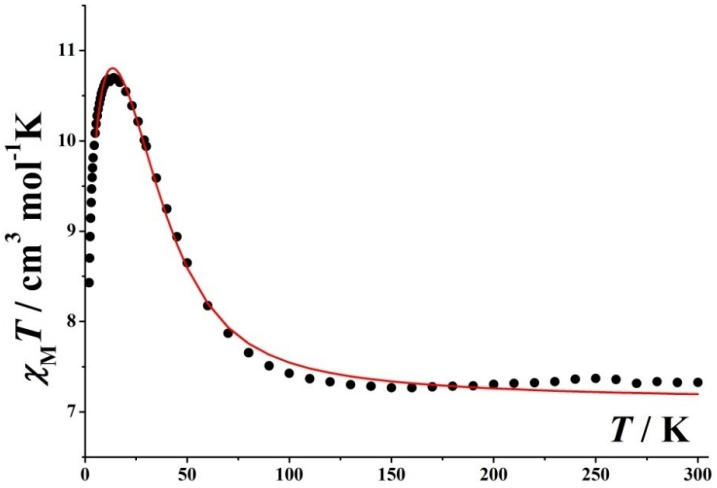


**Figura 25.** Representació de $\chi_M T$ *vs.* $T$ per al compost **11_6**. La línia vermella representa el millor ajust obtingut.

Donat que el bescanvi a traves dels cations sodi es pot considerar quasi negligible, la mesura de susceptibilitat magnètica es va ajustar com si es tractés de dos fragments $\{Ni_6\}$ aïllats, utilitzant el programa PHI[7] i el Hamiltonià:

$$H = -J_1 (S_1 S_2 + S_1 S_3 + S_1 S_5 + S_1 S_6) - J_2 (S_2 S_3 + S_3 S_4 + S_4 S_5 + S_5 S_6)$$

Els millors valors obtinguts d'aquest ajust van ser: $J_1$ = -18,5 $cm^{-1}$, $J_2$ = +22,6 $cm^{-1}$, $g$ = 2,17 i $R = 9{,}7 \cdot 10^{-5}$. Es va incloure un paràmetre per quantificar les interaccions intermoleculars en l'ajust i es va obtenir el valor de $z'J'$ = -0,05 $cm^{-1}$.

El paràmetre $z'J'$ fa referència a les interaccions intermoleculars, però en ocasions engloba altres efectes antiferromagnètics a baixa temperatura. En aquest cas, però, es pot suposar que l'acoblament entre els dos anells $\{Ni_6\}$ a través dels ions sodi tindrà, previsiblement, una major importància que el causat per l'anisotropia magnètica del compost.

Aquests valors generen un estat fonamental $S$ = 4, valor que coincideix amb el proposat a l'article 8 i amb el valor obtingut en ajustar la mesura de la magnetització ($M$). Aquest ajust es va realitzar considerant l'anell $\{Ni_6\}$ com un spin $S$ = 4 amb un valor de $g$ = 2,10 i es va calcular un valor de $D$ = -0,40 $cm^{-1}$ ($R = 1{,}1 \cdot 10^{-3}$), figura 26.

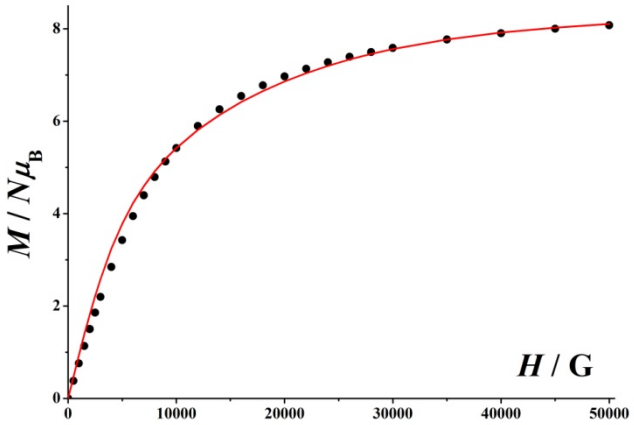


**Figura 26.** Representació de la magnetització ($M$) respecte del camp ($H$) per al compost **11_6**. La línia vermella representa el millor ajust obtingut.

### 3.11.2. Misteris de la ciència

**$DapdoH_2$**

**$[Ni_8(MeOH)_8(dapdo)_4(OH)_4](ClO_4)_4$**. Es va obtenir un compost amb fórmula $[Ni_8(MeOH)_8(dapdo)_4(OH)_4](ClO_4)_4$ (**11_7**) a partir d'1 mmol del lligand $dapdoH_2$ (198 mg), 2 mmols de $Ni(ClO_4)_2{\cdot}6H_2O$ (730 mg) i 2 mmols de $NEt_3$ (202 mg) en 20 mL de metanol. Es va agitar la mescla durant dues hores i posteriorment es va filtrar i procedir a la seva cristal·lització per capes amb 10 mL de dietilèter. Es van obtenir cristalls vermellosos amb forma de prisma adients per a la seva resolució per difracció de raigs-X al cap d'un parell de setmanes. IR ($cm^{-1}$): 3384 (br), 1593 (m), 1520 (w), 1487 (w), 1440(w), 1408(m), 1196 (m), 1109 (s), 1088 (s), 797 (w), 626 (m), 517 (w). Anàlisi elemental calculat per **11_7** ($C_{44}Cl_4N_{12}Ni_8O_{36}H_{72}$): C, 27,01; H, 3,71; N, 8,59 %; trobat: C, 30,1; H, 3,8; N, 9,4 %.

Aquest compost presenta una estructura molt semblant a **2_3**: quatre cations metàl·lics coordinats a lligands $dapdo^{2-}$ en mode de coordinació 3.11111 que presenten un entorn plano-quadrat lleugerament distorsionat, mentre els altres quatre cations $Ni^{II}$ mostren un entorn $NiO_6$ octaèdric, figura 27. La principal diferència entre **11_7** i **2_3** és la substitució dels nitrats coordinats als cations $Ni^{II}$ en entorn octaèdric, per quatre molècules de metanol i quatre anions perclorat que actuen de contraions.

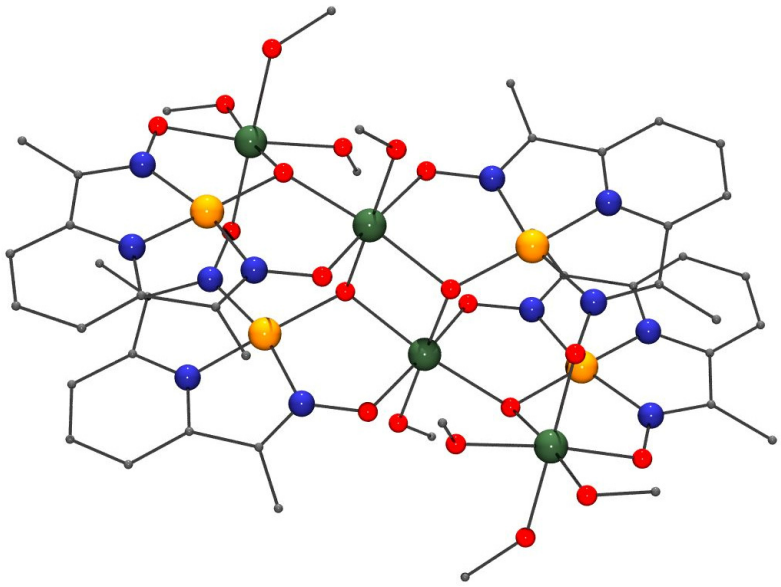

**Figura 27.** Estructura del compost **11_7**. No es mostren els contraions perclorat.

Tot i que aquest producte va ser repetit en diverses ocasions i no es va observar cap variació en els espectres d'IR dels productes, les diverses mesures magnètiques realitzades no van poder ser ajustades d'acord amb l'estructura presentada ja que s'obtenia un valor de $\chi_M T$ a 2 K superior al valor esperat de 0 $cm^3 \cdot K \cdot mol^{-1}$. Aquest fet suggereix la coprecipitació d'impureses paramagnètiques que no es van poder eliminar.

**pyC{CN}NOH**

**$[Ni_2(pyC\{CN\}NOH)_2(3\text{-}ClBzO)_2(pyC\{CN\}NO)_2]\cdot CH_2Cl_2$.** En un dels primers assajos amb el lligand pyC{CN}NOH es va sintetitzar un compost dinuclear amb fórmula $[Ni_2(pyC\{CN\}NOH)_2(3\text{-}ClBzO)_2(pyC\{CN\}NO)_2]$ (**11_8**) a partir de pyC{CN}NOH (1 mmol, 146 mg), $Ni(3\text{-}ClBzO)_2\cdot 3H_2O$ (2 mmols, 847 mg), $NaN_3$ (2 mmols, 130 mg) i $NEt_3$ (2 mmols, 202 mg) en 20 mL de $CH_2Cl_2$. La mescla resultant es va agitar durant 2 h i posteriorment es va filtrar i deixar cristal·litzar en capes amb 10 mL d'hexà. IR ($cm^{-1}$): 3440 (br), 2220 (w), 1602 (s), 1556 (m), 1464 (s), 1422 (m), 1393 (s), 1303 (w), 1263 (w), 1226 (s), 1151 (w), 1107 (w), 1037 (m), 780 (m), 764 (m), 736 (m), 712 (m). Anàlisi elemental calculat per **11_8** ($C_{42}Cl_2N_{12}Ni_2O_8H_{26}$): C, 49,70; H, 2,58; N, 16,56 %; trobat: C, 49,5; H, 2,4; N, 17,0 %.

Com es mostra a la figura 28, els lligands piridiloxima es troben coordinats en dues disposicions diferents: els lligands desprotonats s'uneixen als cations $Ni^{II}$, mitjançant dos àtoms de nitrogen, en el pla equatorial del complex i formen un doble pont oxima (en el mateix pla) entre els dos cations metàl·lics, mentre que els lligands protonats es troben coordinats de forma perpendicular a aquest pla. Els grups oxima protonats es troben encarats als àtoms d'oxigen no-coordinats dels grups carboxilats, establint així ponts d'hidrogen que estabilitzen aquesta disposició dels lligands.

Tot i que la síntesi del compost **11_8** no va presentar cap problema i es va obtenir una fracció cristal·lina ben formada i abundant, per motius desconeguts va resultar ser un compost no reproduïble.

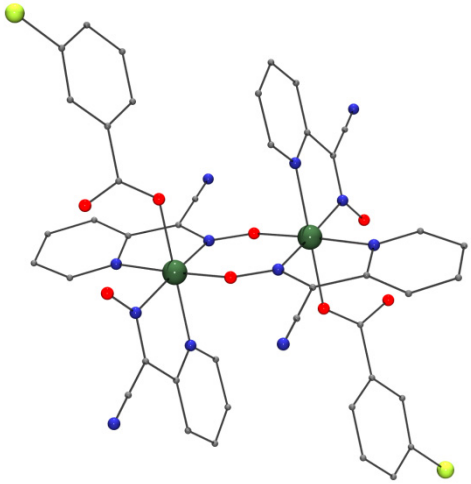

**Figura 28.** Estructura del compost $[Ni_2(pyC\{CN\}NOH)_2(3\text{-}ClBzO)_2(pyC\{CN\}NO)_2]$ (**11_8**).

**$[Ni_5(MeOH)_4(N_3)_4(Ph_2CHCOO)_2(pyC\{CN\}NO)_4]$**. Es va fer reaccionar el lligand pyC{CN}NOH amb $Ni(Ph_2CHCOO)_2{\cdot}xH_2O$, $NaN_3$ i $NEt_3$ en relació 1:1:2:1 (146 mg, 369 mg, 130 mg i 101 mg, respectivament) en 20 mL de MeOH i un cop donada la reacció i filtrada la mescla resultant, aquesta solució es va deixar cristal·litzar en capes amb 10 mL de dietilèter. Es va obtenir el compost pentanuclear $[Ni_5(MeOH)_4(N_3)_4(Ph_2CHCOO)_2(pyC\{CN\}NO)_4]$ (**11_9**), que presenta una estructura amb forma de *bowtie*, figura 29, molt similar a la del compost **4_5**, sent les principals diferències la substitució dels grups $\mu_3\text{-}OH^-$ per $\mu_3\text{-}N_3^-$ i el canvi de carboxilat ($Ph_2CHCOO^-$ enlloc de $BzO^-$).

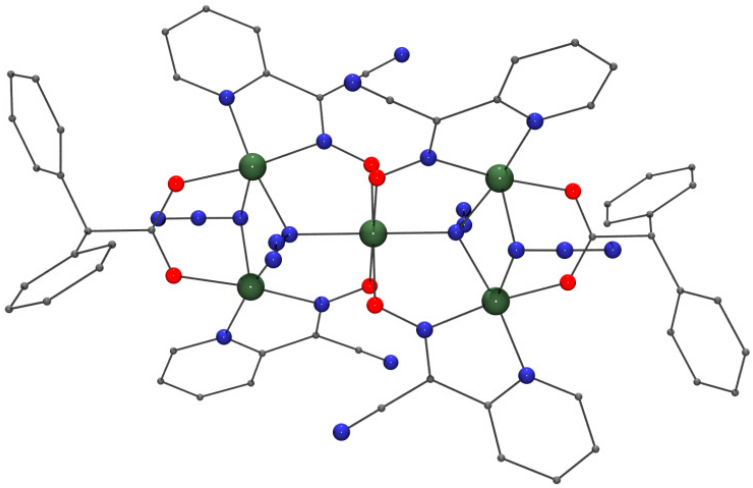

**Figura 29.** Estructura *bowtie* per al compost **11_9** amb ponts $\mu_2\text{-}N_3^-$ i $\mu_3\text{-}N_3^-$.

A la literatura es poden trobar dos compostos amb una estructura semblant a **11_9** i tots ells presenten un estat fonamental d'spin *S* = 5.[130] La mesura de susceptibilitat magnètica no es va poder ajustar satisfactòriament d'acord amb l'estructura mostrada a la figura 29, de la mateixa forma que la mesura de magnetització, que tendeix a 6 electrons, i per tant, un estat *S* = 3. Aquesta divergència, juntament amb el fet que aquesta estructura va ser resolta en un sincrotró a partir d'un cristall de mida molt reduïda (0,14x0,08x0,03 mm), fa pensar que es tracta d'un producte minoritari i que el cristall resolt no és representatiu de la mostra. L'estat fonamental *S* = 3 seria compatible amb un compost pentanuclear amb forma de *bowtie*, com **11_9**, substituint els grups $\mu_3$-$N_3^-$ per $\mu_3$-$OH^-$, és a dir, si aquest compost presentés una estructura anàloga a **4_5**.

**$(NEt_4)_2[Ni_6(N(CN)_2)_2(OH)_2(Ph_2CHCOO)_4(pyC\{CN\}NO)_6]\cdot 3CH_2Cl_2,H_2O$.** Un altre producte mesurat en sincrotró i que, com en el cas anterior, correspon a una fracció minoritària, prové de la reacció que genera el compost pentanuclear **6_1** (pyC{CN}NOH, $Ni(Ph_2CHCOO)_2$, $NaN(CN)_2$ i $NEt_3$ en relació 1:1:2:1 i diclorometà com a solvent) i consisteix en el compost hexanuclear amb fórmula $(NEt_4)_2[Ni_6(N(CN)_2)_2(OH)_2(Ph_2CHCOO)_4(pyC\{CN\}NO)_6]$ (**11_10**), figura 30. Aquest compost es pot descriure com dos triangles $[Ni_3(OH)(Ph_2CHCOO)_2(pyC\{CN\}NO)_3]$ units per dos ponts $\mu_{1,5}$-dicianamida (de forma semblant al compost **4_2**). Els triangles es troben en una disposició alternada.

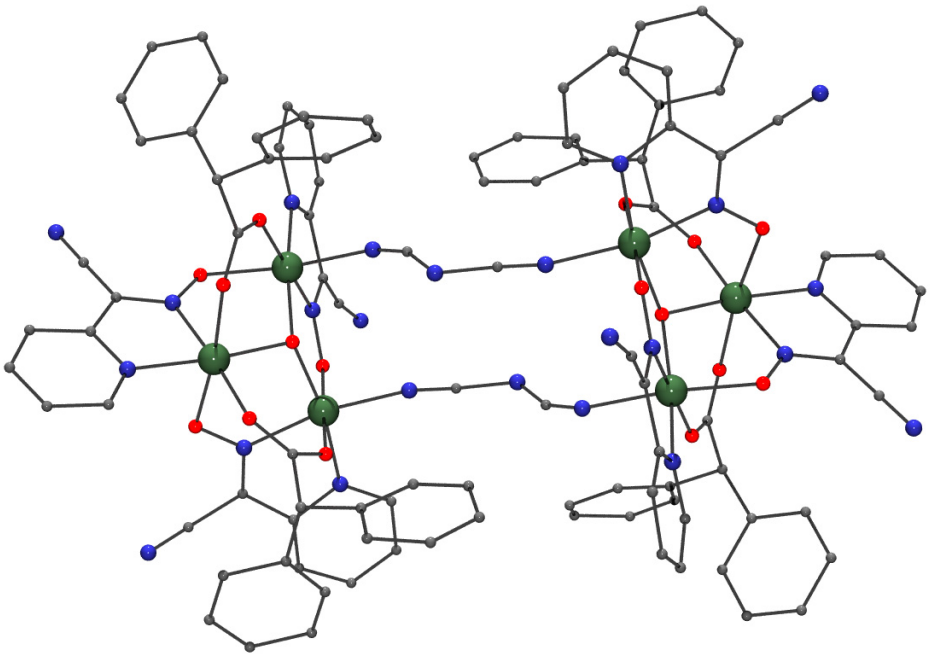

**Figura 30.** Estructura del compost **11_10**: dos triangles units per un doble pont dicianamida.

Els cations tetraetilamoni actuen de contraió i compensen la càrrega negativa dels co-lligands dicianamida. Aquests cations provenen de la reacció d'alquilació que pot patir la trietilamina en $CH_2Cl_2$,[173] que es veu catalitzada en presència de cations metàl·lics (sobretot níquel i manganès) com es troba descrit a la bibliografia.[114,174]

**$[Ni_8(MeOH)_2(N_3)_2(pyC\{CN\}NO)_6(pyC\{tz\}NO)_2(pyC\{tzH\}NO)_2(tfacac)_2]\cdot MeOH\cdot 2H_2O$.** En últim lloc, es va obtenir un compost octanuclear a partir de la reacció: pyC{CN}NOH (0,5 mmols, 73 mg), $Ni(tfacac)_2\cdot xH_2O$ (1 mmol, 362 mg), $NaN_3$ (2 mmols, 130mg) i $NEt_3$ (1 mmol, 101 mg) en 20 mL de MeOH. Es va agitar la mescla durant 2 h, es va filtrar i es va deixar cristal·litzar per capes amb 10 mL de dietilèter. IR ($cm^{-1}$): 3425 (br), 2222 (w), 2068 (s), 1628 (s), 1601 (s), 1461 (s), 1426 (w), 1383 (w), 1291 (m), 1223 (m), 1139 (m), 1064 (w), 1038 (m), 777 (w), 711 (w). Anàlisi elemental calculat per **11_11** ($C_{82}F_6N_{46}Ni_8O_{16}H_{78}$): C, 38,66; H, 3,09; N, 25,29 %; trobat: C, 38,0; H, 2,8; N, 24,9 %.

En aquesta reacció es va produir una modificació parcial del pyC{CN}NOH original que va donar el nou lligand pyC{tzH}NOH (tz = tetrazole), generant així el compost $[Ni_8(MeOH)_2(N_3)_2(pyC\{CN\}NO)_6(pyC\{tz\}NO)_2(pyC\{tzH\}NO)_2(tfacac)_2]$ (**11_11**). Aquest compost presenta dos lligands que contenen el grup tetrazole protonat i monocoordinat mentre que en els altres dos aquest grup està desprotonat i coordina dos cations metàl·lics, unint les dues subunitats tetranuclears que formen el compost, figura 31.

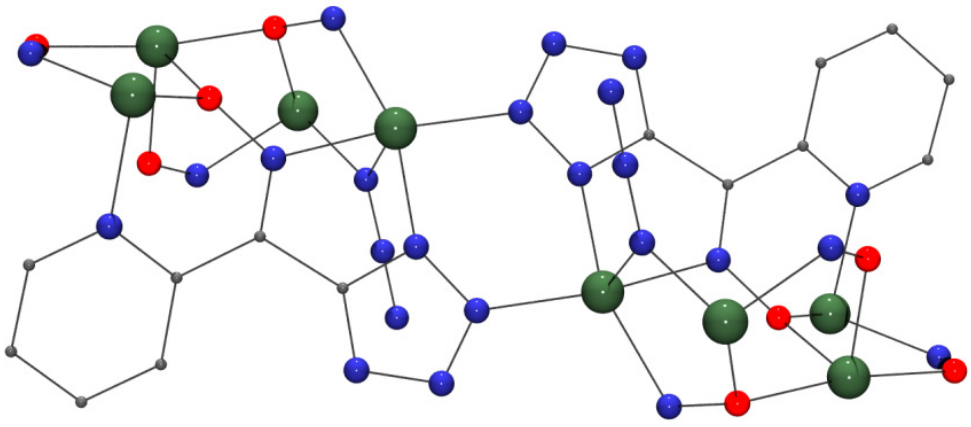

**Figura 31.** *Core* del compost **11_11** amb els lligands $pyC\{tz\}NO^{2-}$ en què els grups tetrazole coordinen els dos ions $Ni^{II}$ centrals.

En la modificació del lligand, es va donar una cicloaddició de nitrils i azidur per formar un grup tetrazole, esquema 10, una reacció ben coneguda en química orgànica,[175] catalitzada en ocasions per cations metàl·lics.[176]

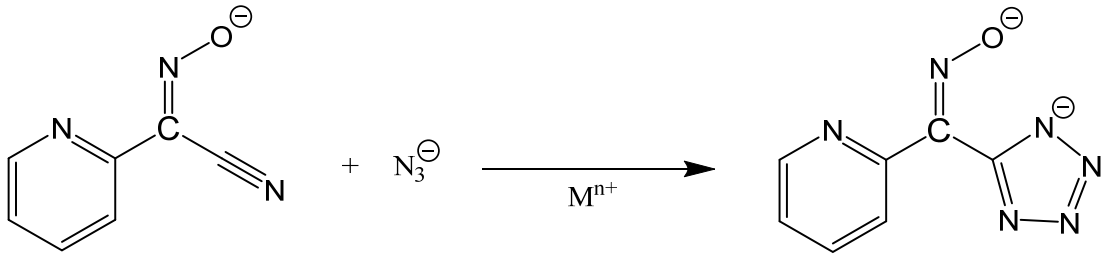


**Esquema 10.** Reacció de formació del lligand pyC{tz}$NO^{2-}$.

La reacció de formació del compost **11_11** és més complexa que la major part de reaccions estudiades anteriorment ja que conté la formació *in situ* del nou lligand. La formació d'aquest lligand és, probablement, el factor que va impedir la repetició d'aquest compost.

Posteriorment, es va provar de sintetitzar directament el lligand pyC{tzH}NOH a partir de pyC{CN}NOH i $NaN_3$ en un reactor microones per tal d'afavorir-ne la formació,[177] però es va recuperar el lligand de partida.

**<u>$DapdoH_2$ + azidur</u>**

En fer reaccionar el lligand $dapdoH_2$ amb l'anió azidur i diverses sals de $Ni^{II}$ (carboxíliques i no carboxíliques) es va observar l'oxidació del $Ni^{II}$ a $Ni^{IV}$ i la formació del compost mononuclear $[Ni(dapdo)_2]$ (**11_12**), caracteritzat el 1973,[89] en què l'ió $Ni^{IV}$ es troba coordinat als sis àtoms de nitrogen dels dos lligands $dapdo^{2-}$, figura 32. La disminució del potencial d'oxidació $Ni^{II}/Ni^{IV}$ és conseqüència de l'elevada energia d'estabilització de la configuració $d^6$ d'spin baix que produeix el lligand $dapdoH_2$ pel seu elevat camp cristal·lí.

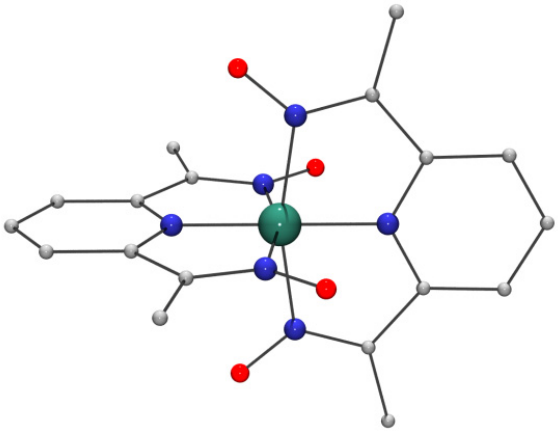

**Figura 32.** Estructura del compost mononuclear **11_12**. L'ió $Ni^{IV}$ es mostra de color verd fosc.

Per tal d'evitar l'oxidació del níquel(II), es van realitzar una sèrie de proves, com ara la reacció en atmosfera inert ($N_2$) o la repetició de les síntesis anteriors en presència d'àcid ascòrbic (un conegut antioxidant), però aquestes reaccions no van donar cap producte caracteritzable.

També es va provar de repetir les síntesis anteriors afegint un agent precipitant com el $NH_4PF_6$ (per tal d'afavorir la formació de compostos iònics i la precipitació d'aquests en combinar-se amb aquest agent), com en la reacció realitzada a partir de $dapdoH_2$, $Ni(3\text{-}ClBzO)_2$, $NaN_3$, $NH_4PF_6$ i $NEt_3$ (en proporció 1:2:2:2:2) en MeOH, que va generar cristalls en forma de petites agulles de color taronja. L'espectre d'IR d'aquesta mostra va permetre determinar que conté el lligand $dapdoH_2$ (en algun dels seus estats) i azidur, i la mesura de susceptibilitat realitzada va posar de manifest que es tracta d'un compost ferrimagnètic (amb presència d'interaccions ferromagnètiques i antiferromagnètiques). Malauradament, l'estructura d'aquest compost no va poder ser resolta en cap de les seves repeticions a causa de la forma i dimensions dels cristalls obtinguts.

# 4

# Discussió global dels resultats

## 4.1. Propietats estructurals i magnètiques dels compostos amb lligand dapdoH$_2$

En aquesta tesi es presenten els següents compostos sintetitzats amb el lligand dapdoH$_2$:

*Article 1*

[Ni$_2$(dapdo)$_2$] (**1_1**)

[Ni$_3$(dapdoH$_2$)(H$_2$O)(OH)(BzO)$_3$(dapdo)] (**1_2**)

[Ni$_3$(H$_2$O)$_2$(AcO)$_4$(dapdoH)$_2$] (**1_3**)

[Ni$_4$(H$_2$O)$_3$(AcO)$_3$(dapdo)(dapdoH)$_2$](AcO) (**1_4**)

*Article 2*

[Ni$_5$(MeOH)$_2$(BzO)$_2$(dapdo)$_2$(dapdoH)$_2$(N(CN)$_2$)$_2$] (**2_1**)

[Ni$_5$(MeOH)$_2$(3-ClBzO)$_2$(dapdo)$_2$(dapdoH)$_2$(N(CN)$_2$)$_2$] (**2_2**)

[Ni$_8$(MeOH)$_4$(dapdo)$_4$(NO$_3$)$_4$(OH)$_4$] (**2_3**)

[Ni$_{10}$(MeOH)(dapdo)$_8$(N(CN)$_2$)$_2$(MeO)](NO$_3$) (**2_4**)

*Article 3*

[Ni$_3$(dapdoH$_2$)(3-ClBzO)(dapdo)(dapdoH)OH](3-ClBzO) (**3_1**)

(Et$_2$NH$_2$)$_6$[Ni$_8$(H$_2$O)$_2$(dapdoH)$_4$(SO$_4$)$_9$] (**3_2**)

(Et$_3$NH)$_2$[Ni$_{10}$(MeOH)$_4$(dapdo)$_8$](BF$_4$)$_6$ (**3_3**)

*Article 10*

[Ni$_4$(Medpt)$_2$(N$_3$)$_4$(dapdo)$_2$] (**10_2**)

*Compostos no publicats*

$[Ni_3(N,N'\text{-}Me_2en)(dapdo)_2(N_3)_2]$ (**11_5**)

$[Ni_8(MeOH)_8(dapdo)_4(OH)_4](ClO_4)_4$ (**11_7**)

$[Ni(dapdo)_2]$ (**11_12**)

En primer lloc, val la pena destacar que aquests compostos no només són els primers exemples reportats de compostos polinuclears de $Ni^{II}$ amb el lligand $dapdoH_2$, sinó que són els únics compostos d'aquest tipus que es poden trobar a la bibliografia en acabar aquesta tesi.

L'anàlisi detallada d'aquests compostos i del seu estudi magnètic ha permès una millor comprensió del comportament d'aquest lligand en la química del $Ni^{II}$:

### 4.1.1. Formació de nous compostos

S'ha observat una clara tendència del lligand $dapdoH_2$ a generar compostos de nuclearitat baixa amb lligands carboxilat i β-dicetonat ($Ni_2$ – $Ni_5$) i en presència d'una amina bidentada ($Ni_3$), mentre que partint de sals amb anions inorgànics es van obtenir compostos de major nuclearitat: $Ni_8$ – $Ni_{10}$.

En fer reaccionar el lligand $dapdoH_2$ amb $Ni(tfacac)_2$ o $Ni(acac)_2$ es va obtenir el compost **1_1**, format únicament pel lligand (en el seu estat $dapdo^{2-}$) i $Ni^{II}$, que presenta una geometria plano-quadrada. Així, es pot dir que no s'ha pogut obtenir cap compost format pel lligand $dapdoH_2$, $Ni^{II}$ i anions β-dicetonat.

Pel què fa als compostos obtinguts a partir de sals carboxíliques, cal comentar que s'han obtingut 6 compostos de baixa nuclearitat: tres compostos trinuclears (**1_2**, **1_3** i **3_1**), un compost tetranuclear (**1_4**) i finalment dos sistemes pentanuclears (**2_1** i **2_2**). Aquests dos últims són, casualment, els únics en què els carboxilats actuen com lligands terminals i no com lligands pont.

D'altra banda, la reacció amb sals no carboxíliques va generar tres compostos de nuclearitat $Ni_8$, **2_3**, **3_2** i **11_7**, i dos compostos de nuclearitat $Ni_{10}$, **2_4** i **3_3**. És remarcable el fet que aquests últims són els compostos de major nuclearitat obtinguts per aquest lligand fins ara.

Aquest augment de la nuclearitat es deu, molt probablement, al fet que aquests anions, o bé no es coordinen ($ClO_4^-$, $BF_4^-$), o bé actuen de lligands terminals ($NO_3^-$), creant així un elevat nombre de vacants a l'esfera de coordinació dels metalls que permet el creixement del compost. L'únic anió no carboxilat que actua com a lligand pont és el sulfat, que és capaç de crear un compost de nuclearitat elevada gràcies a la gran varietat de modes de coordinació trobats (4.1111, 3.2100 i 2.100) i a la seva geometria tetraèdrica, que li permet formar enllaços en diferents direccions i evitar la constricció del compost.

Per últim, comentar que es va obtenir un compost trinuclear ($Ni_3$) en fer reaccionar el lligand dapdo$H_2$ amb $Ni(NO_3)_2$, $NaN_3$ i una amina bidentada (N,N'-$Me_2$en), **11_5**. En aquest cas, l'anió nitrat no es troba coordinat, però és possible que no s'hagi pogut assolir una nuclearitat més elevada per la coordinació de l'amina, que ocupa dues posicions de l'esfera de coordinació.

Un altre aspecte a tenir en compte és la formació d'estructures o fragments d'alta estabilitat, que es repeteixen tot i canviar les condicions de síntesi. Un primer exemple d'aquest fet és el compost **1_4**, que si s'analitza detalladament, es pot veure que està format per la unió de les estructures **1_2** i **1_3**: presenta un grup dapdo$^{2-}$ en mode de coordinació 3.11111 que genera un $Ni^{II}$ plano-quadrat i uneix un catió $Ni^{II}$ per cada pont oxima com al compost **1_2**, però en aquesta ocasió, un d'aquests ions es troba coordinat, mitjançant un pont oxima i dos ponts carboxílics (ponts *syn-syn* 2.11 i 2.20) a un quart ió $Ni^{II}$, de la mateixa forma que al compost **1_3**.

També s'ha observat aquest comportament en dos compostos octanuclears **2_3** i **11_7**, i en els compostos decanuclears **2_4** i **3_3**, i és que la substitució d'un anió coordinant ($NO_3^-$) per un anió no-coordinant ($ClO_4^-$, $BF_4^-$) provoca la coordinació d'una molècula de solvent i fa que aquests nous anions actuïn de contraió; enlloc de generar nous compostos amb noves nuclearitats i topologies.

### 4.1.2. Capacitat coordinativa

S'ha provat la gran capacitat coordinativa d'aquest lligand, pel qual s'han observat fins a cinc modes de coordinació diferents: 1.00111 (**1_2**, **3_1** i **11_12**), 2.10111 (**1_1**, **1_3**, **1_4**, **10_2** i **11_5**), 3.11111 (**1_2**, **1_4**, **2_1**, **2_2**, **2_3**, **2_4**, **3_1**, **3_3** i **11_7**), 3.20111 (**1_4**, **2_1**, **2_2**, **3_2** i **11_7**) i 5.22111 (**2_4** i

**3_3**). És digne de menció el fet que els modes 3.20111 i 5.22111 han estat caracteritzats per primera vegada per aquest lligand durant aquesta tesi; sent el segon mode el de major denticitat trobat fins ara per aquest lligand.

Un aspecte destacable d'aquest lligand és que, quan actua en el mode de coordinació 2.10111 i 3.11111 (en el seu estat desprotonat, dapdo$^{2-}$), presenta una certa tendència a generar un entorn plano-quadrat a l'ió Ni$^{II}$ coordinat pels tres àtoms de nitrogen, com demostren els compostos **1_1**, **10_2** i **11_5** (mode 2.10111) i **1_2**, **1_4**, **2_1**, **2_2**, **2_3**, **2_4**, **3_1**, **3_3** i **11_7** (mode 3.1111). Com s'ha comentat anteriorment, l'estabilització de la geometria plano-quadrada per part d'aquest lligand es deu al fet que és un lligand de camp fort. L'única excepció que s'ha trobat són els compostos **1_3** i **1_4**, que tot i contenir diversos lligands que actuen en el mode de coordinació 2.10111, els centres metàl·lics coordinats a aquests lligands presenten una geometria octaèdrica.

Sorprenentment, el nou mode de coordinació 5.22111 genera entorns octaèdrics en els cations Ni$^{II}$ coordinats al lligand dapdo$^{2-}$. Aquest comportament porta a pensar que hi ha un canvi important en la densitat electrònica del lligand quan el grup oxima coordina el segon ió metàl·lic, que provoca una disminució de l'energia d'estabilització del camp cristal·lí del lligand.

### 4.1.3. Magnetisme

Com s'ha vist, la coordinació del lligand dapdoH$_2$ en els modes de coordinació 2.10111 i 3.11111 genera entorns plano-quadrats en els ions Ni$^{II}$, fet que porta associat la pèrdua del paramagnetisme d'aquests cations. Tot i això, la combinació d'ions Ni$^{II}$ en entorns plano-quadrats ($S$ = 0) i octaèdrics ($S$ = 1) ha permès l'estudi magnètic d'aquests compostos i copsar certes tendències en el comportament magnètic d'aquest lligand.

La primera observació, i més evident, és que tots els compostos obtinguts per aquest lligand presenten un comportament antiferromagnètic (disminució de $\chi_M T$ en disminuir $T$). Així, es confirma que el lligand dapdoH$_2$ genera acoblaments antiferromagnètics ($J$ < 0), d'acord amb el que s'havia trobat a la bibliografia.[86,94-99]

A la bibliografia també es troben una sèrie de correlacions magneto-estructurals per a l'acoblament mitjançant ponts oxima de sistemes de $Cu^{II}$ i $Mn^{III}$, que reflexen que, en el cas del coure, la interacció (antiferromagnètica) disminueix en augmentar la torsió M-N-O-M,[165] i pel manganès, s'observa que *J* també depèn de la torsió M-N-O-M fins a arribar a capgirar el signe de la interacció per certes torsions.[166] L'any 2010, Brechin, Colacio *et al.* van proposar la primera correlació per a l'acoblament Ni-N-O-Ni,[167]en què s'establia que l'antiferromagnetisme disminuïa en augmentar la torsió del pont oxima, i que era possible arribar a canviar el signe de la interacció per valors de torsió lleugerament superiors a 80°.

Analitzant els diversos acoblaments trobats per als compostos formats pel lligand dapdo$H_2$ s'han trobat una sèrie d'acoblaments mediats únicament per ponts oxima que presenten un ampli interval d'angles de torsió Ni-N-O-Ni, taula 2. Si es representa el valor calculat de *J* per a cadascuna d'aquestes interaccions respecte l'angle de torsió, s'obté un tendència parabòlica, figura 33, que confirma les prediccions trobades a la literatura: acoblaments fortament antiferromagnètics per torsions petites, disminució de la interacció en augmentar la torsió fins arribar a un valor màxim (menys antiferromagnètic o fins i tot lleugerament ferromagnètic) per a torsions superiors a 80° (en aquest cas, proper als 90°).

**Taula 2.** Angles de torsió [°] trobats i constants d'acoblament [$cm^{-1}$] calculades per aquestes interaccions.

| Torsió Ni-N-O-Ni | *J* | compost |
|---|---|---|
| 50,0 | -29,6 | **3_3** |
| 92,5 | 1,2 | **1_4** |
| 103,3 | -0,5 | **2_2** |
| 103,5 | -0,4 | **2_1** |
| 117,0 | -4,8 | **2_4** |
| 117,8 | -8,4 | **3_3** |

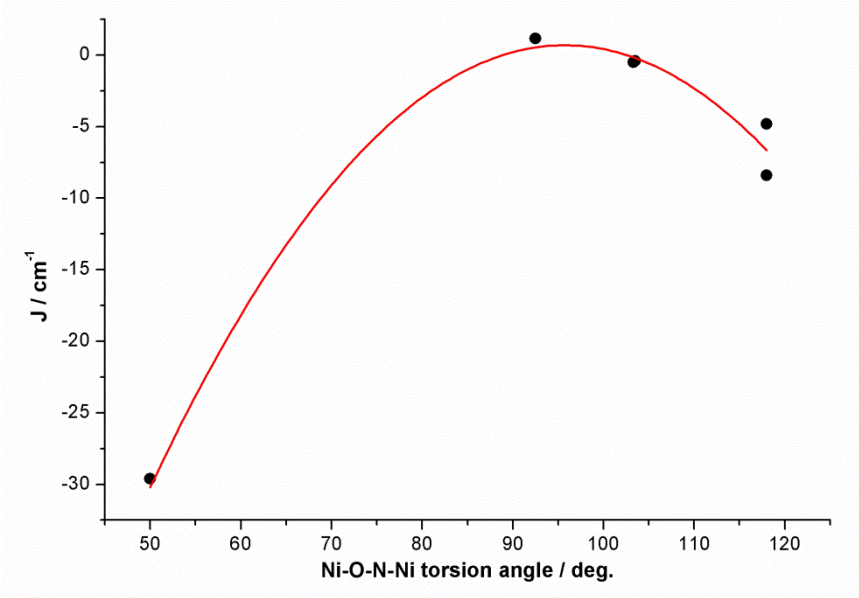


**Figura 33.** Variació del valor de la constant d'acoblament (*J*) en funció de l'angle de torsió.

### 4.1.4. DapdoH$_2$ + azida

És ben coneguda la capacitat de l'anió azidur de generar interaccions ferromagnètiques en actuar de lligand pont en el mode *end-on* o 2.20.[119] Per tal de formar compostos amb un estat fonamental d'spin el més elevat possible es van realitzar un elevat nombre de reaccions amb diferents sals de $Ni^{II}$ i $NaN_3$. En la gran majoria d'ocasions, es van obtenir uns cristalls ròmbics i foscos que malauradament contenien el compost mononuclear de $Ni^{IV}$ **11_12**. La formació d'aquest compost, caracteritzat per Sproul i Stucky fa 40anys,[89] confirma el fet que aquest és un lligand de camp fort, capaç de generar entorns plano-quadrats en cations $Ni^{II}$ per coordinació d'un lligand, i de fomentar la oxidació d'aquest catió en coordinar dos molècules de $dapdo^{2-}$. Es van repetir diverses reaccions que havien generat el compost mononuclear **11_12** en una atmosfera inert ($N_2$) però aquestes síntesis no van donar resultat. En un últim intent, també es va provar d'afegir àcid ascòrbic a les reaccions inicials per tal d'evitar la oxidació d'aquest metall, però, de nou, no es va obtenir cap producte caracteritzable.

Posteriorment, es van obtenir una sèrie de cristalls que contenien $Ni^{II}$, el lligand dapdoH$_2$ i l'anió azidur i presentaven un comportament ferrimagnètic (combinació d'interaccions ferromagnètiques i antiferromagnètiques), que confirma la presència de ponts azida entre centres metàl·lics, però aquests cristalls no van resultar adequats per a la seva resolució estructural.

Finalment, es van caracteritzar els compostos **10_2** i **11_5** que contenen el lligand dapdo$H_2$ i l'anió azidur en el mode desitjat (*end-on*), però en tots dos casos aquest pont s'estableix entre un catió $Ni^{II}$ octaèdric i un catió $Ni^{II}$ plano-quadrat (diamagnètic), de forma que no hi ha acoblament magnètic possible entre ells. El compost **10_2** també presenta un pont azida en el mode *end-to-end* entre un ió $Ni^{II}$ amb entorn octaèdric i un segon ió amb entorn plano-quadrat. Així, aquests compostos es comporten, magnèticament, com compostos mononuclears.

## 4.2. Propietats estructurals i magnètiques dels compostos amb lligand pyC{CN}NOH

Els compostos caracteritzats per aquest lligand són:

*Article 4*

$[Ni_3(MeOH)_2(BzO)(OH)(pyC\{CN\}NO)_4]$ (**4_1**)

$(NEt_3H)[Ni_6(H_2O)(MeOH)(3\text{-}ClBzO)_2(N(CN)_2)(OH)_2(pyC\{CN\}NO)_8]$ (**4_2**)

$[Ni_4(MeOH)_2(tfacac)_2(MeO)_2(pyC\{CN\}NO)_4]$ (**4_3**)

$[Ni_5(MeOH)_4(3\text{-}ClBzO)_4(OH)_2(pyC\{CN\}NO)_4]$ (**4_4**)

$[Ni_5(H_2O)_4(N_3)_2(BzO)_2(OH)_2(pyC\{CN\}NO)_4]$ (**4_5**)

*Article 5*

$[Ni_3(MeOH)_2(AcO)(OH)(pyC\{CN\}NO)_4]$ (**5_1**)

$(NEt_4)[Ni_3(H_2O)(3\text{-}ClBzO)_2(OH)(pyC\{CN\}NO)_4]$ (**5_2**)

$(NEt_3H)[Ni_3(H_2O)_3(OH)(Ph_2CHCOO)_3(pyC\{CN\}NO)_3]$ (**5_3**)

*Article 6*

$NEt_4[Ni_5(H_2O)(OH)_2(Ph_2CHCOO)_5(pyC\{CN\}NO)_4]$ (**6_1**)

$[Ni_5(H_2O)_2Cl_2(pyC\{CN\}NO)_8]$ (**6_2**)

$[Ni_5(MeOH)_6Br_3(MeO)_4(pyC\{CN\}NO)_3]$ (**6_3**)

$[Ni_5(MeOH)_6Cl_3(MeO)_4(pyC\{CN\}NO)_3]$ (**6_3b**)

$[Ni_5(H_2O)_3(NCS)_2(OH)_2(pyC\{CN\}NO)_6]$ (**6_4**)

$[Ni_5(H_2O)_{2,5}(MeOH)(MeO)_2(OH)_{1,5}(pyC\{CN\}NO)_6](NO_3)_{0,5}$ (**6_5**)

*Article 7*

$[Ni_{13}Na_2(H_2O)_2(MeOH)_{14}(OH)_4(pyC\{CN\}NO)_8(SO_4)_8]_n$ (**7_1**)

*Compostos no publicats*

$[Ni(MeOH)_2(pyC\{CN\}NOH)_2]$ (**11_1**)

$[Ni_3(MeOH)_2(CF_3COO)(OH)(pyC\{CN\}NO)_4]$ (**11_2**)

$[Ni(dpt)(N_3)(pyC\{CN\}NO]$ (**11_3**)

$[Ni_2(pyC\{CN\}NOH)_2(3\text{-}ClBzO)_2(pyC\{CN\}NO)_2]$ (**11_8**)

$[Ni_5(MeOH)_4(N_3)_4(Ph_2CHCOO)_2(pyC\{CN\}NO)_4]$ (**11_9**)

$(NEt_4)_2[Ni_6(N(CN)_2)_2(OH)_2(Ph_2CHCOO)_4(pyC\{CN\}NO)_6]$ (**11_10**)

$[Ni_8(MeOH)_2(N_3)_2(pyC\{CN\}NO)_6(pyC\{tz\}NO)_2(pyC\{tzH\}NO)_2(tfacac)_2]$ (**11_11**)

La reactivitat del lligand pyC{CN}NOH amb $Ni^{II}$ era totalment desconeguda a l'inici d'aquesta tesi, sent aquests compostos els primers exemples d'aquesta química. És més, aquests són també els únics compostos caracteritzats per aquest lligand i $Ni^{II}$ fins la data.

Les característiques més importants d'aquests sistemes són:

### 4.2.1. Modes de coordinació

El lligand pyC{CN}NOH ha generat tres modes de coordinació diferents: 1.011 (**4_1**, **4_2**, **6_2**, **11_1**, **11_3** i **11_8**), 2.111 (**4_1**, **4_2**, **4_3**, **4_4**, **4_5**, **5_1**, **5_2**, **5_3**, **6_1**, **6_2**, **6_3**, **6_4**, **6_5**, **7_1**, **11_2**, **11_8**, **11_9**, **11_10** i **11_11**) i 3.211 (**6_2**). D'aquests, els modes de coordinació 1.011 i 3.211 han estat caracteritzats per primera vegada durant l'elaboració d'aquest treball.

Aquest lligand presenta, com s'ha comentat anteriorment, una quarta posició potencialment coordinable: el grup nitril. Cap dels 22 compostos sintetitzats amb al lligand pyC{CN}NOH en aquest treball ni dels 9 trobats a la bibliografia (tots ells sintetitzats al grup) ha pogut assolir la coordinació d'aquest grup. És per aquest motiu que, si bé la terminologia correcta per als modes de coordinació d'aquest lligand hauria de ser 1.0110, 2.1110 i 3.2110, s'ha negligit l'últim número (0), que correspondria al grup -C≡N.

### 4.2.2. Compostos basats en fragments triangulars

La major part dels compostos obtinguts pel lligand pyC{CN}NOH amb $Ni^{II}$ generen estructures triangulars $Ni_3/\mu_3$-OH/oxima (**4_1**, **5_1**, **5_2**, **5_3** i **11_2**) o basades en aquests fragments $Ni_3/\mu_3$-OR/oxima, R = H, Me, (**4_2**, **4_3**, **4_4**, **4_5**, **6_1**, **6_4**, **6_5**, **7_1** i **11_10**), així com un compost format pel fragment $Ni_3/\mu_3$-$N_3$/oxima (**11_9**). El compost pentanuclear **6_2** també està basat en fragments triangulars, però en aquest cas l'àtom d'oxigen que actua de pont prové d'un grup oxima, molt probablement perquè la seva síntesi es va realitzar en $CH_2Cl_2$ i, per tant, no hi havia grups $OR^-$ disponibles. Entre els diferents compostos sintetitzats generats a partir de fragments triangulars $Ni_3/\mu_3$-OR/oxima destaca el compost monodimensional amb nuclearitat $\{Ni_{13}Na_2\}_n$, que serà analitzat amb detall a l'apartat següent.

El fet més destacable d'aquest lligand és que, si bé és cert que els fragments triangulars $Ni_3/\mu_3$-OH/oxima es troben en diversos compostos de nuclearitat elevada prèviament caracteritzats, i que s'havien caracteritzat sistemes triangulars aïllats per coure,[113,115,123a,136,178] manganès,[16,116] ferro[117] i cobalt[118], els compostos **4_1**, **5_1**, **5_2**, **5_3** i **11_2** són els primers exemples de triangles discrets $Ni_3/\mu_3$-OR/oxima. L'acidesa del lligand pyC{CN}NOH és, probablement, el motiu pel qual aquest és l'únic lligand 2-piridiloxima capaç de generar els sistemes triangulars $Ni_3/\mu_3$-OR/oxima aïllats.

Els compostos mononuclears **11_1** i **11_3**, el compost dinuclear **11_8** i els compostos pentanuclear **6_3** i octanuclear **11_11** són els únics compostos derivats d'aquest lligand que no presenten una estructura basada en fragments triangulars.

### 4.2.3. Compost $\{Ni_{13}Na_2\}_n$

Es va caracteritzar un compost monodimensional obtingut a partir del lligand pyC{CN}NOH i $NiSO_4$ que es pot descriure com una subunitat $\{Ni_{12}Na_2\}$ que s'estén a l'espai en coordinar un ió $Ni^{II}$ monomèric, de forma que es genera la cadena $\{Ni_{12}Na_2\text{-}Ni\text{-}\}_n$ (**7_1**). Un dels trets més destacables d'aquest compost és que la subunitat $\{Ni_{12}Na_2\}$ està formada per quatre triangles $\{Ni_3(\mu_3\text{-}OH)(SO_4)(pyC\{CN\}NO)_2\}^+$ que se situen, per efecte plantilla o *template synthesis*, al voltant d'un catió $Na^+$, al qual es coordinen a través dels grups sulfat. La coordinació del segon catió $Na^+$ també es realitza a través d'un grup sulfat, però aquest catió completa la seva esfera de coordinació mitjançant molècules de solvent.

Un altre aspecte a destacar d'aquest compost és que el fragment $\{Ni_{13}Na_2\}$ presenta la major nuclearitat per al sistema sulfat/oxima i la segona més gran per als sistemes Ni/oxima i $Ni/SO_4$.

### 4.2.4. Compostos pentanuclears

Una altra clara tendència que presenta el lligand pyC{CN}NOH és la de formar compostos de nuclearitat $Ni_5$. Així, un 40% dels compostos sintetitzats amb aquest lligand (9 de 22) presenten aquesta nuclearitat: **4_4**, **4_5**, **6_1**, **6_2**, **6_3**, **6_3b**, **6_4**, **6_5** i **11_9**.

Aquests 9 compostos presenten fins a 5 topologies diferents (figura 34): triangles que comparteixen un vèrtex o *bowtie* amb un grup central $\mu_3$-X (X = $OR^-$, $N_3^-$) (**I**), *bowtie* amb un pont oxima central (**II**), *bowtie* fortament distorsionat (**III**), triangle unit a una subunitat dinuclear o triangle amb *nansa* (**IV**) i cubà unit a un catió metàl·lic per un triple pont oxima (**V**).

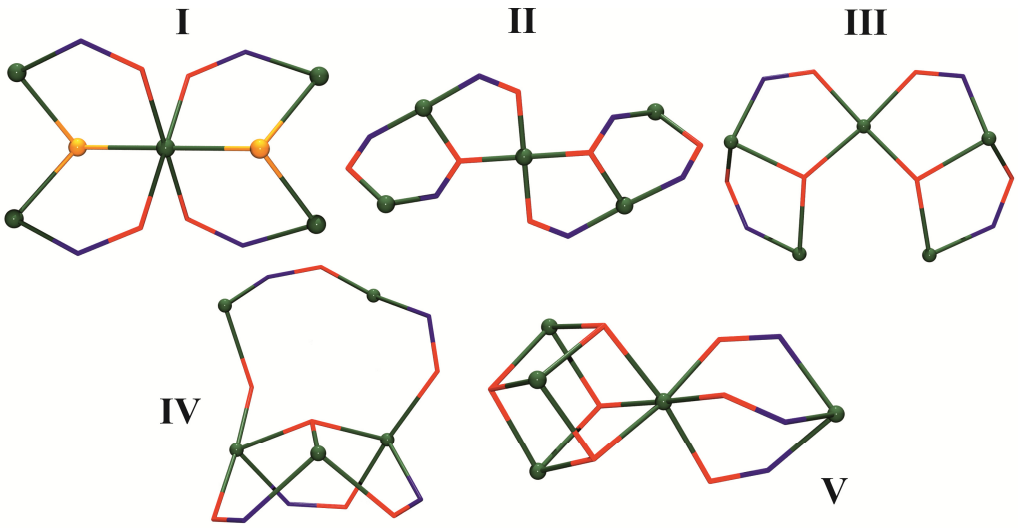


**Figura 34.** Topologies caracteritzades per al sistema $Ni_5$/pyC{CN}NOH.

L'efecte de l'anió de partida sobre la topologia dels compostos pentanuclears serà discutit posteriorment.

### 4.2.5. Magnetisme – sistemes triangulars

Inicialment es van obtenir els compostos **4_1**, **4_2**, **4_3**, **4_4** i **4_5**, en què els dos primers eren els primers exemples de triangles $Ni_3$/$\mu_3$-OH/oxima aïllats (el compost **4_2** està format per dos triangles units per un pont dicianamida però magnèticament es pot considerar com dos triangles aïllats) i els tres últims exemples de sistemes basats en fragments triangulars $Ni_3$/$\mu_3$-OH/oxima amb forma de papallona (**4_3**) i *bowtie* (**4_4** i **4_5**). Per tal d'estudiar el comportament d'aquests sistemes triangulars es van realitzar càlculs per DFT en col·laboració amb el Dr. Eliseo Ruiz que van determinar que els acoblaments mitjançant un grup $\mu_3$-OR i un lligand oxima promouen un acoblament moderadament antiferromagnètic i que la principal via d'acoblament és a través del grup $\mu_3$-OH central (pont Ni-O-Ni), mentre que l'angle de torsió Ni-N-O-Ni no presenta un efecte determinant (de forma similar als triangles de $Cu^{II}$[113] però a l'inrevés que els de $Mn^{III}$[169]), així com el fet que que la interacció mitjançant el grup $\mu_3$-OR és més intensa (més antiferromagnètica) quan el lligand central és un grup alcoxo que no pas quan es tracta d'un grup hidroxo.

Posteriorment, es van obtenir tres nous exemples de triangles $Ni_3/\mu_3$-OH/oxima, compostos **5_1**, **5_2** i **5_3**, i es va realitzar una correlació magneto-estructural que confirmava les tendències apuntades pels càlculs DFT.

Finalment, s'ha ampliat aquesta correlació introduint-hi tots els compostos basats en fragments triangulars $Ni_3/\mu_3$-OH/oxima caracteritzats en aquesta tesi (**6_1**, **6_4**, **6_5**, **7_1** i **11_2**) i s'ha trobat que, en tots ells, la intensitat d'aquest acoblament presenta una dependència directa amb l'angle Ni-O-Ni i una elevada dispersió pel què fa a l'angle de torsió Ni-N-O-Ni, com mostra la figura 35.

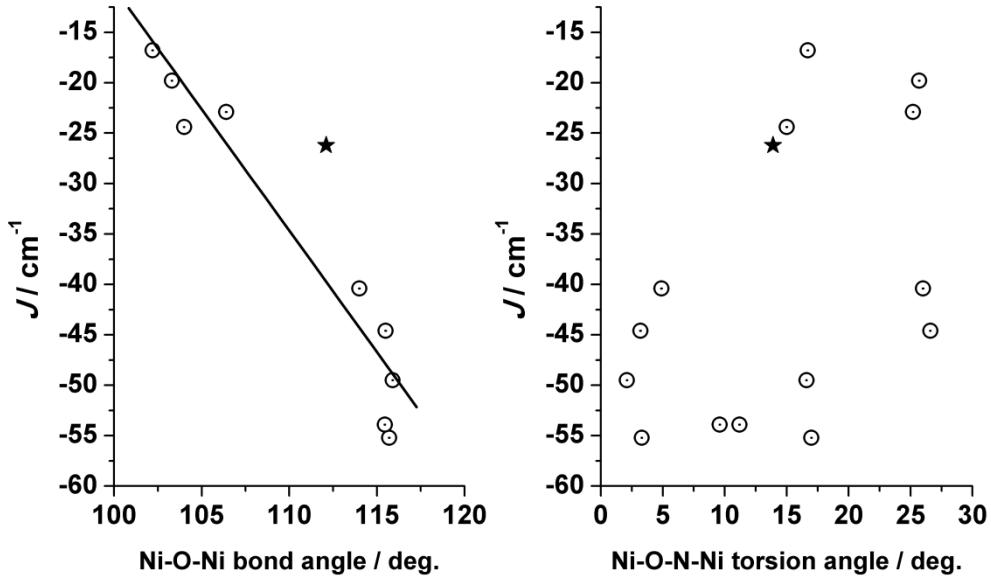


**Figura 35.** Representació de la variació de la constant d'acoblament, *J*, amb l'angle Ni-O-Ni (esquerra) i amb l'angle de torsió Ni-N-O-Ni (dreta) per als sistemes $Ni_3/\mu_3$-OH/oxima obtinguts en aquesta tesi. Els punts marcats amb una estrella representen el triangle equilàter **5_3**.

Per altra banda, s'ha analitzat la relació entre les constants d'acoblament del sistema i l'estat fonamental (*S*) d'aquest. A la introducció s'ha comentat que els sistemes triangulars antiferromagnèticament acoblats són un clar exemple de sistemes magnèticament frustrats, que poden presentar un estat fonamental $S = 1$, $S = 0$ o tots dos alhora, depenent de la relació $J_2/J_1$ (sent $J_1$ la interacció promoguda pel pont $\mu_3$-OH/oxima i $J_2$ l'altra, generalment $\mu_3$-OH/carboxilat). La figura 36 mostra les energies dels diferents nivells d'spin en funció de la relació $J_2/J_1$ i el quocient $J_2/J_1$ per a cadascun dels compostos triangulars caracteritzats.

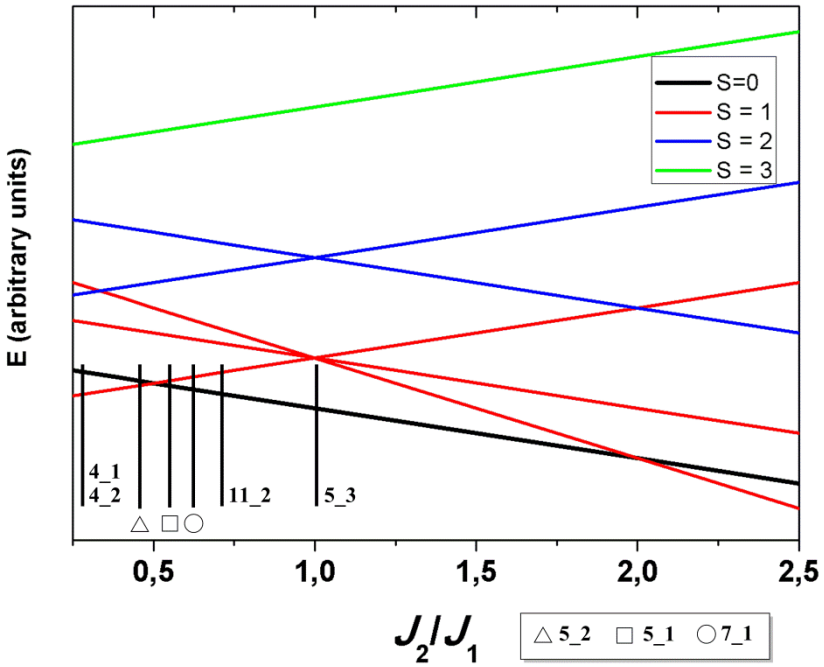


**Figura 36.** Variació de l'energia dels diversos nivells magnètics (per un triangle antiferromagnètic amb $S_1 = S_2 = S_3 = 1$) respecte el quocient $J_2/J_1$. Les línies verticals indiquen el valor de $J_2/J_1$ per a cadascun dels compostos que presenten aquesta topologia.

Els compostos **4_1** i **4_2** tenen uns valors de $J_1$, $J_2$ i $J_2/J_1$ de -55,2 $cm^{-1}$, -16,8 $cm^{-1}$, 0,30 i -53,9 $cm^{-1}$, -19,8 $cm^{-1}$ i 0,36, respectivament, que generen un estat fonamental d'spin $S = 1$ (el compost **4_2** presenta un valor de $\chi_M T$ lleugerament inferior a l'esperat per l'acoblament, a molt baixa temperatura, a través del co-lligand dicianamida).

Els compostos **5_1** i **5_2** presenten un valor de $J_2/J_1$ de 0,55 i 0,46 que provenen dels valors de $J_1$ i $J_2$ següents: -44,6 $cm^{-1}$ i -24,4 $cm^{-1}$ per **5_1** i -49,5 $cm^{-1}$ i -22,9 $cm^{-1}$ per **5_2**. Aquests valors es troben molt propers al punt de frustració $J_2/J_1 = 0,5$ i per tant, en tots dos casos, hi haurà població dels dos nivells magnètics $S = 0$ i $S = 1$ fins i tot a molt baixa temperatura, de forma que s'obté un valor intermedi de $\chi_M T$ de 0,5 $cm^3 \cdot K \cdot mol^{-1}$, entre els valors esperats de $\chi_M T$ de 0 i 0,99 $cm^3 \cdot K \cdot mol^{-1}$ per als estats $S = 0$ i $S = 1$ i $g = 2,00$, respectivament. Tot i presentar uns valors de $\chi_M T$ molt similars, el compost **5_1** presenta un estat fonamental $S = 0$ mentre que **5_2** presenta un estat fonamental $S = 1$.

El sistema monodimensional **7_1** presenta, com a unitat repetitiva, un fragment {$Ni_{12}Na_2$-Ni-} format per quatre triangles units mitjançant ponts sulfat. Com l'acoblament mediat per anions amb una geometria tetraèdrica és molt feble,[132,168] s'ha estimat que aquest compost es pot descriure com quatre triangles aïllats i que la presència d'un mateix grup sulfat unit als tres cations $Ni^{II}$ del triangle no altera els camins de superintercanvi magnètic proposat per als triangles $Ni_3/\mu_3$-OH/oxima. Els valors de $J_1$ i $J_2$ obtinguts per **7_1** són: -22,8 $cm^{-1}$ i -14,3 $cm^{-1}$, que donen un valor de $J_2/J_1$ de 0,62 i un estat $S$ = 0. Així, l'estat fonamental $S$ = 1 del sistema s'explica per la presència de l'ió $Ni^{II}$ de la unitat monomèrica.

Pel compost **11_2** es van calcular unes constants d'acoblament $J_1$ i $J_2$ de -40,4 $cm^{-1}$ i -28,4 $cm^{-1}$, que donen un factor $J_2/J_1$ de 0,70 i un estat fonamental $S$ = 0, que coincideix amb la mesura de $\chi_M T$, que tendeix a un valor de 0,07 $cm^3 \cdot K \cdot mol^{-1}$ a 2 K.

L'últim compost triangular, **5_3**, és un exemple d'un triangle equilàter, de forma que $J_1 = J_2$ = -26,2 $cm^{-1}$ i $J_2/J_1$ és 1. Aquest valor té associat un estat fonamental $S$ = 0, que està d'acord amb el valor de 0,05 $cm^3 \cdot K \cdot mol^{-1}$ a 2 K que s'obté de la mesura de susceptibilitat magnètica.

### 4.2.6. Magnetisme – triangles amb *nansa*

Pel què fa als compostos pentanuclears amb topologia de triangle amb *nansa*, es va trobar que aquests sistemes es poden descriure magnèticament com un sistema amb 3 constants d'acoblament diferents: una constant $J_1$ que fa referència a la interacció dins el triangle, l'acoblament entre dos cations del triangle i els dos ions de la unitat dinuclear, $J_2$, i finalment l'acoblament entre els dos cations de la *nansa*, $J_3$.

L'estudi magnètic dels compostos **6_4** i **6_5** va donar que la principal diferència entre aquests dos compostos és el valor de $J_3$: pel compost **6_4** $J_1$ i $J_2$ presenten un valor similar i més gran que $J_3$ ($J_1 \approx J_2 >> J_3$) mentre que per **6_5** les tres constants presenten el mateix ordre de magnitud ($J_1 \approx J_2 \approx J_3$). És justament la diferència en el valor de $J_3$ la que provoca una variació en l'estat fonamental de cadascun d'aquests compost, sent $S$ = 1 per **6_4** i $S$ = 0 per **6_5**. Per tal d'evitar la sobreparametrització de l'ajust, es va estudiar aquest sistema considerant únicament dues constants d'acoblament: $J_A$ i $J_B$ i dos supòsits: $J_1 = J_2 \equiv J_A$ i $J_3 \equiv J_B$ o $J_1 \equiv J_A$ i $J_2 = J_3 \equiv J_B$, esquema 11.

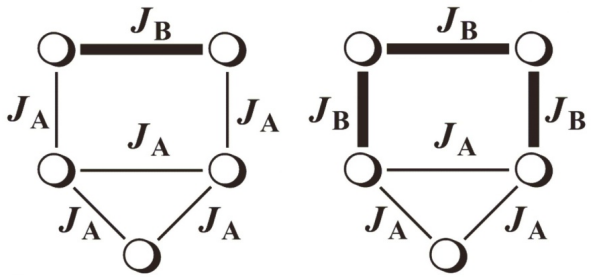


**Esquema 11.** Models per als sistemes pentanuclears basats en un triangle acoblat a un fragment dinuclear.

L'anàlisi dels valors obtinguts en ajustar els compostos **6_4** i **6_5** ($J_1$ = -37,6 $cm^{-1}$, $J_2$ = -41,4 $cm^{-1}$, $J_3$ = -0,7 $cm^{-1}$ i $J_1$ = -39,6 $cm^{-1}$, $J_2$ = -40,4 $cm^{-1}$, $J_3$ = -35,9 $cm^{-1}$, respectivament) fa pensar que aquests exemples es poden descriure amb el model de dos $J$ i el primer cas ($J_1 = J_2 \equiv J_A$ i $J_3 \equiv J_B$). En primer lloc, es va ajustar el compost **6_4** amb aquest nou model i es van obtenir uns valors de $J_A$ = -41,4 $cm^{-1}$ i $J_B$ = -1,6 $cm^{-1}$, mentre que per ajustar el compost **6_5** es va optar per realitzar un ajust amb una única constant d'acoblament ($J_A = J_B = J$ = -37,2 $cm^{-1}$).

Posteriorment, es va representar la variació de l'energia dels diferents nivells magnètics en funció del quocient $J_B/J_A$, mantenint $J_A$ = -40,0 $cm^{-1}$ (un valor aproximat i proper a l'obtingut per **6_4** i **6_5**) i variant el valor de $J_B$, de forma que es va obtenir el diagrama d'energies dels nivells magnètics per aquest sistema en concret, figura 37.

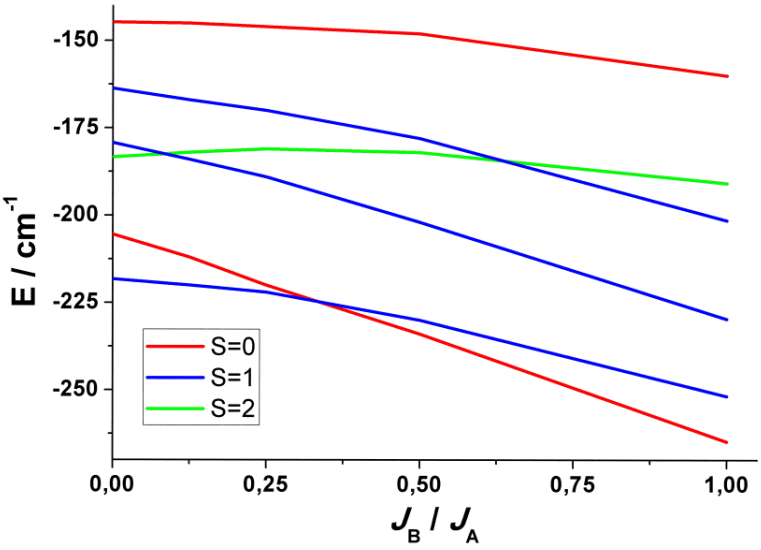


**Figura 37.** Variació de l'energia dels nivells magnètics per a un triangle amb nansa amb $J_A$ = -40 $cm^{-1}$ i $J_B$ variable.

Si es considera que els valors de $J_A$ obtinguts pels compostos **6_4** i **6_5** (-41,4 $cm^{-1}$ i -37,2 $cm^{-1}$, respectivament) són molt propers a -40 $cm^{-1}$, aquests dos compostos poden ser situats en el diagrama d'energies a partir del quocient $J_B/J_A$, obtenint un valor de 0,04 per **6_4** i 1 per **6_5**, que els situa a la zona $S$ = 1 i $S$ = 0, respectivament.

És remarcable el fet que aquests sistemes presenten un punt de frustració d'spin a $J_B/J_A$ = 1/3.

### 4.2.7. Ferrimagnetisme

S'han obtingut dos compostos amb el lligand pyC{CN}NOH que presenten un comportament ferrimagnètic: el primer és el compost **4_5**, un compost amb estructura de *bowtie* que conté quatre interaccions antiferromagnètiques $\mu_3$-OH/oxima entre el $Ni^{II}$ central i els exteriors, i dos acoblaments ferromagnètics $\mu_3$-OH/$N_3$ entre els cations perifèrics.

El segon compost que presenta aquest comportament, **6_3**, està format per un cubà $\{Ni_4(OR)_4\}^{4+}$ unit a un cinquè $Ni^{II}$ per mitjà de tres ponts oxima. Les interaccions observades entre els centres metàl·lics que formen aquest cubà són, totes elles, ferromagnètiques, com es troba a la bibliografia per sistemes similars,[179] mentre que el triple pont oxima genera un acoblament antiferromagnètic.

## 4.3. Propietats estructurals i magnètiques dels compostos derivats del sistema 2-piridiloxima / azida / amina

Els compostos caracteritzats per al sistema quaternari $Ni^{II}$/2-piridiloxima/azida/amina són:

*Article 8*

$[Ni_{13}(N\text{-}Meen)_2(MeOH)_4(6\text{-}MepyC\{H\}NO)_{12}(N_3)_8(OH)_6]$ (**8_1**)

*Article 9*

$[Ni_3(N\text{-}Medpt)_2(py_2CNO)_2(N_3)_4]$ (**9_1**)

$(N_3)\subset[Ni_9(dpt)_6(pyC\{ph\}NO)_6(N_3)_9](NO_3)_2$ (**9_2**)

$(N_3)\subset[Ni_9(dpt)_6(pyC\{ph\}NO)_6(N_3)_9]Cl_2$ (**9_3**)

$Br\subset[Ni_9(dpt)_6(pyC\{ph\}NO)_6(N_3)_9]Br_2$ (**9_4**)

$I\subset[Ni_9(dpt)_6(pyC\{ph\}NO)_6(N_3)_9]I_2$ (**9_5**)

*Article 10*

$[Ni_3(N\text{-}Medpt)_2(py_2CNO)_2(N_3)_4]$ (**9_1**)

$[Ni_4(dpt)_2(N_3)_4(py_2CNO)_2]$ (**10_3**)

$[Ni_4(N,N',N''\text{-}Me_3dpt)_2(N_3)_4(pyC\{ph\}NO)_4]$ (**10_4**)

$[Ni_5(H_2O)_4(AcO)_2(N_3)_2(OH)_2(pyC\{ph\}NO)_4]$ (**10_5**)

$(N_3)\subset[Ni_9(dpt)_6(pyC\{ph\}NO)_6(N_3)_9](NO_3)_2$ (**9_2**)

$(N_3)\subset[Ni_9(dpt)_6(pyC\{ph\}NO)_6(N_3)_9](BF_4)_2$ (**10_7**)

$(N_3)\subset[Ni_9(dpt)_6(pyC\{ph\}NO)_6(N_3)_9]F_2$ (**10_8**)

$(N_3)\subset[Ni_9(dpt)_6(pyC\{ph\}NO)_6(N_3)_9]Cl_2$ (**9_3**)

$Br\subset[Ni_9(dpt)_6(pyC\{ph\}NO)_6(N_3)_9]Br_2$ (**9_4**)

$I\subset[Ni_9(dpt)_6(pyC\{ph\}NO)_6(N_3)_9]I_2$ (**9_5**)

$(N_3)\subset[Ni_9(dpt)_6(py_2CNO)_6(N_3)_9](ClO_4)_2$ (**10_12**)

*Compostos no publicats*

$[Ni(N,N'\text{-}Me_2en)_2(N_3)_2]$ (**11_4**)

$[Ni_{12}Na_2(H_2O)_4(MeOH)_4(6\text{-}MepyC\{H\}NO)_{12}(N_3)_{10}(OH)_4]$ (**11_6**)

La reactivitat de les amines bi- i tridentades juntament amb l'anió azidur i la família de lligands 2-piridiloxima restava totalment inexplorada. En el decurs d'aquesta tesi s'han obtingut diversos compostos sintetitzats a partir del sistema quaternari prèviament esmentat, que són alhora els primers i únics exemples (fins la data) de compostos d'aquest tipus.

Aquesta família de compostos es pot separar en diferents categories en funció del lligand 2-piridiloxima utilitzat en la seva síntesi:

### 4.3.1. Lligand 6-MepyC{H}NOH

Es van caracteritzar tres compostos a partir de la reacció $Ni^{II}$/6-MepyC{H}NOH/azida/amina: en primer lloc es va obtenir el compost mononuclear **11_4**, en què no es va produir la coordinació del lligand 6-MepyC{H}NOH i que presenta dues amines bidentades N,N'-$Me_2$en al pla equatorial i dues azides en *trans*.

Posteriorment, es van obtenir dos compostos de nuclearitat $\{Ni_{12}Na_2\}$ (**11_6**) i $\{Ni_{13}\}$ (**8_1**), que juntament amb els altres dos compostos de nuclearitat $\{Ni_{13}\}$ i $\{Ni_{14}\}$ publicats en l'article 8 (sintetitzats al grup en el treball de Màster de la Sra. Maria Torres-Molina) i els compostos $\{Ni_{12}Na_2\}$ i $\{Ni_{14}\}$ prèviament reportats per Christou *et al.*,[142,170] formen una família de compostos que es pot descriure com dos anells $\{Ni_6\}$ que coordinen un catió metàl·lic ($Ni^{II}$) de forma que s'obté el compost $\{Ni_{13}\}$ ($\{Ni_6\text{-}Ni\text{-}Ni_6\}$), o dos cations metàl·lics ($Na^+$ o $Ni^{II}$) , generant així els sistemes $\{Ni_{12}Na_2\}$ i $\{Ni_{14}\}$ ($\{Ni_6\text{-}M_2\text{-}Ni_6\}$), figura 38.

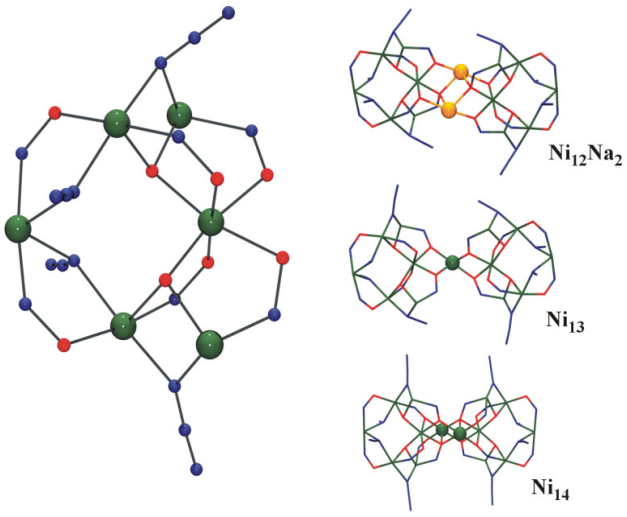


**Figura 38.** Anell de nuclearitat $\{Ni_6\}$ (esquerra), que coordina un o dos ions metàl·lics (dreta).

L'estabilitat d'aquest fragment hexanuclear va permetre la síntesi d'un compost heterometàl·lic $\{Ni_5Mn^{III}\}$ que presenta aquesta mateixa topologia, reportada per Chen *et al*. l'any 2011.[180]

Els fragments de nuclearitat $\{Ni_6\}$ presenten dos ponts oxima/azida, dos ponts $\mu_3$-OH/azida i dos dobles ponts oxima, de forma que s'espera una resposta ferrimagnètica per aquest fragment, que serà analitzada posteriorment.

També és destacable el fet que la coordinació del catió o cations metàl·lics centrals per part dels anells $\{Ni_6\}$ varia en funció del compost: al compost **8_1** s'observa la coordinació del $Ni^{II}$ central a cada fragment $\{Ni_6\}$ per mitjà d'un doble pont oxima, al compost **11_6** la coordinació dels ions $Na^+$ es realitza a través d'un pont oxima i d'un segon pont oxima/azida, mentre que al compost de nuclearitat $\{Ni_{12}Na_2\}$ prèviament publicat la coordinació dels cations sodi no conté cap pont azida i al sistema $\{Ni_{14}\}$ la unió es realitza per un triple pont oxima.

Finalment, comentar que el compost **8_1** presenta la segona nuclearitat més elevada trobada fins la data per als sistemes Ni/oxima (13), superada, precisament, pels compostos de nuclearitat $\{Ni_{14}\}$ d'aquesta família.

### 4.3.2. Lligands $py_2CNOH$ i pyC{ph}NOH

L'objectiu marcat inicialment per aquest apartat era la síntesi de compostos formats exclusivament per diferents lligands 2-piridiloxima, $Ni^{II}$, amina i azidur, per tal de promoure la formació de ponts oxima/azida. Per a realitzar aquestes síntesis es va partir dels compostos dinuclears neutres $[Ni_2(N\text{-}Medpt)_2(N_3)_4]$ i $[Ni_2(dpt)_2(N_3)_4]$ (sintetitzats prèviament al grup),[171] que contenen l'anió azidur com a única espècie amb càrrega negativa i ponts azida/oxima preformats. A partir del primer precursor es van obtenir el compost trinuclear **9_1** amb el lligand $py_2CNOH$ i el compost tetranuclear **10_2** amb el lligand $dapdoH_2$ (que es troba descrit a l'apartat 4.1.), tot i provar aquesta reacció amb diversos lligands 2-piridiloxima. Posteriorment, en provar la síntesi a partir del segon compost dinuclear (que conté l'amina dpt) amb el lligand pyC{ph}NOH es van obtenir uns cristalls que no van poder ser resolts però el seu estudi per IR va indicar que contenien l'anió nitrat (impuresa que provenia de la síntesi del compost dinuclear $[Ni_2(dpt)_2(N_3)_4]$ a partir de $Ni(NO_3)_2$).

Així, es va provar la síntesi directa a partir de pyC{ph}NOH, $Ni(NO_3)_2$, $NaN_3$, dpt i $NEt_3$ com a base i es va obtenir el compost **9_2**. En veure l'èxit d'aquesta síntesi, es va procedir a la síntesi directa dels diferents compostos a partir dels lligands pyC{ph}NOH i $py_2CNOH$, diverses sals de $Ni^{II}$ i amines derivades de dpt, $NaN_3$ i $NEt_3$.

Dels 12 compostos obtinguts a partir de les amines dpt, N-Medpt i N,N',N"-$Me_3$dpt, únicament el compost pentanuclear **10_5** amb forma de *bowtie* no presenta la coordinació de l'amina tridentada (la discussió sobre l'estabilitat d'aquest tipus d'estructures amb anions carboxilat es realitzarà posteriorment en l'apartat 4.4.). Les altres estructures obtingudes en aquest apartat presenten la coordinació del lligand 2-piridiloxima, l'azida i l'amina emprada en cada reacció; i es poden classificar en compostos de baixa nuclearitat ($Ni_3$ i $Ni_4$, **9_1**, **10_3** i **10_4**) i sistemes de nuclearitat elevada ($Ni_9$, **9_2**-**9_5**, **10_7**, **10_8** i **10_12**), esquema 12.

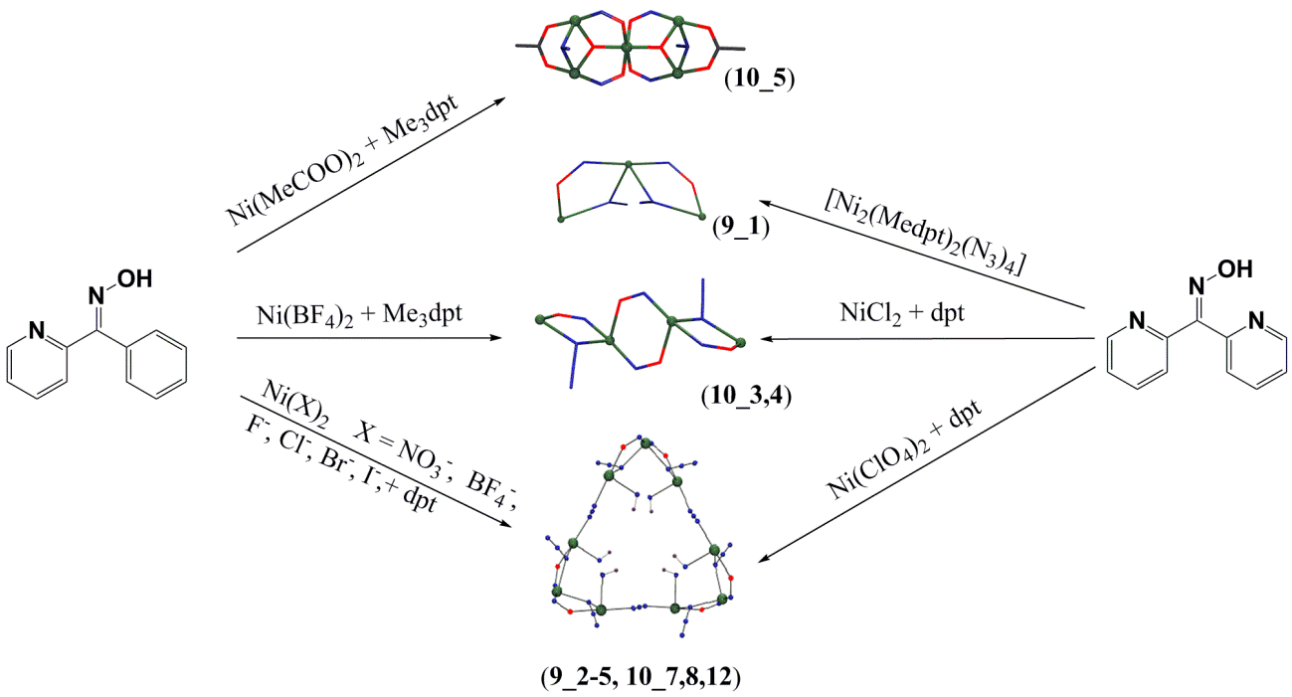


**Esquema 12.** Reactivitat dels lligands $py_2CNOH$ i pyC{ph}NOH amb amines tridentades.

La diferència més notòria que es troba entre els compostos de baixa nuclearitat i la família de $\{Ni_9\}$ és que els primers només presenten els components $Ni^{II}$/oxima/azida/amina a l'estructura, mentre que als segons s'observa, a part dels components anteriors, la presència d'un anió addicional que prové de la sal de partida del $Ni^{II}$ i permet l'augment de la nuclearitat d'aquests compostos.

Com s'ha vist, hi ha una sèrie de compostos que presenten una estructura comuna: l'anell de {$Ni_9$}. Aquest anell, format per *self-assembly* al voltant d'un anió azidur o halur encapsulat a la cavitat creada a l'interior de l'anell per mitjà de ponts d'hidrogen, es pot descriure com un trímer de trímers. Cadascun d'aquests trímers forma una de les cantonades del triangle i s'uneix a les altres dos subunitats trinuclears per mitjà d'un enllaç azida *end-to-end*. Els fragments trinuclears que formen les cantonades del metal·lomacrocicle {$Ni_9$} són molt semblants al compost trinuclear **9_1**, que conté dos lligands azida terminals coordinativament disponibles, així que la formació de l'anell {$Ni_9$} es pot entendre com la reacció que es mostra a l'esquema 13.

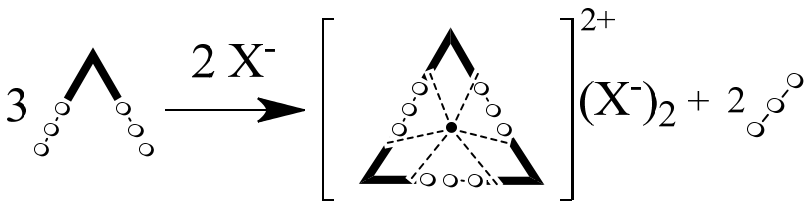


**Esquema 13.** Correlació entre tres fragments trinuclears **9_1** i un anell {$Ni_9$}.

Tot i que aquest esquema no representa estrictament la reacció seguida per a la síntesi d'aquests compostos, queda palès que el trímer de trímers ({$Ni_9$}) presenta càrrega positiva i que necessita de dos contraions per poder formar un compost neutre.

En la síntesi dels diversos anells {$Ni_9$} (**9_2** – **9_5**, **10_7**, **10_8**, **10_12**) s'observa una competència entre els anions nitrat, tetrafluoroborat, perclorat o halur i azidur per tal d'ocupar la cavitat central. Els anions tetraèdrics ($BF_4^-$, $ClO_4^-$) poden ser encapsulats en entorns prismàtics però necessiten una cavitat més gran que la generada pels {$Ni_9$}, de forma que es pot descartar la seva coordinació, així com la dels halurs menys voluminosos, pels quals la cavitat és massa gran com per establir ponts d'H efectius i massa rígida com per reajustar-se de forma més adient. Per aquests motius, i en base als resultats experimentals, es pot dir que l'encapsulament d'anions dins el metal·lomacrocicle depèn de la grandària de la cavitat interna dels {$Ni_9$} i que aquesta té preferència pels anions $Br^-$ i $I^-$ respecte de $N_3^-$.

El comportament dels sistemes {$Ni_9$} és comparable al del (X) ⊂ [BT-6$H^+$] bist-trend criptand reportat per Lehn *et al.* el 1984,[56a] ja que és capaç d'encapsular selectivament anions azidur o halur

variant lleugerament la seva conformació. A diferència del (X) ⊂ [BT-6H$^+$] bist-trend criptand, que crea cavitats prismàtiques o octaèdriques en funció de l'anió encapsulat (azidur i halurs, respectivament), figura 39, els anells {Ni$_9$} creen una cavitat prismàtica trigonal per tots dos casos.

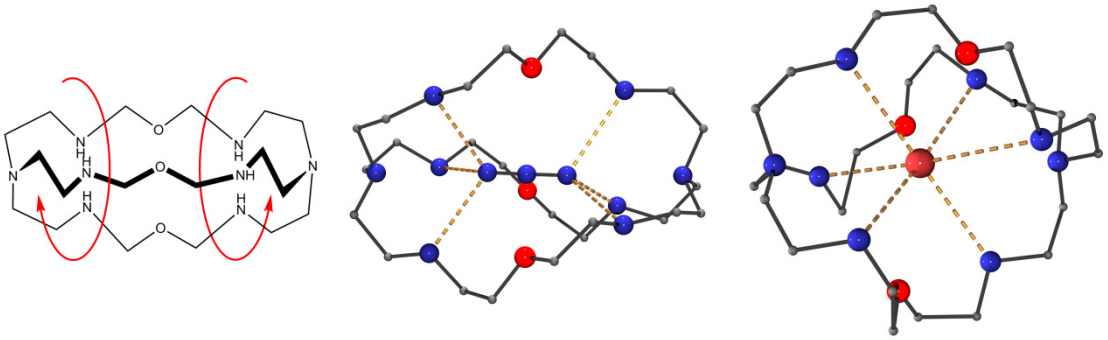

**Figura 39.** D'esquerra a dreta: [BT-6H$^+$] bist-trend criptand, criptand encapsulant un anió azidur en una cavitat prismàtica trigonal i criptand encapsulant un halur en una cavitat octaèdrica. La rotació en sentit contrari dels extrems del criptand permet adaptar l'entorn de coordinació a l'anió encapsulat.

Com s'ha vist, aquests anells estan formats per tres fragments trinuclears formats per un doble pont oxima/azida, que li confereixen una elevada rigidesa, de forma que el reajustament dels anells únicament es podria realitzar variant la torsió Ni-N···N-Ni dels ponts azida *end-to-end*, figura 40, esquerra. Aquest reajustament no és prou important com per modificar la cavitat interior dels anells {Ni$_9$}, de forma que tots tres anions es troben coordinats en un entorn en forma de prisma trigonal, figura 40, dreta.

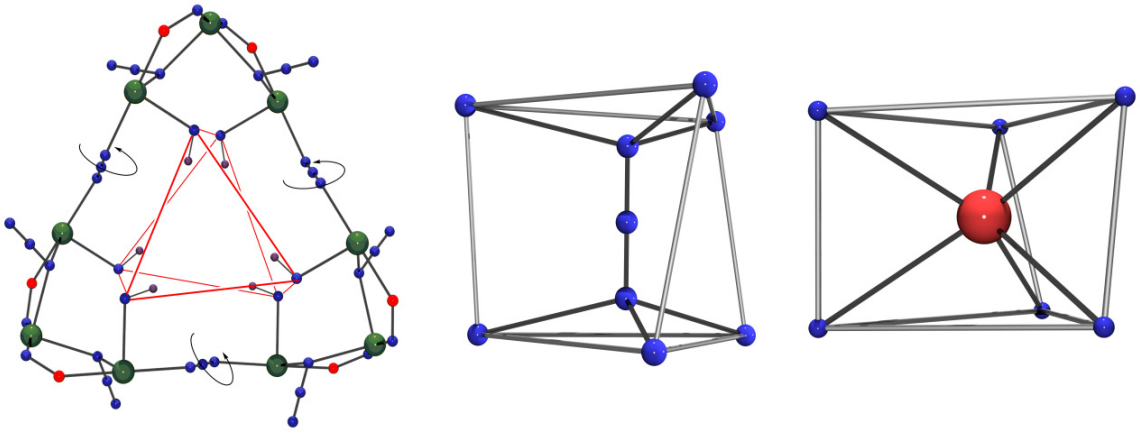

**Figura 40.** D'esquerra a dreta, anell {Ni$_9$} creant la cavitat prismàtica trigonal al seu interior, coordinació de l'anió $N_3^-$ i $Br^-$ a l'interior d'aquesta cavitat.

### 4.3.3. Efecte de l'amina

Un altre punt d'interès que presentava aquesta nova síntesi era determinar l'efecte de l'amina en l'estructura del compost. Aquest efecte es pot estudiar de dues formes diferents: la substitució d'una amina bidentada per una amina tridentada i la modificació (funcionalització) de l'amina emprada.

Els compostos $\{Ni_{12}Na_2\}$ (**11_6**) i $\{Ni_{13}\}$ (**8_1**) són un bon exemple per al primer efecte esmentat: el compost **8_1**, sintetitzat a partir d'una amina bidentada (N-Meen), presenta dues molècules de l'amina coordinades; mentre que el compost **11_6**, sintetitzat en presència d'una amina tridentada (dpt), no presenta aquesta amina en l'estructura. La coordinació de l'amina depèn, clarament, de la seva denticitat: l'amina bidentada només ocupa dues posicions de l'entorn de coordinació (substitueix dues molècules de solvent coordinades a certs ions $Ni^{II}$) i permet la formació dels fragments $\{Ni_6\}$, mentre que la coordinació de l'amina tridentada ocuparia tres posicions de l'entorn de coordinació d'un catió $Ni^{II}$ i impossibilitaria la formació d'aquests anells. La obtenció del compost amb estructura $\{Ni_{12}Na_2\}$ (**1_4**) determina que l'estabilitat i insolubilitat d'aquesta família de compostos és més elevada que no pas la d'un possible compost format pel lligand 6-MepyC{H}NOH, $Ni^{II}$, azida i l'amina dpt.

D'altra banda, els compostos obtinguts a partir dels lligands $py_2CNOH$ i pyC{ph}NOH presentats als articles 9 i 10 (**9_1**, **10_3**-**5**, **9_2**-**9_5**, **10_7**, **10_8** i **10_12**) són un bon exemple dels canvis que es poden produir en funcionalitzar l'amina: els compostos **9_2 – 9_5**, **10_7**, **10_8** i **10_12**, tots ells sintetitzats a partir de l'amina dpt, presenten l'anell de $\{Ni_9\}$ com estructura comuna. Aquest anell es forma selectivament al voltant d'un anió central ($N_3^-$, $X^-$), de forma que aquest queda encapsulat per una sèrie de ponts d'hidrogen establerts per l'amina dpt. Aquests, però, no són els únics ponts d'hidrogen que estableix aquesta amina, ja que també forma diversos ponts d'H intramoleculars que ajuden a mantenir l'estructura compacta. La substitució de l'amina dpt per N-Medpt (que podria establir ponts d'H intra- i intermoleculars però presenta un lleuger impediments estèric per la presència d'un grup Me a l'àtom de N central) i N,N',N"-$Me_3$dpt (que podria interaccionar per ponts d'H amb l'anió central però no generar ponts intramoleculars i presenta una major impediment estèric) provoca un important canvi en la topologia del compost, ja que a partir d'aquestes amines substituïdes s'han obtingut el compost trinuclear **9_1** i el compost tetranuclear **10_3**.

### 4.3.4. Magnetisme – pont oxima/azida

Després d'haver intentat sintetitzar compostos que continguessin ponts oxima/azida sense èxit durant bona part d'aquesta tesi, aquesta nova estratègia sintètica va permetre caracteritzar diversos compostos que presentaven aquest fragment i estudiar-ne la interacció, per la què s'esperava un acoblament ferromagnètic.[59b]

Per una banda, es va ajustar el compost $\{Ni_{12}Na_2\}$ (**11_6**) que, com s'ha vist anteriorment, conté quatre ponts que contenen el lligand azida i dos dobles ponts oxima, com dos fragments $\{Ni_6\}$ aïllats amb un Hamiltonià amb dues constants d'acoblament i un paràmetre *z'J'* que fa referència a les interaccions entre fragments $\{Ni_6\}$. Es va obtenir una constant d'acoblament ferromagnètica per a la interacció oxima/azida ($J_2$) de +22,6 $cm^{-1}$, una constant antiferromagnètica per al doble pont oxima ($J_1$) de -18,5 $cm^{-1}$ i una interacció entre fragments (*z'J'*) de -0,5 $cm^{-1}$. La naturalesa d'aquestes interaccions genera un estat fonamental d'spin $S$ = 4, que concorda amb el resultat observat per als compostos que presenten aquesta mateixa topologia: $\{Ni_{13}\}$ i $\{Ni_{14}\}$,[142,170] $\{Ni_5Mn\}$.[180]

Posteriorment, es va estudiar la resposta magnètica del compost **8_1** ($\{Ni_{13}\}$). Aquest compost no va poder ser ajustat a causa de la seva elevada nuclearitat, però les dades obtingudes pel compost anterior permeten entendre el seu comportament com un sistema $\{Ni_6\text{-}Ni\text{-}Ni_6\}$ amb $S$ = 9 generat per l'acoblament antiferromagnètic entre el catió central i un dels ions de l'anell, d'acord amb la figura 41.

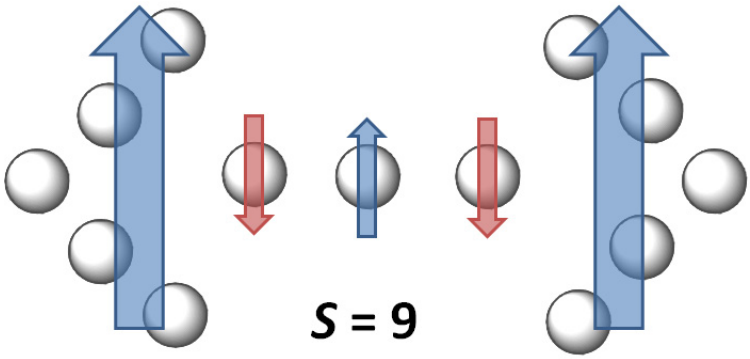


**Figura 41.** Esquema d'acoblament entre cations metàl·lics en el compost **8_1**, generant l'estat fonamental $S$ = 9.

L'ajust de la mesura de magnetització va confirmar que es tracta d'un compost amb un estat fonamental d'spin $S$ = 9 i mitjançant l'ajust de la magnetització reduïda es va obtenir que aquest compost presenta un paràmetre d'anisotropia magnètica $D$ = -0,15 $cm^{-1}$. Per desgràcia, tot i presentar un estat fonamental amb $S$ elevat i un valor de $D$ diferent de zero i negatiu, aquesta anisotropia no és prou gran perquè el compost **8_1** es comporti com un imant uni-molecular per sobre de 2 K, com demostra l'absència de senyals fora de fase ($\chi_M$") dependents de la freqüència en la mesura a corrent altern a aquesta temperatura.

Tot i no comportar-se com un SMM (per sobre de 2 K), el compost **8_1** presenta l'estat fonamental d'spin més elevat ($S$ = 9) caracteritzat fins ara en la química del $Ni^{II}$ amb lligands oxima.

D'altra banda, es va estudiar el compost trinuclear **9_1**, que conté dos ponts oxima/azida (en mode de coordinació *end-on*) i és el primer compost que ha permès l'estudi inequívoc d'aquest acoblament. Es va obtenir una constant d'acoblament ferromagnètica de +9,8 $cm^{-1}$, que presenta un valor molt semblant al calculat pel compost tetranuclear **10_3** (+10,2 $cm^{-1}$) i pels anells $\{Ni_9\}$ **9_3** i **9_4** (+9,9 $cm^{-1}$ i +8,9 $cm^{-1}$, respectivament), que contenen ponts azida/oxima amb paràmetres d'enllaç similars. Aquests valors de $J$ són molt semblants als trobats per fragments similars[141] i estan en consonància amb el comportament proposat per als ponts azida en mode *end-on*.[119] Els fragments trinuclears que actuen de cantonada als anells $\{Ni_9\}$ estan units entre ells, com s'ha comentat, per mitjà de ponts azida *end-to-end*. Es va calcular un acoblament antiferromagnètic de -62,5 $cm^{-1}$ i -53,5 $cm^{-1}$ per **9_3** i **9_4**, respectivament, que cau dins l'interval habitual.[181]

El valor de la constant antiferromagnètica és molt superior a la ferromagnètica, de forma que aquest sistema es pot descriure com un triangle de $Ni^{II}$ antiferromagnèticament acoblat amb les tres constants iguals a causa de la cancel·lació dels spins dels cations $Ni^{II}$ units a través del pont azida *end-to-end*. Com s'ha vist a la introducció, els sistemes triangulars antiferromagnèticament acoblats amb les tres constants iguals tenen associat un estat fonamental d'spin $S$ = 0.

La figura 42 mostra la variació d'energies dels diferents nivells d'spin, considerant la constant d'acoblament $J_1$ (promoguda pel pont oxima/azida) d'un valor fixat de +10 $cm^{-1}$ i variant el valor de la constant $J_2$ (acoblament a través del pont azida en mode *end-to-end*). Es pot observar com, per qualsevol relació de $J_2/J_1$ negativa (és a dir, $J_2$ antiferromagnètica), l'estat fonamental del sistema és $S$ = 0, mentre que per a quocients positius ($J_2$ ferromagnètica) l'estat fonamental és $S$ = 9. El punt $J_2/J_1$ = 0 no es pot considerar un punt de frustració magnètica, ja que per $J_2$ = 0 el sistema es comportaria com tres fragments trinuclears aïllats, cadascun d'ells amb un estat fonamental d'spin $S$ = 3.

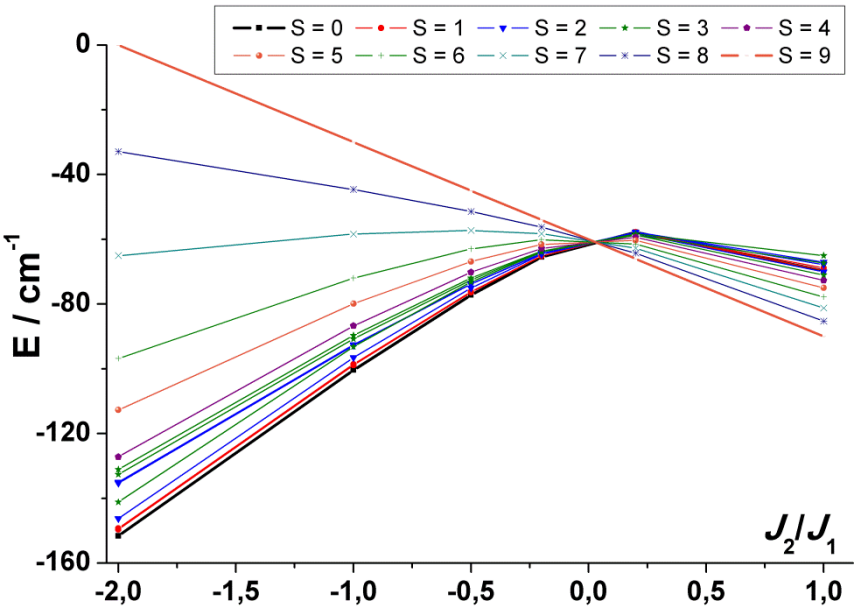


**Figura 42.** Representació dels nivells energètics en funció de la relació $J_2/J_1$.

La presència d'estats excitats amb $S$ superior i propers en energia provoca que la mesura de $\chi_M T$ no arribi al valor esperat de 0 $cm^3 \cdot K \cdot mol^{-1}$ per un compost amb un estat fonamental $S$ = 0.

La figura 43 mostra la variació de la corba de susceptibilitat molar respecte la temperatura en funció de $J_2$, mantenint el valor de $J_1$ fixat en +10 $cm^{-1}$. Com es pot observar, l'increment de $J_2$ comporta una disminució en el valor inicial i final de la corba de $\chi_M T$ i la desaparició del màxim per valors iguals o superiors (en valor absolut) que $J_1$.

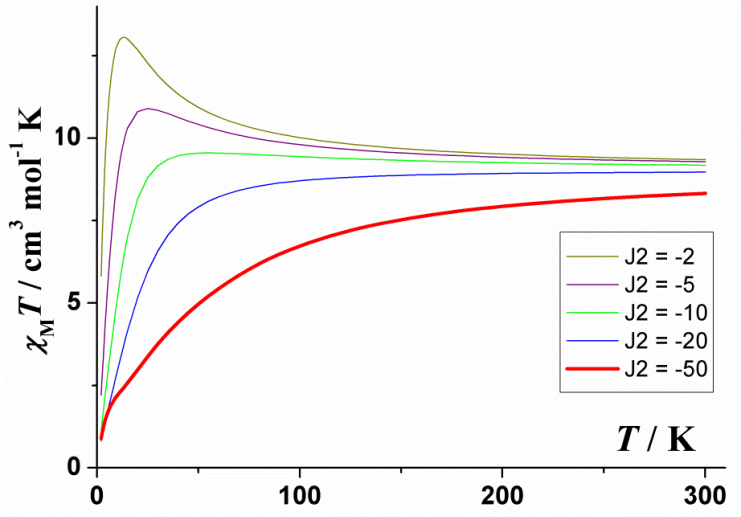


**Figura 43.** Simulació de la variació de la corba de $\chi_M T$ vs. $T$ en funció del valor de $J_2$.

## 4.4. Aspectes sintètics

Com s'ha comentat a la introducció, el treball experimental realitzat al llarg d'aquesta tesi es basa en la reacció entre lligands piridiloxima i sals de níquel(II) en absència o presència de co-lligands i en un solvent orgànic, generalment en medi bàsic. Aquesta reacció, en aparença molt simple, pot generar una gran varietat de productes en modificar qualsevol paràmetre de reacció, ja que cap d'aquests elements es pot considerar innocent. En els apartats anteriors s'ha estudiat l'efecte de cadascun dels lligands piridiloxima emprats, objectiu principal d'aquesta tesi, però l'avaluació de l'efecte dels anions, bases i solvents emprats posa de manifest la necessitat de fer escombrats sistemàtics de cadascun dels paràmetres de reacció per tal d'estudiar adequadament la reactivitat dels corresponents lligands.

### 4.4.1. Efecte de l'anió

Els anions de la sal de níquel(II) poden exercir un efecte determinant, en funció de la seva naturalesa, principalment en dos aspectes: la nuclearitat i la topologia dels compostos obtinguts. Les sals utilitzades al llarg de la tesi es poden separar en dos grans blocs: d'una banda hi ha les que presenten contraions carboxilats i β-dicetonats i, d'altra banda, les formades per anions inorgànics.

Els anions carboxilats presenten una elevada tendència a coordinar-se, sovint en el mode bidentat *syn-syn* encara que no és inusual la seva coordinació amb una denticitat superior. Aquests anions rarament actuen com a contraió d'un complex catiònic, com ho mostra el fet que tots els compostos obtinguts, excepte un, contenen els anions carboxilat coordinats. L'únic exemple d'anió carboxilat que actua de contraió es troba al compost **3_1**, en què l'anió 3-ClBzO$^-$ és estabilitzat per un triple pont d'hidrogen i per interaccions d'apilament π-π. Els anions β-dicetonats tendeixen a la coordinació com a lligand bidentat i, de la mateixa manera que a la bibliografia, no s'ha observat que actuï de contraió en cap compost.

La reactivitat dels carboxilats de níquel amb els lligands dapdo$H_2$ i pyC{CN}NOH mostra una tendència a generar compostos de nuclearitat baixa, sobretot $Ni_3$ i $Ni_5$ (**1_2**, **1_3**, **2_1**, **2_2**, **3_1**, **4_1**, **4_4**, **4_5**, **5_1**, **5_2**, **5_3**, **6_1**, **11_2**, **11_5** i **11_9**), generalment basats en fragments triangulars (**1_2**, **2_1**, **2_2**, **3_1**, **4_1**, **4_4**, **4_5**, **5_1**, **5_2**, **5_3**, **6_1**, **11_2** i **11_9**), en els que, en tots els casos, es troben carboxilats coordinats. També es va obtenir un compost pentanuclear basat en fragments trinuclears a partir del lligand pyC{ph}NOH i l'anió acetat (**10_5**).

D'altra banda, s'han obtingut tres compostos a partir d'anions β-dicetonats: els compostos tetranuclear **4_3** i octanuclear **11_11**, sintetitzats a partir de l'anió tfacac$^-$, i el clúster trinuclear **11_2** obtingut a partir de l'anió hfacac$^-$. Com s'ha vist a l'apartat 3.11. i es comentarà posteriorment, aquest anió ha patit una modificació de forma que l'anió trobat a l'estructura és el $CF_3COO^-$ enlloc del hfacac$^-$ original.

Les sals de níquel amb contraions inorgànics es poden classificar, al seu torn, en dos grups: les que contenen anions inorgànics potencialment coordinants i les formades per anions inorgànics poc o gens coordinants. Dins el segon grup s'hi troben els anions $ClO_4^-$ i $BF_4^-$, que no es troben coordinats en cap de les estructures obtingudes: **10_12** i **11_7** i **3_3** i **10_7**, respectivament, i que, per tant, tendeixen a estabilitzar clústers catiònics. El grup dels anions potencialment coordinants és més extens i s'han emprat halurs, $SCN^-$, $NO_3^-$ i $SO_4^{2-}$. Abans de procedir a l'anàlisi de l'efecte d'aquests anions en l'estructura dels compostos obtinguts, val la pena aclarir que no s'ha tingut en compte els sistemes {$Ni_9$} en aquesta anàlisi, ja que per aquests sistemes es va procedir a la síntesi dirigida dels anells {$Ni_9$} i es va estudiar la capacitat d'aquests anells per encapsular els anions seleccionats enlloc d'estudiar la capacitat coordinativa dels anions. A més, el cas del sulfat serà estudiat de forma separada a la resta d'anions per les seves característiques úniques.

Els anions $Cl^-$, $Br^-$, $SCN^-$ i $NO_3^-$, així com l'anió $MeO^-$ que pot aparèixer en solucions bàsiques de metanol, tendeixen a trobar-se coordinats en els productes resultants, ja sigui com lligands terminals, com és el cas del $NO_3^-$ en el compost **2_3** o dels halurs $Br^-$ i $Cl^-$ en els compostos **6_3** i **6_3b**, respectivament, o bé formant ponts entre dos cations $Ni^{II}$ com el mateix $Cl^-$ en el compost **6_2**, $SCN^-$ en **6_4** i $MeO^-$ en **6_5**. El nitrat és l'anió menys coordinant de tots ells i en ocasions actua de contraió: **2_4** i **6_5**. Així, aquests anions es troben coordinats en sis dels compostos caracteritzats (**2_3**, **6_2**, **6_3**, **6_3b, 6_4** i **6_5**). En el cas dels compostos **6_3**, **6_3b** i **6_5** s'observa la coordinació de l'anió $MeO^-$ procedent de la desprotonació del solvent.

Per últim s'estudiarà el cas de l'anió $SO_4^{2-}$, que presenta unes propietats úniques: una elevada tendència a coordinar-se a cations $Ni^{II}$ així com un elevat nombre de modes de coordinació d'alta denticitat. En aquesta tesi s'han obtingut dos compostos d'elevada nuclearitat que contenen aquest anió (**3_2**, $Ni_8$ i **7_1**, $\{Ni_{13}Na_2\}_n$) i en tots dos casos s'observa com el sulfat actua de pont entre dos o més clústers formats pel lligand piridiloxima en qüestió, el catió $Ni^{II}$ i el propi anió $SO_4^{2-}$. Així, es pot considerar que la nuclearitat i topologia dels compostos venen determinats per l'anió $SO_4^{2-}$ més que no pas pels propis lligands piridiloxima. S'han caracteritzat els modes de coordinació 4.1111, 3.2100 i 2.1100 per al compost **3_2** i els modes 4.2210, 4.1111 i 3.1110 per al compost **7_1**.

Com es pot veure, la principal diferència entre el sulfat i els altres anions inorgànics és que, mentre aquests últims solen actuar d'anions terminals o de pont entre dos cations metàl·lics, el $SO_4^{2-}$ tendeix a coordinar-se formant una gran quantitat i varietat de ponts, dirigint l'estructura del compost final.

A mode de resum de l'efecte de l'anió sobre la nuclearitat, es pot dir que s'han obtingut exemples de totes les nuclearitats igual i inferiors a $Ni_{13}$, excepte $Ni_7$ i $Ni_{11}$, i que s'ha observat una clara tendència per als lligands dapdo$H_2$ i pyC{CN}NOH de generar compostos de major nuclearitat ($Ni_8$-$Ni_{13}$) per anions inorgànics (nitrat, sulfat, perclorat, etc.) que no pas per anions carboxilat ($Ni_2$-$Ni_6$).

Pel què fa a la relació entre l'anió emprat i la topologia del compost obtingut, el cas més clar són els sistemes $Ni_5$/piridiloxima. Si bé és cert que prop del 40% de les reaccions que contenien la mescla de reactius lligand 2-piridiloxima/carboxilat/$Ni^{II}$ van generar compostos d'aquesta nuclearitat, també es van obtenir diversos pentàmers a partir de sals inorgàniques.

Els compostos pentanuclears obtinguts en aquesta tesi presenten una elevada variabilitat topològica, fet que coincideix amb les dades trobades a la bibliografia, ja que els 14 compostos reportats per al sistema $Ni_5$/2-piridiloxima (10 dels quals es presenten en aquesta tesi) presenten fins a 8 topologies diferents, figura 44.

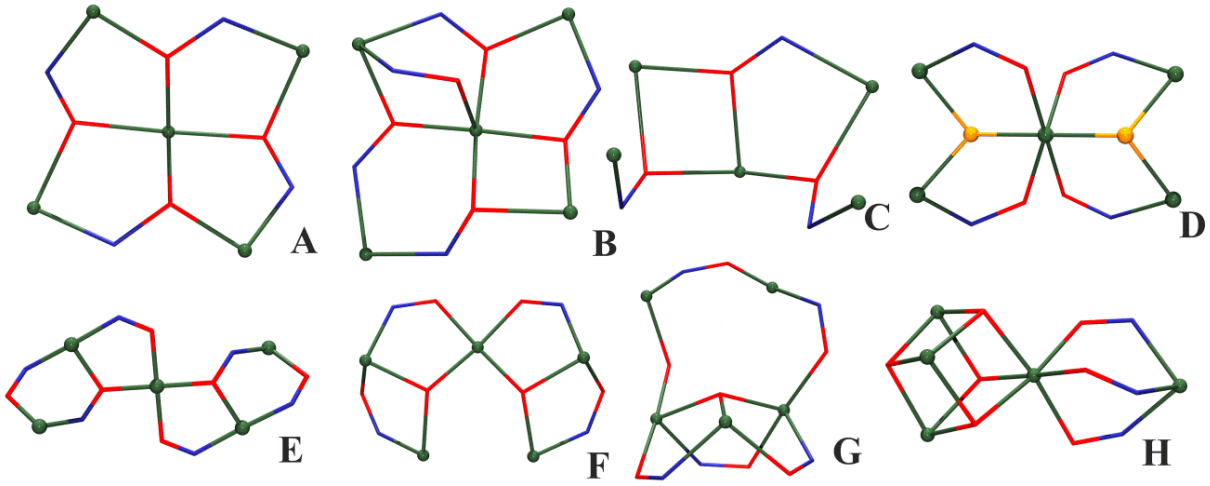


**Figura 44.** Topologies reportades per a sistemes $Ni_5$/2-piridiloxima.

En primer lloc, s'ha observat que, en els casos en què l'anió no es coordina, el lligand $py_2CNOH$ genera les metal·locorones centrades **A** en presència d'àcids hidroxàmics o **B** en absència d'aquests, de forma similar a altres metalls.[67,182] Els lligands indano-1,2,3-trionadioxima i indano-1,2,3-trionatrioxima, que contenen dos i tres grups oxima, respectivament, també generen metal·locorones centrades del tipus **A**.

En segon lloc, s'ha trobat que la major part de lligands 2-piridiloxima ($dapdoH_2$, pyC{ph}NOH, 6-MepyC{H}NOH i pyC{CN}NOH), excepte el lligand $py_2CNOH$, genera estructures tipus *bowtie* en presència d'anions carboxilat. El lligand $py_2CNOH$ genera el nucli irregular **C** amb anions carboxilat, mentre que els lligands esmentats anteriorment generen l'estructura tipus **D** en presència de grups $N_3^-$ o $OH^-$ (**4_4**, **4_5**, **10_5**, **11_9**) o **E** en absència d'aquests grups, situació en què és el propi àtom d'oxigen del grup oxima qui actua com a grup $\mu_3$-donador (**2_1** i **2_2**). L'ús d'anions carboxilat voluminosos, com ara $Ph_2CHCOO^-$, juntament amb el lligand pyC{CN}NOH, genera una estructura tipus *bowtie* fortament distorsionada (**6_1**), que també es pot descriure com un trapezi lleugerament distorsionat, topologia **F**.

Finalment, s'ha vist que la coordinació d'anions inorgànics pot generar noves topologies amb el lligand pyC{CN}NOH. S'han caracteritzat dos triangles amb una *nansa* dinuclear, estructura **G** (**6_4** i **6_5**), en què els anions $SCN^-$ i $MeO^-$ actuen de pont entre els dos ions $Ni^{II}$ de la *nansa* (en el segon cas, no s'ha coordinat l'anió emprat en la síntesi del compost: $NO_3^-$), i partint d'halurs s'han obtingut, en MeOH, dos cubans de $\{Ni_4(MeO)_4\}$ units a un cinquè ió $Ni^{II}$ per mitjà d'un triple pont oxima en què els halurs ($Cl^-$ i $Br^-$) actuen d'anions terminals (**6_3** i **6_3b**), **H**, mentre que en $CH_2Cl_2$ s'ha obtingut un compost *bowtie* del tipus **E**, en què l'anió $Cl^-$ actua de pont entre els cations $Ni^{II}$ perifèrics (**6_2**).

### 4.4.2. Efecte del solvent

Es van utilitzar, principalment, tres solvents diferents al llarg de la tesi: MeOH, MeCN i $CH_2Cl_2$, cadascun dels quals té unes propietats (capacitat coordinativa, polaritat, tendència a formar ponts d'hidrogen, etc.) diferent dels altres. Per aquest motiu, en variar el solvent d'una reacció es poden observar tres resultats diferents: en primer lloc es pot obtenir un producte no cristal·lí o no obtenir cap producte, en segon lloc es pot obtenir el mateix producte que amb el solvent anterior i, finalment, es pot generar un nou compost.

Per norma general, cadascun dels compostos caracteritzats s'ha obtingut a partir d'un únic solvent, la variació del qual impedeix la formació o obtenció del compost original.

En cas d'obtenir el mateix producte amb dos solvents diferents, hi sol haver una variació en el rendiment de la reacció i/o en la cristal·linitat del compost obtingut, fent que s'hagi escollit la síntesi del producte més cristal·lí. Per exemple, el compost **1_2** pot ser sintetitzat tant en MeOH com en MeCN, com demostra l'espectre d'IR realitzat per als productes obtinguts, però amb el primer solvent es van obtenir cristalls vermellosos amb forma hexagonal mentre que amb el segon va aparèixer una pols cristal·lina d'un color semblant però de forma irregular, fent que es decidís reportar la seva síntesi a partir de MeOH enlloc de MeCN. De forma similar, els compostos mononuclear **11_1**, trinuclears **4_1** i **5_1** i octanuclear **11_7** van ser obtinguts en metanol i acetonitril, sent el primer solvent el que donava productes més cristal·lins.

L'última possibilitat és que el canvi de solvent provoqui un canvi en l'estructura del compost sintetitzat. Un primer exemple d'aquesta situació és la reacció entre pyC{CN}NOH, $NiCl_2$ i $NEt_3$, que quan es realitza en metanol genera el compost **6_3b** (cubà de $\{Ni_4(OMe)_4\}^{4+}$ unit a un cinquè $Ni^{II}$ per un triple pont oxima), mentre que en diclorometà aquesta reacció no és possible (per l'absència d'anions metòxid) i dóna el compost **6_2** amb forma de *bowtie*. Per aquest mateix motiu, els clústers que contenen molècules de solvent coordinades (generalment metanol), no es poden obtenir en solvents no coordinants.

Un altre exemple d'aquest últim cas ve donat per la quantitat d'aigua present en el medi: si bé en el medi de reacció sempre hi ha una certa quantitat d'aigua aportada pel solvent i per la pròpia sal de partida, que és important com a font d'anions $OH^-$, resulta interessant el cas de la reacció dapdo$H_2$ + $Ni(AcO)_2$ + $NEt_3$. Inicialment, es va obtenir (de forma repetida i reproduïble) el compost **1_3** a partir de la seva reacció en MeOH, però al cap d'un cert temps aquesta síntesi no es va poder repetir. Després d'una anàlisi detallada de les condicions de reacció, es va trobar que s'havia canviat de proveïdor del solvent, i que el nou MeOH contenia una proporció d'aigua menor que l'anterior. Així, es va repetir aquesta síntesi amb el nou solvent, afegint unes gotes d'aigua, i es va obtenir, de nou, el compost **1_3**. A més, aquesta mateixa reacció dóna el compost **1_4** utilitzant $CH_2Cl_2$ com a solvent.

### 4.4.3. Química supramolecular

Com s'ha introduït anteriorment, la química supramolecular estudia les interaccions febles no covalents. Al llarg d'aquesta tesi s'han obtingut una sèrie de compostos que presenten ponts d'hidrogen intra- i intermoleculars (ja sigui amb molècules veïnes o amb molècules de solvent), per tal d'estabilitzar la seva estructura i generar així el compost en qüestió.

Hi ha dues famílies de compostos presentats en aquesta tesi que destaquen des del punt de vista de la química supramolecular. En primer lloc, el compost monodimensional **7_1** encapsula un catió $Na^+$ mitjançant vuit interaccions electrostàtiques febles (càrrega/dipol) de llarga distància, al voltant de 2,8 Å, establertes pels grups sulfat pont. La presència del catió $Na^+$ al centre del fragment $\{Ni_{12}Na\}$ es pot entendre com el motor de la formació del compost **7_1**, de forma que es pot parlar d'efecte plantilla o *template synthesis*.

El segon cas és la família de compostos amb nuclearitat {$Ni_9$}: **9_2** – **9_5**, **10_7**, **10_8** i **10_12**. Aquests anells de {$Ni_9$} capturen anions ($N_3^-$, $Br^-$ o $I^-$) a través d'una sèrie de ponts d'hidrogen intermoleculars, que varien en funció de l'anió. Al mateix temps, la pròpia estructura d'aquests anells es veu estabilitzada per la presència de diversos ponts d'hidrogen intramoleculars. Així, aquests compostos són alhora exemples de les dues branques de la química supramolecular esmentades a la introducció: en primer lloc, aquests anells estan formats per efecte plantilla (de forma anàloga al compost **7_1**) però alhora s'estableix un reconeixement molecular (receptor-substrat o *host-guest*) entre l'anió encapsulat i l'amina dpt. La substitució o funcionalització d'aquesta amina provoca la desestabilització i trencament de l'estructura en no poder establir aquestes interaccions febles.

### 4.4.4. Reaccions secundàries

Es coneix que els cations metàl·lics actuen de catalitzadors en un gran nombre de reaccions orgàniques. Tot i no ser l'objectiu d'aquest treball, s'han observat diverses reaccions en què s'han format noves espècies, ja sigui per addició o trencament dels reactius.

D'aquestes, la reacció més observada és la modificació de la base $NEt_3$. La bibliografia descriu la reactivitat de di- i trialquilamines en diclorometà i condicions suaus.[190a] El seu ús com a base en dissolucions de $CH_2Cl_2$ en presència de cations $Ni^{II}$ pot generar les noves espècies $NEt_2H_2^+$ i $NEt_4^+$, observades durant aquesta tesi en els compostos **3_2** i **3_3** i **5_2**, **6_1** i **11_10**, respectivament, així com diverses amines amb substituents cloroalquilats.[114,174a]

El compost trinuclear **11_2** presenta una alteració en l'anió de partida: aquest va ser sintetitzat a partir de $Ni(hfacac)_2$ però el compost final presenta l'anió $CF_3COO^-$ enlloc del reactiu original. La descomposició de l'anió $hfacac^-$ de partida en $CF_3COO^-$ en presència de cations metàl·lics (en aquest cas $Ni^{II}$) es troba descrita a la bibliografia i segueix un mecanisme de condensació retro-Claisen.[172]

Finalment, el compost octanuclear **11_11** conté un nou lligand a l'estructura, pyC{tzH}NOH (tzH = tetrazole), que prové de la cicloaddició de nitrils i azidur formant l'anell de tetrazole. Aquesta també és una reacció catalitzada per cations metàl·lics descrita en la bibliografia.[176] Es va provar de sintetitzar aquest nou lligand a partir dels seus components, tant a reflux com en un reactor microones, però no es va donar la reacció, probablement per l'absència de cations metàl·lics.

# 5

# Summary

# 5. Summary

The aim of this thesis was the synthesis and both structural and magnetic characterization of new $Ni^{II}$/2-pyridyloximato polynuclear clusters. For this purpose, the reactivity of different 2-pyiridyloximato ligands in $Ni^{II}$ chemistry was tested, being the 2,6-diacetylpyridine-dioxyme ($dapdoH_2$) and the 2-pyridylcyanoxime (pyC{CN}NOH) the most studied ligands. In a final attempt to generate oximato/azido bridges, which tend to generate ferromagnetic couplings, the behavior of the 2-pyridyloxime/amine/azide system was also studied.

20 new clusters have been characterized with $dapdoH_2$ ligand, as well as the previously reported $[Ni^{IV}(dapdo)_2]$ mononuclear compound,[89] proving the coordinative capacity of this ligand. The following trends can be drawn from these new compounds:

- These clusters are the first $Ni^{II}$ polynuclear compounds obtained with $dapdoH_2$ ligand.
- $Dapdo^{2-}$ ligand tends to generate square-planar environments in $Ni^{II}$ cations when it coordinates in 2.10111 and 3.11111 modes.
- Inorganic anions generate higher nuclearity clusters ($Ni_8$-$Ni_{10}$) than carboxylate and β-dicetonate anions ($Ni_2$-$Ni_5$).
- On basis of diverse examples of oximato-mediated couplings with different bond parameters, the relation between the Ni-N-O-Ni torsion angle and the *J* value has been demonstrated, confirming previous correlations:[167] strong antiferromagnetic interaction for low torsion angles, decrease of the antiferromagnetic coupling when enlarging the torsion angle reaching a maximum *J* value (close to zero or even slightly ferromagnetic) for torsion angles close to 90°.

PyC{CN}NOH ligand have yielded 22 new clusters, being their most notable features:

- The presented clusters are the first $Ni^{II}$ polynuclear compounds obtained with this ligand.
- First examples of isolated $Ni_3$/$\mu_3$-OH/oximate triangular clusters have been obtained for this ligand, together with several $\mu_3$-OR-centered triangular based compounds with $Ni_4$ to $Ni_{13}$ nuclearities. The magneto-structural correlation derived from the magnetic study of these clusters, in addition to DFT calculations, permitted to establish that the main magnetic pathway for triangular units goes through the central $\mu_3$-OR bridge and the key parameter is the Ni-O-Ni angle.
- The $\{Ni_{13}Na_2\}_n$ chain possesses the highest nuclearity observed for sulfate/oximate clusters and the second highest in Ni/oximate and $Ni^{II}/SO_4$ clusters.
- $Ni_5$ nuclearity clusters represent 40% of the characterized compounds for pyC{CN}NOH ligand (9 out of 22). These clusters exhibit five different topologies, three of them observed in this thesis

for the first time: strongly distorted bowtie, triangle with dinuclear *handle* and a cubane coordinated to the fifth $Ni^{II}$ cation by a triple oximato bridge.

Finally, one mononuclear and 13 polynuclear new clusters were generated from the $Ni^{II}$/pyridyloximato/amine/azide quaternary system, all of the latter possessing azido-mediated interactions. Two main families of clusters were obtained, depending on the ligand used:

- PyC{ph}NOH and $py_2$CNOH ligands have generated a series of $\{Ni_9\}$ rings able to encapsulate azide and halide anions selectively by means of a set of H-bonds that come from the tridentate amine used in its synthesis and generate a prismatic environment in both anions.
- 6-MepyC{H}NOH ligand have formed two $\{Ni_{12}Na_2\}$ and $\{Ni_{13}\}$ clusters that can be described like two $\{Ni_6\}$ subunits that coordinate one or two metal ions. Each of these subunits contains four $\mu_3$-OH/azide and oximate/azide bridges that confer them an $S$ = 4 ground spin state and allow the generation of large spin clusters like the $\{Ni_{13}\}$, that exhibits an $S$ = 9 ground state, the highest observed among all $Ni^{II}$/oximato systems.

# 6

# Conclusions

The next conclusions can be drawn from the work presented in this thesis:

- The first polynuclear compounds from Nickel(II) and dapdo$H_2$ ligand have been obtained.

- The great coordinative capacity and variability of dapdo$H_2$ ligand and its derivatives have been proven: 1.00111, 2.10111, 3.11111, 3.20111 and 5.22111 coordination modes were characterized. 3.20111 and 5.22111 coordination modes have been characterized for the first time in this thesis.

- Dapdo$^{2-}$ ligand usually generates square-planar environments in $Ni^{II}$ cations when it coordinates in 2.10111 and 3.11111 modes.

- The mixture of $Ni^{II}$, dapdo$H_2$ and azide, in absence of polydentate amines, tends to generate the $[Ni^{IV}(dapdo)_2]$ mononuclear compound.

- Reaction of Nickel(II) with dapdo$H_2$ ligand has yielded higher nuclearity clusters for inorganic anions ($Ni_8$-$Ni_{10}$) than for carboxylate and β-dicetonate anions ($Ni_2$-$Ni_5$).

- The first $Ni^{II}$ compounds from pyC{CN}NOH ligand have been obtained. Moreover, the compounds obtained during this thesis are the only reported examples for this system.

- PyC{CN}NOH and pyC{CN}$NO^-$ ligands have shown 1.011, 2.111 and 3.211 coordination modes. Coordination of the nitrile group has not been observed in any case.

- This ligand tends to generate $\mu_3$-OR centered triangular-based clusters with carboxylate and β-dicetonate anions. Furthermore, the unique examples of isolated $Ni_3$/$\mu_3$-OR/oximato triangles reported until date were obtained from pyC{CN}NOH ligand.

- The great coordinative properties of the sulfate anion have been corroborated in the $\{Ni_8\}$ cluster and the $\{Ni_{13}Na_2\}_n$ chain. The latter shows the highest nuclearity for the sulfato/oximato system, as well as the second highest for both $Ni^{II}$/oximato and $Ni^{II}$/$SO_4$ systems.

- PyC{CN}$NO^-$ ligand is prone to the $Ni_5$ nuclearity, as proven by 40% of the compounds obtained with it. This trend is independent of the anion used in the synthesis. Moreover, these clusters exhibit up to 9 different nuclearities, 3 of them reported for the first time in this dissertation.

- The $Ni^{II}$/pyridyloximato/amine/azide quaternary system has demonstrated to be adequate to synthesize polynuclear compounds with azido-containing bridges. The $\{Ni_{13}\}$ system was obtained by this approach and exhibits the second highest nuclearity for $Ni^{II}$/oximato clusters.

- The nuclearity and topology of the final cluster depend basically on the pyridyloximato ligand and the amine used in its synthesis. However, the presence of carboxylate anions in the reaction medium affects the nature of the product.

- It has been confirmed that the oximato Ni-N-O-Ni torsion angle marks the intensity of the magnetic coupling.

- The Ni-O-Ni angle (with the central $\mu_3$-OR group) determines the coupling intensity in triangular systems while the Ni-N-O-Ni torsion angle has a minor effect in it. This dependency has been stated by means of the $Ni_3/\mu_3$-OR/oximato isolated triangles and confirmed by both DFT calculations and magneto-structural correlations.

- Several examples of rare $S$ = 0 $Ni_3/\mu_3$-OR/oximato triangles have been presented in this thesis. The ground state was justified by the $J_2/J_1$ ratio.

- The magnetic ground state of the pentanuclear systems described like triangle with *handle* depend on the $J_B/J_A$ ratio, being $J_A$ and $J_B$ the magnetic interactions inside and outside the triangle, respectively.

- Finally, it has been confirmed that oximato/azido and $\mu_3$-OR/azido mediated interactions (when the azide bridges in the *end-on* conformation) are ferromagnetic. The unambiguous determination of this interaction was fulfilled in basis of the first isolated oximato/azido bridged cluster.

- The $\{Ni_{13}\}$ system, formed by 6-MepyC{H}NO/azido and $\mu_3$-OR/azido bridges achieved the highest ground spin state among all $Ni^{II}$/oximato systems to date: $S$ = 9.

# 7

# Bibliografia

1. O. Khan, *Molecular Magnetism*, VCH Publishers, New York, **1993**.

2. J. Ribas, *Coordination Chemistry*, Wiley-VCH Verlag GmbH & Co. KGaA, Weinheim **2008**.

3. P. Pascal, *Ann. Chim. Phys.*, **1910**, 19, 5.

4. J. H. Van Vleck, *The theory of electric and magnetic susceptibilities*, Oxford University Press, Oxford, UK, **1932**.

5. D. Gatteschi, L. Pardi, *Gazz. Chim. Ital.* **1993**, 123, 231

6. Magpack: J. J. Borrás-Almenar, J. M. Clemente-Juan, E. Coronado, B. S. Tsukerblat, *J. Comput. Chem.* **2001**, *22*, 985. Fit: DSTEPIT program. Program 66, Quantum Chemistry Program Exchange, Indiana University, Bloomington, IN, **1965**.

7. N. F. Chilton, R. P. Anderson, L. D. Turner, A. Soncini, K. S. Murray, *J. Comput. Chem.* **2013**, *34*, 1164.

8. H. Giacomini, H. T. Diep, *Frustrated spin systems,* World Scientific Publishing Co. Pte. Ltd, USA, **2005**.

9. M. B. Ketchen, J. M. Jaycox, *Appl. Phys. Lett.* **1982**, *40*, 736.

10. T. Lis, *Acta Crystallographica Section B* **1980**, *36*, 2042.

11. A. Caneschi, D. Gatteschi, R. Sessoli, *J. Am. Chem. Soc*. **1991**, *113*, 5874.

12. (a) R. Sessoli, H. L. Tsai, A. R. Schake, S. Wang, J. B. Vincent, K. Folting, D. Gatteschi, G. Christou, D. N. Hendrickson, *J. Am. Chem. Soc.* **1993**, *115*, 1804; (b) R. Sessoli, D. Gatteschi, A. Caneschi, M. A. Novak, *Nature* **1993**, *365*, 141.

13. p.e. (a) G. Aromí, E. K. Brechin, *Struct. Bond*, **2006**, *122*, 1. (b) M. Andruh, J.-P. Costes, C. Diaz, S. Gao, *Inorg. Chem.* **2009**, *48*, 3342. (c) D. N. Woodruff, R. E. P. Winpenny, R. A. Layfield, *Chem. Rev*. **2013**, *113*, 5110. (d) P. Zhang, Y.-N. Guoa, J. Tang, *Coord. Chem. Rev.* **2013**, *257*, 1728.

14. S. L. Castro, Z. M. Sun, J. C. Bollinger, D. N. Hendrickson, G. Christou, *J. Chem. Soc.-Chem. Commun.* **1995**, 2517.

15. H. Miyasaka, R. Clérac, W. Wernsdorfer, L. Lecren, C. Bonhomme, K.-I. Sugiura, M. Yamashita, *Angew. Chem., Int. Ed.* **2004**, *43*, 2801.

16. T. C. Stamatatos, D. Foguet-Albiol, S.-C. Lee, C. C. Stoumpos, C. P. Raptopoulou, A. Terzis, W. Wernsdorfer, S. O. Hill, S. P. Perlepes, G. Christou, *J. Am. Chem. Soc.* **2007**, *129*, 9484.

17. C. J. Milios, A. Vinslava, W. Wernsdorfer, A. Prescimone, P. A. Wood, S. Parsons, S. P. Perlepes, G. Christou, E. K. Brechin, *J. Am. Chem. Soc.* **2007**, *129*, 6547.

18. C. Boskovic, E. K. Brechin, W. E. Streib, K. Folting, J. C. Bollinger, D. N. Hendrickson, G. Christou, *J. Am. Chem. Soc.* **2002**, *124*, 3725.

19. E. E. Moushi, A. Masello, W. Wernsdorfer, V. Nastopoulos, G. Christou, A. J. Tasiopoulos, *Dalton Trans.* **2010**, *39*, 4978.

20. M. Murugesu, M. Habrych, W. Wernsdorfer, K. A. Abboud, G. Christou, *J. Am. Chem. Soc.* **2004**, *126*, 4766.

21. A. J. Tasiopoulos, A. Vinslava, W. Wernsdorfer, K. A. Abboud, G. Christou, *Angew. Chem., Int. Ed.* **2004**, *116*, 2169.

22. A. Caneschi, A. Cornia, A. C. Fabretti, S. Foner, D. Gatteschi, R. Grandi, L. Schenetti, *Chem. Eur. J*. **1996**, *2*, 1379.

23. A. L. Barra, P. Debrunner, D. Gatteschi, C. E. Schulz, R. Sessoli, *Europhys. Lett.* **1996**, *35*,133.

24. L. F. Jones, E. K. Brechin, D. Collison, M. Helliwell, T. Mallah, S. Piligkos, G. Rajaraman, W. Wernsdorfer, *Inorg. Chem.* **2003**, *42*, 6601.

25. A. K. Boudalis, B. Donnadieu, V. Nastopoulos, J. M. Clemente-Juan, A. Mari, Y. Sanakis, J.-P. Tuchagues, S. P. Perlepes, *Angew. Chem.* **2004**, *116*, 2316.

26. E. K. Brechin, S. G. Harris, S. Parsons, R. E. P. Winpenny, *Chem. Commun.* **1996**, 1439.

27. M. Murrie, S. J. Teat, H. Stoeckli-Evans, H. U. Güdel, *Angew. Chem., Int. Ed.* **2003**, *42*, 4653.

28. M. Moragues-Cánovas, M. Helliwell, L. Ricard, E. Rivière, W. Wernsdorfer, E. K. Brechin, T. Mallah, *Eur. J. Inorg. Chem.* **2004**, 2219.

29. J. Ribas, A. Escuer, M. Monfort, R. Vicente, R. Cortes, L. Lezama, T. Rojo, *Coord. Chem. Rev.* **1999**, *195*, 1027.

30. G. S. Papaefstathiou, S. P. Perlepes, *Comments Inorg. Chem.* **2002**, *23*, 249.

31. C. Cadiou, M. Murrie, C. Paulsen, V. Villar, W. Wernsdorfer, R. E. P. Winpenny, *Chem. Commun.* **2001**, 2666.

32. S. T. Ochsenbein, M. Murrie, E. Rusanov, H. Stoeckli-Evans, C. Sekine, H. U. Güdel, *Inorg. Chem.* **2002**, *41*, 5133.

33. (a) A. Morello, O. N. Bakharev, H. B. Brom, L. J. de Jongh, *Polyhedron* **2003**, *22*, 1745. (b) E. K. Brechin, C. Boskovic, W. Wernsdorfer, J. Yoo, A. Yamaguchi, E. C. Sanudo, T. R. Concolino, A. L. Rheingold, H. Ishimoto, D. N. Hendrickson, G. Christou, *J. Am. Chem. Soc.* **2002**, *124*, 9710. (c) D. Gatteschi, R. Sessoli, *Angew. Chem., Int. Ed.* **2003**, *42*, 268. (e) D. Ruiz, Z. Sun, B. Albela, K. Folting, J. Ribas, G. Christou, D. N. Hendrickson, *Angew. Chem., Int. Ed.* **1998**, *37*, 300.

34. (a) W. Wernsdorfer, R. Sessoli, *Science* **1999**, *284*, 133. (b) W. Wernsdorfer, S. Bhaduri, C. Boskovic, G. Christou, D. N. Hendrickson, *Phys. Rev. B* **2002**, *65*, 180403.

35. (a) W. Wernsdorfer, N. E. Chakov, G. Christou, *Phys. Rev. Lett.* **2005**, *95*, 037203. (b) W. Wernsdorfer, M. Soler, G. Christou, D. N. Hendrickson, *J. Appl. Phys.* **2002**, *91*, 7164.

36. (a) Y. Suzuki, M. P. Sarachik, E. M. Chudnovsky, S. McHugh, R. Gonzalez-Rubio, N. Avraham, Y. Myasoedov, E. Zeldov, H. Shtrikman, N. Chakov, G. Christou, *Phys. Rev. Lett.* **2005**, *95*, 147201. (b) A. Hernández-Mínguez, J. M. Hernández, F. Macià, A. García-Santiago, J. Tejada, P. V. Santos, *Phys. Rev. Lett.* **2005**, *95*, 217205. (c) F. Macià, J. M. Hernandez, J. Tejada, S. Datta, S. Hill, C. Lampropoulos, G. Christou, *Phys. Rev. B* **2009**, *79*, 092403.

37. (a) M. N. Leuenberger, D. Loss, *Nature* **2001**, *410*, 789. (b) J. Tejada, E. M. Chudnovsky, E. del Barco, J. M. Hernández, T. P. Spiller, *Nanotechnology* **2001**, *12*, 181. (c) L. Bogani, W. Wernsdorfer, *Nature Mat.* **2008**, *7*, 179.

38. E. Warburg, *Ann. Phys.* **1881**, *249*, 141.

39. (a) P. Weiss, A. Piccard, *C. R. Hebd. Seances Acad. Sci.* **1918**, *166*, 352. (b) P. Debye, *Ann. Phys.* **1926**, *81*, 1154. (c) W. F. Giauque, *J. Am. Chem. Soc.* **1927**, *49*, 1864.

40. (a) V. K. Pecharsky, K. A. Gschneidner Jr., *J. Magn. Magn. Mater.*, **1999**, *200, 44.* (b) K. A. Gschneidner Jr., V. K. Pecharsky, *J. Appl. Phys.* **1999**, *85*, 5365. (c) J. Tejada, *Polyhedron* **2001**, *20*, 1751. (d) M. Evangelisti, E. K. Brechin, *Dalton Trans.*, **2010**, *39*, 4672. (e) V. Franco, J.S. Blázquez, B. Ingale, A. Conde, *Annu. Rev. Mater. Res.* **2012**, *42*, 305. (f) J. W. Sharples, D. Collison, *Polyhedron* **2013**, *54*, 91.

41. (a) F. Torres, J.M. Hernandez, X. Bohigas, J. Tejada, *Appl. Phys. Lett.* **2000**, *77*, 3248. (b) F. Torres, X. Bohigas, J.M. Hernandez, J. Tejada, *J. Phys. Condens. Mater.* **2003**, *15*, 119. (c) Y.I. Spichkin, A.K. Zvezdin, S.P. Gubin, A.S. Mischenko, A.M. Tishin, *J. Phys. D-Appl. Phys.* **2001**, *34*, 1162.

42. (a) M. Evangelisti, A. Candini, A. Ghirri, M. Affronte, S. Piligkos, E.K. Brechin, E.J.L. McInnes, *Polyhedron* **2005**, *24*, 2573. (b) I. A. Gass, E. K. Brechin, M. Evangelisti, *Polyhedron* **2013**, *52*, 1177.

43. (a) S. Nayak, M. Evangelisti, A.K. Powell, J. Reedijk, *Chem. Eur. J.* **2010**, *16*, 12865. (b) J.-L. Liu, J.-D. Leng, Z. Lin, M.-L. Tong, *Chem. Asian J*. **2011**, *6*, 1007. (c) M. Manoli, R. D. L. Johnstone, S. Parsons, M. Murrie, M. Affronte, M. Evangelisti, E. K. Brechin, *Angew. Chem., Int. Ed.* **2007**, *46*, 4456.

44. M. Evangelisti, A. Candini, M. Affronte, E. Pasca, L.J. de Jongh, R.T.W. Scott, E.K. Brechin, *Phys. Rev. B* **2009**, *79*, 104414.

45. L. J. Batchelor, M. Sander, F. Tuna, M. Helliwell, F. Moro, J. van Slageren, E. Burzuri, O. Montero, M. Evangelisti, F. Luis, E. J. L. McInnes, *Dalton Trans.* **2011**, *40*, 5278.

46. (a) G. Karotsis, M. Evangelisti, S.J. Dalgarno, E.K. Brechin, *Angew. Chem., Int. Ed.* **2009**, *48*, 9928. (b) C.-M. Liu, D.-Q. Zhang, D.-B. Zhu, *Dalton Trans.* **2010**, *39*, 11325. (c) Y.-Z. Zheng, E.M. Pineda, M. Helliwell, R.E.P. Winpenny, *Chem. Eur. J.* **2012**, *18*, 4161.

47. (a) Y.-Z. Zheng, M. Evangelisti, R.E.P. Winpenny, *Chem. Sci.* **2011**, *2*, 99. (b) Y.-Z. Zheng, M. Evangelisti, F. Tuna, R.E.P. Winpenny, *J. Am. Chem. Soc.* **2012**, *134*, 1057. (c) J.-B. Peng, Q.-C. Zhang, X.-J. Kong, Y.-Z. Zheng, Y.-P. Ren, L.-S. Long, R.-B. Huang, L.-S. Zheng, Z. Zheng, *J. Am. Chem. Soc.* **2012**, *134*, 3314.

48. (a) Y.-Z. Zheng, M. Evangelisti, R.E.P. Winpenny, *Angew. Chem., Int. Ed.* **2011**, *50*, 3692. (b) T.N. Hooper, J. Schnack, S. Piligkos, M. Evangelisti, E.K. Brechin, *Angew. Chem., Int. Ed.* **2012**, *51*, 4633. (c) J.-B. Peng, Q.-C. Zhang, X.-J. Kong, Y.-P. Ren, L.-S. Long, R.-B. Huang, L.-S. Zheng, Z. Zheng, *Angew. Chem., Int. Ed.* **2011**, *50*, 10649.

49. (a) A.S. Dinca, A. Ghirri, A.M. Madalan, M. Affronte, M. Andruh, *Inorg. Chem.* **2012**, *51*, 3935. (b) J.-D. Leng, J.-L. Liu, M.-L. Tong, *Chem. Commun.* **2012**, *48*, 5286.

50. M. Evangelisti, O. Roubeau, E. Palacios, A. Camon, T.N. Hooper, E.K. Brechin, J.J. Alonso, *Angew. Chem., Int. Ed.* **2011**, *50*, 6606.

51. (a) R.J. Blagg, F. Tuna, E.J.L. McInnes, R.E.P. Winpenny, *Chem. Commun.* **2011**, *47*, 10587. (b) J.W. Sharples, Y.-Z. Zheng, F. Tuna, E.J.L. McInnes, D. Collison, *Chem. Commun.* **2011**, *47*, 7650.

52. L.-X. Chang, G. Xiong, L. Wang, P. Cheng, B. Zhao, *Chem. Commun.* **2013**, *49*, 1055.

53. (a) T. Numazawa, K. Kamiya, T. Okano, K. Matsumoto, *Physica B* **2003**, *329*, 1656. (b) M.-J. Martinez-Perez, O. Montero, M. Evangelisti, F. Luis, J. Sese, S. Cardona-Serra, E. Coronado, *Adv. Mater.* **2012**, *24*, 4301.

54. (a) G. Christou, D. Gatteschi, D. N. Hendrickson, R. Sessoli, *MRS Bull.* **2000**, *25*, 66. (b) G. Aromi, E. K. Brechin, *Struct. Bonding* **2006**, *122*, 1. (c) G. Christou, *Polyhedron* **2005**, *24*, 2065.

55. J. Gómez-Segura, J. Veciana, D. Ruiz-Molina, *Chem. Commun.* **2007**, 3699.

56. (a) B. Dietrich, J. Guilhem, J. M. Lehn, C. Pascard, E. Sonveaux, *Helv. Chim. Acta* **1984**, *67*, 91. (b) S. Ulrich, A. Petitjean, J. M. Lehn, *Eur. J. Inorg. Chem.* **2010**, 1913.

57. (a) M. Yoneya, T. Yamaguchi, S. Sato, M. Fujita, *J. Am. Chem. Soc.* **2012**, *134*, 14401. (b) D. Fujita, K. Suzuki, S. Sato, M. Yagi-Utsumi, Y. Yamaguchi, N. Mizuno, T. Kumasaka, M. Takata, M. Noda, S. Uchiyama, K. Kato, M. Fujita, *Nature Commun.* **2012**, *3*, 1093.

58. (a) S. M. Biros, R. M. Yeh, K. N. Raymond, *Angew. Chem., Int. Ed.* **2008**, *47*, 6062. (b) C. J. Brown, G. M. Miller, M. W. Johnson, R. G. Bergman, K. N. Raymond, *J. Am. Chem. Soc.* **2011**, *133*, 11964.

59. (a) R. E. P. Winpenny, *J. Chem. Soc*., *Dalton Trans*. **2002**, 1. (b) A. Escuer, G. Aromí, *Eur. J. Inorg. Chem.* **2006**, 4721. (c) T. C. Stamatatos, V. Tangoulis, C. P. Raptopoulou, A. Terzis, G. S. Papaefstathiou, S. P. Perlepes, *Inorg. Chem.* **2008**, *47*, 7969. (d) S. Mukherjee, P. S. Mukherjee, *Acc. Chem. Res.* **2013**, *46*, 2556.

60. (a) J. M. Lehn, *Supramolecular Chemistry: Concepts and Perspectives*, Wiley-VCH, Weinheim, Germany, **1995**. (b) J. W. Steed, D. R. Turner, K. J. Wallace, *Core Concepts in Supramolecular Chemistry and Nanochemistry*, Wiley, Chichester, UK, **2007**. (c) J. W. Steed, J. L. Atwood, *Supramolecular Chemistry*, Wiley, Chichester, UK, **2009**.

61. (a) J. M. Lehn, *Angew. Chem., Int. Ed. Eng.* **1988**, *27*, 89. (b) J. M. Lehn, *Angew. Chem., Int. Ed. Eng.* **1990**, *29*, 1304.

62. (a) P. A. Gale, T. Gunnlaugsson, *Chem. Soc. Rev.* **2010**, *39*, 3595. (b) J. Steed, *Chem. Soc. Rev.* **2009**, *38*, 506. (c) J. L. Sessler, P. A. Gale, W.-S. Cho, *Anion Receptor Chemistry*; Royal Society of Chemistry, Cambridge, U.K., **2006**. (d) S. O. Kang, R. A. Begum, K. Bowman-James, *Angew. Chem., Int. Ed.* **2006**, *45*, 7882. (e) K. Bowman-James, *Acc. Chem. Res.* **2005**, *38*, 671.

63. D. Philp, J. F. Stoddart, *Angew. Chem., Int. Ed. Engl.* **1996**, *35*, 1154.

64. N. V. Gerbeleu, V. B. Arion, J. Burgess, *Template Synthesis in Macrocyclic Chemistry*, Wiley, Chichester, UK, **1999**.

65. (a) C. J. Pedersen, *J. Am. Chem. Soc.* **1967**, *89*, 2495. (b) C. J. Pedersen, *J. Am. Chem. Soc.* **1967**, *89*, 7017.

66. (a) J. H. Hartley, T. D. James, C. J. Ward, *J. Chem.Soc., Perkin Trans.,* **2000**, *1*, 3155. (b) A. W. Kleij, J. N. H. Reek, *Chem. Eur. J.* **2006**, *12*, 4218. (c) C. D. Gutsche, *Calixarenes Revisited*, The Royal Society of Chemistry, Cambridge, UK, **1997**.

67. G. Mezei, C. M. Zaleski, V. L. Pecoraro, *Chem. Rev.* **2007**, *107*, 4933.

68. H. E. Simmons, C. H. Park*, J. Am. Chem. Soc.* **1968**, *90*, 2428.

69. (a) E. Graf, J. M. Lehn, *J. Am. Chem. Soc.* **1976**, *98*, 6403. (b) J. M. Lehn, S. H. Pine, E. I. Watanabe, A. K. Willard, *J. Am. Chem. Soc.* **1977**, *99*, 6766. (c) J. M. Lehn, *Acc. Chem. Res.* **1978**, *11*, 49.

70. (a) N. Gimeno, R. Vilar, *Coord. Chem. Rev.* **2006**, *250*, 3161. (b) S. O. Kang, J. M. Llinares, V. W. Day, K. Bowman-James, *Chem. Soc. Rev.,* **2010**, **39**, 3980. (c) P. A. Gale, *Chem. Commun.* **2011**, *47*, 82.

71. S. J. Rosenberg, *Nickel and Its Alloys,* National Bureau of Standards, **1968**.

72. M. E. Weeks, *J. Chem. Educ.* **1932**, *9*, 22.

73. *Nickel*. U.S. Geological Survey, Mineral Commodity Summaries, **2013**.

74. J. R. Davis, *Nickel, Cobalt, and Their Alloys*, ASM Specialty Handbook, ASM International, **2000**, 7–13.

75. C. J. Milios, T. C. Stamatatos, S. P. Perlepes, *Polyhedron* **2006**, *25*, 134.

76. L. Tschugaeff, *Chem. Ber.* **1890**, *23*, 1.

77. (a) D. T. Rosa, J. A. Krause Bauer, M. J. Baldwin, *Inorg. Chem.* **2001**, *40*, 1606. (b) E. Abele, R. Abele, E. Lukevics, *Chem. Heter. Comp.* **2003**, *39*, 825. (c) E. S. Koumousi, M. Zampakou, C. P. Raptopoulou, V. Psycharis, C. M. Beavers, S. J. Teat, G. Psomas, T. C. Stamatatos, *Inorg. Chem.* **2012**, *51*, 7699

78. S. Akine, T. Taniguchi, T. Saiki, T. Nabeshima, *J. Am. Chem. Soc.* **2005**, *127*, 540.

79. (a) M. J. Goldcamp, S. E. Robison, J. A. Krause Bauer, M. J. Baldwin, *Inorg. Chem.* **2002**, *41*, 2307. (b) M.N. Kopylovich, V. Y. Kukushkin, M. Haukka, J. J. R. F. da Silva, A. J. L. Pombeiro, *Inorg. Chem.* **2002**, *41*, 4798.

80. J. M. Thorpe, R. L. Beddoes, D. Collison, C. D. Garner, M. Helliwell, J. M. Holmes, P. A. Tasker, *Angew. Chem., Int. Ed.* **1999**, *38*, 1119.

81. p.e.: P. Chaudhuri, *Coord. Chem. Rev.* **2003**, *243*, 143.

82. C.J. Milios, C.P. Raptopoulou, A. Terzis, F. Lloret, R. Vicente, S.P. Perlepes, A. Escuer, *Angew. Chem., Int. Ed.* **2004**, *43*, 210.

83. (a) R. Clérac, H. Miyasaka, M. Yamashita, C. Coulon, *J. Am. Chem. Soc.* **2002**, *124*, 12837. (b) A. Escuer, G. Vlahopoulou, F. A. Mautner, *Inorg. Chem.* **2011**, *50*, 2717.

84. R. A. Coxall, S. G. Harris, D. K. Henderson, S. Parsons, P. A. Tasker, R. E. P. Winpenny, *J. Chem. Soc., Dalton Trans.* **2000**, 2349.

85. C. W. Glynn, M. M. Turnbull, *Transition Met. Chem.* **2002**, *27*, 822.

86. G. I. H. Hanania, D. H. Irvine, F. Shurayh, *J. Chem. Soc.* **1965**, 1149.

86. I. V. Vasilevsky, R. E. Stenkamp, E. C. Lingafelter, N. J. Rose, *J. Coord. Chem.* **1988**, *19*, 171.

87. (a) B. A. Bovenzi, G. A. Pearse Jr., *J. Chem. Soc., Dalton Trans.* **1997**, 2793. (b) M. Salonen, H. Saarinen, I. J. Mutikainen, *Coord. Chem.* **2008**, *61*, 1462.

88. (a) K.A. Abboud, R.C. Palenik, G.J. Palenik, *Acta Crystallogr., Sect. C 50* **1994**, 525. (b) M. A. Halcrow, C. A. Kilner, J. Wolowska, E. J. L. McInnes, A. J. Bridgeman, *New J. Chem.* **2004**, *28*, 228.

89. G. Sproul, G. D. Stucky, *Inorg. Chem.* **1973**, *12*, 2898.

90. H. Namli, A. D. Azaz, S. Karabulut, S. Celen, R. Kurtaran, C. Kazak, *Transition Met. Chem.* **2007**, *32*, 266.

91. (a) B.C. Unni Nair, J.E. Sheats, R. Ponteciello, D. Van Engen, V. Petrouleas, G.C. Dismukes, *Inorg. Chem.* **1989**, *28*, 1582. (b) R.E. Marsh, *Inorg. Chem.* **1990**, *29*, 572.

92. A. Escuer, B. Cordero, X. Solans, M. Font-Bardia, T. Calvet, *Eur. J. Inorg. Chem.* **2008**, 5082.

93. I.V. Vasilevsky, R.E. Stenkamp, E.C. Lingafelter, V. Schomaker, R.D. Willet, N.J. Rose, *Inorg. Chem.* **1989**, *28*, 2619.

94. G.A. Nicholson, C.R. Lazarus, B.J. McCormick, *Inorg. Chem.* **1980**, *19*, 192.

95. T.C. Stamatatos, G. Christou, *Inorg. Chem.* **2009**, *48*, 3308.

96. (a) T. C. Stamatatos, B. S. Luisi, B. Moulton, G. Christou, *Inorg. Chem.* **2008**, *47*, 1134. (b) S. Khanra, T. Weyhermüller, P. Chaudhuri, *Dalton Trans.* **2008**, 4885.

97. A. Escuer, B. Cordero, M. Font-Bardia, T. Calvet, O. Roubeau, S. J. Teat, F. F. de Biani, *Dalton Trans.* **2010**, *39*, 4817.

98. S. Khanra, T. Weyhermüller, P. Chaudhuri, *Dalton Trans.* **2007**, 4675.

99. C. Lampropoulos, T. C. Stamatatos, K. A. Abboud, G. Christou, *Inorg. Chem.* **2009**, *48*, 429.

100. E. I. Baucom, R. S. Drago, *J. Am. Chem. Soc.* **1971**, *93*, 6469.

101. (a) V. V. Skopenko, N. N. Gerasimchuk, S. I. Tyukhtenko, H. Kohler, *Z. Anorg. Allg. Chem.* **1986**, *542*, 65. (b) T. V. Guskova, M. S. Tchernoviants, K. N. Bagdasarov, *Ukr. Khim. Zhurn.* **1984**, *50*, 982.

102. (a) A. Hubele, M. Kuehne, *Patent of the USA,* US 4063921, **1977**. (b) J. E. Engelhart, *Patent of the USA*, US 3780085, **1973**; US 3787579, **1974**.

103. (a) AG. Ciba-Geigy, *Patent of Austria* #367268, **1982**. (b) AG. Ciba-Geigy, *Patent of Poland* #127786, **1985**.

104. (a) G. K. Paliy, V. V. Skopenko, N. N. Gerasimchuk, O. A. Domashevskaya, E. F. Makats, R. V. Rakovskaya, *Patent of the USSR* #1405281, **1988**. (b) G. K. Paliy, V. V. Skopenko, N. N. Gerasimchuk, O. A. Domashevskaya, E. F. Makats, R. V. Rakovskaya, *Patent of the USSR* #1405282, **1988**. (c) S.H. Davidson, *Patent of the USA*, US 3957847, **1976**. (d) S.H. Davidson, *Brit. Patent*, GB 1470740, **1977**. (d) N. N. Gerasimchuk, A. Garmian, *Patent of the USA*, US 20130096098, **2013**.

105. (a) N. Gerasimchuk, A. N. Esaulenko, K. N. Dalley, C. Moore, *Dalton Trans.* **2010**, *39*, 749. (b) N.N. Gerasimchuk, V.V. Skopenko, V.V. Ponomareva, K.V. Domasevich, *Russ. J. Inorg. Chem.* **1993**, *38*, 964.

106. V.V. Skopenko, V.V. Ponomareva, Yu.A. Simonov, K.V. Domasevich, *Russ. J. Inorg. Chem.* **1994**, *39*, 1332.

107. N.N. Gerasimchuk, Yu.A. Simonov, A.A. Dvorkin, N. Rebrova, *Russ. J. Inorg. Chem.* **1993**, *38*, 247.

108. H. A. Charlier, N. Gerasimchuk, *Patent of the USA*, US 20070225238, **2007**; US 20080182804, **2008**; US 20080227731, **2008**.

109. (a) N. N. Gerasimchuk, V. V. Skopenko, K. V. Domasevich, O. A. Zhmurko, *Ukr. Khim. Zhurn. (Russian Edition)* **1992**, *58*, 935. (b) A. A. Mokhir, K. V. Domasevich, N. K. Dalley, X. Kou, N. N. Gerasimchuk, O. A. Gerasimchuk, *Inorg. Chim. Acta* **1999**, *284*, 85.

110. M.S. Tchernoviants, T.V. Guskova, K.N. Bagdasarov, *Russ. J. Anal. Chem.* **1984**, *39*, 797.

111. (a) N. Gerasimchuk, L. Nagy, H. G. Schmidt, M. Notlemeyer, R. Bohra, H. Roesky, *Z. Naturforsch. B* **1992**, *47*, 1741. (b) K.V. Domasevich, N.N. Gerasimchuk, E.V. Rusanov, O.A. Gerasimchuk, *Russ. J. Gen. Chem.* **1996**, *66*, 635.

112. N.N. Gerasimchuk, O.A. Zhmurko, S.I. Tykhtenko, *Russ. J. Inorg. Chem.* **1993**, *38*, 282.

113. A. Escuer, G. Vlahopoulou, S. P. Perlepes, F. A. Mautner, *Inorg. Chem.* **2011**, *50*, 2468.

114. L. Alcázar, B. Cordero, J. Esteban, V. Tangoulis, M. Font-Bardia, T. Calvet, A. Escuer, *Dalton Trans.* **2013**, *42*, 12334.

115. p.e: (a) R. Beckett, B. F. J. Hoskins, *Chem. Soc. Dalton Trans.* **1972**, 291. (b) T. C. Stamatatos, J. C. Vlahopoulou, Y. Sanakis, C. Raptopoulou, V. Psycharis, A. K. Boudalis, S. P. Perlepes, *Inorg. Chem. Commun.* **2006**, *9*, 814. (c) T. Afrati, C. Dendrinou-Samara, C. Raptopoulou, A. Terzis, V. Tangoulis, A. Tsipis, D. P. Kessissoglou, *Inorg. Chem.* **2008**, *47*, 7545.

116. (a) T. C. Stamatatos, D. Foguet-Albiol, C. C. Stoumpos, C. P. Raptopoulou, A. Terzis, W. Wernsdorfer, S. P. Perlepes, G. Christou, *J. Am. Chem. Soc.* **2005**, *127*, 15380. (b) T. C. Stamatatos, D. Foguet-Albiol, C. C. Stoumpos, C. P. Raptopoulou, A. Terzis, W. Wernsdorfer, S. P. Perlepes, G. Christou, *Polyhedron* **2007**, *26*, 2165.

117. Y.-L. Miao, J.-L. Liu, Z.-J. Lin, Y.-C. Ou, J.-D. Leng, M.-L. Tong, *Dalton Trans.* **2010**, *39*, 4893.

118. C. P. Raptopoulou, V. Psycharis, *Inorg. Chem. Commun*. **2008**, *11*, 1194.

119. E. Ruiz , J. Cano , S. Alvarez , P. Alemany, *J. Am. Chem. Soc.* **1998**, *120*, 11122.

120. J. S.-Y. Wong, W.-T. Wong, *New J. Chem.* **2002**, *26*, 94.

121. W.-Q. Chen, Y.-M. Chen, T. Lei, W. Liu, Y. Li, *Inorg. Chem. Commun.* **2012**, *19*, 4.

122. J. Martinez, I. Aiello, A. Bellusci, A. Crispini, M. Ghedini, *Inorg. Chim. Acta* **2008**, *361*, 2677.

123. (a) T. Afrati, C. Dendrinou-Samara, C. Raptopoulou, A. Terzis, V. Tangoulis, D.P. Kessissoglou, *Dalton Trans*. **2007**, 5156. (b) T. Afrati, A.A. Pantazaki, C. Dendrinou-Samara, C. Raptopoulou, A. Terzis, D.P. Kessissoglou, *Dalton Trans.* **2010**, 765. (c) G.-X. Liu, W. Guo, S. Nishihara, X.-M. Ren, *Inorg. Chim. Acta* **2011**, *368*, 165.

124. (a) T.C. Stamatatos, A. Bell, P. Cooper, A. Terzis, C.P. Raptopoulou, S.L. Heath, R.E.P. Winpenny, S.P. Perlepes, *Inorg. Chem. Commun.* **2005**, *8*, 533. (b) T.C. Stamatatos, C. Papatriantafyllopoulou, E. Katsoulakou, C.P. Raptopoulou, S.P. Perlepes, *Polyhedron* **2007**, *26*, 1830. (c) T.C. Stamatatos, E. Katsoulakou, A. Terzis, C.P. Raptopoulou, R.E.P. Winpenny, S.P. Perlepes, *Polyhedron* **2009**, *28*, 1638.

125. (a) M. Holynska, J. Klak, *Z. Kristallogr.* **2012**, *227*, 635. (b) C.J. Milios, S. Piligkos, A.R. Bell, R.H. Laye, S.J. Teat, R. Vicente, E. McInnes, A. Escuer, S. P. Perlepes, R. E. P. Winpenny, *Inorg. Chem. Commun.* **2006**, *9*, 638. (c) M. Holynska, S. Dehnen, *Inorg. Chem. Commun.* **2011**, *14*, 1290.

126. C. C. Stoumpos, R. Inglis, O. Roubeau, H. Sartzi, A. A. Kitos, C. J. Milios, G. Aromi, A. J. Tasiopoulos, V. Nastopoulos, E. K. Brechin, S. P. Perlepes, *Inorg. Chem.* **2010**, *49*, 4388.

127. (a) C .J. Milios, E. Kefalloniti, C. P. Raptopoulou, A. Terzis, R. Vicente, N. Lalioti, A. Escuer, S. P. Perlepes, *Chem. Commun.* **2003**, 819. (b) C. J. Milios, T. C. Stamatatos, P. Kyritsis, A. Terzis, C. P. Raptopoulou, R. Vicente, A. Escuer, S. P. Perlepes, *Eur. J. Inorg. Chem*. **2004**, *14*, 2885. (c) D. I. Alexandropoulos, M. J. Manos, C. Papatriantafyllopoulou, S. Mukherjee, A. J. Tasiopoulos, S. P. Perlepes, G. Christou, T. C. Stamatatos, *Dalton Trans.* **2012**, *41*, 4744.

128. P. Chaudhuri, T. Weyhermuller, R. Wagner, S. Khanra, B. Biswas, E. Bothe, E. Bill, *Inorg. Chem.* **2007**, *46*, 9003.

129. C. Papatriantafyllopoulou, C. G. Efthymiou, C. P. Raptopoulou, A. Terzis, E. Manessi-Zoupa, S. P. Perlepes, *Spectrochim. Acta, Part A*, **2008,** *70*, 718.

130. C. G. Efthymiou, C. P. Raptopoulou, A. Terzis, S. P. Perlepes, A. Escuer, C. Papatriantafyllopoulou, *Polyhedron* **2010**, *29*, 627.

131. C. Papatriantafyllopoulou, T. C. Stamatatos, W. Wernsdorfer, S. J. Teat, A. J. Tasiopoulos, A. Escuer, S. P. Perlepes, *Inorg. Chem.* **2010**, *49*, 10486.

132. (a) C. Papatriantafyllopoulou, G. Aromi, A. J. Tasiopoulos, V. Nastopoulos, C. P. Raptopoulou, S. J. Teat, A. Escuer, S. P. Perlepes, *Eur. J. Inorg. Chem.* **2007**, 2761. (b) C. G. Efthymiou, A. A. Kitos, C. P. Raptopoulou, S. P. Perlepes, A. Escuer, C. Papatriantafyllopoulou, *Polyhedron* **2009**, *28*, 3177.

133. (a) E. O. Schlemper, J. Stunkel, C. Patterson, *Acta Crystallogr., Sect. C* **1990**, *46*, 1226. (b) A. J. Stemmler, J. W. Kampf, V. L. Pecoraro, *Inorg. Chem.* **1995**, *34*, 2271. (c) S. O. Sommerer, B. L. Westcott, A. J. Jircitano, K. A. Abboud, *Inorg. Chim. Acta* **1995**, *238*, 149.

134. C. Dendrinou-Samara, C. M. Zaleski, A. Evagorou, J. W. Kampf, V. L. Pecoraro, D. P. Kessissoglou, *Chem. Commun.*, **2003**, 2668.

135. T. C. Stamatatos, S. Dionyssopoulou, G. Efthymiou, P. Kyritsis, C. P. Raptopoulou, A. Terzis, R. Vicente, A. Escuer, S. P. Perlepes, *Inorg. Chem.* **2005**, *44*, 3374.

136. T. Afrati, C. M. Zaleski, C. Dendrinou-Samara, G. Mezei, J. W. Kampf, V. L. Pecoraro, D. P. Kessissoglou, *Dalton Trans*. **2007**, 2658.

137. M. Alexiou , C. Dendrinou-Samara , C. P. Raptopoulou , A. Terzis , D. P. Kessissoglou, *Inorg. Chem*. **2002**, *41*, 4732.

138. (a) F. Mori , T. Nyui, T. Ishida , T. Nogami , K.-Y. Choi , H. Nojiri, *J. Am. Chem. Soc.* **2006**, *128*, 1440. (b) A. Okazawa, T. Nogami, H. Nojiri, T. Ishida, *Inorg. Chem.* **2008**, *47*, 9763. (c) A. Okazawa, R. Watanabe, M. Nezu, T. Shimada, S. Yoshii, H. Nojiri, T. Ishida, *Chemistry Letters* **2010**, *39*, 1331. (d) A. Okazawa, H. Nojiri, T. Ishida, N. Kojima, *Polyhedron* **2011**, *30*, 3140.

139. M. Alexiou, I. Tsivikas, C. Dendrinou-Samara, A. A. Pantazaki, P. Trikalitis, N. Lalioti, D. A. Kyriakidis, D. P. Kessissoglou, *J. Inorg. Biochem.* **2003**, *93*, 256.

140. (a) G. Psomas, A. J. Stemmler, C. Dendrinou-Samara, J. J. Bodwin, M. Schneider, M. Alexiou, J. W. Kampf, D. P. Kessissoglou, V. L. Pecoraro, *Inorg. Chem*. **2001**, *40*, 1562. (b) M. Alexiou, C. Dendrinou-Samara, C. P. Raptopoulou, A. Terzis, V. Tangoulis, D. P. Kessissoglou, *Eur. J. Inorg. Chem.* **2004**, 3822. (c) A. Audhya, M. Maity, K. Bhattacharya, R. Clerac, M. Chaudhury, *Inorg.Chem.* **2010**, *49*, 9026. (d) E. Moushi, C. G. Efthymiou, S. P. Perlepes, C. Papatriantafyllopoulou, *Int. J. Inorg. Chem.* **2011**, 606271.

141. T. C. Stamatatos, E. Diamantopoulou, C. P. Raptopoulou, V. Psycharis, A. Escuer, S. P. Perlepes, *Inorg. Chem*. **2007**, *46*, 2350.

142. (a) T. C. Stamatatos, A. Escuer, K. A. Abboud, C. P. Raptopoulou, S. P. Perlepes, G. Christou, *Inorg. Chem.* **2008**, *47*, 11825.

143. G. Psomas, C. Dendrinou-Samara, M. Alexiou, A. Tsohos, C. P. Raptopoulou, A. Terzis, D. P. Kessissoglou, *Inorg. Chem.* **1998**, *37*, 6556.

144. F. Mori, T. Ishida, T. Nogami, *Polyhedron* **2005**, *24*, 2588.

145. D. W. Phelps, W. F. Little, D. J. Hodgson, *Inorg. Chem.* **1976**, *15*, 2263.

146. T. Lynde-Kernell, E. O. Schlemper*, J. Coord. Chem.* **1988**, *16*, 347.

147. (a) K. Riggle, T. Lynde-Kernell, E. O. Schlemper, *J. Coord. Chem.* **1992**, *25*, 117. (b) A. Pajunen, M. Orama, H. Saarinen, *Acta Crystallogr., Sect. C: Cryst. Struct. Commun*. **1999**, *C55*, 2075.

148. G. C. Chiumia, D. C. Craig, Imdadullah, D. J. Phillips, *Inorg. Chim. Acta*, **1993**, *209*, 213.

149. G. C. Chiumia, D. J. Phillips, A. D. Rae, *Inorg. Chim. Acta* **1995**, *238*, 197.

150. D. C. Fariati, C.C. Craig, D.J. Phillips, *Inorg. Chim. Acta* **1998**, *268*, 135.

151. (a) C. C. Stoumpos, T. C. Stamatatos, V. Psycharis, C. P. Raptopoulou, G. Christou, S. P. Perlepes, *Polyhedron* **2008**, *27*, 3703. (b) C. C. Stoumpos, T. C. Stamatatos, H. Sartzi, O. Roubeau, A. J. Tasiopoulos, V. Nastopoulos, S. J. Teat, G. Christou, S. P. Perlepes, *Dalton Trans.* **2009**, *6*, 1004. (c) C. Lampropoulos, T. C. Stamatatos, M. J. Manos, A. J. Tasiopoulos, K. A. Abboud, G. Christou, *Eur. J. Inorg. Chem.* **2010**, *15*, 2244.

152. H.-S. Wang, Z.-C. Zhang, X.-J. Song, J.-W. Zhang, H.-B. Zhou, J. Wang, Y. Song, X.-Z. You, *Dalton Trans*. **2011**, *40*, 2703.

153. C. Gkioni, A. K. Boudalis, Y. Sanakis, V. Psycharis, C. P. Raptopoulou, *Polyhedron* **2009**, *28*, 32216.

154. X.-M. Qiu, S.-N. Wang, J. Lu, L.-Q. Kong, D.-C. Li, J.-M. Dou, *J. Coord. Chem.* **2012**, *65*, 3308.

155. (a) C. Papatriantafyllopoulou, M. Estrader, C. G. Efthymiou, D. Dermitzaki, K. Gkotsis, A. Terzis, C. Diaz, S. P. Perlepes, *Polyhedron* **2009**, *28*, 1652. (b) C. D. Polyzou, H. Nikolaou, C. Papatriantafyllopoulou, V. Psycharis, A. Terzis, C. P. Raptopoulou, A. Escuer, S. P. Perlepes, *Dalton Trans*. **2012**, *41*, 13755.

156. C. Papatriantafyllopoulou, L. F. Jones, T. D. Nguyen, N. Matamoros-Salvador, L. Cunha-Silva, F. A. Almeida Paz, J. Rocha, M. Evangelisti, E. K. Brechin, S. P. Perlepes, *Dalton Trans*. **2008**, *24*, 3153.

157. (a) C.-M. Ji, H.-J. Yang, C.-C. Zhao, V. Tangoulis, A.-L. Cui, H.-Z. Kou, *Cryst. Growth Des.* **2009**, *9*, 4607. (b) H.-Z. Kou, G.-Y. An, C.-M. Ji, B.-W. Wang, A.-L. Cui, *Dalton Trans*. **2010**, *39*, 9604. (c) X.-H. Deng, J.-W. Ran, *Acta Crystallogr., Sect. E: Struct. Rep. Online* **2012**, *68*, m40.

158. (a) J. Ran, X. Li, Q. Zhao, Y. Hou, W. Teng, G. Chen, *Inorg. Chem. Commun.* **2010**, *13*, 1527. (b) G.-Y. An, B. Yuan, J. Tao, A.-L. Cui, H.-Z. Kou, *Inorg. Chim. Acta* **2012**, *387*, 401.

159. X.-H. Deng, J.-W. Ran, *Acta Crystallogr., Sect. E: Struct. Rep. Online* **2011**, *67*, m1323.

160. K. F. Konidaris, V. Bekiari, E. Katsoulakou, C. P. Raptopoulou, V. Psycharis, S. P. Perlepes, T. C. Stamatatos, E. Manessi-Zoupa, *Inorg. Chim. Acta* **2011**, *376*, 470.

161. A. Pajunen, I. Mutikainen, H. Saarinen, M. Orama, *Z. Kristallogr.- New Cryst. Struct.* **1999**, *214*, 217.

162. A. Escuer, G. Vlahopoulou, F. A. Mautner, *Dalton Trans*. **2011**, *40*, 10109.

163. G. Vlahopoulou, A. Escuer, M. Font-Bardia, T. Calvet, *Inorg. Chem. Commun.* **2012**, *16*, 78.

164. A. Escuer, G. Vlahopoulou, F. Lloret, F. A. Mautner, *Eur. J. Inorg. Chem.* **2014**, *1*, 83.

165. (a) A. Escuer, G. Vlahopoulou, S. P. Perlepes, M. Font-Bardia, T. Calvet, *Dalton Trans.* **2011**, *40*, 225. (b) R. Ruiz, F. Lloret, M. Julve, M. C. Munoz, C. Bois, *Inorg. Chim. Acta* **1994**, *219*, 179. (c) E. Colacio, J. M. Dominguez-Vera, A. Escuer, M. Klinga, R. Kivekas, A. Romerosa, *J. Chem. Soc., Dalton Trans.* **1995**, 343. (d) J. M. Dominguez-Vera, E. Colacio, A. Escuer, M. Klinga, R. Kivekas, A Romerosa, *Polyhedron* **1997**, *16*, 281.

166. (a) C. J. Milios, R. Inglis, A. Vinslava, R. Bagai, W. Wernsdorfer, S. Parsons, S. P. Perlepes, G. Christou, E. K. Brechin, *J. Am. Chem. Soc.* **2007**, *129*, 12505. (b) R. Inglis, L. F. Jones, C. J. Milios, S. Datta, A. Collins, S. Parsons, W. Wernsdorfer, S. Hill, S. P. Perlepes, S. Piligkos, E. K. Brechin, *Dalton Trans.* **2009**, 3403.

167. M. A. Palacios, A. J. Mota, J. E. Perea-Buceta, F. J. White, E. K. Brechin, E. Colacio, *Inorg. Chem.* **2010**, *49*, 10156.

168. (a) C. Papatriantafyllopoulou, E. Manessi-Zoupa, A. Escuer, S. P. Perlepes, *Inorg. Chim. Acta* **2009**, *362*, 634. (b) C. Papatriantafyllopoulou, C. G. Efthymiou, C. P. Raptopoulou, R. Vicente, E. Manessi-Zoupa, V. Psycharis, A. Escuer, S. P. Perlepes, *J. Mol. Struct*. **2007**, *829*, 176.

169. J. Cano, T. Cauchy, E. Ruiz, C. J. Milios, C. C. Stoumpos, T. C. Stamatos, S. P. Perlepes, G. Christou, E. K. Brechin, *Dalton Trans.* **2008**, 234.

170. T. C. Stamatatos, K. A. Abboud, S. P. Perlepes, G. Christou, *Dalton Trans*. **2007**, 3861.

171. A. Escuer, R. Vicente, J. Ribas and X. Solans, *Inorg. Chem*. **1995**, *34*, 1793.

172. (a) S. R. Drake, A. Lyons, D. J. Otway, D. J. Williams, *Inorg. Chem.* **1994**, *33*, 1230. (b) S. Wang, Z. Pang, K. D. L. Smith, Y.-S. Hua, C. Deslippe, M. J. Wagner, *Inorg. Chem.* **1995**, *34*, 908.

173. W. C. Davies, E. B. Evans, F. L. Hulbert, *J. Chem. Soc.* **1939**, 412.

174. (a) C. Lampropoulos, K. A. Abboud, T. C. Stamatatos, G. Christou, *Inorg. Chem.* **2009**, *48*, 813. (b) J. Esteban, M. Font-Bardia, A. Escuer, *Eur. J. Inorg. Chem.* **2013**, 5274. (c) J. Esteban, M. Font-Bardia, J. Sanchez Costa, S. J. Teat, A. Escuer, *Inorg. Chem.* **2014**, *53*, 3194.

175. (a) J. S. Mihina , R. M. Herbst, *J. Org. Chem.* **1950**, *15*, 1082. (b) F. Himo, Z. P. Demko, L. Noodleman, K. B. Sharpless, *J. Am. Chem. Soc.* **2002**, *124*, 12210.

176. (a) D.P. Matthews, J.E. Green, A.J. Shuker*, J. Comb. Chem.* **2000**, *2*, 19. (b) Z. P. Demko, K. B. Sharpless, *J. Org. Chem.* **2001**, *66*, 7945. (c) L. Bosch, J. Vilarrasa, *Angew. Chem.* **2007**, *46*, 3926. (d) T. Jin, K. S. Kitahara, Y. Yamamoto, *Tetrahedron Lett*. **2008**, *49*, 2824. (e) G. Venkateshwarlu, A. Premalatha, K. C. Rajanna, P. K. Saiprakash, *Synth. Commun*. **2009**, *39*, 4479. (f) J. Bonnamour, C. Bolm, *Chem. Eur. J.* **2009**, *15*, 4543. (g) M. Nasrollahzadeh, Y. Bayat, D. Habibi, S. Moshaee, *Tetrahedron Lett*. **2009**, *50*, 4435.

177. (a) C. O. Kappe, *Angew. Chem., Int. Ed.* **2004**, *43*, 6250. (b) N. E. Leadbetter, *Chem. Commun.* **2005**, 2881.

178. A. Escuer, B. Cordero, M. Font-Bardia, T. Calvet, *Inorg. Chem.* **2010**, *49*, 9752.

179. (a) W. L. Gladfelter, M. W. Lynch, W. P. Schaefer, D. N. Hendrickson, H. B. Gray, *Inorg. Chem.* **1981**, *20*, 2390. (b) A. Escuer, M. Font-Bardıa, S. B. Kumar, X. Solans, R. Vicente, *Polyhedron* **1999**, *18*, 909. (c) E.-C. Yang, W. Wernsdorfer, S. Hill, R. S. Edwards, M. Nakano, S. Maccagnano, L. N. Zakharov, A. L. Rheingold, G. Christou, D. N. Hendrickson, *Polyhedron* **2003**, *22*, 1727. (d) E.-C. Yang, W. Wernsdorfer, L. N. Zakharov, Y. Karaki, A. Yamaguchi, R. M. Isidro, G.-D. Lu, S. A. Wilson, A. L. Rheingold, H. Ishimoto, D. N. Hendrickson, *Inorg. Chem.* **2006**, *45*, 529. (e) H.-S. Wang, Y. Song, *Inorg. Chem. Commun.* **2013**, *35*, 86.

180. H. Chen, C.-B. Ma, D.-Q. Yuan, M.-Q. Hu, H.-M. Wen, Q.-T. Liu, C.-N. Chen, *Inorg. Chem.* **2011**, *50*, 10352.

181. A. Escuer, R. Vicente, J. Ribas, M. S. El Fallah, X. Solans, M. Font-Bardia, *Inorg. Chem*. **1994**, *33*, 1842.

182. (a) J. Herring, M. Zeller, C. M. Zaleski, *Acta Cryst.* **2011**, *E67*, m41. (b) M. S. Lah, V. L. Pecoraro, *J. Am. Chem. Soc.* **1989**, *111, 7258. (*c) C. Dendrinou-Samara, A. N. Papadopoulos, D. A. Malamatri,A. Tarushi, C. P. Raptopoulou, A. Terzis, E. Samaras, D. P. Kessissoglou, *Journal of Inorganic Biochemistry*, **2005**, *99*, 864.